The early-stage structural evolution of the Barmer Basin rift, Rajasthan, northwest India

Andrew John Bladon

Submitted for the degree of Doctor of Philosophy
November 2014
Keele University

Keele University

Declaration Part 1. To be bound in the thesis

SUBMISSION OF THESIS FOR A RESEARCH DEGREE

Part I. DECLARATION by the candidate for a research degree. To be bound in the thesis

Degree for which thesis being submitted **Doctor of Philosophy in Earth Science**
Title of thesis **The early-stage structural evolution of the Barmer Basin rift, Rajasthan, northwest India.**

This thesis contains confidential information and is subject to the protocol set down for the submission and examination of such a thesis: NO

Date of submission **3rd November 2014** Original registration date **1st August 2011**
(Date of submission must comply with Regulation 2D)

Name of candidate **Andrew John Bladon**

Research Institute **EPSAM** Name of Lead Supervisor **Dr Stuart Clarke**

I certify that:

(a) The thesis being submitted for examination is my own account of my own research
(b) My research has been conducted ethically. Where relevant a letter from the approving body confirming that ethical approval has been given has been bound in the thesis as an Annex
(c) The data and results presented are the genuine data and results actually obtained by me during the conduct of the research
(d) Where I have drawn on the work, ideas and results of others this has been appropriately acknowledged in the thesis
(e) Where any collaboration has taken place with one or more other researchers, I have included within an 'Acknowledgments' section in the thesis a clear statement of their contributions, in line with the relevant statement in the Code of Practice (see Note overleaf).
(f) The greater portion of the work described in the thesis has been undertaken subsequent to my registration for the higher degree for which I am submitting for examination
(g) Where part of the work described in the thesis has previously been incorporated in another thesis submitted by me for a higher degree (if any), this has been identified and acknowledged in the thesis
(h) The thesis submitted is within the required word limit as specified in the Regulations

Total words in submitted thesis (including text and footnotes, but excluding references and appendices): **55,000**

Signature of candidate …… Date……

Note
Extract from Code of Practice: If the research degree is set within a broader programme of work involving a group of investigators – particularly if this programme of work predates the candidate's registration – the candidate should provide an explicit statement (in an 'Acknowledgments' section) of the respective roles of the candidate and these other individuals in relevant aspects of the work reported in the thesis. For example, it should make clear, where relevant, the candidate's role in designing the study, developing data collection instruments, collecting primary data, analysing such data, and formulating conclusions from the analysis. Others involved in these aspects of the research should be named, and their contributions relative to that of the candidate should be specified (*this does not apply to the ordinary supervision, only if the supervisor or supervisory team has had greater than usual involvement*).

Abstract

The structural evolution of the Barmer Basin and the context of the rift within the northwest Indian region are poorly understood, despite being a prolific hydrocarbon province. In this work an integrated basin analysis is presented covering the outcrop-, seismic-, and lithosphere-scales. The early-stage structural evolution and the origin of poorly understood structural complications in the Barmer Basin subsurface are assessed. Subsequently, the findings are placed within the wider context of the northwest Indian region and the implications for continued hydrocarbon exploration within the Barmer Basin are discussed.

Two non-coaxial extensional structural regimes are exposed at outcrop. Rift-perpendicular (≈ northeast-southwest) extension is demonstrably Paleocene in age and corresponded to the main episode of rifting in the Barmer Basin. A previously unrecognised, rift-oblique (≈ northwest-southeast) extensional event is poorly age constrained, and is suggested to have occurred during the Lower Cretaceous Epoch. Expansion of the investigation into the subsurface substantiates that rift-oblique extension preceded rift-perpendicular extension. The present day structural architecture of the Barmer Basin, therefore, resulted from the superimposition of two non-coaxial rifting events. Further structural analyses and lithosphere-scale forward modelling demonstrate that structural complications in the Barmer Basin subsurface arise from structural inheritance, and lithosphere flexure may have been substantial during Paleogene rifting.

The results demonstrate active rifting throughout northwest India prior to the Cretaceous-Paleogene boundary and eruption of the Deccan Traps. Lower Cretaceous (northwest-southeast) extension within the Barmer Basin may be an intra-continental manifestation of transtension between the Greater Indian and Madagascan continents during Gondwana fragmentation. Subsequently, relocation of the plate boundary between the Greater Indian and African continents in the wake of the rapidly migrating Greater Indian continent initiated northeast-southwest extension. Mesozoic sub-basins and the improved understanding of structural geometries with proven trapping potential are important considerations for ongoing hydrocarbon exploration within the Barmer Basin.

Acknowledgements

In submitting this thesis I am indebted to my academic supervisor Dr Stuart M. Clarke and my industrial supervisor Prof. Stuart D. Burley. I thank you both sincerely for giving me this opportunity, for your guidance and inspiration, and for your time and patience. I would have achieved little without your support. I hope that you will both look back upon this project with fond memories.

I am also grateful to many others who have helped shape me personally and professionally; Stuart Egan for his supervision and humour; Nicholas Whiteley for his unwavering support and kindness while in India; V. Kothari and Pinakadhar Mohapatra for their time and assistance; I am especially grateful to Bhanwar Lal for his companionship and logistical support while on fieldwork in Rajasthan; Jamie Pringle and the Mellor-Pringle family for their friendship; Richard Burgess for his invaluable technical support; Hazel Beaumont for her friendship and assistance while on fieldwork, and; members of the Basin Dynamics Research Group (BDRG) for many helpful discussions.

Cairn India Limited and Keele University provided funding and logistical support; Schlumberger Information Systems, Midland Valley, and Badleys Geoscience are thanked for providing Petrel, Move, and Stretch software packages respectively under academic licences, and; Faultkin7 and GEOrient stereoplotting software were also used. Crayola LLC is also thanked for producing some cracking colouring pencils.

Finally, nothing would be possible without the love and support of my parents Simon and Gabrielle and my sisters Toni and Jenny.

Contents

List of figures

List of tables

1. Introduction

The Barmer Basin rift; Summary hydrocarbon exploration history; Project rationale; Research aims and objectives; Thesis structure.

In this introduction, the Barmer Basin rift is briefly introduced, the broad aims and objectives of this thesis are outlined, and the structure of the subsequent chapters is described.

1.1 The Barmer Basin rift

Several giant oilfields were discovered in the Barmer Basin in 2004, predominantly situated within the crests of faulted blocks, and the basin is now an established oil and gas producing province with an estimated eight billion barrels (BBL) of stock tank oil in place (STOIIP), and over two hundred thousand barrels of oil per day (bopd) production. The extent and geometry of many fault blocks within the rift are controlled by poorly understood rift-oblique faults that are variably imaged throughout the subsurface. Today the rift has negligible topographic expression (Dolson *et al.* in press), and the tectonics, extent, and relationship of the Barmer Basin with the rifted margins remain undocumented. However, a substantial subsurface dataset acquired during hydrocarbon exploration within the Barmer Basin provides an unrivalled tool to investigate the evolution of the Barmer Basin and the tectonic evolution of the northwest Indian region.

Located within the Thar Desert of Rajasthan, northwest India, the Barmer Basin is a long (200 km), narrow (< 40 km) and deep (≤ 6 km), north-northwest trending, low-strain ($1.2 \leq \beta \leq 1.5$), failed continental rift (**Figure 1.1**). To date, the Barmer Basin has been interpreted as a latest Cretaceous (Maastrichtian) to mid-Paleogene (Lutetian) rift that opened in response to rifting of the Seychelles microcontinent from the Greater Indian continent near to the Cretaceous-Paleogene boundary (Compton 2009), contemporaneous with the main phase of Deccan eruptions. Despite 70% coverage of the rift by three-dimensional seismic data, a regional two-dimensional seismic dataset, four hundred and twenty wells, and an associated 4 km of core (Dolson *et al.* in press), an abundance of structural complications and rift-oblique faults are variably imaged on seismic datasets throughout the rift (**Figure 1.1b**), the origin of which remains elusive.

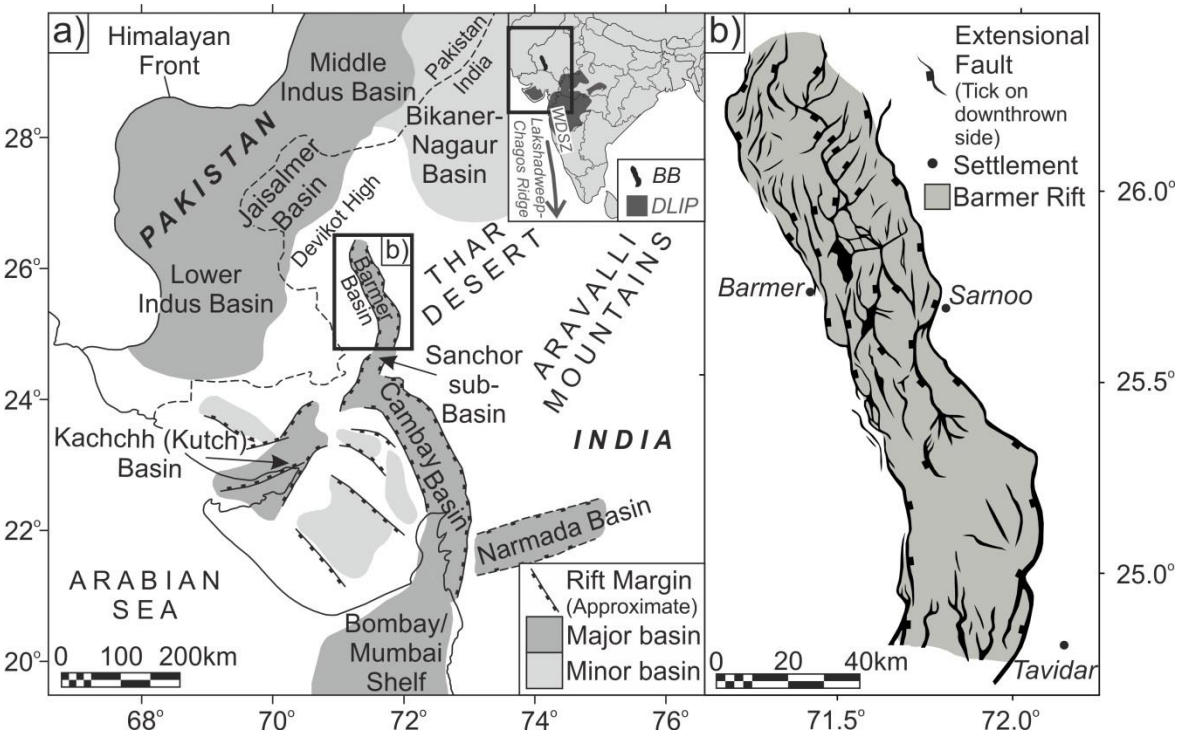

Figure 1.1 – **a)** Northwest Indian basins (location map inset). WDSZ = Western Deccan Strike-Slip Zone, BB = Barmer Basin, DLIP = Deccan Large Igneous Province; **(b)** Structure map of the Barmer Basin at the top Fatehgarh Formation (Paleocene) based on subsurface data (after Dolson *et al*. in press).

Despite the paucity of outcrop exposure within the Barmer Basin (< 1% by area), the available outcrop is situated at pivotal locations along the rifted margins, and can be closely correlated with subsurface seismic data. The lack of exposure precludes a detailed understanding of rift evolution being attained from outcrop exposure alone. However, in conjunction with the wealth of available subsurface seismic and well data, a multi-component analysis combining outcrop and subsurface studies, as well as lithosphere-scale forward modelling, provides critical insights into Barmer Basin rift evolution and the evolution of the West Indian Rift System as a whole. The Barmer Basin, therefore, is a truly excellent natural laboratory to undertake an integrated basin analysis, investigate complex tectono-stratigraphical relationships within a continental rift setting, and apply the findings to regional tectonic processes. Furthermore, the findings are highly applicable industrially and will aid ongoing hydrocarbon exploration within the Barmer Basin.

1.2 Summary hydrocarbon exploration history

Gravity data and poor quality two-dimensional seismic data prompted acquisition of 150 km of forty-eight fold two-dimensional seismic data across the south of the rift in 1989, which led to

formation of an exploration partnership between Shell India Petroleum Development, the Oil and Natural Gas Commission of India (ONGC), and the Government of India, and acquisition of a further 1613 km of two-dimensional seismic data and a small three-dimensional seismic survey (Dolson *et al.* in press). In 1995, Cairn Energy India Limited (CEIL) joined the exploration partnership with 27.5% equity, which increased to 50% in 1999 (Dolson *et al.* in press). Initial disappointing results prompted the transfer of operatorship to CEIL in 2000, who acquired a further 1267 km and 650 km^2 of two- and three-dimensional seismic data respectively, and discovered the Saraswati Field in 2001 and the Raageshwari Field in 2003 (Dolson *et al.* in press). However, these initial discoveries were considered small, and Shell India Petroleum Development and ONGC withdrew from the rift, leaving Cairn Energy India Limited (CEIL) as sole operator (Dolson *et al.* in press). In 2004 CEIL considered withdrawing from the rift, until an exploration well testing a large, shallow fault-block encountered the giant Mangala field with 360 m of overall pay (Dolson *et al.* in press). To date, thirty-six discoveries have been made, including five major fields, with the current joint venture partnership shared 70% to 30% between Cairn India Limited and the Oil and Natural Gas Commission (ONGC) respectively.

1.3 Project rationale

The poor understanding of Barmer Basin rift evolution needs to be improved. The Barmer Basin, and the West Indian Rift System as a whole (**Figure 1.1**), is an established and prosperous hydrocarbon province, and furthering the current understanding of rift, and rift-system evolution is essential for continued successful hydrocarbon exploration and efficient extraction of reserves.

Further to this, the West Indian Rift System is situated within a geologically fascinating and diverse setting. Rifts in the south of the West Indian Rift System are situated within the Deccan Large Igneous Province (DLIP; **Figure 1.1a inset**), where the Réunion plume is commonly invoked to explain the large outpouring of continental flood basalts and the onset of rifting throughout northwest India around the time of the Cretaceous-Paleogene boundary. However, the relationship between rifting and the eruption of flood basalts is speculative. Moreover, in the north of the West Indian Rift System, the Barmer Basin is situated within 400 km of the Himalayan Front, and the end of rifting in the Barmer Basin was approximately coincident with the onset of the collision between the Greater Indian and Eurasian continents. The geology and structural evolution of the West Indian Rift System, therefore, is exciting and influential, but remains largely undocumented. This

investigation will begin to unravel the structural evolution of the West Indian Rift System using a detailed, multi-component, integrated structural analysis of the Barmer Basin. The improved understanding of the structural evolution of the Barmer Basin will be discussed within the wider context of the northwest Indian region, and the implications of the work with respect to continued hydrocarbon exploration in the Barmer Basin will be assessed.

1.4 Research aims and objectives

In this work, the structural evolution of the Barmer Basin is investigated using combined outcrop and subsurface data, with a specific focus on structural complications evident within the deeper and older, early-stage sedimentary succession. A progressive and integrated basin analysis spanning three scales of investigation, namely the outcrop (small), basin (seismic), and lithosphere-scales, is presented in order to address the poorly understood evolution of the Barmer Basin rift, and place the findings within the wider context of the northwest Indian region. Explicitly, the main aims of this research are:

1. To further the current understanding of the structural evolution of the Barmer Basin.
2. To investigate the origin of poorly understood structural complications and rift-oblique faults imaged throughout the subsurface of the Barmer Basin.
3. To place Barmer Basin rift evolution within the wider context of the northwest Indian region.
4. To assess how the findings can aid ongoing hydrocarbon exploration within the Barmer Basin.

In order to achieve these aims, the initial objective of this research is to gain an understanding of the structure of the rift from the limited outcrop exposure within the Barmer Basin. Subsequently, upon gaining an understanding of the structure of the rift at outcrop, the objective is to expand the findings into the subsurface of the Barmer Basin using two-dimensional seismic data across a broad area of the central Barmer Basin, and additionally to clarify and refine the findings by conducting a targeted investigation of a rift-oblique subsurface structure using three-dimensional seismic data. Upon augmenting outcrop and subsurface investigations, the final objective is to investigate the flexural response of the lithosphere to extensional deformation, and to validate that shallow deformational processes constrained from outcrop and subsurface investigations are compatible with deformational processes at the lithosphere-scale.

1.5 Thesis structure

To achieve the aims and objectives of this research, a literature review is provided to support the results and interpretations presented in the subsequent chapters. This is followed by two chapters outlining the results of field-based investigations on opposing rift margins of the Barmer Basin, one chapter extending the investigation into the subsurface adjacent to one of the field sites using two-dimensional seismic data in conjunction with wireline log data, an application chapter where the results of the field- and subsurface seismic (two-dimensional) investigations are clarified and refined using three-dimensional seismic data, and one final chapter assessing the flexural response of the lithosphere and lithosphere deformational processes using the flexural-cantilever forward model. Finally, the findings of the integrated structural analysis of the Barmer Basin are discussed within the wider context of the northwest Indian region and with respect to ongoing hydrocarbon exploration within the Barmer Basin, and the conclusions of the work are presented. The content of each of the subsequent chapters is summarised below:

- **Chapter 2** presents a literature review in which background theory relevant to this investigation is introduced, including: 1) Brittle extensional deformation; 2) The onshore rift basins of northwest India, and 3) The Barmer Basin rift.
- In **Chapter 3** the results of an investigation into outcrop (small) scale, rift-parallel structures, exposed along the central western rift margin of the Barmer Basin, in the Barmer Hills, are presented. The main aim of this study is to assess the validity of the common assumption that deformation during the main phase of subsidence in the Barmer Basin during the Paleogene Period, namely the Barmer Basin rift event, accommodated approximately rift-perpendicular, northeast-southwest orientated regional extension.
- In **Chapter 4** the results of an investigation into outcrop (small) scale, rift-oblique structures, exposed along the central eastern rift margin of the Barmer Basin in the Sarnoo Hills, are presented in conjunction with the results of a sedimentological analysis of the sedimentary succession exposed. The main aims of this study are to characterise a rift-oblique fault network that is apparent nowhere else in the region and a sedimentary succession that accumulated prior to the main Barmer Basin rift event.
- In **Chapter 5** the results of an investigation into seismic (basin) scale tectono-stratigraphical relationships in the subsurface of the central Barmer Basin are presented.

The main aims of this study are to build upon the tectonic framework constructed from the two previous outcrop (small-scale) investigations using two-dimensional seismic data, and to investigate poorly understood spatio-temporal tectono-stratigraphical relationships between rift-parallel and rift-oblique faults in the subsurface of the Barmer Basin.

- In **Chapter 6** the results of a targeted investigation into a rift-oblique (north-south) seismic-scale structure, the Kaameshwari Fault, are presented. The main aim of this study is to clarify and refine the findings of the preceding outcrop (small) and seismic (basin) scale investigations using three-dimensional seismic data.
- In **Chapter 7** the results of an investigation into deformational processes at the lithosphere-scale are presented. The main aims of this study are to investigate the flexural response of the lithosphere during the main Barmer Basin rift event, validate that shallow deformational processes constrained from outcrop and subsurface investigations are compatible with deformational processes at the lithosphere-scale, constrain poorly understood mechanical lithosphere parameters, and complete the integrated structural analysis of the Barmer Basin.
- **Chapter 8** is a discussion in which the combined results of the integrated basin analysis presented in the preceding chapters are discussed together in the context of Barmer Basin rift evolution, and subsequently within the wider context of the northwest Indian region. The discussion is concluded with the implications of the work for continued hydrocarbon exploration within the Barmer Basin.
- In **Chapter 9** the thesis is concluded. The main results are summarised and some recommendations for further research are made.

2 Literature synthesis

Brittle extensional deformation; The onshore rift basins of northwest India; The Barmer Basin rift

In this literature review, the general theory of extensional deformation is introduced, followed by a summary evolution of the basins of northwest India, and finally the current understanding of the geology of the Barmer Basin is introduced.

2.1 Brittle extensional deformation

Deformation, namely a change in the form (e.g. shape/size/volume/orientation) of a body, results from the application of force to a body (Turcotte & Schubert 2002). Deformation is an expression of an applied force and depends upon numerous governing factors including material strength, material homogeneity, and the orientation and magnitude of the applied force. Deformation is quantified by 'strain', defined as the "the relative displacement of neighbouring elements in a rock mass" (Turcotte & Schubert 2002; Allen & Allen 2005; Jaeger *et al.* 2007). This section concentrates on relatively high-strain, brittle, deformational structures that occur within the shallow, brittle portion of the crust, namely extensional (normal) faults, that result from the application of an extensional force to a body, with specific focus on the structure and evolution of continental rift basins. A summary of models describing the geometries, evolution, and characteristics of extensional fault systems is introduced, followed by a description of continental rift basin evolution and interaction, and the section is concluded with a summary of structural complexities that may arise during fault or continental rift evolution in the presence of pre-existing planes of weakness (structural inheritance), or the application of an extensional force that is oblique to an evolving continental rift (transtensional or oblique rifts).

2.1.1 Extensional faulting

Faults, namely a surface or narrow zone with a distinct sense of shear displacement (Fossen 2010), are not laterally continuous and segmented fault arrays are common features of faults at all scales (Walsh *et al.* 2003). For the idealised case of an isolated fault, fault displacement, defined as the relative motion between two points that were originally adjacent before deformation, generally increases from zero at the fault tip points to a maximum at the centre of the fault

(**Figure 2.1**; Watterson 1986; Schlische 1991; Dawers & Anders 1995; Walsh *et al.* 2002). The length and maximum displacement of a fault display the following displacement-length relationship:

$$D = cL^n \qquad \textit{Equation 2.1}$$

where D = maximum fault displacement; L = fault trace length; c = is a constant that varies between fault populations (generally between 0 and 1), and; n = between 1 and 1.5, often simplified as 1 (Watterson 1986; Walsh & Watterson 1988; Schlische 1991; Cowie & Scholz 1992; Dawers & Anders 1995; Walsh *et al.* 2002; Kim & Sanderson 2005). Graphically, this idealized relationship is depicted as a symmetrical profile with maximum displacement (D_{max}) at the centre of the fault that decreases to zero towards the fault tip points (**Figure 2.1**). Analysis of fault displacement-length profiles provide key insights into the evolution of extensional fault systems, due to the distortion of fault displacement-length profiles as a result of kinematic interaction between adjacent fault segments (e.g. Trudgill & Cartwright 1994; Mcleod *et al.* 2000; Giba *et al.* 2012; Conneally *et al.* 2014).

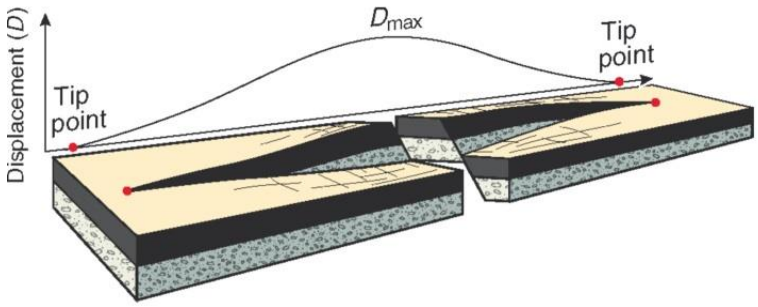

Figure 2.1 – Idealized fault displacement-length relationship with maximum displacement (D_{max}) at the centre of the fault that decreases to zero at the fault tip points. Image reproduced from Fossen (2010)

The relationship described (**Equation 2.1**) is widely accepted, and assumes a progressive increase in fault trace length as fault displacement increases (Walsh *et al.* 2002). In this manner, an array of faults may evolve from a series of initially isolated faults (**Figure 2.2a**; fault segments) by the lateral propagation of the fault tip points associated with increasing fault displacement, and the subsequent incidental lateral overlap of isolated fault segments (**Figure 2.2b**; Dawers & Anders 1995; Trudgill & Cartwright 1994; Schlische *et al.* 1996; Gupta *et al.* 1998; McLeod *et al.* 2000; Gawthorpe & Leeder 2000; Giba *et al.* 2012). Upon overlap, fault segments kinematically interact and may eventually link to form a through-going fault system (**Figure 2.2c**). 'Hard-linked' fault segments are physically joined, and 'soft-linked' fault segments are not physically joined, that is fault segments remain isolated, but are kinematically linked by ductile strain of the rock volume that

separates the fault segments (Trudgill & Cartwright 1994). At the scale of an array of normal faults, the formation, growth, and linkage of a normal fault system from a series of initially isolated faults into a through-going fault system by fault tip propagation, overstep, and hard-linkage (**Figure 2.2**), is termed an 'isolated fault model' (**Figure 2.3**; e.g. Dawers & Anders 1995; Trudgill & Cartwright 1994; Schlische *et al.* 1996; Gawthorpe & Leeder 2000; McLeod *et al.* 2000; Giba *et al.* 2012).

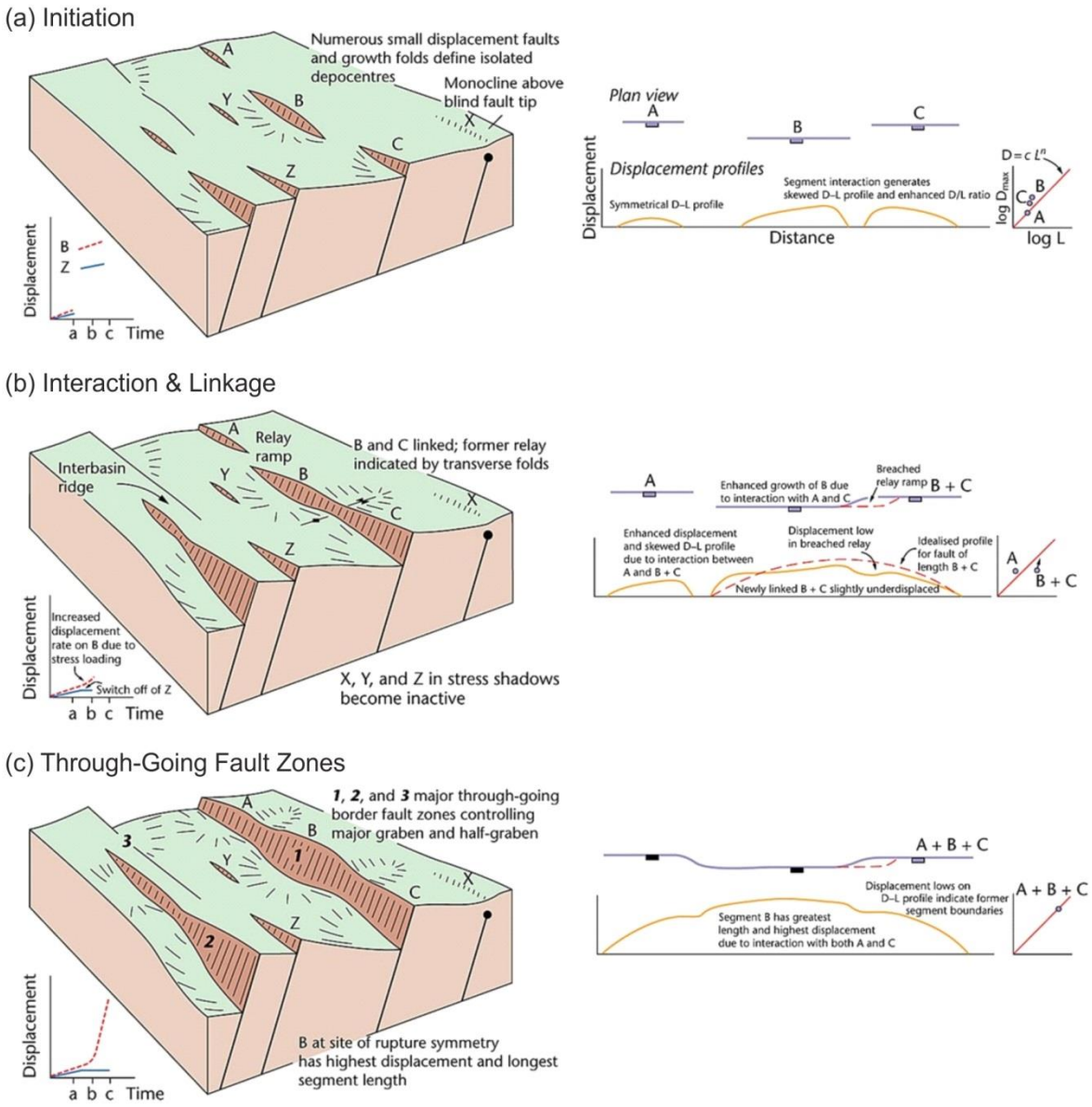

Figure 2.2 – Fault array evolution from a series of initially isolated fault segments [e.g. A, B, & C] **(a)** that grow and link at the expense of unfavourably positioned faults [e.g. X, Y, & Z] **(b)** to form through-going fault systems [e.g. 1, 2, & 3] **(c)** (after Gawthorpe & Leeder 2000). Schematic fault displacement-length profiles and map-view evolution of faults A, B, & C are shown to the right of the corresponding block-diagram. Image reproduced from Allen & Allen (2013).

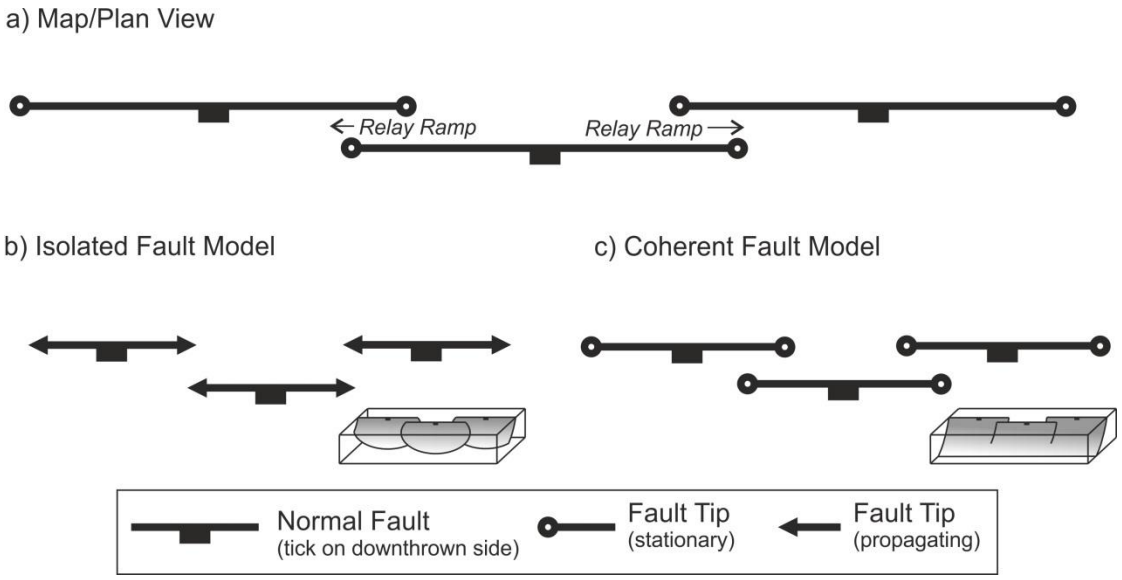

Figure 2.3 – In map view it is hard to distinguish whether a series of isolated fault segments **(a)** evolved by lateral fault-tip propagation, overstep, and subsequent hard-linkage (isolated fault model; **b**) or whether faults are kinematically related components of the same fault at depth (coherent model; **c**; after Giba *et al.* 2012).

Inherent in the isolated fault model is the predominance of lateral fault tip propagation and subsequent linkage between fault segments. However, fault planes propagate in three-dimensions, and where there is a significant vertical component of fault tip propagation, the map-view length of a fault segment may become rapidly established with relatively little increase in maximum fault displacement (Morley 1999a; Giba *et al.* 2012). Subsequent deformation will be dominated by displacement accumulation and subdued lateral fault-tip propagation in order to re-equilibrate the fault with the idealised displacement-length relationship (**Equation 2.1**; Morley 1999a; Walsh *et al.* 2002). An array of faults associated with a significant component of vertical fault-tip-propagation may be kinematically related components of the same structure, and may even be linked at depth (Giba *et al.* 2012). Such a scenario is termed the coherent fault model (**Figure 2.3c**; Childs *et al.* 1995; Walsh *et al.* 2002; Walsh *et al.* 2003). In map view it is difficult to distinguish whether a laterally segmented fault system evolved according to an isolated or coherent fault model, and it is often assumed that fault-tip propagation is within the plane of inspection favouring the isolated fault model (Giba *et al.* 2012).

Regardless of whether an array of normal faults evolved according to an isolated or coherent fault model, faults are inherently three-dimensional and fault growth is associated with both lateral and vertical propagation of the fault tip points. Lateral propagation and the subsequent interaction

between adjacent fault segments results in lateral segmentation in normal fault systems. However, the vertical variation in deformation mechanism (brittle vs ductile) caused by mechanical heterogeneity and rheological contrasts within a sedimentary succession also promotes vertical segmentation within fault systems and occurs at all scales (Childs *et al.* 1996). At the large scale, where ductile sedimentary rocks are present within a sedimentary basin, a complete decoupling may occur between shallow and deep-seated deformation (Withjack *et al.* 1990; Hardy & McClay 1999). However, fault systems are often viewed in map- (plan-) view, and vertical segmentation within fault systems is less well documented. It is critical to understand the geometrical evolution of an array of faults in three-dimensions in order to predict gross-depositional environments, sedimentary architectures, and thickness of basin fill sediments, which are often structurally controlled in an extensional terrane (Gawthorpe & Leeder 2000).

2.1.2 Displacement transfer and fault segment linkage within an extensional fault system

Inherent in the evolution of an extensional fault system is the vertical and lateral growth and linkage of fault segments. Fault systems containing two or more fault segments (segmented fault systems) are common across all scales (Walsh & Watterson 1989; Peacock & Sanderson 1991; Peacock & Sanderson 1994; Childs *et al.* 1995; Walsh *et al.* 2003; Giba *et al.* 2012). A primary feature of extensional fault systems, therefore, is the segmentation of the fault system into offset fault segments separated by discrete zones of displacement transfer. The rock volume between adjacent fault segments are zones of high strain that accommodate the transfer of displacement between fault segments, and are termed ‘relay zones’ (Childs *et al.* 1995; Kristensen *et al.* 2008). The relay zone between two overlapping faults can be classified as extensional or contractional in vertical cross-section depending upon the type of volumetric strain within the relay zone, while fault segments that overlap along-strike are associated with no volumetric strain and are referred to as neutral (**Figure 2.4**; Childs *et al.* 1996; Walsh *et al.* 1999; Kristensen *et al.* 2008). In this study the plane of inspection is predominantly in map (plan) view, and here a summary of lateral segmentation within extensional fault systems is presented, that is neutral relay zones (**Figure 2.4**).

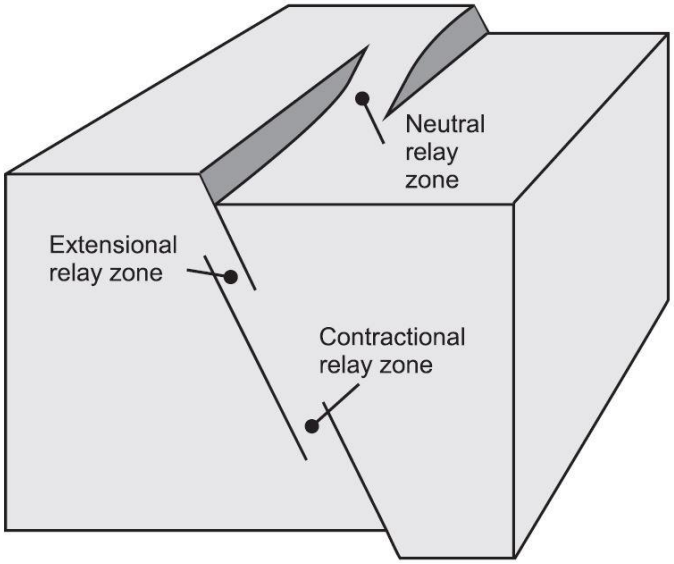

Figure 2.4 – Relay zones between overlapping fault segments are classified as extensional, contractional, or neutral dependent upon the type of volumetric strain within the relay zone. Image reproduced from Kristensen *et al.* (2008).

In the simple case of two synthetic normal faults, that is normal faults of sub-parallel orientation and comparable dip-direction, that overlap along strike, ductile strain in the intervening rock mass will cause rotation of the relay zone into the subsiding region and formation of a ramp (**Figure 2.5**; Fossen *et al.* 2005). The ramp-like structure that separates the offset fault segments is called a 'relay ramp' and accommodates the soft-linkage of synthetic normal faults (**Figures 2.5b & c**; Morley *et al.* 1990). With continued extension, propagation of the overlapping fault tip points is locally retarded due to the presence of a localised 'stress-shadow' within the hanging-wall or footwall of the adjacent fault segment (e.g. Cowie *et al.* 1993; Hodgkinson *et al.* 1996; Willemse 1997; Gupta *et al.* 1998; Cowie *et al.* 2000), that is an area of locally subdued stress resulting from proximity to an actively deforming fault (**Figure 2.6**). Subsequently, continued deformation is accommodated through an increase in fault displacement and supressed propagation of the fault tip points, resulting in progressively severe ramp rotation into the subsiding region. Strike-parallel (axial) rotation and attenuation of a relay-ramp produces extensional forces within the ramp, locally perturbing the stress-field and promoting the formation of second-order faults that are orientated obliquely to the adjacent fault segments, that breach the intervening relay ramp, and directly (hard) link the two offset fault segments (**Figure 2.5d & e**). Relay ramps are well documented, with many examples preserved globally within extensional fault systems, and are important locations of sediment input and migration pathways within extensional basins due to the subdued topographical relief associated with relay-ramp structures (e.g. Morley *et al.* 1990; Gawthorpe & Hurst 1993; Peacock & Sanderson 1994; Trudgill & Cartwright 1994; Faulds & Varga 1998; Gawthorpe &

Leeder 2000; Crider & Peacock 2004; Fossen 2010). Conversely, relay ramps may also form a pathway for hydrocarbons to migrate away from a depocentre when buried.

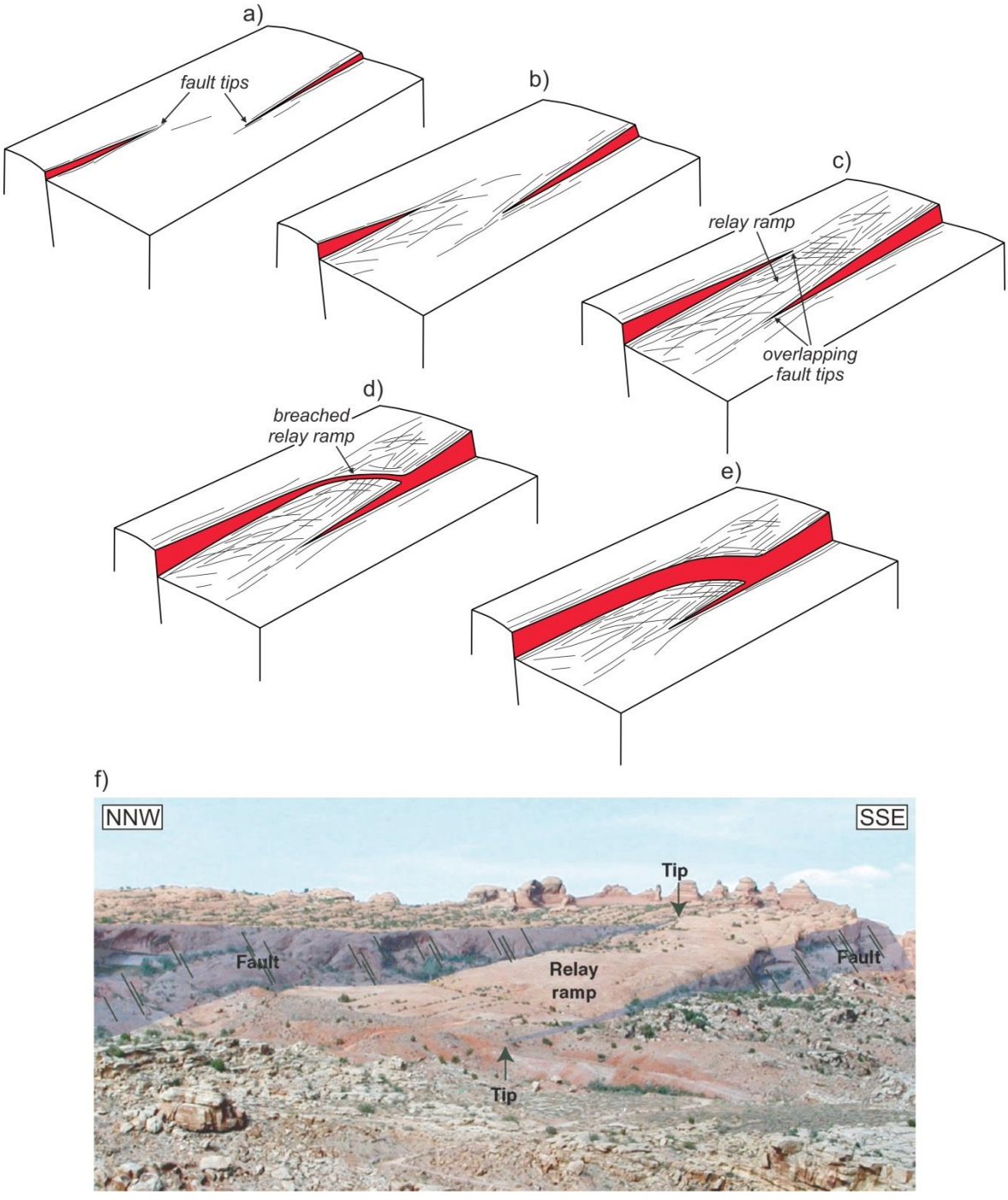

Figure 2.5 – **(a)** to **(e)** schematic diagrams of linkage between two sub-parallel normal faults by fault tip propagation, overstep, and breaching of the intervening relay ramp structure (after Fossen *et al.* 2005). **(f)** Photograph of an intact relay-ramp structure at Delicate Arch, Arches National Park, Utah, USA, corresponding to **(c)** (reproduced from Fossen 2010).

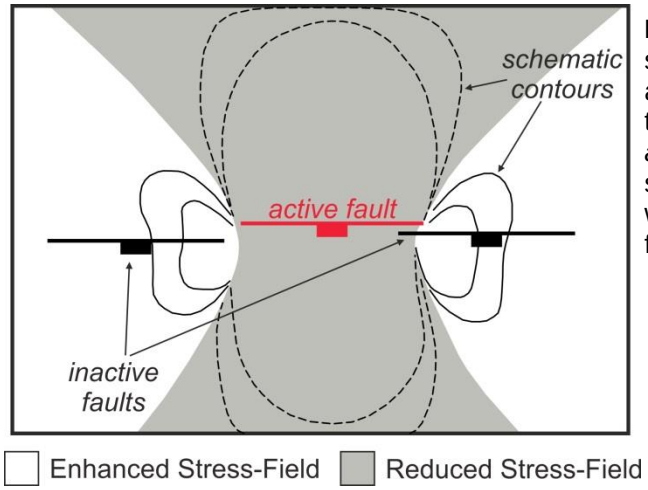

Figure 2.6 – Changes to the stress field after slip on an active fault inclined at 60° to the horizontal (after Gupta *et al.* 1998). Note the reduced stress-field in the hanging-wall and footwall of the active fault (stress-shadow).

Evolution of a fault system from a series of initially isolated fault segments that grow and link to form a through-going fault system results in a stress-feedback within an evolving fault network (Cowie *et al.* 1993; Cowie *et al.* 2000; Gawthorpe & Leeder 2000). Faults that are favourably orientated with comparable strike and dips, and positioned favourably within the evolving fault array (e.g. A, B, & C on **Figure 2.2**), will grow and link by the incidental lateral propagation, overlap, and linkage of isolated fault segments to form through-going fault systems (e.g. 1, 2, & 3 on **Figure 2.2**). However, faults that are either unfavourably orientated with an antithetic (opposite) dip or an unfavourable fault-strike, or faults that are favourably orientated but unfavourable positioned within the fault array, will become inactive (e.g. X, Y, & Z on **Figure 2.2**), further promoting growth of the evolving system of favourably positioned and orientated faults (Cowie *et al.* 1993; Cowie *et al.* 2000; Gawthorpe & Leeder 2000).

Upon establishment of a normal fault system comprising multiple, linked fault segments, the fault system will conform to the idealised displacement-length relationship described for an isolated fault (**Equation 2.1; Figure 2.1**), namely the fault system will have a maximum displacement near the centre that decreases to zero towards either end of the fault system (**Figure 2.7**; e.g. Willemse 1997). Individual fault segments within a fault system, therefore, will have displacement-length profiles that do not conform to the idealised relationship of an isolated fault (**Equation 2.1; Figure 2.1**), and may be skewed or accommodate a disproportionately large displacement relative to the length of the fault segment (**Figure 2.7**). However, fault segments within a fault system are no longer isolated, and mechanical linkage and interaction between individual fault segments facilitates the linked fault system to resemble the idealised displacement-length relationship.

During linkage of synthetic fault segments, rotation of the intervening relay ramp represents a ductile-type of non-recoverable strain accommodation that is not expressed as fault displacement. Any permanent ductile strain within the relay ramp between two offset fault segments during soft-linkage will persist as a low in aggregate displacement relative to the adjacent fault segments upon hard-linkage, and will indicate the location of relay zones and the extent of individual fault segments within a fault system (roman numerals in **Figure 2.7b**; e.g. Anders & Schlische 1994; Contreras *et al.* 2000; McLeod *et al.* 2000). Analysis of the displacement-length relationships of a fault system, therefore, provides critical insights into fault system evolution.

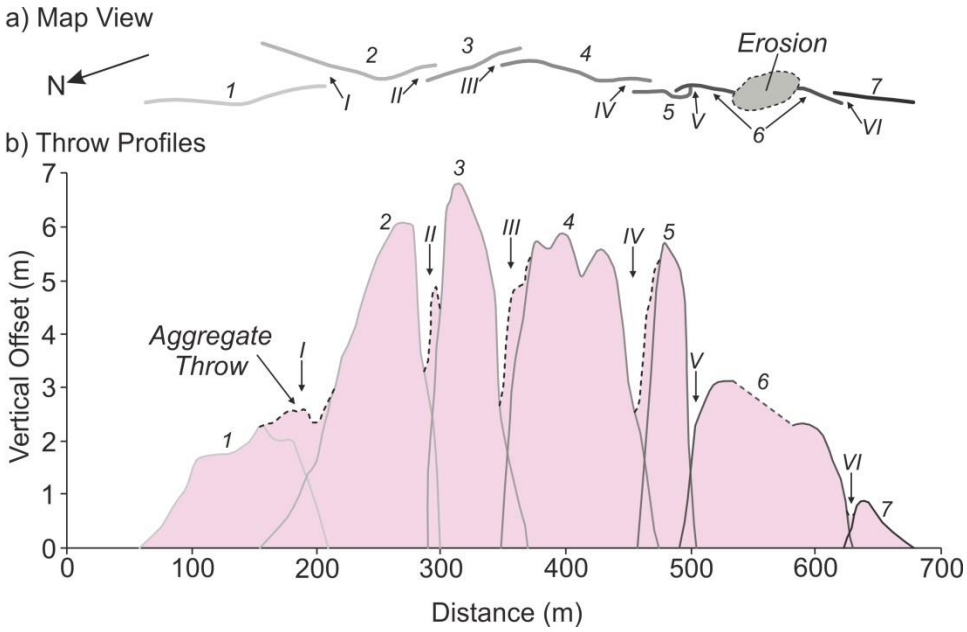

Figure 2.7 – Small- (metre) scale segmented fault system exposed at outcrop in California, USA, comprising seven individual fault segments (Arabic numerals) separated by six relay zones (Roman numerals; after Willemse 1997). **(a)** Map view of segmented fault system (north arrow inset). For scale see horizontal axis of **(b)**; **(b)** fault throw (vertical stratigraphical offset) profiles indicating individual fault segments within a fault system may have skewed profiles (1, 2, 6 & 7) or unusually high throw to length ratios (2, 3, 4, & 5) in order to form an aggregate throw profile (shaded in pink) which tends towards the idealised profile, namely maximum throw at the centre of the fault system decreasing to zero at either end. Note the low aggregate throw corresponding to each relay zone.

2.1.3 Continental rift basins

Continental rift basins occur as part of a suite of extensional basins resulting from lithosphere extension, with each classification of extensional basin defined by the degree of crustal stretching or thinning (**Figure 2.8**; Allen & Allen 2005). Crustal stretching and thinning is defined by the Beta (β) factor, namely “the factor by which a unit length of uniformly deforming material is extended and

unit thickness is thinned" (Kusznir *et al.* 1995), and is accommodated by brittle faulting in the shallow crust, and ductile thinning in the lower crust and mantle lithosphere (Kusznir & Egan 1989; Kusznir *et al.* 1991; Kusznir & Ziegler 1992; Kusznir *et al.* 1995). During continental rifting, crustal thinning induces localised uplift of the moho beneath the rift basin emplacing hot, comparatively low-density material beneath the rift causing a negative Bouguer gravity anomaly (raw gravity data corrected for elevation; c.f. Kearey & Brooks 1991), high heat flow, and magmatism (Allen & Allen 2005). The negative Bouguer gravity anomaly is accentuated by the low density sedimentary fill of the rift. Superficially, continental rift basins comprise normal sense, dip-slip faults, with a varying degree of strike-slip faults depending on the orientation of the rift axis with relation to the extension direction, and actively extending continental rift systems often have topographically elevated rift flanks bordering the subsiding region (e.g. the Great Rift Valley of East Africa; Allen & Allen 2005).

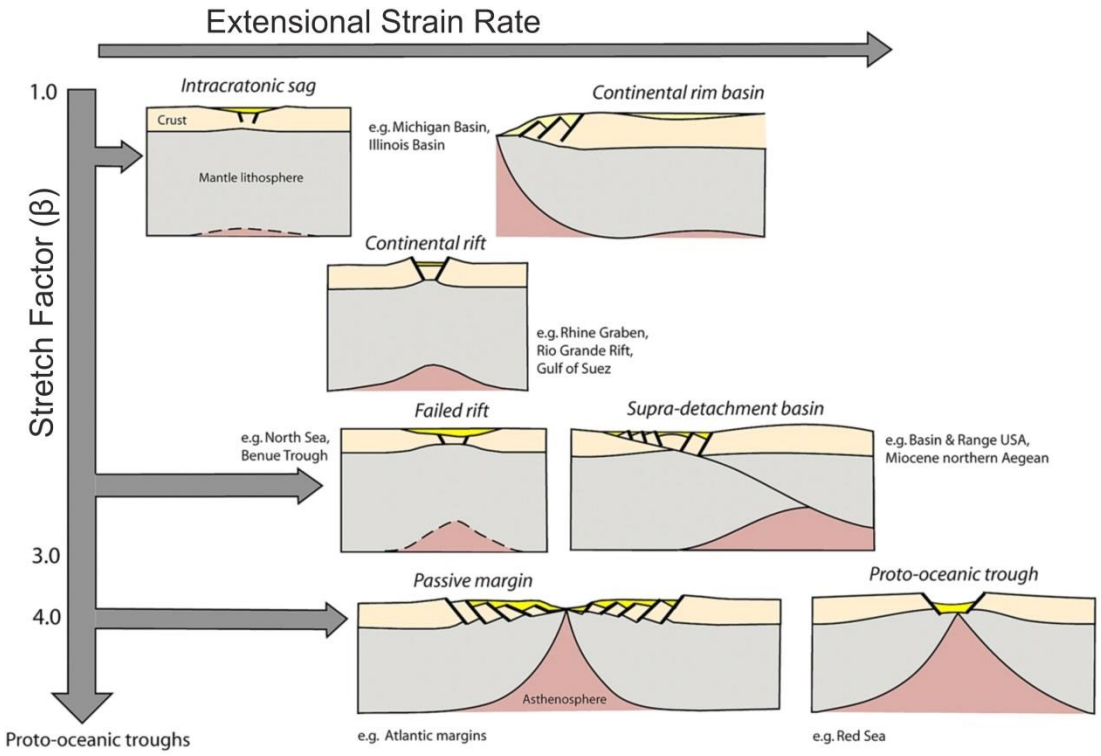

Figure 2.8 – The rift to drift suite of extensional basins, which categorises basins based upon the amount of crustal stretching [stretch or Beta (β) factor] and the strain rate (reproduced from Allen & Allen 2013). Continental rifts such as the Barmer Basin are situated between intra-cratonic sag and failed rift basins.

Crustal thinning in the shallow portion of the crust is facilitated by brittle faulting. Upon lithosphere extension, the establishment of through-going fault systems, comprising offset fault segments linked across discrete zones of displacement transfer, facilitates subsidence of a broad region and

formation of a localised rift basin in the hanging-wall of the active fault system. In the simplest case, a localised rift-basin in the hanging-wall of a major fault system may form an asymmetrical rift, termed a 'half-graben' (**Figure 2.9a**; Morley 1995; Fossen 2010). Asymmetrical half-graben form the fundamental building blocks of continental rift systems, and comprise a single, dominant rift-margin fault system opposed by a flexural rift-margin that may be largely unfaulted (Rosendahl 1987; Kusznir & Egan 1989; Morley 1995). Alternatively, a rift bound by antithetic rift-margin fault systems on either side forming a symmetrical rift is termed a 'graben' (**Figure 2.9b**; Morley 1995; Fossen. 2010). Similar to evolution of extensional fault systems from a series of initially isolated fault segments that grow and link to form a through-going fault system (**Figure 2.2**), through-going continental rift systems form by the propagation and linkage of initially isolated pockets of extension, termed 'rift segments' (Nelson *et al.* 1992). More specifically, continental rifts may form in one area and propagate in one or more directions away from that area (e.g. eastern branch of the East African Rift System), or multiple rift segments may initiate simultaneously along the length of a continental rift and propagate and link within the rift system (e.g. western branch of the East African Rift System; Nelson *et al.* 1992).

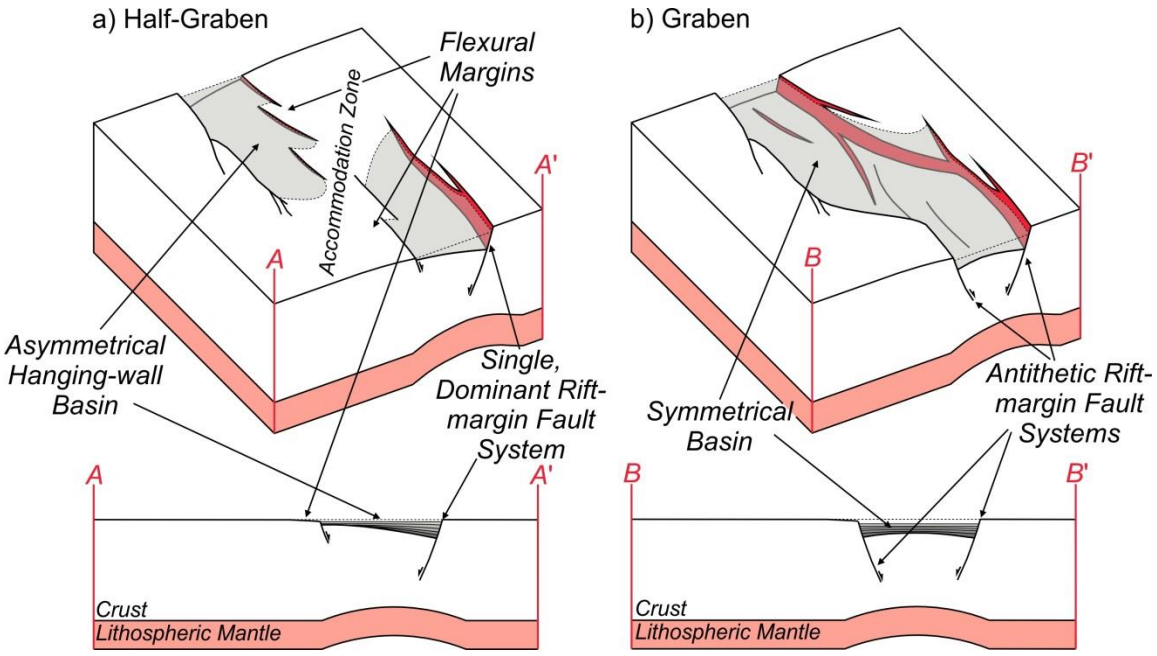

Figure 2.9 – Three-dimensional block diagrams and two-dimensional cross-sections of half-graben **(a)** and graben **(b)** rift geometries.

2.1.4 Displacement transfer and rift-segment linkage within an evolving rift system

As with the evolution of an extensional fault system, it is implicit that the evolution of a continental rift system from a series of isolated rift segments involves the interaction and eventual linkage of adjacent rift segments. The zones of displacement transfer between adjacent rift segments are analogous to those between offset fault segments, and have been classified in the literature using various terms, predominantly transfer and accommodation zones (e.g. Rosendahl 1987; Scott & Rosendahl 1989; Morley *et al.* 1990; Gawthorpe & Hurst 1993; Faulds & Varga 1998). Here, both 'accommodation zone' and 'transfer zone' are used to classify these regions depending upon the nature of displacement transfer (e.g. Faulds & Varga 1998). Normal fault systems are assumed to terminate in one of two types of structure: 1) strike-slip or oblique-slip fault zones that generally link spatially separated pockets of extension, termed a 'transfer zone' (**Figure 2.10**), or; 2) diffuse belts of overlapping fault terminations between adjacent rift segments, termed an 'accommodation zone' (**Figure 2.11**; Faulds & Varga 1998). Further sub-classifications of transfer and accommodation zones are defined by the relationship of the dip-direction of the dominant fault systems, namely similarly (synthetic) or oppositely (antithetic) dipping, and accommodation zones can be further classified based upon the degree of overlap between fault systems (**Figures 2.10 & 2.11**). As occurs during soft-linkage of two offset fault segments within an evolving fault system, non-recoverable ductile (rotational) strain within accommodation zones results in aggregate displacement measurement minima.

2.1.5 Structural complications

Many natural examples of extensional fault and continental rift systems do not display the geometrical characteristics and relationships described previously. Disparities between predicted and observed geometries are generally attributed to two broad phenomena, namely the interaction of structures inherent in the crust with the evolving structural systems during extensional deformation, known as structural inheritance, or an extension direction that is oblique (non-perpendicular) to the deforming structure, known as transtensional (oblique) rifting. In this sub-section these two phenomena are introduced.

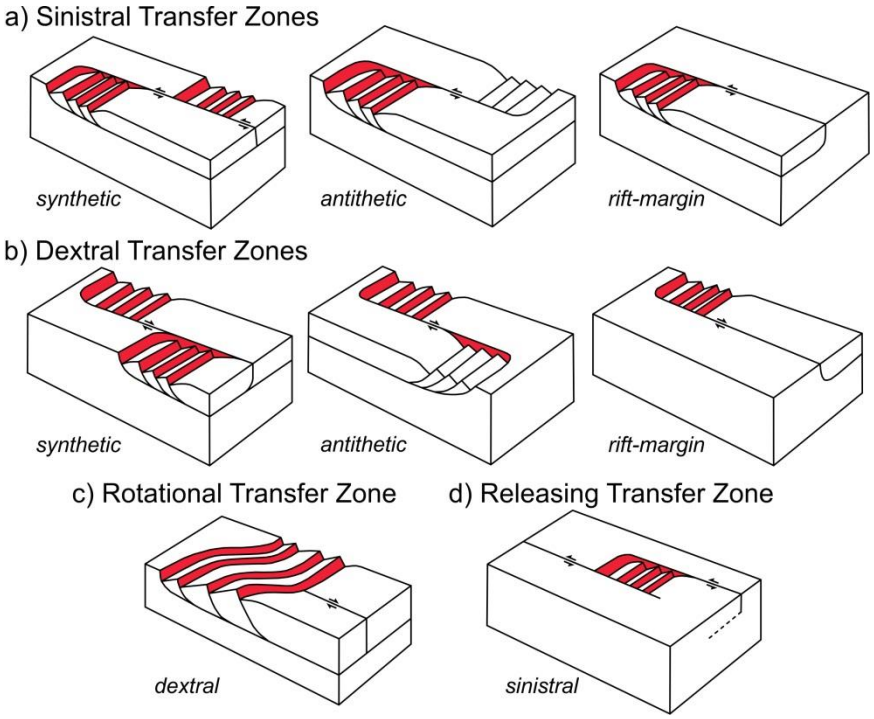

Figure 2.10 – Transfer zone classification (after Faulds & Varga 1998). Transfer zones are classified based upon the relative dip directions of normal fault systems within the linked domains of extension (synthetic or antithetic) and the sense of motion along the zone separating linked zones (sinistral or dextral).

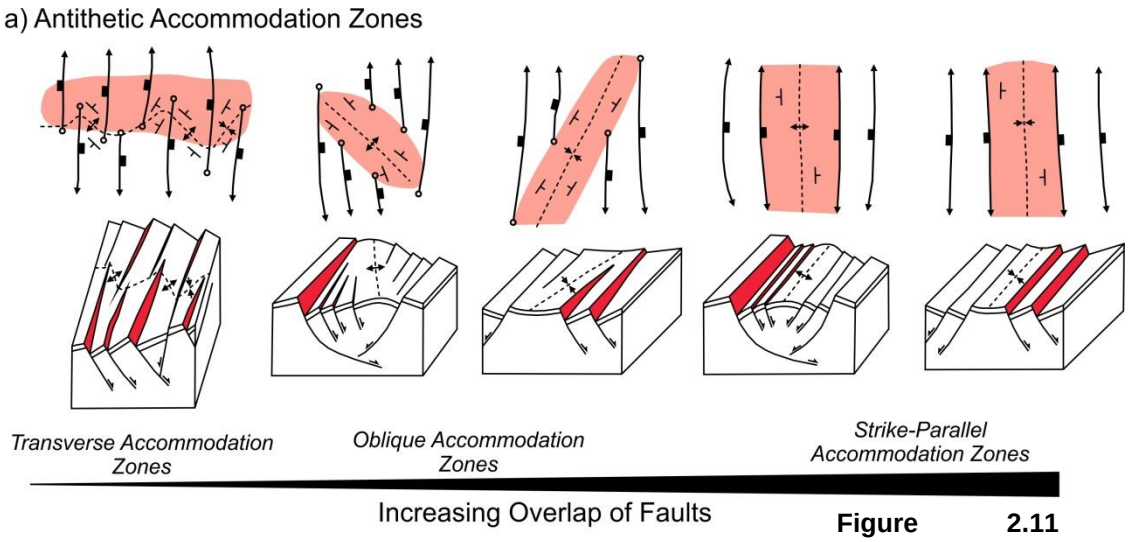

Figure 2.11 – Accommodation zone classification (after Faulds & Varga 1998). The geometry of accommodation zones varies significantly depending upon the degree of overlap (transverse, oblique, and strike-parallel) and the relative dip directions (synthetic or antithetic) between adjacent normal fault systems.

2.1.5.1 Structural inheritance

The involvement of pre-existing structures that are inherent in the crust during extension has been investigated extensively through combined experimental, seismic, and outcrop studies (Lezzar *et al.* 2002; Younes & McClay 2002; McClay *et al.* 2002; Morley *et al.* 2004; Bellahsen & Daniel 2005; Bellahsen *et al.* 2006; Henza *et al.* 2010; Henza *et al.* 2011; Giba *et al.* 2012; Chattopadhyay & Chakra 2013; Reeve *et al.* 2014; Whipp *et al.* 2014; Nixon *et al.* 2014). However, few detailed studies exist that characterise the affect that structures inherent in the crust can have on an evolving extensional fault network based on outcrop-data alone (e.g. McClay & Khalil 1998). Pre-existing faults are ubiquitous throughout continental crust and it is likely that structural inheritance will occur at some scale within all extensional fault systems. Multiple extensional deformational events may be localised onto discrete, weak sections of continental crust resulting in superimposition of rift events, and complex interactions between large-scale rift structures (e.g. Keep & McClay 1997; Bonini *et al.* 1997; Morley *et al.* 2007; Henza *et al.* 2010; Henza *et al.* 2011; Nixon *et al.* 2014). Where superimposed extensional events are non-coaxial, that is the extension direction changes between successive rifting events, complex and unexpected three-dimensional structural geometries and relationships often develop (**Figure 2.12**).

Extensional faulting occurs in a low mean-stress environment, and pre-existing fabrics within the crust may be reactivated at high angles (60°) to the extension direction (Morley 1995). Shear failure of an intact rock takes place along a plane due to the shear stress acting on the rock (Jaeger *et al.* 2007). Motion on an existing plane is resisted by a frictional-type force that arises due to the normal stress ($\boldsymbol{\sigma_n}$) acting on the shear plane, with a magnitude defined by multiplying the normal stress by the coefficient of sliding friction of the plane ($\boldsymbol{\mu_s}$). However, in the case of intact rock, shear failure is also resisted by the strength of the intact material, termed the cohesive rock strength ($\boldsymbol{C}$), and the magnitude of friction is defined by the coefficient of internal friction ($\boldsymbol{\mu}$), namely the coefficient of friction along an imaginary surface within the intact rock before failure occurs. It follows that failure of most upper crustal rocks is defined by:

$$\boldsymbol{\tau = C + \mu\sigma_n} \qquad \textit{Equation 2.2}$$

where $\boldsymbol{\tau}$ = shear stress acting on failure plane; $\boldsymbol{C}$ = cohesive strength of the rock; $\boldsymbol{\mu}$ = coefficient of internal friction, and; $\boldsymbol{\sigma_n}$ = normal stress acting on failure plane (Jaeger *et al.* 2007; Henza *et al.* 2010).

Shear failure of intact rock will occur when:

$$\tau > C + \mu\sigma_n \qquad \textit{Equation 2.3}$$

Upon formation of a shear plane, the rock is considered to retain no cohesive strength across the failure plane (C = 0) and continued shear along the plane is controlled by frictional-sliding:

$$\tau = \mu_s\sigma_n \qquad \textit{Equation 2.4}$$

where μ_s = coefficient of sliding friction (Jaeger *et al.* 2007; Henza *et al.* 2010). Reactivation of a pre-existing plane of weakness, therefore, will occur if the ratio of shear stress to normal stress acting on a plane exceeds the coefficient of sliding friction (Henza *et al.* 2010):

$$\tau > \mu_s\sigma_n \quad or \quad \frac{\tau}{\sigma_n} > \mu_s \qquad \textit{Equation 2.5}$$

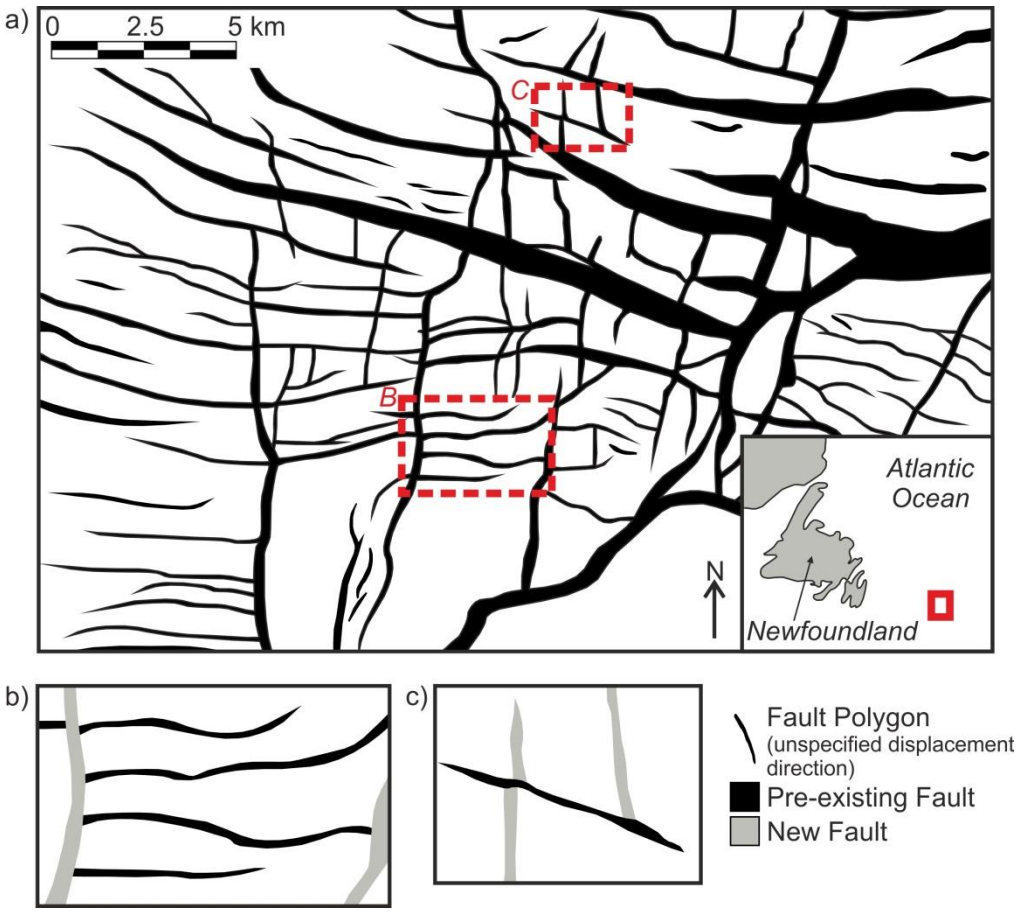

Figure 2.12 – **(a)** Map view of complex and unusual three-dimensional fault geometries preserved within early Cretaceous strata in the Jeanne d'Arc Basin, offshore Newfoundland. Location map inset. Faults formed during a more recent deformational event ('new fault') are interpreted to both abut **(b)** and offset **(c)** older, pre-existing faults. Fault interactions, therefore, are variable. The locations of **(b)** and **(c)** are indicated on **(a)**. After Henza *et al.* (2010).

It follows that, assuming $\boldsymbol{\mu \approx \mu_s}$, shear failure of a pre-existing plane of weakness requires a lower value of shear stress than is required to form a new shear plane. The value of shear stress necessary for reactivation of a pre-existing plane will differ from that required for formation of a new shear-plane by a value equivalent to the cohesive rock strength ($\boldsymbol{C}$). However, the strength of a pre-existing plane of weakness ($\boldsymbol{\mu_s}$) will vary from structure to structure within an extending province, with factors such as cementation or cataclasis increasing fault strength (strain hardening) and shale gouge decreasing fault strength (strain weakening). While some faults may be reactivated during extension, others of comparable orientation might not. Further to this, the orientation of a pre-existing plane of weakness relative to the principal stress axes ($\sigma_1 > \sigma_2 > \sigma_3$) dictates the magnitudes of the shear ($\boldsymbol{\tau}$) and normal ($\boldsymbol{\sigma_n}$) stresses acting on the plane. A complex interplay exists, therefore, between the many factors that dictate the reactivation of weak structures inherent in the crust, which include: 1) the strength of the fabric relative to intact rock; 2) the dip and strike of the fabric relative to the stress field, and 3) the sense of slip (shear) upon reactivation (Morley *et al.* 2004).

During extension, reactivated structures inherent in the crust may affect rift basins at all scales (e.g. Lezzar *et al.* 2002; Younes & McClay 2002; Morley *et al.* 2004; Bellahsen & Daniel 2005; Corti 2012; Autin *et al.* 2013; Whipp *et al.* 2014). However, it should not be assumed that inherited fabrics controlled rift geometry in all cases (Reeve *et al.* 2014). Pre-existing fabrics are most prevalent during the earliest stages of extension, at which time strain is accommodated on competing pre-existing and rift-generated faults (Morley *et al.* 2004). As extension proceeds rift-generated faults become dominant (**Figure 2.13**; Lezzar *et al.* 2002; Bellahsen & Daniel 2005). Where pre-existing faults interact with evolving fault systems, fault geometries tend not to display that expected from classical and idealized models, but instead often form 'crooked X-shapes' and 'zig-zag' patterns (**Figure 2.14**; Morley 1995). As faults grow and link, such irregularities may become smoothed out or obliterated (Morley 1995). Reactivated fault segments may only be active along a portion of their length, and may deviate, link or have no effect on the evolving rift-generated faults (Bellahsen & Daniel 2005). Even if inactive (or slightly active), pre-existing fabrics may hinder the evolution of rift-generated faults (Bellahsen & Daniel 2005). As such, pre-existing fabrics are classified as pervasive or discrete based upon their characteristics (**Figure 2.15**), and as active or passive based upon their behaviour (Morley 1999b). Active fabrics act as a through-going structure

with a unique sense of shear (e.g. a through-going strike-slip zone) and passive fabrics locally influence fault terminations and orientations (Morley 1999b).

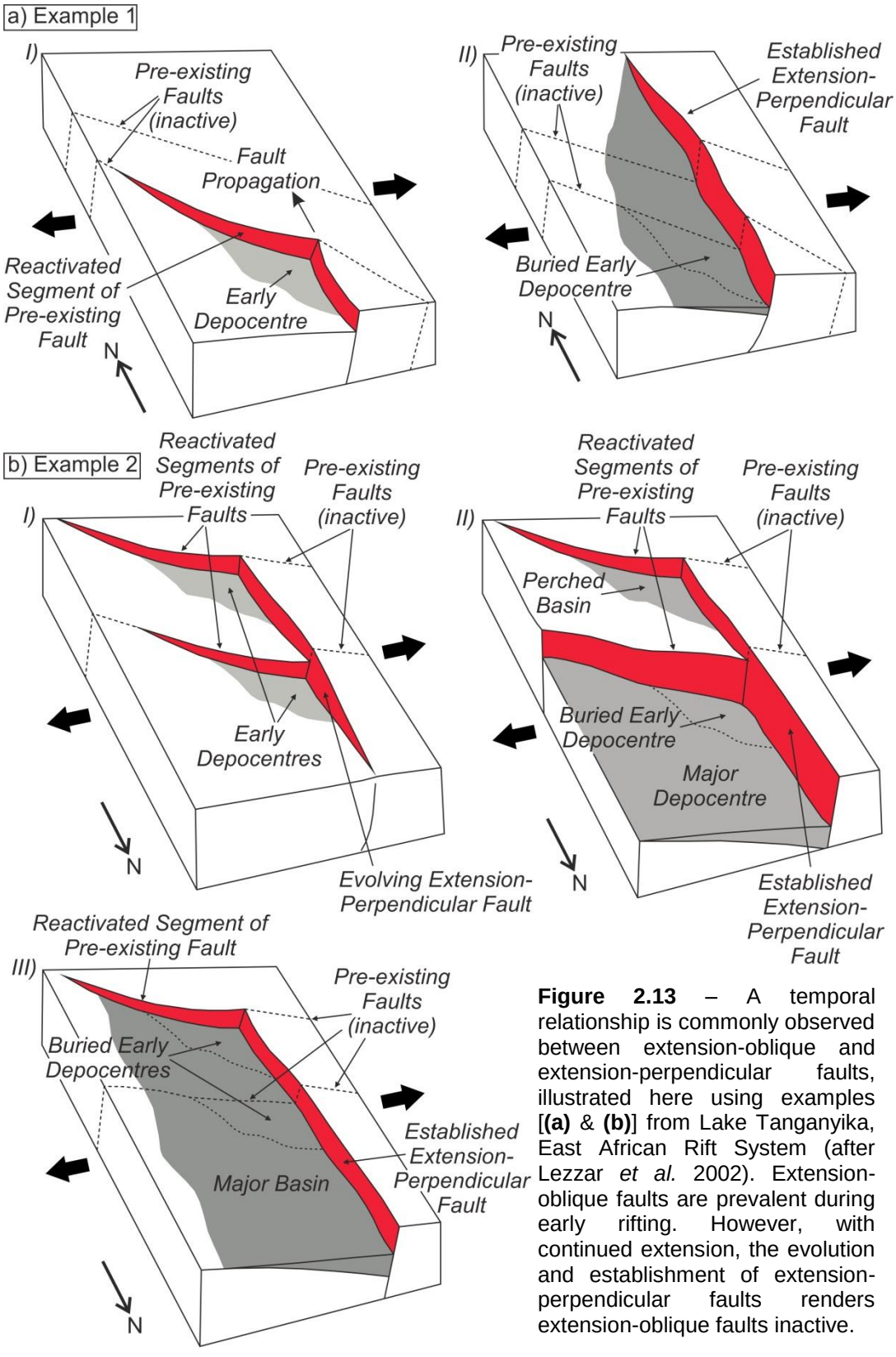

Figure 2.13 – A temporal relationship is commonly observed between extension-oblique and extension-perpendicular faults, illustrated here using examples [**(a)** & **(b)**] from Lake Tanganyika, East African Rift System (after Lezzar *et al.* 2002). Extension-oblique faults are prevalent during early rifting. However, with continued extension, the evolution and establishment of extension-perpendicular faults renders extension-oblique faults inactive.

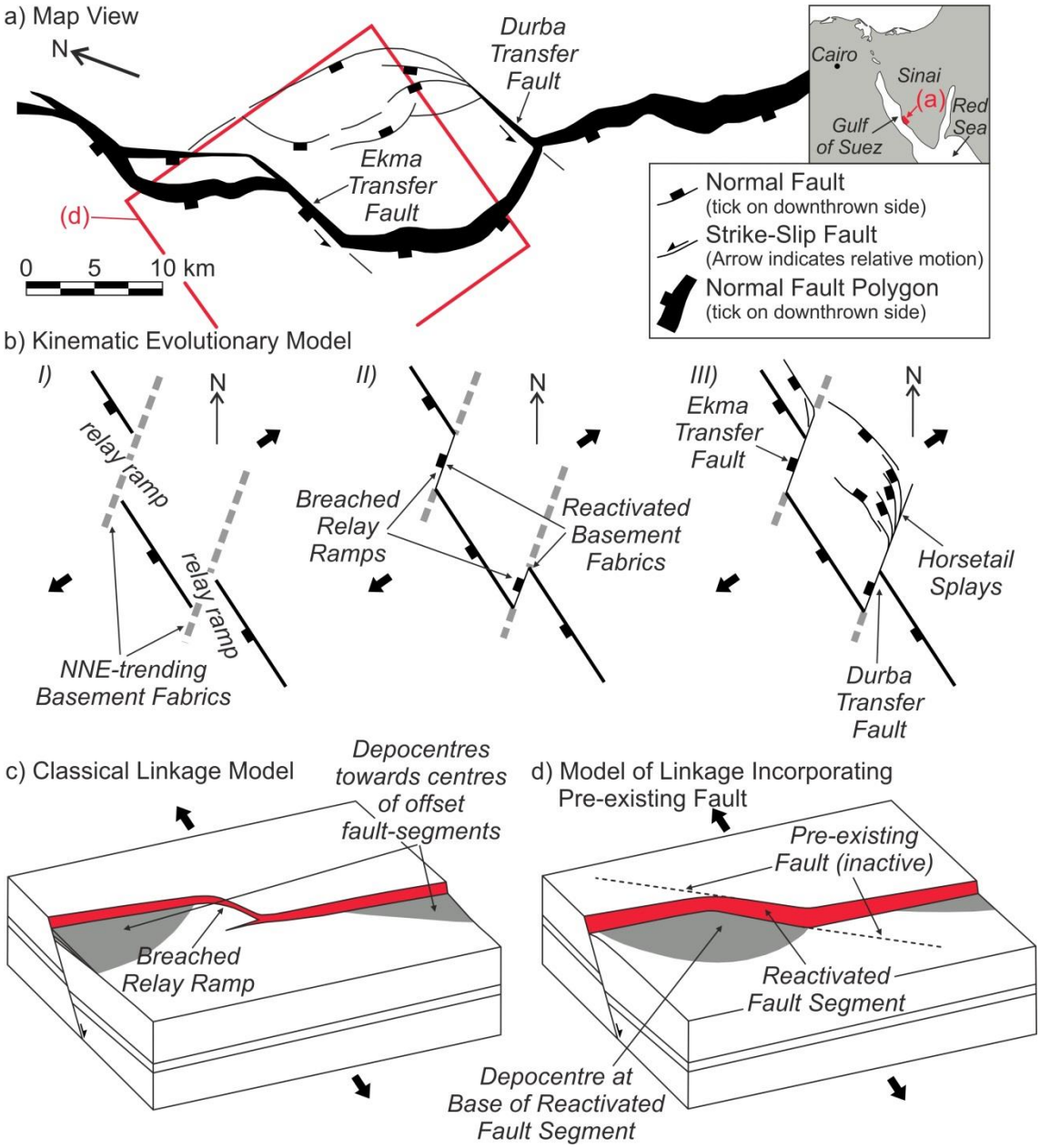

Figure 2.14 – Unusual 'zig-zag' fault geometries arising from the incorporation of pre-existing, extension-oblique faults into an evolving extension-perpendicular fault system [**(a)** & **(b)** after McClay & Khalil (1998); **(c)** & **(d)** after Bellahsen & Daniel (2005)]. **(a)** Simplified fault map of the Durba and Ekma transfer faults, eastern Gulf of Suez, based on geological field mapping (location map inset); **(b)** plan view kinematic evolutionary model for the Durba and Ekma transfer faults; **(c)** block diagram of a classical model of linkage between two sub-parallel fault segments; **(d)** block diagram of a structural inheritance linkage model (based on analogue modelling) similar to the Ekma transfer fault in the eastern Gulf of Suez (see **a**).

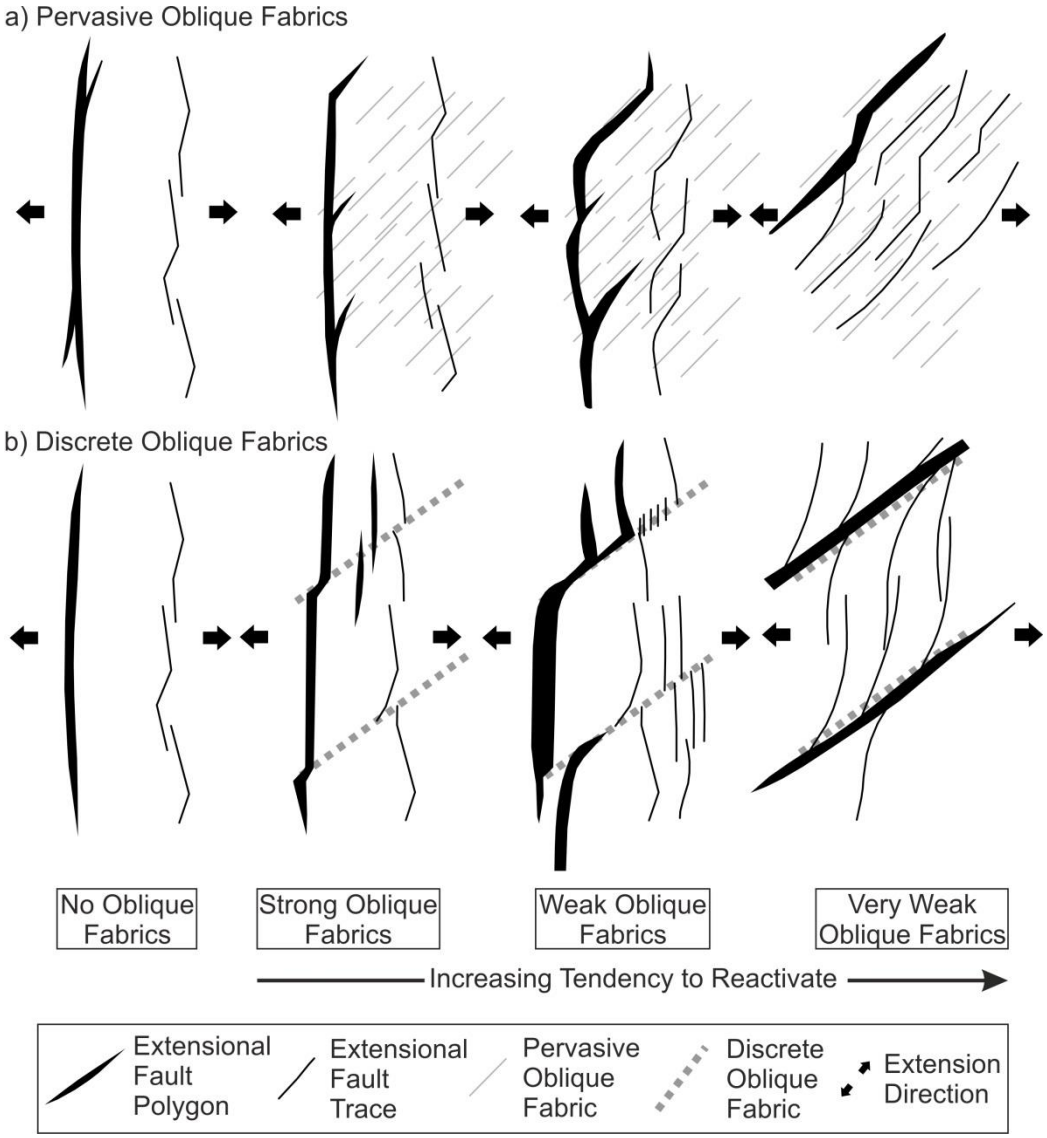

Figure 2.15 – Schematic plan view diagrams of the impact of pre-existing, extension-oblique fabrics of different type (pervasive or discrete) and different strengths (weak fabrics have a higher tendency to reactivate) on the evolution of extension-perpendicular faults (after Morley *et al.* 2004).

2.1.5.2 Transtensional (oblique) rifts

Where the direction of extension is orientated obliquely to a deforming structure, transtensional, or oblique, deformation occurs (**Figure 2.16**; e.g. Withjack & Jamison 1986, Tron & Brun 1991; McClay & White 1995; Clifton *et al.* 2000; Clifton & Schlische 2001; McClay *et al.* 2002; Autin *et al.* 2013; Bellahsen *et al.* 2013). At the rift-scale, a pre-existing crustal weakness may dictate the orientation of a rift or rift system, and strain localisation onto an extension-oblique crustal weakness produces rift-systems characterised by a regular series of intra-rift extension perpendicular (rift-oblique) faults and rift-parallel fault systems along the rifted margins (**Figures 2.16 & 2.17**; Withjack & Jamison 1986, Tron & Brun 1991; McClay & White 1995; Clifton *et al.* 2000; McClay *et*

al. 2002). The orientations of rift-margin faults are controlled by the orientation of the underlying ductile zone of stretching, which is rift-parallel, whereas intra-rift faults form perpendicularly to the regional extension direction, which is rift-oblique (**Figure 2.16**; McClay & White 1995).

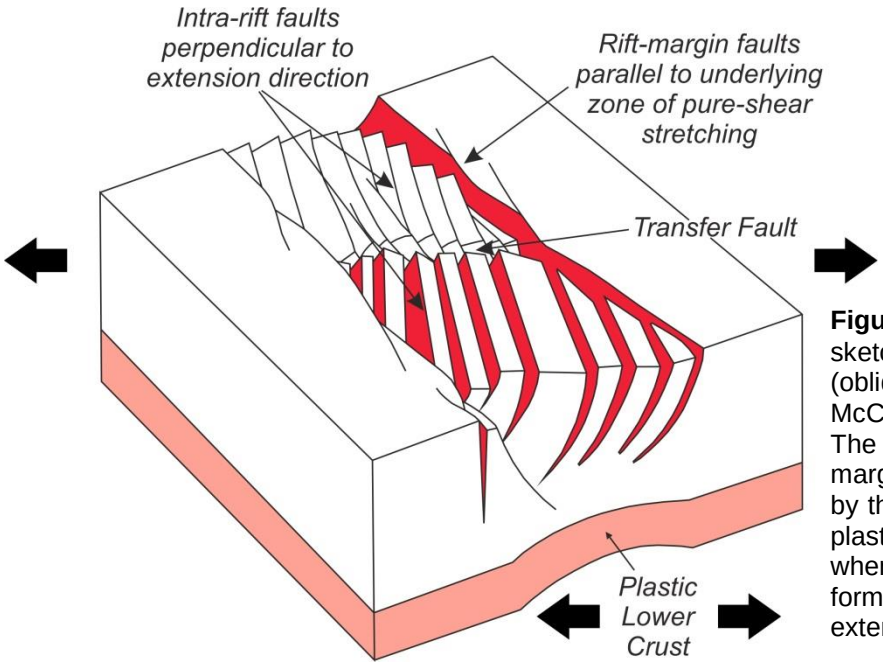

Figure 2.16 – Cartoon sketch of a transtensional (oblique) rift (after McClay & White 1995). The orientation of the rift margin faults is controlled by the underlying zone of plastic stretching, whereas intra-rift faults form perpendicular to the extension direction.

Fault systems within oblique rift systems are often highly segmented (**Figure 2.17**; McClay & White 1995; Clifton *et al.* 2000; Clifton & Schlische 2001). Extension perpendicular (rift-oblique) faults are commonly active during early rifting with rift-parallel faults becoming progressively dominant with continued extension (Bellahsen *et al.* 2013). Further to this, experimental modelling indicates the degree of rift-obliquity results in characteristic fault kinematics and fault population systematics (Clifton *et al.* 2000; Clifton & Schlische 2001). For rifting with an extension direction orientated more than 45° relative to the trend of the rift (90° = rift-perpendicular extension), namely moderately oblique rifting, a unimodal population of predominantly dip-slip faults with a normal sense of displacement will form. However, during rifting with an extension direction that is orientated at an angle less than 45° to the rift trend, namely highly oblique rifting, deformation will be accommodated on an increasingly bimodal fault population, with rift-parallel faults defining the rift-margins and extension perpendicular (rift-oblique) faults within the rift (e.g. **Figures 2.16 & 2.17**), and an increasing proportion of oblique- and strike-slip faults (Withjack & Jamison 1986, Tron & Brun 1991, Clifton *et al.* 2000, Henza *et al.* 2010, Henza *et al.* 2011).

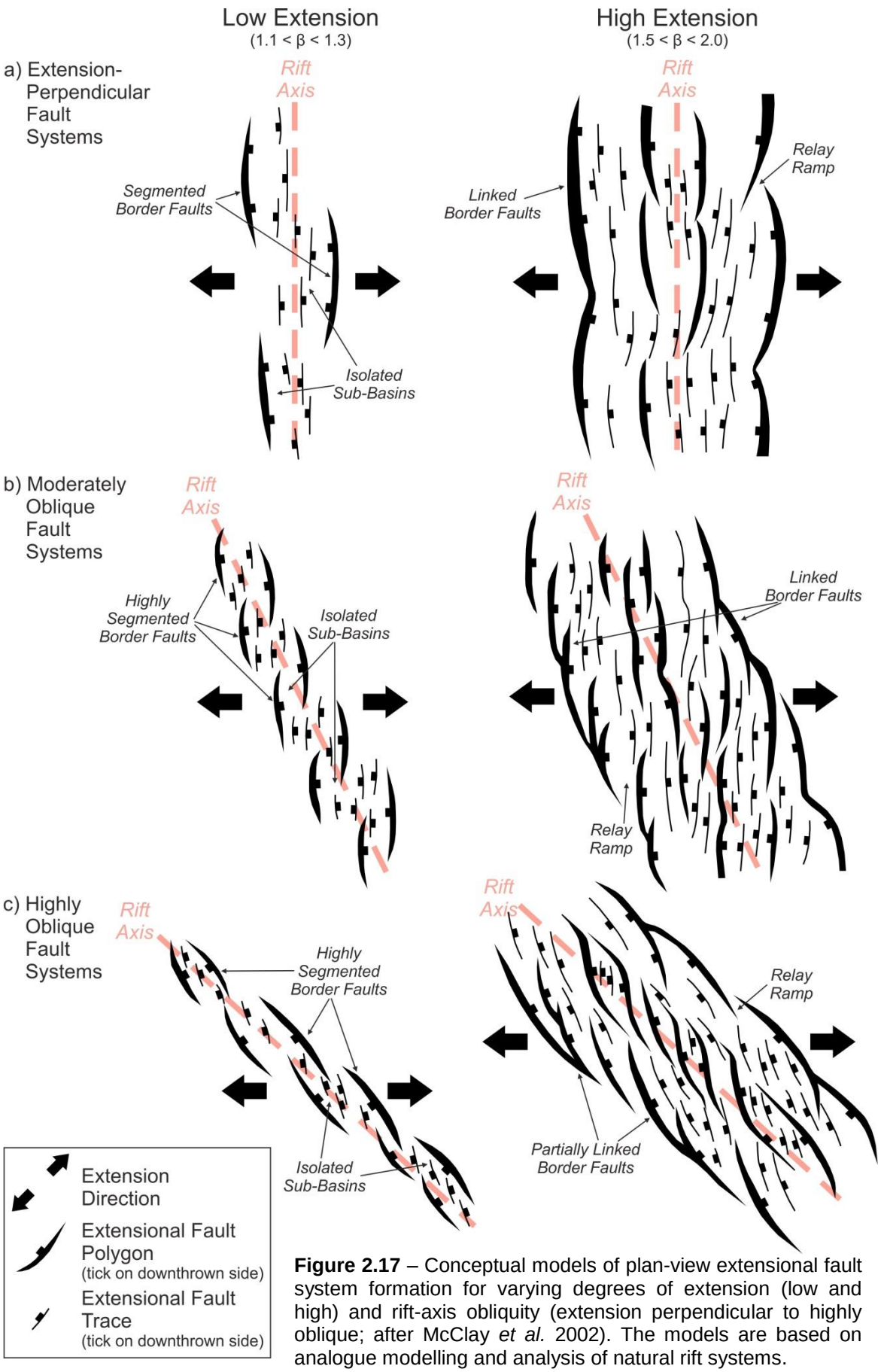

Figure 2.17 – Conceptual models of plan-view extensional fault system formation for varying degrees of extension (low and high) and rift-axis obliquity (extension perpendicular to highly oblique; after McClay *et al.* 2002). The models are based on analogue modelling and analysis of natural rift systems.

Successful continental rifting is enhanced under an oblique extensional regime due to oblique deformation requiring less tectonic force to reach the plastic yield limit than rift-perpendicular deformation (Brune *et al.* 2012). Oblique rifts, therefore, are mechanically preferred to extension perpendicular rifts and are the locus of greater strain localisation (Brune *et al.* 2012; Heine & Brune 2014).

2.2 The onshore rift basins of northwest India

The rifted north-western margin of India (**Figure 2.18**), active since the early Mesozoic Era, remains poorly understood despite many hydrocarbon discoveries (Biswas 1982; Gombos *et al.* 1995; Compton 2009; Dolson *et al.* in press). Onshore rift basins within the West Indian Rift System include the Kachchh (Kutch), Cambay, and Narmada basins (**Figure 2.18**). The Barmer Basin is the most northerly rift within the West Indian Rift System. Together, the Barmer and Cambay basins form a north-northwest trending rift system that extends some six-hundred kilometres into the Indian continent. To the north of the Barmer Basin, the Jaisalmer Basin forms the eastern slopes of the larger Indus Basin (Singh 2006; Singh 2007). The Barmer and Jaisalmer basins are separated by a basement structural high, the Devikot High (**Figure 2.18**). In this section the context of the West Indian Rift System is described within the currently understood regional tectonic framework, followed by a brief summary geology of the Kachchh, Cambay, Narmada and Jaisalmer basins.

2.2.1 Plate tectonic setting

During the multi-stage fragmentation of Gondwana throughout the Mesozoic Era, the Greater Indian continent became isolated from the African, Antarctic and Australian continents through a series of rift-drift events involving changes in plate motion, spreading-centre relocations, failed rifting, and mantle plumes (**Figure 2.19**; e.g. Patriat & Achache 1984; Storey *et al.* 1995; Collier *et al.* 2008; Cande *et al.* 2010; Cande & Stegman 2011; Torsvik *et al.* 2013; Reeves 2014; Eagles & Hoang 2014). The West Indian Rift System is the result of this long-lived succession of regional tectonic events. The orientation and configuration of rifts was, in part, controlled by major Precambrian trends and metamorphic fabrics (Gombos *et al.* 1995). Mesozoic Era rift events throughout northwest India are attributed to successive stages of India's northwards drift, accompanied by an anti-clockwise rotation of the Greater Indian continent, and formed a network of failed rift-basins that opened sequentially from north to south (Biswas 1982; Biswas 1987; Gombos

et al. 1995; Sheth 2005a). Rifting was long-lived, possibly beginning as early as the late Triassic Period, and involved multiple rift events that continued into the Paleogene Period (Biswas 1982; Sharma 2007).

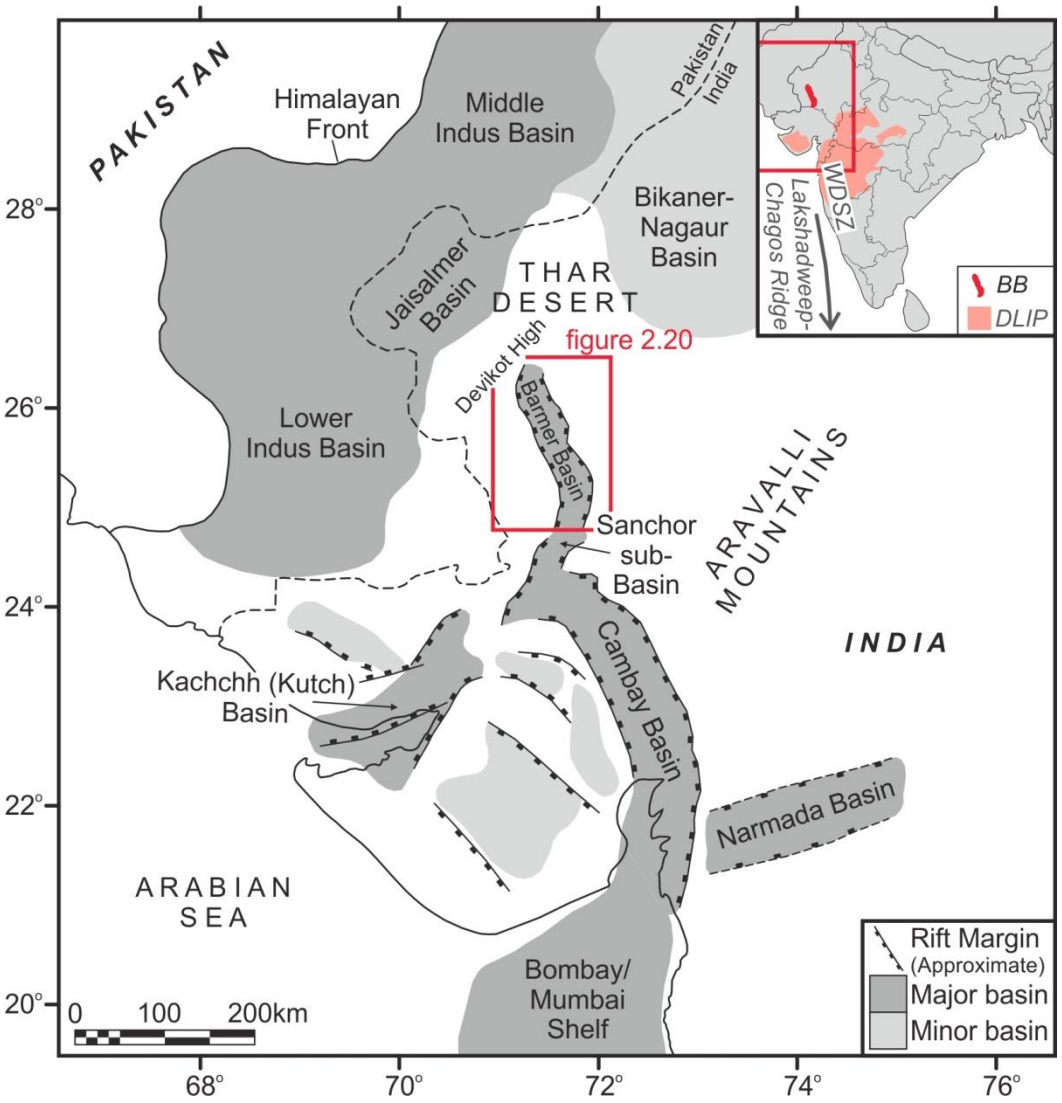

Figure 2.18 – Basins of northwest India (location map inset). The location of the Barmer Basin fault map shown in **figure 2.20** is also indicated. WDSZ = Western Deccan Strike-Slip Zone, BB = Barmer Basin, DLIP = Deccan Large Igneous Province.

East and west Gondwana separated during the early to middle Jurassic Period, facilitated by opening of the Mozambique and Somali proto-oceans (**Figure 2.19a**; Reeves & de Wit 2000; Reeves 2014). Relative motion between the Madagascan and Greater Indian (c.f. Ali & Aitchison 2014) continents may have generated transtension in the region between them during separation (Mascarene Rift of Bastia *et al.* 2010, Reeves 2014). Accelerated sea-floor spreading between the Greater Indian and Antarctic continents occurred during the early Cretaceous Period at the

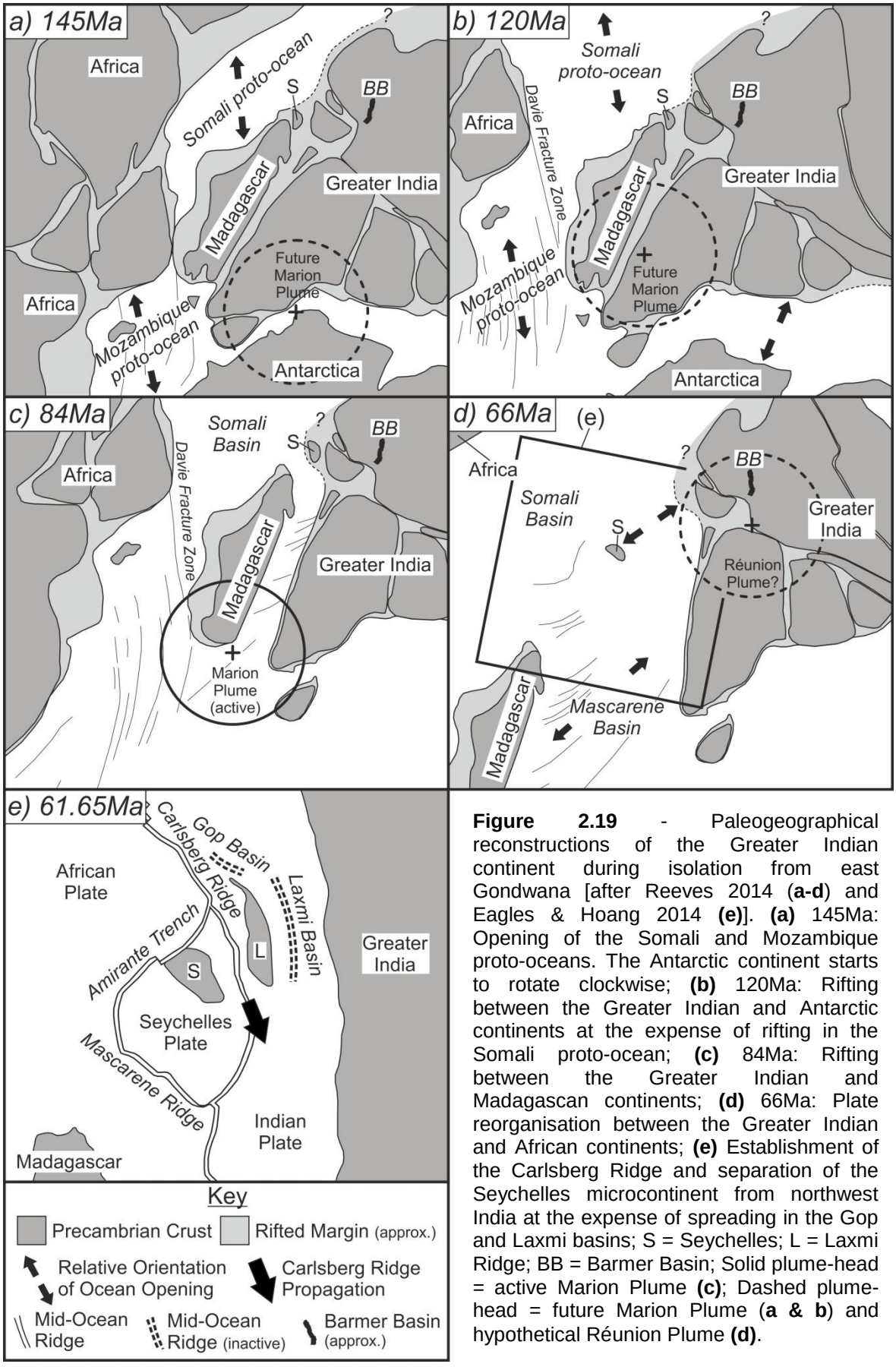

Figure 2.19 - Paleogeographical reconstructions of the Greater Indian continent during isolation from east Gondwana [after Reeves 2014 (**a-d**) and Eagles & Hoang 2014 **(e)**]. **(a)** 145Ma: Opening of the Somali and Mozambique proto-oceans. The Antarctic continent starts to rotate clockwise; **(b)** 120Ma: Rifting between the Greater Indian and Antarctic continents at the expense of rifting in the Somali proto-ocean; **(c)** 84Ma: Rifting between the Greater Indian and Madagascan continents; **(d)** 66Ma: Plate reorganisation between the Greater Indian and African continents; **(e)** Establishment of the Carlsberg Ridge and separation of the Seychelles microcontinent from northwest India at the expense of spreading in the Gop and Laxmi basins; S = Seychelles; L = Laxmi Ridge; BB = Barmer Basin; Solid plume-head = active Marion Plume **(c)**; Dashed plume-head = future Marion Plume (**a & b**) and hypothetical Réunion Plume **(d)**.

expense of rifting in the Somali Basin (**Figure 2.19b**; Gombos *et al.* 1995; Reeves & de Wit 2000; Reeves 2014). Prior to cessation of rifting in the Somali Basin during the Aptian Age (120 Ma), a period of mutual spreading to the north and south of the Greater Indian continent, combined with a clockwise rotation of the Antarctic continent with respect to the African continent, represents the most likely period during which transtensional rifting occurred between the Greater Indian and Madagascan continents (Bastia *et al.* 2010; Reeves 2014). Subsequently to the cessation of spreading in the Somali Basin, little relative motion occurred between the Greater Indian, African, and Madagascan continents, until the Greater Indian continent separated from the Madagascan continent during the Coniacian Age (88 Ma), a rifting event attributed to the Marion Plume (**Figure 2.19c**; Storey *et al.* 1995; Reeves 2014). Thereafter, the Greater Indian continent drifted rapidly northwards (Reeves & de Wit 2000; Reeves 2014), with the spreading centre in the Mascarene Basin undergoing three major southwest ridge jumps at 80 Ma, 73.6 Ma and 70 Ma (Torsvik *et al.* 2013).

The Greater Indian continent was isolated from all fragments of east Gondwana by rifting of the Seychelles microcontinent from northwest India around the time of the Cretaceous-Paleogene boundary (**Figure 2.19d**; Collier *et al.* 2008; Armitage *et al.* 2010; Armitage *et al.* 2011; Reeves 2014). Accelerated divergence between the Indian and African continents caused rapid propagation of the Carlsberg Ridge during the Maastrichtian Age (69 Ma-65 Ma; **Figure 2.19e**; Eagles & Hoang 2014). The Mascarene Basin (**Figure 2.19d**) was progressively abandoned in favour of short-lived spreading in the Laxmi and Gop basins (**Figure 2.19e**; Malod *et al.* 1997; Chaubey *et al.* 2002; Collier *et al.* 2008; Yatheesh *et al.* 2009; Armitage *et al.* 2011), prior to stabilisation of the Carlsberg Ridge between the Seychelles microcontinent and northwest India during the Danian Age that facilitated successful Seychelles rifting (Cox 1989; White & McKenzie 1989; Collier *et al.* 2008; Armitage *et al.* 2011; Torsvik *et al.* 2013; Eagles & Hoang 2014). A period of contemporaneous spreading along the Carlsberg and Mascarene ridges isolated the Seychelles Plate (**Figure 2.19e**), which rotated rapidly anticlockwise between 64 Ma and 59 Ma, and caused compression along the Amirante Trench (Cande *et al.* 2010; Eagles & Hoang 2014). The common assumption of perpendicular rifting between the Seychelles microcontinent and northwest India has been challenged, with some authors (Misra *et al.* 2014) suggesting oblique rifting based upon outcrop work in the Western Deccan Strike-slip Zone. Successful separation of the Seychelles

microcontinent from the Greater Indian continent was followed by two further jumps of the Carlsberg Ridge at 56 Ma and 41 Ma (Torsvik *et al.* 2013).

Extrusion of the voluminous Deccan Traps (68 Ma-60 Ma) was contemporaneous, and closely associated with rifting of the Seychelles microcontinent from the Greater Indian continent (Cox 1989; White & McKenzie 1989; Sheth 2005a; Sheth 2005b; Sheth 2007; Collier *et al.* 2008), with volcanism commonly thought to have instigated rifting (Morgan 1971; Plummer & Belle 1995; Sen & Chandrasekharam 2011). Evidence presented in support of the presence of a mantle plume beneath northwest India at the Cretaceous-Paleogene boundary (**Figure 2.19d**; e.g. Sen and Chandrasekharam 2011) include: 1) the characteristic trap-and-tail geometry of the Deccan Large Igneous Province and the Lakshadweep-Chagos Ridge (**Figure 2.18** inset; White and McKenzie 1989; Campbell and Griffiths 1990); 2) radial drainage centred in western India (e.g. Cox 1989; Rainbird and Ernst 2001); 3) surface uplift (e.g. Campbell and Griffiths 1990); 4) rapid extrusion (e.g. Borges *et al.* 2014) that predated rifting (Hooper *et al.* 2010); 5) a postulated Cambay triple junction (Sheth and Chandrasekharam 1997); 6) primitive Deccan Large Igneous Province geochemistry (Srivastava *et al.* 2014); 7) a southwards age progression of Deccan Trap lavas; 8) Deccan-age kimberlites within the extent of the postulated Réunion plume head (e.g. Chalapathi Rao & Lehmann 2011); .9) a 'plume scar' beneath the Seychelles microcontinent (e.g. Hammond *et al.* 2012), and; 10) the presence early melts of the Réunion Mantle Plume in Pakistan (e.g. Kerr *et al.* 2010).

Although widely accepted, a plume origin for the Deccan Traps has been shown to match poorly with many of the features of Deccan Large Igneous Province (DLIP; **Figure 2.18 inset**) geology (Sheth 2005a; Sheth 2007). Evidence for post-volcanic uplift - not confined to the Deccan province - with antecedent drainage patterns, long-lived eruptions (≥ 8 Ma-9 Ma; Sheth & Pande 2014), pre-Deccan planation surfaces that suggest tectonic stability, a 10° Réunion Mantle Plume palaeolatitude disparity, and a lack of evidence for thinned, sub-Deccan lithosphere, are all inconsistent with the plume-head model (Sheth 2005a; Sheth 2007). Seychelles rifting is also suggested to have resulted from plate reorganisations underway long before the arrival of the Réunion Mantle Plume (Sharma 2007; Collier *et al.* 2008) and continued after the main Deccan eruptions (Armitage *et al.* 2011). Similarly, rather than being formed as part of the Réunion Mantle

Plume 'tail,' the Mascarene Plateau (and possibly Lakshadweep-Chagos Ridge) may be underpinned by thinned Proterozoic continental lithosphere that was situated between the Greater Indian and Madagascan continents prior to successful separation (Torsvik *et al.* 2013). This microcontinent (Mauritia) has since been concealed beneath flood basalts, fragmented by multiple mid-ocean ridge-jumps, and isolated in the Indian Ocean upon establishment of the Central Indian Ridge (Torsvik *et al.* 2013; Reeves 2014). A postulated alternative model (Sheth 2005b) invokes the passive release of fertile lithosphere material, trapped within ancient lithosphere sutures, upon extension, to provide a significant contribution to the voluminous Deccan Trap magmatism. Similar processes have been suggested for other Large Igneous Provinces (e.g. Iceland, Foulger *et al.* 2005; Foulger & Anderson 2005).

Post India-Seychelles rifting, the Indian peninsula continued to drift northwards, undergoing variable plate-motions (Cande & Stegman 2011), and directional changes resulting from the initial interactions of the Indian and Eurasian continents (Patriat & Achache 1984) that collided between 56.5 Ma and 50.5 Ma (Patriat & Achache 1984; Beck *et al.* 1995; Leech *et al.* 2005; Green *et al.* 2008; Liebke *et al* 2013).

2.2.2 Summary geology of the onshore rift basins of northwest India

Extension within the West Indian Rift System may have begun as early as the Triassic Period in the Kachchh Basin (Biswas 1982; Biswas 1987). However, significant basin-wide deposition did not occur in the Kachchh Basin until the Jurassic Period (Jhurio/Kaladongar Formation; **Figure 2.18**; Krishna 1987; Fürisch & Pandey 2003; Pandey *et al.* 2009). Adjacent to the Kachchh Basin, sub-Deccan strata within the Cambay Basin are poorly imaged and largely unknown in the subsurface (Rohrman 2007). Based upon surface exposures, Mesozoic sedimentation within the Cambay rift is thought to have occurred in shallow marine, brackish and deltaic environments on an occasionally emergent platform (Raju 1968; Chowdhary 1975). To the east of the Cambay Basin, subsidence and deposition within the Narmada Basin began during the Lower Cretaceous Epoch. Deposition of the continental Nimar Sandstone occurred prior to a marine transgression throughout the Narmada rift, until eruption of the Deccan Traps (Akhtar & Ahmad 1991; Khosla *et al.* 2003; Jaitly & Ajane 2013). The preservation of Mesozoic Era deposits throughout the West Indian Rift System alludes to established Mesozoic rifting throughout northwest India that pre-dated the main phase of Deccan eruptions.

In the Jaisalmer Basin (**Figure 2.18**) deposition of the fluvio-deltaic Lathi Formation (≤ 500 m thick) during the Jurassic Period preceded marine deposition that endured until the Upper Cretaceous Epoch (Torsvik *et al.* 2005; Singh 2006; Pandey *et al.* 2012; Rai *et al.* 2013). However, continental deposits that are Jurassic in age occur at outcrop within the Jaisalmer Basin, indicating that marine deposition was intermittent. During the Cretaceous Period, therefore, the south-western periphery of the Marwar Craton separated a series of marine-embayed rifts to the south (Kachchh, Cambay and Narmada basins), from a shallow-marine passive margin shelf to the north (Jaisalmer Basin). It is across this three-hundred kilometre wide area that the Barmer Basin rift subsequently developed

2.3 The Barmer Basin rift

The Barmer Basin is a long, narrow, and deep (200 km, < 40 km, & ≤ 6 km respectively), late Cretaceous Period to mid-Eocene Epoch, low strain ($1.2 \leq \beta \leq 1.5$), failed continental rift, that is linked with the Cambay Basin to the south via the poorly defined Sanchor sub-Basin (**Figures 2.18 & 2.20**; Compton 2009; Dolson *et al.* in press). Until recently, the extent, structure and geology of the Barmer Basin were poorly constrained, and only since subsurface data became available over the last decade has an appreciation of the scale and significance of the rift been achieved (Dolson *et al.* in press). However, an abundance of complex structures and rift-oblique faults are variably imaged on subsurface data throughout the rift (**Figure 2.20**), the origin of which remain elusive, and a detailed understanding of the structural evolution of the rift is yet to be attained. In this section the current understanding of the structural evolution and structure of the rift are summarised, along with a description of the Barmer Basin stratigraphical succession.

2.3.1 Structural evolution

The main phase of fault controlled subsidence in the Barmer Basin initiated during the latest Cretaceous Period (Maastrichtian Age) and continued into the mid-Eocene Epoch (Lutetian Age; Compton 2009; Dolson *et al.* in press; Farrimond *et al.* in review). Rift evolution is thought to have responded to regional, approximately rift-perpendicular (≈ northeast-southwest) extension that was related to rifting of the Seychelles microcontinent from the Greater Indian continent near to the Cretaceous-Paleogene boundary (e.g. Collier *et al.* 2008; Reeves 2014; Eagles & Hoang 2014).

Maximum syn-rift displacement occurred in the late Paleocene Epoch during deposition of the Barmer Hill Formation, and is marked by establishment of a basin-wide lake (Compton 2009;

Dolson *et al.* in press; Farrimond *et al.* in review). In the southern part of the rift, rifting was accompanied by a thermal pulse with a geothermal gradient of 50°C km^{-1} that has since stabilised at 30°C km^{-1} (Dolson *et al.* in press; Farrimond *et al.* in review). By comparison, the geothermal gradient has remained at a relatively constant 30°C km^{-1} in the northern part of the rift throughout rift evolution. Although the main phase of subsidence occurred during the Paleogene Period, small, rift-oblique (northeast-southwest) depocentres are thought to underlie the Barmer Basin, and are suggested to be Mesozoic in age (Dolson *et al.* in press). The suggestion that Mesozoic sub-basins underlie the rift is supported by the presence of an active Mesozoic petroleum system (Farrimond *et al.* in review) that may have affinities with the Kachchh Basin to the west (Dolson *et al.* in press).

Recently, large-scale uplift in the north of the basin (> 1 km) likely resulted from the collision between the Greater Indian and Eurasian continents, with the Present Day peneplanation of the northern Barmer Basin being the current expression of this uplift (Dolson *et al.* in press). In contrast to the northern part of the Barmer Basin, the southern part of the basin has undergone continuous subsidence since the end of extension in the late Eocene Epoch, which, when coupled with uplift in the north, has resulted in a gentle tilting of the basin to the southeast.

2.3.2 Rift structure

Subsurface structural maps of the Barmer Basin (**Figure 2.20**) reveal many features typical of intra-continental rifts, such as faulted margins, uplifted flanks, deep troughs, intra-rift horsts, and distinct rift-onset and post-rift stratigraphical successions (Dolson *et al.* in press), as well as atypical structural geometries. The rift deepens to the south (**Figure 2.21**), and asymmetrical (deepening to the east) and symmetrical rift geometries characterise northern and southern provinces, respectively (**Figure 2.22**; Compton 2009; Dolson *et al.* in press; Farrimond *et al.* in review). The coincidence of an abrupt southwards deepening of the rift with the boundary between structural domains, suggests a major transverse structural boundary may underlie the rift. In the northern part of the rift, large, rotated faulted blocks are separated by deep, asymmetrical, fault-controlled depocentres (**Figures 2.22a-c**). In the southern province, a large rift-parallel structural high runs along the west-central section of the rift and is flanked by very deep, undrilled depocentres (**Figures 2.22f & g**; Dolson *et al.* in press). Rift-margin faults accommodated the majority of displacement (Compton 2009), and exhibit normal-displacement, are hard-linked, and form well-developed zones of linkage (accommodation/transfer zones; Dolson *et al.* in press). Faults became

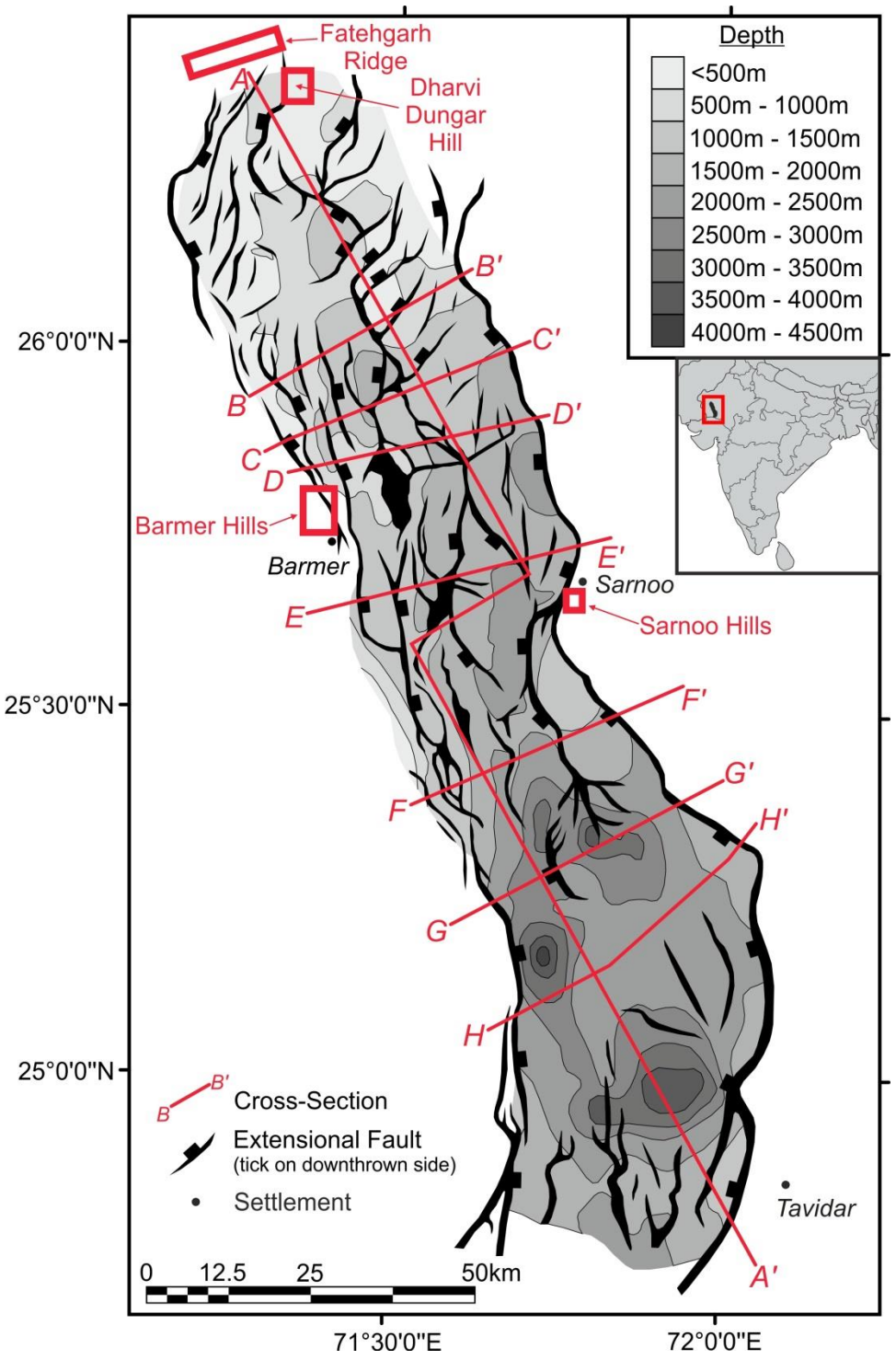

Figure 2.20 – Large-scale structure of the Barmer Basin at the top Fatehgarh Formation horizon based on subsurface data (after Dolson *et al.* in press). Location map within India inset. Cross-sections shown in **figures 2.21 and 2.22** are indicated.

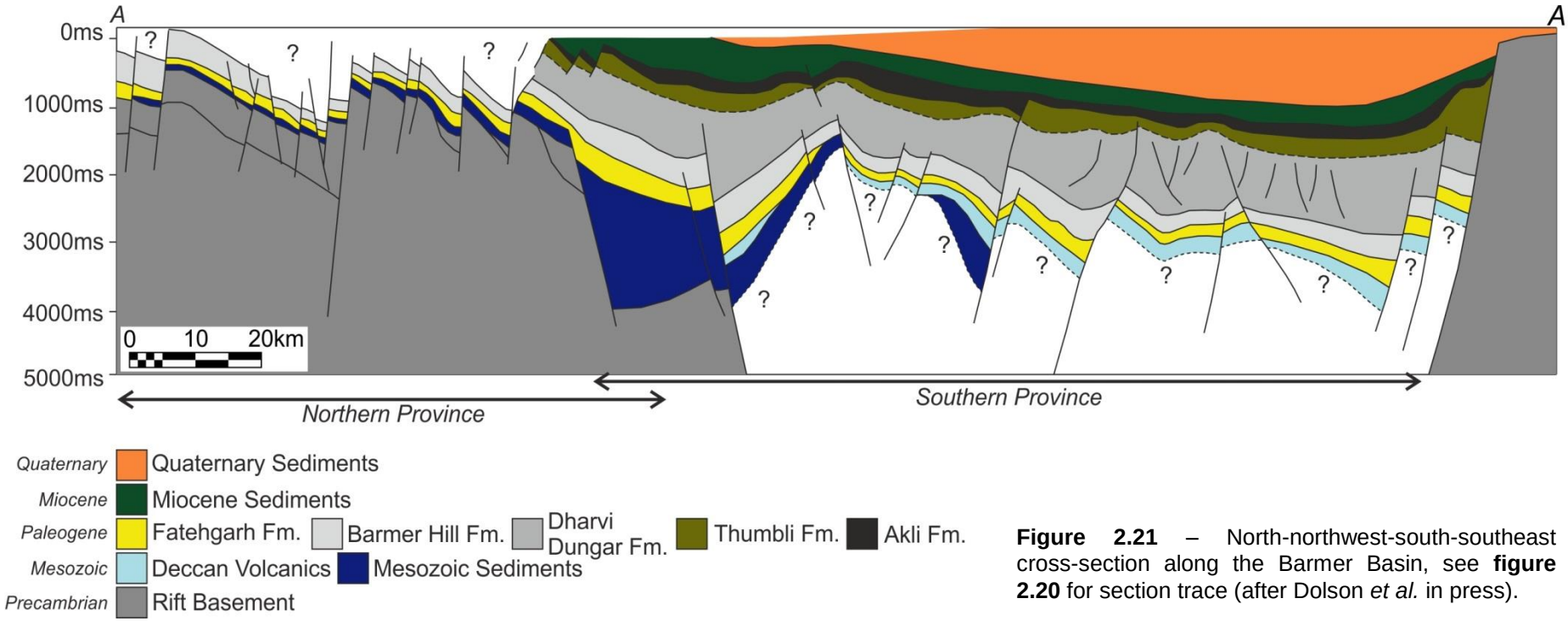

Figure 2.21 – North-northwest-south-southeast cross-section along the Barmer Basin, see **figure 2.20** for section trace (after Dolson *et al.* in press).

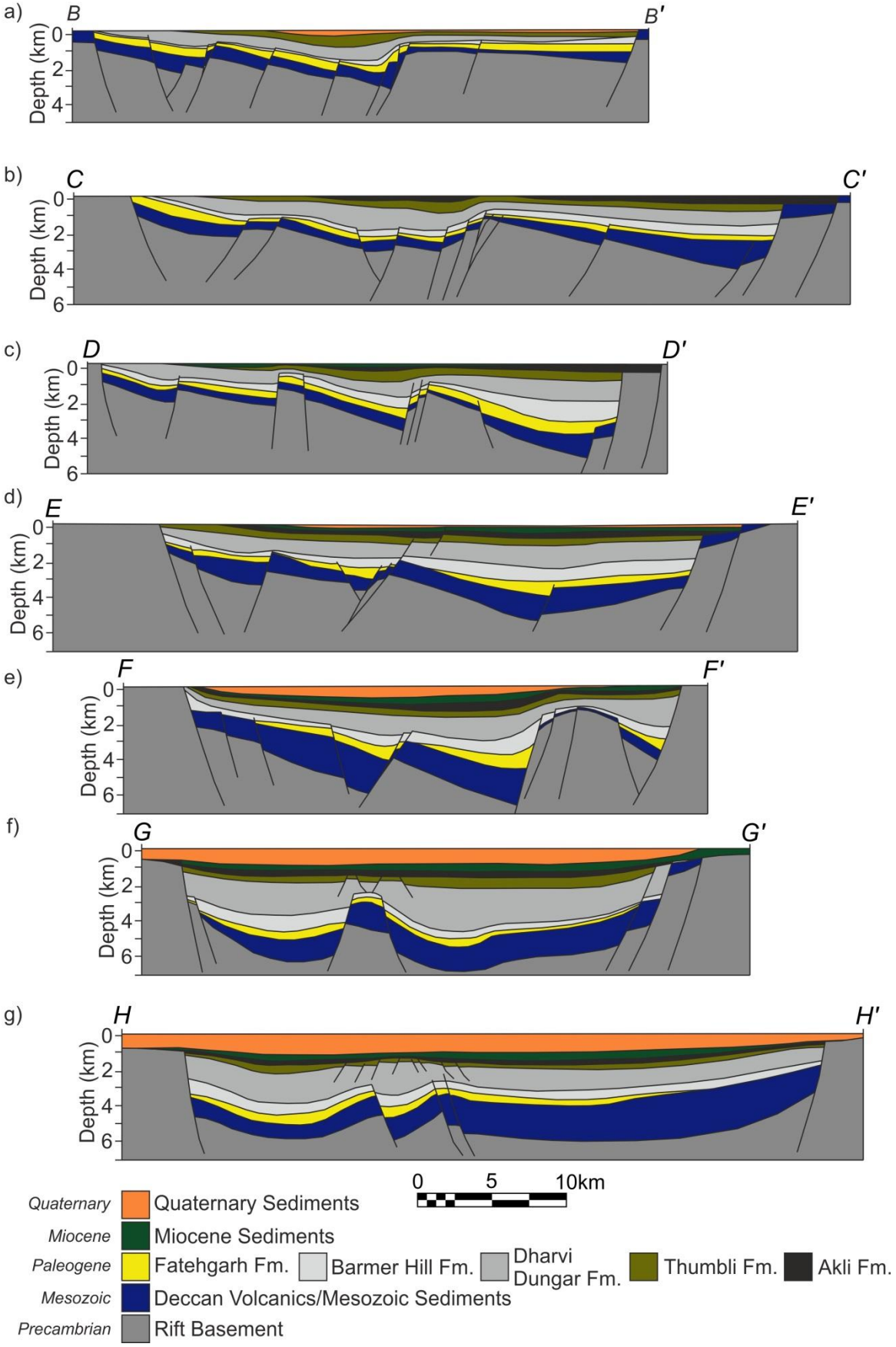

Figure 2.22 – East-northeast-west-southwest cross-sections across the Barmer Basin, see **figure 2.20** for section traces (after Dolson *et al.* in press).

hard linked in the late Paleocene to early Eocene epochs during deposition of the late Barmer Hill and Dharvi Dungar formations, and terminate vertically upwards within the mudstones of the Dharvi Dungar Formation (Dolson *et al.* in press). In conjunction with dominant rift-parallel faults, large rotated fault-blocks are characterised by an older series of rift-oblique, northeast-southwest faults (Dolson *et al.* in press).

2.3.3 Barmer Basin stratigraphical succession

Rift-basement rocks in the Barmer Basin comprise the Precambrian Malani Igneous Suite (c.f. Pareek 1981; **Figure 2.23**). Overlying the Malani Igneous Suite, the sedimentary succession can be categorised into three broad depositional groups, defined by the timing of deposition relative to Paleogene rifting, namely pre-, syn-, and post-rift.

2.3.3.1 Pre-rift formations

Unconformably overlying the Malani Igneous Suite, exposures of the Jurassic Lathi Formation in the north Barmer Basin (Fatehgarh Ridge; **Figure 2.20**), and the Lower Cretaceous Ghaggar-Hakra Formation along the central eastern rift margin (Sarnoo Hills; **Figure 2.20**; Sisodia & Singh 2000; Dolson *et al.* in press), indicate that Mesozoic deposition occurred in the Barmer region prior to the main Barmer Basin rift event. A poorly understood suite of volcanic strata are exposed intermixed with the Ghaggar-Hakra Formation at outcrop (Karentia Volcanic Formation; **Figure 2.23**). Although unknown in the Barmer Basin, the Neoproterozoic (≈ 650 Ma) Marwar Supergroup sediments, which are of substantial thickness in some areas of Rajasthan (< 2000 m in the Bikaner-Nagaur Basin; **Figure 2.18**), are likely to underlie the Mesozoic succession within the subsurface of the Barmer Basin (Dolson *et al.* in press)

2.3.3.2 Syn-rift formations

The syn-rift sedimentary succession in the Barmer Basin is predominantly Paleocene to Eocene in age, and comprises a progression from fluvial, through shallow lacustrine to deep lacustrine deposition, prior to post-rift infilling of the Barmer Basin lake with low-energy fluvial and flood plain sediments (Dolson *et al.* in press). Syn-rift deposition was strongly affected by active tectonism, with faulting contributing to cyclicity in the basin fill as well as rapid facies variations (Dolson *et al.* in press). Further to this, minor Deccan-related volcanic strata crop out along the eastern rift margin in the Sarnoo (Sarnu[sic]-Dandali Suite) and Tavidar areas (Basu *et al.* 1993; Roy & Jakhar

2002; Sen *et al.* 2012), as well as in the subsurface (Raageshwari Volcanic Formation; **Figure 2.23**; Dolson *et al.* in press).

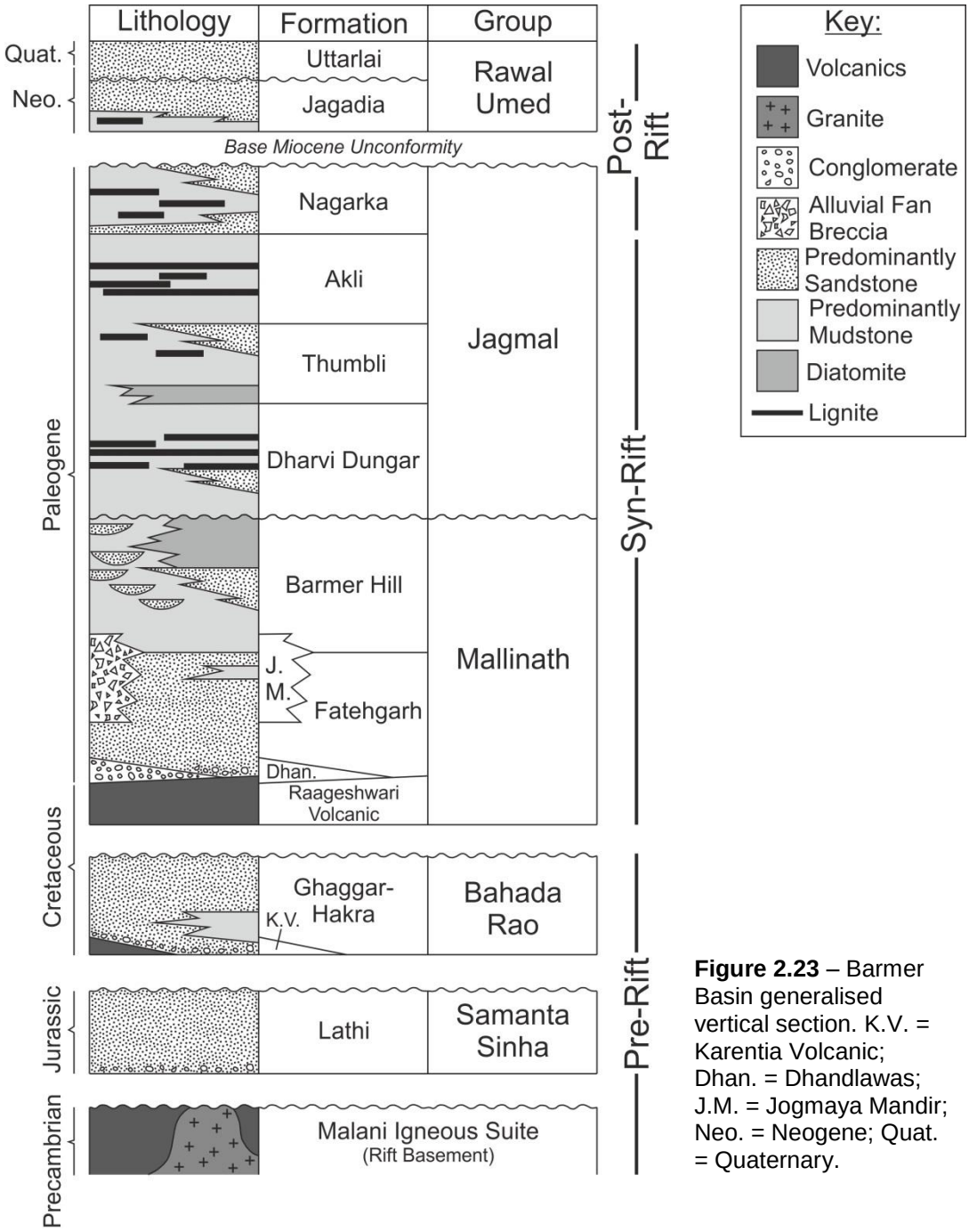

Figure 2.23 – Barmer Basin generalised vertical section. K.V. = Karentia Volcanic; Dhan. = Dhandlawas; J.M. = Jogmaya Mandir; Neo. = Neogene; Quat. = Quaternary.

The earliest syn-rift sediments of the Fatehgarh Formation were deposited within a broad fluvial plain in the northern Barmer Basin and a deep-water lake setting in the southern Barmer Basin, with deposits grading from stacked fluvial sandstones in the north, through isolated, single-storey channels into deep water turbidites in the south of the rift (**Figure 2.23**; Compton 2009; Dolson *et al.* in press). Sediments in the Fatehgarh Formation had a north to north-easterly provenance, were

probably derived from re-working of Cretaceous or older sediments, and form high-quality reservoirs that contain the bulk of the oil reserves within the rift. Negligible variations in the thickness of the Fatehgarh Formation across rift structures in the northern Barmer Basin indicate deposition in the north of the rift within a pre-rift to early syn-rift tectono-stratigraphical setting (Dolson *et al.* in press). Along the rift margins the Fatehgarh Formation interdigitates with the Jogmaya Mandir Formation (**Figure 2.23**), which is inferred to be of Paleocene age, and comprises proximal rift-margin facies (Dolson *et al.* in press). In the south of the rift the Dhandlawas Formation is locally associated with lava flows of the Raageshwari Volcanic Formation, and comprises muddy debris flows and alluvial fan deposits that represent the progressive burial of the irregular upper surface of the Raageshwari Volcanic Formation (**Figure 2.23**).

The Fatehgarh Formation transitions upwards into the Barmer Hill Formation, which comprises the thickest and best developed lacustrine deposits within the rift (**Figure 2.23**; Dolson *et al.* in press). The Barmer Hill Formation displays rapid thickness variations across active faulting and indicates deposition within a tectonically active setting. A prominent maximum flooding surface towards the base of the Barmer Hill Formation marks a widespread deepening of the rift. Overriding the Barmer Hill Formation, the Dharvi Dungar, Thumbli, and Akli formations (**Figure 2.23**) are sand poor and are represented by several depositional cycles of lacustrine mudstones and siltstones, fluvial sandstones, and swamp lignites, and contain many pronounced unconformities related to variable sediment input (Dolson *et al.* in press). The Dharvi Dungar, Thumbli, and Akli formations have a distinct cyclic seismic character, with high-amplitude lignite intervals separated by low-amplitude, homogeneous lacustrine mudstones and siltstones. Mudstone and siltstone deposits are predominantly freshwater lacustrine. However, the occasional presence of dinoflagellates indicates marine incursions from either the north or south (Dolson *et al.* in press). The absence of oil shows, that is any indication of oil during drilling, above the Thumbli Formation indicates that the Akli Formation forms the regional seal (Dolson *et al.* in press).

2.3.3.3 Post-rift formations

Post-rift deposition in the Barmer Basin comprises the middle Eocene Nagarka Formation, and the Miocene to recent Jagadia and Uttarlai formations. Oligocene Epoch strata are missing in the Barmer Basin due to erosion (Compton 2009; Dolson *et al.* in press). However, post-rift deposition was re-instated during the Miocene Epoch with deposition of the Jagadia and Uttarlai formations

above the base Miocene unconformity (**Figure 2.23**). The occurrence of a thick succession of Quaternary sediments in the south of the rift indicates rapid sedimentation coeval with non-deposition in the north of the rift during the Quaternary Period (**Figure 2.21**). However, the cause of rapid Quaternary subsidence in the south of the rift is unknown.

3 The Barmer Hills

Structural geology of a section of the central western rift margin of the Barmer Basin

Coincident with rifting of the Seychelles microcontinent from the west coast of India, and extrusion of the Deccan flood basalts, the main phase of subsidence in the Barmer Basin, the Barmer Basin rift event, was fault-controlled and commonly assumed to have accommodated regional, approximately rift-perpendicular (≈ northeast-southwest) extension. However, no evidence other than the orientation and geometries of rift-scale structures mapped in the subsurface has been presented to support this assumption. In this chapter, outcrop- (small) scale structures exposed along a section of rift-parallel faulting of the western rift margin of the Barmer Basin, in the Barmer Hills (**Figure 3.1**), are investigated to refine the findings of previous work, and place the structural evolution of the study area within the wider context of Barmer Basin rift evolution. The findings provide direct outcrop-based evidence supporting the assumption of rift-perpendicular extension during the Paleogene Barmer Basin rift event.

3.1 Geological setting

Located along the central section of the western rift margin of the Barmer Basin (**Figure 3.1**), the Barmer Hills are a scattered series of hills situated to the west of the town of Barmer (**Figure 3.2**). Exposure occurs sporadically across an area of 800 km^2. However, the largest series of hills covers approximately 330 km^2 (**Figure 3.2a**).

Exposures in the Barmer Hills are dominated by the Precambrian Malani Igneous Suite (Pareek 1981) that forms the rift-basement of the Barmer Basin (**Figure 3.3**). The third largest felsic igneous province in the world, the Malani Igneous Suite consists of bimodal, dominantly felsic deposits that are largely undeformed and un-metamorphosed (Pareek 1981; Torsvik *et al.* 2001; Roy & Jakhar 2002; Sharma 2004). Malani magmatism occurred during the Tonian Period (770 Ma to 750 Ma), and commenced with extrusion of large volumes of rhyolite and rhyolitic tuff, followed by intrusion of granite, and finished with emplacement of porphyries and quartz veins (Pareek 1981; Torsvik *et al.* 2001; Sharma 2004). Magmatism is related to the fragmentation of the Rodinian Supercontinent, with some authors suggesting an intra-continental plume or rift-setting

(Plummer & Belle 1995; Sharma 2004), while others prefer subduction-related magmatism in an Andean-type arc setting on the edge of the Rodinian Supercontinent (Torsvik *et al.* 2001).

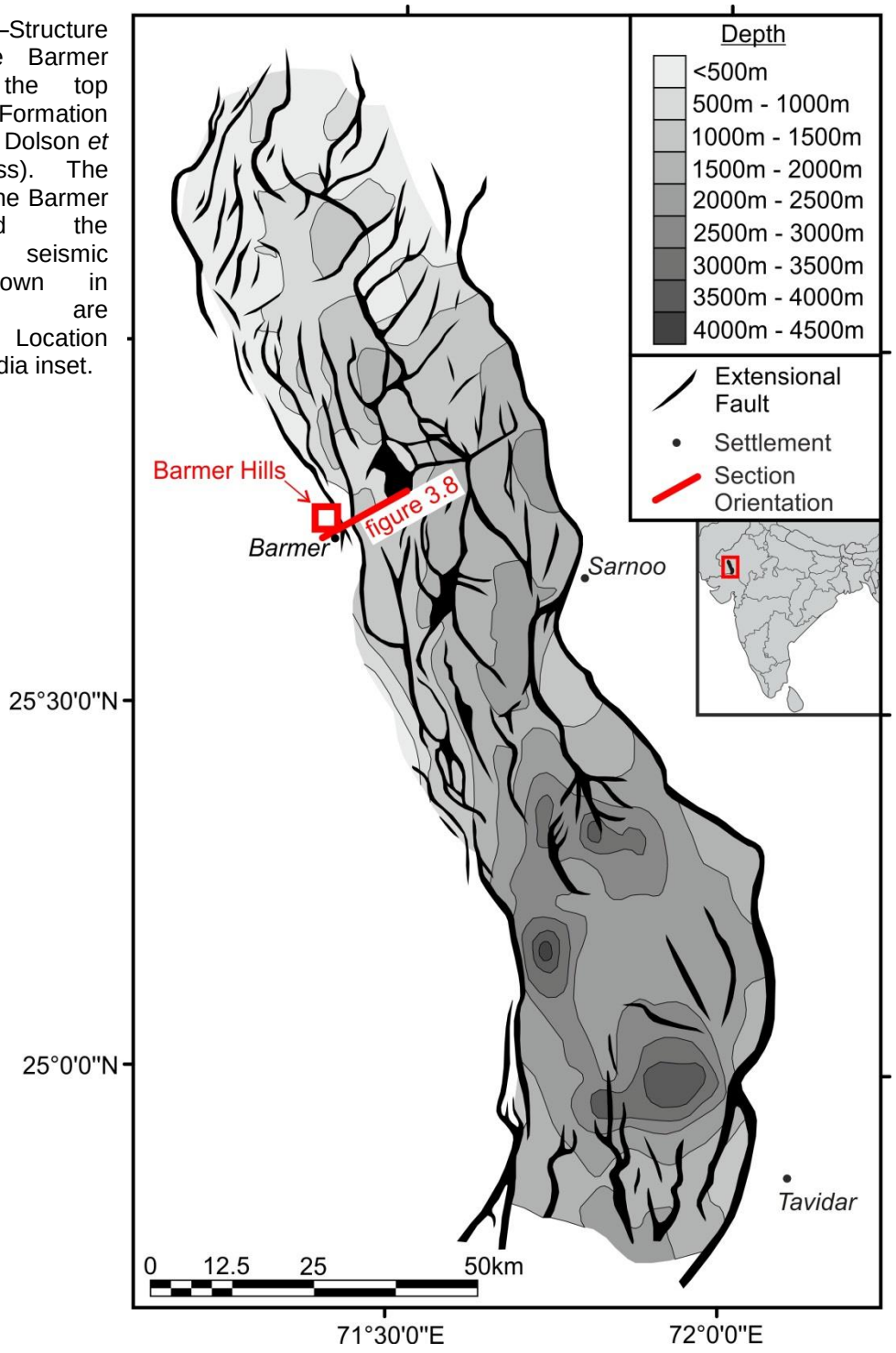

Figure 3.1 –Structure map of the Barmer Basin at the top Fatehgarh Formation horizon (after Dolson *et al.* in press). The locations of the Barmer Hills and the interpreted seismic section shown in **Figure 3.8** are indicated. Location map within India inset.

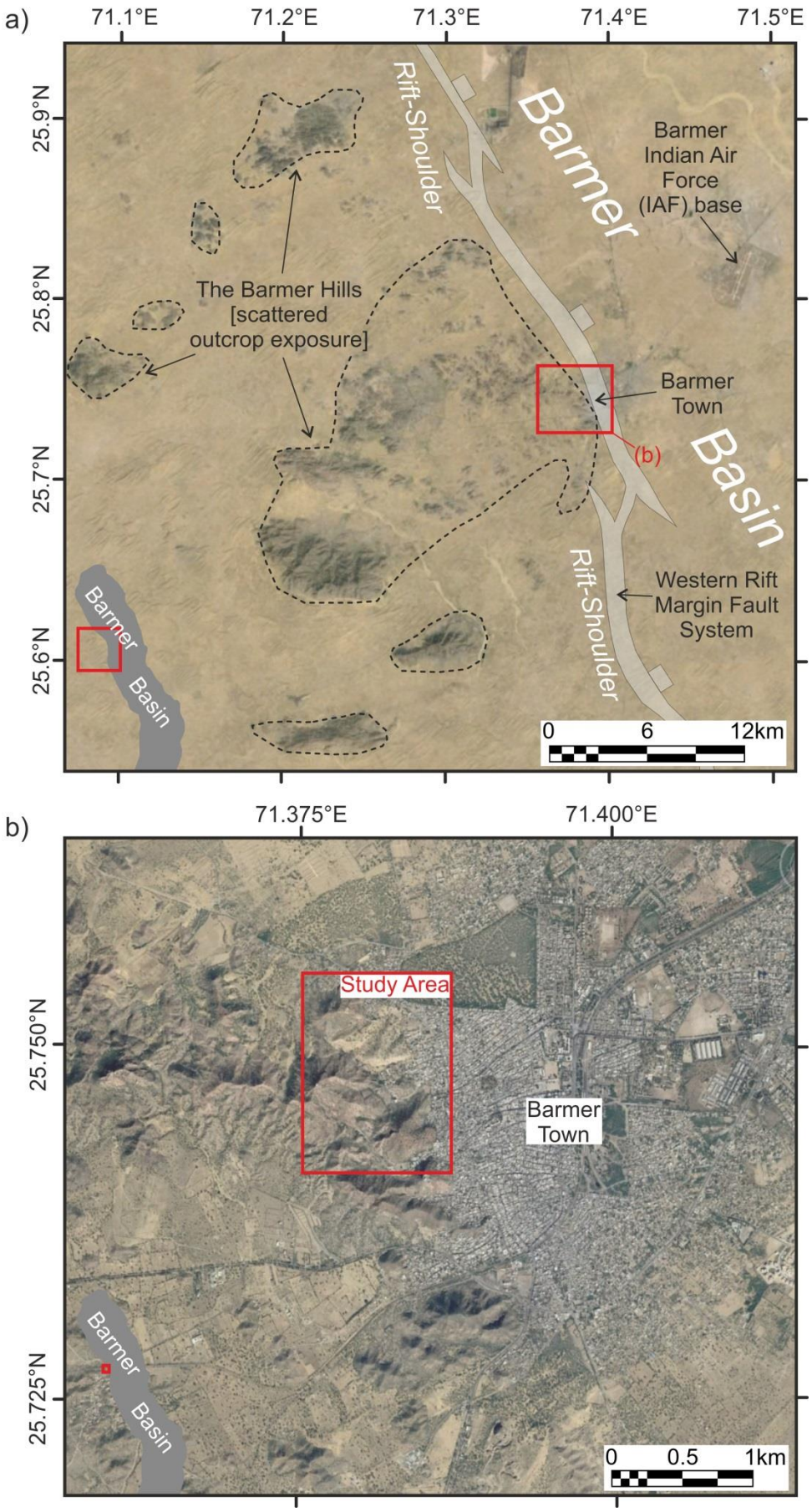

Figure 3.2 – Satellite images of the Barmer Hills with notable features and fault polygons of the western rift margin fault system (mapped commercially using subsurface data) indicated **(a)** along with the Barmer Hills study area (see **Figure 3.1** for image location) **(b)**. Images courtesy of Google™ earth

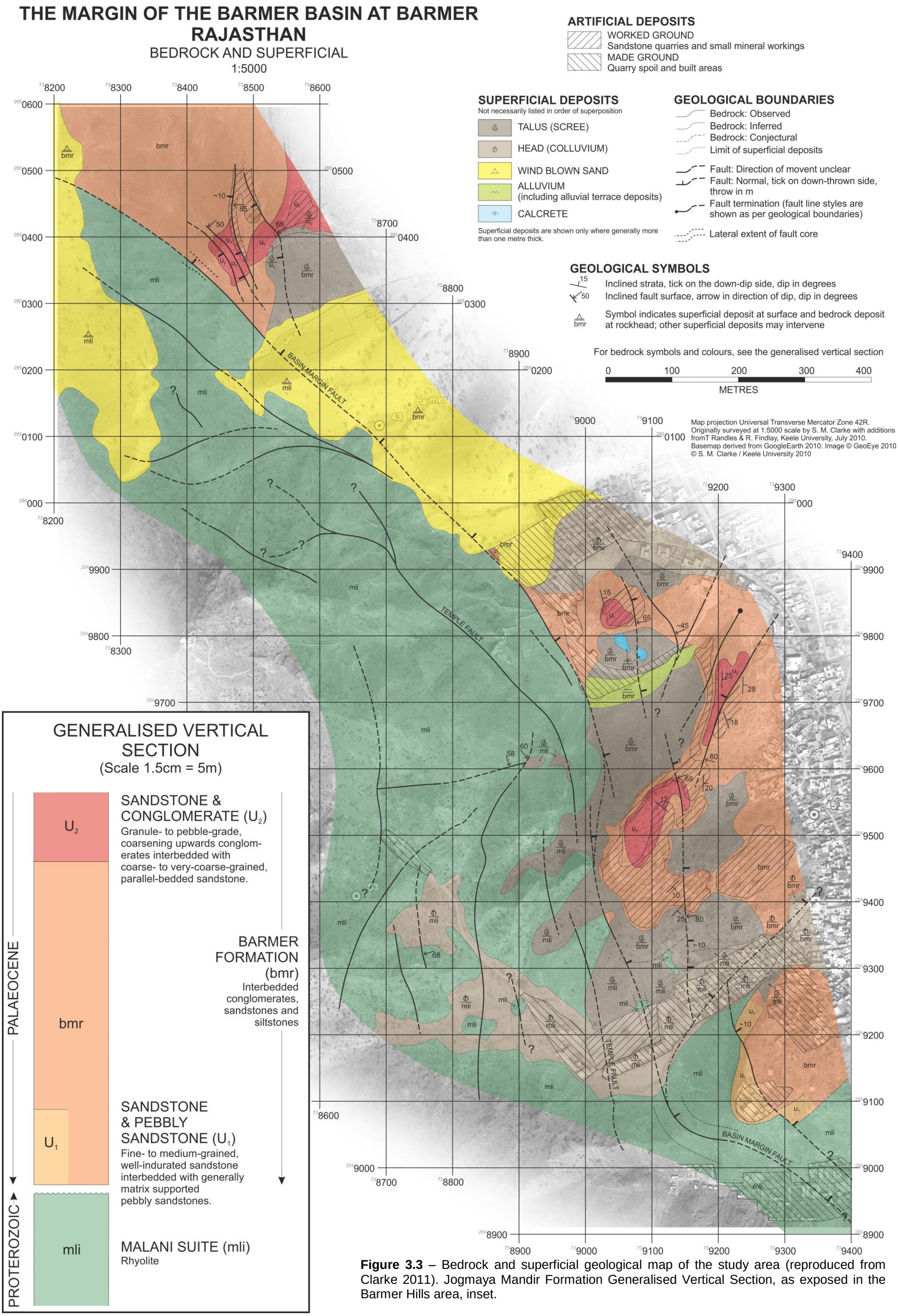

Figure 3.3 – Bedrock and superficial geological map of the study area (reproduced from Clarke 2011). Jogmaya Mandir Formation Generalised Vertical Section, as exposed in the Barmer Hills area, inset.

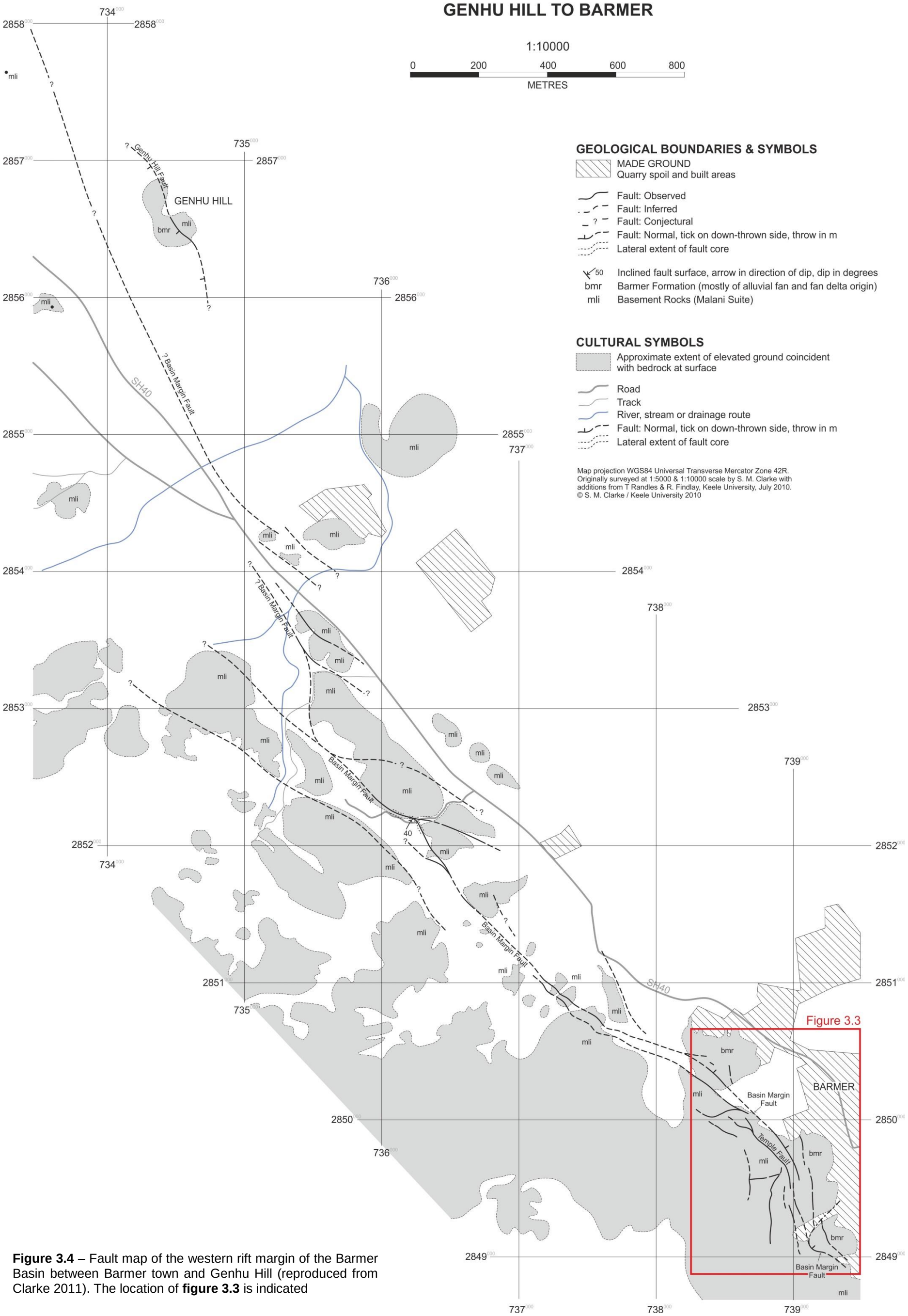

Figure 3.4 – Fault map of the western rift margin of the Barmer Basin between Barmer town and Genhu Hill (reproduced from Clarke 2011). The location of **figure 3.3** is indicated

Unconformably overlying, and juxtaposed against, the Malani Igneous Suite across the western rift margin fault system, the Jogmaya Mandir Formation (Dolson *et al.* in press; **Figure 2.23**) was previously part of the Barmer Formation (Sisodia & Singh 2000; Clarke 2011), and comprises a series of interbedded conglomerates, sandstones, and siltstones (**Figure 3.3 inset**) that form coarse-grained facies and facies associations typical of deposition within alluvial fans proximal to the rift-margins (Clarke 2011; Dolson *et al.* in press). Conglomeratic deposits comprise monomictic clasts of Malani Igneous Suite detritus up to cobble and boulder grade. A Paleocene age is inferred for the Jogmaya Mandir Formation on the basis that it interdigitates with and locally overlies the Fatehgarh Formation in the subsurface (Dolson *et al.* in press). However, a lack of fossils, limited lateral extent, and the poorly-defined base mean that in places, the Jogmaya Mandir Formation may be older or younger than currently interpreted (Dolson *et al.* in press).

Initial mapping of the study area (**Figure 3.2b**) indicated that faults defining the western rift margin in the Barmer Hills are predominantly northwest-striking (rift-parallel), northeast-dipping, en-echelon, and anastomosing structures, with arcuate fault segments that are both hard- and soft-linked at the level of the exposure (**Figure 3.3 & 3.4**; Clarke 2011). Where hard-linked, offset fault segments are connected by zones of north-northwest to north-striking faults that form a broad series of anastomosing fault splays within the intervening accommodation zone (**Figure 3.4**). The lack of a consistent marker horizon in this succession precludes determination of displacement from field observations alone. Hanging-wall faulting is both syn- and antithetic to the main rift-margin fault, predominantly north-northwest- and northeast-striking, and accommodates significantly less deformation (Clarke 2011). Dominant fracture sets are north-northwest and northeast-trending, and three inconsistent fault-plane kinematic indicators were recorded that indicated fault-slip towards the west-northwest, east-northeast, and south-southeast, with a significant component of oblique-slip (Clarke 2011; Mukhopadhyay 2011).

3.2 Methodology

High resolution (1:5000) fault mapping was conducted throughout the study area (≈ 2 km^2; **Figure 3.2b**). The same study area used in previous studies (Clarke 2011; Mukhopadhyay 2011) was chosen as it is the only known area where syn-rift sediments of the Jogmaya Mandir Formation are exposed juxtaposed against the western rift margin fault. Further to this, previous work (**Figure 3.3**; Clarke 2011) provided a framework to build upon. Georeferenced satellite

images of the study area were combined with a 90 m Digital Elevation Model to generate the basemaps used for field mapping. Elevation is in metres above sea level. The Digital Elevation Model encompassed the entire area of the Barmer Hills, with maximum and minimum values of 380 m and 215 m in the study area respectively.

3.2.1 Kinematic analysis

Under low confining pressures (e.g. deformation in the shallow crust), the simple case of uniaxial tension (extension) results in formation of extensional fractures (fissures, joints, and veins), defined as a clean separation between two opposing halves of a deforming rock with no shear between the two surfaces, that is no fracture-parallel displacement (Turcotte & Schubert 2002; Jaeger *et al.* 2007). Extensional fractures form perpendicular to the minimum principal stress axis (σ3) once the applied deviatoric stress locally exceeds the strength of the rock. The orientation of extensional fractures, therefore, provides a simple method of estimating the orientation of the minimum principal stress axis (σ3) during deformation.

When the shear stress exceeds the frictional strength of an existing shear plane or the cohesive strength of the rock (**Equations 2.2 to 2.5**) shear failure results in mechanical interaction and scouring between adjacent blocks and generates slickenline lineations. Slickenlines, combined with the orientation of the fault plane and the sense of fault slip (e.g. normal/reverse), characterise the kinematics of a fault (Angelier *et al.* 1982; Angelier 1984; Huang & Angelier 1989; Angelier 1990; Marrett & Allmendinger 1990; Doblas 1998). Fault-plane slip sense indicators indicate the sense of shear during the most recent deformational event, and include steps, crescentic markings, trailed material, mineralogical or crystallographic orientations, and fractures situated on a fault plane (Doblas 1998). During field mapping, extensional fracture plane, fault plane, and fault-plane slickenline lineation data were recorded where available in order to assess the kinematics of the exposed fault network.

3.2.2 Fault-slip inversion

The stress acting on a plane in any stress system, comprising three perpendicular principal stress axes (σ1 > σ2 > σ3), can be broken into two components, the component of stress acting perpendicularly to the plane [normal ($\boldsymbol{\sigma_n}$) stress] and the stress acting within (parallel) to the plane [shear ($\boldsymbol{\tau}$) stress; Wallace 1951; Jaeger *et al.* 2007]. For any arbitrary plane within a stress system,

the shear stress reaches a maximum, and thus shear failure is most likely to occur (**Equation 2.3**), when the arbitrary plane is orientated at 45° to the maximum (σ1) and minimum (σ3) principal stress axes, and is parallel to the intermediate (σ2) principal stress axis (e.g. Mohr's representation of stress; **Figure 3.5**; Wallace 1951; Jaeger *et al.* 2007).

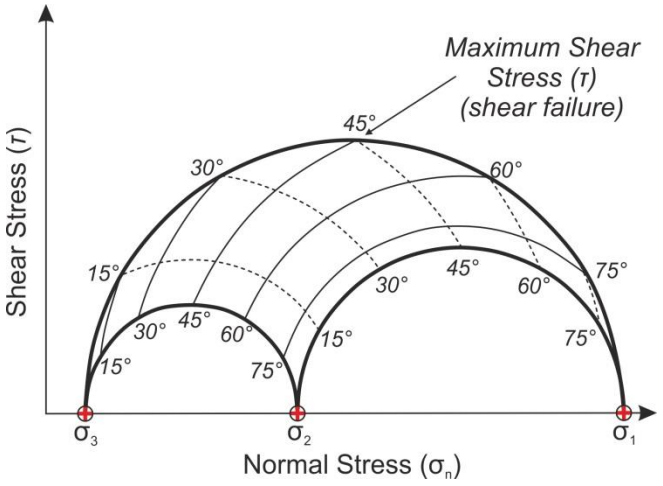

Figure 3.5 – Mohr's relationship between normal ($\boldsymbol{\sigma_n}$) stress acting perpendicularly to a plane and shear ($\boldsymbol{\tau}$) stress acting within a plane in three-dimensions (after Wallace 1951). Shear stress on a plane within a stress system is greatest, and therefore shear failure of a plane is most likely (**Equation 2.3**), when a plane is orientated at 45° to the maximum (σ1) and minimum (σ3) principal stress axes within a stress system (annotated).

Using this simple geometrical relationship, if the orientation of a fault plane and the direction and sense of shear failure (fault-slip) are known from field measurements, fault-slip data can be used to estimate the relative orientation of compressional (shortening) and tensional (extensional) strain during deformation under a series of assumptions in a process termed fault-slip inversion (Angelier *et al.* 1982; Angelier 1984; Huang & Angelier 1989; Angelier 1990; Marrett & Allmendinger 1990). The direction of shortening and extension define the shortening (P) and extensional (T) kinematic axes. Kinematic axes, namely the extensional (T), shortening (P), and neutral (N) axes represent the principal axes of strain during deformation, are perpendicular, and are often assumed to parallel the principal stress axes (σ1 > σ2 > σ3; Marrett & Allmendinger 1990). Assuming: 1) that stress is homogeneous; 2) that faults do not interact mechanically; 3) that shear failure occurs when the shear (fault) plane is orientated at 45° to the direction of shortening and extension (P & T kinematic axes) and that the intermediate stress axis (σ2) lies within the active fault plane, that is shear failure occurs when shear stress is at a maximum (Mohr's relationship; **Figure 3.5**), and; 4) that fault-slip parallels the direction of shear stress projected within the fault plane (e.g. Wallace 1951; Bott 1959; Marrett & Allmendinger 1990), the P and T kinematic axes during deformation can be estimated using a stereographic projection (**Figures 3.6 & 3.7**).

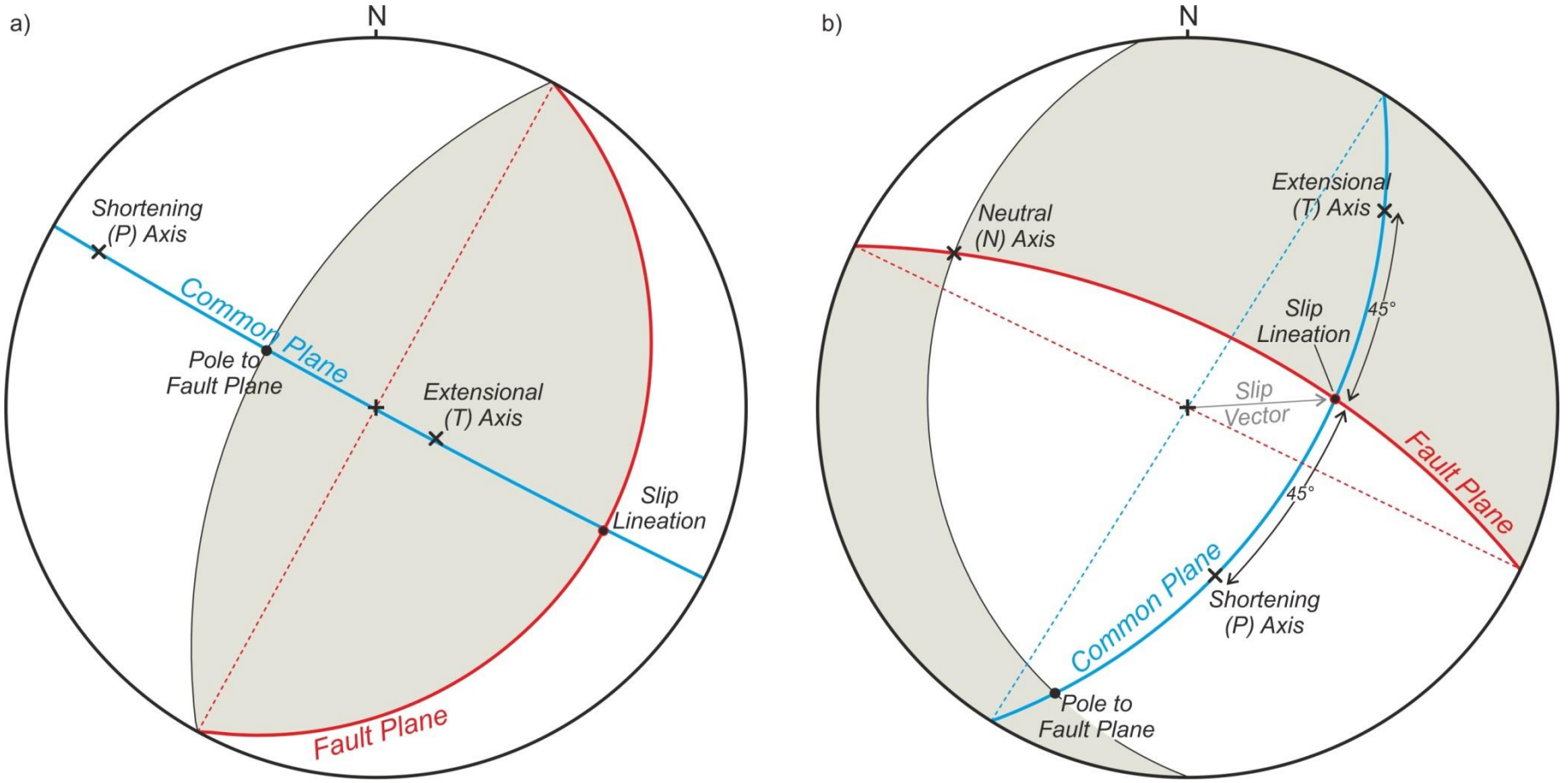

Figure 3.6 – Representation of fault-slip data in terms of kinematic [shortening (P), extensional(T), and neutral (N)] axes; **(a)** Simple example depicting a shallow-dipping fault plane with a reverse-sense slip lineation resulting in sub-horizontal and sub-vertical shortening and extensional axis respectively (after Marrett & Allmendinger 1990). The slip-lineation, pole to fault plane, and shortening (P) and extensional (T) kinematic axes lie within a common 'movement' plane. **(b)** worked example of a fault-slip measurement from the Barmer Hills depicting the three kinematic axis (P, T, & N) and fault-plane solution. Fault Plane = 296°/73°NE; Slickenline Pitch = 116°; Displacement = normal-sense. Grey = extensional first motions; white = compressional first motions

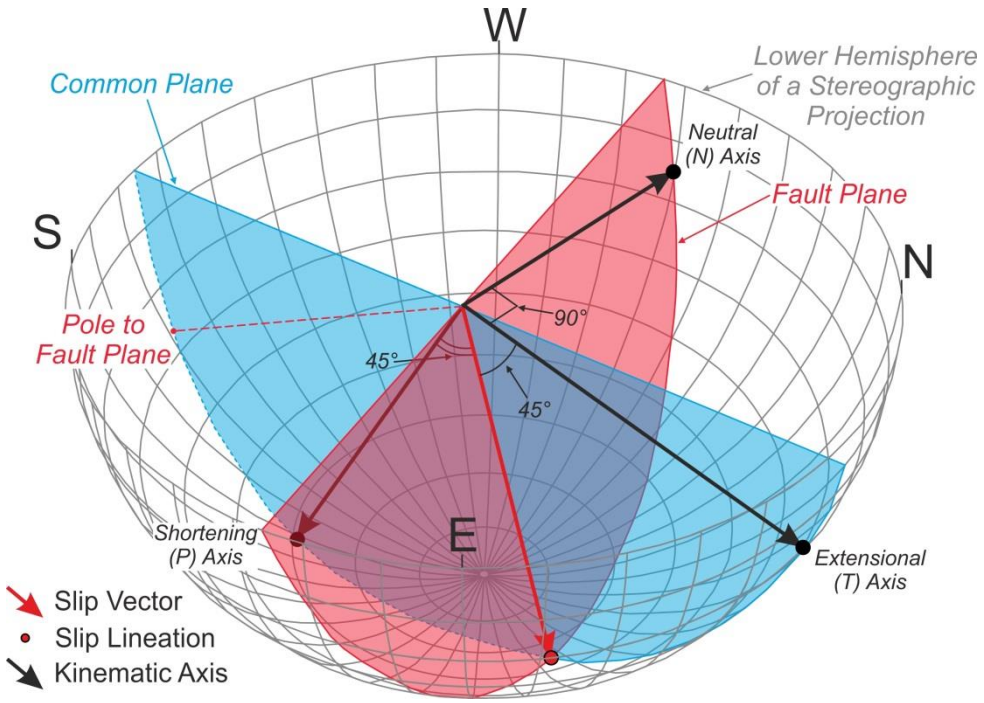

Figure 3.7 – Oblique, three-dimensional view of the lower hemisphere of a stereographic projection depicting the fault plane solution shown in **Figure 3.6b** (key to symbols inset). Kinematic axes (P, T, & N; black arrows) are orthogonal, and lie within two perpendicular planes, the fault plane (red) and a common (or movement) plane (blue). The extensional (T) and shortening (P) kinematic axes are situated 45° either side of the fault slip lineation within the common plane, which is defined by the slip lineation and the pole to the fault plane.

Graphically, the shortening (P) and extensional (T) kinematic axes are approximated by plotting a fault plane, the pole to the fault plane, and the associated fault slip lineation on a stereographic projection (**Figure 3.6**). The shortening (P) and extensional (T) kinematic axes are perpendicular and, therefore, lie within a common plane, which must also contain the displacement (slip) vector. The slip lineation within a fault plane on a stereographic projection is a graphical representation of the intersection between the direction of shear displacement (slip vector) and the fault plane. Combining Mohr's relationship, namely that the shortening (P) and extensional (T) kinematic axes are orientated at 45° to a shear plane upon shear failure (**Figure 3.5**; Wallace 1951; Jaeger *et al.* 2007), with the requirement that the P and T axes, as well as the displacement (slip) vector must lie within a common (or movement) plane, indicates that the P and T axes are situated 45° either side of the slip lineation within the common plane (**Figures 3.6 & 3.7**). The common (movement) plane must also contain the pole to the fault plane, that is the vector normal to the fault plane, to ensure perpendicularity between the common and fault planes, and orthogonality between kinematic axes

(P, T, & N). Essentially, a fault-plane-solution is generated as conducted in seismology. The extensional (T) and shortening (P) axes are situated within the extensional and compressional quadrants of the fault-plane solution respectively (**Figure 3.6**). The sense of fault slip, therefore, is necessary to define these quadrants and determine which of the kinematic axes situated 45° either side of the slip lineation within the common (movement) plane correspond to the direction of shortening and extension. Critically, no interpretation is involved in this procedure and the kinematic axes are an alternative representation of the original data (Marrett & Allmendinger 1990).

Using open source software (FaultKin7), measurements of fault-slip recorded in the Barmer Hills study area (c.f. **Figure 3.2b**; **Appendix A**) were used to generate orthogonal (perpendicular) shortening (P), extensional (T), and neutral (N) kinematic axes. Subsequently, the software contoured (Kamb 1959) all kinematic axes to indicate the directional distribution of the principal strain axes during deformation (T, P, & N axes; Marrett & Allmendinger 1990). Directional maxima were also calculated using Bingham distribution statistics (c.f. Marrett & Allmendinger 1990).

3.3 Structures exposed in the Barmer Hills

Subsurface data reveal the study area is situated in the immediate footwall of the western rift margin fault system that is locally north-northwest-striking, east-northeast-dipping (rift-parallel; **Figure 3.2a**), and accommodated up to 1 km of subsidence (**Figure 3.8**). At outcrop, the cores of fault zones (**Figure 3.9**) comprise a spectrum of fault rocks from fault (crush) breccia (**Figure 3.9b**) to fault gouge (**Figure 3.9a**) and are surrounded by brittle damage zones in the adjacent footwall and hanging-wall blocks. Dominant faults are northwest-striking and northeast-dipping (**Figure 3.10**). Two right-stepping rift-margin fault segments in the northwest and southeast of the study area are separated by a diffuse zone of north-trending faults (**Figure 3.10**). In the north of the study area Jogmaya Mandir Formation sediments are juxtaposed directly against the rift margin fault, and the basal contact of the Jogmaya Mandir Formation is not exposed (**Figures 3.9c, d, & e**). However, in the southeast of the study area, within the diffuse zone of north-trending faults, the basal contact of the Jogmaya Mandir Formation is exposed, revealing Jogmaya Mandir formation sediments unconformably overlying the Malani Igneous Suite (**Figure 3.10**).

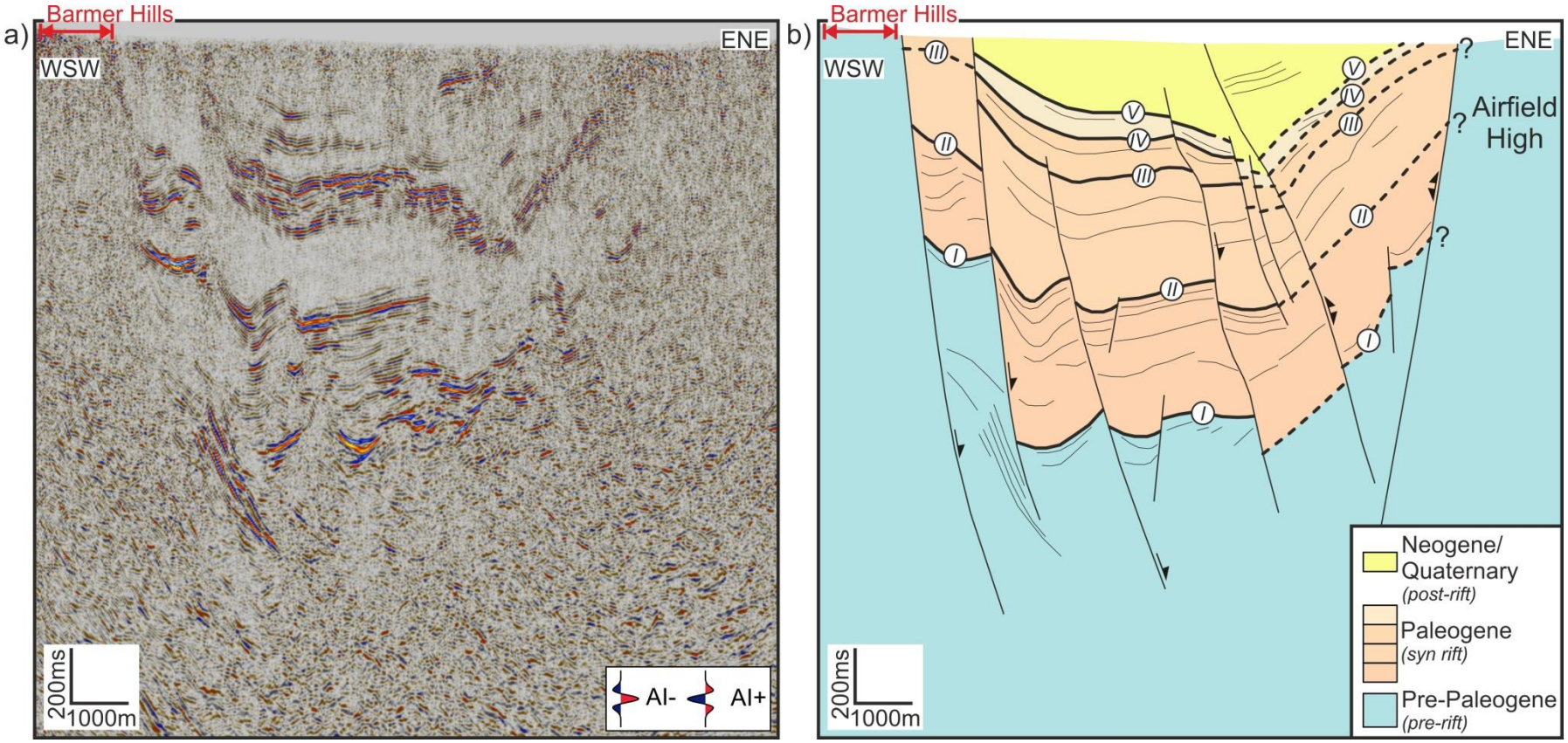

Figure 3.8 – Un-interpreted **(a)** and interpreted **(b)** cross-line (061°) seismic section depicting the relationship of outcrop exposure in the Barmer Hills (highlighted in red) to the Barmer Basin subsurface. For section location see **figure 3.1**.

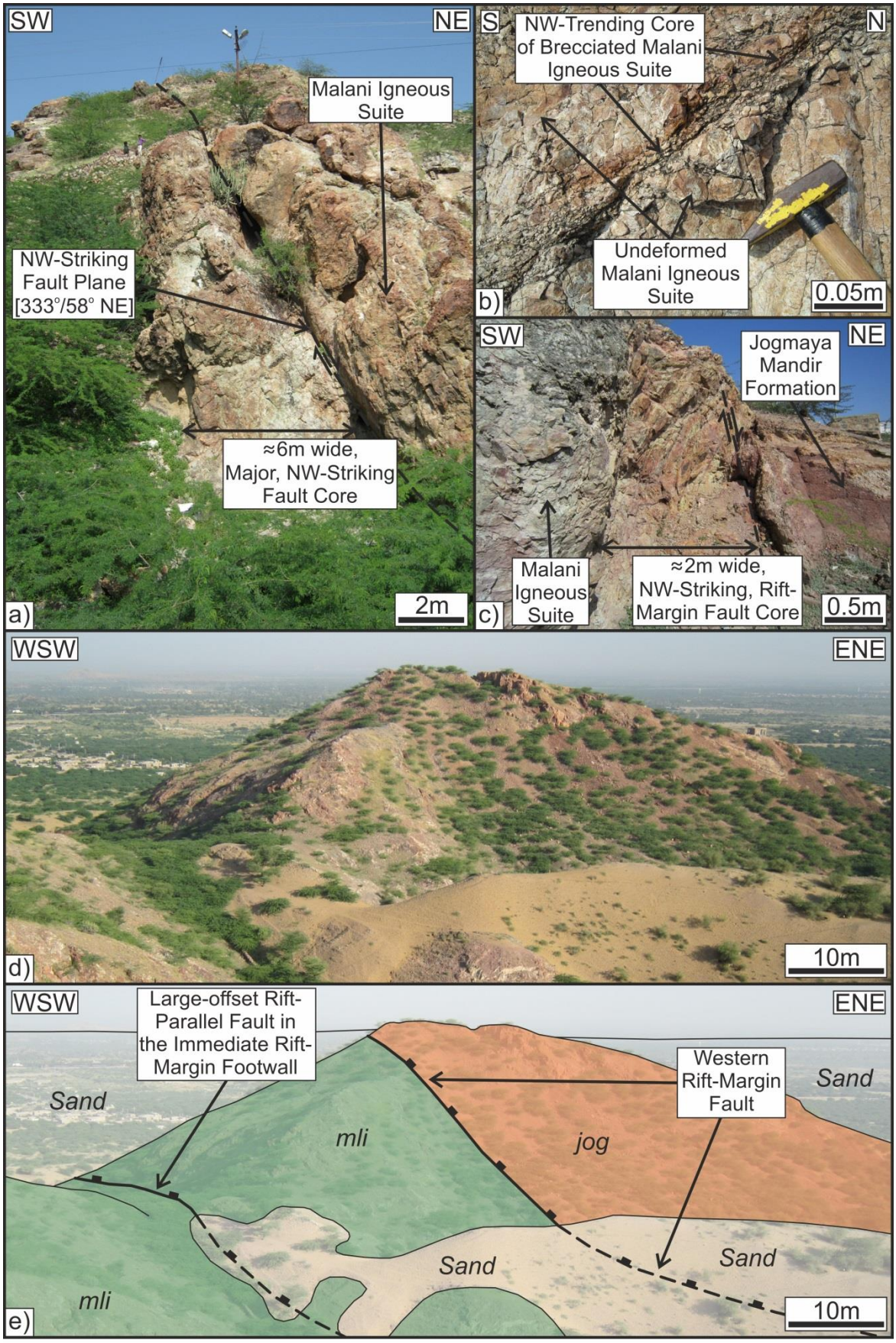
SW
NE
Malani Igneous Suite
NW-Striking Fault Plane [333°/58° NE]
≈6m wide, Major, NW-Striking Fault Core
2m
a)
S
N
NW-Trending Core of Brecciated Malani Igneous Suite
Undeformed Malani Igneous Suite
0.05m
b)
SW
NE
Jogmaya Mandir Formation
Malani Igneous Suite
≈2m wide, NW-Striking, Rift-Margin Fault Core
0.5m
c)
WSW
ENE
10m
d)
WSW
ENE
Large-offset Rift-Parallel Fault in the Immediate Rift-Margin Footwall
Western Rift-Margin Fault
Sand
mli
jog
Sand
Sand
mli
10m
e)
Malani Igneous Suite
(Rift-Basement)
Jogmaya Mandir Formation
Extensional Fault
(tick on downthrown side)

Figure 3.9 (*previous page*) – **(a)** NW-striking, NE-dipping fault in the immediate (≤ 100 m) footwall of the western rift margin fault system; **(b)** Tectonic breccia in a narrow (≈ 0.2 m) shear zone within the Malani Igneous Suite (note the lack of fault-gouge); **(c)** Malani Igneous Suite rift basement juxtaposed against footwall-derived alluvial fan sediments of the Paleocene Jogmaya Mandir Formation; **(d)** un-interpreted and **(e)** interpreted landscape depicting the western rift-margin fault. See **figure 3.10** for photograph locations.

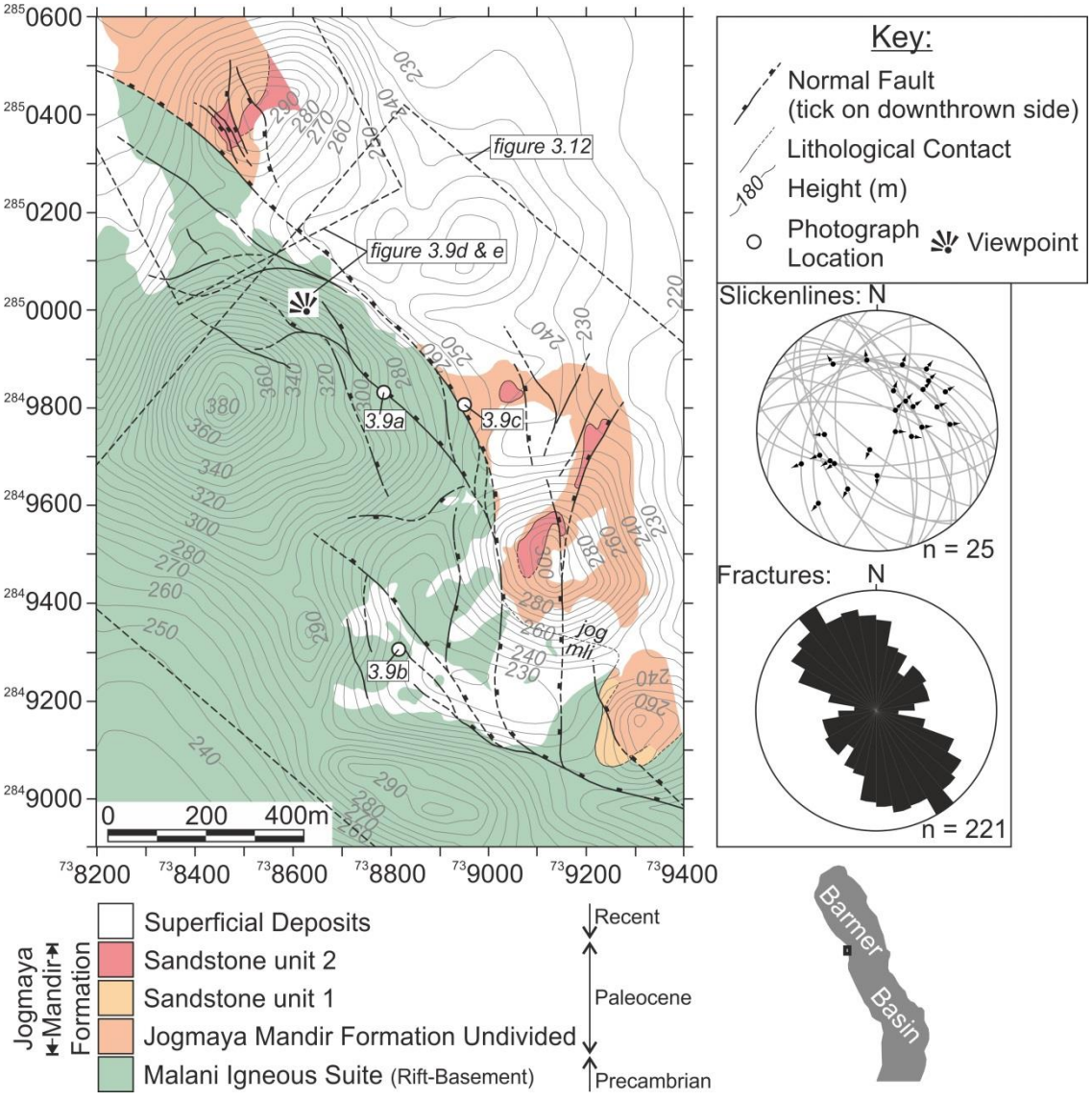

Figure 3.10 – Updated fault map of the study area, situated west of Barmer town. Topographical contours are at 5 metre intervals. Reference grids are UTM zone 42N. Location map inset. The locations of photographs shown in **figure 3.9**, and the area of block diagrams depicted in **figure 3.12** are also shown. Structural data indicate faulting facilitated NE & SW dip-slip movement and dominant extensional fractures are NNW – SSE trending (rift-parallel). See **Appendix A** for raw structural data.

Dominant extensional fractures are north-northwest trending and kinematic indicators (slickenlines) are rare, but show predominantly dip-slip movement towards the northeast and southwest (**Figure 3.10**). However, north-south and east-west orientated slickenline measurements are also evident. Slip-sense indicators (**Section 3.2.1**; e.g. Doblas 1998) are uncommon. However, the proximity and sub-parallel orientation of faulting in the study area to the large-offset (< 1 km) normal-sense rift-margin fault (**Figures 3.2 & 3.8**) suggests faulting in the study area and the rift-margin fault are genetically linked. As such, faulting in the study area was attributed a normal-sense where slip-sense was uncertain. Fault-plane solutions indicate shortening (P) axes dip steeply and extensional (T) axes are sub-horizontal, with an average extensional axis that is sub-horizontal and northeast (047.6°) trending, and a sub-vertical average shortening (P) axis (**Figure 3.11**).

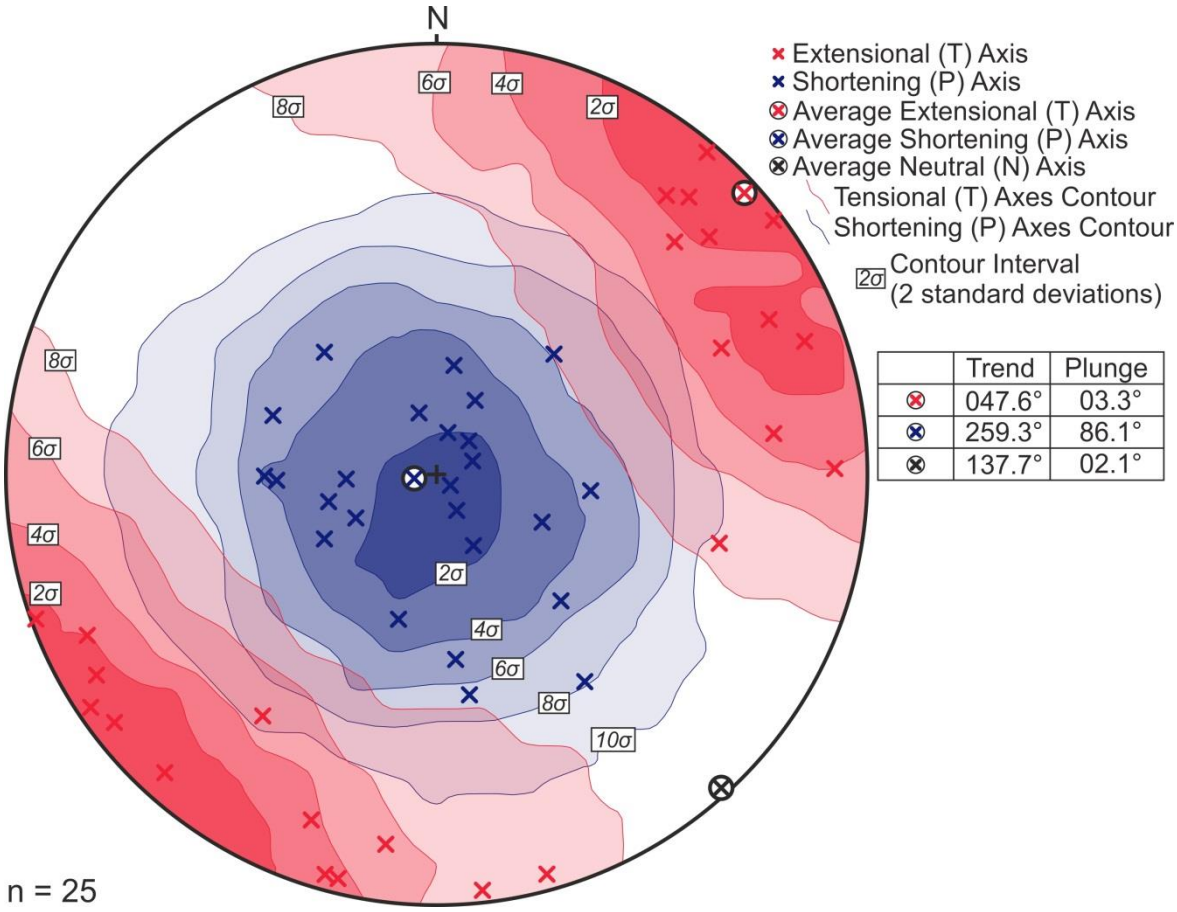

Figure 3.11 – Contoured kinematic [shortening (P) and extensional (T)] axes of fault-slip data measured in the Barmer Hills giving an indication of the directional distribution of the average strain axes during deformation in the Barmer Hills. Data are plotted on a lower hemisphere, equal area stereonet. Key to symbols inset. Contour interval is two standard deviations, and the trend and plunge of each average kinematic axes are tabulated inset. See **Appendix A** for raw structural data.

3.4 Structural evolution of the Barmer Hills

Assuming the upper surface of the Malani Igneous Suite approximated a peneplaned surface prior to deformation, exposure of the basal contact of the Jogmaya Mandir Formation within the diffuse zone of north-trending faults in the south of the study area (**Figure 3.10**) suggests a southwards reduction of displacement on the western rift margin fault within the study area. This reduction of displacement, coincident with the diffuse zone of faulting that is orientated obliquely and situated between the adjacent northwest-striking rift-margin fault segments, suggests displacement transfer between offset faults within an evolving fault system (**Figure 3.12**; Gawthorpe & Hurst, 1993). It follows that the diffuse zone of north trending faults represents the relay zone separating offset, rift-parallel, rift-margin fault segments (**Figure 3.12**). Such relationships, specifically offset fault segments linked by discrete zones of displacement transfer, commonly occur in areas of active extension (e.g. Basin and Range Province, East African Rift System, and Gulf of Suez; **Section 2.1**). Further to this, the presence of hard-linked fault segments within the study area, and soft-linked fault segments to the north (**Figure 3.4**; Clarke 2011), suggests evolution of the western rift margin from a series of isolated, northwest-striking, northeast-dipping fault segments that linked to form a single, through-going fault system (**Section 2.1.1**; **Figure 3.12**; e.g. Peacock & Sanderson, 1994; Cartwright *et al.*, 1995; Cowie *et al.*, 2000; Walsh *et al.*, 2003; Giba *et al.*, 2012). Such fault geometries resemble those predicted to form in a perpendicular extensional regime, that is where faults evolve in an orientation that is perpendicular to the extension direction.

In conjunction with fault geometries suggesting a perpendicular extension direction relative to faulting (≈ northeast-southwest; **Figure 3.10**), kinematic indicators including; 1) the rift-parallel (north-northwest-south-southeast) orientation of extensional fractures (**Figure 3.10**); 2) fault-slip data recording dip-slip movement to the northeast and southwest (**Figure 3.10**), and; 3) fault-plane solutions indicating an average sub-horizontal, northeast (047.6°) trending extensional (T) kinematic axis, and a sub-vertical average shortening (P) kinematic axis (**Figure 3.11**), demonstrate that the extensional strain axis, and therefore under the assumption that kinematic axes parallel the principal stress axes (**Section 3.2.2**), the minimum principal stress axis (σ3), was northeast-southwest orientated (047.6°-227.6°) during the most-recent slip event in the study area. However, the presence of north-south and east-west orientated slickenline measurements alludes to additional, poorly classified deformational events within the study area.

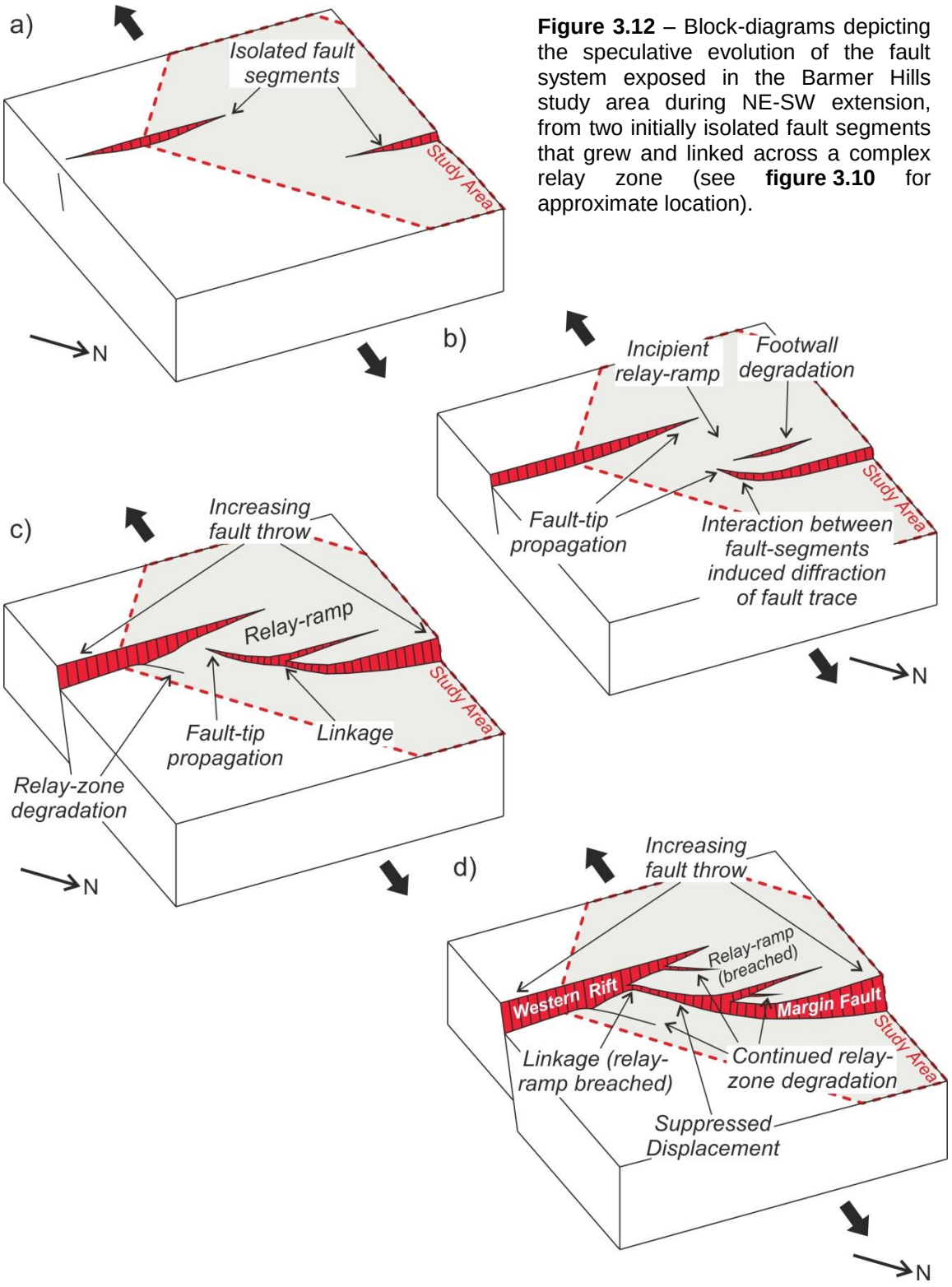

Figure 3.12 – Block-diagrams depicting the speculative evolution of the fault system exposed in the Barmer Hills study area during NE-SW extension, from two initially isolated fault segments that grew and linked across a complex relay zone (see **figure 3.10** for approximate location).

3.5 Discussion

The kinematic analysis of structures exposed in the study area demonstrates that the extensional strain axis during the most recent slip event was northeast-southwest orientated. However, fault-plane slickenlines only preserve the most recent part of the deformation history (i.e. the most

recent slip-event), and many shear-sense indicators are ambiguous. Further to this, many of the assumptions made during fault-slip inversion, including: 1) stress homogeneity; 2) non-interacting faults, and; 3) shear failure when the shear plane is orientated at 45° to the shortening (P) and extensional (T) kinematic axes, may not be appropriate in natural examples. The results of quantitative methods of fault-slip inversion, therefore, should be used with caution and supported by other kinematic criteria (Marrett & Allmendinger 1990). In order to mitigate against the uncertainties inherent to methods of fault-slip inversion, the kinematic analysis presented is multi-component and reduces the ambiguity implicit with any single kinematic criterion. The dominant north-northwest trend of extensional fractures in conjunction with the northeast and southwest orientation of normal-sense dip-slip displacement accommodated by faults in the study area supports the results of the fault slip inversion performed.

The monomictic, highly immature clast array of the Jogmaya Mandir Formation exposed within the study area, comprising clasts of the Malani Igneous suite (c.f. Clarke 2011), indicate the alluvial fan deposits are proximal to the sediment source region and were derived locally. The most likely hinterland of Jogmaya Mandir Formation sediments is the rift-margin footwall, situated immediately adjacent and to the west of exposures of Jogmaya Mandir Formation deposits within the study area. Active faulting induces uplift of the footwall relative to the hanging-wall, and where the footwall is exposed or situated above the local base-level the footwall crest degrades. Subsequently, periodic mobilisation of the detritus produced from the degrading footwall facilitates a ‘shedding’ of material into the adjacent subsiding regions within debris flows. Progressive debris flows originating from a common origin (nick-point) are preserved within alluvial fan deposits, as exposed in sediments of the Jogmaya Mandir Formation within the study area. This proximal source-sink relationship, and the Paleocene age of Jogmaya Mandir Formation deposits (Dolson *et al.* in press), indicate that fault activity in the study area occurred during the Paleocene Epoch, and was contemporaneous with deposition of the basin fill. It follows that structures in the Barmer Hills were active during the main Barmer Basin rift event. Combined, the findings substantiate the common assumption that deformation during the main Paleogene Barmer Basin rift event accommodated approximately northeast-southwest (rift-perpendicular) regional extension.

3.6 Summary

This chapter investigated the validity of the common assumption that deformation during the Paleogene Barmer Basin rift event accommodated regional extension that was perpendicular (≈ northeast-southwest) to the north-northwest trending Barmer Basin. High resolution mapping of the western rift margin fault system in the Barmer Hills built on the findings of previous work and was conducted in conjunction with collection of structural data. Faults are predominantly northwest-striking, northeast-dipping, with dominant north-northwest-trending (rift-parallel) extensional fractures. Rare fault-plane slickenlines show predominantly dip-slip movement towards the northeast and southwest. Fault plane solutions demonstrate extensional (T) kinematic axes are sub-horizontal and northeast trending, and shortening (P) kinematic axes are sub-vertical. Combined, kinematic indicators and characteristics of the fault network (displacement transfer between faults and hard-linkages) demonstrate the western rift margin fault system evolved from a series of isolated fault segments during approximately northeast-southwest (rift-perpendicular) extension. The juxtaposition of proximal fan sediments of the Paleocene Jogmaya Mandir Formation, derived from the rift margin footwall, against the Malani Igneous Suite in the rift margin, indicate that faults were active in the study area during the Paleocene Epoch. Tectono-stratigraphical relationships exposed along the eastern edge of the southeast Barmer Hills, therefore, support that deformation during the main Paleogene Barmer Basin rift event accommodated approximately northeast-southwest (rift-perpendicular) regional extension.

4 The Sarnoo Hills

Structural and sedimentological analysis of a rift-oblique fault network and Lower Cretaceous sediments exposed along the central eastern rift margin of the Barmer Basin

In conjunction with the rift-parallel, basin-bounding fault systems, seismic data variably image an abundance of rift-oblique faults throughout the subsurface of the Barmer Basin (**Figure 4.1**). In this chapter, a rift-oblique fault network that is apparent nowhere else in the region, and a sedimentary succession that accumulated prior to the main Barmer Basin rift event, are characterised using exposure along the eastern rift margin of the Barmer Basin, in the Sarnoo Hills. High resolution mapping and subsequent structural analysis unveil a previously unrecognised extensional structural regime that accommodated northwest-southeast extension, and was influenced by weak fabrics inherent in the crust. The northwest-southeast extensional regime exposed in the Sarnoo Hills is highly oblique (near-perpendicular) to the extensional structural regime exposed along the western rift margin in the Barmer Hills (≈ northeast-southwest; **Chapter 3**). The exposed sedimentary succession is part of the Lower Cretaceous Ghaggar-Hakra Formation, and comprises a series of maturing upwards fluvial sandstone successions, separated by thick packages of floodplain mudstone and siltstone. The findings document an extensional structural regime that was previously unrecognised throughout the northwest Indian region and, in conjunction with the findings of investigations along the central western rift margin of the Barmer Basin (**Chapter 3**), establish a robust outcrop-based tectonic framework for the Barmer Basin, which will be built upon in subsequent chapters at the seismic- (basin-) and lithosphere-scales.

4.1 Geological setting

Situated along the central eastern rift margin of the Barmer Basin (**Figure 4.1**), the Sarnoo Hills are a prominent series of northeast-trending ridges in the vicinity of the village of Sarnoo (alternatively spelled ‘Sarnu’ or ‘Saranu’; **Figure 4.2**). Exposure predominantly occurs across an area of 2 km^2. Previous fieldwork in the north Sarnoo Hills (Clarke 2011) indicated that dominant faults are southwest-striking and define southeast-dipping rotated normal fault blocks compartmentalised by faulting oblique to the block-bounding faults (**Figure 4.3**).

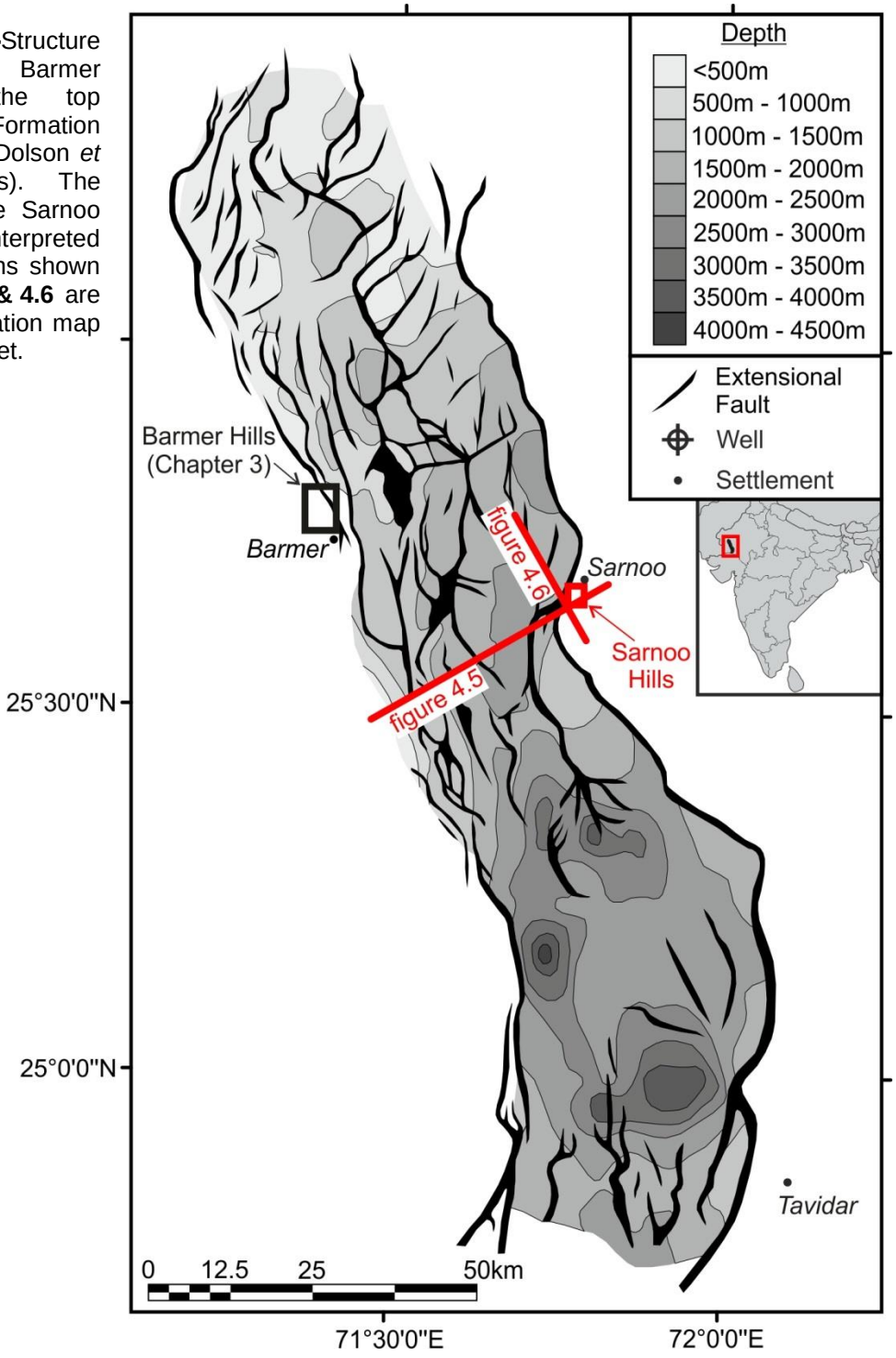

Figure 4.1 –Structure map of the Barmer Basin at the top Fatehgarh Formation horizon (after Dolson *et al.* in press). The location of the Sarnoo Hills and the interpreted seismic sections shown in **figures 4.5 & 4.6** are indicated. Location map within India inset.

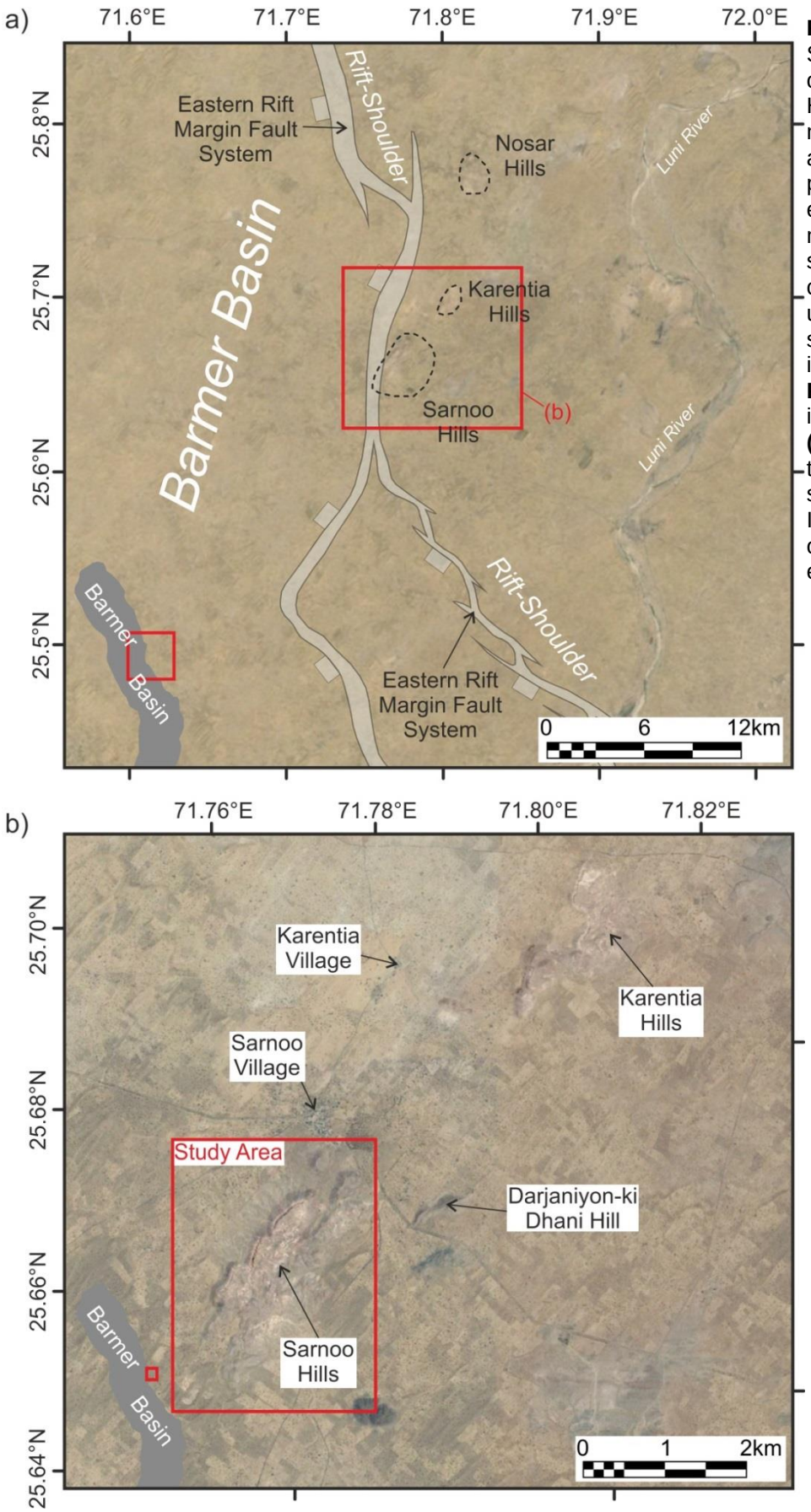

Figure 4.2 – Satellite images of the Sarnoo Hills with notable features and fault polygons of the eastern rift margin fault system (mapped commercially using subsurface data) indicated (see **Figure 4.1** for image location) **(a)** along with the Sarnoo Hills study area **(b)**. Images courtesy of Google™ earth

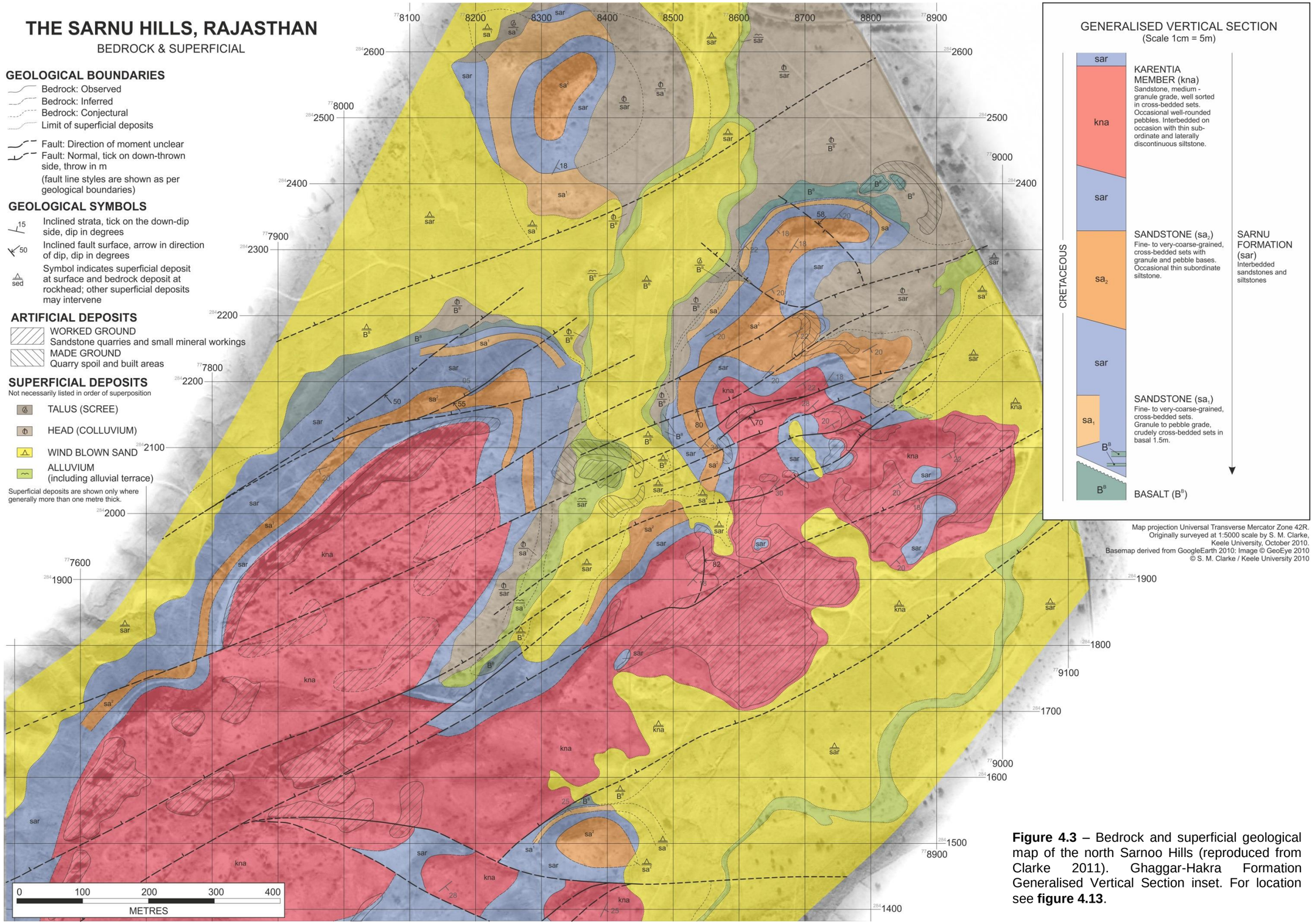

Figure 4.3 – Bedrock and superficial geological map of the north Sarnoo Hills (reproduced from Clarke 2011). Ghaggar-Hakra Formation Generalised Vertical Section inset. For location see **figure 4.13**.

Exposure in the Sarnoo area is dominated by rhyolite and rhyolitic tuff of the Precambrian Malani Igneous Suite (Roy & Jakhar 2002) that forms the rift basement of the Barmer Basin. Alkali olivine basalt, hawaiites, trachy-andesite, and trachyte of poorly-constrained age immediately overlie the Malani Igneous Suite (Roy & Jakhar 2002). An Aptian age has been suggested for these mildly alkaline igneous rocks (120 Ma), with a genesis associated with regional extension arising from Gondwana fragmentation (Sharma 2007). An intrusive origin has also been postulated (Sisodia & Singh 2000). In-turn, this suite of mafic igneous rocks is overlain by interbedded sands and silts of the Ghaggar-Hakra Formation (**Figure 2.23**; Baksi & Naskar 1981; Sisodia & Singh 2000; Roy & Jakhar 2002; Clarke 2011). Subsequent to deposition of the Ghaggar-Hakra Formation, a diverse suite of acid, intermediate, and alkaline plug-like bodies (Sarnu[sic]-Dandali Suite), associated with an early phase of Deccan igneous activity (68.57 ± 0.08 Ma; Basu *et al.* 1993), were emplaced and are exposed throughout the Sarnoo area (Basu *et al.* 1993; Simonetti *et al.* 1995, Simonetti *et al.* 1998; Roy & Jakhar 2002; Roy 2003; Sen *et al.* 2012).

Previously part of the Sarnu[sic] Formation (also termed the Sarnu Sandstone), the Ghaggar-Hakra Formation was assigned a poorly constrained Middle Jurassic to Lower Cretaceous age based on plant fossils recovered from the Sarnoo Hills (Baksi & Naskar 1981). Exposures of the Ghaggar-Hakra Formation in the Sarnoo Hills comprise three fluvial sandstone successions interbedded with thick successions of parallel-bedded and laminated very-fine-grained sandstones and siltstones (**Figure 4.3 inset**; Sisodia & Singh 2000; Clarke 2011). The sandstone unit at the base of the succession (sa_1; **Figure 4.3 inset**) is granule- to pebble-grade, erosive, comprises planar and trough cross-bedded sets up to 0.5 m in thickness, and was deposited within a high-energy, poorly confined braided fluvial system (Clarke 2011). Separated from the lowermost sandstone succession (sa_1) by a thick package of siltstone (< 20 m), the second sandstone succession (sa_2; **Figure 4.3 inset**) is 10 m to 20 m thick, fine- to medium-grained, and comprises 0.5 m to 1 m thick cyclic packages of planar and trough cross-bedded sets, parallel-bedded sandstone, and laminated and cross-ripple laminated sandstone, which occasionally culminate in siltstone. The facies associations of this second sandstone succession are typical of a fluvial meandering system (Clarke 2011). Separated from the second sandstone succession (sa_2) by a thick siltstone succession (< 15 m), the uppermost sandstone succession (kna; **Figure 4.3 inset**) has a strongly erosive base, comprises medium- to coarse-grained sand, is normally graded, and occurs in 1 m to

5 m thick planar and trough cross-bedded sets. Facies associations are typical of a well-developed, sinuous meandering fluvial system (Clarke 2011). Although the sandstone successions are characteristically fluvial, the preserved thickness of fine-deposits within the sedimentary succession is atypical for a continental fluvial depositional environment (Clarke 2011), and it is tentatively suggested that such deposits may represent deposition within an immature lacustrine setting. In the subsurface, the Ghaggar-Hakra Formation comprises fluvial and lacustrine sandstones, siltstones, and mudstones that often display abundant exposure surfaces and palaeosols (Dolson *et al.* in press).

4.2 Methodology

High resolution geological mapping was conducted throughout the Sarnoo Hills (≈ 2 km^2; **Figure 4.2**) under a lithostratigraphical mapping scheme, in association with interpretation of satellite imagery. Georeferenced satellite images of the study area, in conjunction with a 30 m Digital Elevation Model, were used to generate the basemaps used for field mapping. Elevation is in metres above sea level. The Digital Elevation Model covered an area of approximately 24 km^2 with minimum and maximum values of 108 m and 239 m above sea level respectively. Where available, extensional fracture plane, fault plane, and fault-plane slickenline lineation (kinematic) data were recorded. Logging of the sedimentary succession accompanied geological mapping, as well as architectural, textural, and petrographical (thin-section) descriptions of each mapping unit.

4.2.1 Sedimentological analysis

Microscopic textural descriptions of each mapping unit, constrained from thin sections, and architectural descriptions of macroscopic sedimentary features exposed at outcrop (e.g. channel geometries, ripple structures) were used in conjunction with graphical sedimentary logs to generate a broad depositional framework for each mapping unit, that is each mapping unit was attributed a broad depositional environment. Subsequently, megascopic (outcrop-scale) architectures and the associations between the broad depositional frameworks defined for each mapping unit were combined into a depositional model describing the exposed sedimentary succession.

4.2.2 Qualitative kinematic analysis of faulting

Quantitative kinematic analysis, such as methods of fault-slip inversion, assume that fault slip (strain) parallels the principal stress axes, that stress is homogeneous, and that faults do not

interact mechanically (c.f. **section 3.2.2**; Marrett & Allmendinger 1990). In the Sarnoo Hills, deformation incorporated multiple orientations of mutually slipping fault planes, invalidating the assumption of non-interacting faults applied during quantitative methods of fault-slip inversion (Marrett & Allmendinger 1990; Nieto-Samaniego & Alaniz-Alvarez 1997). As such, the calculation of the three principal strain axes (T, P, & N axes) using fault-slip data, as conducted for data recorded in the Barmer Hills (**Chapter 3**), is inappropriate for fault slip data recorded in the Sarnoo Hills. However, a more qualitative kinematic analysis of the exposed fault population is undertaken using fault-slip statistics.

In conjunction with fault plane measurements, the trend and sense (normal or reverse) of fault slip characterise the kinematics of a fault (Marrett & Allmendinger 1990; Doblas 1998). Although fault-slip data is inherently three-dimensional, and comprises a plunge and trend, qualitatively the azimuth (trend) of fault slip alludes to the direction of shear stress (**Section 3.2.2**; Wallace 1951; Bott 1959). Where fault slip is normal-sense, therefore, the azimuth of fault slip alludes to the direction of extension. While linear geological features (e.g. fold axes, fault traces) have a bimodal orientation, for example north-south or northwest-southeast, directional (vector) geological data, such as the trend of fault slip, are spherically distributed with a unimodal trend or azimuth (Davis 1986). The dominant (average) trend of a suite of directional or vector data can be calculated using:

$$\tan \overline{\theta} = \frac{\sum_{n=1}^{N} \sin \theta_n}{\sum_{n=1}^{N} \cos \theta_n} \qquad \textit{Equation 4.1}$$

$$\overline{\theta} = \tan^{-1} \left\{ \frac{\sum_{n=1}^{N} \sin \theta_n}{\sum_{n=1}^{N} \cos \theta_n} \right\} \qquad \textit{Equation 4.2}$$

where $\overline{\theta}$ = Azimuth of the vector mean; θ_n = azimuth of fault-slip measurement 'n'; and N = total number of fault slip measurements (Davis 1986). Azimuth is measured clockwise from north. All natural data, directional or data with magnitude only (scalar data; e.g. fault dip), will display variation and dispersion (spread) around the mean of the data sample, possibly substantial. The variation within a dataset should be quantified to assess the scatter, or randomness, of the data, especially when the data is being used to investigate common or dominant trends. Distribution within a scalar data sample is quantified using the 'variance' and 'standard deviation' parameters. The variance is defined as "the average squared deviation of all possible observations from the

population mean" (Davis 1986). The standard deviation is the square root of the variance and provides a statistic describing the dispersion around the mean of the data sample:

$$\boldsymbol{\sigma^2 = \frac{\sum_{i=1}^{n}(X_i - \bar{X})^2}{n}} \qquad \textit{Equation 4.3}$$

$$\boldsymbol{\sigma = \sqrt{\frac{\sum_{i=1}^{n}(X_i - \bar{X})^2}{n}}} \qquad \textit{Equation 4.4}$$

where σ^2 = variance; σ = standard deviation; X_i = scalar data measurement 'i' within a data sample of 'n' measurements (X_1, X_2;…….X_n); n = total number of measurements within the data sample, and; $\bar{X}$ = mean value of data sample (Davis 1986). Similarly, for a suite of directional (vector) data, the magnitude (length) of the resultant average vector (vector mean) will depend upon the amount of dispersion in the data, and is analogous to the standard deviation of a sample of scalar values:

$$\boldsymbol{r = \sqrt{(\sum_{n=1}^{N} \sin \theta_n)^2 + (\sum_{n=1}^{N} \cos \theta_n)^2}} \qquad \textit{Equation 4.5}$$

where r = magnitude of the vector mean (Davis 1986). The magnitude of the vector mean can be converted to a percentage to define a parameter known as the dispersion:

$$\boldsymbol{dispersion}\ (\%) = \mathbf{100} \times \left(\frac{r}{N}\right) \qquad \textit{Equation 4.6}$$

where r = magnitude of the vector mean, and; N = total number of readings. A dispersion of 0% indicates the data is completely random, and a dispersion of 100% indicates all data trend in the same direction, that is a unimodal data population.

To assess the dominant direction of shear stress (≈ direction of extension) accommodated on faults exposed in the Sarnoo Hills, the azimuth of the vector mean (**Equation 4.2**) was calculated using all measurements of fault-slip recorded (n = 231), and the randomness of the data assessed by calculating the dispersion (**Equations 4.5 & 4.6**). Further to this, insights into the kinematics of faults of specific orientations within the Sarnoo Hills fault network were gained by categorising fault slip data by fault strike (**Table 4.1**), and calculating the dominant direction of shear stress (≈ direction of extension; **Equation 4.2**) and randomness (**Equations 4.5 & 4.6**) of these sample datasets. Finally, the qualitative kinematic analysis of faulting in the Sarnoo Hills was concluded by investigating the obliquity of each fault slip measurement, which was achieved by graphically plotting the pitch (measured from strike) of each measurement of fault slip against the strike of the corresponding fault plane.

Orientation	Fault Strike (°)
North	337.5°-22.5°
Northeast	22.5°-67.5°
East	67.5°-112.5°
Southeast	112.5°-157.5°
South	157.5°-202.5°
Southwest	202.5°-247.5°
West	247.5°-292.5°
Northwest	292.5°-337.5°

Table 4.1 – Categorisation of fault strike measurements into strike orientations.

4.2.3 Construction of a structural outcrop model from balanced two-dimensional cross-sections

When working with limited or two-dimensional data (e.g. maps or cross-sections), problems may arise from poor data quality (e.g. poor outcrop exposure or limited correlation of data between subsurface seismic sections) or poor data interpretation (Groshong 2006). In the Sarnoo Hills, the limited (≈ 2 km^2) and sporadic exposure (**Figure 4.2**) often prevented direct interpretation of the geology throughout the study area. In order to combine discontinuous two-dimensional map-view interpretations throughout the study area into a coherent, internally consistent, three-dimensional interpretation, map-view interpretations were used to construct twenty two-dimensional cross-sections, prior to using interpretations on serial two-dimensional cross-sections to construct a three-dimensional structural model of the exposure. To reduce the errors associated with limited and two-dimensional data it is important to demonstrate that interpretations are internally consistent and geometrically valid through balancing and structural restorations (Groshong 2006). Two-dimensional cross-sections, therefore, were structurally balanced.

4.2.3.1 Quality control

During primary interpretation of datasets (outcrop and subsurface), unrealistic stratigraphical and fault geometries introduce inconsistencies into a geological model. When interpreting datasets it is commonly assumed that bed thickness is constant, varies smoothly, or represents a realistic growth history, and that undeformed faults are approximately planar and smooth at the large scale (Groshong 2006). Completed interpretations should be inspected for data errors (e.g. localised highs and lows, and seismic mis-ties), edge effects (e.g. closure of contours where open contours are favoured), and contouring artefacts (e.g. extension of structure maps beyond limit of input data, excessive detail, and trend artefacts; Groshong 2006).

4.2.3.2 Structural balancing and restoration

When a satisfactory interpretation is complete it should be demonstrated to be internally consistent and geometrically plausible through structural balancing and restoration. Although a restorable structure validates that the interpretation is internally consistent, restorations are non-unique (Schultz-Ela 1992; Groshong 2006) and the interpretation belongs to a set of possible correct interpretations. However, critical insights into an interpretation are gained through balancing attempts (Gibbs 1983). Sections to be restored should have equal vertical and horizontal scales (i.e. no vertical exaggeration) and the vertical axis should be in depth (Gibbs 1983; Hart 2012). A valid restoration will conserve surface area or volume between the deformed and undeformed states in three-dimensions (Gibbs 1983; Groshong 2006). However, the restoration of three-dimensional structures is often simplified into two-dimensions under the assumption of plane strain, namely the assumption that the displacement vector occurs within the plane of the restored section (Gibbs 1983, Groshong 2006). Where restorations are simplified into two-dimensions, the conservation of surface area or volume in three-dimensions is represented by conservation of line-length or cross-sectional area respectively in two-dimensions. Restorations conducted under the assumption of plane strain are termed palinspastic.

Where the assumption of plane strain is invalid, three-dimensional restorations, for example 'jigsaw' fit restorations (Williams *et al.* 1997; Buddin *et al.* 1997), are more applicable. Alternatively, non-palinspastic restorations, that is a two-dimensional restoration on a cross-section that does not contain the displacement vector, termed geometrical restorations, validate that an interpretation is internally consistent; however, the units in the section are not returned to the exact undeformed state (Groshong 2006). In extensional settings where deposition accompanies deformation, many of the assumptions made during two-dimensional restorations are invalid (e.g. conservation of bed-length or area, uniform bed thickness, and correlateable hanging-wall and footwall strata; Schultz-Ela 1992). However, syn-deformation deposition introduces incremental strain-markers that can be used to sequentially restore a section and constrain deformational processes (Schultz-Ela 1992).

4.2.3.3 Cross-section construction

Using the lithological contacts and faults mapped at outcrop, structural data, and general field observations, twenty 1.8 km long two-dimensional cross sections, bearing 125° with a spacing of approximately 140 m, were constructed. Surface data, including dip measurements and lithological

contacts with X and Y coordinates, were projected vertically onto the Digital Elevation Model and given an elevation attribute (Z coordinate). Further to this, surface data situated within a 70 m zone either side of each cross-section were projected laterally into the plane of each cross-section to constrain each interpretation with as much surface data as possible. Lithological contacts were interpreted across each cross-section and faults were assumed to dip at a constant 61° in accordance with structural data recorded in the Sarnoo Hills. The thicknesses of stratigraphical units were assumed constant, with the exception of the Ghaggar-Hakra Formation undivided mapping unit (gha), the thickness of which was thickened to the west between the Sarnoo and Nosar sandstone mapping units in accordance with field-observations. Observations made at outcrop were used to make sensible interpretations in areas of no exposure.

4.2.3.4 Cross-section validation

Interpretations made on two-dimensional cross-sections were validated and assessed for internal consistency by performing a simple rigid-block restoration of each cross-section (**Appendix B**). If deformation is facilitated by the displacement of rigid-blocks, with negligible deformation occurring within faulted blocks, then a cross-section can be restored by rigid body translation and rotation of rigid-blocks, preserving all lengths and angles within fault blocks between the deformed and undeformed states (**Figure 4.4**; Groshong 2006). Rigid body restorations are conducted by separating a cross-section into rigid fault blocks, removing the offset across a fault, and reassembling the cross-section so that the reference horizon is the required shape (**Figure 4.4**; Groshong 2006). The base Nosar Sandstone surface was used as the reference surface and restorations were conducted to return the base Nosar Sandstone surface approximately to the horizontal. Upon performing rigid body restorations an interpretation was deemed satisfactory if bed-thickness (≈ cross-sectional area) remained constant, or if the interpretation represented a realistic growth history (Groshong 2006).

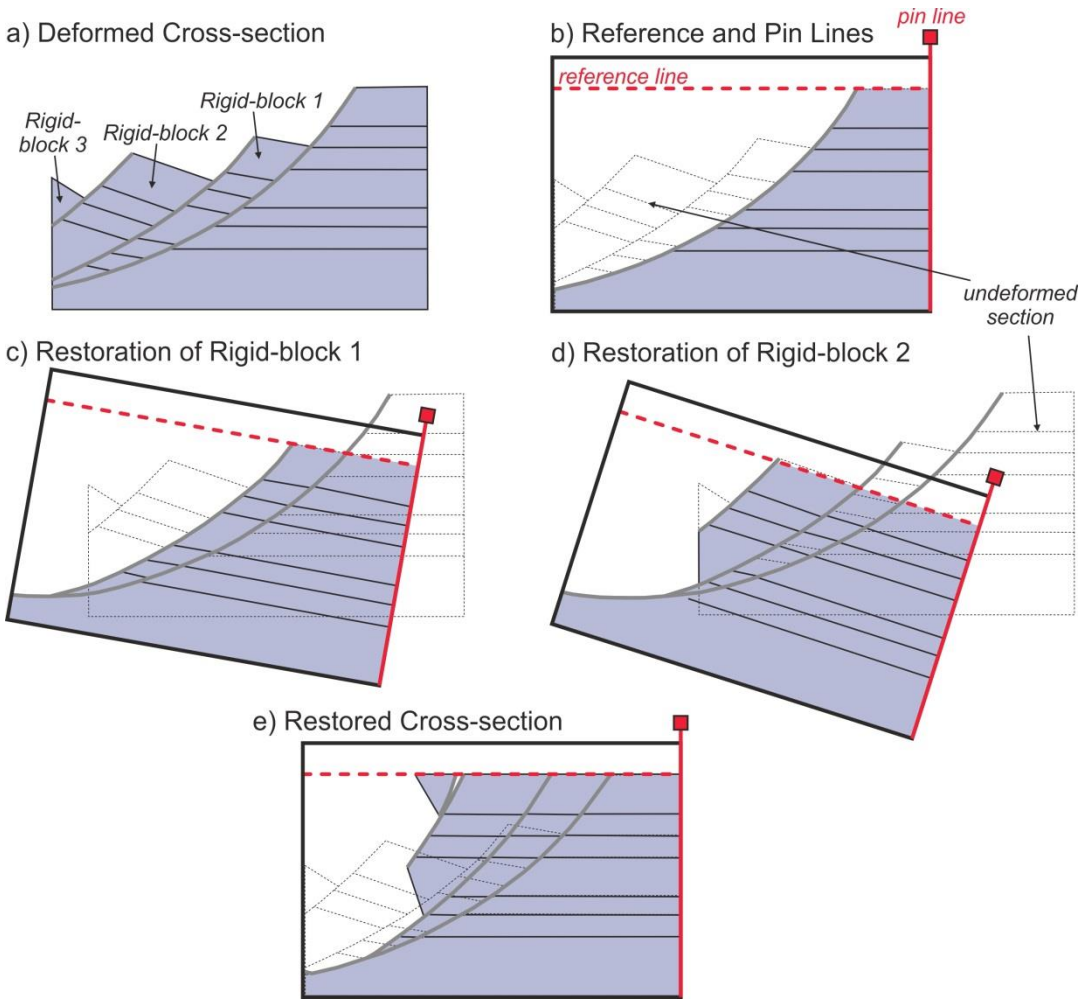

Figure 4.4 – Rigid-block restoration of a cross-section deformed on a series of listric faults (after Groshong 2006). A deformed cross-section comprising multiple rigid fault blocks **(a)** is restored using a reference line and pin line **(b)** by sequentially removing the offset across each fault **(c)** & **(d)**, and reassembling the cross-section so that the reference horizon is the required shape **(e)**.

4.2.3.5 Structural outcrop model

Fault and horizon interpretations on serial two-dimensional balanced cross-sections established a three-dimensional framework (**Appendix B**), which was used to construct a three-dimensional structural model of the outcrop. The model covered an area of 4.8 km^2. A fault model was constructed by connecting equivalent fault interpretations on adjacent cross-sections in accordance with the corresponding fault trace mapped at surface. Subsequently, lithological contacts interpreted on serial two-dimensional cross-sections were gridded using a convergent gridding algorithm that converges upon the solution by adding resolution with each iteration in areas of sparse data, while honouring the input data where present. During gridding, data was deleted within a symmetrical 20 m zone either side of the fault (step-back-distance) and projected back

onto the fault plane to remove uncertainties in the zones immediately adjacent to faults. During construction and upon completion, the model was quality controlled and visually inspected to ensure its compatibility with the outcrop.

Upon construction, the structural model was used to generate artificial (model-generated) fault displacement-length profiles for key faults within the Sarnoo Hills fault network. Displacement measurements were recorded at 10 m to 20 m intervals along each fault trace and were plotted against distance along the fault trace.

4.3 The Sarnoo Hills

Subsurface data reveal that the Sarnoo Hills are situated in the immediate footwall of the eastern rift-margin fault system that is locally southwest-striking (rift-oblique) and northwest-dipping (**Figure 4.2a**), and has accommodated up to 3 km of subsidence (**Figures 4.5 & 4.6**).

4.3.1 Stratigraphy

The mafic crystalline rocks at the base of the succession comprise predominantly microcrystalline plagioclase laths and sphene, with some interstitial glass (**Figure 4.7a**). In some samples, irregular chlorite-filled enclaves are observed (**Figure 4.7a**). Occasionally, a heavily altered, poorly consolidated, light green crystalline unit appears interbedded within the lowermost Ghaggar-Hakra Formation (**Figure 4.8a**). However, a superficially similar unit often displays cross-cutting relationships within the sedimentary succession (**Figure 4.8b**). Overlying the crystalline rocks, the Ghaggar-Hakra Formation comprises three arenaceous successions separated by thick mudstone and siltstone packages (≤ 30 m) that contain thin arenite interbeds (≤ 0.5 m; **Figure 4.7b**). The mudstone and siltstone packages are generally red and horizontally laminated, but contain both symmetrically and asymmetrically ripple cross-laminated units, mottled and rooted horizons, and rare soft-sediment deformation.

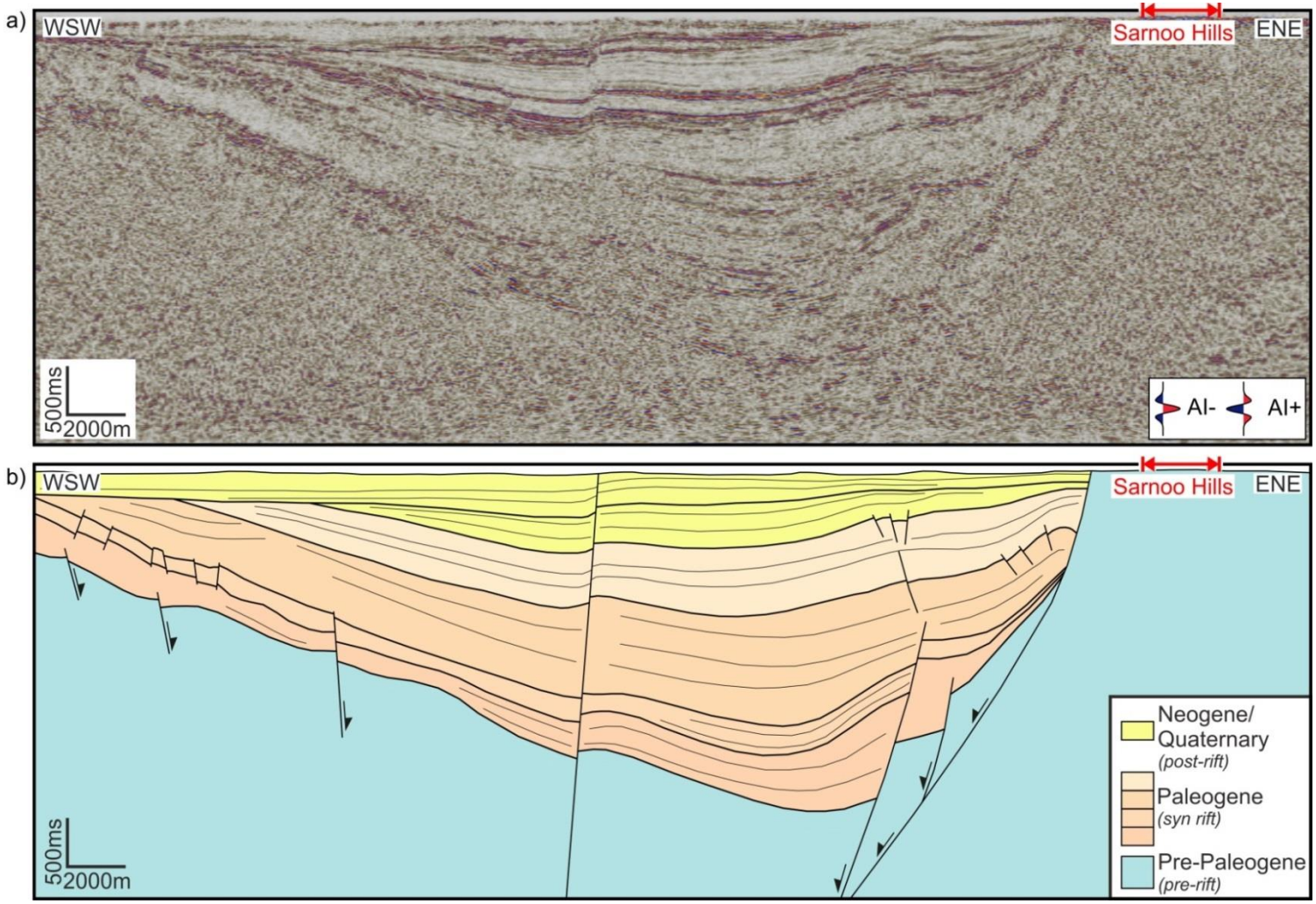

Figure 4.5 – Un-interpreted **(a)** and interpreted **(b)** cross-line (061°) seismic section depicting the relationship of exposure in the Sarnoo Hills (highlighted in red) to the Barmer Basin subsurface. For section location see **figure 4.1**.

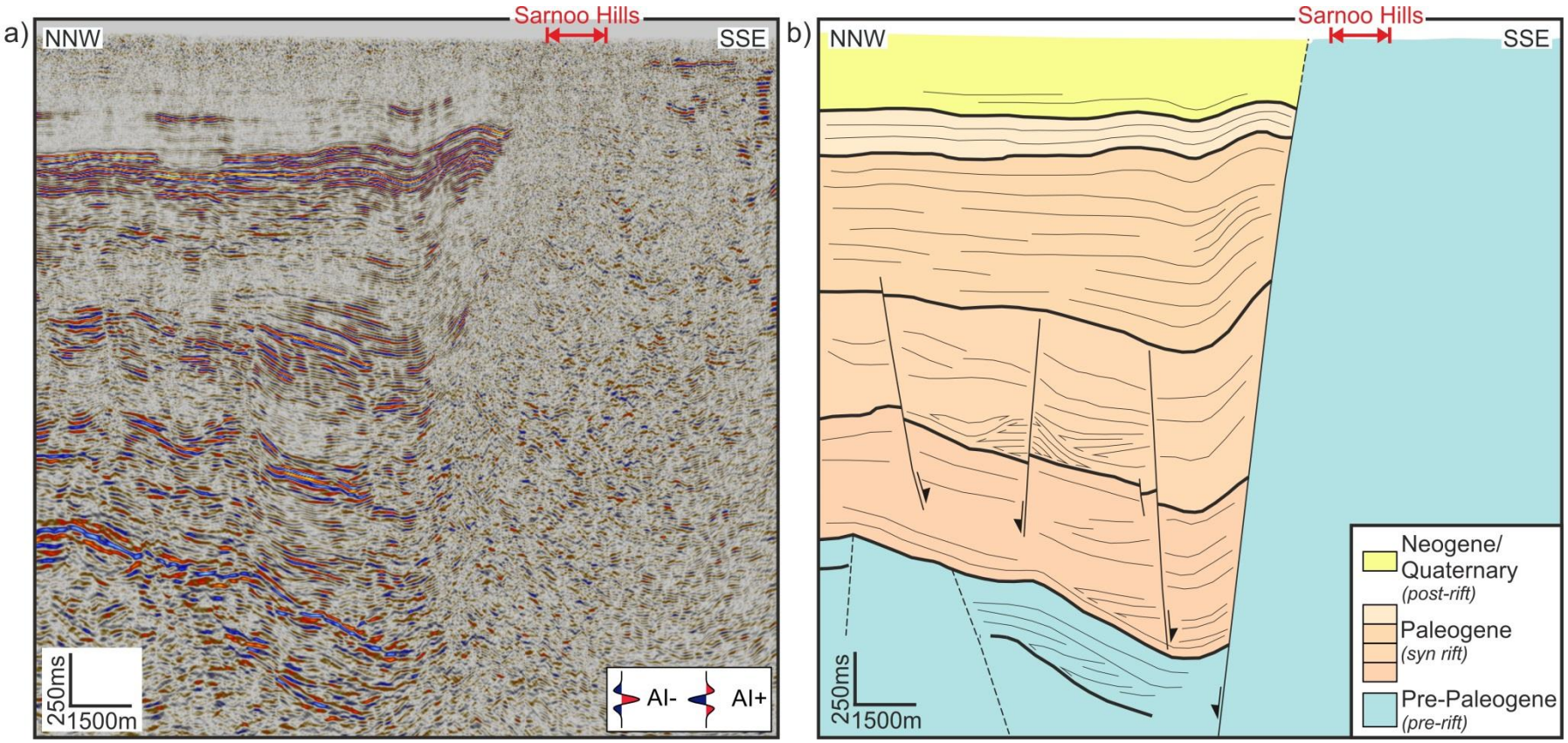

Figure 4.6 – Un-interpreted **(a)** and interpreted **(b)** in-line (151°) seismic section depicting the relationship of exposure in the Sarnoo Hills (highlighted in red) to the Barmer Basin subsurface. For section location see **figure 4.1**.

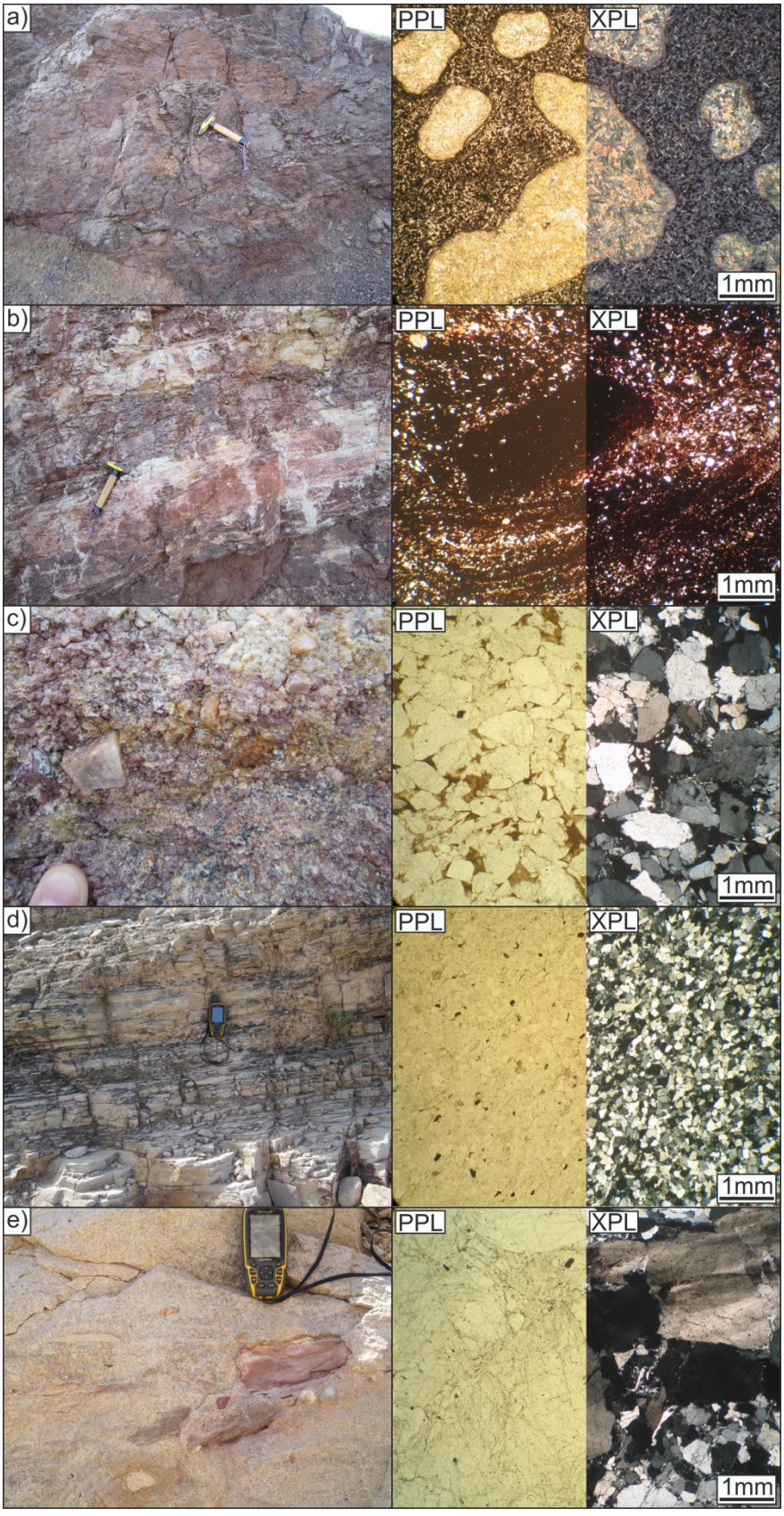

Figure 4.7 - Outcrop (left) and thin section (right; PPL = Plane Polarised Light; XPL = Cross-Polarised Light) images of each mapping unit exposed in the Sarnoo Hills: **(a)** basalt at the base of the succession; **(b)** mudstone and siltstone packages of the Ghaggar-Hakra Formation (gha); **(c)** the Darjaniyon-ki Dhani Sandstone (dar); **(d)** the Sarnoo Sandstone (sar); **(e)** the Nosar Sandstone (nos).

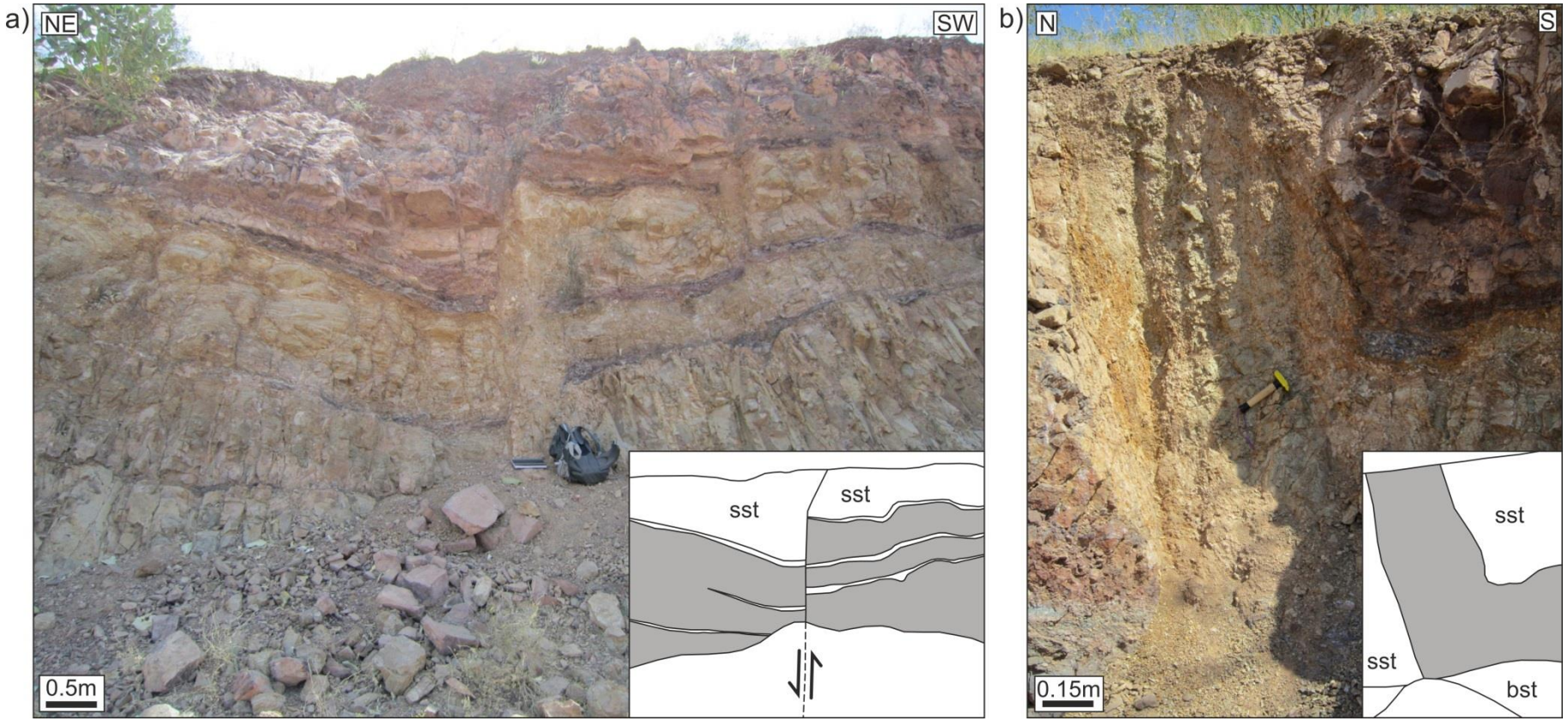

Figure 4.8 - A heavily altered, poorly consolidated, light green crystalline unit is exposed towards the base of the sedimentary succession, and appears both interbedded **(a)** [GR 0779583 2841933 UTM zone 42N] and to intrude into **(b)** [GR 0779992 2842124 UTM zone 42N] the lowermost Ghaggar-Hakra Formation. Photos were taken from Darjaniyon-ki Dhani, approximately 500 m east of the north Sarnoo Hills. Sketch interpretations of each photograph are inset; grey = heavily altered, poorly consolidated, light green crystalline unit; sst = sandstone; bst = basalt.

The lowermost lithic arenite succession, the Darjaniyon-ki Dhani Sandstone (dar; sa_1 of Clarke 2011; **Figures 4.9a, 4.9b & 4.10**), comprises a poorly-sorted, clast-supported, coarse- to granule-grade litharenite containing polymictic, angular clasts (**Figure 4.7c**). Crude planar and trough cross-bedded sets are 0.5 m to 1 m thick, and show strongly erosive bases, crude channel geometries, and are generally normally graded. The middle arenite succession, the Sarnoo Sandstone (sar; sa_2 of Clarke 2011; **Figures 4.9c & 4.10**), is a well-sorted, clast-supported and fine- to medium-grained quartz arenite, with well-rounded, monomictic quartz clasts (**Figure 4.7d**). Coarse- to very-coarse, occasionally granule-grade clasts occur in lags at the base of channel geometries, alongside abundant siltstone rip-up clasts. Beds are 0.5 m to 2 m thick and generally planar cross-bedded or horizontally bedded. However, trough cross-bedding and erosive bases are occasionally evident. Thick beds (≤ 2 m) of fine- to very fine-grained extensively rippled and ripple cross-laminated units are also observed. The uppermost quartz arenite succession, the Nosar Sandstone (nos; kna of Clarke 2011; **Figures 4.9d & 4.10**) that caps the prominent hills, is poorly-sorted, clast-supported and coarse- to very coarse-grained and contains abundant granules and pebbles, with sub-angular to sub-rounded, predominantly quartzitic clasts (**Figure 4.7e**). Cross-bedded sets are 0.5 m to 3 m thick, highly erosive with abundant siltstone rip-up clasts, and are both planar and trough cross-bedded. Foresets are commonly normally graded from pebble- to coarse-grained, and authigenic illite and kaolinite cement gives the sandstone a striking white colour. Although no upper contact is preserved, the Nosar Sandstone is at least 30 m thick in some exposures. Nowhere in the Sarnoo Hills do syn-sedimentary growth successions occur, or do the sedimentary units show thickness variations across faults.

4.3.2 Structure

Three structural trends are evident on satellite imagery; 1) northeast-southwest; 2) east-west, and; 3) east-northeast-west-southwest, as well as three prominent outcrop-dissecting topographical depressions (**Figure 4.11**). Field observations confirm that southwest-striking (≈ 210°-220°), northwest-dipping, ridge-parallel faults are dominant, defining ridge-parallel valleys in the north and south of the exposure. Southwest-striking faults accommodate large displacements (≤ 80 m) on discrete slip-surfaces that form narrow (< 5 m) damage zones (**Figure 4.12a**). West-striking (≈ 270°-280°), north-dipping faults accommodate less displacement (≤ 25 m; **Figures 4.12b & c**),

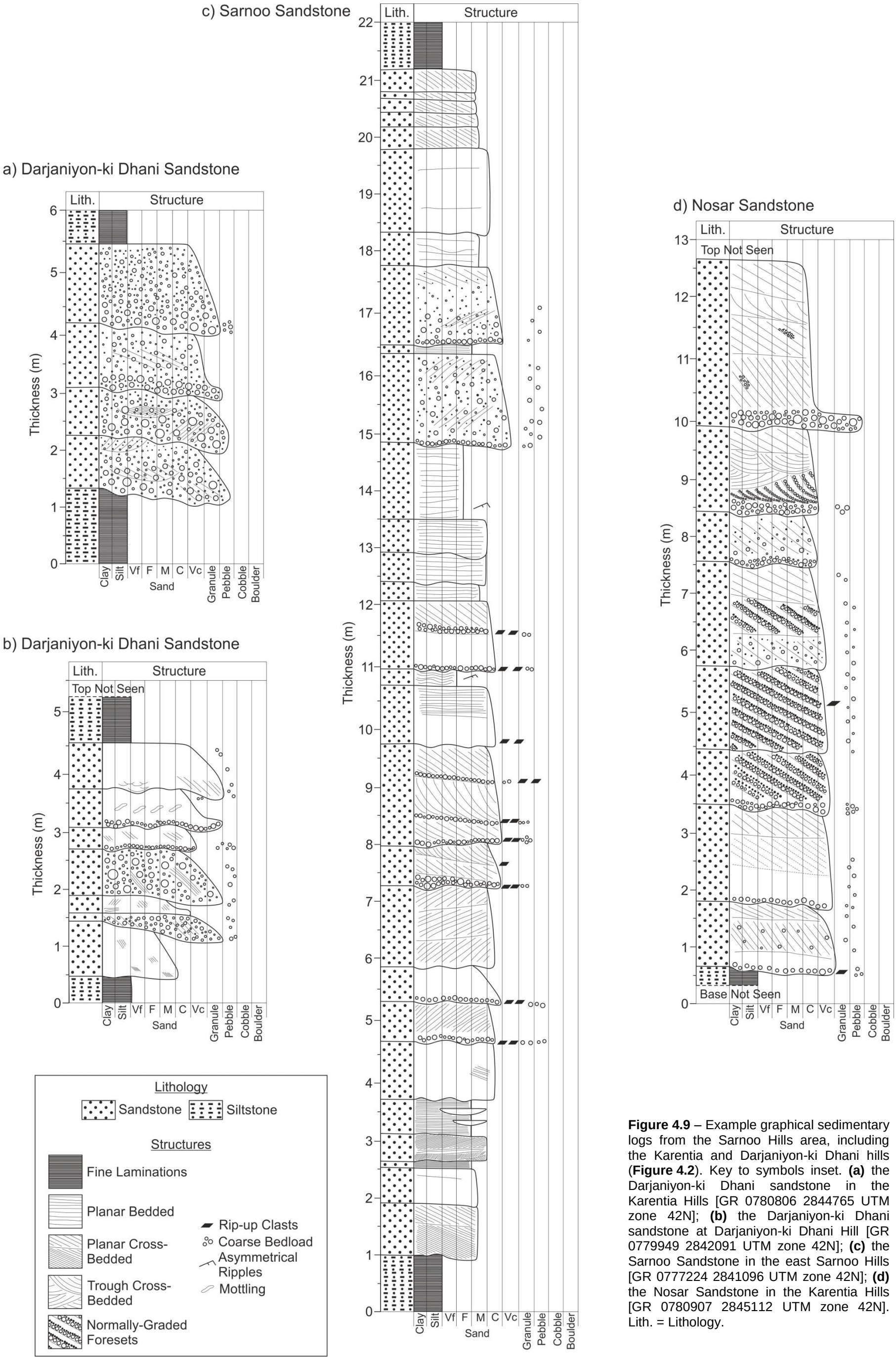

Figure 4.9 – Example graphical sedimentary logs from the Sarnoo Hills area, including the Karentia and Darjaniyon-ki Dhani hills (**Figure 4.2**). Key to symbols inset. **(a)** the Darjaniyon-ki Dhani sandstone in the Karentia Hills [GR 0780806 2844765 UTM zone 42N]; **(b)** the Darjaniyon-ki Dhani sandstone at Darjaniyon-ki Dhani Hill [GR 0779949 2842091 UTM zone 42N]; **(c)** the Sarnoo Sandstone in the east Sarnoo Hills [GR 0777224 2841096 UTM zone 42N]; **(d)** the Nosar Sandstone in the Karentia Hills [GR 0780907 2845112 UTM zone 42N]. Lith. = Lithology.

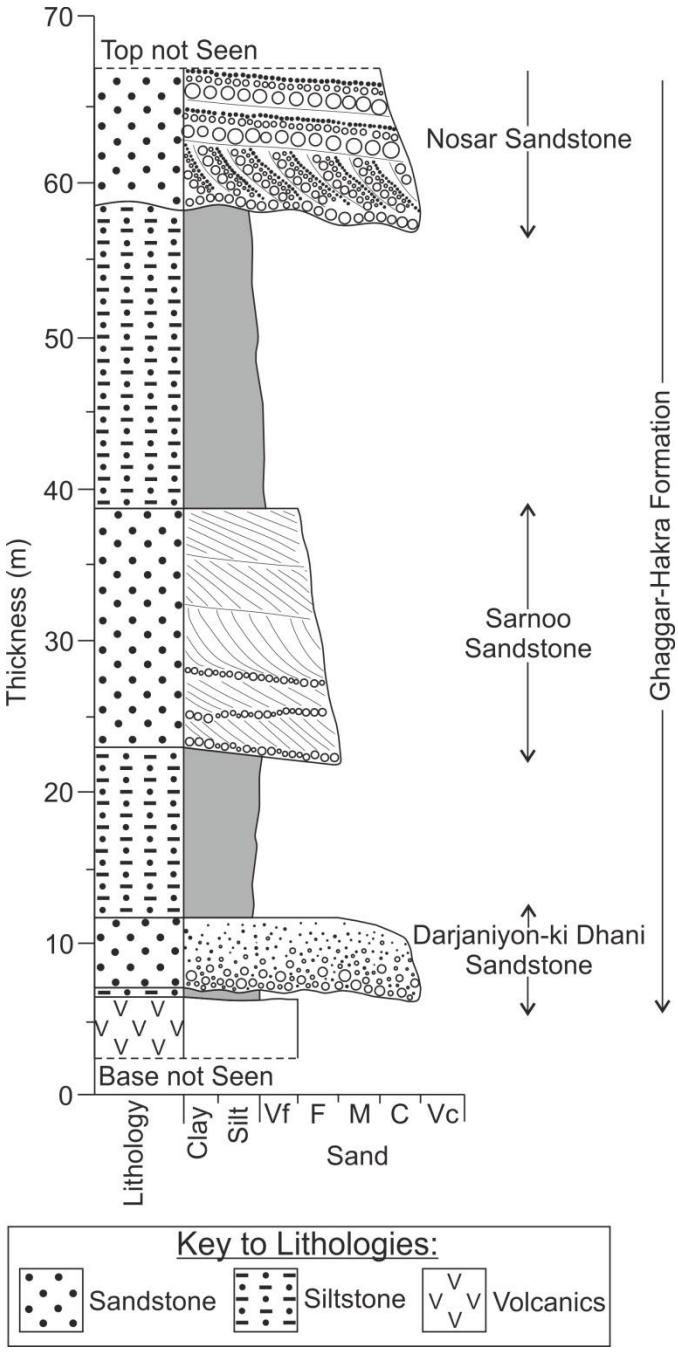

Figure 4.10 – Composite sedimentary log through the Lower Cretaceous Ghaggar-Hakra Formation, comprising three sandstone successions, the Nosar Sandstone, Sarnoo Sandstone, and Darjaniyon-ki Dhani Sandstone, interbedded with thick packages of mudstone and siltstone. Vf = Very fine; F = Fine; M = Medium; C = Coarse; Vc = Very coarse.

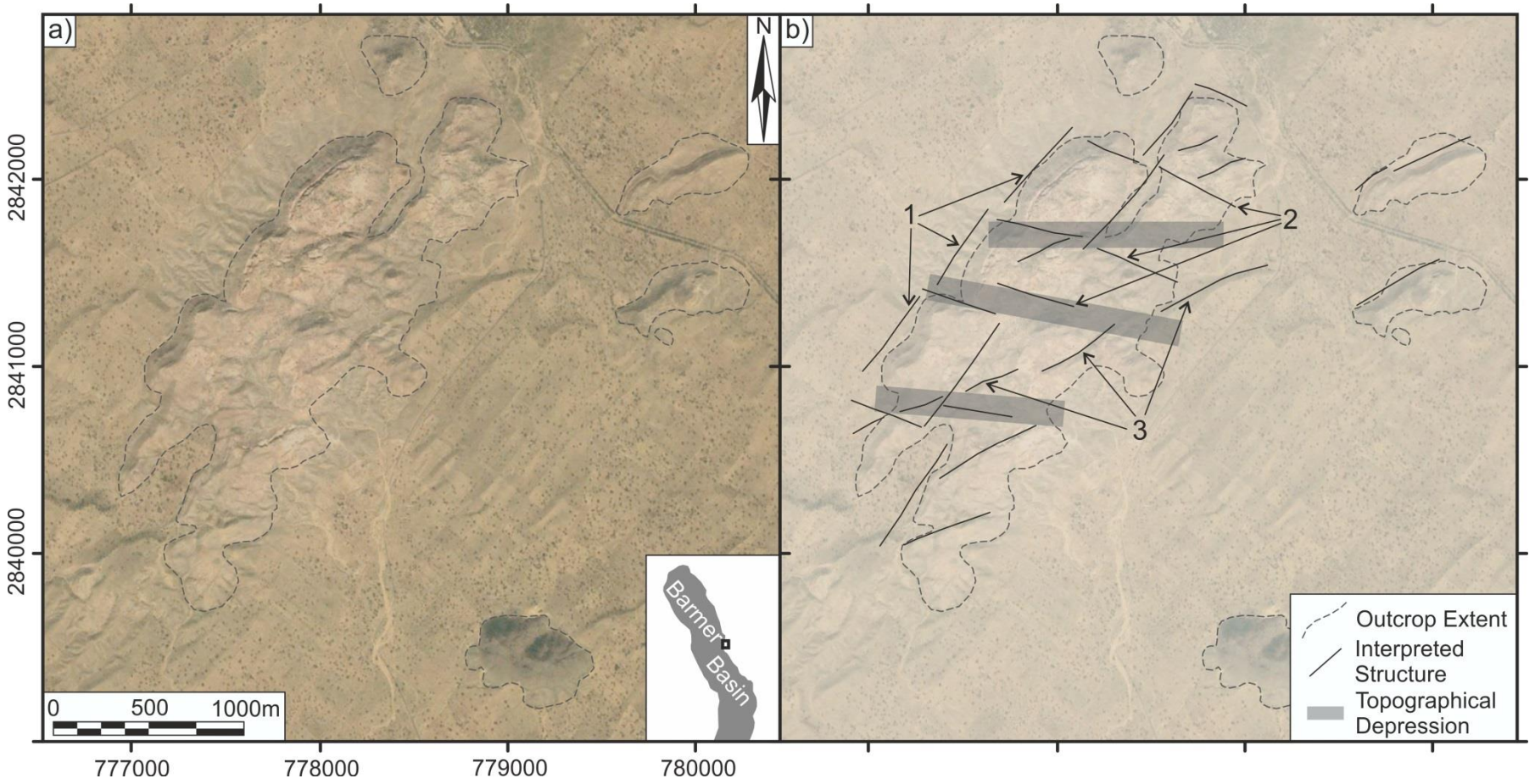

Figure 4.11 - **(a)** Satellite image of exposure at the Sarnoo Hills (location map inset). Image courtesy of Google™ earth. The limit of the exposure is dashed; **(b)** Interpretation of **(a)** indicating three main structural trends (1, 2, & 3). Three prominent outcrop-dissecting topographical depressions are also indicated (key inset).

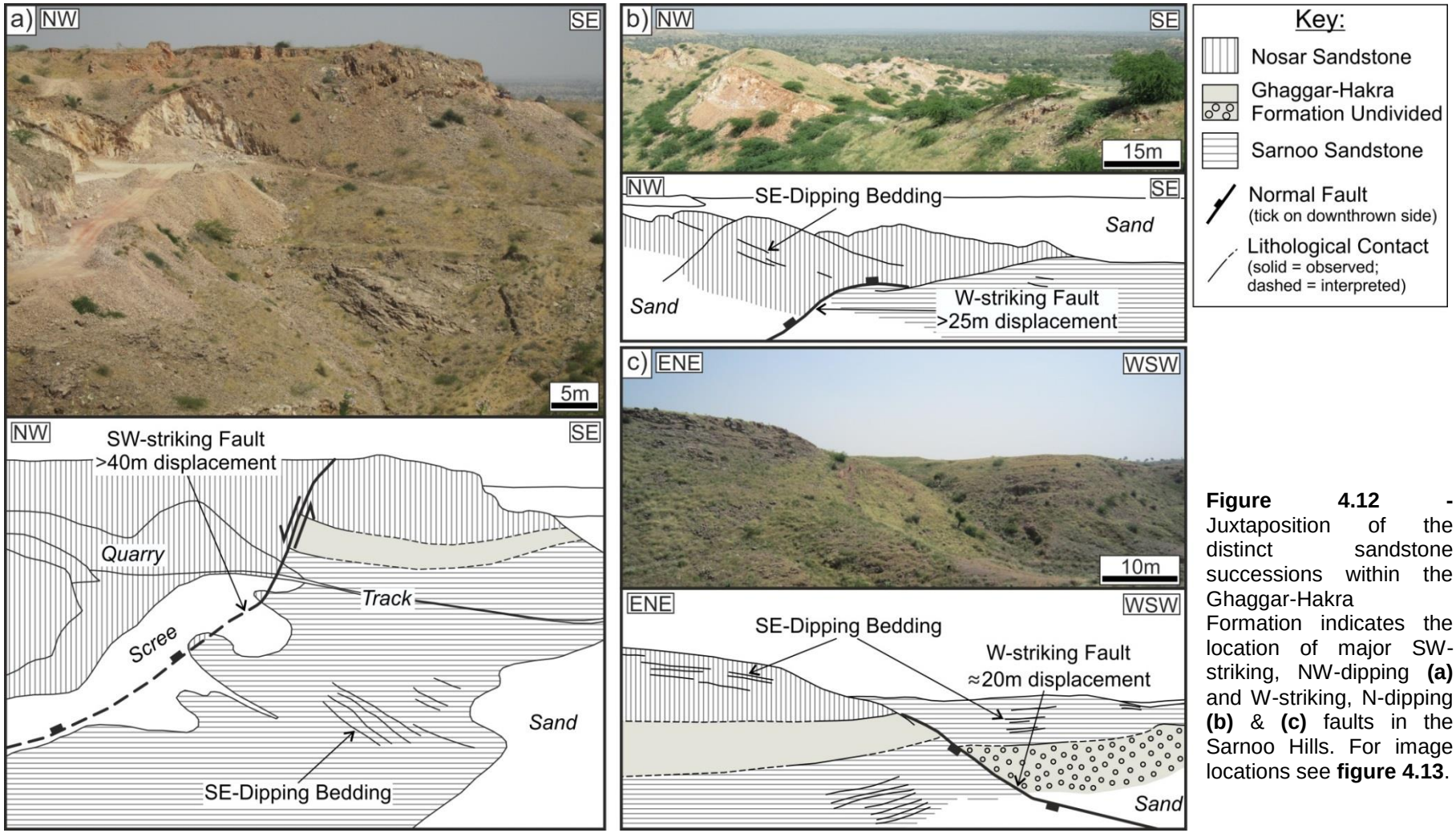

Figure 4.12 - Juxtaposition of the distinct sandstone successions within the Ghaggar-Hakra Formation indicates the location of major SW-striking, NW-dipping **(a)** and W-striking, N-dipping **(b)** & **(c)** faults in the Sarnoo Hills. For image locations see **figure 4.13**.

and correspond to the outcrop-dissecting topographical depressions evident on satellite imagery (**Figure 4.11**). Although discrete west-striking faults do not occur everywhere along the outcrop-dissecting depressions, these topographical features are characterised by a broad zone of concentrated, low-strain deformation features (e.g. fractures, small-offset faults) that accommodate negligible aggregate displacement. Combined, west- and southwest-striking faults form a zig-zag fault network (**Figure 4.13**). Fault blocks are largely rigid with negligible internal deformation, brittle or ductile (**Figures 4.14**; **Appendix B**), and satisfactory restorations can be achieved using a rigid-block restoration (**Figure 4.15**; **Appendix B**). Where observed, deformation within faulted blocks is accommodated on west-southwest-striking (≈ 240°-250°) faults.

On average, the dip of the strata is 15° to the southeast (126° dip-azimuth), with north-northwest-trending fractures, and east-trending faults most prevalent (**Figure 4.16**). Although variable, the average dip of the faults is 61° (n = 337; standard deviation = 15°; **Equation 4.4**). Rift-parallel fractures were commonly observed oblique to large fault cores (**Figure 4.17c**). Within the competent sandstone successions, fault zones typically comprise thick packages of fault-gouge (≤ 1 m), with brittle damage zones being variably present (**Figures 4.17a-c**). Occasionally, gouge thickness is disproportionately large for observed fault displacement (e.g. 1 m wide for 0.9 m offset). In contrast, within the thick mudstone and siltstone packages faults are obscure, and deformation occurs on discrete slip-planes.

Excellent exposure of in-plane fault kinematic (slickenline) data (**Figures 4.17d-f**) shows predominantly normal-sense, dip-slip movement to the northwest, with a mean resultant slip direction of 308° (**Figure 4.18a**; **Equation 4.2**). Fault-plane slickenlines occur almost exclusively in one consistent orientation (single-generation; **Figures 4.17d-f**) rather than as several, cross-cutting slickenline sets (multiple-generation). Insights into the kinematics of the fault network were attained by categorising slip data by fault-strike (**Table 4.1**; **Figures 4.18b & c**). Both southwest- and west-striking faults accommodated unimodal slip to the northwest (313° and 326° respectively); however, a 013° disparity exits between average slickenline trends (**Figure 4.18**). Fault-slip on southwest-striking faults is predominantly dip-slip (i.e. slickenline pitch ≈ 90°), with average pitch measurements of 87° (3° component of sinistral oblique slip), whereas fault-slip on west-striking faults displays a significant component (15°) of sinistral-oblique slip (average pitch = 75°;

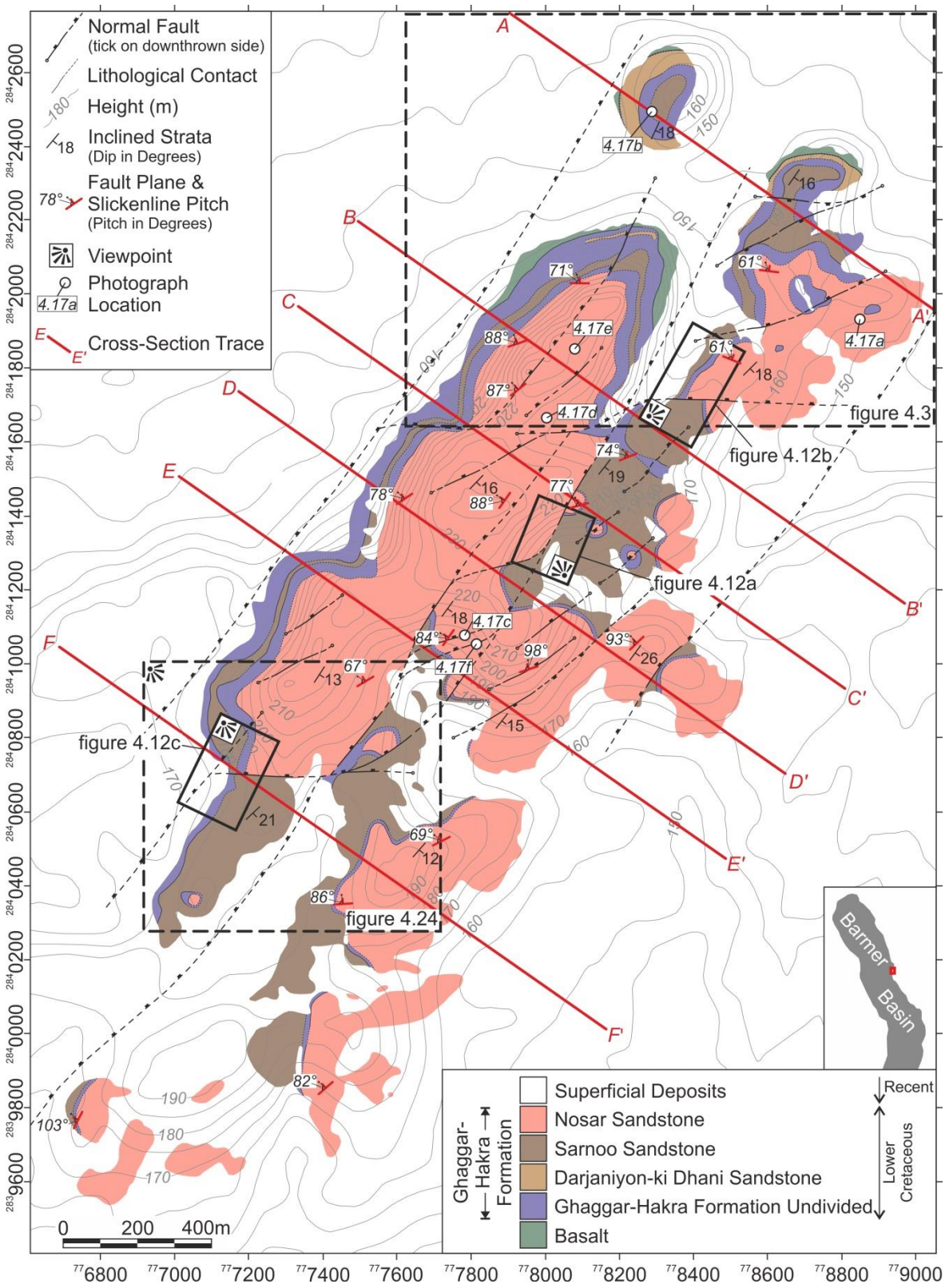

Figure 4.13 - The Sarnoo Hills, east Barmer rift (location map, stratigraphy and key to symbols inset). Topographical contours are at 5 metre intervals. Reference grid is UTM zone 42N. The locations and viewpoints of **figures 4.3, 4.12 & 4.24** are indicated, alongside the locations of photographs shown in **figure 4.17** and the orientations of cross-sections shown in **figures 4.14 & 4.15**. Fault slip data for selected (often minor) faults are also shown.

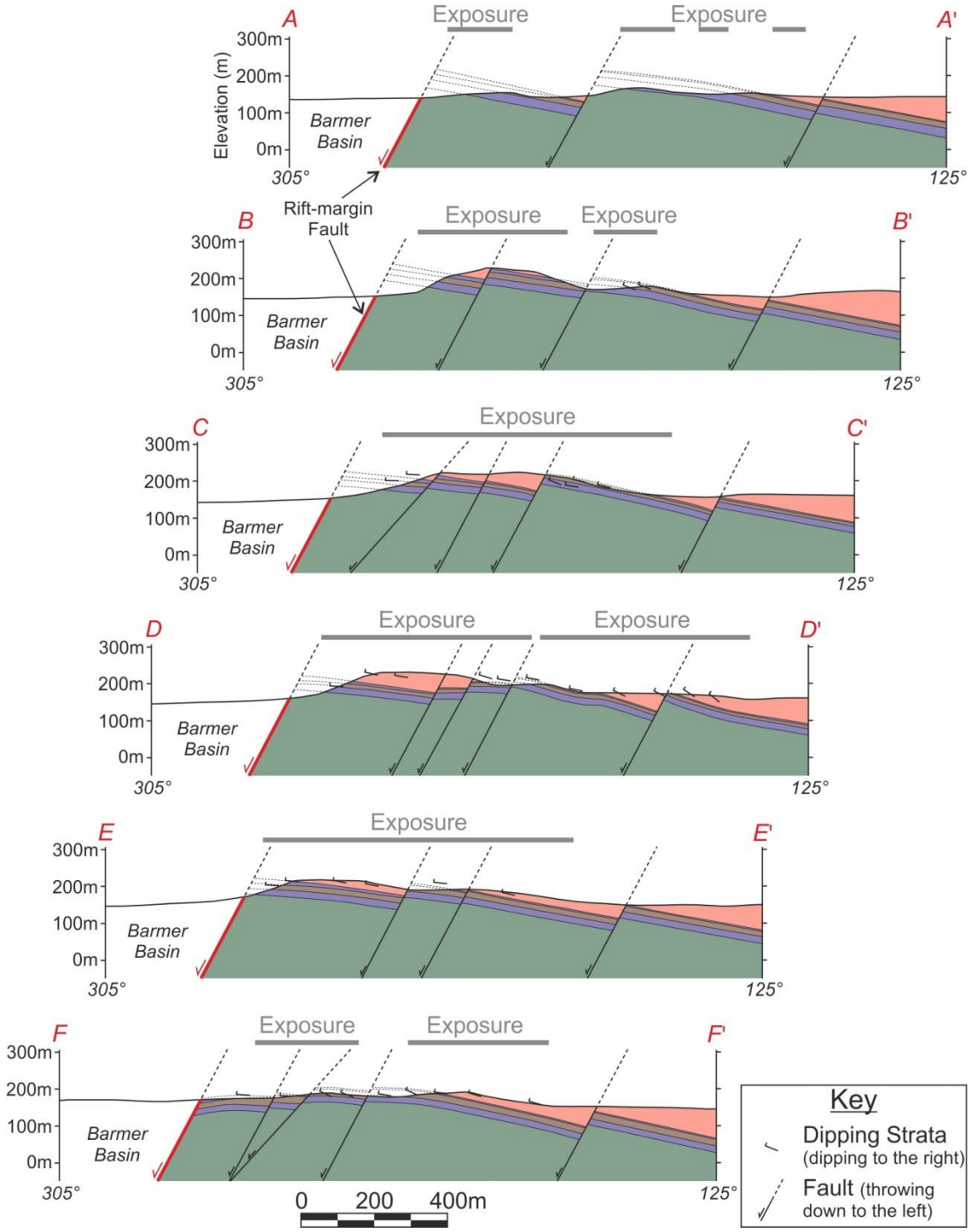

Figure 4.14 – Representative cross-sections across the Sarnoo Hills (key to symbols inset). Cross-sections were used to construct a structural model of the outcrop. See **figure 4.13** for key to colours and cross-section locations. Sections redrawn from Midland Valley's Move software. For all cross-sections see **Appendix B**.

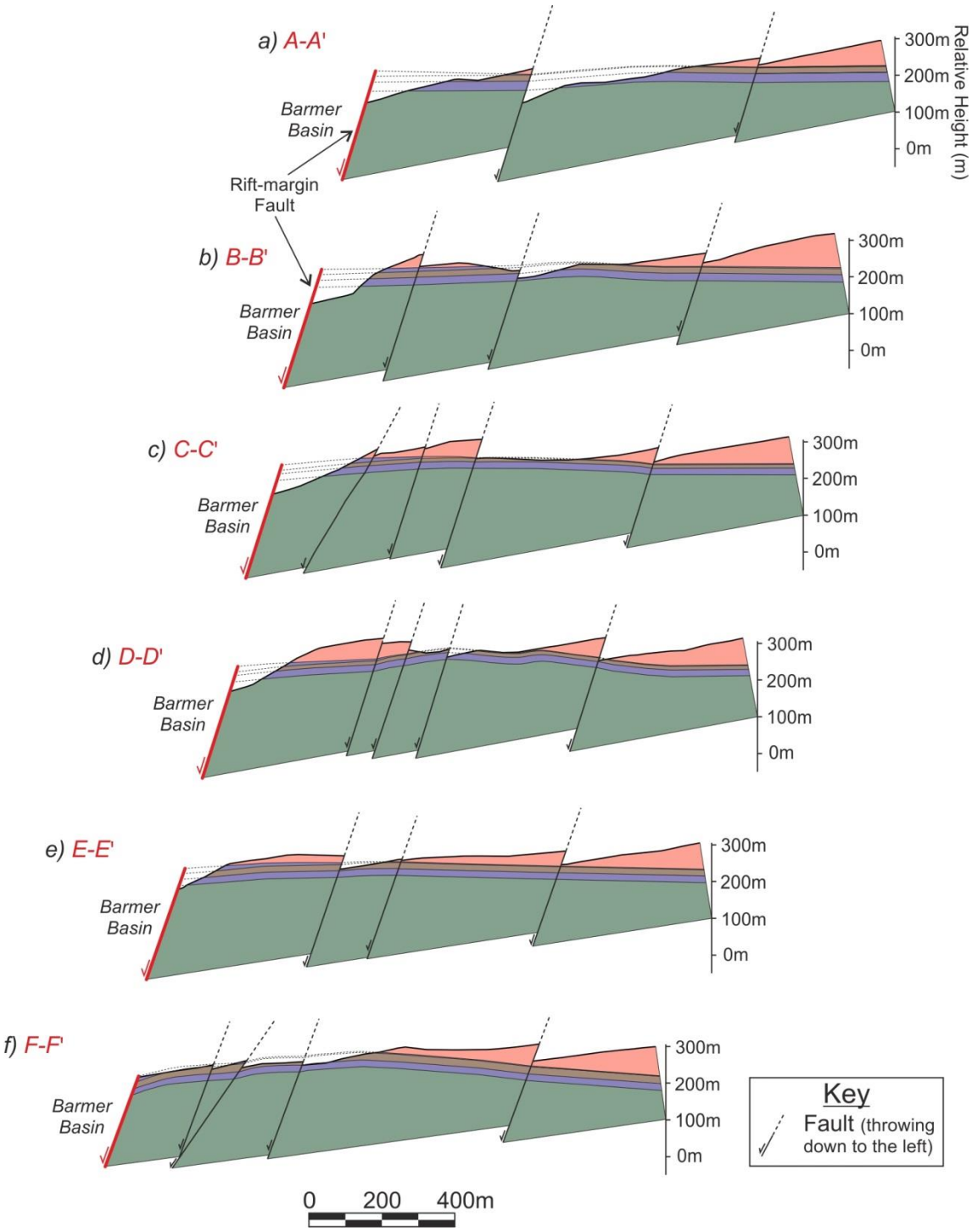

Figure 4.15 – Rigid-block restored cross-sections across the Sarnoo Hills (key to symbols inset). Rigid-block restorations were conducted using Midland Valley's Move software package. See **figure 4.13** for key to colours and cross-section locations, and **figure 4.14** for unrestored cross-sections. Sections redrawn from Midland Valley's Move software. For all restored cross-sections see **Appendix B**.

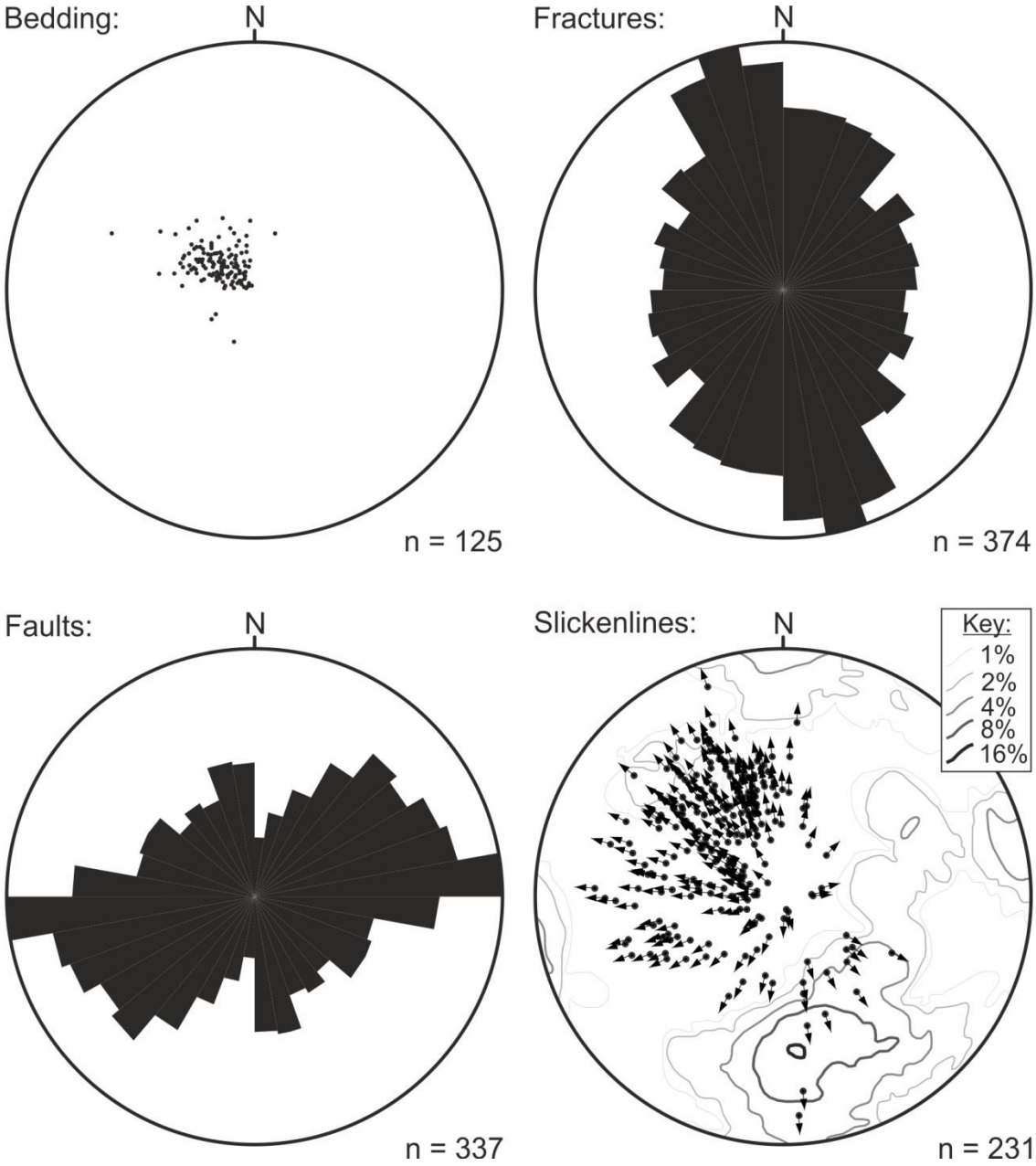

Figure 4.16 - Structural data from the Sarnoo Hills, indicating a gentle stratigraphical dip to the southeast, a predominance of north-northwest trending fractures and west-trending faults, and fault slip to the northwest. Contours on slickenline plot represent density of poles-to-fault plane measurements by area (key inset). All stereographic projections are lower hemisphere, equal area. Rose diagrams are equal area. See **Appendix C** for raw structural data.

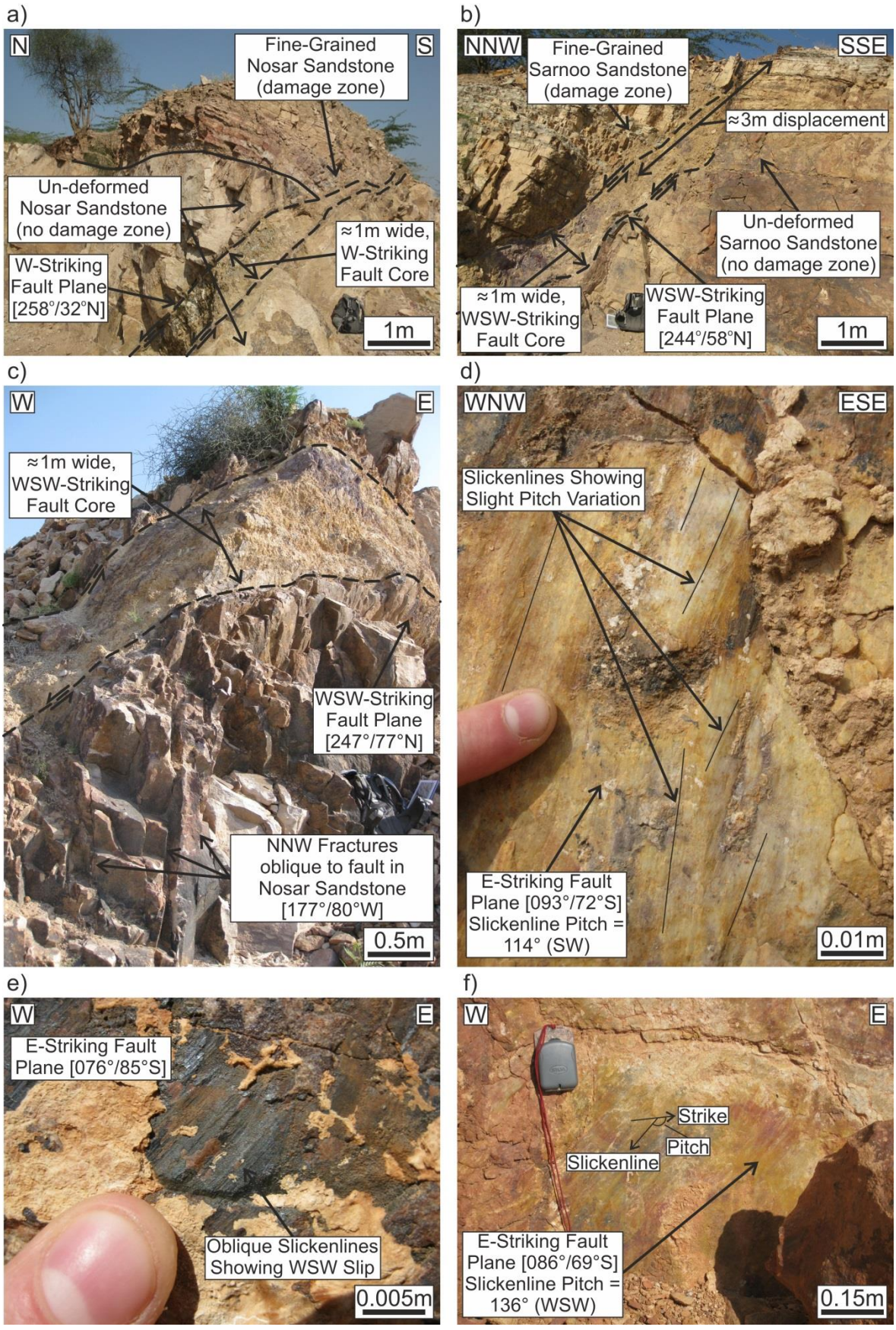
a)
N
S
Fine-Grained
Nosar Sandstone
(damage zone)
Un-deformed
Nosar Sandstone
(no damage zone)
≈1m wide,
W-Striking
Fault Core
W-Striking
Fault Plane
[258°/32°N]
1m
b)
NNW
SSE
Fine-Grained
Sarnoo Sandstone
(damage zone)
≈3m displacement
Un-deformed
Sarnoo Sandstone
(no damage zone)
≈1m wide,
WSW-Striking
Fault Core
WSW-Striking
Fault Plane
[244°/58°N]
1m
c)
W
E
≈1m wide,
WSW-Striking
Fault Core
WSW-Striking
Fault Plane
[247°/77°N]
NNW Fractures
oblique to fault in
Nosar Sandstone
[177°/80°W]
0.5m
d)
WNW
ESE
Slickenlines Showing
Slight Pitch Variation
E-Striking Fault
Plane [093°/72°S]
Slickenline Pitch =
114° (SW)
0.01m
e)
W
E
E-Striking Fault
Plane [076°/85°S]
Oblique Slickenlines
Showing WSW Slip
0.005m
f)
W
E
Strike
Pitch
Slickenline
E-Striking Fault
Plane [086°/69°S]
Slickenline Pitch =
136° (WSW)
0.15m

Figure 4.17 (*previous page*) **-** Structures exposed in the Sarnoo Hills (see **figure 4.13** for photograph locations). Fault measurements are recorded as strike/dip/sense and pitch-in-plane is measured from fault strike, with the general lineation trend shown in brackets. **(a)** Southwest-striking fault within the Nosar Sandstone; **(b)** West-southwest-striking fault within the Sarnoo Sandstone; **(c)** north-northwest -trending fractures abutting obliquely against a southwest-striking fault; **(d)** Multiple slickenline sets on an exposed fault plane; **(e)** Slickenlines displaying highly-oblique slip towards the west-southwest; **(f)** Slickenlines exposed on an east-striking fault displaying dextral oblique-slip towards the west-southwest.

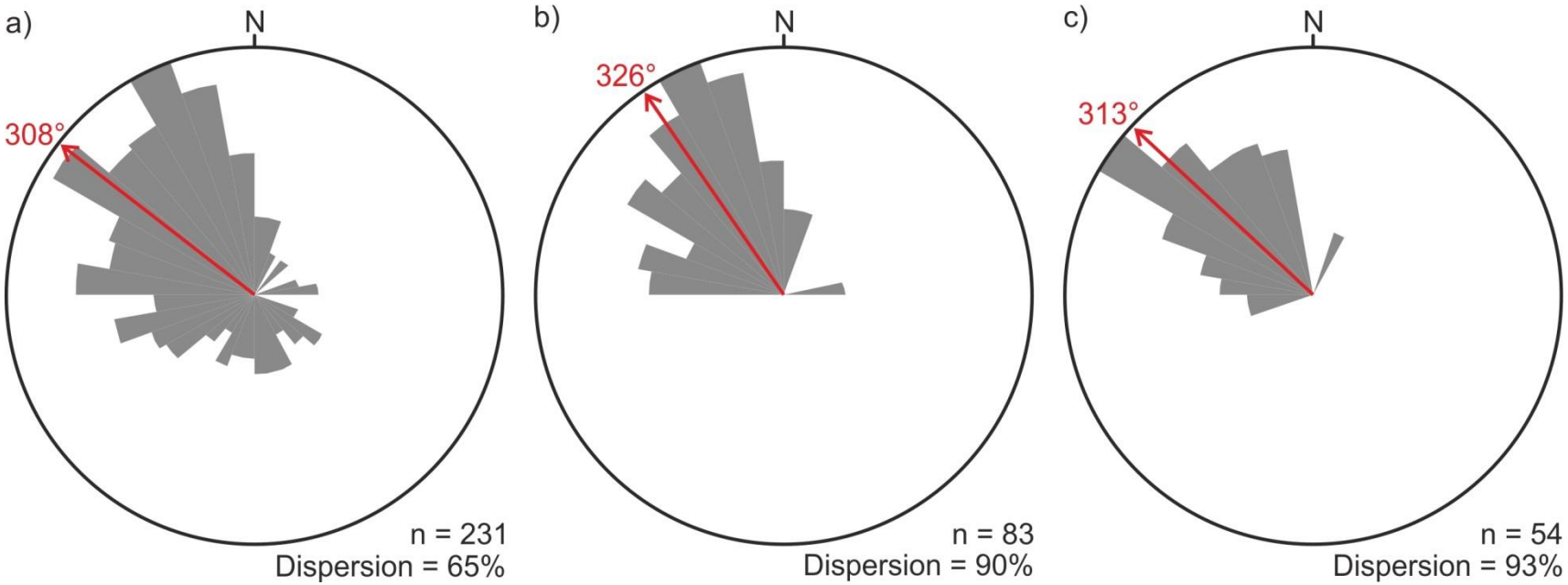

Figure 4.18 - Fault slip data from the Sarnoo Hills. The azimuth of the vector mean (arrowed; **Equation 4.2**) and dispersion (**Equations 4.5 & 4.6**) are shown for each dataset. All rose plots are equal area. **(a)** all Sarnoo slickenlines; **(b)** slickenlines measured on west-striking (247.5°-292.5°; **Table 4.1**) faults; **(c)** slickenlines measured on southwest-striking (202.5°-247.5°; **Table 4.1**) faults. See **Appendix C** for raw structural data.

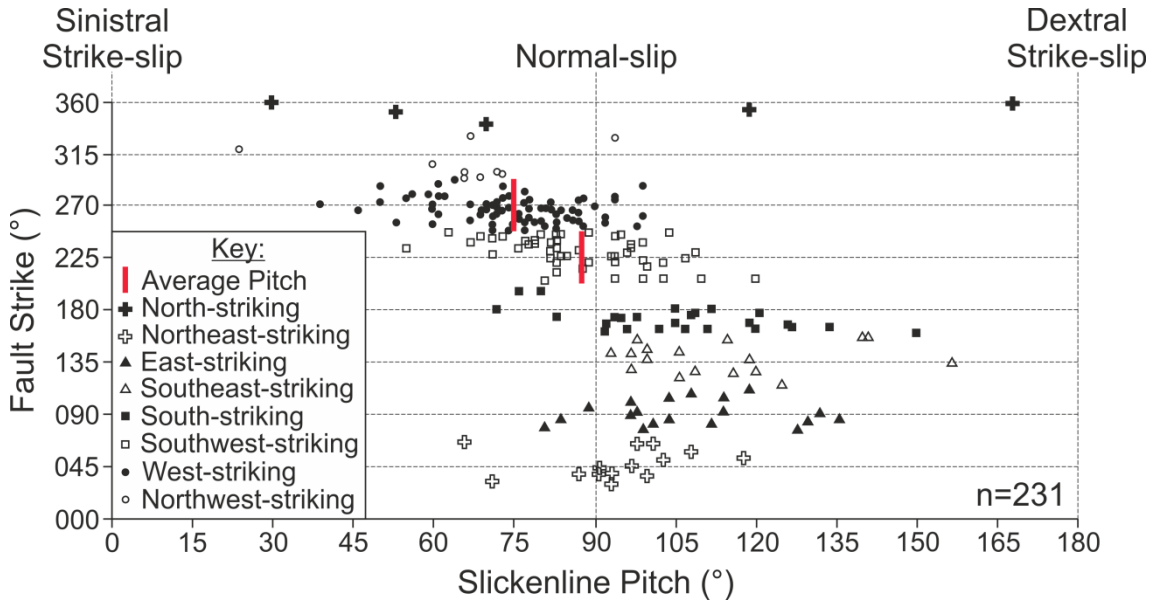

Figure 4.19 - Slickenline pitch vs. fault strike plot. Average fault slip on SW-striking, NW-dipping faults displays a 3° component of sinistral oblique slip (average pitch = 87°). In contrast, average W-striking, N-dipping faults display a significantly larger (15°) component of sinistral oblique slip (average pitch = 75°). See **Appendix C** for raw structural data and **Table 4.1** for fault strike categorisation.

Figure 4.19). Little evidence of fault reactivation is observed in the Sarnoo Hills, despite the recent collision between India and Eurasia, and the associated inversion recorded elsewhere in the Barmer Basin (Dolson *et al.* in press).

4.3.3 Structural model of the outcrop

Construction of a three-dimensional structural model of the outcrop from a framework of serial two-dimensional cross-sections (**Figure 4.20**) reproduced a satisfactory replication of the fault network exposed at outcrop (**Figure 4.21**). Artificial (model-generated) fault displacement-length profiles were generated using the base Nosar Sandstone surface, the most significant and consistent surface exposed (**Figure 4.22**). Although the base Nosar Sandstone surface is erosive (≤ 4 m), it can be used reliably to correlate across faults because deposition pre-dates deformation. Fault displacement-length profiles are generally smooth, and display gradual profiles that progressively increase or decrease in displacement along strike. In some examples (**Figures 4.22a, b, & d**) displacement profiles are arcuate, and displacement decreases from a displacement maxima (D_{max}; **Section 2.1.1**) towards zero along strike. However, in areas where southwest- and west-striking faults interact, fault displacement-length profiles are erratic (**Figure 4.22**). Maximum and minimum displacement values are approximately 100 m and 0 m respectively. An important feature is the

near complete loss of displacement on some sections of southwest-striking faults towards west-striking faults (starred in **Figure 4.22**).

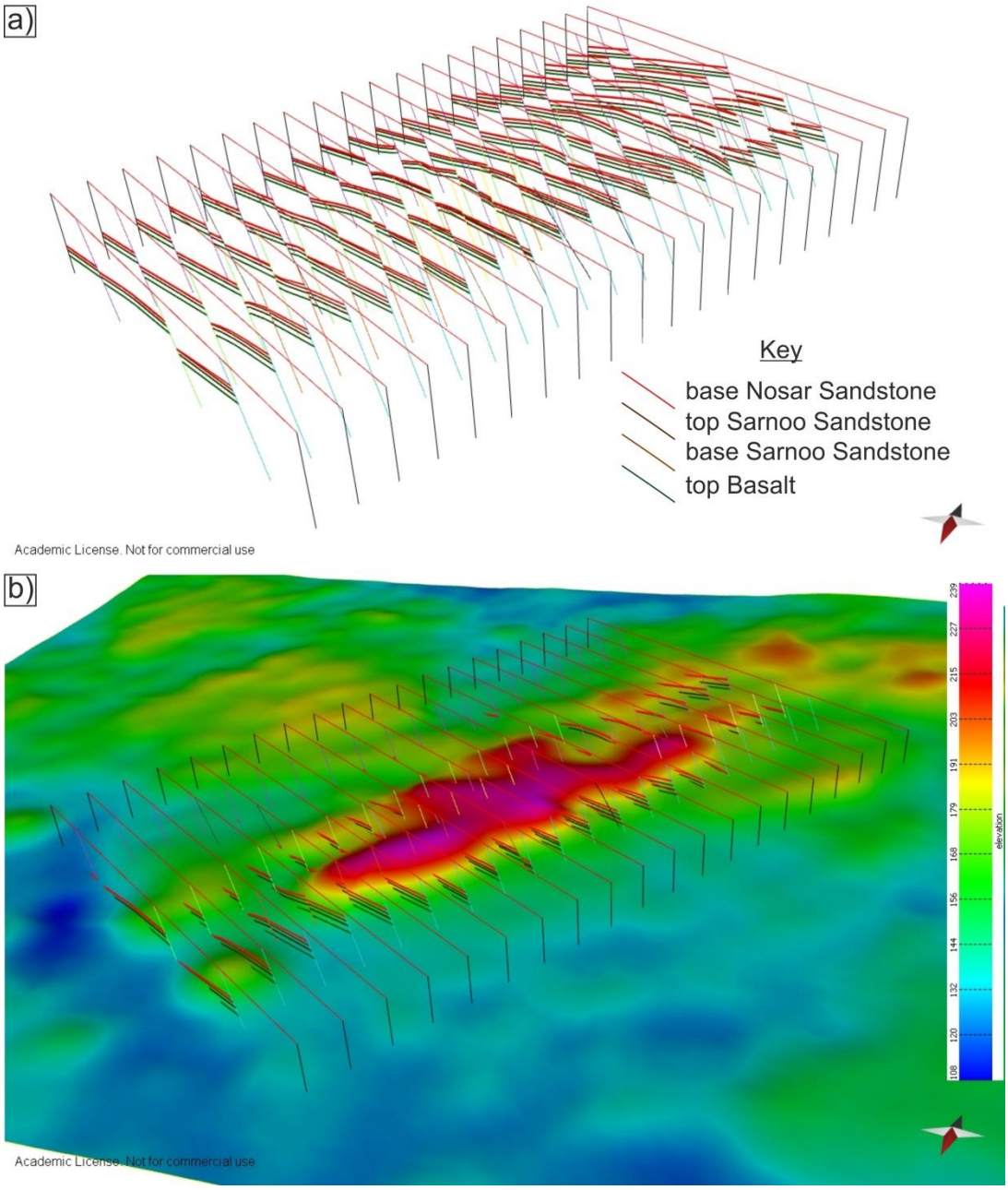

Figure 4.20 – Oblique, three-dimensional images depicting the construction of the three-dimensional model of the outcrop. **(a)** Three-dimensional framework comprising lithological contacts and faults interpreted on twenty two-dimensional cross-sections bearing 125° (**Appendix B**); **(b)** as (a) with 30 m DEM overlain (key to colours inset). Images from Midland Valley's Move software.

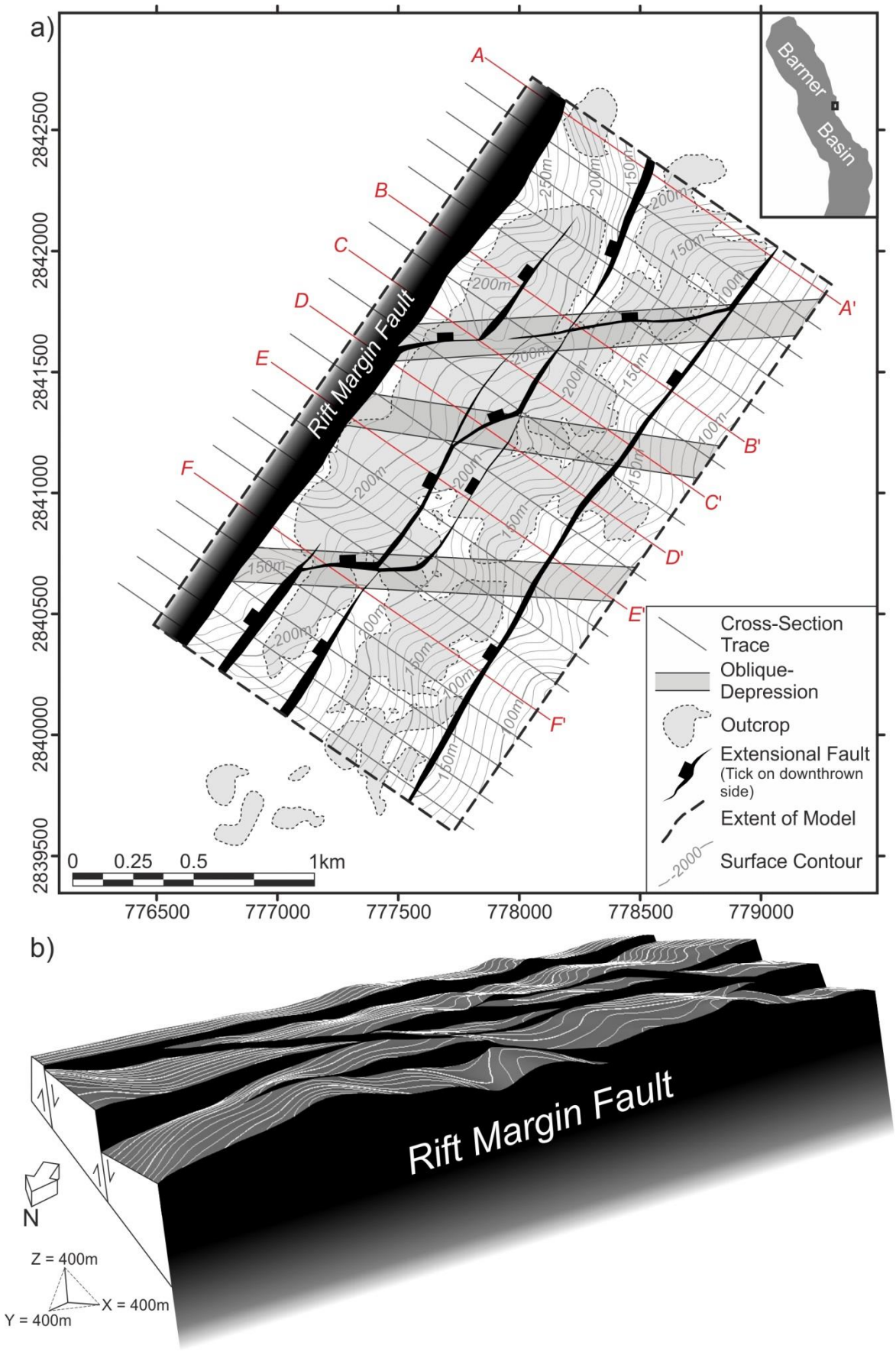
a)
Barmer
Basin
A
B
C
D
E
F
A'
B'
C'
D'
E'
F'
Rift Margin Fault
Cross-Section Trace
Oblique-Depression
Outcrop
Extensional Fault
(Tick on downthrown side)
Extent of Model
Surface Contour
0 0.25 0.5 1km
2842500
2842000
2841500
2841000
2840500
2840000
2839500
776500
777000
777500
778000
778500
779000
b)
Rift Margin Fault
N
Z = 400m
X = 400m
Y = 400m

Figure 4.21 (*previous page*) - **(a)** Contoured base Nosar Sandstone surface from the structural model of the outcrop. Fault polygons from the base Nosar Sandstone surface are overlain. Reference grid is UTM Zone 42N. Contours are of elevation in metres (location within the Barmer Basin inset), and cross-section traces from which the model was constructed (**Appendix B**), including those depicted in **figures 4.14 & 4.15**, are also displayed; **(b)** oblique three-dimensional view of the base Nosar Sandstone surface, taken from the structural model of the outcrop. Image courtesy of Schlumberger Information Systems Petrel software.

4.4 Deposition of the Ghaggar-Hakra Formation

The mafic crystalline rock underlying the Ghaggar-Hakra Formation has characteristic basaltic mineralogy in accordance with previous interpretations (Roy & Jakhar 2002). Within this unit the irregular chlorite-filled enclaves (**Figure 4.7a**) are interpreted as infilled vesicles, supporting shallow emplacement or sub-aerial extrusion. A distinct lack of evidence for thermal interaction between the basalt and the overlying sediments of the Ghaggar-Hakra Formation (chilled/baked margins) suggests the former is not intrusive and deposition occurred directly onto the exposed upper surface of the basalt. Although apparently interbedded with the Ghaggar-Hakra Formation in places (**Figure 4.8a**), the heavily altered, light green crystalline unit at the base of the succession is interpreted as intrusive based on the definite cross-cutting relationship displayed with the sedimentary succession (**Figure 4.8b**) and, therefore, is the youngest unit within the exposed succession.

The lowermost sandstone succession, the Darjaniyon-ki Dhani Sandstone (dar; **Figures 4.10 & 4.23**), represents immature, braided fluvial deposition with a high sediment load, in mobile, erosive channels. The middle sandstone succession, the Sarnoo Sandstone (sar; **Figures 4.10 & 4.23**), displays deposition within a much larger fluvial system, as indicated through stacked channel elements and an increase in the maturity of clasts. Sedimentary logs show facies associations characteristic of waning fluid flow successions, with lags and siltstone rip-up clasts indicative of channel migration or a seasonally recharged system (**Figure 4.9c**). Thick, extensively rippled units (0.5 m – 2 m) represent unconfined deposition within sheetfloods. The Sarnoo Sandstone reflects deposition within a mobile, meandering fluvial system. Preservation of stacked accreting channel systems with highly erosive bases, a lack of preserved channel geometries, and siltstone rip-up clasts (**Figure 4.9d**), suggests deposition of the uppermost sandstone succession, the Nosar Sandstone (nos; **Figures 4.10 & 4.23**) occurred within an active, rapidly migrating fluvial system that was dominantly braided. Although moderately sorted and medium- to very coarse-

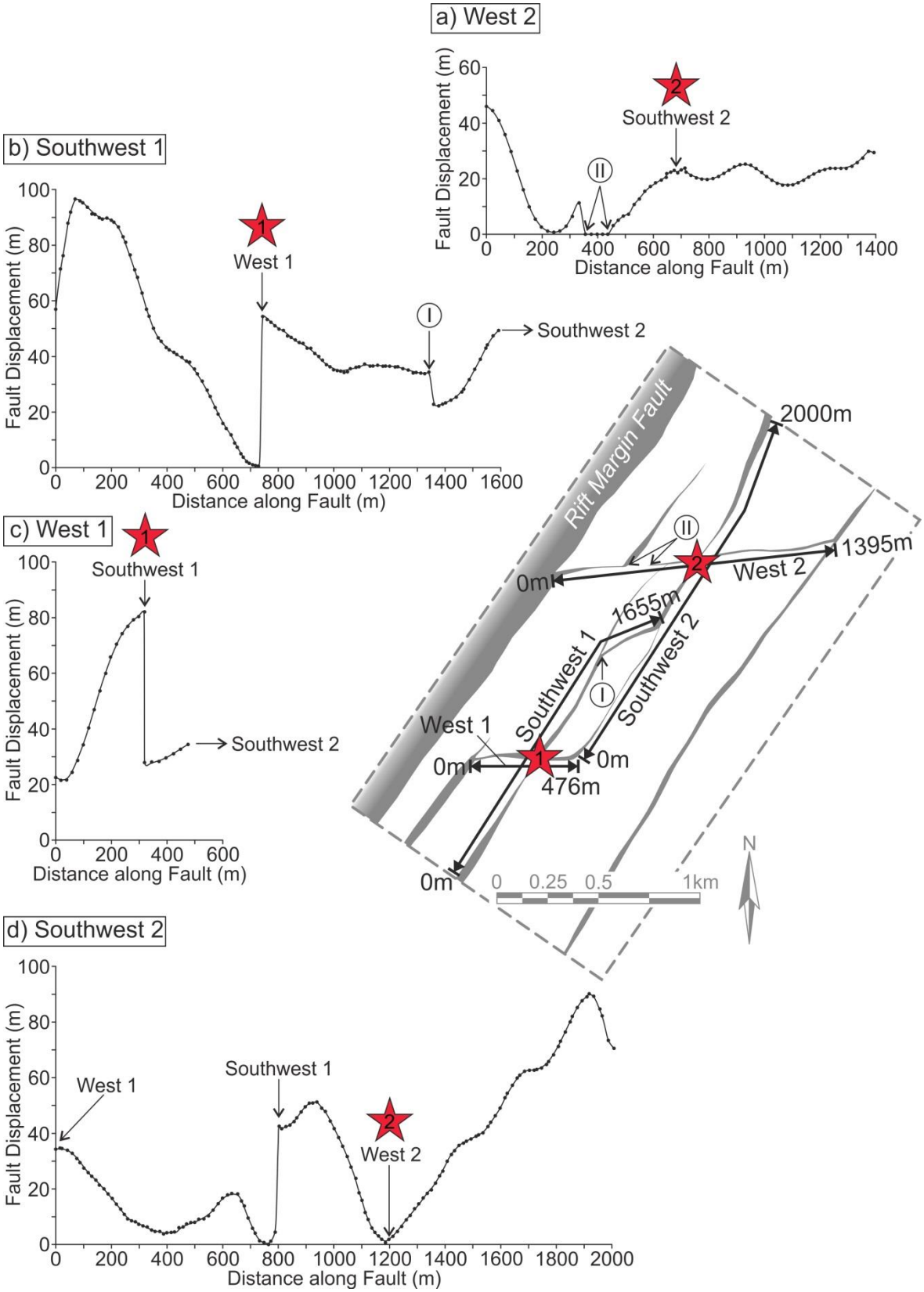

Figure 4.22 – Artificial (model-generated) fault-displacement length profiles constructed from the base Nosar Sandstone surface in the structural outcrop model. Displacement measurements (dots) were taken at 10-20 metre intervals. Stars indicate where a reactivated, extension-oblique fault segment intersects an extension perpendicular fault.

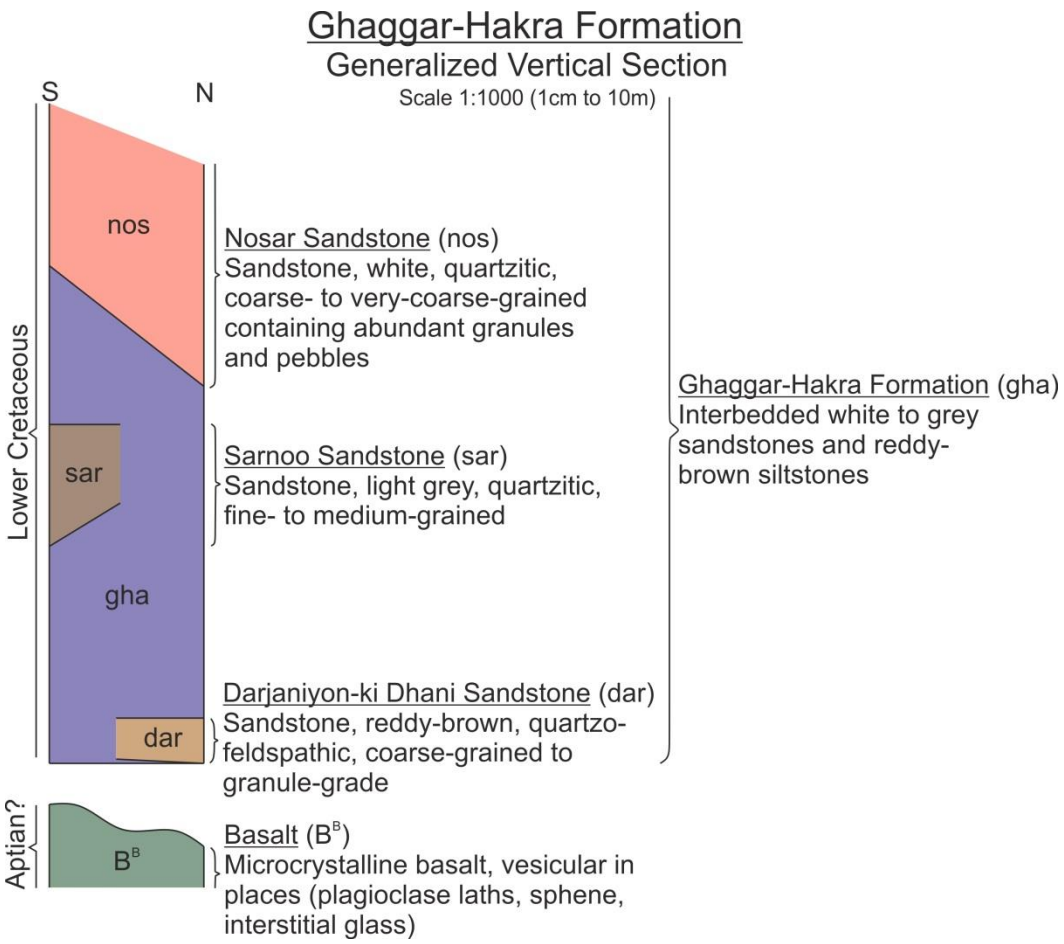

Figure 4.23 - Generalised vertical section depicting the spatial relationship of mapping units within the Lower Cretaceous Ghaggar-Hakra Formation sedimentary succession, as exposed in the Sarnoo Hills area, east Barmer Basin (updated from Clarke 2011; **Figure 4.3 inset**). Three channelised fluvial sandstone successions (dar; sar; nos) are separated by a thick (< 50 m) package of floodplain mudstones and siltstones (gha). The high proportion of fine deposits within the succession suggests floodplain aggradation, possibly due to rapid subsidence and a high sediment supply.

grained, the mature clast array may indicate intraformational reworking. The lack of in-situ overbank material and channel geometries suggests that channel migration was rapid, or that sediment input was high relative to subsidence. Overall, the sandstone successions of the Ghaggar-Hakra Formation show deposition within a maturing-upwards, mobile fluvial succession that displays a temporal increase in the size of the system.

Relative to the sandstone successions, the intervening mudstones and siltstones occur in unusually thick packages (≤ 30 m) and likely represent the floodplain environment that accompanied the Darjaniyon-ki Dhani and Sarnoo sandstone fluvial systems. Rooted horizons within the siltstone and mudstone packages allude to sub-aerial exposure and the beginning of

pedogenesis. The maturity of a (palaeo) soil is an important time-constraint on surface exposure prior to burial (Miall 1996), and may be used to approximate rates of deposition under the assumption that soil maturity increases with decreasing rates of deposition (Bridge 2003). Even the most weakly developed, immature soils, namely entisols (very weakly developed) and inceptisols (weakly developed), require long (100 to 1000 years) periods of time where sedimentation rate is low (< 1 mm $year^{-1}$) in order to develop (Bridge 2003). The paucity of well-developed palaeosols within exposures of the Ghaggar-Hakra Formation in the Sarnoo Hills indicates a lack of long-term floodplain stability. Further to this, rapid subsidence and a high sediment supply, resulting in floodplain aggradation, may account for the preservation of a high proportion of fine deposits relative to the sandstone successions. Rapid rates of floodplain aggradation (> 0.5 cm $year^{-1}$) limit soil formation and pedogenic assimilation (Daniels 2003), and is consistent with the limited evidence for long-term floodplain stabilisation within the exposed sedimentary succession. Deposition of the mudstones and siltstones within ephemeral lakes during long-lived periods of flooding may also account for high proportion of fines within the Sarnoo Hills sedimentary succession. In summary, the sedimentary succession exposed in the Sarnoo Hills likely represents fluvial deposition within a rapidly subsiding continental alluvial plain system that, at times (Nosar Sandstone), had a high sediment supply.

4.5 Structural Evolution of the Sarnoo Hills

The near-exclusive trend of single-generation, normal-sense slickenlines towards the northwest, and the southwest-striking orientation of major faults, indicates fault activity during a single phase, or multiple co-axial phases, of northwest-southeast extension. The presence of a dominant north-northwest trending extensional fracture set (**Figure 4.16**), however, indicates that the Sarnoo Hills underwent a period of northeast-southwest orientated extensional deformation. The abutting rather than cross-cutting relationship of rift-parallel extensional fractures with southwest-striking faults (**Figure 4.17c**) suggests that southwest-striking faults predate north-northwest-trending extensional fractures. A lack of growth faulting and fault-related stratigraphical thickness changes signifies that deformation post-dates deposition. The depth of deformation is unknown; however, the large component of mode-one (pure-shear) opening evident on many faults suggests deformation was shallow. A combination of block-rotations during deformation, and tilting during the recent uplift and

subsidence of the northern and southern rift respectively, rotated the strata towards the southeast by an average 15°.

The average 15° component of sinistral oblique-slip of west-striking faults exposed in the Sarnoo Hills (**Figure 4.19**) suggests these faults were orientated obliquely to the extension direction. By comparison, the near pure normal slip of southwest-striking faults (average 87° pitch; **Figure 4.19**), and the larger displacement accommodated by these faults, indicates they were orientated approximately perpendicular to the direction of extension. It follows that west-striking faults were influenced by pre-existing, extension oblique, rift basement faults that acted passively as breach faults between the evolving, extension-perpendicular (southwest striking) faults, and were incorporated into the evolving southwest-striking fault systems during northwest-southeast extension (**Figure 4.24**). The concomitance between west-striking faults and the outcrop dissecting topographical depressions (**Figure 4.21**), suggests that the depressions are a subtle indicator of a discrete rift-basement fabric at depth. West-striking faults do not occur everywhere along the length of the topographical depressions (**Figure 4.21**) indicating partial, not complete reactivation of the underlying rift-basement fabric. The incorporation of west-striking faults within the evolving southwest-striking fault network indicates that both fault trends were active contemporaneously and underwent a mutual slip. Deformation accommodated by contemporaneous slip of multiple, kinematically interacting fault planes of different orientation results in the formation of multiple slickenline sets during a single deformational event (Nieto-Samaniego & Alaniz-Alvarez 1997). A mutual slip of southwest- and west-striking faults, therefore, may account for the 013° disparity in average slickenline trends (e.g. Nieto-Samaniego & Alaniz-Alvarez 1997; **Figure 4.18**).

The correspondence of erratic displacement profiles with the zones of interaction between west- and southwest-striking faults (**Figure 4.22**) indicates displacement transfer between faults and kinematic interaction (e.g. Nixon *et al.* 2014). The near complete loss of displacement on some sections of the extension-perpendicular (southwest-striking) faults towards the reactivated, extension-oblique (west-striking) fault segments (starred on **Figures 4.22b & d**), indicates that reactivated fault segments restricted the evolution of the extension-perpendicular (southwest-striking) fault systems (**Figure 4.24**). This relationship is illustrated where the faults ‘West 2’ and ‘Southwest 2’ interact (star no. 2 on **Figure 4.22**). The displacement-length profile of ‘West 2’ is

comparable to that expected of an isolated fault, namely maximum displacement towards the centre of the fault decreasing towards the fault tip points (**Section 2.1.2; Figure 4.22a**). Further to this, the displacement profile of 'West 2' is unaffected where the fault intersects 'Southwest 2' indicating no displacement transfer occurred between 'West 2' and 'Southwest 2' during deformation. The characteristics of the displacement profile of 'West 2', coupled with the lack of evidence supporting kinematic interaction and the complete loss of displacement on 'Southwest 2' towards 'West 2', indicate that 'West 2' was active during deformation and did not interact kinematically with 'Southwest 2', despite the more favourable orientation of the 'Southwest 2' to accommodate extension (extension-perpendicular). Similar relationships have been observed experimentally (Bellahsen & Daniel 2005), and were attributed to the reactivated pre-existing fault acting as a 'stress barrier' that inhibited the lateral propagation of the evolving faults due to a perturbed stress field (e.g. Willemse 1997; **Figure 2.6**).

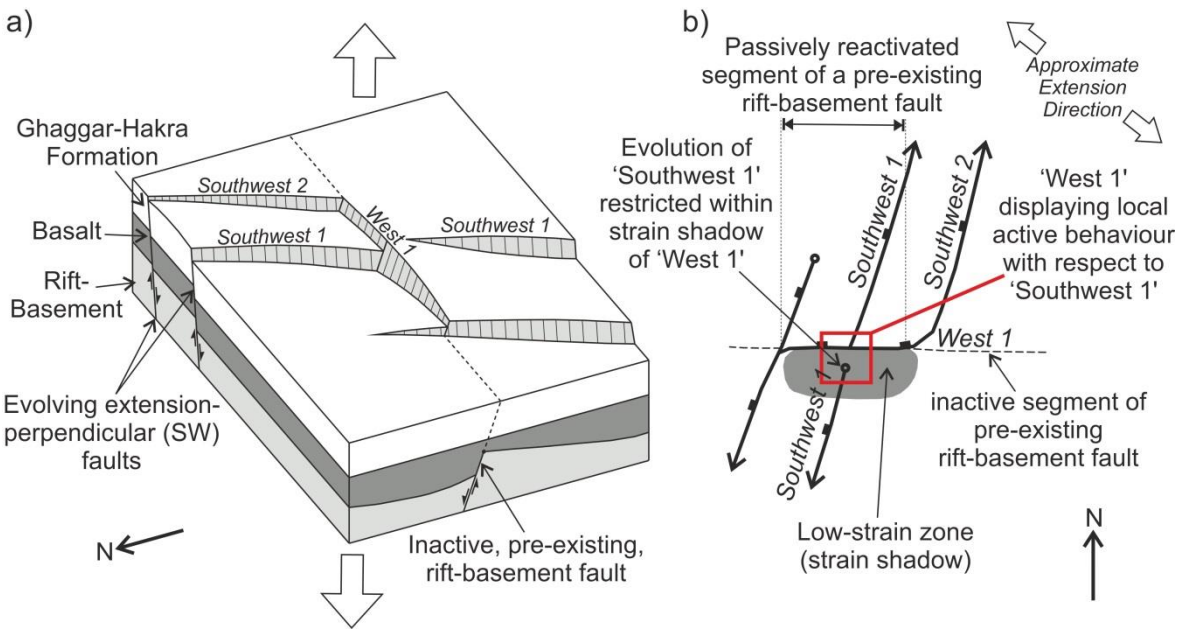

Figure 4.24 - In the Sarnoo Hills, pre-existing west-striking, extension-oblique rift-basement faults acted passively as breach faults between the evolving, extension-perpendicular (SW-striking) faults. However, where a passively reactivated segment of a pre-existing, extension-oblique fault (e.g. West 1) intersected an extension perpendicular (SW-striking) fault (e.g. Southwest 1), the passively reactivated segment of the extension-oblique fault segment restricted the evolution of the extension-perpendicular fault and locally displayed active behaviour. See **figure 4.13** for location. Light grey = Malani Igneous Suite rift basement; dark grey = basalt; white = Ghaggar-Hakra Formation; **(a)** Block diagram; **(b)** annotated sketch map of **(a)**.

4.6 Discussion

If the Aptian age proposed for the basalt underlying the Ghaggar-Hakra Formation is credible (120 Ma; Sharma 2007), Ghaggar-Hakra Formation deposition cannot have occurred prior to this time. Such an age inference falls within the poorly constrained Middle Jurassic to Lower Cretaceous estimate proposed for the Ghaggar-Hakra Formation previously based on plant fossils (Baksi & Naskar 1981), and further constrains deposition to the Aptian and Albian ages. Additional sample dating is required to validate and refine these limits. The intrusions within the Ghaggar-Hakra Formation sedimentary succession are the youngest unit exposed in the Sarnoo Hills and most likely correspond to the early phase of Deccan igneous activity (68.57 ± 0.08Ma; Basu *et al.* 1993) exposed locally as scattered plug-like bodies (Basu *et al.* 1993; Simonetti *et al.* 1995; Simonetti *et al.* 1998; Roy & Jakhar 2002; Roy 2003; Sen *et al.* 2012).

The initially immature deposits, rapid subsidence, and high sediment input of the Ghaggar-Hakra Formation sedimentary succession exposed in the Sarnoo Hills, suggests that deposition marked a sudden change to long-lived, tectonic stability on the craton interior, as indicated by the significant regional unconformity above Malani Igneous Suite deposits throughout northwest India (Sisodia & Singh 2000; Dolson *et al.* in press). The origin of tectonic destabilisation is unknown. Further to this, no data currently exists constraining the sediment source region of Gaggar-Hakra Formation sediments exposed in the Sarnoo Hills. It is tentatively suggested that the Aravalli Mountains, immediately east and southeast of the Barmer Basin, which formed during the Proterozoic Eon (Mamtani *et al.* 2000; Vijaya Rao *et al.* 2000), are a probable hinterland for Ghaggar-Hakra Formation deposits. The seasonal Luni river, situated 20 km to the east of the Sarnoo Hills (**Figure 4.2a**), drains the western slopes of the Aravalli Mountains with a south-westerly flow local to exposure in the Sarnoo Hills (**Figure 4.25**; Kale *et al.* 2000; Jain *et al.* 2005), and may be an analogous or equivalent fluvial system to that exposed in deposits of the Ghaggar-Hakra Formation in the Sarnoo Hills.

Partial reactivation of the underlying west-striking rift-basement fabric indicates passive behaviour (c.f. Morley 1999b) of pre-existing structures during northwest-southeast extension. However, where reactivated west-striking fault segments restricted the evolution of southwest-striking faults, the reactivated fault segment acted as a through-going fault with a distinct sense of shear, and locally exhibited active behaviour (**Figure 4.24**). Characteristics of the Sarnoo Hills fault network,

including; 1) the high degree of involvement of reactivated fault segments; 2) the strong influence that reactivated fault segments had on the evolving extension-ideal (southwest-striking) fault systems, and; 3) the prominent zig-zag geometry, indicate that extension perpendicular faults did not become dominant, nor was the zig-zag geometry 'smoothed out,' as is expected to occur during fault network maturation (Morley 1999b; Lezzar, *et al.* 2002; Bellahsen & Daniel 2005). Such traits indicate that fault activity occurred during incipient northwest-southeast extension, and the fault network did not mature from the incipient stages of formation.

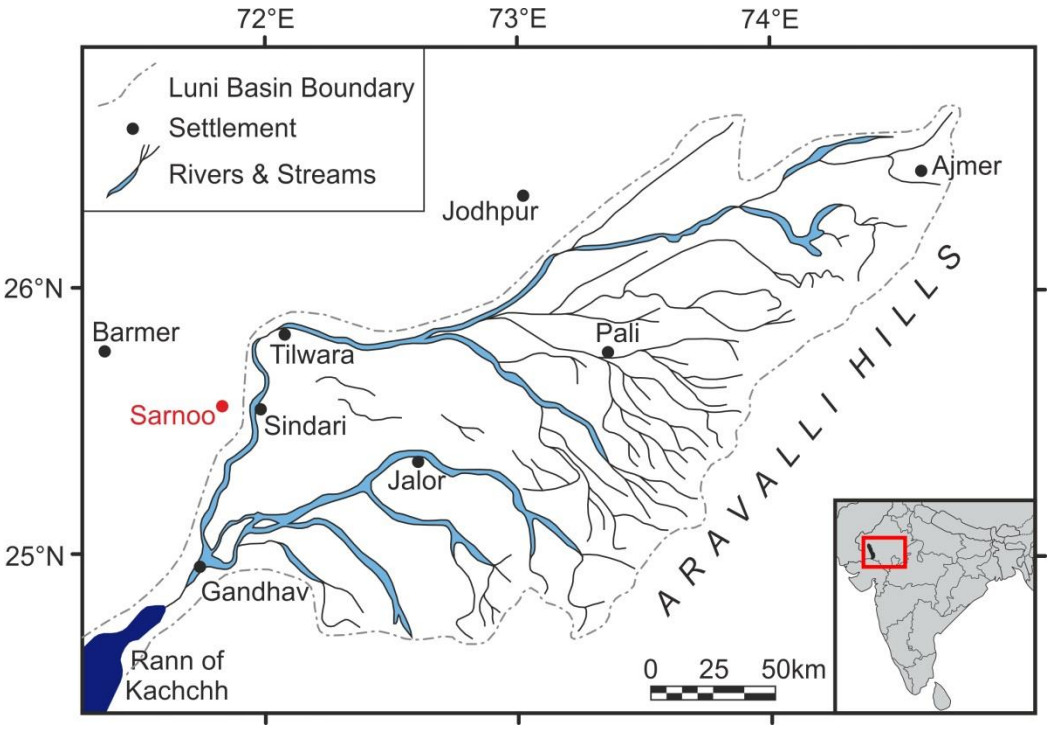

Figure 4.25 – The present day Luni River may be an analogous or equivalent fluvial system to that exposed in deposits of the Ghaggar-Hakra Formation in the Sarnoo Hills (after Kale *et al.* 2000).

4.7 Summary

This chapter investigated a rift-oblique fault network and sedimentary succession that accumulated prior to the main Barmer Basin rift event, which are situated along the central eastern rift margin of the Barmer Basin, in the Sarnoo Hills. High resolution geological mapping was conducted throughout the Sarnoo Hills alongside graphical logging of the exposed sedimentary succession. Sedimentary logs, sedimentary architectures, and petrographical descriptions were used to establish a broad depositional framework for each mapping unit, which were subsequently used to construct a depositional model describing the exposed sedimentary succession. Mapped

lithological contacts, structural data, and a 30 m Digital Elevation Model were combined to construct twenty 1.8 km long, northwest-southeast orientated (125°) cross-sections that were validated using rigid-block restorations and were used to build a structural model of the outcrop. In turn, the outcrop model was used to generate artificial (model-generated) displacement-length profiles for key faults within the Sarnoo Hills fault network.

The exposed sedimentary succession is part of the Lower Cretaceous Ghaggar-Hakra Formation, and comprises a series of fluvial sandstone successions separated by thick packages of mudstone and siltstone. Sediments were deposited within a maturing fluvial system, and deposition likely marked a sudden change to long-lived stability on the craton interior, possibly due to tectonic destabilisation. Dominant faults are southwest-striking, northwest-dipping and form a zig-zag fault network with west-striking, north-dipping faults, which evolved under a northwest-southeast extensional regime. Northwest-southeast extension was previously unrecognised within the Barmer Basin. During northwest-southeast extension, west-striking faults were influenced by pre-existing rift-basement structures, and the evolution of extension-perpendicular (southwest-striking) faults was restricted by reactivated segments of pre-existing rift basement (west-striking) faults. The lack of outcrop exposure within the Barmer Basin precludes further, outcrop-based investigation into the relationship between the northwest-southeast and northeast-southwest (non-coaxial) extensional structural regimes exposed in the Sarnoo and Barmer hills respectively. Further investigation into the spatial and temporal relationship between the extensional regimes exposed on opposing rift margins of the Barmer Basin requires that subsurface data be employed.

5 Tectono-stratigraphical evolution of the central Barmer Basin

Investigation into the e*arly-stage tectono-stratigraphical evolution of the central Barmer Basin using subsurface datasets*

The paucity of outcrop exposure in the Barmer Basin precludes direct, outcrop-based observation of the relationship between the two non-coaxial extensional regimes exposed on opposing rift margins (**Figure 5.1**). In this chapter, the tectonic framework established at the outcrop- (small) scale is built upon at the basin-scale using subsurface (two-dimensional seismic & well) datasets. Tectono-stratigraphical relationships in the central Barmer Basin provide the pivotal link to the poorly understood spatio-temporal relationship between non-coaxial extensional regimes (**Chapters 3 & 4**). Fresh interpretations of two-dimensional seismic data are used to construct a three-dimensional tectono-stratigraphical model of early syn-rift deposits in the central Barmer Basin (**Figure 5.2**). Subsequently, two- and three-dimensional structural restorations demonstrate that interpretations of two-dimensional seismic sections, and the three-dimensional model, are geometrically valid.

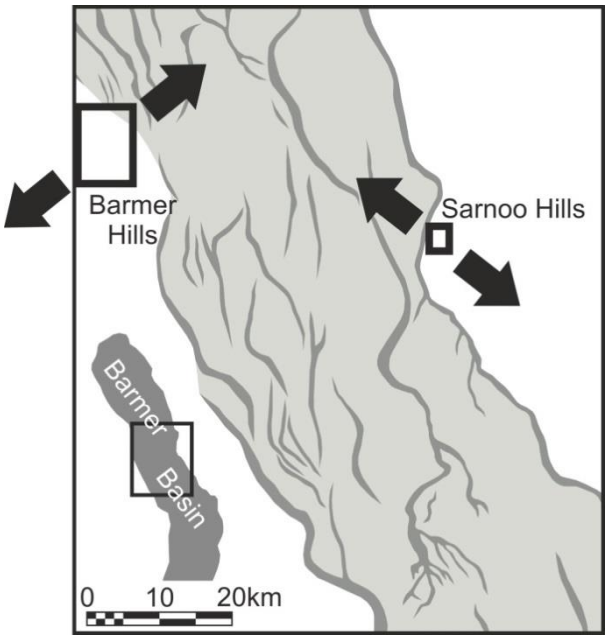

Figure 5.1 – Outcrop exposure in the Barmer (**Chapter 3**) and Sarnoo (**Chapter 4**) hills reveal two non-coaxial extensional structural regimes on opposing rift margins of the Barmer Basin.

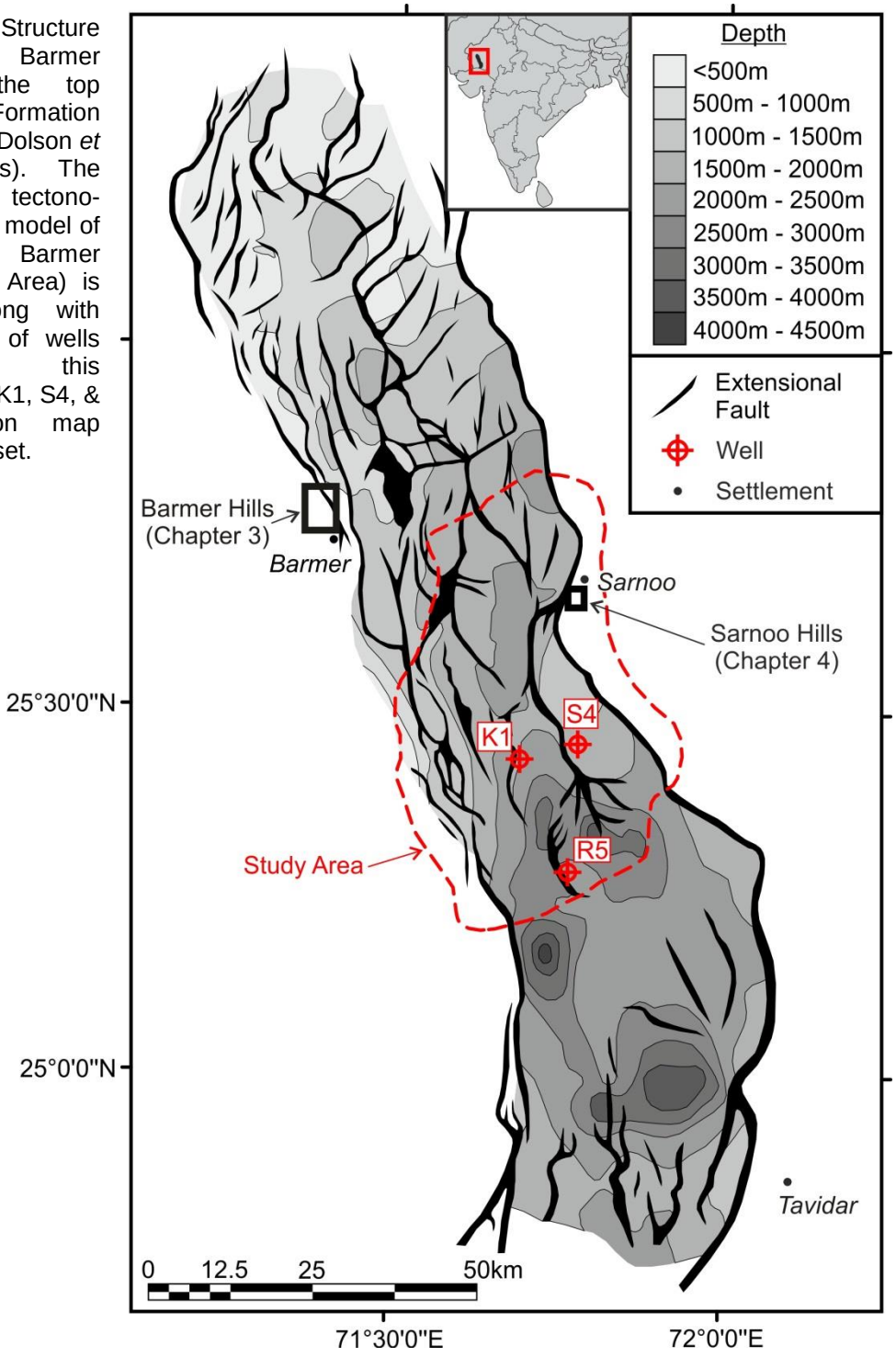

Figure 5.2 – Structure map of the Barmer Basin at the top Fatehgarh Formation horizon (after Dolson *et al.* in press). The extent of the tectono-stratigraphical model of the central Barmer Basin (Study Area) is indicated along with the locations of wells used in this investigation (K1, S4, & R5). Location map within India inset.

As exposed at outcrop, rift-parallel (≈ north-northwest) and rift-oblique (≈ southwest) faults are evident in the subsurface. Subsurface sediment thickness maps highlight activity on southwest-trending (rift-oblique) faults predated activity on north-northwest-trending (rift-parallel) faults. It follows that the northwest-southeast extensional structural regime exposed in the Sarnoo Hills (**Chapter 4**) predated the northeast-southwest Paleogene Barmer Basin rift event, as exposed in the Barmer Hills (**Chapter 3**). Further to this, a rift-oblique (southwest-trending) fault that was active

during early oblique (≈ northwest-southeast) rifting was incorporated into the evolving eastern rift margin fault system, and formed an atypical eastern rift-margin accommodation structure not predicted by conventional accommodation zone, transfer zone, or extensional structural models. The findings demonstrate that northwest-southeast extensional deformation (Sarnoo Hills; **Chapter 4**) predated the northeast-southwest orientated Barmer Basin rift event (Barmer Hills; **Chapter 3**), indicate that structural inheritance provides a robust explanation of structural complications and rift-oblique faults variably imaged throughout the Barmer Basin subsurface, and illustrate one further example of how extensional fault systems may evolve during rifting within a changing stress-field.

5.1 Dataset

The study area encompasses 1850 km^2 in the centre of the Barmer Basin, and is covered by a network of two-dimensional seismic surveys that image a total horizontal distance of approximately 1500 km within the study area (**Figure 5.3**). Data quality varies, but is generally moderate to poor (**Figure 5.3b**), and contains frequencies up to 60 Hz. Seismic sections are presented with reverse (international) polarity whereby a downward increase in acoustic impedance, that is a positive reflection coefficient, is represented by a trough (blue reflection). Each seismic survey is pre-stack time-migrated with the survey comprising in-lines (≈ rift-parallel) bearing 151° and cross-lines (≈ rift-perpendicular) bearing 061°. Spacing between adjacent seismic lines varies between 1 km and 2.5 km. The vertical axis of the seismic surveys is in two-way travel time (TWT) with maximum and minimum values of 202 ms and -6000 ms respectively.

Average interval velocity logs from three exploration wells situated within the study area (K1, R5, and S4) were utilised in conjunction with two-dimensional seismic data (**Figure 5.3**). Well-logs are presented in true vertical depth (TVD), and penetrate the entire sedimentary succession within the rift. Important lithostratigraphical boundaries interpreted from well-data, with a vertical axis in two-way travel time (TWT) to correlate with seismic data, were used to aid horizon interpretations within the deeper sedimentary succession. No biostratigraphical or similar age data were available for these, or any other wells throughout the rift, and the ages of lithostratigraphical boundaries are poorly constrained.

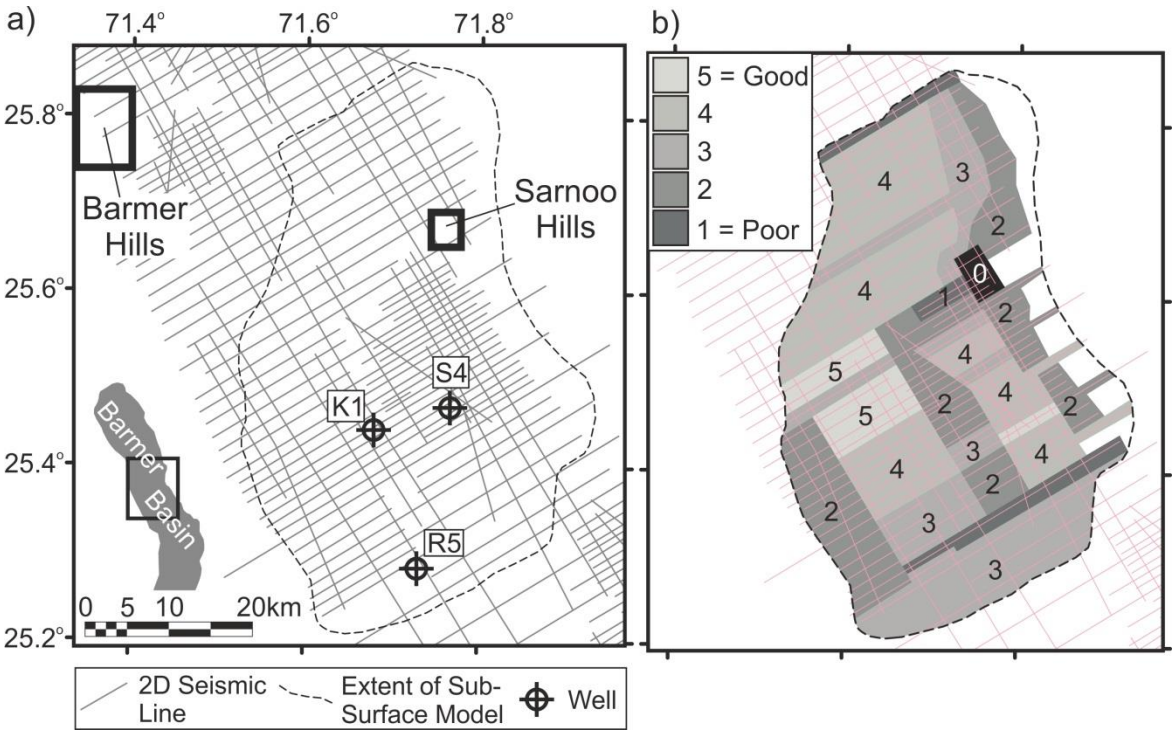

Figure 5.3 – Subsurface data set; **(a)** two-dimensional seismic data (location map inset). The locations of fieldwork, the Barmer and Sarnoo hills, are also shown; **(b)** approximate seismic data quality. 1 = poor quality, 5 = good quality (key to colours shown inset).

5.2 Methodology

5.2.1 Seismic interpretation

Eight poorly age-constrained, syn-rift seismic horizons, including the pre-rift unconformity, were interpreted throughout the study area in conjunction with mapping of the subsurface fault network (**Figure 5.4**; seismic interpretation was conducted using Schlumberger Information Systems Petrel software package). Techniques such as flattening and seismic attribute (e.g. envelope amplitude) analysis aided the interpretation process. The shallowest four horizons (chronostratigraphical horizons on **Figure 5.4**) were interpreted based upon seismic character alone, and followed bright, consistent seismic reflectors within shallow deposits throughout the study area. Correlation of seismic reflectors with key lithostratigraphical boundaries constrained from wells aided interpretation of the four deepest horizons (lithostratigraphical horizons on **Figure 5.4**). Excluding the uppermost horizon (Yellow), all stratigraphical intervals are situated within the rift, and negligible deposition is preserved on the rift margins. Syn-rift intervals are characterised by wedged-shaped packages of seismic reflectors, and thickness changes across active faulting.

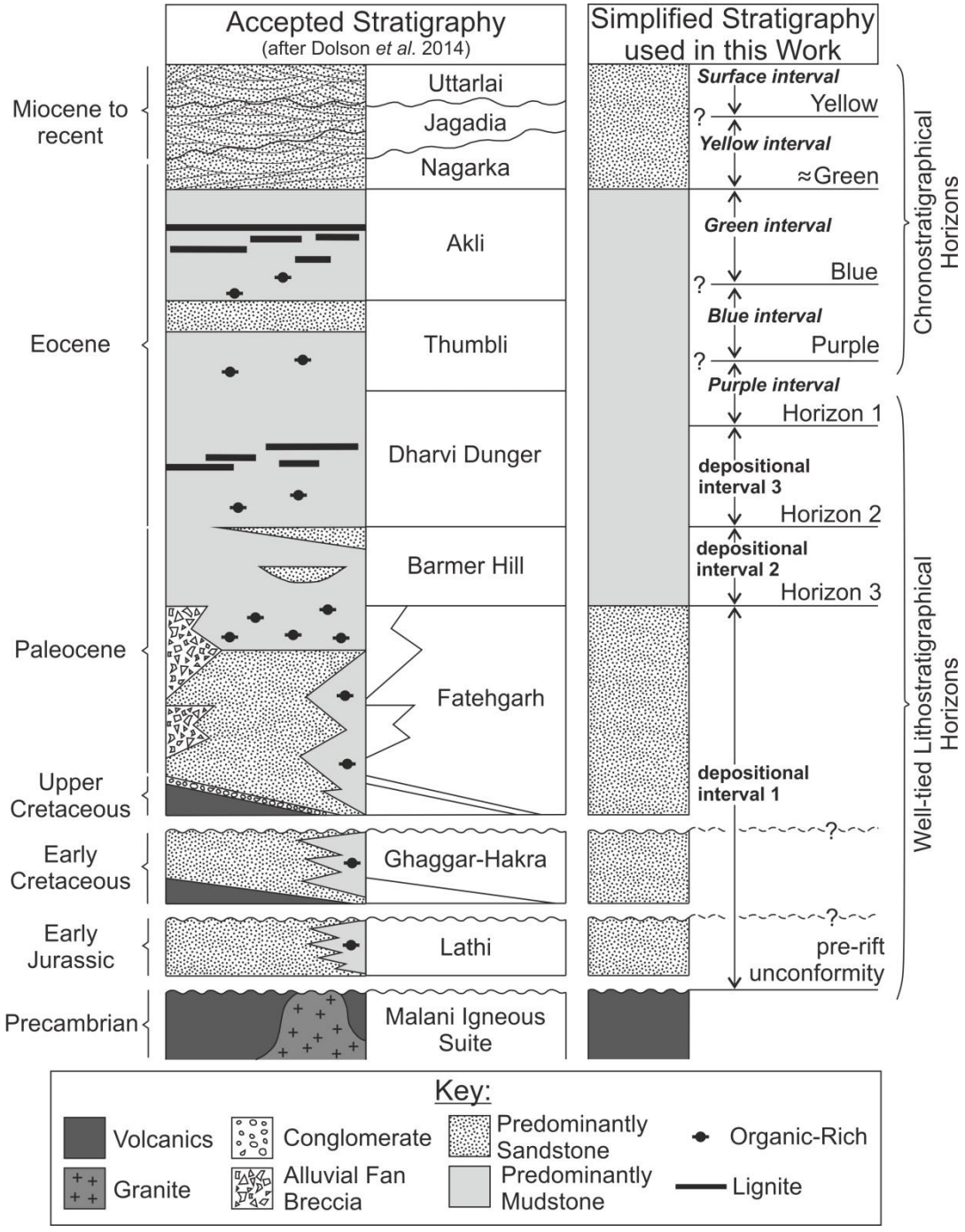

Figure 5.4 – Stratigraphical comparison between the currently accepted stratigraphy of the Barmer Basin (Dolson *et al.* in press) and the chronostratigraphical and lithostratigraphical horizons used in this study.

5.2.2 Validation of interpretations and structural restoration

Interpretations of three rift-perpendicular seismic sections were interrogated to ensure internal consistency and geometrical plausibility (**Section 4.2.3.2**). Interpreted seismic sections were depth converted and sequentially backstripped, decompacted, structurally restored (two-dimensional cross-sectional area-balanced), and flattened on the uppermost horizon, that is sections were

sequentially restored (all steps were conducted using Midland Valley's Move software package). For restoration purposes interpretations were simplified, and where horizons had been removed by erosion, horizon interpretations were projected to the edge of the cross-section. Exposure of rift-oblique (≈ northwest-southeast) extension in the Sarnoo Hills (**Chapter 4**) indicated that the assumption of plane-strain may not be satisfied on cross-line seismic sections (061°). Hence, restorations are classified as geometrical rather than palinspastic (**Section 4.2.3.2**). The isostatic component of subsidence was not removed during backstripping, namely the flexural response of the lithosphere to extension was not accounted for (flexural backstripping; e.g. Roberts *et al.* 1993; Roberts *et al.* 1997), because: 1) negligible syn-rift deposits were preserved on the rift shoulders that could be used to constrain rift-shoulder palaeo-depth during deformation, and; 2) flexural backstripping is applicable to post-rift successions, which are largely absent in the study area.

5.2.2.1 Depth conversion

The vertical axis of subsurface seismic data is often presented in time, that is the travel time of the seismic signal, and it is common to map stratigraphical horizons and faults in the time domain (Hart 2012). However, horizon and fault interpretations mapped in time should be converted into the depth domain (depth conversion) in order to perform structural restorations (Gibbs 1983; Hart 2012). Two methods of depth conversion are commonly used. The 'average velocity' method correlates known seismic reflectors (in time) with the corresponding feature on borehole data (in depth) to calculate the average velocity from the seismic datum (e.g. surface) to that reflector using:

$$\boldsymbol{v} = \frac{\boldsymbol{d}}{\boldsymbol{t}} \qquad \textit{Equation 5.1}$$

where v = average velocity (m s^{-1}); d = distance (m), and; t = one-way travel time (s). Depth conversion is achieved by combining time-structure maps with average velocity contour maps (Hart 2012). Alternatively, a subsurface velocity model can be constructed by combining horizon interpretations with subsurface interval travel-times at well-locations (using check-shot surveys or sonic logs) or with stacking velocities (Hart 2012). Velocity models are versatile and can include layers of constant velocity, layers with a velocity gradient, a linearly changing velocity structure, or a combination of these.

Upon establishing the velocity gradient for a succession, or for a unit within a succession, the velocity at a particular depth within the unit or succession can be calculated using:

$$V_{(z)} = V_0 + kz \qquad \textit{Equation 5.2}$$

where $V_{(z)}$ = velocity at depth z; V_0 = velocity at the top of the succession or unit; k = rate of change of velocity with depth (empirically defined), and; z = depth.

In order to convert the vertical axis of interpreted seismic sections from two-way travel time (TWT) into depth, as is necessary to perform structural restorations (e.g. Gibbs 1983; Hart 2012), a simple subsurface velocity model was constructed for the study area using average interval velocity logs (**Figure 5.5**; **Table 5.1**). For simplicity, velocities for each stratigraphical interval (**Figure 5.5**) were assumed constant (k = 0 m s^{-1}, **Equation 5.2**).

Horizon	Dominant Rock Type	Velocity at Horizon [V_o (m s^{-1})]				Rate of change of velocity (k)
		K1	R5	S4	Average	
Surface	*Sand*	2300	2300	2000	2200	0
Yellow	*Sand*	2300	2300	2000	2200	0
Green	*Mudstone (Shale)*	2300	2300	2000	2200	0
Blue	*Mudstone (Shale)*	2300	2300	2000	2200	0
Purple	*Mudstone (Shale)*	2300	2300	2000	2200	0
Horizon 1	*Mudstone (Shale)*	2850	2700	2300	2617	0
Horizon 2	*Mudstone (Shale)*	3100	3300	2900	3100	0
Horizon 3	*Sand*	3400	3700	3800	3633	0
pre-rift unconformity	*Malani Igneous Suite*	-	4700	-	4700	0

Table 5.1 – Parameters used to generate simple subsurface velocity model using interval velocities constrained from wells.

5.2.2.2 Backstripping and decompaction

Compaction (due to burial) of sediments deposited during deformation results in syn-deformational changes to surface area and volume (line-length and cross-sectional area in two-dimensions respectively; Sclater & Christie 1980; Gibbs 1983; Schultz-Ela 1992). With the exception of tectonic deformation, compaction may be the largest finite strain during deformation (Gibbs 1983) and it is essential that such strain is accounted for during structural restorations in extensional settings where deposition accompanies deformation.

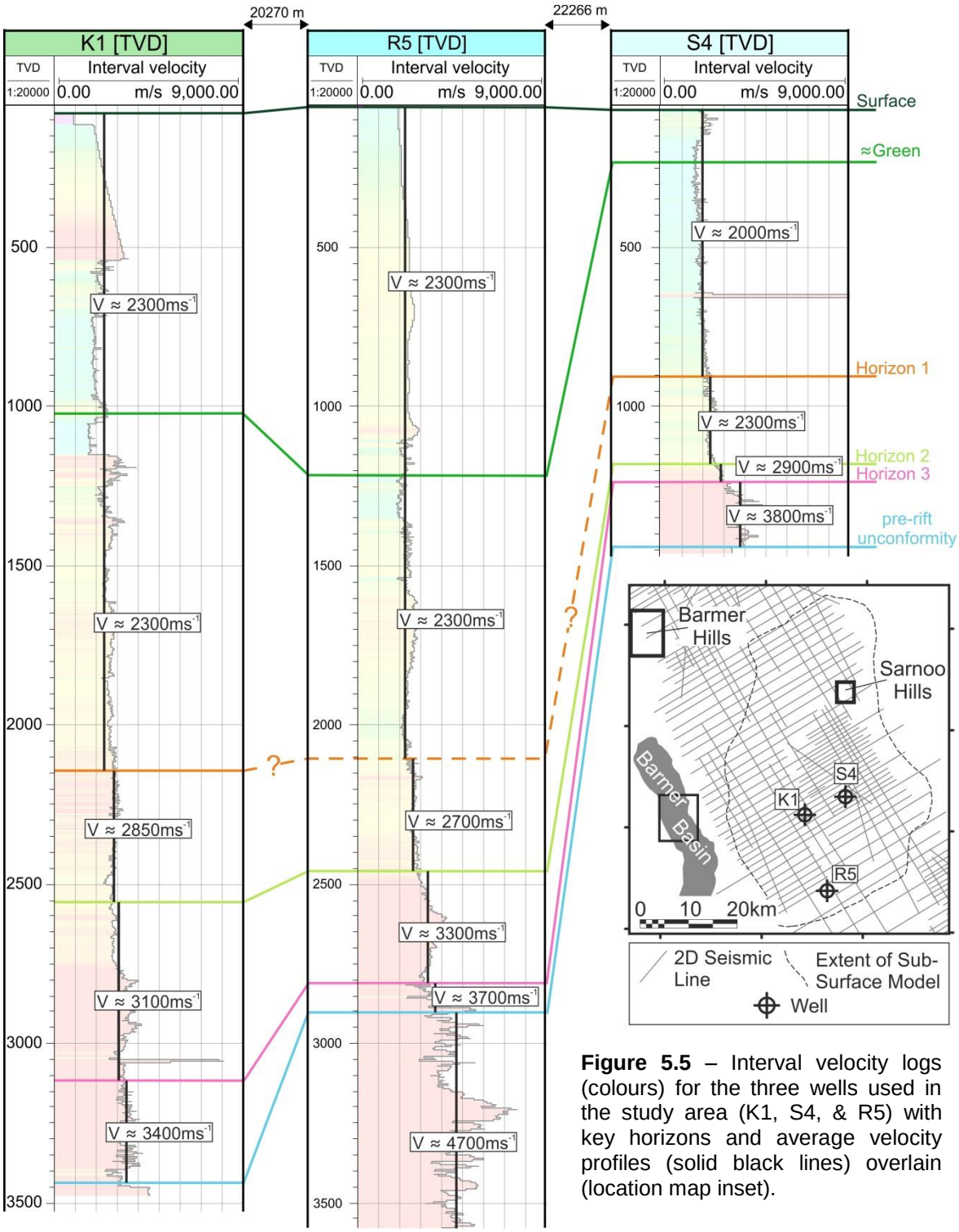

Figure 5.5 – Interval velocity logs (colours) for the three wells used in the study area (K1, S4, & R5) with key horizons and average velocity profiles (solid black lines) overlain (location map inset).

The volume of sedimentary grains (V_s) is assumed constant with burial, so changes to total volume (V_t) of a sediment layer result from changes to pore-space volume (V_p) or porosity:

$$\boldsymbol{V_t = V_S + V_p} \qquad \textit{Equation 5.3}$$

During burial, porosity (pore-space volume) is reduced due to the increased effective (overburden) stress, and porosity variations with depth are calculated using:

$$\emptyset = \emptyset_0 e^{-cy} \qquad \textit{Equation 5.4}$$

where $\emptyset$ = porosity at depth 'y', $\emptyset_0$ = surface porosity, y = depth, and c = coefficient determining the slope of the resultant porosity-depth curve that is estimated from a number of porosity measurements for different lithologies within a particular basin (e.g. Sclater & Christie, 1980; Allen & Allen 2005). Subsequently, thickness or volume loss during burial is accounted for by sequentially stripping away the shallowest stratigraphical interval (backstripping) and adding the appropriate porosity to each underlying stratigraphical interval, i.e. the sediment layer is translated up or down the appropriate porosity depth curve to approximate the reduction in effective (overburden) stress induced by removal of the topmost stratigraphical interval (Allen & Allen 2005).

Such a process is termed decompaction. In the absence of extensive porosity data that are necessary to calculate the coefficient of the porosity-depth curve for each stratigraphical interval (parameter 'c' in **Equation 5.4**), 'standard' parameters and porosity-depth curves defined for specific lithologies in the North Sea (Sclater & Christie 1980) have been used for decompaction in this study (**Table 5.2**). Each stratigraphical interval was broadly categorised as predominantly sandstone or mudstone based upon the currently accepted Barmer Basin stratigraphy (**Figure 5.4**; c.f. Dolson *et al.* in press) and assigned the appropriate decompaction curve (**Table 5.2**).

Horizon	Dominant Rock Type	Surface Porosity (Φ_0)	Depth Coefficient (c) (km^{-1})	Compaction Curve
Surface	*Sand*	0.49	0.27	Sclater & Christie (1980)
Yellow	*Sand*	0.49	0.27	Sclater & Christie (1980)
Green	*Mudstone (Shale)*	0.63	0.51	Sclater & Christie (1980)
Blue	*Mudstone (Shale)*	0.63	0.51	Sclater & Christie (1980)
Purple	*Mudstone (Shale)*	0.63	0.51	Sclater & Christie (1980)
Horizon 1	*Mudstone (Shale)*	0.63	0.51	Sclater & Christie (1980)
Horizon 2	*Mudstone (Shale)*	0.63	0.51	Sclater & Christie (1980)
Horizon 3	*Sand*	0.49	0.27	Sclater & Christie (1980)
pre-rift unconformity	*Malani Igneous Suite*	N/A	N/A	N/A

Table 5.2 – Parameters used for decompaction

5.2.2.3 Structural restoration

Backstripping and decompaction of the uppermost stratigraphical interval exposed the underlying horizon. Any remaining offset of the underlying horizon across faults represented the total subsidence that accumulated during deposition of the overriding stratigraphical interval, that is the combined effects of fault-induced (tectonic) subsidence and subsidence generated by the weight of the sedimentary succession that accumulates within the rift (isostatic component). Upon exposure, total subsidence was restored using a simple-shear move-on-fault restoration algorithm.

Simple shear is the concept that a cross-section deforms as if the cross-section comprised an infinite number of planar slices that were free to slip past one another (**Figure 5.6**; Groshong 2006). The angle of simple shear (α) is defined by a shear angle measured from a reference datum (regional), that is a reference datum that does not change during deformation and is usually horizontal. Simple shear perpendicular (α = 90°) to the datum is termed 'vertical simple shear,' and simple shear orientated at an angle other than perpendicular (α ≠ 90°) to the datum is termed 'inclined simple shear' (**Figure 5.6**). Restoration of extensional structures was conducted using a simple shear restoration algorithm, which models diffuse simple-shear deformation throughout the hanging-wall, and geometrically models the relationship between fault geometry and hanging-wall deformation (**Figure 5.7**). Vertical simple shear restorations comprise the vertical displacement of vertical slices of a cross-section in order to restore a reference horizon to a defined datum (**Figure 5.7a**; Groshong 2006). Similarly, restoration of a cross-section using inclined simple-shear comprises the displacement of oblique slices of a cross-section to restore a reference horizon to a regional datum (**Figure 5.7b**; Groshong 2006). Bed-length (surface area in three-dimensions) is not preserved during simple-shear restorations. However, the technique balances cross-sectional area, and thus balances volume in three-dimensions (**Section 4.2.3.2**).

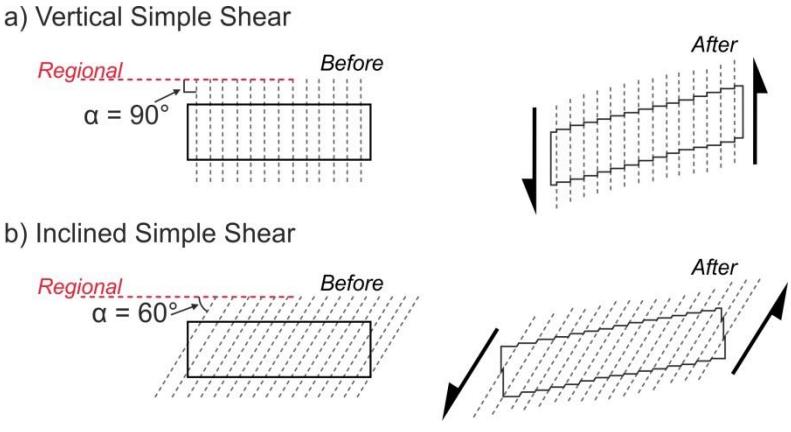

Figure 5.6 – Vertical **(a)** and inclined **(b)** simple shear deformation (after Groshong 2006). Dashed grey lines represent planes of simple shear allowing adjacent 'slices' of the deforming body (black) to slip past one another. α = angle of simple shear.

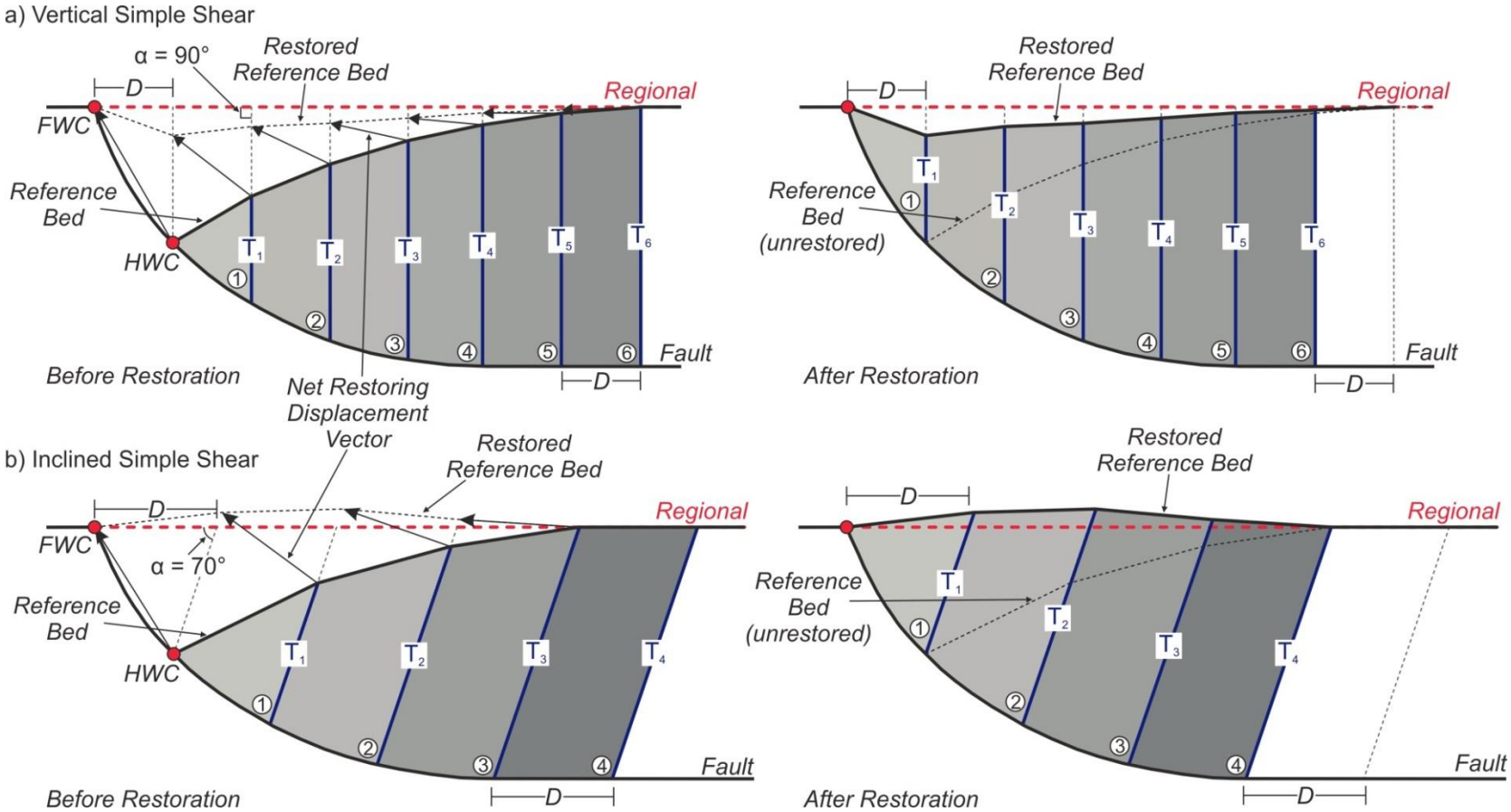

Figure 5.7 – Restoration of a cross-section by vertical **(a)** and inclined **(b)** simple shear of a rollover anticline within the hanging-wall of a listric fault (after Groshong 2006). A deformed reference bed (labelled) is restored to a regional datum (regional), by removing the horizontal component of extension (D) through translating each hanging-wall block (numbered) along the fault plane towards the fault footwall along a restoring displacement vector (arrows). In order to preserve cross-sectional area, the base of each hanging-wall segment must remain in contact with the fault plane, which is facilitated by sliding adjacent hanging-wall blocks past one another along vertical **(a)** or inclined **(b)** shear planes. During deformation the bed thickness (T_1, T_2, T_3, …..) in the direction of shear remains constant. α = shear angle; D = the horizontal component of extension; T_n = thickness of the body being restored in the shear direction; FWC = Footwall cut-off; HWC = Hanging-wall cut-off.

Simple shear restorations are highly sensitive to shear angle (e.g. Buddin *et al.* 1997), which may be highly variable (e.g. Schultz-Ela 1992; Groshong 2006). Due to the lack of constraint on shear angle in the study area, simple-shear restorations were conducted using a universal antithetic simple-shear inclined at 62° to the horizontal, because: 1) a simple shear angle of 62° to the horizontal is similar to the angle of normal sense-shear failure derived for many rock types in laboratory experiments (≈ 60°; e.g. Reches & Lockner 1994), and; 2) the average dip of faults measured at outcrop exposure in the Sarnoo Hills was 61° providing some outcrop-based constraint on the angle of shear within the study area (**Chapter 4**). During sequential restorations, inconsistencies and errors in an interpretation were highlighted where restorations resulted in horizons within the deeper succession restoring with a reverse sense of movement.

5.2.2.4 Flattening

After backstripping, decompacting, and structurally restoring each stratigraphical interval, the section was flattened to the uppermost horizon using vertical simple shear (two-dimensional cross-sectional area balanced; **Figure 5.8**). Assuming depositional horizontality, this returns the section to the geometry at the time of deposition.

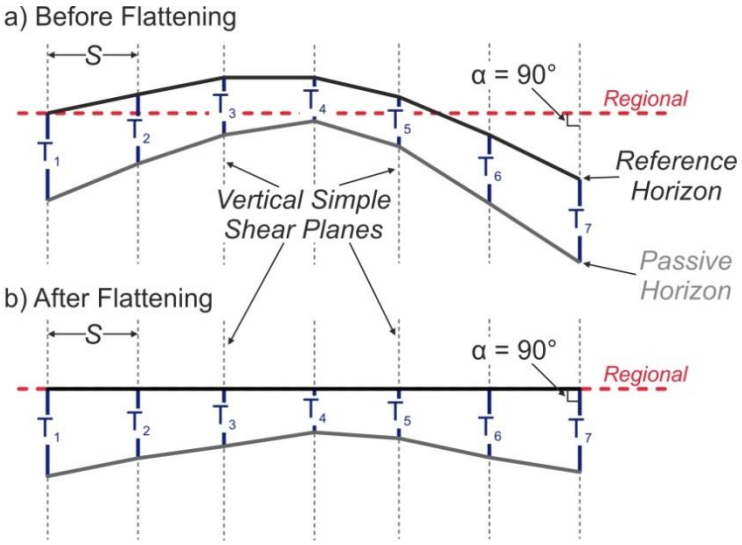

Figure 5.8 – Flattening of a non-planar reference horizon to a horizontal datum (regional) using vertical simple shear (after Groshong 2006). Bed thickness (T_1, T_2, T_3, …..) remains constant during flattening preserving cross-sectional area, but not bed-length. S = arbitrary spacing between shear planes; α = shear angle.

5.2.3 Three-dimensional model of the central Barmer Basin

Stratigraphical horizon and fault interpretations, mapped throughout the study area on two-dimensional seismic sections, were used to construct a three-dimensional tectono-stratigraphical model of the central Barmer Basin. Surfaces (horizons and faults) were gridded using a convergent gridding algorithm. A dislocation between deep and shallow faulting in the study area necessitated

separate fault models. However, because this investigation focused on early-stage rift evolution, a model was constructed for the three earliest stratigraphical intervals only (depositional intervals 1 to 3; **Figure 5.4**).

Fault interpretations on adjacent seismic lines were connected to produce realistic fault geometries and displacement profiles (c.f. **Section 2.1**). The spacing between seismic sections did not allow segmentation of the fault system into individual fault segments, hence, faults have been connected into through-going fault systems. For simplicity, rift-margin faults and the pre-rift unconformity in the rift-margin footwall were projected to surface due to the lack of correlateable deposits on the rift-shoulders. Stratigraphical horizon interpretations were pre-processed prior to gridding by generating and manipulating a dense three-dimensional point cloud. This allowed the input data to be quality controlled and for removal of any erroneous points or gridding artefacts. During gridding within the model, further processing of the input data comprised a deleting of data within a symmetrical zone either side of a fault (step-back distance). Subsequently, the horizon was extrapolated (projected) back onto the fault plane to generate the hanging-wall and footwall cut-offs. This removed interpretation uncertainties in the zones immediately adjacent to faults. Globally, a 'step-back' distance of 500 m produced the best results with the least amount of input data deleted. A step-back distance of 500 m resulted in the deletion of all input data where faults were situated within 1000 m of each other. However, in the only section of the model where this occurred, the artificial result simplified structural complexities and satisfactorily re-created the desired structure.

5.2.4 Model validation

Subsequent to construction of the three-dimensional tectono-stratigraphical model of the central Barmer Basin, the model was interrogated to ensure internal consistency and geometrical plausibility (all steps were conducted using Midland Valley's Move software package). Three-dimensional models can be restored and geometrically validated in map-view by conducting a jigsaw-fit restoration (e.g. Rouby *et al.* 1996; Williams *et al.* 1997; Buddin *et al.* 1997). The main aim of a jigsaw fit restoration is to reconstruct the undeformed, map-view state of an interpreted seismic horizon, which is dissected by an extensional fault network (Rouby *et al.* 1996). Fault heave maps, namely the horizontal component of extension, are generated by vertical projection of the hanging-wall and footwall cut-offs at the deformed horizon onto a horizontal plane, that is the

horizon is flattened using vertical simple shear (**Figure 5.8**; Rouby *et al.* 1996). Jigsaw fit restorations rely on three main assumptions (Rouby *et al.* 1996): 1) the deformed horizon is divided into distinct, fault-bounded blocks; 2) fault blocks are rigid or deform internally by vertical simple shear, and; 3) map-view restorations do not restore any rotational deformation, such as folding or fault-block tilting. In order to perform a jigsaw-fit restoration fault heave maps should be modified to generate a fault heave map comprising fault blocks completely surrounded by faults (**Figure 5.9**; Rouby *et al.* 1996). Subsequently, fault blocks are translated in map view to remove the horizontal component of extension between adjacent fault blocks and restore the horizon to the undeformed state (**Figure 5.9**). Gaps and overlaps remaining after performing a jigsaw fit restoration indicate inconsistencies in the model (misfit; **Figure 5.9d**) and are quantified by determining the misfit area (m^2).

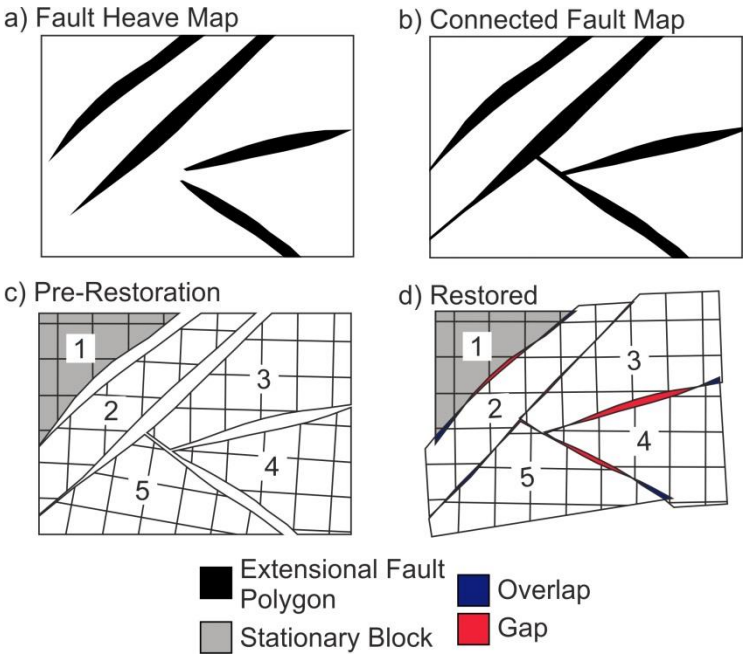

Figure 5.9 – Map view jigsaw-fit restoration of a horizon dissected by extensional faulting (after Rouby *et al.* 1996). A fault heave map **(a)** is modified by extrapolating fault traces to form a connected fault map defining fault blocks completely surrounded by faults **(b)**. Fault blocks are numbered and a stationary bock is defined **(c)** with the map-view restoration achieved by packing fault blocks against the stationary block **(d)**. Gaps (red) and overlaps (blue) remaining after restoration indicates inconsistencies in the model (misfit).

For restoration purposes, the fault network in the three-dimensional model of the central Barmer Basin was simplified to generate a connected fault heave map, and the model was depth converted using the simple velocity model constructed for the study area from interval velocity logs (**Figure 5.5; Table 5.1**). The entire sedimentary succession was sequentially backstripped and decompacted, and the exposed pre-rift unconformity was flattened using vertical simple shear prior to performing a map-view jigsaw-fit restoration (e.g. Rouby *et al.* 1996; Williams *et al.* 1997; Buddin *et al.* 1997). Flattening the pre-rift unconformity using vertical simple shear does not preserve

three-dimensional surface area. However, the plan (map) view extent of each fault block remained constant and the loss of surface area is minimal for shallow-dipping surfaces. In conjunction with a visual assessment of the jigsaw fit restoration, the change in misfit area between the deformed and undeformed state was calculated to quantify the effectiveness of the restoration.

5.2.5 Stratigraphical analysis

Time-thickness [True Vertical Thickness (TVT) or isochore] maps were generated throughout the study area for the three earliest syn-rift stratigraphical intervals (depositional intervals 1 to 3; **Figure 5.4**). Correlation of stratigraphical horizons used in this study with the currently accepted stratigraphy of the Barmer Basin (**Figure 5.4**) indicate that depositional interval 1 incorporates all deposition between the pre-rift unconformity and Horizon-3 (Top Fatehgarh Formation), including any Mesozoic deposits if present (e.g. Lathi and Ghaggar-Hakra formations; **Figure 5.4**). Depositional intervals 2 and 3 (**Figure 5.4**) were deposited during the early stages of the main Paleogene Barmer Basin rift event. Thickness variations within stratigraphical intervals reflect spatial and temporal changes in accommodation space and/or sedimentation rates, and are often used to examine the spatial and temporal development of faulting (Whipp *et al.* 2014). In conjunction with time-thickness maps of stratigraphical intervals, seismic-stratigraphical geometries, such as wedging packages of hanging-wall reflectors and onlap-relationships between seismic reflectors, provided further insights into the tectono-stratigraphical evolution of the central Barmer Basin.

5.2.6 Fault analysis

In order to investigate cumulative deformation since the onset of extension, palinspastic (extension parallel) fault heave profiles were constructed using hanging-wall and footwall cut-offs at the pre-rift unconformity surface in the three-dimensional model. The horizontal stratigraphical offset of the pre-rift unconformity was measured across each fault in the direction of the extension vector during the main Barmer Basin rift event, namely northeast-southwest in accordance with outcrop exposure in the Barmer Hills (**Chapter 3**). Subsequently, measurements of palinspastic fault heave were plotted against a universal axis that paralleled the trend of the rift, that is orientated perpendicular to the extension direction, in order to generate inter-fault heave profiles that were aligned in the direction of extension (≈ northeast-southwest). The resultant palinspastic fault heave profiles provided critical insights into strain partitioning during the approximately rift-perpendicular Barmer

Basin rift event. However, it is important to note that; 1) footwall uplift and erosion may have removed an unknown amount of material that is unaccounted for in fault-heave measurements, and; 2) palinspastic fault-heave measurements will overestimate heave on polyphase faults reactivated obliquely during the main Barmer Basin rift event, although the relative profile geometries will remain constant.

5.3 Structural framework of the central Barmer Basin

5.3.1 Rift structure

The central Barmer Basin is 30 km wide and up to 5 km deep throughout the study area, with a symmetrical geometry in the south (**Figure 5.10**), a structurally complex central region (**Figure 5.11**), and an asymmetrical geometry in the north (deepening to the east; **Figure 5.12**). In the southeast of the study area, a 'terrace-like' feature that is up to 10 km wide and buried beneath 1500 m to 2500 m of syn-rift sediments is situated adjacent to the eastern rift margin fault system (**Figure 5.11**). The terrace dips to the south-southeast, displays minor faulting, and is overlain by a condensed sedimentary succession at the northern end of the terrace that thickens towards the south-southeast (**Figure 5.13**). Northwards towards the structurally complex central section of the study area, the terrace becomes increasingly narrow, westerly-dipping, and eventually heavily faulted such that the terrace becomes more attenuated (**Figure 5.11**). In some areas of the study area, the earliest syn-rift deposits (depositional interval 1) display pronounced 'wedging' towards rift-oblique rift-basement faulting (**Figures 5.14 & 5.15**), with occasional pronounced progradational sedimentary packages observed (**Figures 5.15c & d**), and are imaged buried beneath younger, tabular stratigraphical intervals. Variable post-extensional processes are also evident, with thermal subsidence packages in the south (**Figure 5.10**), and erosional truncation of the upper horizons in the west to northwest of the study area (**Figures 5.11 & 5.12**). Negligible syn-rift deposition is preserved on the rift-shoulders.

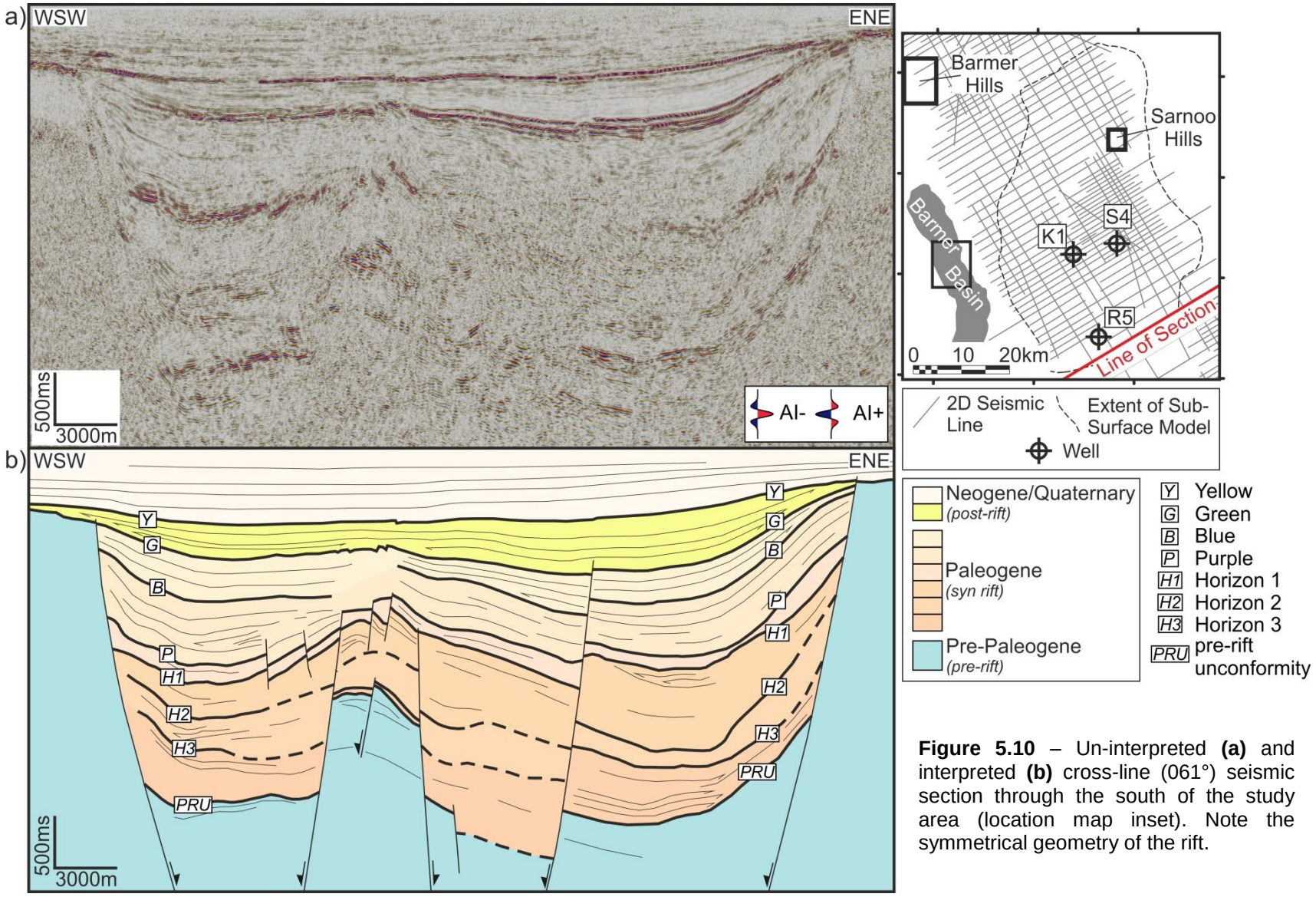

Figure 5.10 – Un-interpreted **(a)** and interpreted **(b)** cross-line (061°) seismic section through the south of the study area (location map inset). Note the symmetrical geometry of the rift.

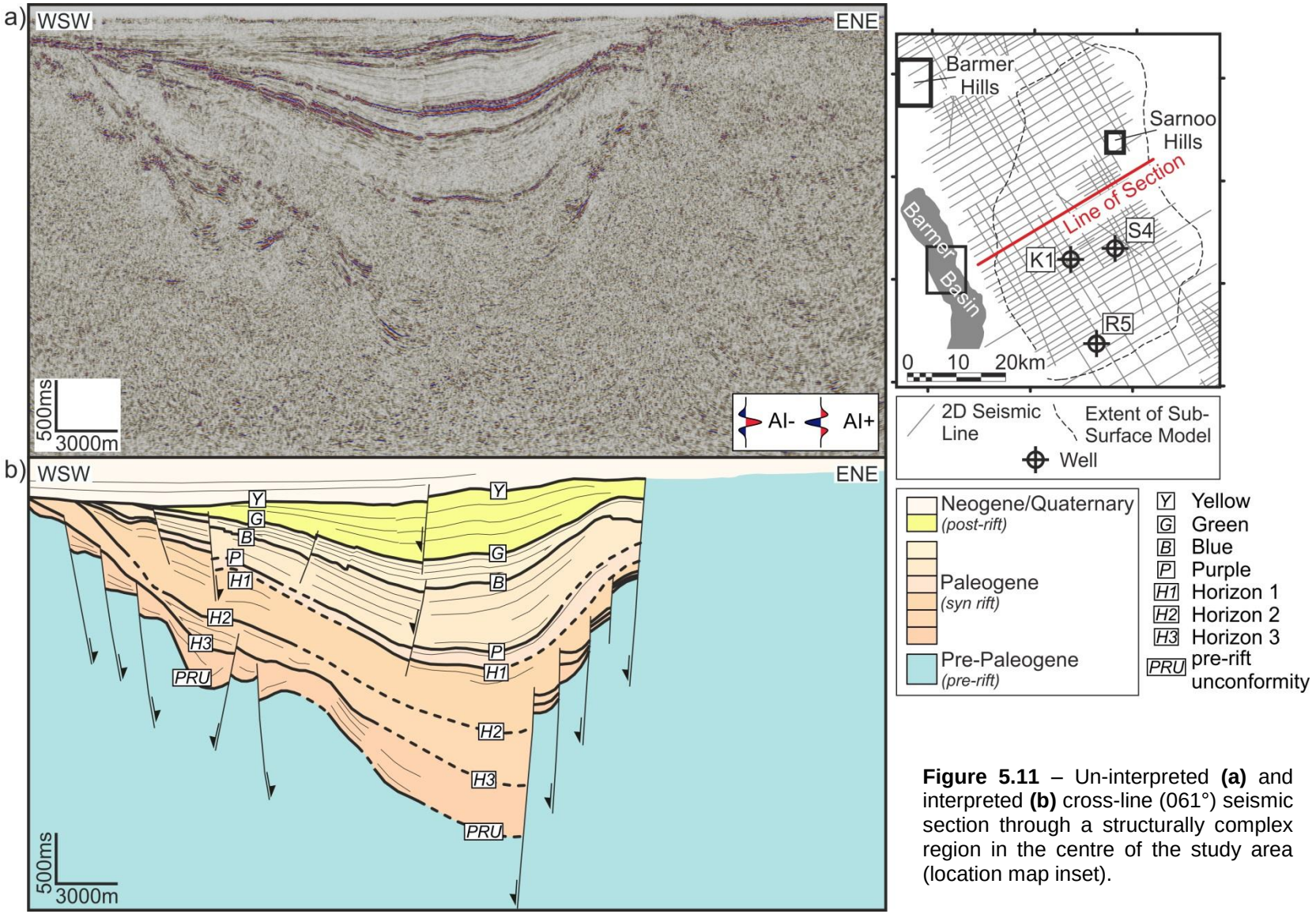

Figure 5.11 – Un-interpreted **(a)** and interpreted **(b)** cross-line (061°) seismic section through a structurally complex region in the centre of the study area (location map inset).

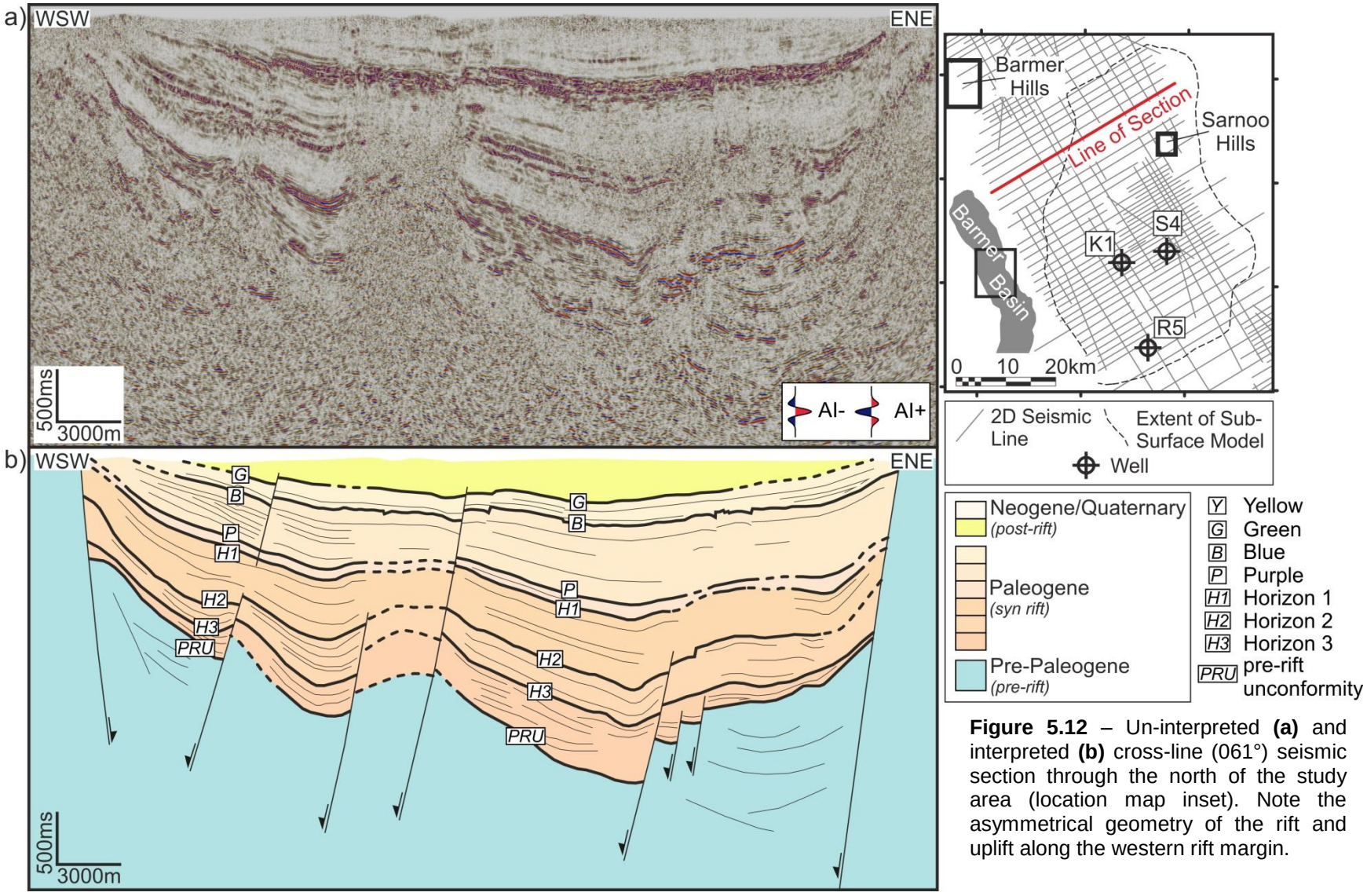

Figure 5.12 – Un-interpreted **(a)** and interpreted **(b)** cross-line (061°) seismic section through the north of the study area (location map inset). Note the asymmetrical geometry of the rift and uplift along the western rift margin.

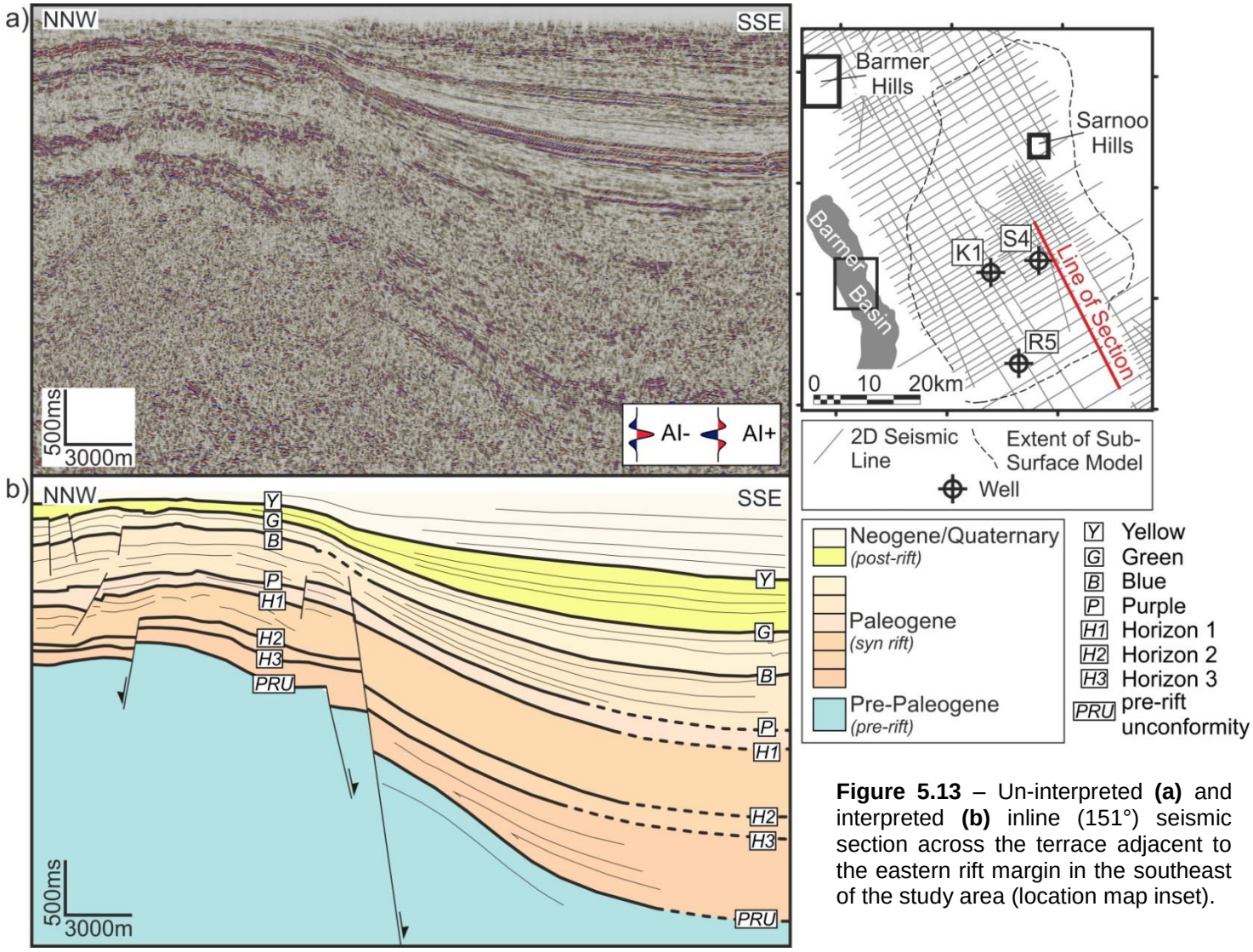

Figure 5.13 – Un-interpreted **(a)** and interpreted **(b)** inline (151°) seismic section across the terrace adjacent to the eastern rift margin in the southeast of the study area (location map inset).

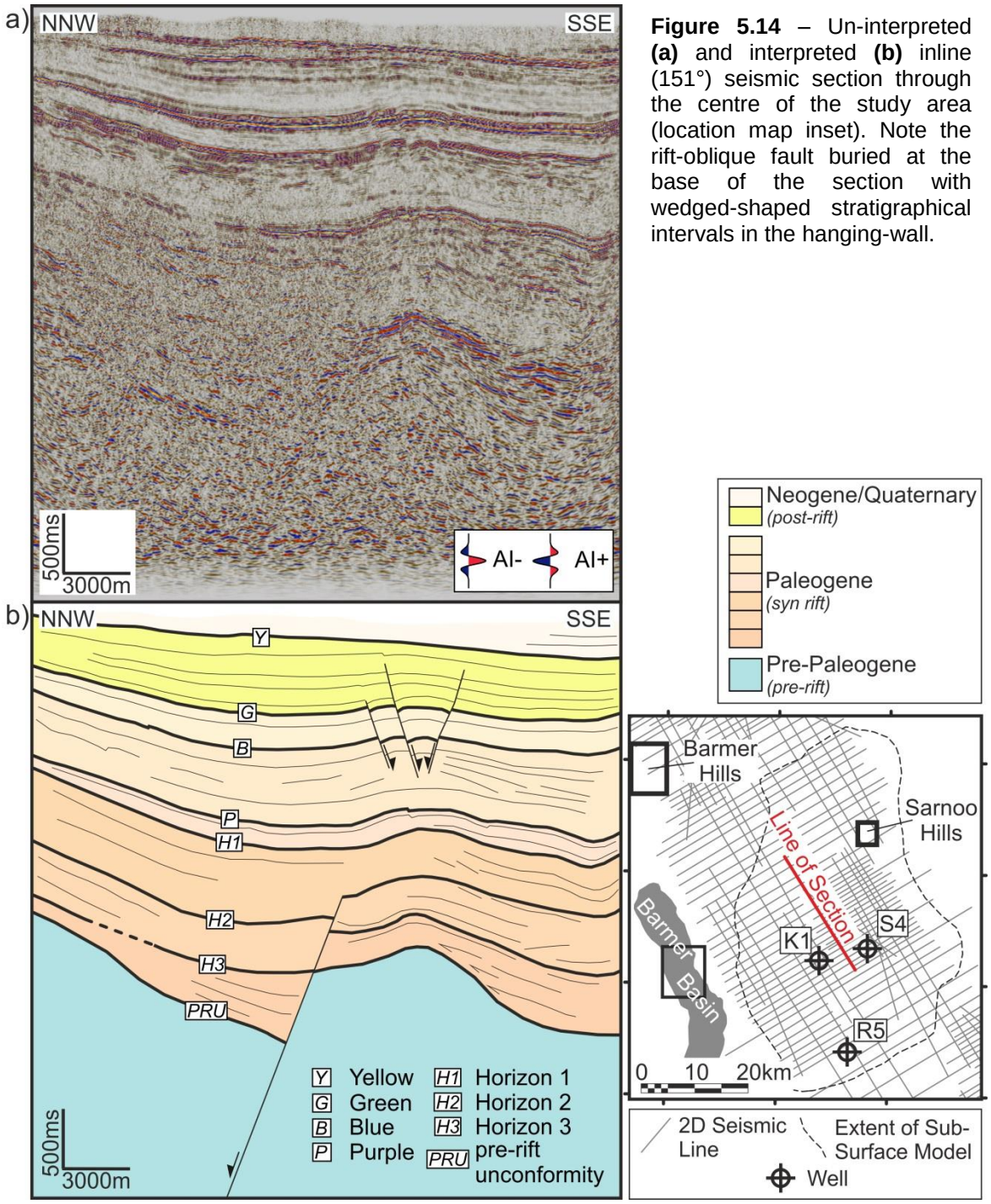

Figure 5.14 – Un-interpreted **(a)** and interpreted **(b)** inline (151°) seismic section through the centre of the study area (location map inset). Note the rift-oblique fault buried at the base of the section with wedged-shaped stratigraphical intervals in the hanging-wall.

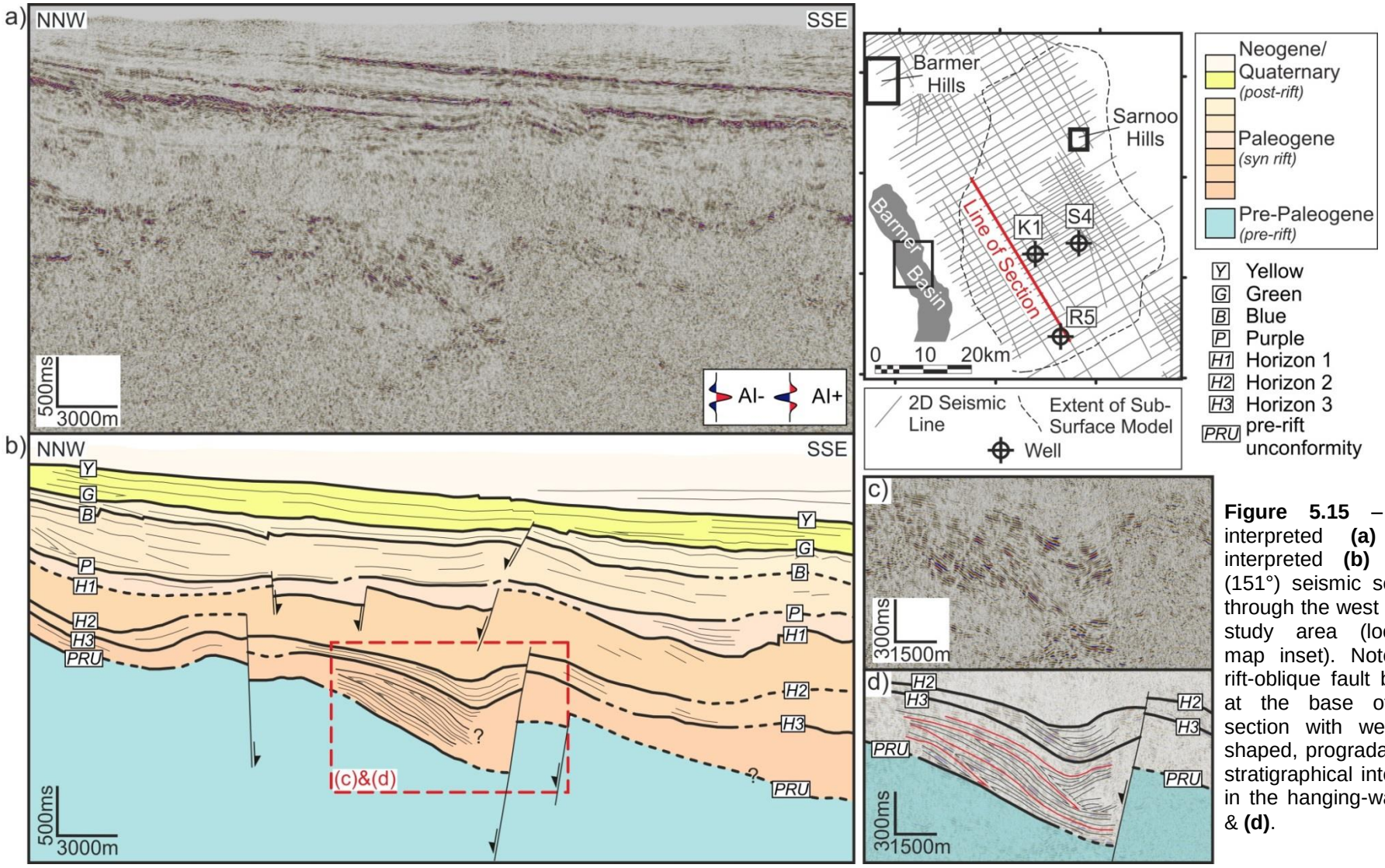

Figure 5.15 – Un-interpreted **(a)** and interpreted **(b)** inline (151°) seismic section through the west of the study area (location map inset). Note the rift-oblique fault buried at the base of the section with wedged-shaped, progradational stratigraphical intervals in the hanging-wall **(c)** & **(d)**.

5.3.2 Two-dimensional sequential restorations

All three sequentially restored cross-line (061°) seismic sections encountered few problems (**Figures 5.16, 5.17, & 5.18**), validating that the interpretations are internally consistent and geometrically plausible. Subsidence in the south of the study area was uniform across the rift throughout rift evolution (**Figure 5.16**). The early rift comprised a large, mid-rift horst block and two adjacent sub-basins (**Figure 5.16h**) that were buried during depositional interval 2 (**Figure 5.16g**), and became inactive during depositional interval 3 (**Figure 5.16f**). Subsequent to burial of the mid-rift horst block, deformation was predominantly accommodated on the rift-margin fault systems (**Figures 5.16a-e**).

In the centre of the study area (**Figure 5.17**), early rift geometry was strongly asymmetrical, and the rift margin was situated along the western edge of the terrace adjacent to the eastern rift margin (**Figure 5.17j**). The terrace became dissected by a series of westerly-dipping normal faults and was rotated towards the centre of the rift, such that the terrace rotated basinwards during depositional interval 3 (**Figures 5.17i-h**). Subsequently, deformation was accommodated on the eastern rift margin fault system (**Figures 5.17d-g**) signifying a 5 km to 10 km migration of deformation eastwards into the rift-margin footwall (footwall degradation).

In the north of the study area significant mid-rift rift-basement-faulting is largely absent (**Figure 5.18**). The earliest syn-rift deposits (depositional interval 1) formed a broad elliptical sedimentary package that was largely devoid of faulting (**Figure 5.18i**). Fault-controlled subsidence initiated along the rift-margins during depositional interval 2. Subsequently, the rift-margin faults accommodated extension and remained active for the duration of rifting (**Figures 5.18c-h**).

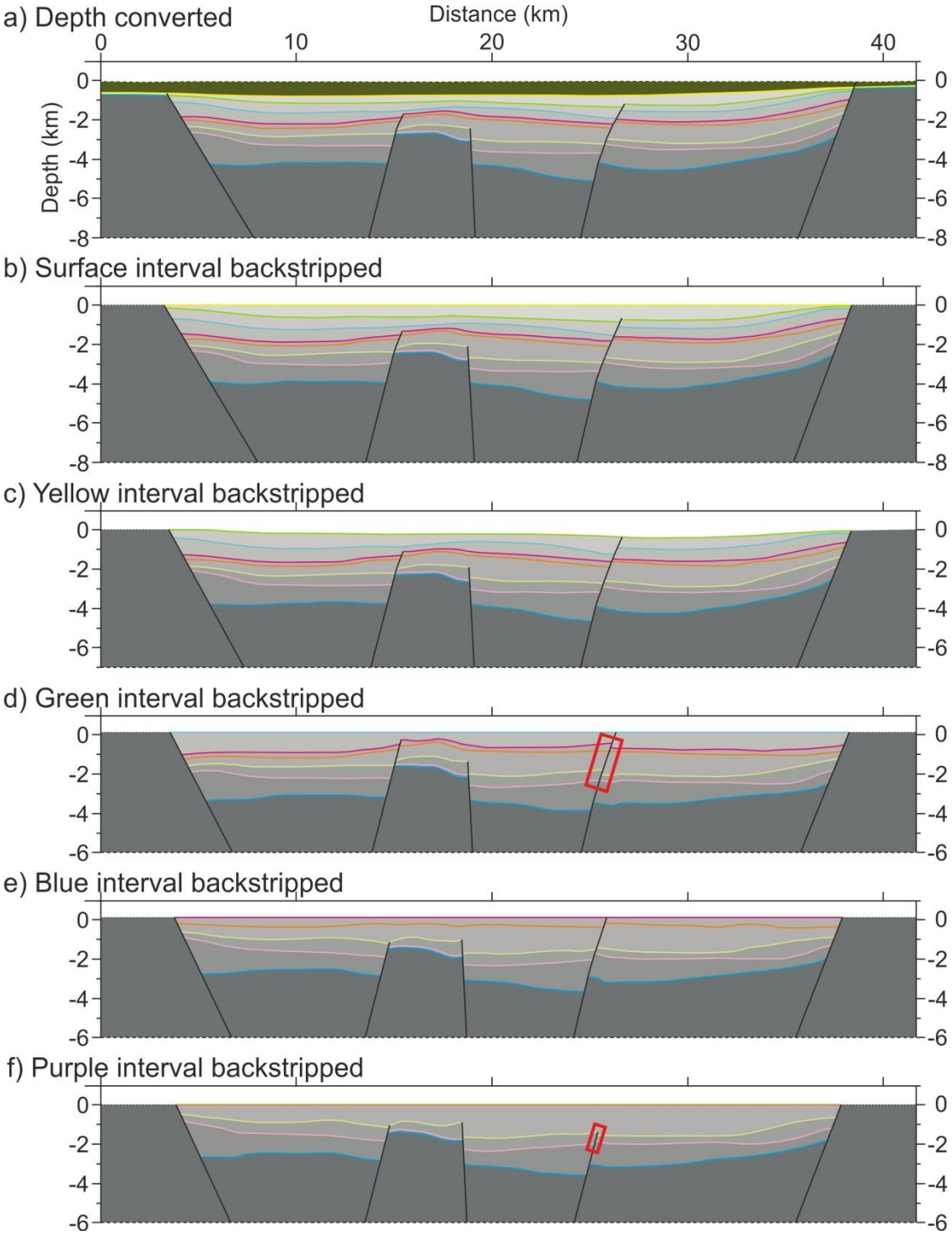

Figure 5.16 – Sequentially decompacted, backstripped, and move-on-fault restored cross-line (061°) seismic depth-section through the south of the study area (location map inset). See **figure 5.10** for interpreted seismic section.

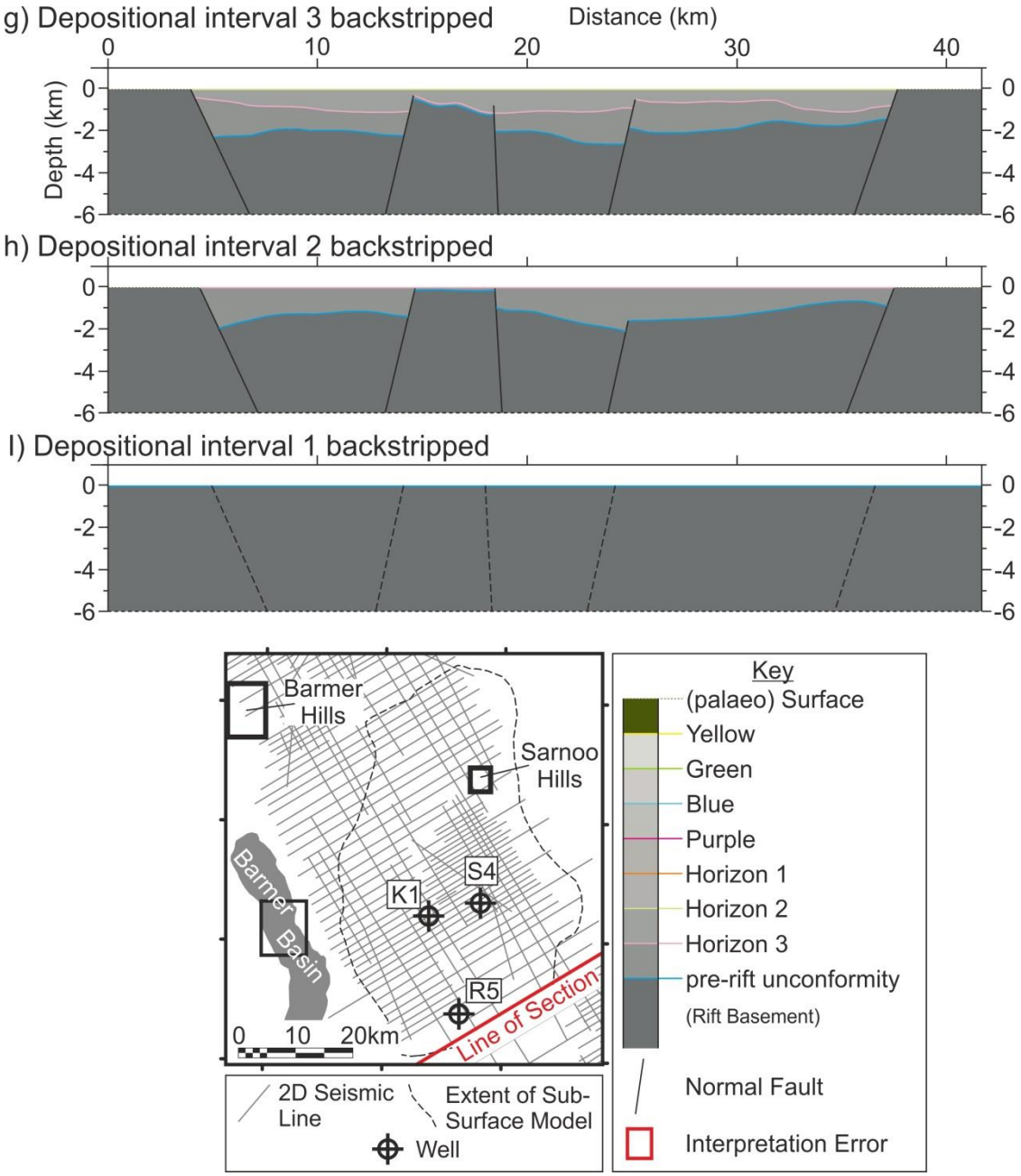

Figure 5.16 cont.

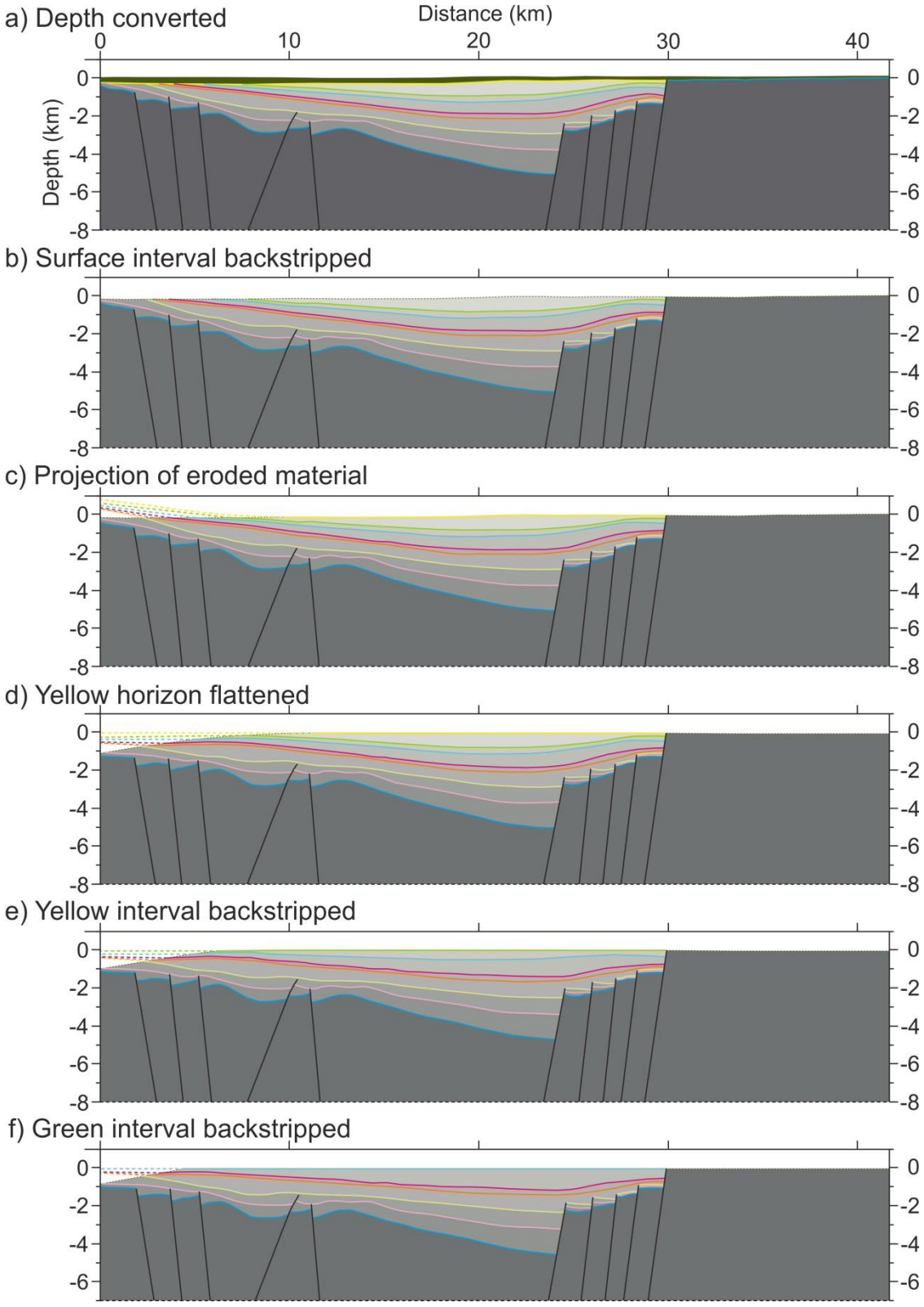

Figure 5.17 - Sequentially decompacted, backstripped, and move-on-fault restored cross-line (061°) seismic depth-section through the structurally complex centre of the study area (location map inset). See **figure 5.11** for interpreted seismic section.

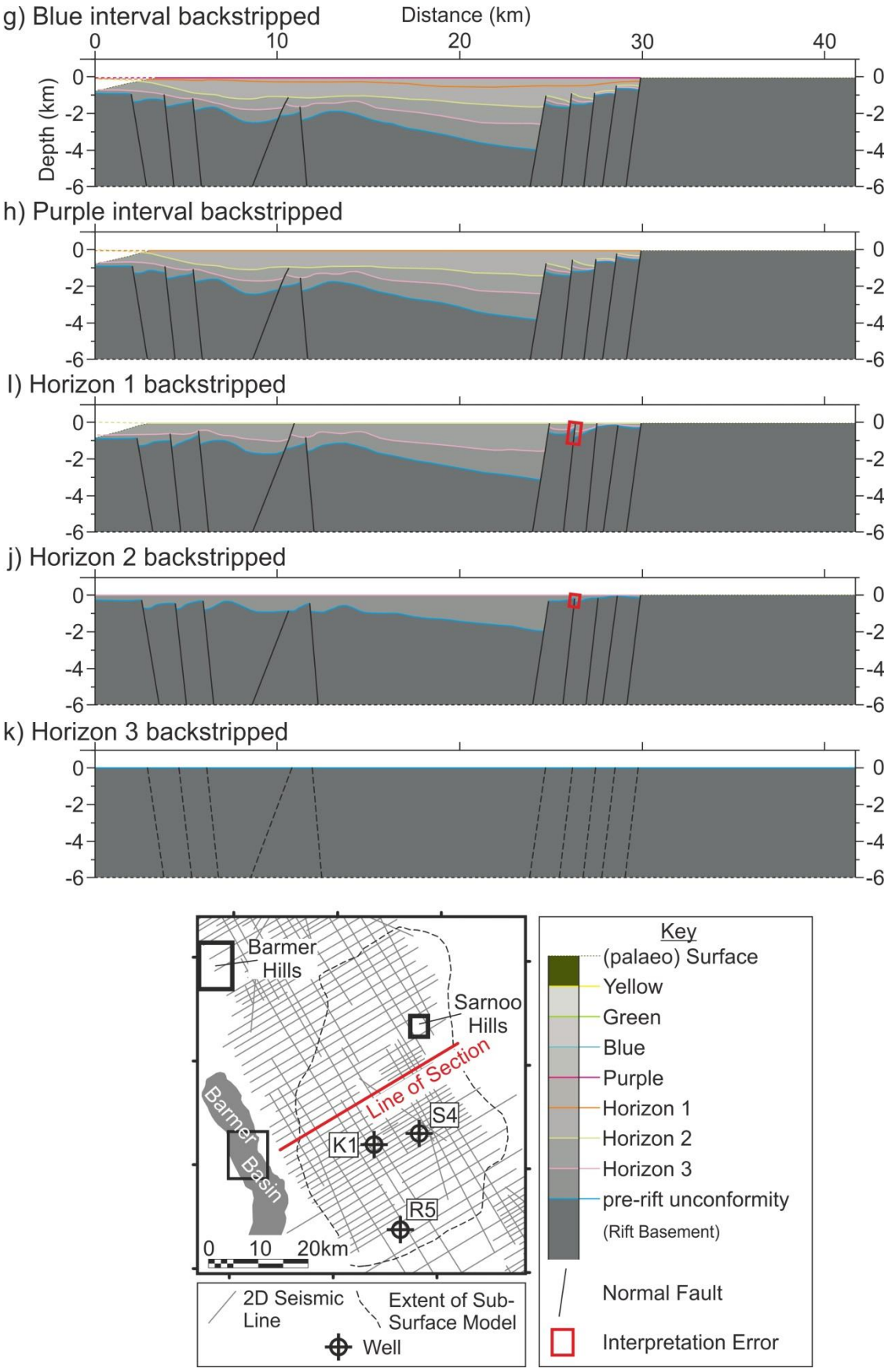

Figure 5.17 cont.

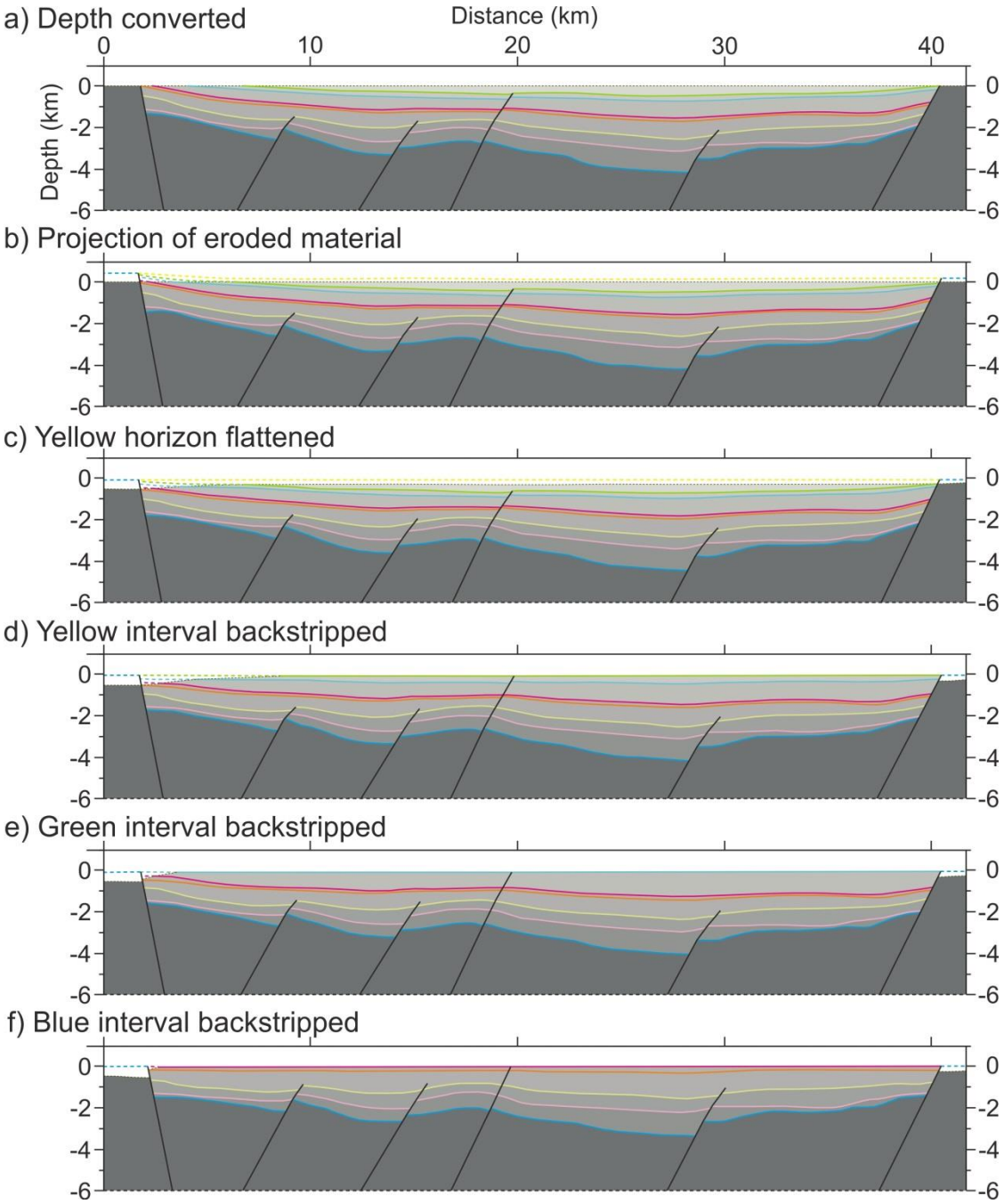

Figure 5.18 - Sequentially decompacted, backstripped, and move-on-fault restored cross-line (061°) seismic depth-section through the north of the study area (location map inset). See **figure 5.12** for interpreted seismic section.

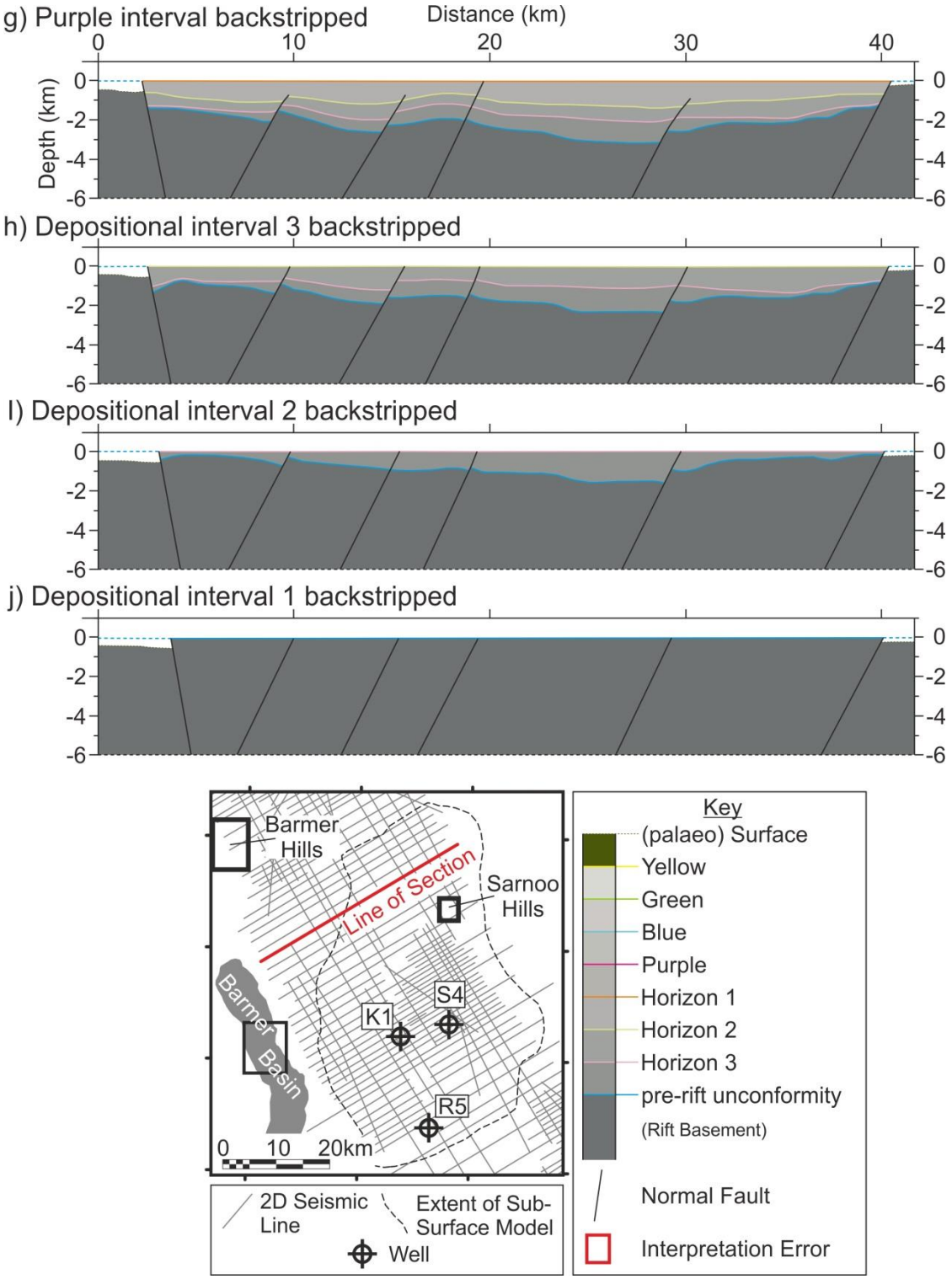

Figure 5.18 cont.

5.3.3 Seismic stratigraphical relationships

Above the terrace adjacent to the eastern rift margin in the southeast of the study area, seismic reflectors onlap towards the eastern rift margin within a sedimentary package deposited during depositional interval 3, which displays a wedge-shaped geometry and thickens towards the west, that is thickens basinwards (**Figure 5.19**). Sequential restoration (**Figure 5.20**) demonstrates an approximately 10 km migration of deformation eastwards into the rift-margin footwall during depositional interval 3, accompanied by a basinwards (westwards) rotation of the intervening terrace (**Figure 5.20f**). This tectono-stratigraphical relationship is similar and temporally equivalent to that observed approximately 5 km to the north (**Figures 5.11 & 5.17h**).

5.3.4 Three-dimensional model

A time-structure map at the pre-rift unconformity illustrates the structure of the Barmer Basin in the study area (**Figure 5.21**). Eastern rift margin fault systems in the north and south of the study area (North Eastern Rift Margin Fault System and South Eastern Rift Margin Fault System) are separated by a major displacement (up to 3000 m), southwest-striking, northeast-dipping, rift-oblique fault (Major Rift-Oblique Fault) situated immediately adjacent to outcrop exposure in the Sarnoo Hills (**Figure 5.21a**). The Major Rift-Oblique Fault coincides with a prominent rightwards-step ('kink') in the eastern rift margin and is extensively splayed towards the southern end of the fault (**Figure 5.21a**). Along the eastern rift margin, two sub-parallel and rift-parallel fault systems accommodated extension, generating terrace-like structures adjacent to the eastern rift margin (Northern Terrace and Southern Terrace; **Figure 5.21**). The Southern Terrace constitutes a significant, southeast-dipping, rift-internal ramp adjacent to the South Eastern Rift Margin Fault System (**Figure 5.21b**). Along the western rift margin, extension was accommodated on a single, rift-parallel fault system (Western Rift Margin Fault System; **Figure 5.21a**).

5.3.5 Three-dimensional restorations: jigsaw fitting

When the entire sedimentary succession was backstripped and decompacted, and the pre-rift unconformity surface flattened, gaps and overlaps (misfits) in the map-view jigsaw fit restoration were negligible throughout the study area (**Figure 5.22**). However, two regions displayed significant misfits coincident with areas of linkage between a rift-oblique fault and a rift-parallel fault (1' & '2' on **Figure 5.22h**).

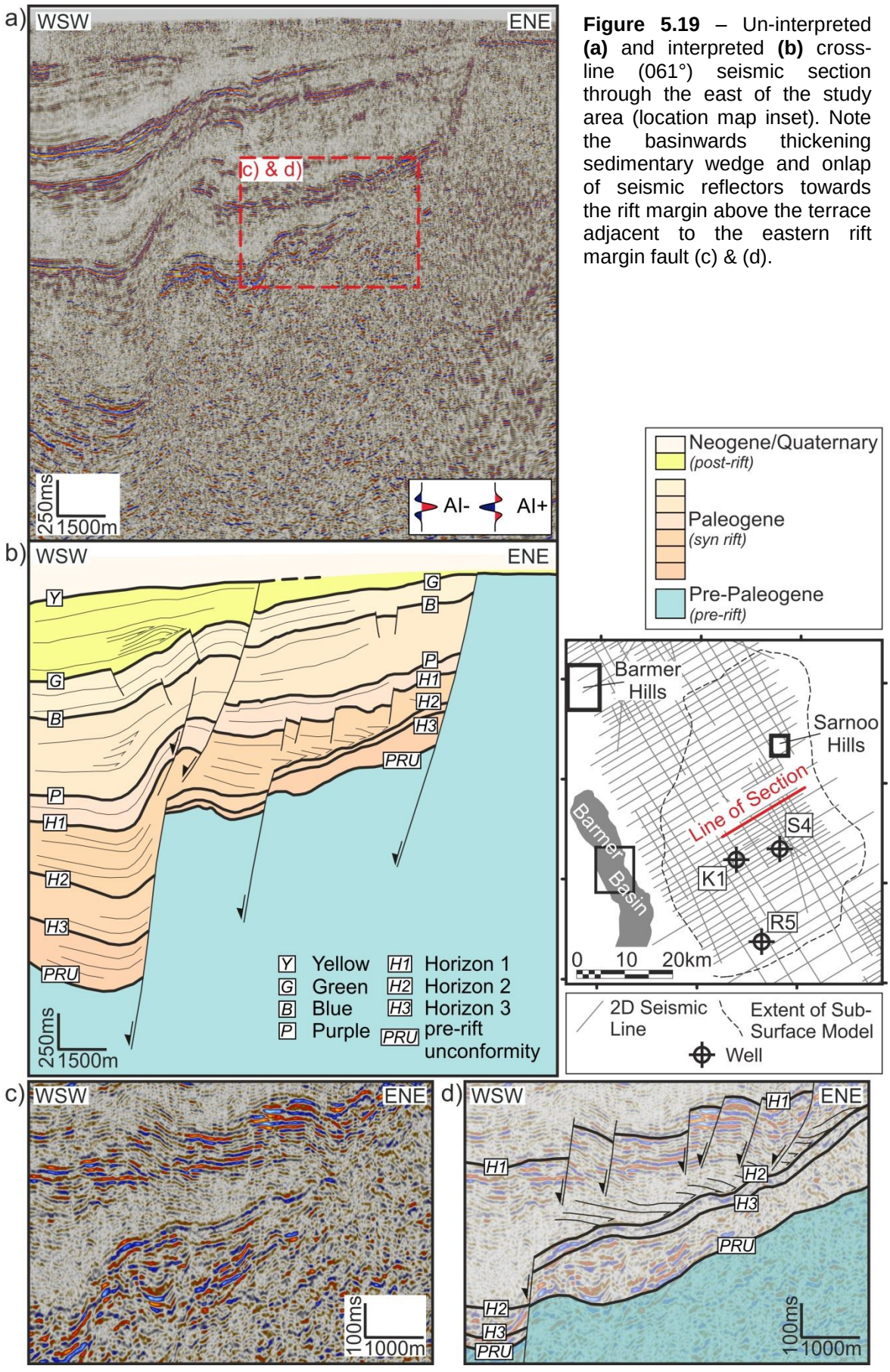

Figure 5.19 – Un-interpreted **(a)** and interpreted **(b)** cross-line (061°) seismic section through the east of the study area (location map inset). Note the basinwards thickening sedimentary wedge and onlap of seismic reflectors towards the rift margin above the terrace adjacent to the eastern rift margin fault (c) & (d).

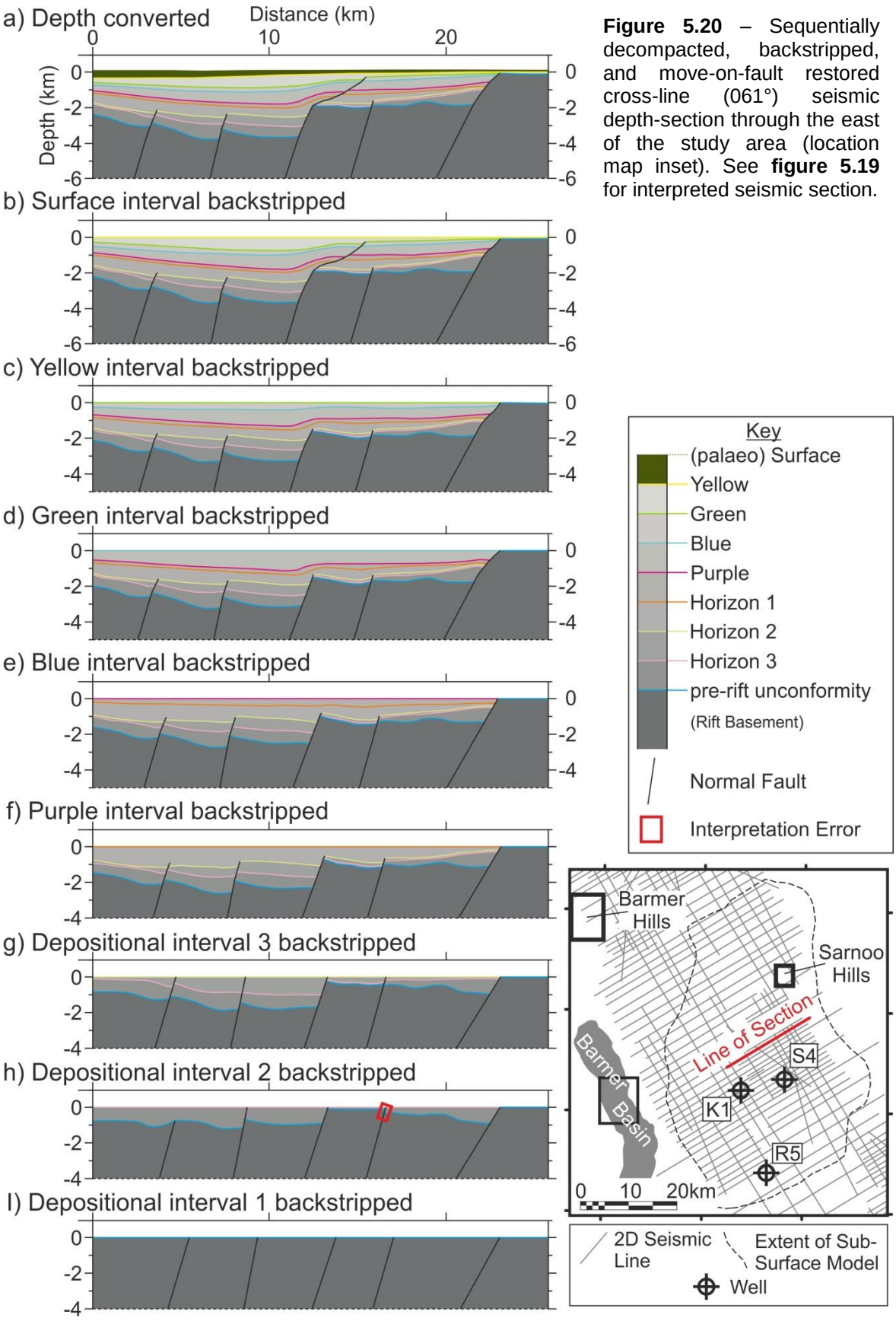

Figure 5.20 – Sequentially decompacted, backstripped, and move-on-fault restored cross-line (061°) seismic depth-section through the east of the study area (location map inset). See **figure 5.19** for interpreted seismic section.

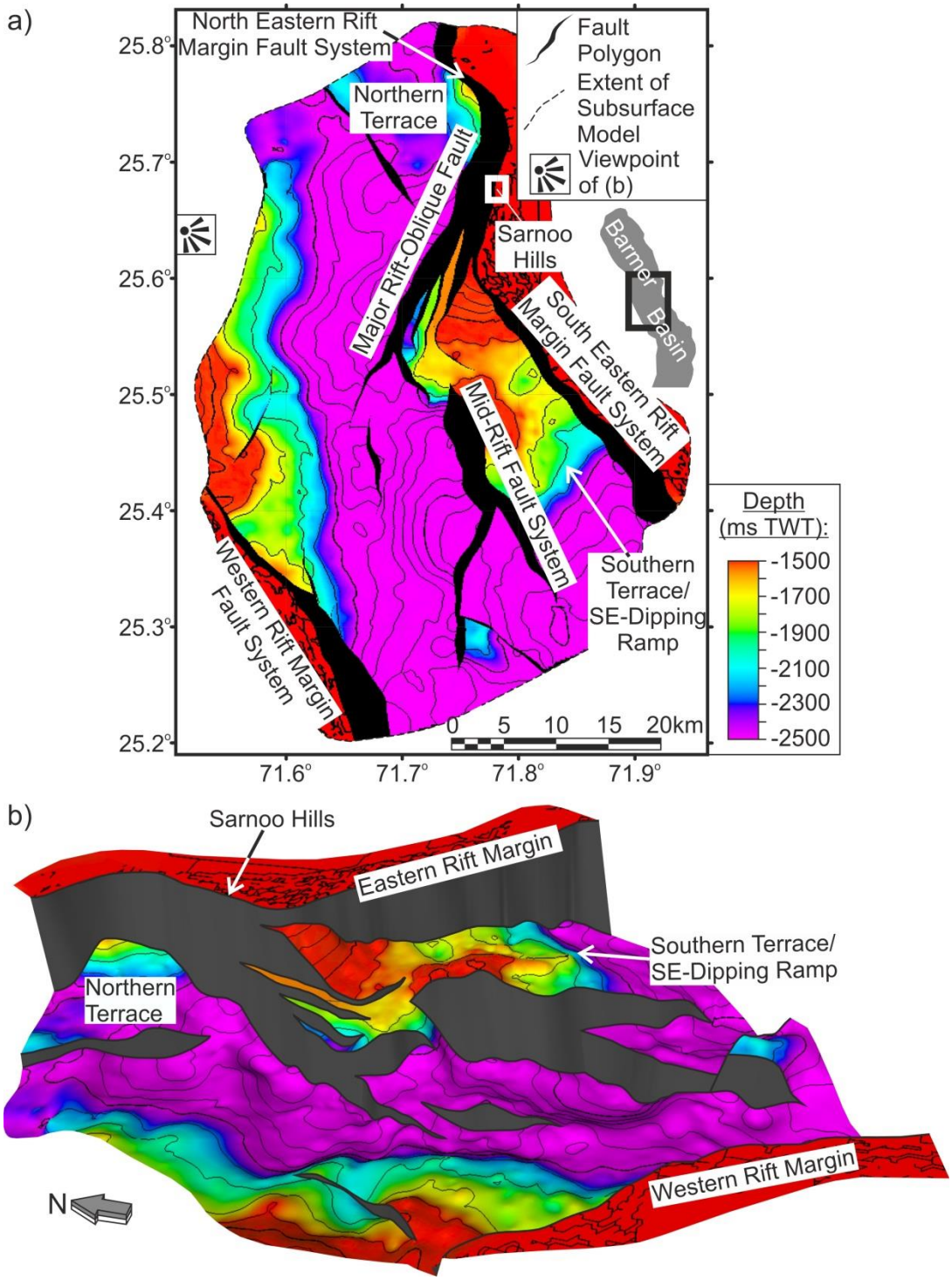

Figure 5.21 – **(a)** Time-structure map of the pre-rift unconformity surface (location map and key to colours inset). Key structural systems referred to in the text are labelled and the location of the Sarnoo Hills and the viewpoint of **(b)** are shown. **(b)** Oblique three-dimensional image of **(a)** (3x vertical exaggeration).

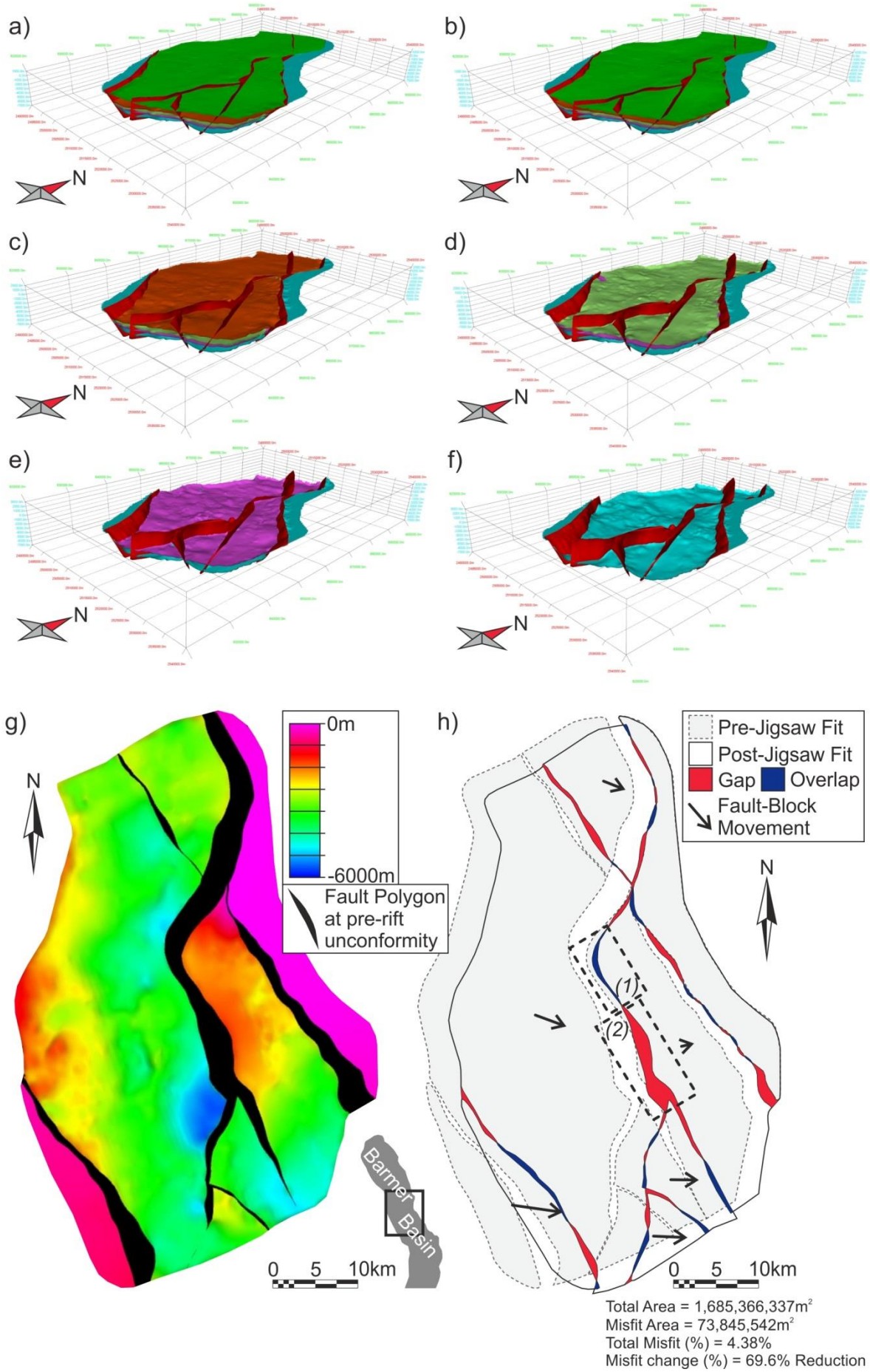
a)
b)
c)
d)
e)
f)
N
g)
0m
-6000m
Fault Polygon at pre-rift unconformity
Barmer Basin
0 5 10km
h)
Pre-Jigsaw Fit
Post-Jigsaw Fit
Gap
Overlap
Fault-Block Movement
(1)
(2)
0 5 10km
Total Area = 1,685,366,337m²
Misfit Area = 73,845,542m²
Total Misfit (%) = 4.38%
Misfit change (%) = 69.6% Reduction

Figure 5.22 (*previous page*) – Oblique three-dimensional images of the tectono-stratigraphical model of the central Barmer Basin **(a)** in time; **(b)** depth converted; **(c)** Green backstripped; **(d)** Horizon 1 backstripped; **(e)** Horizon 2 backstripped; **(f)** Horizon 3 backstripped exposing the pre-rift unconformity surface **(g)**. Map-view of the flattened pre-rift unconformity surface in depth before jigsaw-fit restoration (key to colours inset), and; **(h)** after jigsaw-fit restoration showing misfit areas (key to colours inset). All steps were conducted using Midland Valley's Move software package

5.3.6 Stratigraphical analysis

Thick (< 1200 ms), southwest-trending, elongate, and partially-isolated depocentres are preserved in the hanging-walls of rift-oblique faults during depositional interval 1 (**Figure 5.23a**), alongside thinner (< 700 ms) depocentres in the hanging-walls of rift-parallel faults in the north and south of the study area. In the succeeding depositional interval, depositional interval 2 (**Figure 5.23b**), broad depocentres (< 600 ms) in the north and south of the study area, situated in the hanging-walls of rift-parallel faults and the Major Rift-Oblique Fault, indicate that two large, approximately rift-parallel depocentres were separated by a transverse area of non-deposition, possibly a structural high (**Figure 5.23b**). Subsequently, rift-wide deposition occurred during the youngest depositional interval within the model, depositional interval 3 (**Figure 5.23c**). However, two prominent depocentres prevailed in the north and south, and relative structural highs remained in the east and west of the central study area. The thickest sedimentary accumulations (> 800 ms) occurred in the hanging-wall of the Major Rift-Oblique Fault (**Figure 5.23c**).

5.3.7 Fault analysis

Along the eastern rift margin, a combined 4 km of aggregate palinspastic fault heave was accommodated on fault systems bounding the southern terrace in the study area (**Figure 5.24a**). A northwards reduction in palinspastic fault heave on the South Eastern Rift Margin Fault System (fault '8' on **Figure 5.24a**) was coupled with a northwards increasing palinspastic fault heave on the Mid-Rift Fault System to the west (fault '9' on **Figure 5.24a**). In the north of the study area, aggregate palinspastic fault heave on fault systems bounding the Northern Terrace (faults '1' & '2' on **Figure 5.24a**) approached 4 km towards the north. It follows that a consistent minimum of 4 km of aggregate palinspastic fault heave was accommodated along the modelled length of the eastern rift margin (**Figure 5.24a**). However, two lows in aggregate palinspastic fault heave occur at either end of the Major Rift-Oblique Fault, which is characterised by a peak in palinspastic fault heave towards the centre of the fault, with a corresponding decrease towards the fault tips (fault '3' on

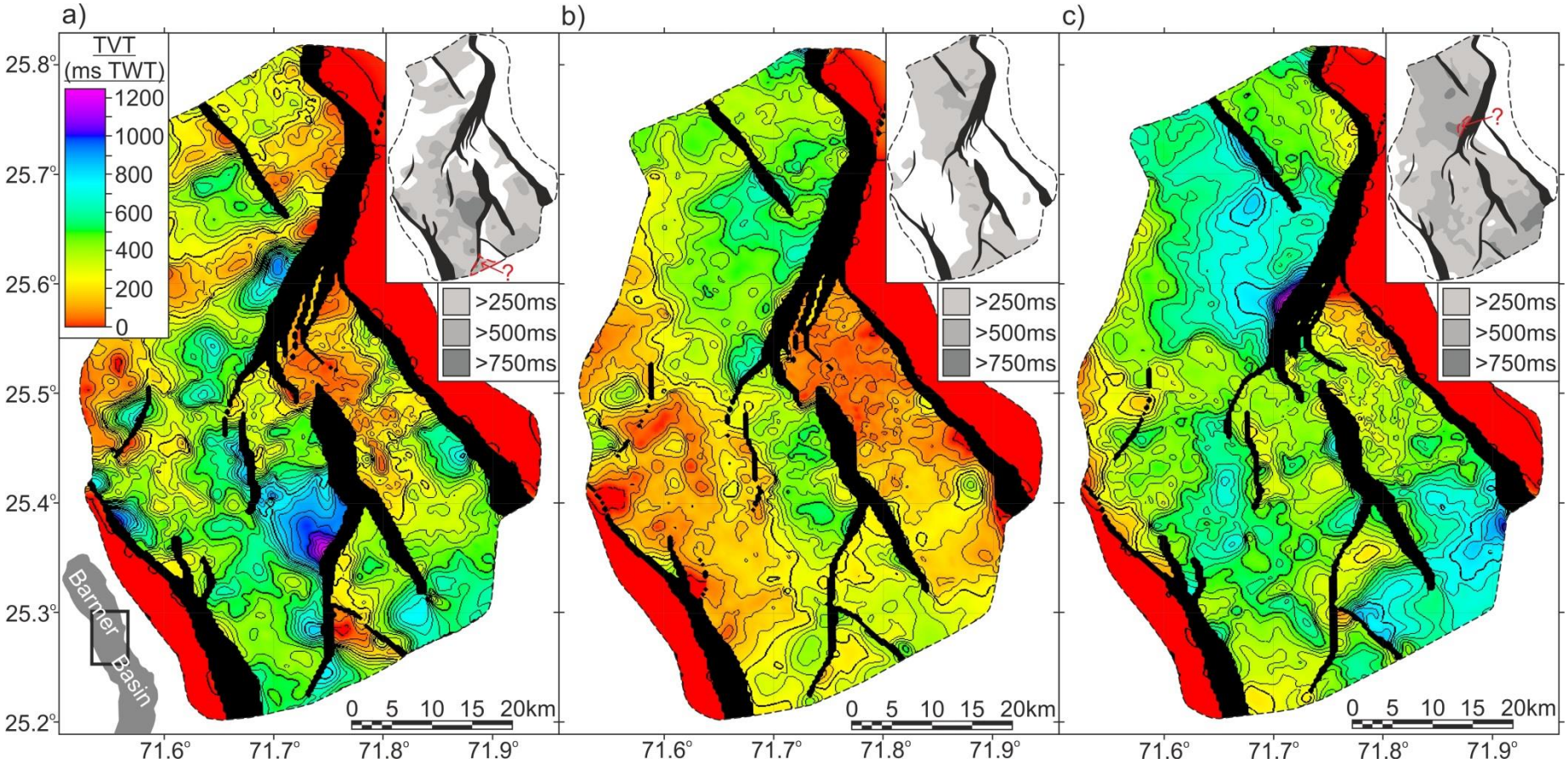

Figure 5.23 – Contoured subsurface sediment thickness [True Vertical Thickness (TVT) or isochore] maps. Simplified contour maps and key to colours are shown inset. **(a)** Depositional interval 1: Thick deposits occur at the base of rift-oblique faults. Minimal activity is evident on rift-parallel fault systems; **(b)** Depositional interval 2: two depocentres in the north and south of the study area are separated by a transverse structural high; **(c)** Depositional interval 3: Rift-wide deposition. A basinwards thickening sedimentary wedge at the northern end of the Southern Terrace is an important tectono-stratigraphical feature (see **figure 5.19**).

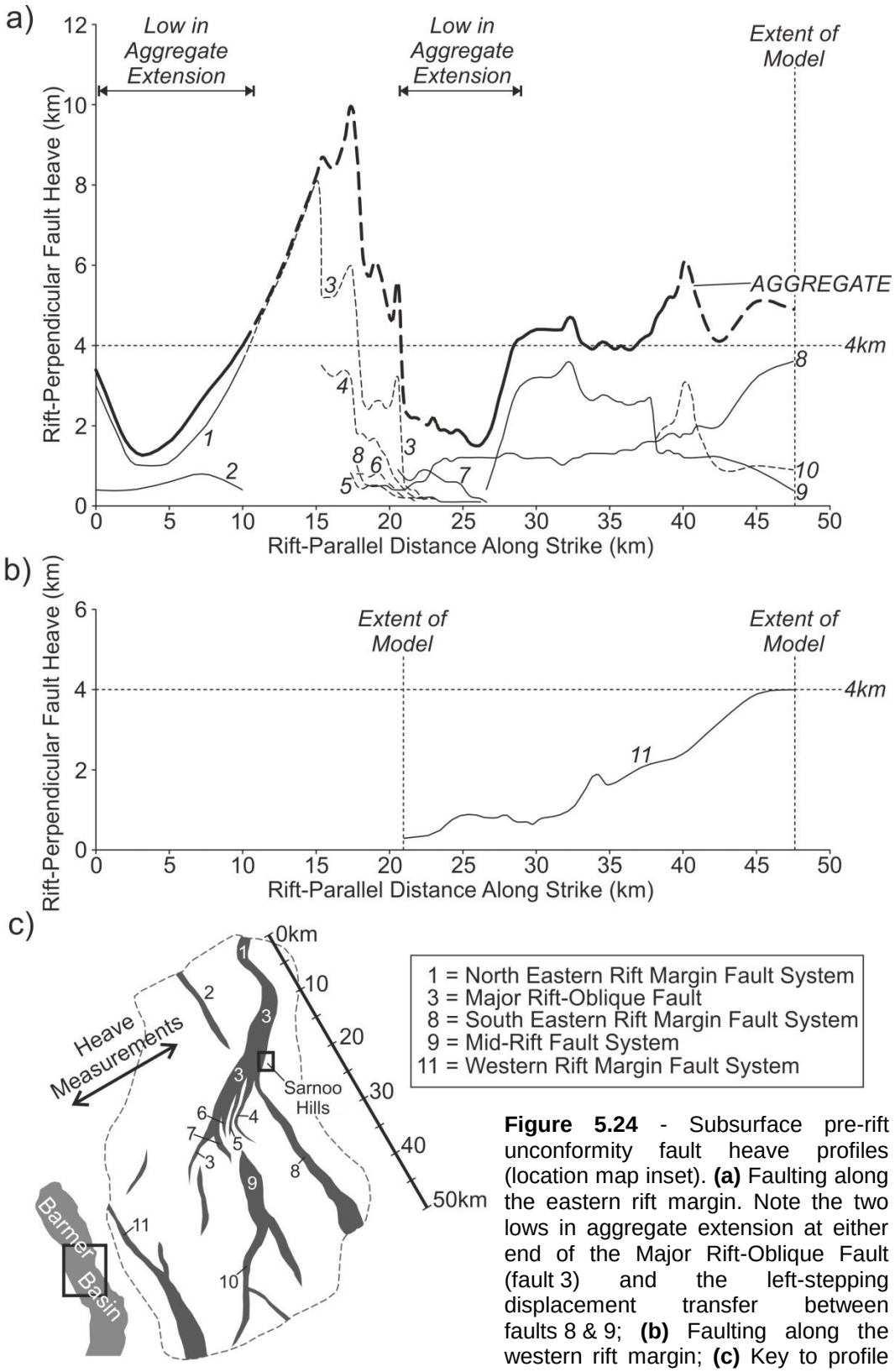

Figure 5.24 - Subsurface pre-rift unconformity fault heave profiles (location map inset). **(a)** Faulting along the eastern rift margin. Note the two lows in aggregate extension at either end of the Major Rift-Oblique Fault (fault 3) and the left-stepping displacement transfer between faults 8 & 9; **(b)** Faulting along the western rift margin; **(c)** Key to profile labels. The orientation of heave and distance measurements are indicated, and key to numbering of important fault systems is shown inset

Figure 5.24a). Along the western rift margin, extension was accommodated on a single, rift-parallel fault system with palinspastic fault heave increasing towards the south (Western Rift Margin Fault System; fault '11' on **Figure 5.24b**).

5.4 Early-stage tectono-stratigraphical evolution of the central Barmer Basin

The structural framework constructed for the central Barmer Basin is used to constrain the spatio-temporal evolution of faulting within the study area.

5.4.1 Early Jurassic Period to mid-Paleocene Epoch (depositional interval 1)

Minor deposition in the hanging-walls of rift-parallel faults (< 700 ms) in comparison to the thick deposits in the hanging-walls of rift-oblique faults (< 1200 ms; **Figure 5.23a**) indicates that cumulative subsidence on rift-oblique faults exceeded that of rift-parallel faults between the early Jurassic Period to the mid-Paleocene Epoch. Assuming thickness variations reflect the spatial and temporal development of faulting (e.g. Whipp *et al.* 2014), southwest-trending (rift-oblique) faults predominated over north-northwest-trending (rift-parallel) faults during this depositional interval (**Figure 5.25a**). Wedge-shaped geometries (**Figures 5.14 & 5.15b**) and progradation towards southwest-trending (rift-oblique) faults (**Figures 5.15c & d**), further supports that rift-oblique faults were active.

5.4.2 Mid to late-Paleocene Epoch (depositional interval 2)

Deposition within the hanging-walls of rift-parallel (rift-margin) faults in the north and south of the study area indicates rift-parallel faulting was active by the mid- to late-Paleocene Epoch. However, thick deposits in the hanging-wall of the Major Rift-Oblique Fault (< 600 ms) also indicate continued activity on some sections of rift-oblique faults (**Figure 5.23b**). The lack of significant wedging towards rift-internal faults in the north and south of the study area (**Figures 5.16g & 5.18h**) indicates tectonic inactivity. Subsidence was accommodated on the rift-margin fault systems. However, eastwards thickening towards rift-internal faulting in the structurally complex central section of the study area, (**Figures 5.17i & 5.20g**) emphasizes that the current eastern rift margin fault system was not established. Thus, areas of active rift-parallel faulting in the north and south of the study area (**Figure 5.25b**), where subsidence was accommodated on the rift margin fault systems, were separated by a structurally complex region (**Figures 5.11 & 5.21**). Such a scenario is common during rift evolution, i.e. initially isolated fault-controlled depocentres separated by a

structural high or structurally complex region (c.f. **Section 2.1.4**; accommodation zone, e.g. Morley *et al.* 1990; Nelson *et al.* 1992; Gawthorpe & Hurst 1993; Faulds & Varga 1998).

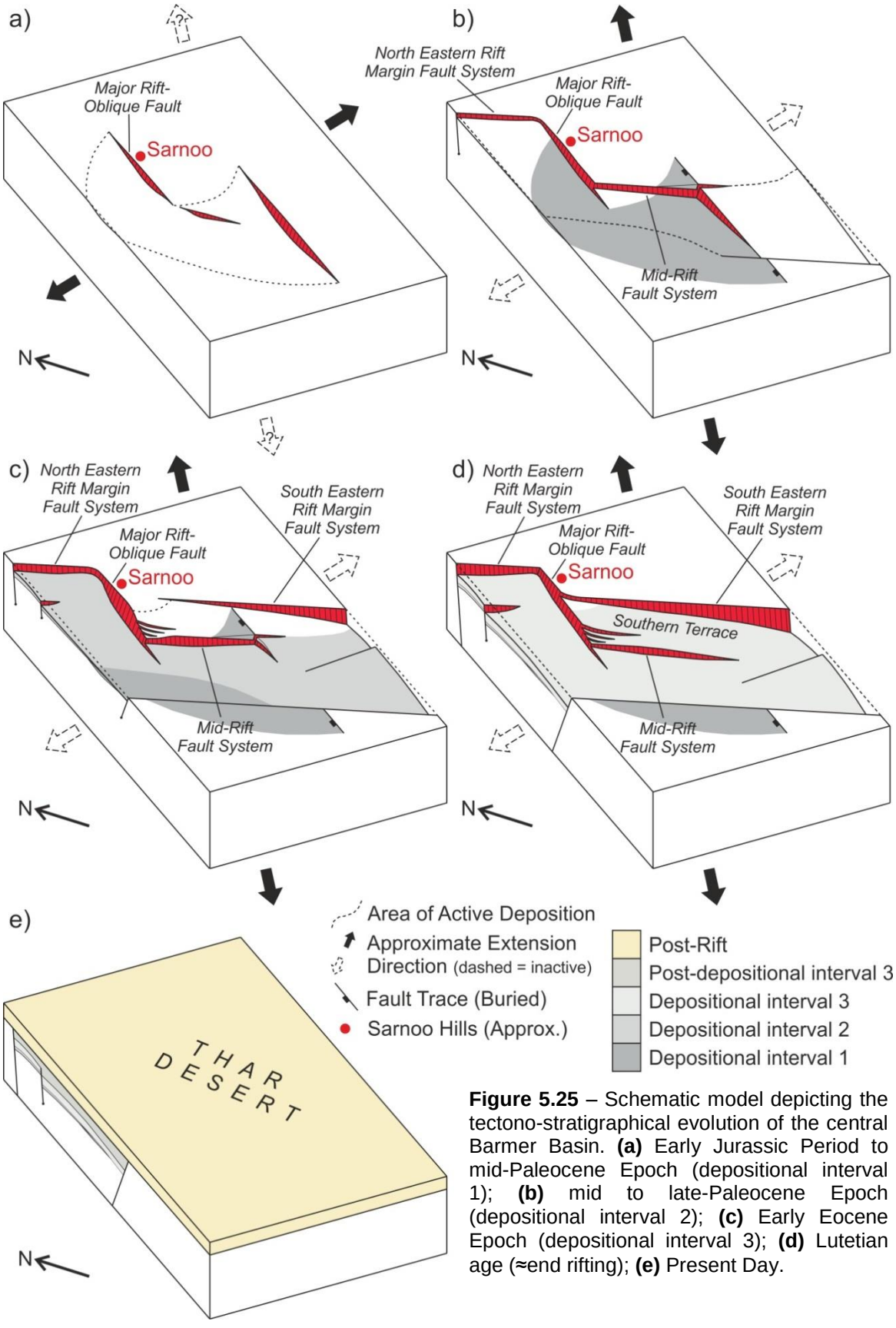

Figure 5.25 – Schematic model depicting the tectono-stratigraphical evolution of the central Barmer Basin. **(a)** Early Jurassic Period to mid-Paleocene Epoch (depositional interval 1); **(b)** mid to late-Paleocene Epoch (depositional interval 2); **(c)** Early Eocene Epoch (depositional interval 3); **(d)** Lutetian age (≈end rifting); **(e)** Present Day.

5.4.3 Early Eocene Epoch (depositional interval 3)

Deposition throughout the study area (**Figure 5.23c**) indicates the onset of rift-wide subsidence, and ubiquitous establishment of the rift-margin fault systems (**Figure 5.25c**). However, deposition in the hanging-wall of the Major Rift-Oblique Fault indicates this fault remained active. In the north and south of the study area, the majority of subsidence continued to be accommodated on the rift margin fault systems (**Figures 5.16f & 5.18g**), and in the centre of the study area, the Eastern Rift Margin Fault System was established by migration of deformation eastwards into the rift-margin footwall (**Figures 5.17i-h & 5.20f-g**) forming the Southern Terrace (**Figure 5.21**). Ubiquitous establishment of the Eastern Rift Margin Fault System by-passed structural complexities in the centre of the study area (**Figures 5.25c & d**), likely in order to minimize the work required to continue accommodating rift-perpendicular extension (e.g. Cooke & Madden 2014). The eastwards migration of deformation into the rift-margin footwall was accompanied by a basinwards rotation of the Southern Terrace (**Figures 5.17h, 5.19, & 5.20f**), and degradation (collapse) of the northern end of the terrace through extensive rotation and faulting (**Figure 5.17h**).

5.4.4 Late-stage structural evolution of the central Barmer Basin

Upon establishment of the rift margin fault systems, deformation localised onto the rift-margins, which accommodated the majority of subsidence for the remainder of rifting (**Figure 5.25d**). Subsequently, upon the cessation of rifting, the rift was buried beneath post-rift sediments prior to variable uplift and erosion (**Figure 5.25e**).

5.4.5 Temporal relationship of extensional regimes exposed at outcrop

Under the assumption that thickness variations reflect the spatial and temporal development of faulting (e.g. Whipp *et al.* 2014) rift-oblique depocentres preceding rift-parallel depocentres indicates rift-oblique faults were active prior to establishment of rift-parallel faults (**Figure 5.25**). The oblique (northwest-southeast) extensional structural regime exposed in the Sarnoo Hills (**Chapter 4**), therefore, predated the main, approximately rift-perpendicular Barmer Basin rift event as exposed in the Barmer Hills (**Chapter 3; Figure 5.1**).

5.5 Early-stage structural evolution of the central Barmer Basin

Exposure in the Sarnoo Hills (**Chapter 4**) provides direct, outcrop-based evidence for active rift-oblique faulting during early northwest-southeast extension. It follows that rift-oblique faults were inherent in the crust upon the main northeast-southwest Barmer Basin rift event.

5.5.1 Major Rift-Oblique Fault

The proximity and sub-parallel orientation of the Major Rift-Oblique Fault to dominant southwest-striking faults in the Sarnoo Hills suggests evolution of the two is closely linked. The complete syn-rift sedimentary succession within the hanging-wall of the Major Rift-Oblique Fault (**Figure 4.6**) highlights fault activity endured for the duration of rifting. A peak in palinspastic fault heave measurements towards the centre of the fault, with a corresponding decrease towards the fault tip points (fault '3' on **Figure 5.24a**), suggests evolution as an isolated fault (**Section 2.1.1**). Further to this, lows in aggregate palinspastic fault heave at either end of the Major Rift Oblique Fault, commonly associated with zones of fault-linkage (accommodation/transfer zones) in natural datasets (**Section 2.1.2**), suggest linkage of the Major Rift-Oblique Fault with the North Eastern Rift Margin Fault System and Mid-Rift Fault System to the north and south, respectively. Thus, the genetic link between the Major Rift-Oblique Fault and the fault network exposed in the Sarnoo Hills that evolved under northwest-southeast extension, indicate evolution of the Major Rift-Oblique Fault as an isolated fault during early rift-oblique extension. Zones of linkage at the fault tips indicate the Major Rift-Oblique Fault transferred displacement between the North Eastern Rift Margin Fault System and the Mid-Rift Fault System to the north and south, respectively.

5.5.2 Southern Terrace

The corresponding northwards reduction and gain in palinspastic fault heave of the South Eastern Rift Margin Fault System and the Mid-Rift Fault System respectively (faults '8' & '9' on **Figure 5.24a**) indicate that strain was increasingly accommodated on the Mid-Rift Fault System northwards towards the Major Rift-Oblique Fault (i.e. soft-linkage). The Southern Terrace represents the intervening relay ramp structure. Ramp-rotation (**Figures 5.19 & 5.20f**) and faulting (**Figure 5.17h**) of the Southern Terrace, associated with the eastwards migration of deformation into the rift-shoulder during depositional interval 3, signifies evolution of the South Eastern Rift Margin Fault System, and soft-linkage with the Mid-Rift Fault System during the early Eocene

Epoch. Attenuation of the northern parts of the Southern Terrace (**Figure 5.11**), manifest as rotation and faulting, suggest proximity to a high-strain zone, such as an accommodation zone.

5.5.3 Evolution of the eastern rift margin fault system within a changing stress field

Incorporation (via inheritance) of the Major Rift-Oblique Fault into the evolving eastern rift margin fault system facilitated displacement transfer between right-stepping rift margin fault systems to the north and south (**Figures 5.26a & b**). Such a scenario has been described previously, both experimentally (Bellahsen & Daniel 2005; Henza *et al.* 2010; Henza *et al.* 2011) and in nature (McClay & Khalil 1998; Lezzar *et al.* 2002; Younes & McClay 2002; Bellahsen *et al*. 2006; Whipp *et al.* 2014). However, the structural geometries and characteristics described from the central Barmer Basin are not in accordance with a model of passive inheritance of a discrete, rift-oblique, pre-existing fault that transferred extension directly between offset rift margin fault systems (**Figure 5.26d**). Significantly, the Southern Terrace (**Figure 5.21**), comprising a major southeast-dipping, rift-internal ramp, is not predicted by this, or any accepted extensional margin, accommodation or transfer zone models (e.g. Morley *et al.* 1990; Gawthorpe & Hurst 1993; Faulds & Varga 1998), which instead predict a northwest dipping ramp between two right-stepping, southwest-dipping, synthetic fault systems (**Figure 5.26c**).

The data indicate that the Major Rift-Oblique Fault transferred extension between the North Eastern Rift Margin Fault System and the Mid-Rift Fault System to the north and south respectively, rather than between right-stepping, rift margin fault systems directly (e.g. Bellahsen & Daniel 2005; **Figure 5.26d**). Subsequently, displacement was transferred from the Mid-Rift Fault System onto the South Eastern Rift Margin Fault System to the east by soft-linkage, forming a southeast-dipping relay ramp (Southern Terrace; **Figures 5.26a & b**). Linkage of the Major Rift-Oblique Fault with the Mid-Rift Fault System, rather than direct linkage of the North and South Eastern Rift Margin Fault Systems, as proposed, accounts for the numerous splays (**Figures 5.11 & 5.21a**), low in aggregate palinspastic fault heave (**Figure 5.24a**), and basinwards thickening sedimentary wedge (**Figure 5.19**) in the accommodation zone between them (**Figure 5.26a**). This unusual accommodation structure (**Figure 5.26**) illustrates one further example of how extensional fault systems may evolve during rifting within a changing stress-field (e.g. Morley *et al.* 2007).

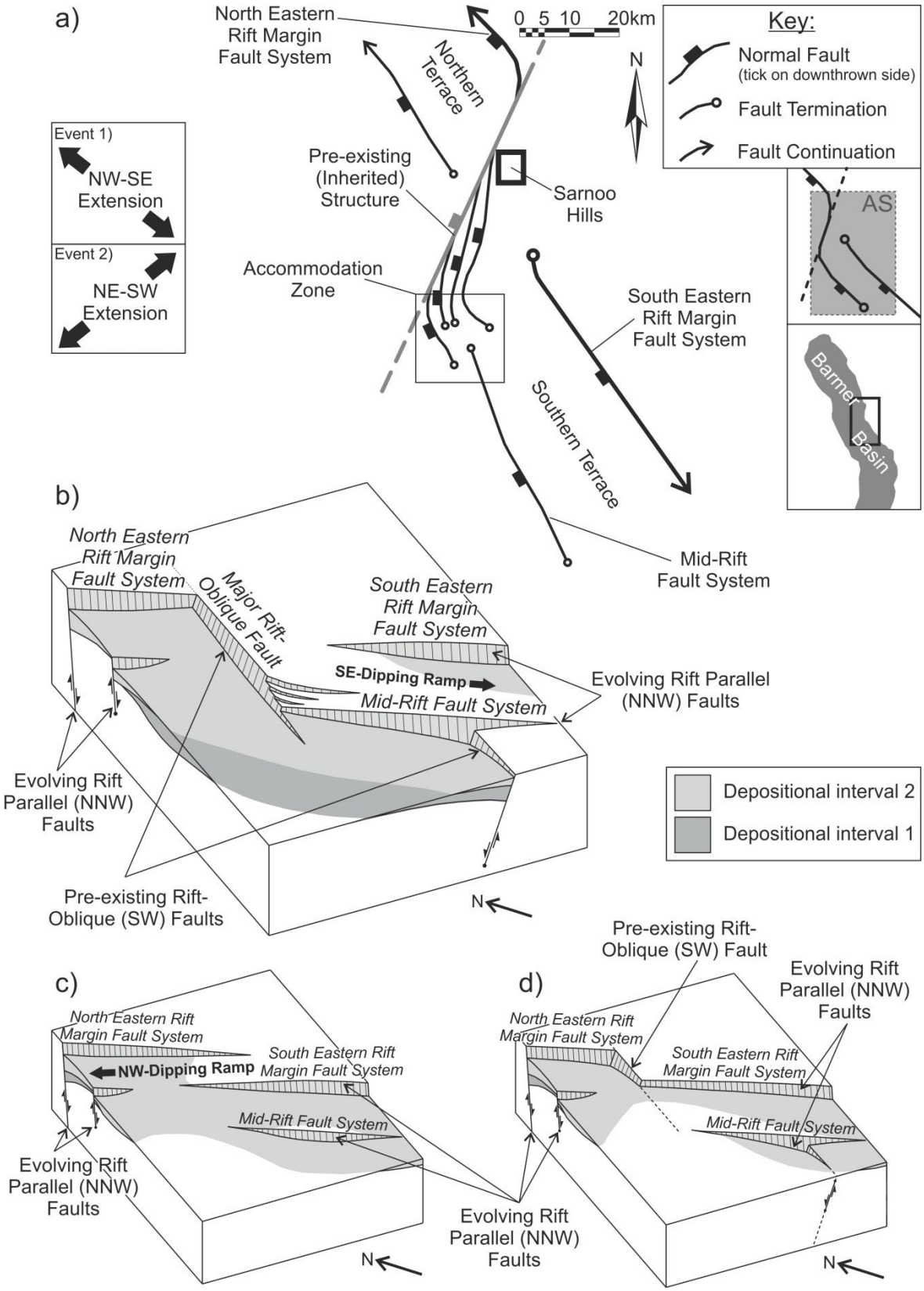

Figure 5.26 - Incorporation of a pre-existing, rift-oblique fault (Major Rift-Oblique Fault) into the evolving eastern margin fault system formed an atypical eastern rift margin accommodation structure (AS):**(a)** Cartoon sketch map (location map and extensional events inset; AS = Accommodation Structure); **(b)** Block diagram of (a); **(c)** Conventional model of linkage between two sub-parallel synthetic faults; **(d)** Passive inheritance of a discrete pre-existing structure as a transfer fault between offset fault systems (e.g. Bellahsen & Daniel 2005; c.f. **Figure 2.14d**).

5.6 Discussion

A three-dimensional tectono-stratigraphical model of the central Barmer Basin was successfully constructed and validated from interpretations of seismic horizons and faults using a network of two-dimensional seismic data at a spacing of between 1 km and 2.5 km. However, problems associated with two-dimensional seismic data, including; 1) limited well data; 2) poor seismic imaging, especially with depth; 3) faulting below the resolution of the seismic data, and; 4) faulting oblique to the seismic section, are all potential sources of error in the analyses presented. Further to this, the inherent uncertainties and resolution limits (> 10 m vertical and > 30 m lateral) of seismic data result in a large degree of subjectivity in any resulting model (Bond *et al.* 2012), which may be exacerbated when a structural setting (e.g. extensional, compressional, or strike-slip) is presumed by the interpreter, or if the interpretations are made using pre-conceived models. In an attempt to mitigate against these inherent errors, significant emphasis has been placed on balancing and restoring two-dimensional cross-sections and the three-dimensional model, to ensure internal consistency and geometrical plausibility. Furthermore, the success of a depth conversion is highly sensitive to the subsurface velocity model employed. In order to ensure realistic parameters were used during depth conversion, subsurface velocities were constrained from interval velocity logs in the study area.

Time-thickness [True Vertical Thickness (TVT) or isochore] maps provided the pivotal link to the poorly understood spatio-temporal relationship between the two non-coaxial extensional events exposed at outcrop on opposing rift margins of the Barmer Basin, a relationship which could not be investigated at outcrop. However, the absence of differentiation between Mesozoic Era and Paleocene Epoch deposits within the early-Jurassic Period to mid-Paleocene Epoch depositional interval (depositional interval 1), due to the lack of subsurface constraint on the positioning of this reflector, precludes attaining a detailed spatio-temporal tectono-stratigraphical understanding of early rift-oblique extension. Furthermore, it has been assumed that no uplift and erosion removed any of the underlying pre-Paleogene stratigraphy, and that the thickness of depositional interval 1 reflects the creation of accommodation space by active faulting alone. Until new data is available detailing the Cretaceous-Paleogene boundary, resolving this depositional interval into packages of definitive age is problematic.

Subsurface structural geometries along the central eastern rift margin differ from that predicted by a model of passive incorporation of a discrete, rift-oblique, pre-existing structure between two right-stepping rift margin fault systems (e.g. Bellahsen & Daniel 2005; **Figure 5.26d**). These disparities have important implications for early sediment routing and depocentre evolution. Conventional models of linkage between two southwest-dipping, synthetic, right-stepping faults predict formation of a northwest-dipping relay ramp (e.g. Morley *et al.* 1990; Gawthorpe & Hurst 1993; Faulds & Varga 1998), with northwest-orientated sediment inputs, and depocentres towards the centres of each fault segment (**Figure 5.26c**). However, in the east Barmer Basin, activity of the Major Rift-Oblique Fault during early rifting (**Figure 5.23a**), and the subsequent incorporation of this fault into the evolving Eastern Rift Margin Fault System during the main Barmer Basin rift event (**Figures 5.26a & b**), resulted in an early depocentre at the base of the inherited structure (e.g. Bellahsen & Daniel 2005; **Figures 5.23b**), and formation of a southeast-dipping ramp (**Figure 5.26b**). This structure is likely to have directed sediment input towards the southeast rather than to the northwest, as predicted by conventional models.

5.7 Summary

This chapter investigated how the two non-coaxial extensional regimes exposed on opposing rift-margins of the Barmer Basin (**Chapters 3 & 4**) were related both spatially and temporally using subsurface datasets. Eight seismic horizons and the associated fault network were mapped across an 1850 km^2 area in the central Barmer Basin using a network of two-dimensional seismic data. Interpretations of three two-dimensional cross-line seismic sections (061°) in the south, central, and north of the study area were validated by sequentially backstripping and decompacting the uppermost stratigraphical interval, move-on-fault restoring any remaining subsidence, and flattening to the exposed upper horizon for the entire sedimentary succession within the rift. Subsequently a three-dimensional model was constructed that was, in-turn, validated with a three-dimensional jigsaw-fit restoration at the pre-rift-unconformity surface. Upon construction of a geometrically valid model, a structural framework of the central Barmer Basin was established, and the resultant stratigraphical and structural analyses, as well as the interpretation of key seismic stratigraphical relationships imaged on seismic sections, were used to interpret the early-stage tectono-stratigraphical evolution of the study area.

The central Barmer Basin has asymmetrical and symmetrical geometries in the north and south of the study area respectively, separated by a structurally complex region. Significant rift-parallel (≈ north-northwest) and rift-oblique (≈ southwest) faults occur in the subsurface that are sub-parallel to dominant fault trends exposed at outcrop in the Barmer (**Chapter 3**) and Sarnoo (**Chapter 4**) hills respectively. Along the eastern rift margin, right-stepping, rift-parallel, rift margin fault systems are separated by a significant rift-oblique (southwest-trending) fault, and a large southeast-dipping ramp is situated adjacent to the eastern rift margin in the southeast of the study area. Sediment thickness maps indicate that activity on southwest-trending (rift-oblique) faults preceded that on northwest-trending (rift-parallel) faults. It follows that northwest-southeast extension preceded northeast-southwest extension. The incorporation (via inheritance) of a significant rift-oblique fault, active during early rift-oblique extension, into the eastern rift margin during the Barmer Basin rift event (≈ northeast-southwest), formed an atypical accommodation structure not predicted by conventional models as a result of structural inheritance. Rift-oblique faults variably imaged throughout the subsurface of the Barmer Basin, therefore, likely result from the incorporation of rift-oblique faults into the evolving rift-parallel fault systems during the Paleogene Barmer Basin rift event. Rift-oblique faults may have formed during early, oblique (≈ northwest-southeast) extension. However, the lack of differentiation within the early-Jurassic Period to mid-Paleocene Epoch depositional interval resulted in a rudimentary spatio-temporal understanding of the early episode of northwest-southeast extension. Further to this, the interpretation that structural complications in the Barmer Basin subsurface result from structural inheritance should be clarified and evaluated due to the inherent problems, uncertainties, and resolution limits associated with two-dimensional seismic data. Such limitations and uncertainties would be reduced if the base Paleogene surface were defined and three-dimensional seismic data were utilized.

6 The Kaameshwari Fault

Targeted investigation of a rift-oblique fault in the Barmer Basin subsurface

The lack of differentiation within the early Jurassic Period to mid-Paleocene Epoch depositional interval of the tectono-stratigraphical model of the central Barmer Basin (**Chapter 5**) introduces ambiguity into the interpretation that rift-oblique (≈ northwest-southeast) extension pre-dated the Barmer Basin rift event. Further to this, inherent problems and uncertainties associated with two-dimensional seismic data suggest that the interpretation attributing rift-oblique faults to structural inheritance should be clarified. In this chapter, a targeted investigation of a seismic-scale structure within the tectono-stratigraphical model of the central Barmer Basin, the Kaameshwari Fault, was conducted using three-dimensional seismic data. The study incorporates newly available interpretations of the base Cretaceous and base Paleogene horizons, improving resolution within the deep syn-rift sedimentary succession. This investigation evaluates and refines the findings of previous outcrop- (small) and seismic- (basin) scale work (**Chapters 3, 4, & 5**), and will support or refute: 1) that deformation during the main Barmer Basin rift event accommodated northeast-southwest regional extension (**Chapter 3**); 2) the existence of an early episode of non-coaxial extensional deformation that predated the main Barmer Basin rift event (**Chapters 4 & 5**), or; 3) that structural complications arise from the inheritance of pre-existing structures (**Chapter 5**). A three-dimensional tectono-stratigraphical model was constructed for the early-stage (deep) sedimentary succession surrounding the Kaameshwari Fault, and high-resolution mapping of a late-stage (shallow) fault system was conducted. Subsequently, the temporal evolution of deformation was assessed by conducting a geometrical comparison of early- and late-stage fault systems.

Seismic- and tectono-stratigraphical relationships indicate that the rift-oblique (≈ north-south) Kaameshwari Fault accommodated large fault-controlled subsidence during incipient rifting, but became rapidly inactive during the mid-Paleocene Epoch. The cessation of Kaameshwari Fault activity was coeval with the establishment of the main rift-parallel, rift-margin fault systems, suggesting the Kaameshwari Fault was orientated obliquely to the regional extension direction. Such a relationship is characteristic in areas of structural inheritance, supporting previous

suggestions. However, a lack of thickness variations across the Kaameshwari Fault within the Cretaceous depositional interval indicates tectonic inactivity. Subsequently, the Kaameshwari Fault was buried beneath a thick succession of lacustrine deposits, detaching late-stage (shallow) fault systems from early-stage (deep) structural complexities. A geometrical comparison between early- and late- stage fault systems indicate late-stage faults tended towards a more rift-parallel orientation, alluding to regional rift-perpendicular (≈ northeast-southwest) extension during the Barmer Basin rift event. The findings support previous suggestions that rift-oblique faults in the subsurface of the Barmer Basin result from the inheritance of pre-existing structures during rift-perpendicular Paleogene extension. Inactivity of the Kaameshwari Fault during the Cretaceous depositional interval, however, suggests pre-existing fabrics of multiple origins were incorporated into the evolving rift-parallel fault systems.

6.1 Geological setting

Within the north-northwest trending Barmer Basin (≈ 330°), the north trending (≈ 360°) Kaameshwari Fault is oblique (≈ 30°) to the rift-trend (**Figure 6.1**). The Kaameshwari Fault is situated to the west and immediately adjacent to the K1 well, and is in the hanging-wall of a large-displacement, rift-parallel extensional fault defining the western edge of the Saraswati Terrace. (**Figure 6.2**; 'Southern Terrace' of **Chapter 5**). The fault is buried beneath a thick (< 2500 ms) succession of syn-rift sediments that display large-scale, wedge-shaped geometries that thicken towards the Saraswati Terrace (**Figure 6.2**).

6.2 Dataset

The study area is covered by a three-dimensional seismic survey that encompasses 215 km^2 of the central Barmer Basin in the vicinity of the K1 well (**Figure 6.1**). The data is of moderate quality and contains frequencies up to 60 Hz. Seismic sections are presented with reverse (international) polarity whereby a downward increase in acoustic impedance, that is a positive reflection coefficient, is represented by a trough (blue reflection). The seismic survey is pre-stack time-migrated, and the three-dimensional migrated volume comprises 951 in-lines bearing 151° and 1451 cross-lines bearing 061°, each with a spacing of 12.5 m. The vertical axis of the seismic survey is in two-way travel time (TWT), with maximum and minimum values of 202 ms and -4802 ms respectively, and all measurements regarding depth are in TWT. The depths (TWT) of important lithostratigraphical boundaries for the only exploration well in the study area, the K1 well

that penetrates the entire sedimentary succession within the rift, were provided by the operator, as well as pre-existing interpretations of the base Cretaceous (bC) and base Paleogene (bP) horizons (**Figures 6.3 & 6.4**; Clemson 2014) from a regional dataset. The base Cretaceous (bC) horizon is assumed to be the base of the sedimentary fill within the rift.

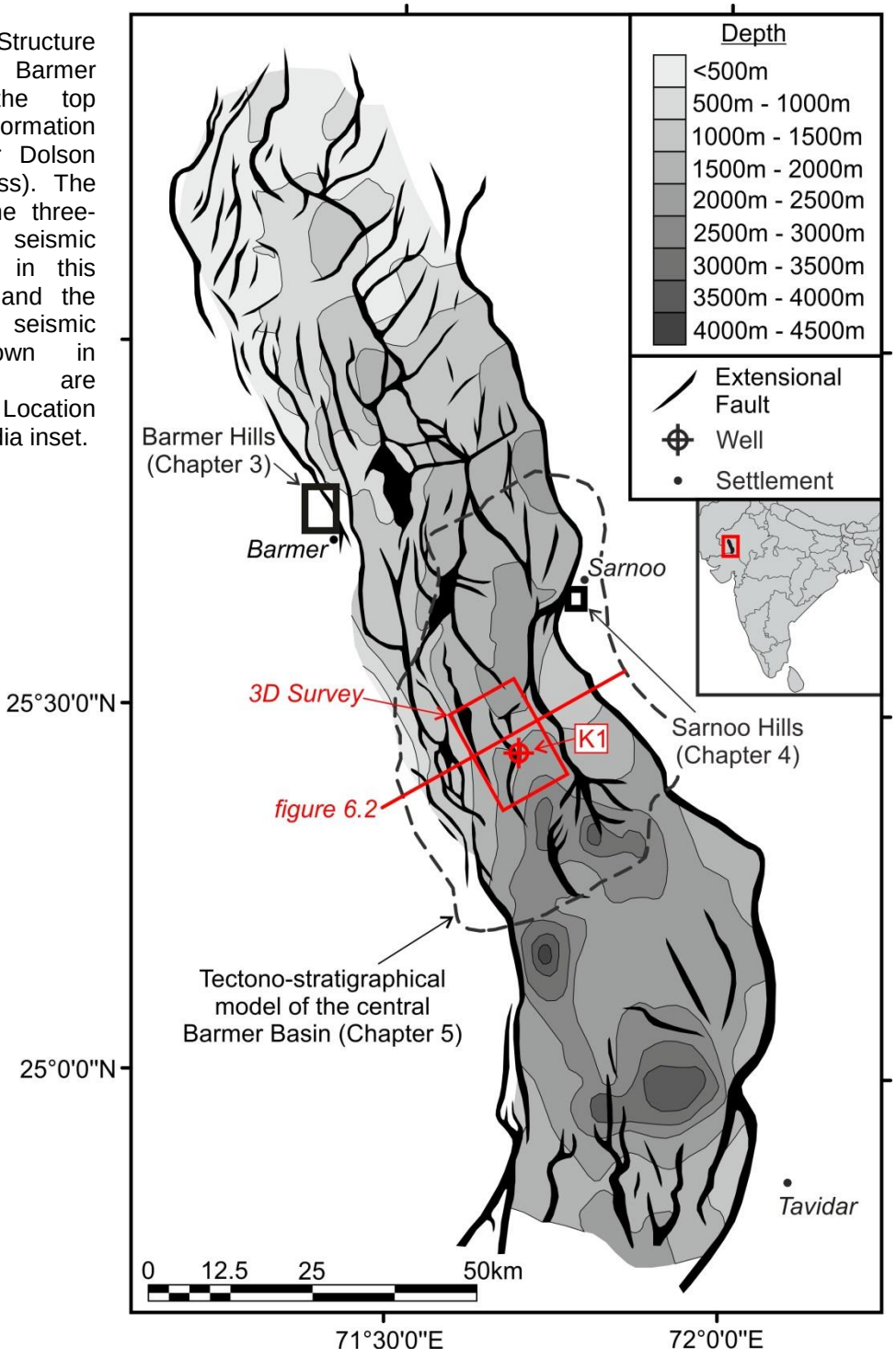

Figure 6.1 – Structure map of the Barmer Basin at the top Fatehgarh Formation horizon (after Dolson *et al.* in press). The location of the three-dimensional seismic survey used in this investigation and the interpreted seismic section shown in **figure 6.2** are indicated. Location map within India inset.

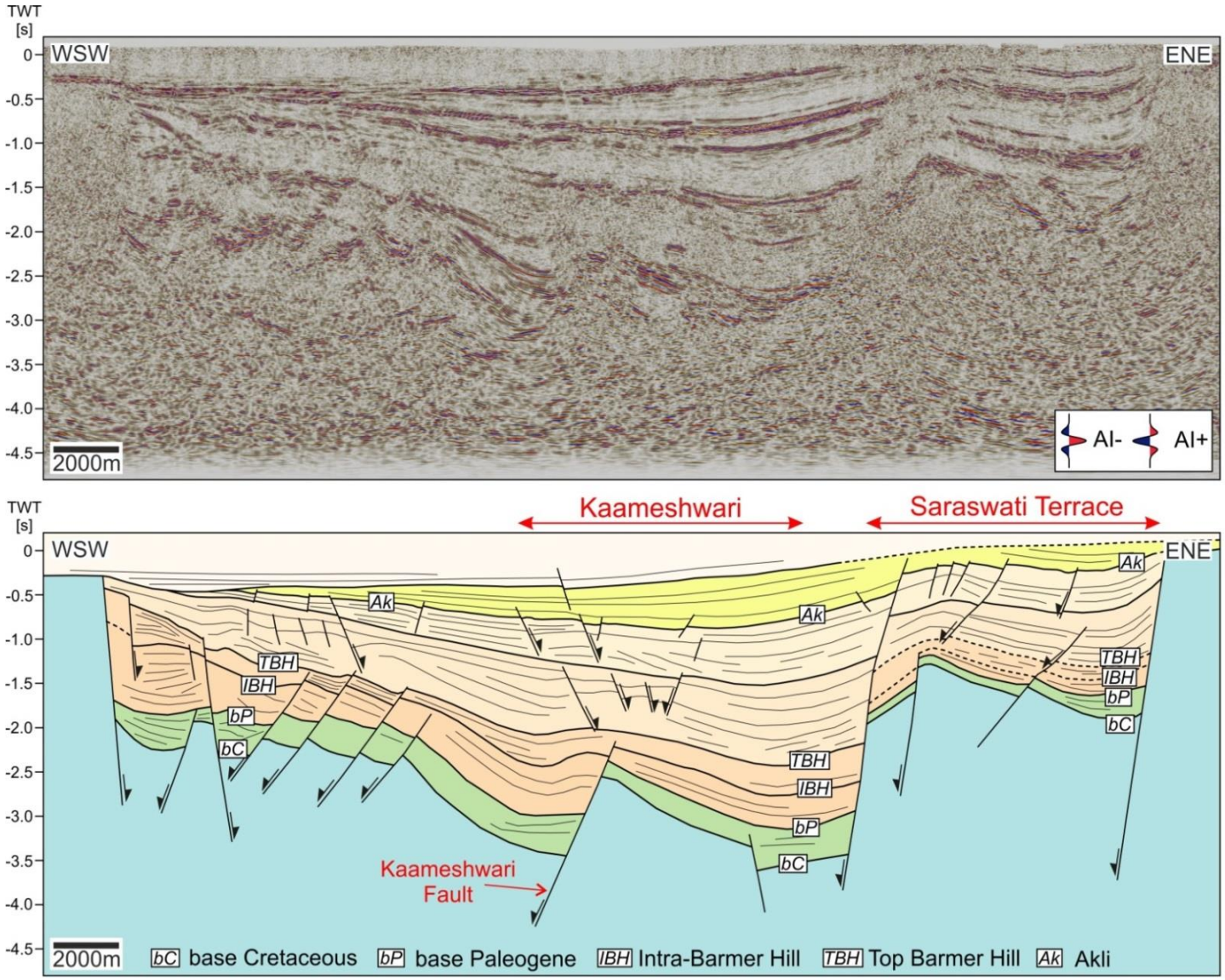

Figure 6.2 – Un-interpreted **(top)** and interpreted **(base)** cross-line (061°) seismic section across the central Barmer Basin. The location of the Kaameshwari Fault is highlighted. See **figure 6.1** for section location. Interpretations at the base Cretaceous and base Paleogene horizons are reproduced from Clemson (2014).

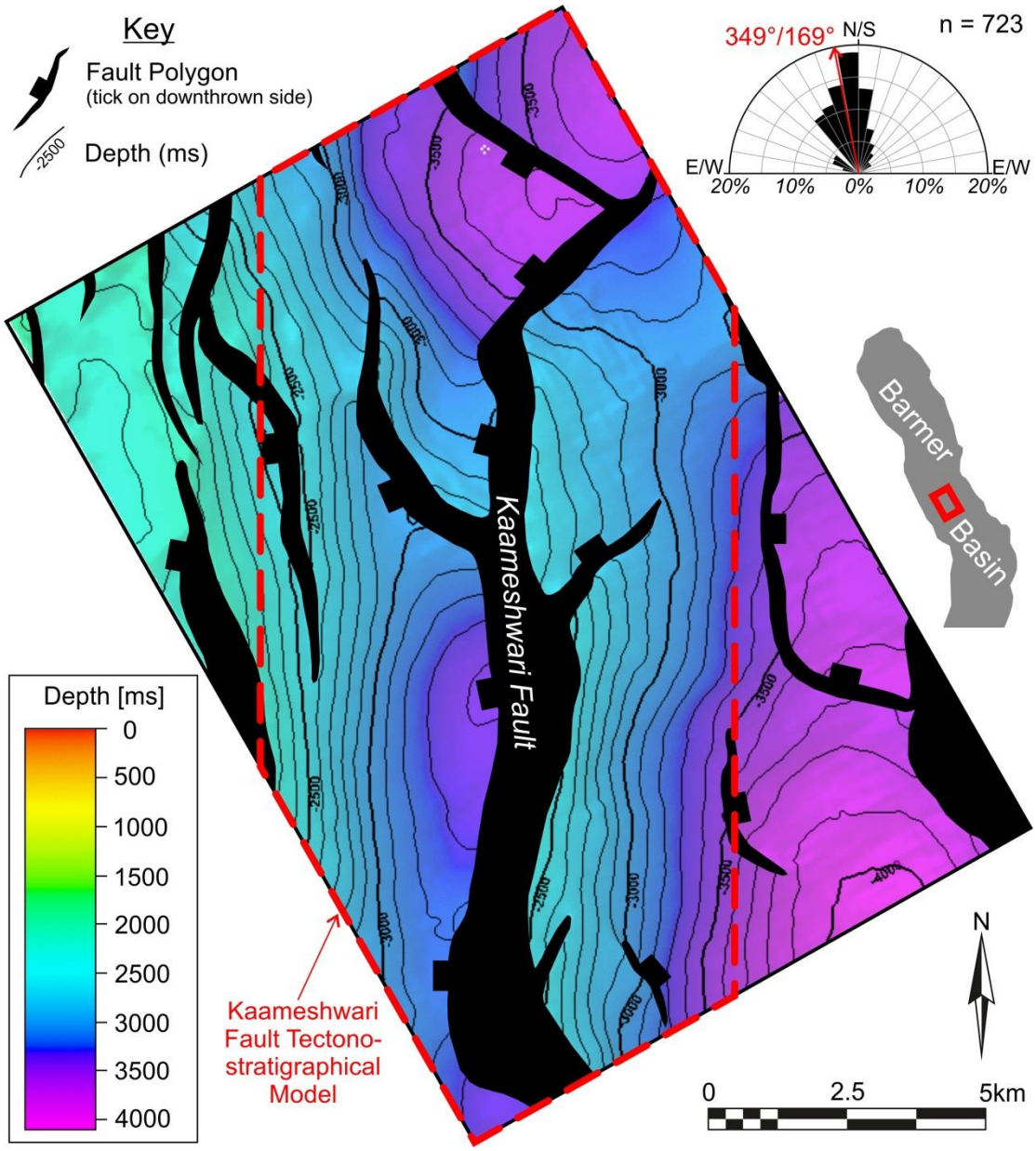

Figure 6.3 – Time-structure map of the base Cretaceous (bC) horizon (reproduced from Clemson 2014). Normalised half-rose diagram of fault azimuths recorded at the centre of each 100m long footwall segment is shown inset demonstrating that mean fault azimuth is 349°/169°, with a population mode of 350°-360° (for raw structural data see **Appendix D**). Key to colours and location map are also shown inset. The extent of the Kaameshwari Fault study area is also shown.

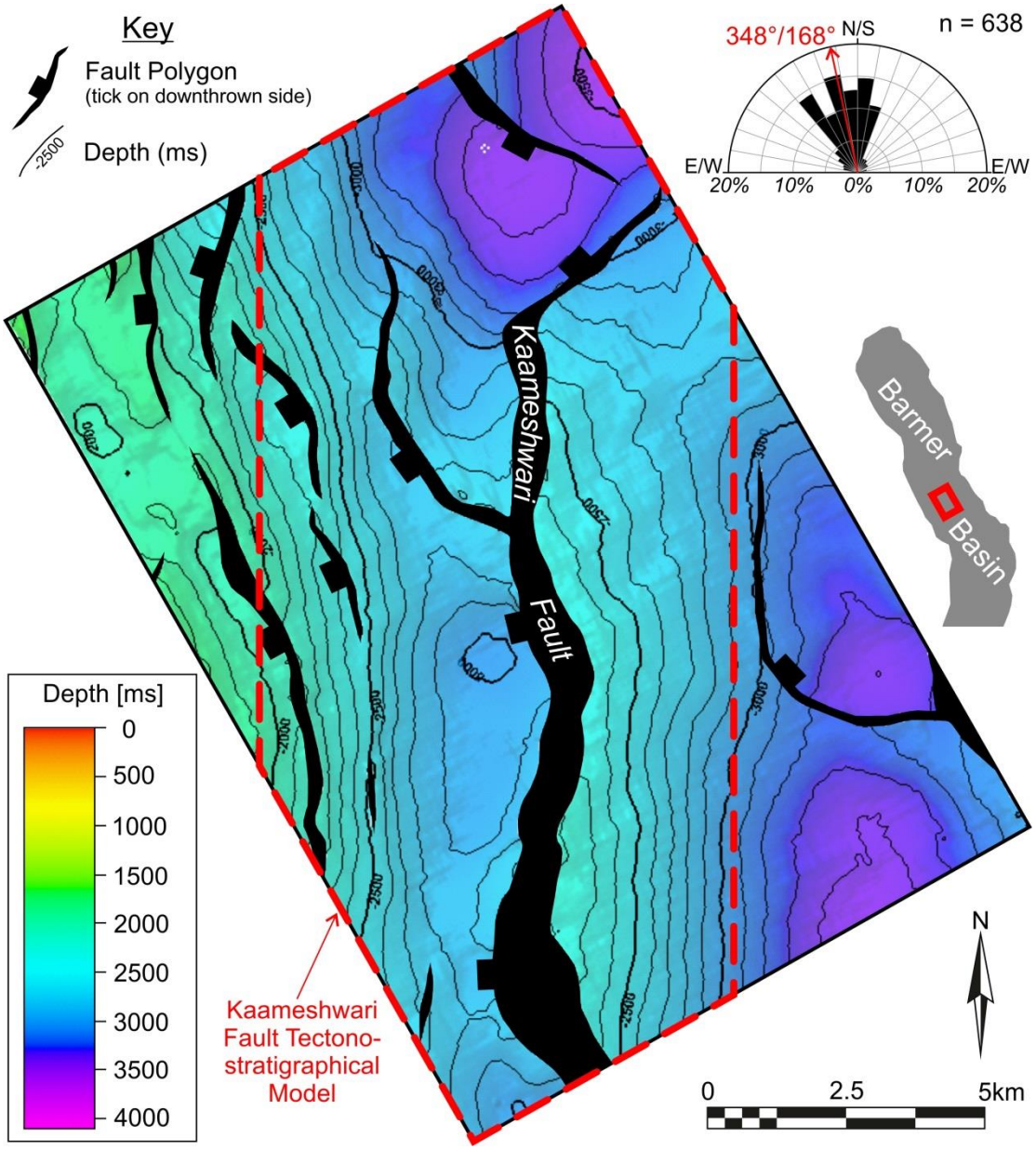

Figure 6.4 – Time-structure map of the base Paleogene (bP) horizon (reproduced from Clemson 2014). Normalised half-rose diagram of fault azimuths recorded at the centre of each 100m long footwall segment is shown inset demonstrating that mean fault azimuth is 348°/168°, with a population mode of 340°-350° (for raw structural data see **Appendix D**). Key to colours and location map are also shown inset. The extent of the Kaameshwari Fault study area is also shown.

6.3 Methodology

6.3.1 The vertical resolution of seismic data

The vertical resolution of a seismic signal is defined as the minimum thickness of a subsurface body that can be identified as two separate and distinct signals corresponding to the upper and lower interfaces of the body. In this chapter the vertical resolution of a seismic signal will be calculated to evaluate the minimum detectable stratigraphical offset of a seismic reflector across a

fault. Subsequently, in **Chapter 7** the vertical resolution of a seismic signal will be calculated to determine the vertical error associated with a seismic interpretation. The vertical resolution of a seismic signal can be calculated if the velocity (m s^{-1}) and frequency (s^{-1} or Hz) of the signal are known at the target depth. Using:

$$\boldsymbol{v = \frac{d}{t} \ \ or \ \ d = v \times t} \qquad \textit{Equation 6.1}$$

where v = compressional wave velocity (m s^{-1}); d = distance (m), and; t = time (s), the wavelength of the seismic signal can be calculated. Frequency and wave period, the latter defined as the duration of a single wavelength, are related by:

$$\boldsymbol{p = \frac{1}{f}} \qquad \textit{Equation 6.2}$$

where p = wave period (s), and; f = frequency (Hz). Hence, substituting wave period (p) and the velocity of the seismic signal into **equation 6.1**, the wavelength (distance) of a seismic signal can be calculated:

$$\boldsymbol{\lambda = v \times p = \frac{v}{f}} \qquad \textit{Equation 6.3}$$

where λ = wavelength (m), and; v = compressional wave velocity (m s^{-1}; Hart 2012). Subsequently, the vertical resolution of the seismic signal at the target depth is approximated using:

$$\boldsymbol{Vertical\ Resolution \approx \frac{\lambda}{4}} \qquad \textit{Equation 6.4}$$

If the thickness of the subsurface body is less than λ/4, reflections from the top and base of the body destructively interfere and cannot be resolved separately (Hart 2012). However, it is possible to detect a bed of thickness less than λ/4, with detectability dependent upon the signal-to-noise ratio of the seismic dataset.

6.3.2 Seismic interpretation

In conjunction with the base Cretaceous (bC) and base Paleogene (bP) horizon interpretations provided (**Figures 6.3 & 6.4**; Clemson 2014), two further horizons were interpreted within the deep sedimentary succession in the vicinity of the Kaameshwari Fault (**Figure 6.2**; interpretations were conducted using Schlumberger Information Systems Petrel software package). Based on the lithological boundaries constrained from the K1 well the lower horizon occurred within the Barmer Hill Formation (Intra-Barmer Hill or IBH; **Figure 6.5**), and the upper horizon represented the top Barmer Hill Formation (Top Barmer Hill or TBH; **Figure 6.5**). Both horizons are mid- to late-

Paleocene in age. High resolution mapping of a further horizon was conducted across the entire seismic survey within a cyclic package of moderate to high-amplitude, continuous, shallow seismic reflectors (Akli or Ak; **Figure 6.5**). Based on lithological boundaries constrained from the K1 well, and corroboration of the properties of the seismic reflectors with lithological descriptions outlined in technical publications (Sunder *et al.* 2013), the horizon is situated within the lignite succession of the Akli Formation, and is early- to middle-Eocene in age.

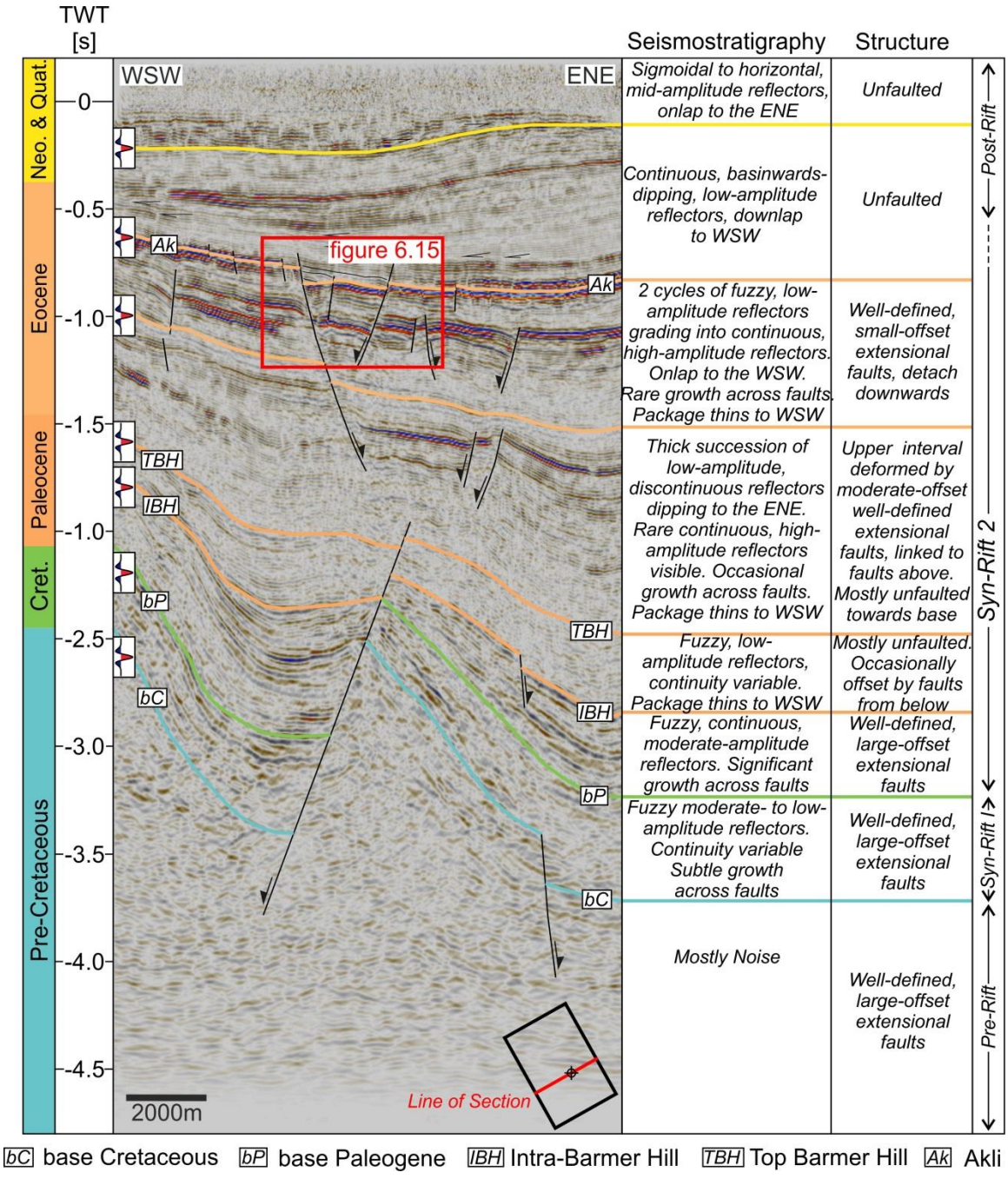

Figure 6.5 – Seismostratigraphy of the Kaameshwari study area. Interpretations at the base Cretaceous and base Paleogene horizons are reproduced from Clemson (2014).

Horizons comprising high-amplitude seismic reflectors (Ak & IBH; **Figure 6.5**) were interpreted on every tenth in-line (151°) and cross-line (061°) section. However, in structurally complex regions every fifth in-line and cross line was used in conjunction with arbitrary interpretation sections orientated perpendicular to the local structural trend. The low-amplitude nature of the Top Barmer Hill (TBH) horizon (**Figure 6.5**) prevented high resolution mapping, and a general sense of the horizon topography was attained using sparse interpretations on every fiftieth in-line (151°) and cross-line (061°) section.

Fault planes were identified using offsets and terminations of seismic reflections. Horizon interpretations were continued into the fault plane to generate hanging-wall and footwall cut-offs. Upon generation of a tight grid of horizon interpretations, fault polygons were drawn in map-view for the Ak horizon using the interpreted hanging-wall and footwall cut-offs, generating a fault network map. The resultant fault map was validated with a stratal (dip-parallel) slice through a variance (edge effect) cube.

6.3.3 Tectono-stratigraphical model of the Kaameshwari Fault

Interpretations of the base-Cretaceous (bC), base Paleogene (bP), Intra-Barmer Hill (IBH), and top Barmer Hill (TBH) horizons were used to construct a three-dimensional tectono-stratigraphical model of the early-stage sedimentary succession surrounding the Kaameshwari Fault (for model area see **Figure 6.3**; modelling was conducted using Schlumberger Information Systems Petrel software package). Upon construction of a fault model from fault interpretations, horizons were gridded using a convergent gridding algorithm. During gridding, input horizons were processed by deleting data within a user-defined symmetrical zone either side of the fault (step-back distance). Globally, a ‘step-back’ distance of 200m was used. Time-thickness [TVT (True Vertical Thickness) or isochore] maps were generated for the Cretaceous depositional interval (bC to bP) and the two depositional intervals within the Paleocene, to examine the spatial and temporal development of the Kaameshwari Fault (e.g. Whipp *et al.* 2014).

6.3.4 Geometrical comparison of early- and late-stage fault systems

The temporal evolution of deformation in the Barmer Basin was further constrained by comparing the fault populations at the base Cretaceous (bC; Clemson 2014) and Akli (Ak) horizons, that is by comparing fault maps at horizons within the early- and late-stage syn-rift sedimentary succession.

The geometrical properties of each fault population were represented by plotting measurements of fault azimuth on normalized half-rose diagrams. Fault traces were defined using footwall cut-offs, and were separated into linear segments 100 m in length. Subsequently, fault strike was recorded at the centre of each 100 m segment using the convention that fault dip is always to the right of fault strike. Fault azimuth was represented by plotting measurements of fault strike on the northern half (180°) of each normalised rose diagram, namely clockwise between bearings of 270° and 090°. For example, fault segments striking 013° and 205° as fault azimuths would plot as 013°and 025°, respectively.

6.4 The Kaameshwari area of the Barmer Basin

6.4.1 Structure

The study area is dominated by a large-displacement, approximately north-south trending fault (the Kaameshwari Fault; **Figures 6.3 & 6.4**) that displaces the deep sedimentary succession within the rift, namely the base Cretaceous (bC), base Paleogene (bP), Intra Barmer Hill (IBH), and Top Barmer Hill (TBH) horizons (**Figures 6.6 to 6.10**). The Kaameshwari Fault displaced horizons with an extensional sense and accommodated large deformation (> 800 ms throw; **Figures 6.6 to 6.10**). Horizon offset decreases upwards, that is younger horizons are offset to a lesser degree. In some areas the Kaameshwari fault dies out vertically into monoclinal structures that are mapped at the Top Barmer Hill (TBH), and occasionally intra-Barmer Hill (IBH) horizons (**Figures 6.7, 6.10, & 6.11**). The two deepest horizons, the base-Cretaceous (bC) and base-Paleogene (bP) horizons, dip steeply to the east with structural lows at the base of the Kaameshwari Fault, and are offset by large-displacement, approximately north-south to north-northwest-south-southeast trending extensional faults that are few in number (Clemson 2014; **Figures 6.3 & 6.4**). The base Cretaceous (bC) and base Paleogene (bP) fault populations have mean fault azimuths of 349°/169° and 348°/168° respectively, and population modes of 350°-360° and 340°-350° (**Figures 6.3 & 6.4**). However, the base Paleogene (bP) horizon is also deformed by significant faulting with azimuths between 320°-330° and 000°-010° (**Figure 6.4**). Within the area of the Kaameshwari Fault tectono-stratigraphical model, the intra-Barmer Hill (IBH) and Top Barmer Hill (TBH) horizons form gently folded, largely unfaulted surfaces, with structural lows in the east and in a north-south trending synformal structure above the Kaameshwari Fault (**Figure 6.11c & 6.11d**).

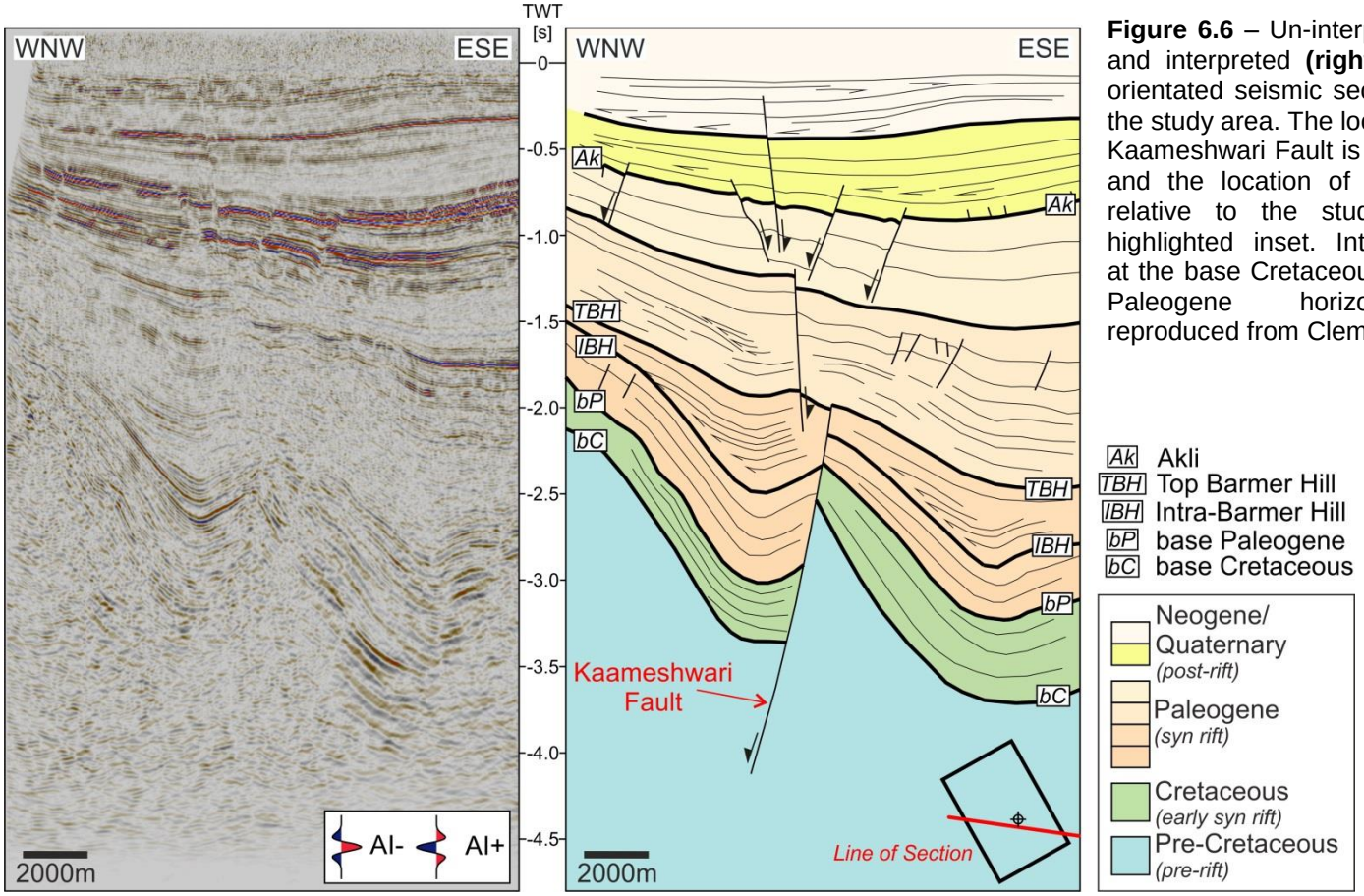

Figure 6.6 – Un-interpreted **(left)** and interpreted **(right)** randomly orientated seismic section across the study area. The location of the Kaameshwari Fault is highlighted, and the location of the section relative to the study area is highlighted inset. Interpretations at the base Cretaceous and base Paleogene horizons are reproduced from Clemson (2014).

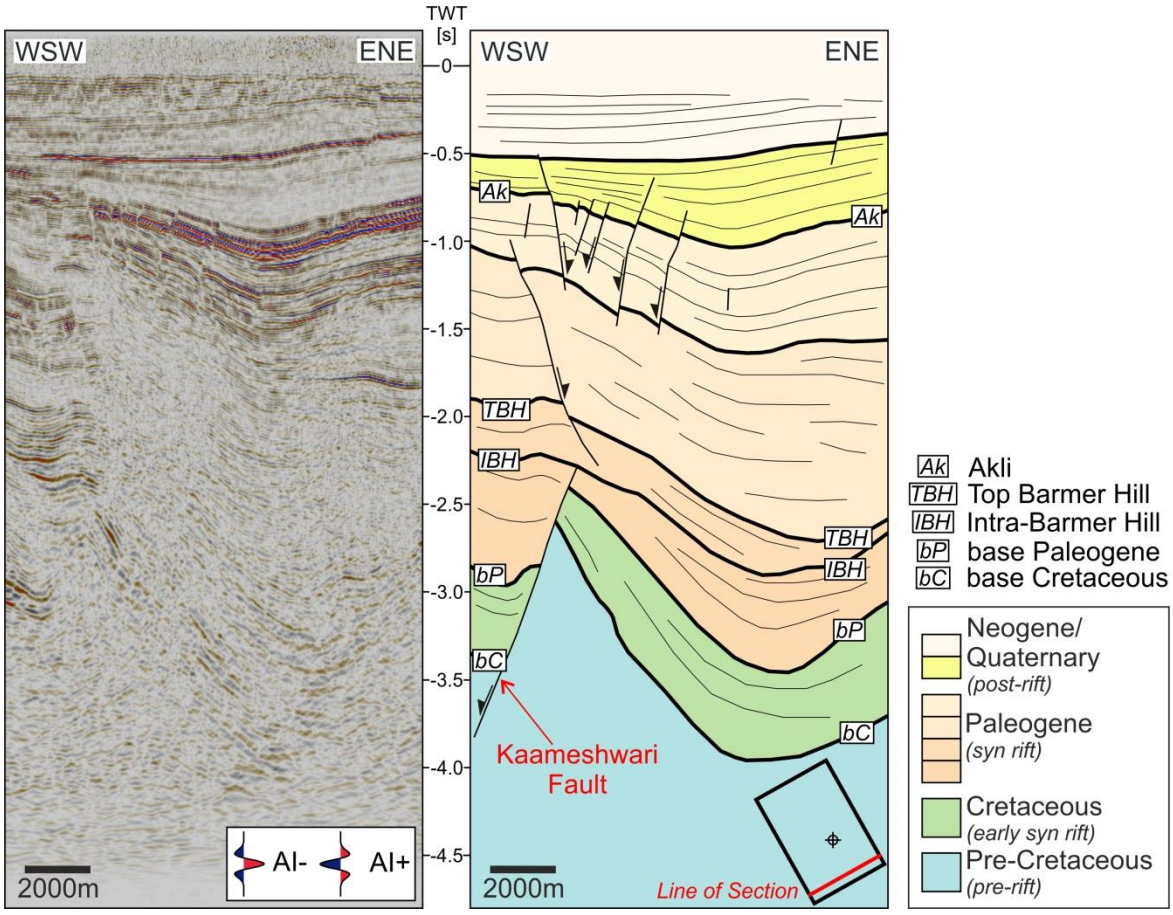

Figure 6.7 – Un-interpreted **(left)** and interpreted **(right)** cross-line seismic section across the south of the study area. The location of the Kaameshwari Fault is highlighted, and the location of the section relative to the study area is highlighted inset. Interpretations at the base Cretaceous and base Paleogene horizons are reproduced from Clemson (2014).

Overlying the Top Barmer Hill (TBH) horizon is a thick package of low-amplitude, discontinuous reflectors that characterise the Dharvi Dungar Formation and is largely devoid of seismically imaged through-going faulting (**Figures 6.8, 6.9, & 6.10**). However, in the south of the study area this package is offset by a through-going fault that is antithetic to the underlying Kaameshwari Fault (**Figures 6.6 & 6.7**). Occasionally, high-amplitude, continuous reflectors are imaged within this succession and are deformed by small-offset faults (**Figures 6.6 & 6.10**). Where the Top Barmer Hill horizon is penetrated by the Kaameshwari Fault, the Kaameshwari Fault terminates rapidly upwards within this nondescript package of seismic reflectors.

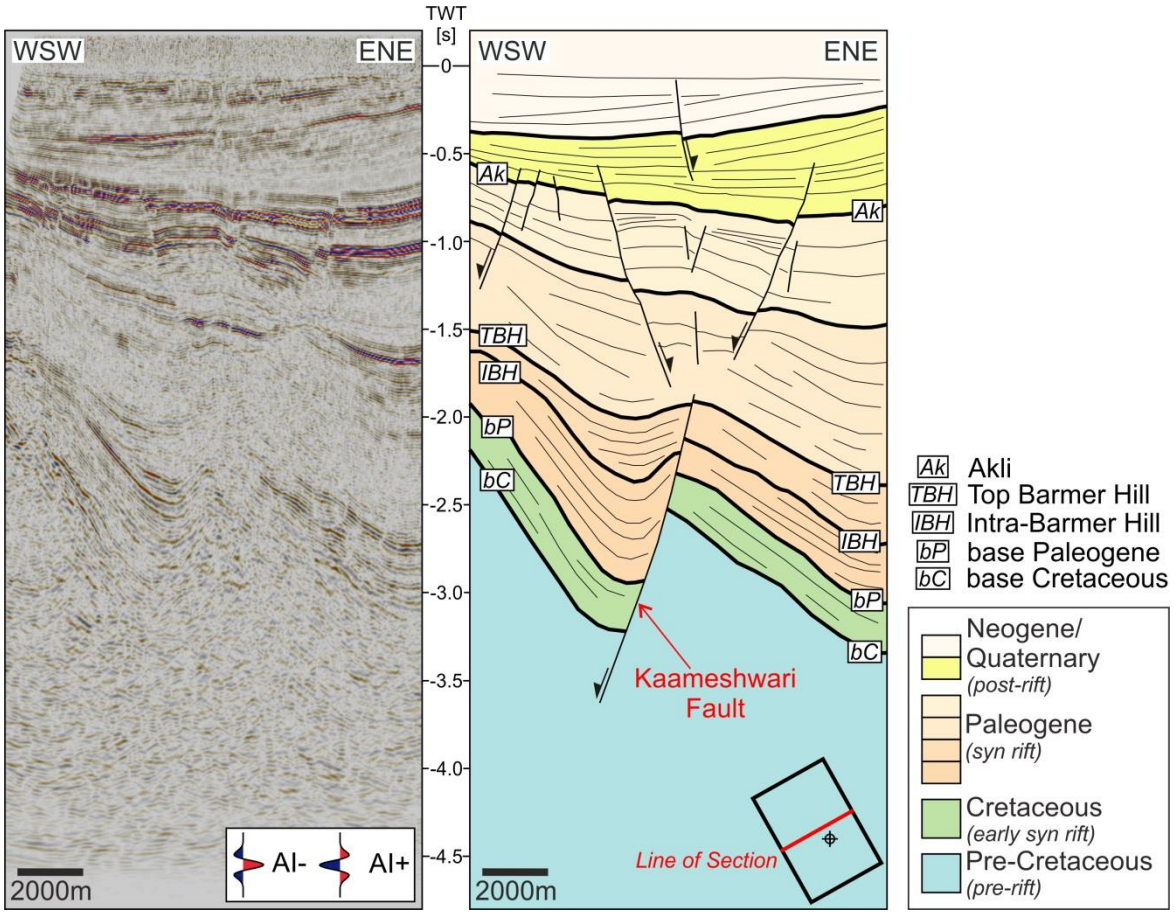

Figure 6.8 – Un-interpreted **(left)** and interpreted **(right)** cross-line seismic section across the centre of the study area. The location of the Kaameshwari Fault is highlighted, and the location of the section relative to the study area is highlighted inset. Interpretations at the base Cretaceous and base Paleogene horizons are reproduced from Clemson (2014).

Above the thick package of low-amplitude seismic reflectors (Dharvi Dungar Formation), a shallow fault system accommodated minor deformation in comparison to the underlying Kaameshwari Fault (**Figures 6.6 to 6.10**). Numerous small-offset faults deform two cyclic packages of low- to high-amplitude seismic reflectors, capped by the Akli (Ak) horizon (**Figure 6.5**), and terminate downwards within the underlying low-amplitude reflectors of the Dharvi Dungar Formation (**Figures 6.6 to 6.10**). The dominant seismic signal frequency at the Ak horizon is approximately 40Hz, and the average interval velocity as constrained from the K1 well is 2300 m s^{-1} (**Figure 5.5**). From **equations 6.3 & 6.4**, therefore, the vertical resolution at the Ak horizon is approximately 14 m. The Akli (Ak) horizon dips shallowly to the east-northeast, and is offset by numerous small-offset (up to 30 ms TWT; ≈ 34.5 m when v = 2300 m s^{-1}), isolated faults that form arcuate, some highly curved, fault traces, and occur in two dominant orientations; north-northwest-south-southeast (rift-parallel) and northeast-southwest (rift-oblique) trending (**Figure 6.12**). Two structural

lows are present in the southeast and north of the study area (**Figure 6.12**). The mean fault azimuth of the fault population that deforms the Akli (Ak) horizon is 351°/171°, with a population mode between 330° and 340° (**Figure 6.12**). In the northwest of the study area faulting is almost exclusively rift-parallel (north-northwest-south-southeast). However, in a north-south trending zone across the centre of the study area, both rift-parallel and rift-oblique (northeast-southwest) faults occur (**Figure 6.12**). In cross-section, shallow faulting is often localised above the Kaameshwari Fault (**Figures 6.6, 6.7, 6.8, & 6.10**), specifically where the Intra Barmer Hill (IBH) and Top Barmer Hill (TBH) horizons are offset by the Kaameshwari Fault (**Figures 6.6 & 6.8**). Rarely, small-offset faulting deforms the post-rift succession (**Figures 6.6, 6.8, & 6.10**).

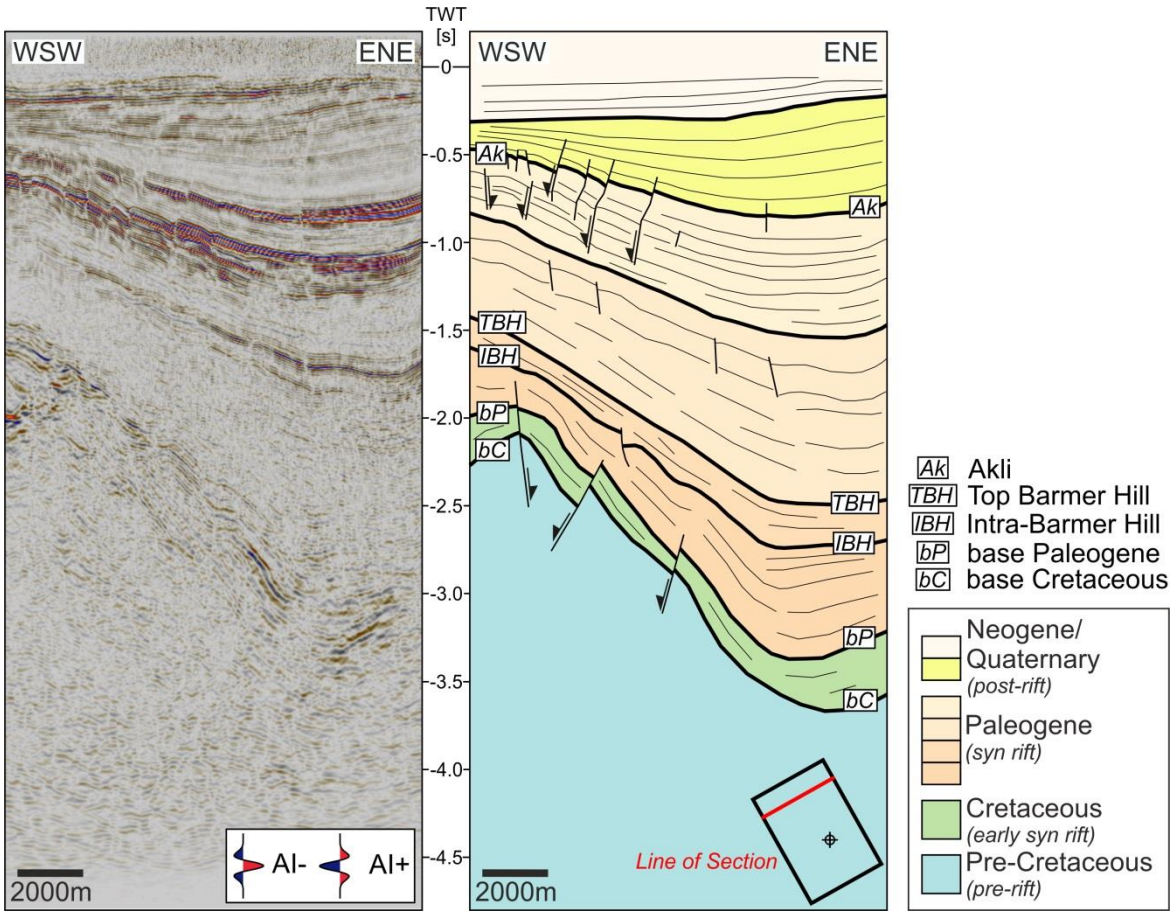

Figure 6.9 – Un-interpreted **(left)** and interpreted **(right)** cross-line seismic section across the north of the study area. The location of the section relative to the study area is highlighted inset. Interpretations at the base Cretaceous and base Paleogene horizons are reproduced from Clemson (2014).

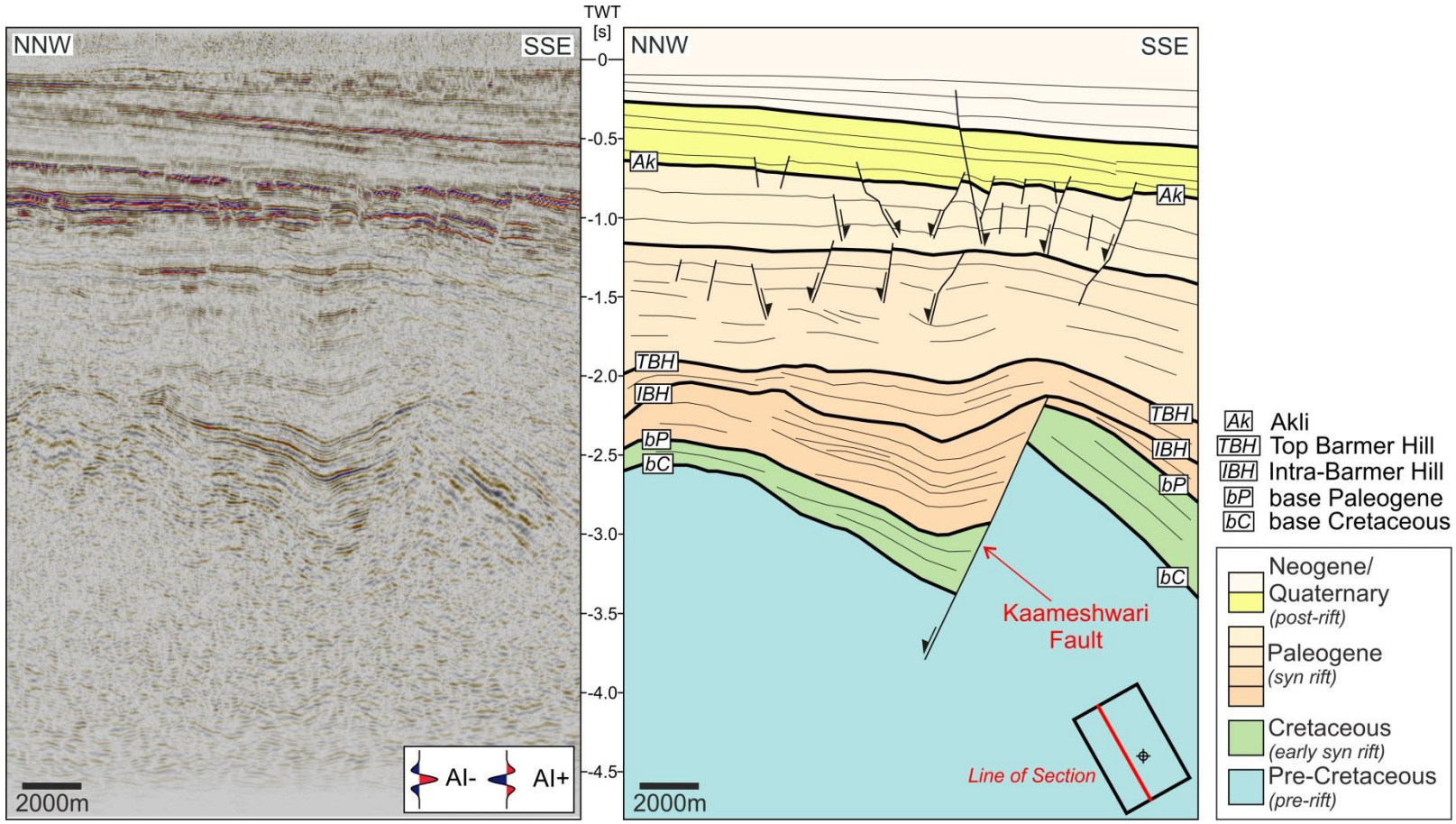

Figure 6.10 – Un-interpreted **(left)** and interpreted **(right)** inline seismic section across the centre of the study area. The location of the Kaameshwari Fault is highlighted, and the location of the section relative to the study area is highlighted inset. Interpretations at the base Cretaceous and base Paleogene horizons are reproduced from Clemson (2014).

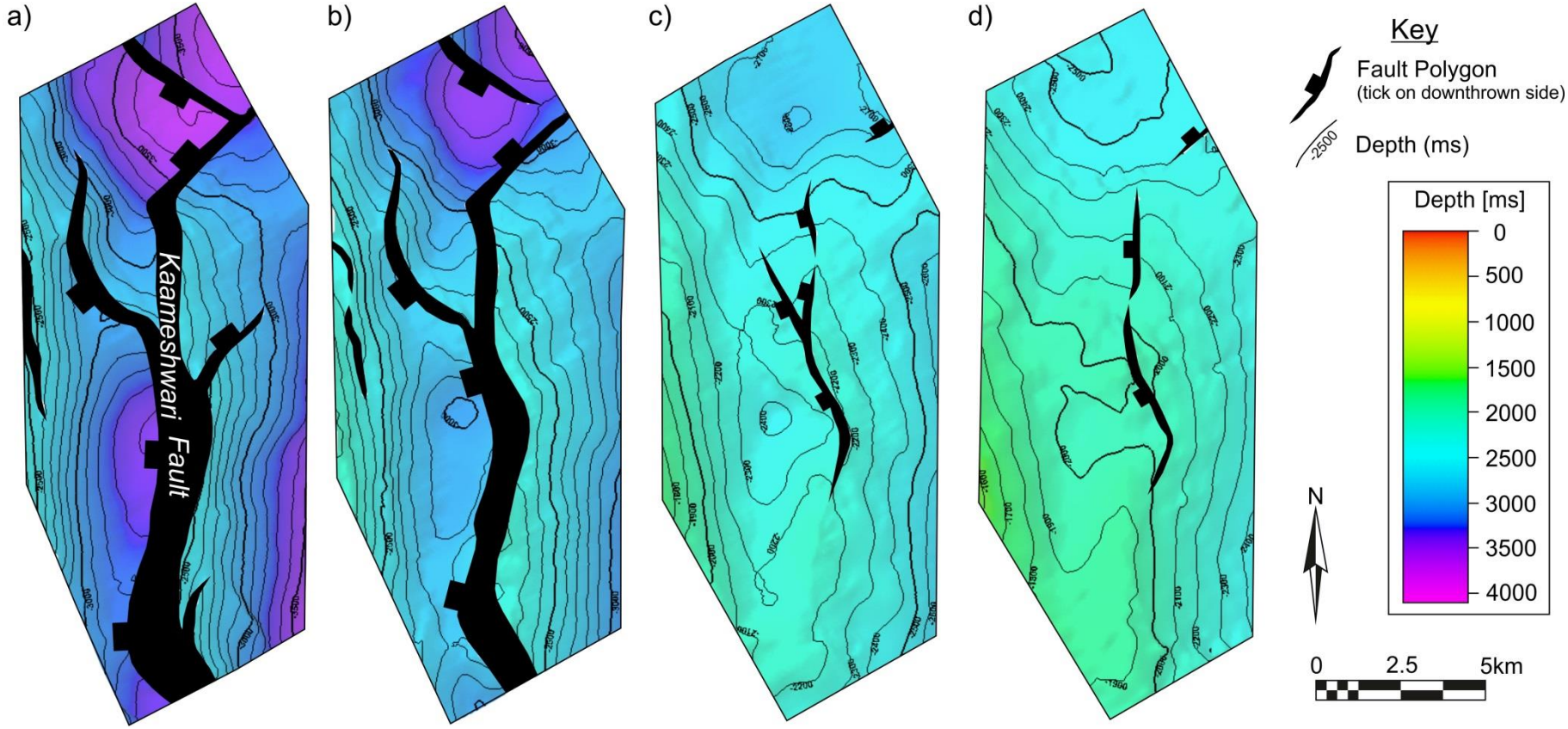

Figure 6.11 – Time-structure maps of the base Cretaceous **(a)**, base Paleogene **(b)**, Intra-Barmer Hill (IBH) **(c)**, and Top Barmer Hill (TBH) **(d)** surfaces within the Kaameshwari Fault study area. (a) & (b) reproduced from Clemson (2014). Key to colours inset. For location see **figure 6.3**.

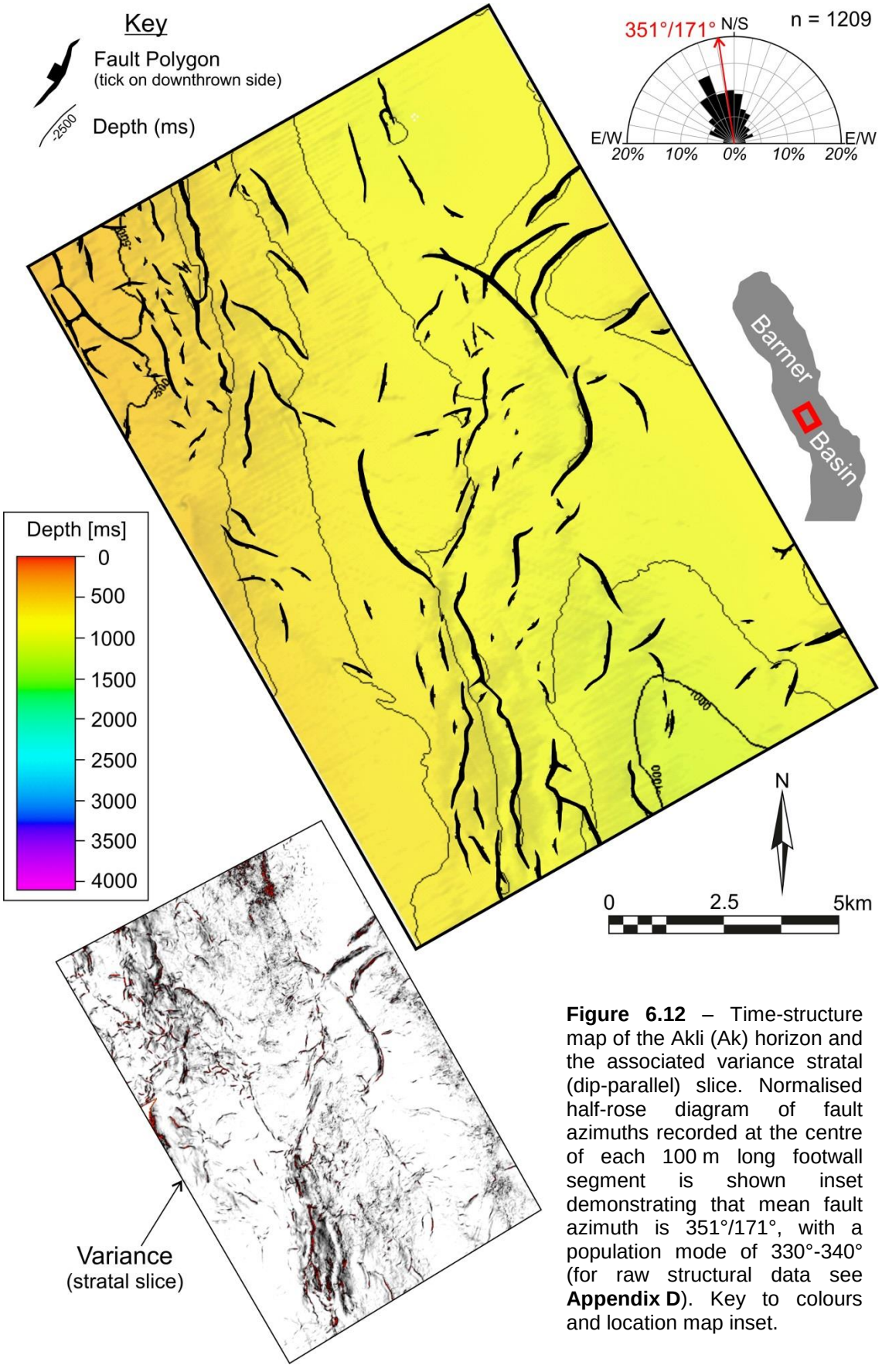

Figure 6.12 – Time-structure map of the Akli (Ak) horizon and the associated variance stratal (dip-parallel) slice. Normalised half-rose diagram of fault azimuths recorded at the centre of each 100 m long footwall segment is shown inset demonstrating that mean fault azimuth is 351°/171°, with a population mode of 330°-340° (for raw structural data see **Appendix D**). Key to colours and location map inset.

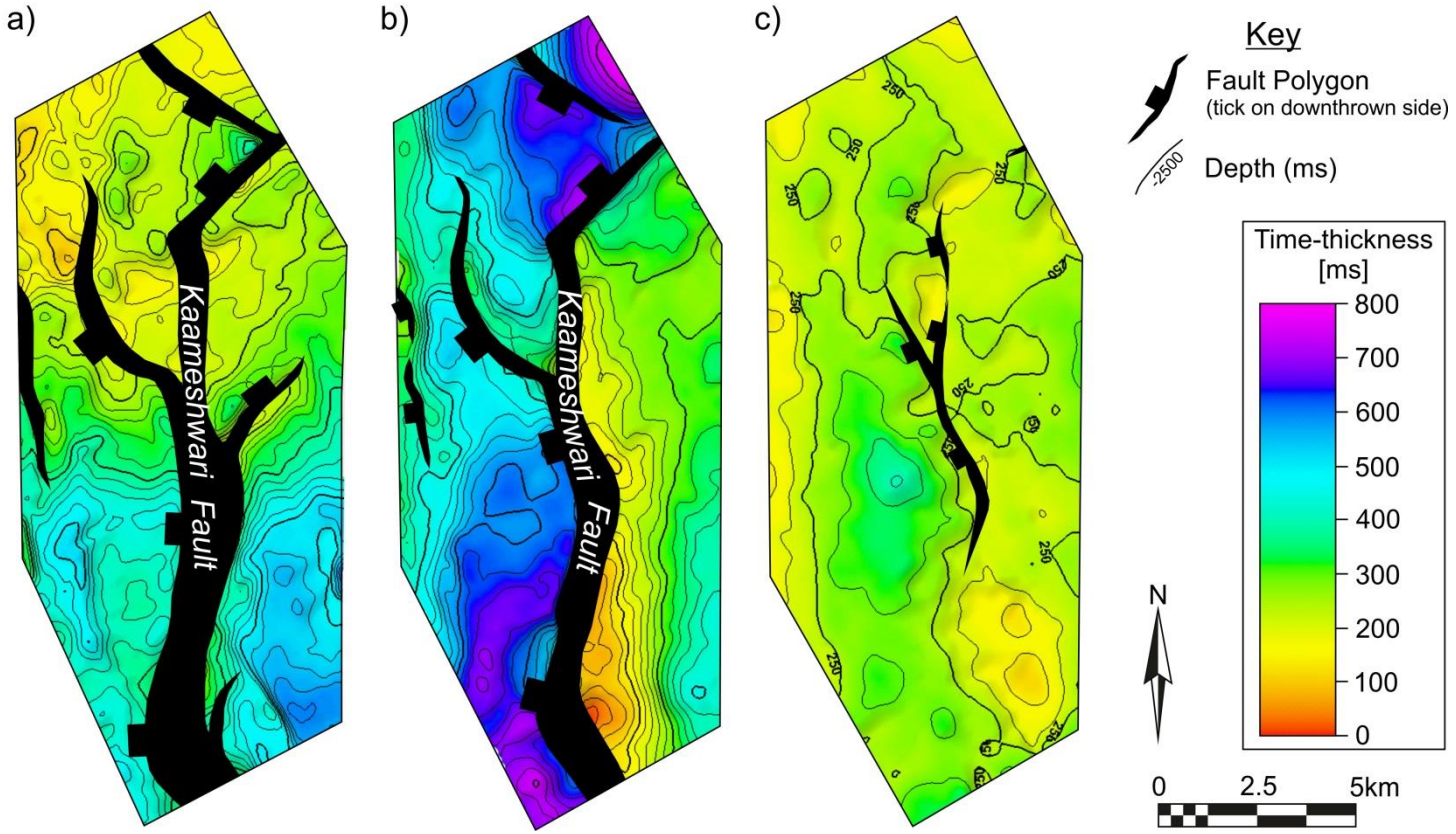

Figure 6.13 – Sediment thickness [True Vertical Thickness (TVT) or isochore maps of the Cretaceous (bC to bP) **(a)**, the base Paleogene (bP) to Intra-Barmer Hill (IBH) **(b)**, and the Intra-Barmer Hill (IBH) to Top Barmer Hill (TBH) **(c)** depositional intervals in the Kaameshwari Fault study area. Key to colours inset. For location see **figure 6.3**.

6.4.2 Seismic stratigraphy

Seismic reflectors within the Cretaceous depositional interval (bC to bP) are broadly laminar (**Figures 6.6 to 6.10, & 6.14**). The package shows little significant variation in thickness across the Kaameshwari Fault (**Figure 6.13a**) but thickens substantially (< 400 ms) from north to south.

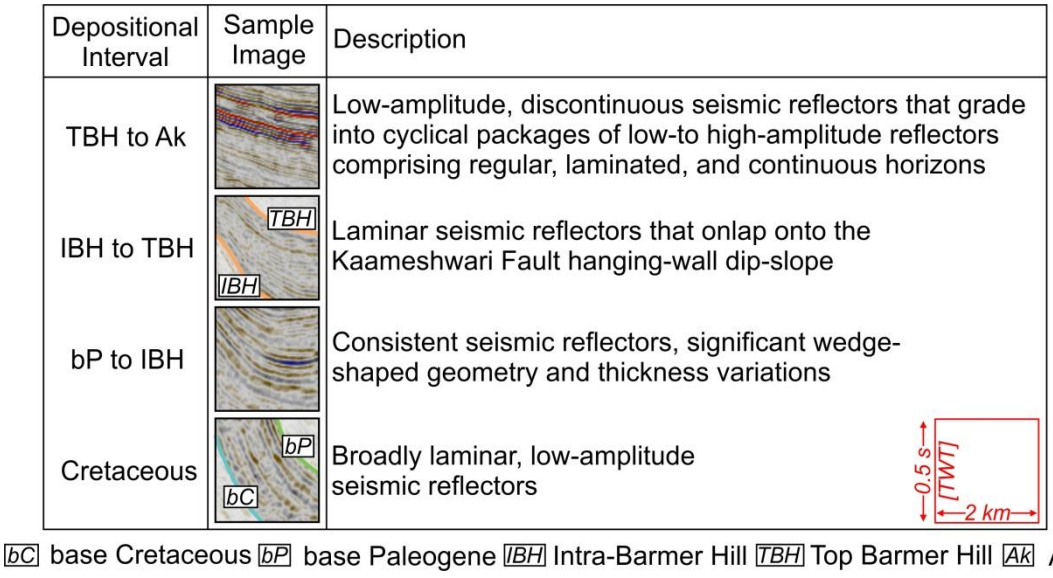

Figure 6.14 – Representative seismic stratigraphical images of each depositional interval used in the Kaameshwari study. Key to horizon labels and the scale of each sample image are shown.

The depositional interval between the base Paleogene (bP) and Intra-Barmer Hill (IBH) horizons is characterised by prominent seismic reflectors that are constant along the hanging-wall dip-slope and fan towards the Kaameshwari Fault (**Figures 6.6 to 6.10, & 6.14**). This interval has the most pronounced wedge-shaped geometry throughout the study area and thickens significantly (< 700 ms) across the Kaameshwari Fault (**Figure 6.13b**). Thickening occurs through addition of seismic reflectors between prominent reflectors towards the Kaameshwari Fault (**Figure 6.14**), rather than through a gradual onlap of seismic reflectors up the Kaameshwari Fault hanging-wall dip-slope. In the south of the study area, steeply-dipping reflectors within the Cretaceous interval (bC to bP) that occur in the footwall of the Kaameshwari Fault are truncated against the uppermost reflectors within the bP to IBH interval (**Figure 6.15**). Occasionally the IBH horizon onlaps across the truncation surface (**Figure 6.15**).

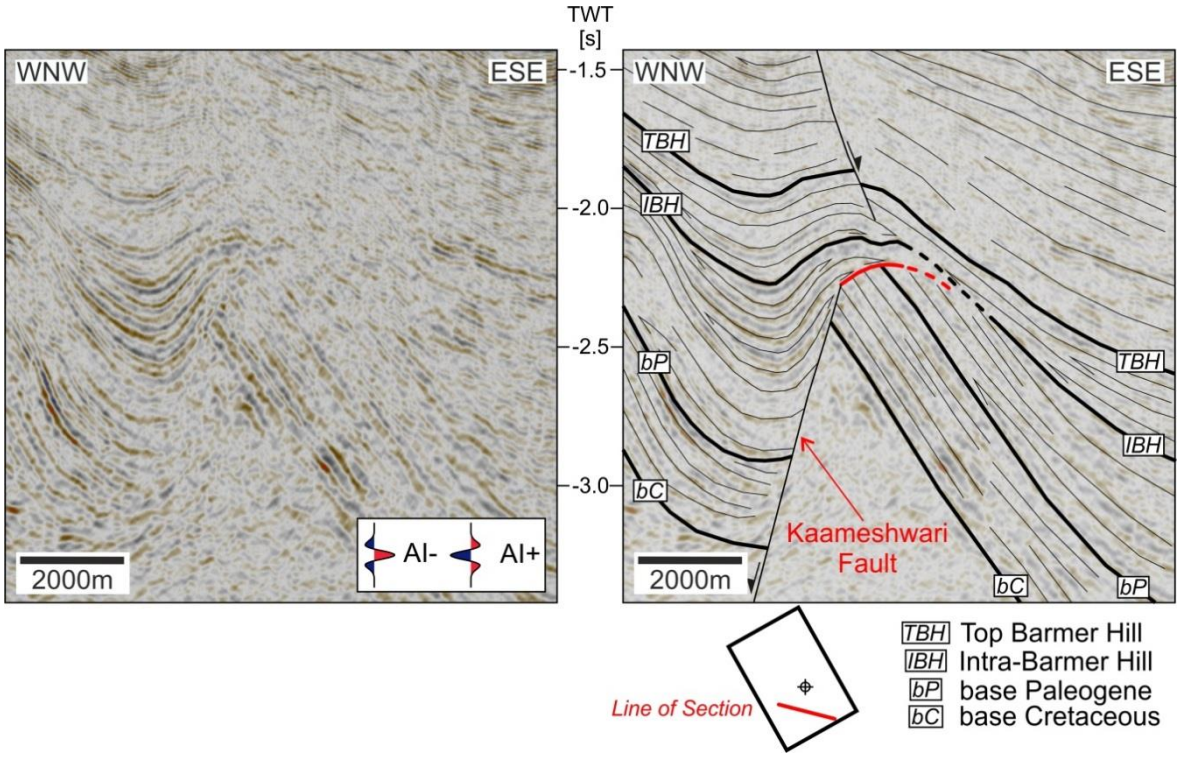

Figure 6.15 – Un-interpreted **(left)** and interpreted **(right)** seismic images depicting truncated seismic reflectors in the Kaameshwari Fault footwall and onlap of the Intra-Barmer Hill (IBH) horizon onto the truncation surface. The location of the Kaameshwari Fault is highlighted, and the location of the section relative to the study area is highlighted inset. Interpretations at the base Cretaceous and base Paleogene horizons are reproduced from Clemson (2014).

Within the depositional interval between the IBH and TBH horizons seismic reflectors are relatively laminar and progressively onlap up the Kaameshwari Fault hanging-wall dip slope (**Figures 6.6, 6.8, 6.9 & 6.14**). The depositional interval between the intra-Barmer Hill (IBH) and Top Barmer Hill (TBH) horizon is relatively uniform in thickness. However, an approximately north-south trending zone occurs across the centre of the study area where deposits are thicker (<100ms; **Figure 6.13c**).

A significant and prominent reduction in the continuity of seismic reflectors occurs across the Top Barmer Hill (TBH) horizon within the Dharvi Dungar Formation. Reflectors are low-amplitude, fuzzy, and discontinuous (**Figure 6.5 & 6.14**). However, a general dip and thickening of the package towards the east-northeast is apparent. Fuzzy, discontinuous reflections grade upwards into two cyclic, low-to high-amplitude reflector packages comprising regular, laminated, and continuous horizons capped by the Akli (Ak) horizon (**Figure 6.5 & 6.14**). Rarely, small-scale growth of stratigraphical intervals is apparent across faults (growth faulting; **Figure 6.16**).

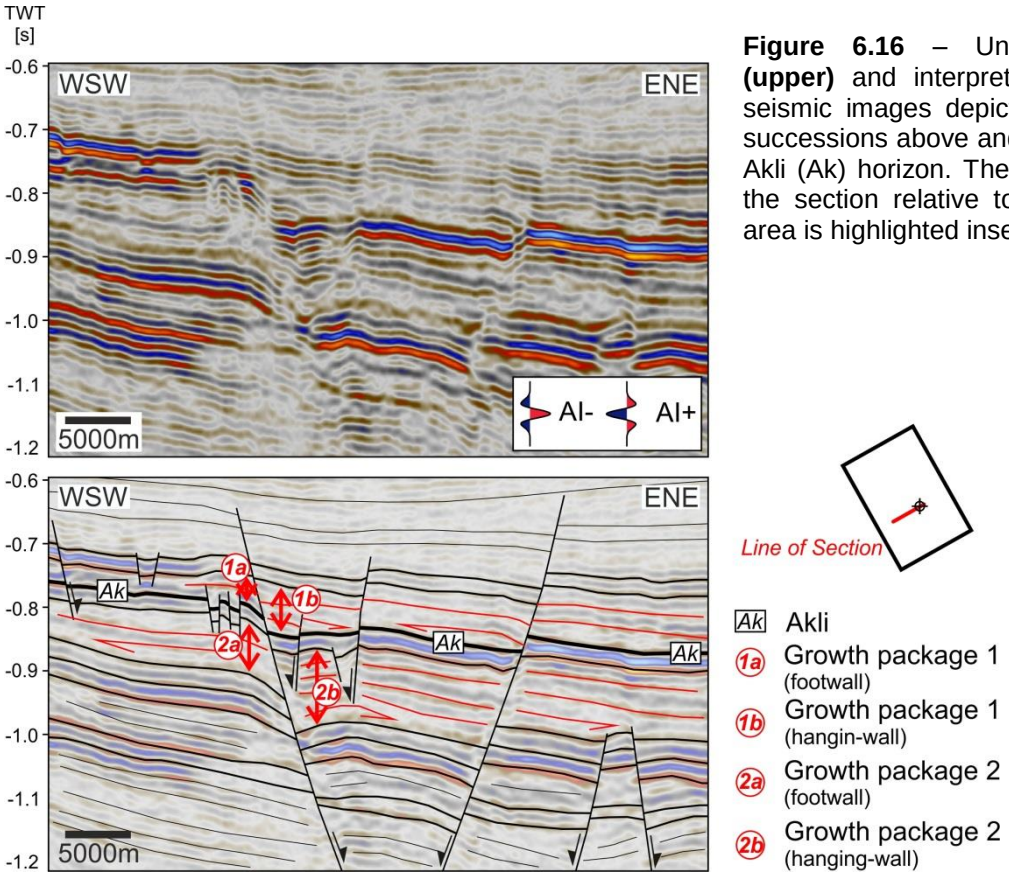

Figure 6.16 – Un-interpreted **(upper)** and interpreted **(lower)** seismic images depicting growth successions above and below the Akli (Ak) horizon. The location of the section relative to the study area is highlighted inset.

6.5 Tectono-stratigraphy

6.5.1 Early-stage faulting: the Kaameshwari Fault

The lack of significant thickness variations across the Kaameshwari fault during the Cretaceous depositional interval (bC to bP; **Figure 6.13a**) indicates tectonic inactivity, corroborated by the broadly laminar seismic reflectors imaged on seismic sections (**Figures 6.6 to 6.10**), despite previous suggestions of an early, rift-oblique (≈ northwest-southeast) extensional event (**Chapter 5**). However, the substantial thickening (< 400 ms) of the Cretaceous interval to the south alludes to active faulting elsewhere in the region.

The significant thickening of the depositional interval between the base Paleogene (bP) and intra-Barmer Hill (IBH) horizon in the Kaameshwari Fault hanging-wall, and the associated condensed sedimentary succession in the footwall (**Figure 6.13b**), indicates substantial fault-controlled subsidence and the onset of deformation during the Paleogene Period. The wedge of seismic reflectors that fan towards the Kaameshwari Fault represents deposition during a gradual rotation of the hanging-wall dip-slope. In the south of the study area, truncation of the base Paleogene horizon (bP) in the Kaameshwari Fault footwall, and onlap of the intra-Barmer Hill horizon (IBH)

onto the truncation surface indicate exposure, erosion and burial was rapid, and occurred between deposition of the base Paleogene (bP) and intra-Barmer Hill (IBH) horizons. The negligible offset of the intra-Barmer Hill horizon by the Kaameshwari Fault throughout the study area (**Figure 6.6 to 6.10, & 6.15**) indicates that the Kaameshwari Fault was largely inactive by the time of deposition of the Intra-Barmer Hill (IBH) horizon.

The minor thickness variations between the Intra-Barmer Hill (IBH) and the Top Barmer Hill (TBH) horizons (**Figure 6.13c**) and lack of discrete faulting of the intra-Barmer Hill (IBH) and Top Barmer Hill (TBH) horizons (**Figures 6.11c & d**) indicate negligible active faulting throughout the study area during this depositional interval. The progressive onlap of laminar seismic reflectors up the Kaameshwari Fault hanging-wall dip-slope (**Figures 6.6 & 6.8**), as well as the occasionally unfaulted succession of reflectors that are draped across the Kaameshwari Fault (**Figures 6.10 & 6.15**), indicate subsidence rates had exceeded the sedimentation rate and the inactive Kaameshwari Fault was buried. The transition from a wedged package of fanning seismic reflectors in the bP to IBH depositional interval, into a package of laminated seismic reflectors that onlap over the underlying intra-Barmer Hill (IBH) horizon, suggests a sudden deepening event coincident with the establishment of the main rift-parallel extensional fault systems (Dolson *et al.* in press). The north-south trending zone of thicker sediments (**Figure 6.13c**) may reflect an infilling of irregular topography or deposition within a subtle flexural basin during the concluding stages of deformation on the Kaameshwari Fault.

In summary, the rift-oblique (north-south) Kaameshwari Fault accommodated significant extensional deformation during the earliest-stages of the main Barmer Basin rift event. However, the fault rapidly became inactive, and was buried by the end of Barmer Hill Formation deposition.

6.5.2 Dharvi Dungar Formation detachment

The transition from continuous reflectors of variable amplitude beneath the Top Barmer Hill (TBH) horizon, into discontinuous fuzzy reflectors above, marks an important mechanical boundary. The lack of regular seismic reflections of notable amplitude suggests the overlying depositional interval comprises a broadly homogeneous sedimentary package at the scale of seismic resolution. The positioning of this package immediately above the Top Barmer Hill (TBH) horizon indicates this nondescript interval corresponds to the fine-grained, sand-poor lacustrine deposits of the Dharvi

Dungar Formation (c.f. Dolson *et al.* in press). Importantly, the lack of faulting resolved within this interval, and the termination of faults into it from both above and below, indicates the incompetency of the lithology for seismically resolvable, systematic brittle failure, and suggests a tendency to fail in a more ductile manner at the scale of seismic resolution. Such a mechanically incompetent unit likely forms an important detachment within the syn-rift sedimentary succession of the Barmer Basin. The lack of seismically resolved faulting may reflect a temporary cessation of rifting. However, as an alternative, continued extension may be manifest through a lithologically-controlled variation in deformation mechanism and a vertically segmented fault system (e.g. Childs *et al.* 1996) resulting from the mechanical incompetence of the Dharvi Dungar Formation and the apparent inability of this interval to deform on seismically resolvable brittle faults.

6.5.3 Late-stage Akli Formation fault system

Low-strain deformation features within the Akli Formation (Ak horizon; **Figure 6.12**) comprise faults with characteristic extensional fault geometries. The presence of small-scale growth faulting (**Figure 6.16**) supports the interpretation that deformation is late-stage syn-rift, and not related to post-rift compressional structures observed elsewhere in the rift (e.g. Dolson *et al.* in press). However, some faults that offset the Akli (Ak) horizon cut upwards into the shallow, post-rift succession (**Figures 6.6, 6.8, & 6.10**) indicating recent deformation, likely the manifestation of recent inversion. Significant offset (< 200 ms) of the Akli (Ak) horizon at the edge of the Saraswati Terrace to the east, as well as the wedge-shaped geometry of the underlying stratigraphical interval (**Figure 6.2**) provide further support for active rifting until this time.

Despite the comparable mean fault azimuths of early- (bC) and late-stage (Ak) fault systems, a significant (20°-30°) anticlockwise rotation in the modes of the fault populations (**Figure 6.17**) demonstrates late-stage fault systems tended towards a more rift-parallel orientation. It follows that the presence of the underlying Dharvi Dungar Formation detachment package isolated (detached) late-stage faulting from the underlying early-stage structural complexities (e.g. Withjack *et al.* 1990; Hardy & McClay 1999), and facilitated the nucleation and growth of late-stage brittle deformation structures in response to the regional state of stress. The northwest-southeast mode of the Akli (Ak) fault population suggests faulting accommodated approximately northeast-southwest (rift-perpendicular) extension.

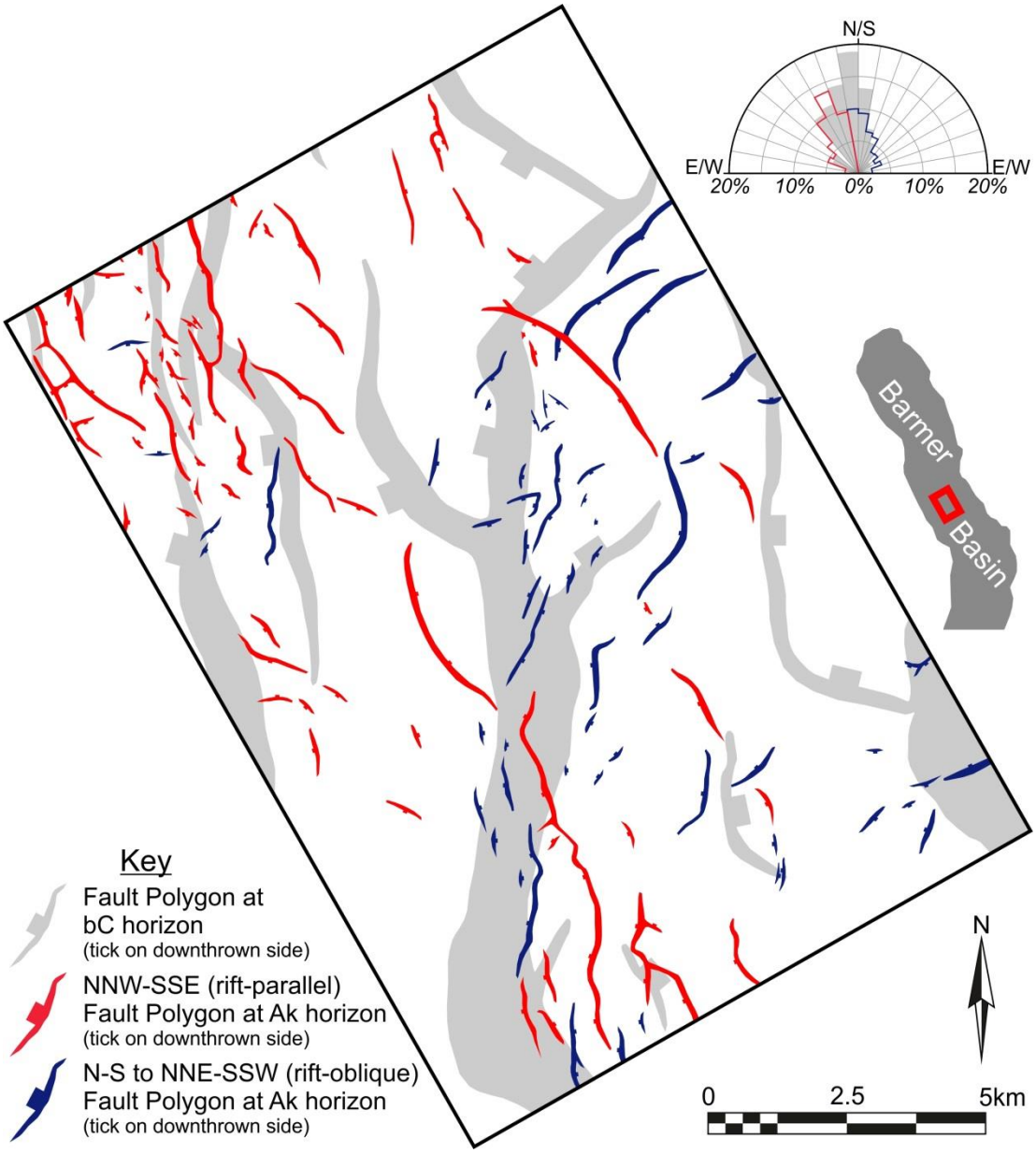

Figure 6.17 – Comparison of early-stage and late-stage fault geometries mapped at the base Cretaceous (bC) and Akli (Ak) horizons respectively. Normalised half-rose diagram of fault azimuths recorded at the centre of each 100m long footwall segment at the base Cretaceous (bC) and Akli (Ak) horizons is shown inset (see key for colours). Despite the comparable mean fault azimuths of the bC and Ak horizon fault populations, a significant (20°-30°) anticlockwise rotation of the modes of the fault populations is evident between early- and late-stage fault systems. Interpretations at the base Cretaceous horizon are reproduced from Clemson (2014). Location map and key to colours inset.

Although separated from the underlying Kaameshwari Fault system by the Dharvi Dungar Formation detachment package (**Figure 6.5**), a spatial correlation is evident between the early-stage (deep) Kaameshwari Fault, and rift-oblique (north-south) faulting within the late-stage (shallow) fault system (**Figure 6.17**). Rift-oblique (north-south to northeast-southwest) faulting is dominant at the northern end of the Kaameshwari Fault likely indicating coupled deformation

processes between early-stage and late-stage fault systems. During deformation the competency contrast between the incompetent Dharvi Dungar Formation, which likely deformed in a ductile manner at the scale of seismic resolution, and the comparatively competent sandstone and lignite successions of the Thumbli and Akli formations, likely promoted brittle deformation. Although not mechanically linked, early- (deep) and late- (shallow) stage fault systems may have been kinematically linked by ductile (at the scale of seismic resolution) deformation within the intervening Dharvi Dungar Formation, accounting for the spatial correlation between early- and late-stage fault systems in some sections of the study area.

6.6 Discussion

Without invoking a substantial rotation (≈ 30°) of the regional extension vector, it is hard to resolve such an active fault during incipient rifting becoming inactive at such an early stage of rift evolution. The concomitance between Kaameshwari Fault inactivity, and the establishment of the major rift-parallel (north-northwest-south-southeast) rift-margin fault systems, suggests the latter formed a more efficient means of accommodating extension. This relationship, namely rift-oblique faulting that is active during early rifting superseded by rift-parallel faulting, is a characteristic relationship in areas of structural inheritance (**Figure 2.13**; e.g. Morley 1995; Lezzar *et al.* 2002; Morley *et al.* 2004; Bellahsen & Daniel 2005). The tectono-stratigraphical evolution of the Kaameshwari Fault, therefore, supports previous suggestions that rift-oblique faults and structural complications interpreted in the subsurface throughout the Barmer Basin, are a manifestation of structural inheritance. However, robust evidence indicating oblique-slip of rift-oblique faults during the main Barmer Basin rift event, which would indicate that rift-oblique faulting was orientated obliquely (unfavourable) to the extension direction, remains elusive. Further to this, inactivity of the Kaameshwari Fault during the Cretaceous depositional interval (bC to bP), but inheritance of this fault during the early-stages of Paleogene rifting suggests weak fabrics of multiple orientations are pervasive throughout the northwest Indian crust. Northeast-southwest faults formed during early, rift-oblique (northwest-southeast) extension, as exposed at outcrop in the Sarnoo Hills, are likely only one of multiple trends of weak fabrics inherited during Barmer Basin rift evolution.

The discovery of growth faulting in early- to middle-Eocene Epoch strata (Ak horizon; **Figure 6.16**) indicates active extensional deformation occurred in the Barmer Basin until at least this time. The dominant rift-parallel orientation of faulting in the Akli (Ak) fault system, and the mechanical

independence of this shallow fault system from deeply buried, early-stage structural complexities, suggest deformation during the late-stages of Barmer Basin rift evolution accommodated approximately rift-perpendicular (≈ northeast-southwest) regional extension. Late-stage rift-perpendicular extension is coaxial to that suggested for early-stage deformation based on outcrop exposure in the Barmer Hills (**Chapter 3**). However, evidence coupling early- and late-stage deformation that accommodated rift-perpendicular (≈ northeast-southwest) extension to a common mechanism, for example long-lived regional extension, is lacking. Regional extension in the Barmer Basin from the latest Upper Cretaceous Epoch into the early- to middle-Eocene Epoch may signify an unusually long period of rifting (< 20 Ma) if early- and late-stage extension were related to a common mechanism. Late-stage deformation at the Akli (Ak) horizon coincides with, or post-dates, the onset of collision between the Indian and Eurasian continents (55 Ma; Green *et al.* 2008), and may signify a late extensional pulse related to tectonism in the foreland of the collision zone. Further to this, the potential for an early collision between the northwest Indian and Eurasian continents, possibly as early as the Cretaceous-Paleogene boundary (66 Ma; Beck *et al.* 1995), suggest that a complex interplay may have existed between regional extension and deformation in the foreland of the India-Eurasia collision zone.

6.7 Summary

This chapter investigated the north trending Kaameshwari Fault that is oblique (≈ 30°) within the north-northwest trending (330°) Barmer Basin to evaluate and refine previous interpretations. In combination, seismic- and tectono-stratigraphical relationships demonstrated that the Kaameshwari Fault accommodated significant fault-controlled subsidence during incipient Paleogene rifting, but became largely inactive by the time of deposition of the intra-Barmer Hill (IBH) horizon during the mid-Paleocene Epoch. The cessation of Kaameshwari Fault activity was coeval with the establishment of the main rift-parallel, rift-margin fault systems, suggesting the rift-oblique (≈ north-south) Kaameshwari Fault was orientated obliquely (non-ideal) to the extension direction. It follows that the Kaameshwari Fault comprises an inherited structure providing further support to previous suggestions that rift-oblique faults and structural complications in the Barmer Basin subsurface arise from the inheritance of pre-existing structures. However, despite a substantial thickening of sediments within the Cretaceous depositional interval towards the south (< 400 ms), a pronounced lack of thickness variations across the Kaameshwari Fault indicates tectonic inactivity. Northeast-

southwest trending faults, therefore, were likely only one of multiple trends of weak pre-existing fabrics that were inherited during the Paleogene Barmer Basin rift event. The formation of faults that tended toward a more rift-parallel orientation within the mechanically independent, early- to middle-Eocene Epoch Akli Formation alludes to northeast-southwest orientated (rift-perpendicular) regional extension as exposed in the Barmer Hills (**Chapter 3**). The potential for early collision between the Indian and Eurasian continents suggest that a complex interplay may have existed between regional extension and extensional deformation in the foreland of the India-Eurasia collision zone.

7 Lithosphere-scale deformation

Lithosphere-scale forward modelling of extensional deformation in the central Barmer Basin using the flexural-cantilever model

A complete basin analysis should incorporate the flexural response of the lithosphere to extension, and it should be demonstrated that shallow deformational processes constrained from outcrop and subsurface investigations, are compatible with deformational processes at the lithosphere-scale. Lithosphere flexure was unaccounted for during backstripping and restoration of two-dimensional cross-sections and the three-dimensional tectono-stratigraphical model of the central Barmer Basin due to a lack of syn-rift deposits preserved on the rift-shoulders (**Chapter 5**). Further to this, large, lithosphere-scale deformational and geodynamical processes are poorly known for the northwest Indian region at the Cretaceous-Paleogene boundary. In this chapter, the flexural response of the lithosphere during the Paleogene Barmer Basin rift event is assessed, and the integrated structural analysis of the Barmer Basin, incorporating outcrop- (small), seismic- (basin) and lithosphere-scale deformation, is completed using a flexural-cantilever forward modelling approach (e.g. Kusznir & Egan 1989; Kusznir *et al.* 1991; Kusznir & Ziegler 1992; Kusznir *et al.* 1995). Two seismic sections across the central Barmer Basin are modelled (profiles 1 & 2; **Figure 7.1**), with models constrained by a geometrical comparison with depth-converted seismic sections and a subsidence history plot adjacent to one of the modelled sections. A model of coupled simple- and pure-shear deformation in the shallow and deep lithosphere respectively, with the zone of pure-shear deformation situated beneath the rift, produced satisfactory results and is an appropriate approximation of Paleogene extension in the Barmer Basin. The findings predict large (< 3 km) flexural rebound induced footwall uplift, indicating: 1) that the Barmer Basin comprised a significant topographical feature during the Paleogene Period; 2) sedimentary environments and sediment facies distributions during early-stage rifting were structurally and geodynamically controlled, and; 3) erosion of uplifted footwall material may have formed an important source of sediment.

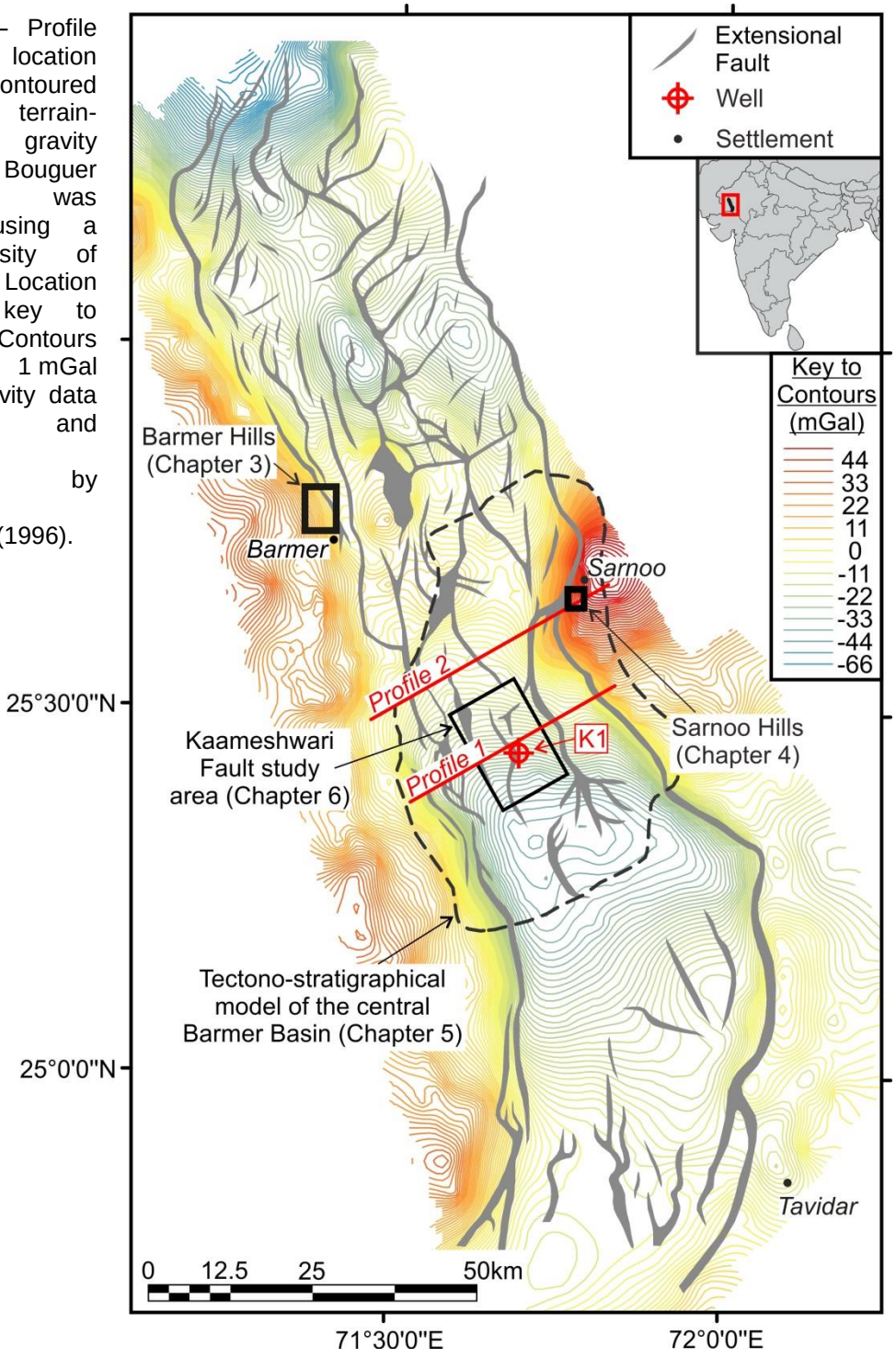

Figure 7.1 – Profile and K1 well location overlying a contoured Bouguer and terrain-corrected gravity dataset. Bouguer correction was conducted using a crustal density of 2.67 g cm^{-3}. Location map and key to colours inset. Contours are at 1 mGal intervals. Gravity data acquired and processed commercially by EDCON-PRJ Incorporation (1996).

7.1 Geological setting

The onset of subsidence in the central Barmer Basin occurred at the Jurassic-Cretaceous boundary and comprised a gradual and progressive deepening to a maximum of 500 m, as demonstrated by sediments preserved in the K1 well (**Figure 7.2**; Dolson *et al.* in press). A sudden and pronounced deepening (2500 m) occurred between the mid-Paleocene (≈ 62 Ma) and mid-Eocene (≈ 48 Ma) epochs, before approximately 25 Myr of gradual subsidence that slowed

progressively with time (**Figure 7.2**). This was followed by a period (< 10 Myr) of gradual and varied uplift during the early- to middle-Miocene Epoch (< 600 m; **Figures 7.2 & 7.3**). Between 400 m and 1200 m of non-uniform uplift in the north of the rift since the late Oligocene and Pliocene epochs is manifest as occasional minor inversion of normal faulting, strike-slip faulting and the associated flower structures (Dolson *et al.* in press). Subsequently to uplift and erosion, subsidence and deposition were re-instated, burying the erosional surface and producing the Base Miocene Unconformity (BMU; Compton 2009), and preserving 500 m of post-uplift deposition in the K1 well (**Figure 7.2**; Dolson *et al.* in press).

The elastic thickness, nature of deformation in the lower crust and mantle lithosphere, and asthenosphere temperature are poorly known for the Barmer Basin at the Cretaceous-Paleogene boundary. However, immediately to the south of the Barmer Basin, work in the Sanchor Basin suggested that the Present Day crustal thickness is 31 - 33 km and the thickness of the upper crust does not exceed 15 km based upon seismic refraction and wide angle reflection data (Kaila *et al.* 1990).

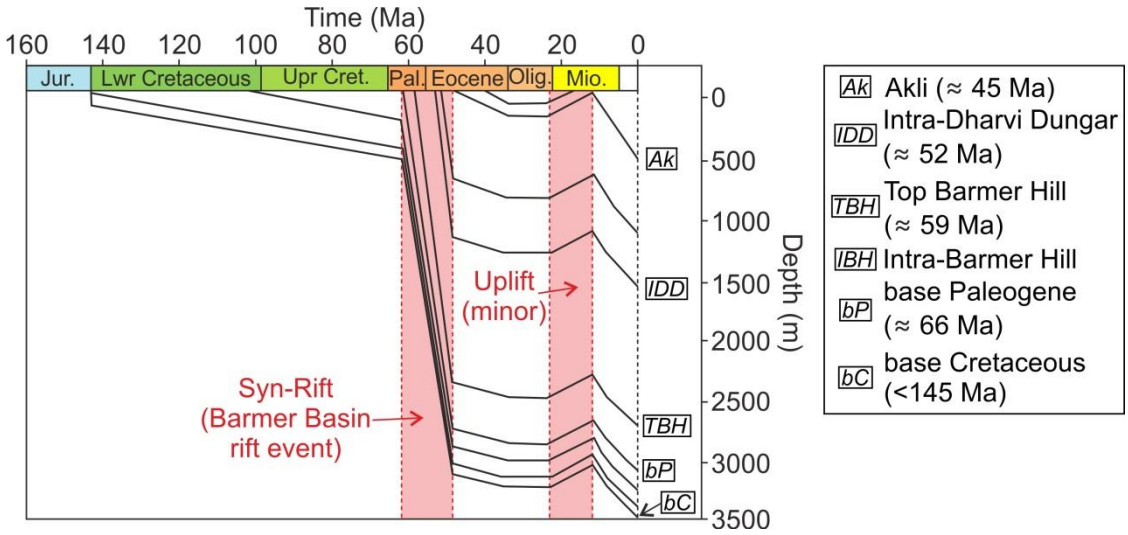

Figure 7.2 – Subsidence history of the central Barmer Basin region, constrained from the K1 well. (after Dolson *et al.* in press). Key to horizons inset. See **figure 7.1** for approximate location of the K1 well.

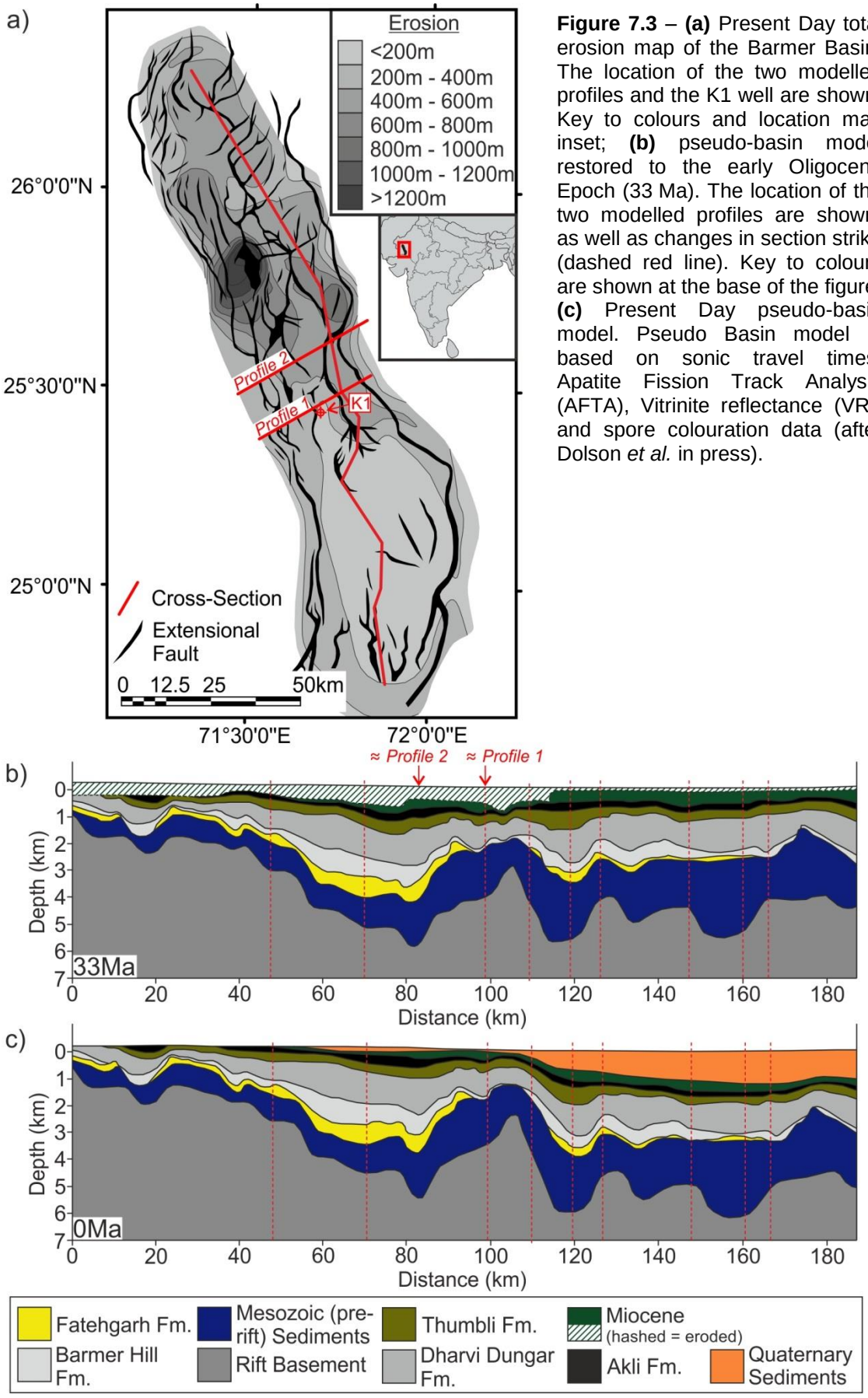

Figure 7.3 – **(a)** Present Day total erosion map of the Barmer Basin. The location of the two modelled profiles and the K1 well are shown. Key to colours and location map inset; **(b)** pseudo-basin model restored to the early Oligocene Epoch (33 Ma). The location of the two modelled profiles are shown, as well as changes in section strike (dashed red line). Key to colours are shown at the base of the figure; **(c)** Present Day pseudo-basin model. Pseudo Basin model is based on sonic travel times, Apatite Fission Track Analysis (AFTA), Vitrinite reflectance (VR), and spore colouration data (after Dolson *et al.* in press).

7.2 The flexural-cantilever forward model

Two end-member forward models (moving forwards in time) approximate lithosphere-scale extensional deformation, namely lithosphere extension by entirely pure-shear (plastic/ductile deformation; McKenzie 1978) or simple-shear (elastic/brittle deformation; Wernicke 1985) deformation (**Figure 7.4**). However, such models are not in accordance with relationships imaged on deep seismic reflection profiles, which indicate that brittle deformational structures in the shallow crust terminate towards the base of the brittle seismogenic layer, that is the shallow portion of the crust that deforms elastically on planar faults inducing seismicity (Kusznir & Egan1989; Kusznir *et al.* 1991; Kusznir & Ziegler 1992; Kusznir *et al.* 1995). A two-layered model of brittle (elastic) deformation (simple-shear) within the shallow crust giving way to ductile (plastic) deformation (pure-shear) within the deep crust and mantle lithosphere, therefore, is more appropriate for modelling lithosphere-scale extensional deformation (**Figure 7.5**; Kusznir & Egan1989; Kusznir *et al.* 1991; Kusznir & Ziegler 1992; Kusznir *et al.* 1995). The zone of brittle (simple-shear) deformation is commonly 10 – 20 km thick, with brittle deformational structures soling-out or detaching within the underlying zone of ductile (pure-shear) deformation (Kusznir & Egan1989).

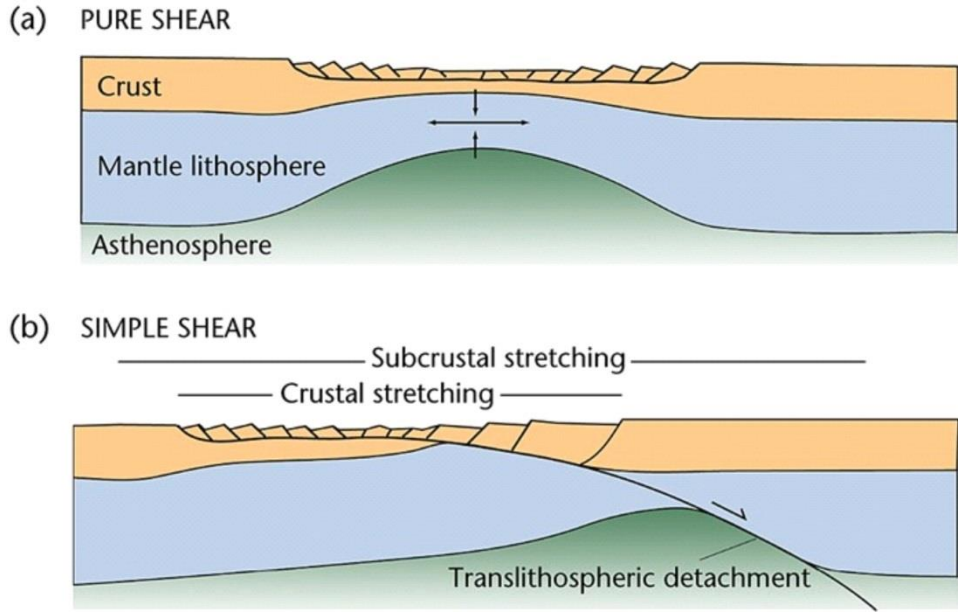

Figure 7.4 – Two end-member models approximating lithosphere extension, accommodated by entirely pure- **(a)** and simple- **(b)** shear deformation (reproduced from Allen & Allen 2013).

The flexural-cantilever model (**Figure 7.5**; Kusznir & Egan1989; Egan 1990; Kusznir *et al.* 1991; Kusznir & Ziegler 1992; Kusznir *et al.* 1995) is a numerical forward model that incorporates the

geometrical, thermal, and flexural isostatic consequences of continental lithosphere extension, accommodated by combined simple and pure-shear deformation in the upper and lower lithosphere respectively (Kusznir & Egan 1989). The model approximates basin geometry, subsidence history, and stratigraphy for lithosphere extension, can incorporate multiple faults, and calculates Moho topography and crustal structure (Kusznir & Egan 1989). Lithosphere extension is quantified by measurements of fault heave, that is the horizontal component of extension across a fault. Within the model, tectonic deformation (faulting) and isostatic equilibration of the positive load applied by syn-deformational deposition is assumed to be instantaneous, and may be followed by a period of lithospheric thermal re-equilibration inducing further, non-tectonic, post-rift thermal subsidence. Detailed descriptions of the mathematics used in the flexural-cantilever model are well documented (Kusznir & Egan 1989; Egan 1990; Kusznir *et al.* 1991; Kusznir & Ziegler 1992), and have been applied in both rift basin and passive margin settings (Kusznir & Egan 1989; Kusznir *et al.* 1991; Kusznir & Ziegler 1992; Roberts *et al.* 1993; Kusznir *et al.* 1995; Roberts *et al.* 1997; Roberts *et al.* 1998; Meredith & Egan 2002; Kusznir *et al.* 2004; Li *et al.* 2014).

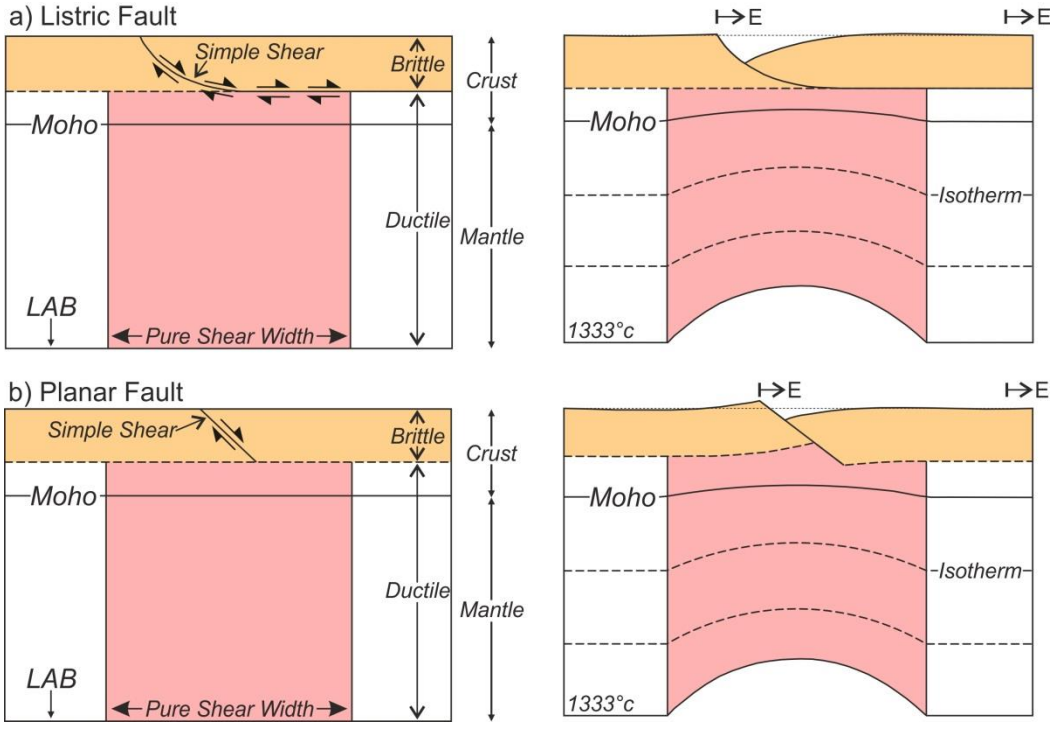

Figure 7.5 – The flexural-cantilever model of lithosphere extension. Extension is accommodated by pure and simple-shear in the shallow and deep lithosphere respectively (after Kusznir *et al.* 1991). Simple-shear deformation may be accommodated on a Listric **(a)** or planar **(b)** fault. LAB = lithosphere-asthenosphere boundary.

Within the flexural-cantilever model, lithosphere-scale extensional deformation and basin formation consists of three distinct but related components (Kusznir & Egan1989; Kusznir *et al.* 1991): 1) the geometrical response of the lithosphere to extension; 2) perturbation of the lithosphere temperature field during deformation and its subsequent re-equilibration after deformation, and; 3) the isostatic response of the lithosphere, both during and after deformation.

7.2.1 Geometrical response of lithosphere extension

The geometrical response of the lithosphere to extension is highly sensitive to multiple factors, including: 1) the degree of lithosphere stretching, quantified by the beta (β) factor, namely "the factor by which a unit length of uniformly deforming material is extended and unit thickness is thinned" (Kusznir *et al.* 1995); 2) the geometry (listric/planar), spacing, and orientation of faults; 3) crustal thickness; 4) the flexural rigidity of the lithosphere, quantified by the conceptual effective elastic thickness (T_e) parameter, defined as "the thickness of an unbroken, perfectly elastic lithosphere plate that would have the same effective flexural rigidity as the lithosphere" (Kusznir *et al.* 1991); 5) the temperature of the underlying asthenosphere; 6) the density of the crust (ρ_c) and mantle (ρ_m); 7) the degree of syn-deformational sediment fill, and; 8) the width and positioning of the zone of pure-shear deformation. Under the assumption of uniform stretching with depth, strain accommodated by simple-shear (faulting) in the shallow crust must be balanced in the underlying crust by pure-shear (ductile) deformation (Kusznir & Egan1989). However, a greater amount of extension may be accommodated in the underlying zone of pure-shear deformation (non-uniform stretching; e.g. Roberts *et al.* 1997; Kusznir *et al.* 2004; Allen & Allen 2005), and geometrically the width of the zone that undergoes pure-shear deformation (pure-shear width) may be wider than the overlying zone of brittle deformation (**Figure 7.5**).

7.2.2 Thermal perturbation

Thinning associated with lithosphere extension perturbs the geothermal gradient (**Figure 7.6**; Kusznir & Egan 1989; Egan 1990). In the shallow crust, faulting (simple-shear) juxtaposes hotter material in the fault footwall against relatively cooler material in the hanging-wall generating a temperature discontinuity across the fault (Egan 1990). Beneath the zone of simple-shear deformation, pure-shear results in thinning of the lithosphere and raises deep, hot rocks to shallower levels of the lithosphere (McKenzie 1978; Egan 1990). Contemporaneous with thinning of the lithosphere, expansion associated with the promotion of hot rocks to shallower crustal levels

induces surface uplift (McKenzie 1978; Egan 1990). However, post-extensional re-equilibration (cooling) of the lithosphere involves a thermal contraction causing a thermally-induced post-rift thermal subsidence that decreases exponentially with time (McKenzie 1978; Egan 1990). In general, a higher asthenospheric temperature generates larger syn-extensional uplift supressing deposition, induces greater volumes of melt production by decompression melting dependent upon the degree of thinning (β-dependent; White & McKenzie 1989; Kusznir & Ziegler 1992), and results in greater degrees of post-rift thermal contraction and re-equilibration generating thick, post-rift thermal sedimentary successions. The presence of a large-offset detachment fault may significantly impact upon the location of the post-rift thermal subsidence package relative to the zone of simple-shear (fault-controlled) deformation (Kusznir & Egan 1989).

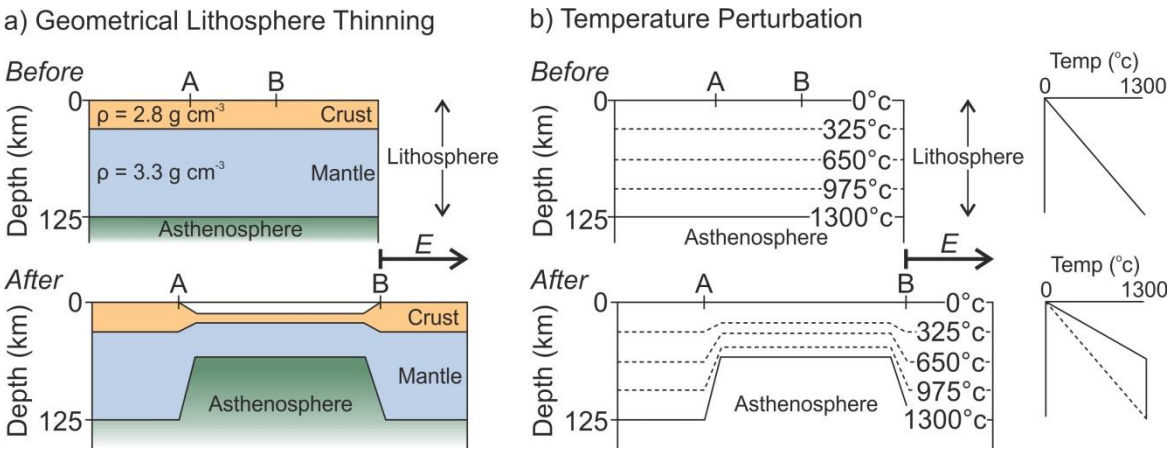

Figure 7.6 – Thermal perturbation associated with entirely pure-shear lithosphere thinning (after McKenzie 1978; Kusznir *et al.* 1995). **(a)** the geometrical response of the lithosphere to entirely pure-shear thinning; **(b)** thermal perturbation associated with lithosphere thinning. E = extension.

7.2.3 Isostatic response of the lithosphere

The simplest form of isostatic correction uses one-dimensional Airy compensation, namely isostatic compensation through changes in the thickness of the lithosphere immediately underlying the applied load (Allen & Allen 2005). However, forward models using Airy compensation poorly reproduce many geometrical features of the modelled structures (e.g. fault geometries & basin depth; Kusznir & Egan1989; Kusznir *et al.* 1991). Giving the lithosphere a finite flexural strength (flexural rigidity), thus allowing loads to be distributing laterally, provides a more favourable geometrical reproduction of the modelled structure (Kusznir & Egan1989; Kusznir *et al.* 1991). Detailed forward models, therefore, incorporate the flexural response of the lithosphere during

deformation (flexural isostasy; e.g. Kusznir & Egan1989; Kusznir *et al.* 1991; Kusznir & Ziegler 1992; Roberts *et al.* 1993; Kusznir *et al.* 1995; Roberts *et al.* 1997; Roberts *et al.* 1998; Fletcher *et al.* 2013).

The flexural strength of the lithosphere is quantified by the conceptual effective elastic thickness (T_e). During deformation, bending stresses induced by flexure are distributed throughout the lithosphere (Kusznir *et al.* 1991). Crustal rocks are unlikely to sustain deviatoric stresses greater than a few kilobars (kB; Byerlee 1968) and, as a result, bending stresses during deformation induce extensive fracturing that occurs within the shallow, brittle (elastic), seismogenic portion of the crust (Kusznir *et al.* 1991). Such fracturing greatly reduces the strength of the lithosphere and, therefore, the thickness of the conceptual, unbroken, perfectly elastic lithosphere plate with the same effective flexural rigidity as the lithosphere (T_e), is greatly reduced during deformation (generally $T_e < 10$km; Kusznir *et al.* 1991; Kusznir *et al.* 1995). If unknown, the effective elastic thickness (T_e) of the lithosphere can be constrained experimentally. The appropriate T_e value will reproduce model geometries (e.g. basin depth and fault-block dip angle) that closely resemble those of the profile being modelled (Kusznir *et al.* 1995). However, the plausibility of the effective elastic thickness constrained using this method should be assessed by ensuring the model predicts realistic amounts of footwall uplift (& erosion rates) and bending stresses (≤ 3 kB; Kusznir *et al.* 1995). Lithosphere with an effective elastic thickness of zero has no flexural strength (Egan 1990), that is the lithosphere is isostatically balanced by Airy compensation.

During extension, simple-shear deformation (faulting) of the shallow crust creates a mass-deficit (negative load; **Figure 7.7**; Egan 1990; Kusznir & Ziegler 1992). The mass deficit induces a short-wavelength (local) buoyancy force that is distributed laterally by the flexurally rigid lithosphere (flexural rebound) which acts as a comparatively long-wavelength filter (**Figure 7.7**; Egan 1990; Kusznir & Ziegler 1992). Lithosphere with a greater flexural rigidity and a low rebound capacity will disperse the negative load across a greater lateral distance (longer wavelength) than weakly rigid lithosphere with a high rebound capacity (**Figure 7.7**; Egan 1990). Flexural rebound of the lithosphere produces uplift of footwall crests and shallowing of the adjacent basin (**Figure 7.7**; Kusznir & Egan 1989; Egan 1990; Kusznir *et al.* 1991; Kusznir & Ziegler 1992; Kusznir *et al.* 1995). Significant footwall uplift is rarely preserved, specifically at the margins of rift basins where uplifted

footwall crests may be exposed and undergo erosion, commonly assumed to be contemporaneous with rifting (e.g. Roberts & Yielding 1991). Where footwall uplift is not preserved, the extension measured on a fault will be an underestimate and needs to be accounted for during forward modelling by the addition of artificial fault heave until the model satisfactorily reproduces the desired basin geometry. Erosion of substantial material uplifted in the footwall of a major fault increases the negative load applied to the lithosphere, promoting further buoyant uplift and continued erosion (Kusznir & Ziegler 1992). In many basins, buoyant uplift related to the erosion of exposed footwall crests may induce erosion of the syn-rift sedimentary succession resulting in an erosional unconformity marking the end of active rifting (Kusznir & Egan 1989).

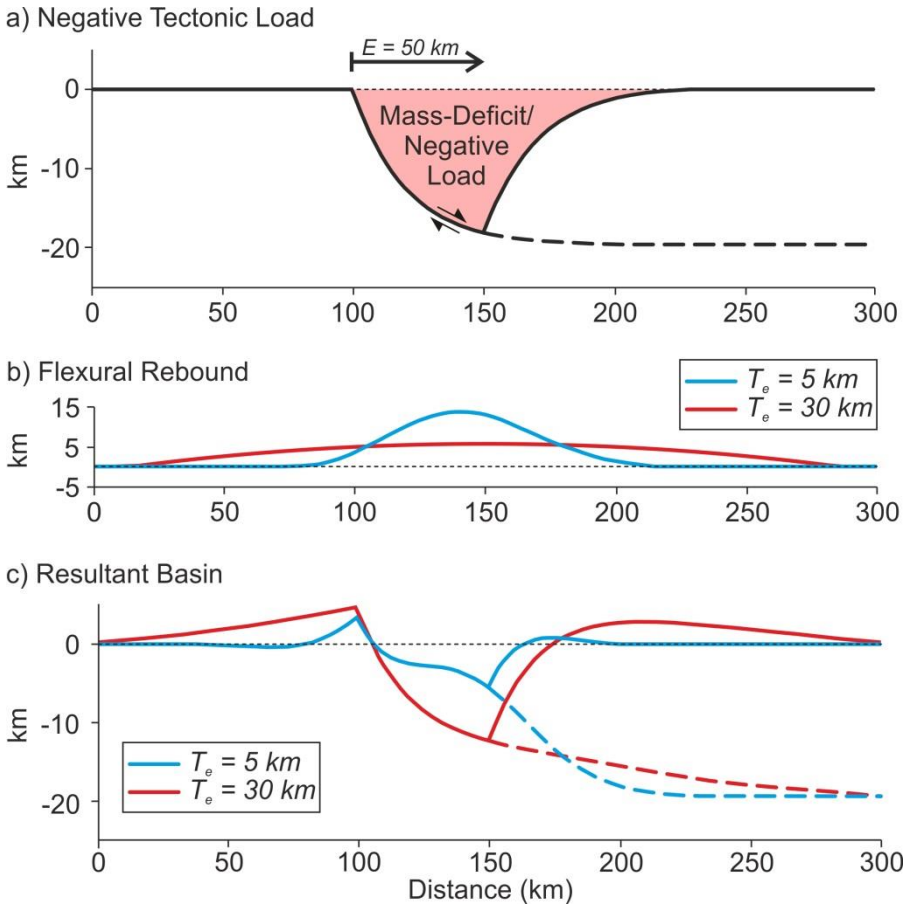

Figure 7.7 – Flexural uplift associated with lithosphere extension (after Egan 1990). **(a)** Simple-shear deformation replaces crust with air and generates a mass deficit or negative load; **(b)** the buoyancy force generated by this mass deficit is distributed laterally by the flexurally rigid lithosphere. The lateral extent by the buoyancy force is dependent upon the flexural strength of the lithosphere (T_e); **(c)** the combined geometrical result of an applied negative load for lithosphere of different flexural strengths (T_e = 5 km & 30 km).

7.2.4 Model constraint

A satisfactory flexural-cantilever forward model will reproduce simple-shear fault geometries similar to those imaged on seismic depth-sections, including basin depth, the dip angle of fault blocks, and amount of fault heave preserved after erosion of uplifted footwall material (Kusznir & Egan 1989; Kusznir *et al.* 1991; Kusznir & Ziegler 1992; Kusznir *et al.* 1995). Further to this, the erosion rates required to remove the necessary footwall uplift, as well as the lithosphere bending stresses associated with deformation, should be assessed for plausibility. Bathymetric markers within the syn-rift sedimentary succession, such as buried erosion surfaces and coal beds, should also be honoured in a satisfactory forward model (Roberts *et al.* 1993; Kusznir *et al.* 1995).

7.3 Seismic dataset and interpretation

Two seismic cross-sections bearing 061° were provided across the central Barmer Basin rift (profiles 1 & 2 on **Figure 7.1**). The sections are 36 km (profile 1) and 42 km (profile 2) in length, and situated approximately 14 km apart. The seismic surveys are pre-stack time-migrated, with a vertical axis in two-way travel time (TWT) imaging between 202 ms and -4500 ms, with sections presented with reverse (international) polarity. An average interval velocity log was also provided for the K1 well (**Figure 5.5**).

7.3.1 Interpretation

The seismic sections were interpreted using the seismostratigraphical scheme employed in the tectono-stratigraphical model of the Kaameshwari Fault (**Figure 6.5**), and were depth converted using interval velocities constrained from the K1 well (**Figures 7.8 & 7.9**; c.f. **Section 5.2.2.1**). The vertical resolution (**Section 6.3.1**), and therefore the vertical error associated with interpretations of the base syn- and post-rift surfaces (bP & Ak horizons respectively), was calculated to assess the potential impact of measurement error on the model results. Below the vertical resolution, seismic signals from the upper and lower contacts of a bed destructively interfere, and eventually cancel each other out. The upper and lower contacts of the bed with a thickness of less than the vertical

Figure 7.8 (*next page*) – Depth conversion of profile 1. See **figure 7.1** for profile location. The interpretations **(b)** of an un-interpreted **(a)** seismic time section were combined with the interval velocity log in the K1 well to construct a subsurface velocity model **(c)**, which was used to convert the vertical axis of the seismic survey from the time into the depth domain **(d)**. Key to colours and labels shown at base of figure and approximate location of burial history shown in **figure 7.2** is also indicated.

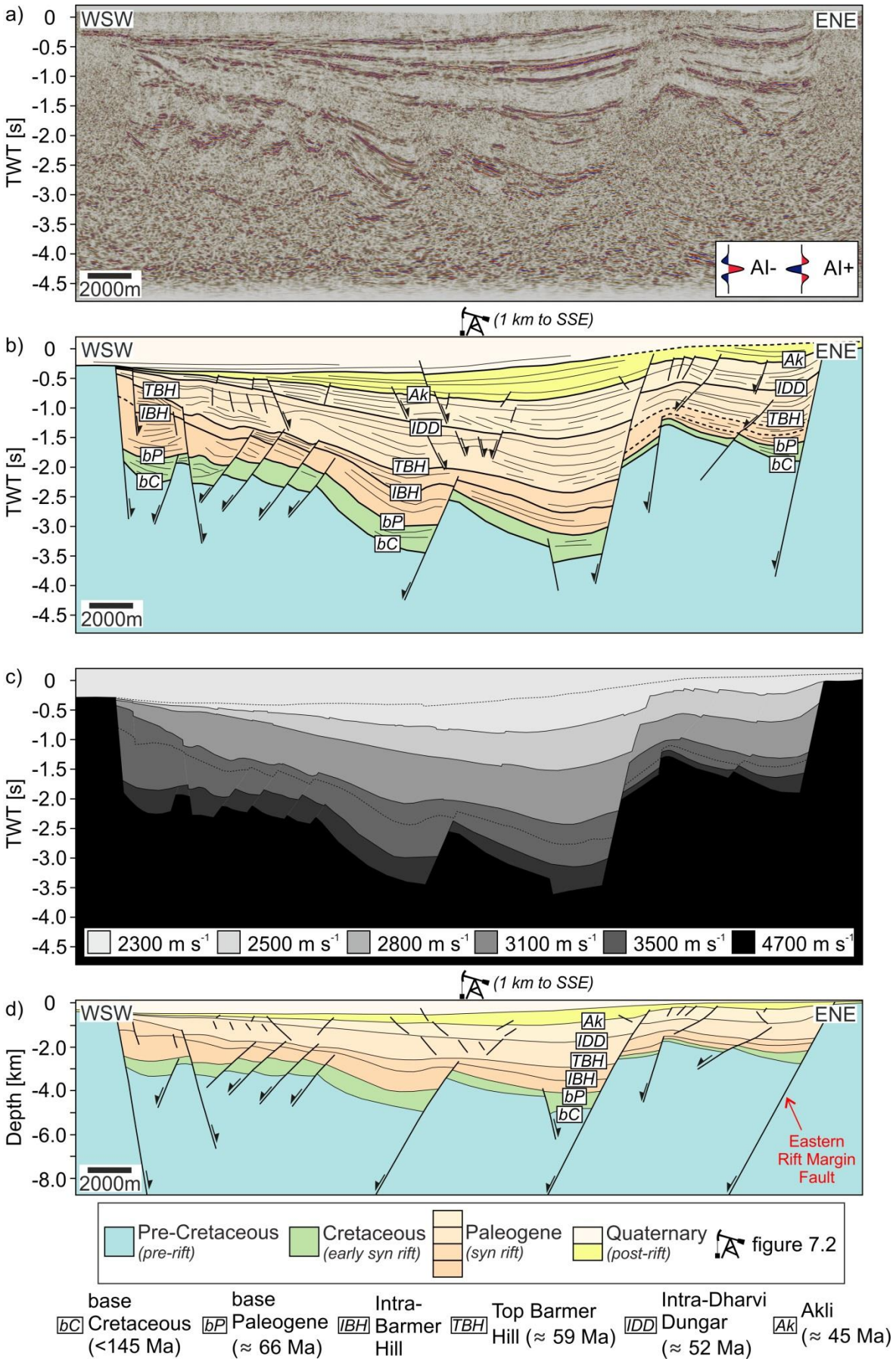
a)
WSW
ENE
TWT [s]
0
-0.5
-1.0
-1.5
-2.0
-2.5
-3.0
-3.5
-4.0
-4.5
2000m
AI-
AI+
(1 km to SSE)
b)
TBH
IBH
bP
bC
Ak
IDD
2000m
c)
2300 m s-1
2500 m s-1
2800 m s-1
3100 m s-1
3500 m s-1
4700 m s-1
d)
Depth [km]
0
-2.0
-4.0
-6.0
-8.0
Eastern Rift Margin Fault
Pre-Cretaceous (pre-rift)
Cretaceous (early syn rift)
Paleogene (syn rift)
Quaternary (post-rift)
figure 7.2
bC base Cretaceous (<145 Ma)
bP base Paleogene (≈ 66 Ma)
IBH Intra-Barmer Hill
TBH Top Barmer Hill (≈ 59 Ma)
IDD Intra-Dharvi Dungar (≈ 52 Ma)
Ak Akli (≈ 45 Ma)

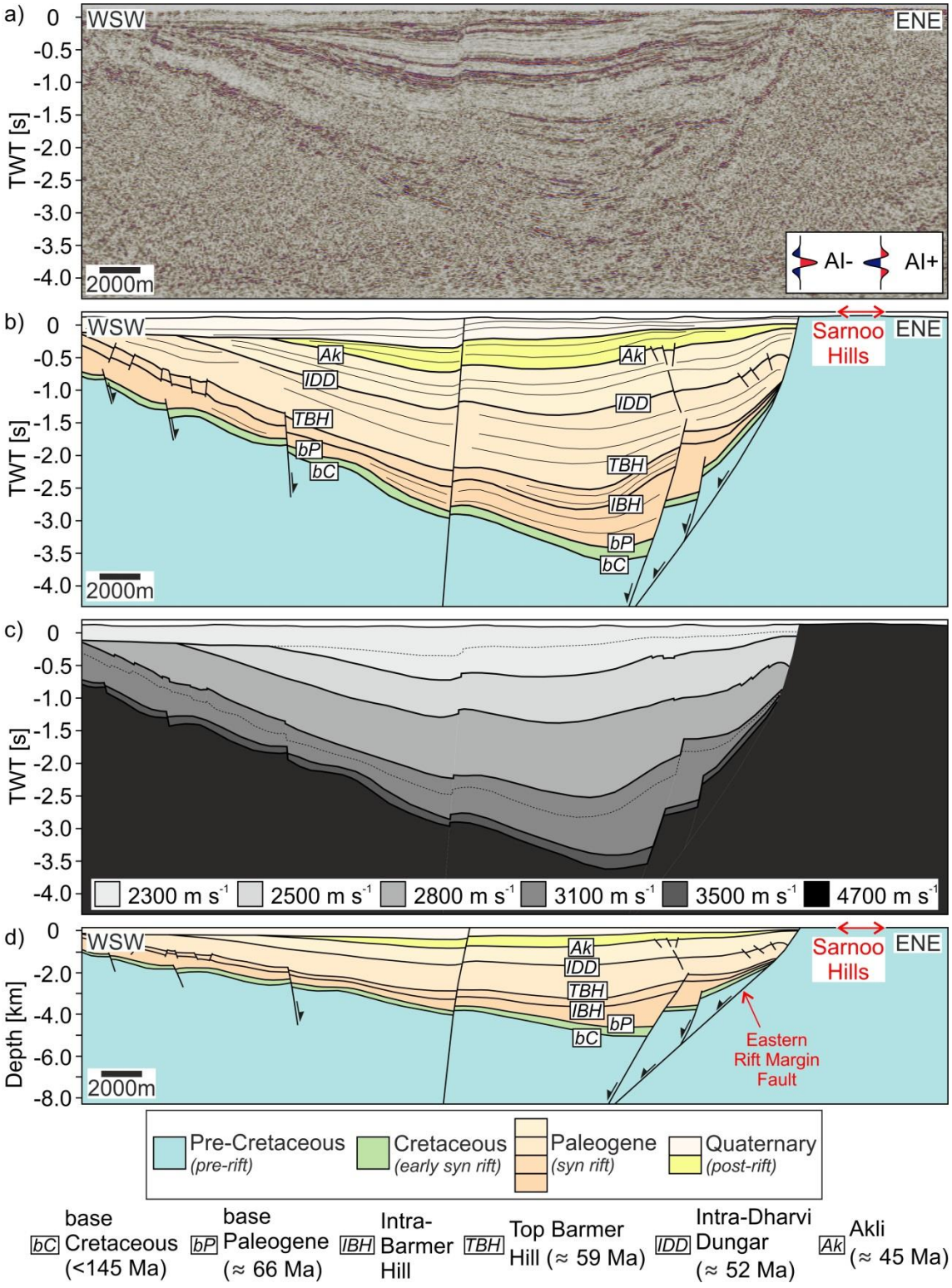

Figure 7.9 – Depth conversion of profile 2, with the location of outcrop exposure in the Sarnoo Hills shown. See **figure 7.1** for profile location. The interpretations **(b)** of an un-interpreted **(a)** seismic time section were combined with the interval velocity log in the K1 well to construct a subsurface velocity model **(c)**, which was used to convert the vertical axis of the seismic survey from the time into the depth domain **(d)**. Key to colours and labels shown at base of figure.

resolution therefore, are un-resolvable as separate seismic signals, but the bed may still be 'detectable' to a degree dependent upon factors such as the signal-to-noise ratio (Hart 2012). It will not be possible, therefore, to place the vertical positioning of an individual seismic signal to an accuracy greater than the vertical resolution. An instantaneous frequency attribute was generated for the raw seismic time-sections of both profiles to approximate the signal frequency at the depth of the interpretation. In the deepest section of both profiles, the approximate frequency at the base-Paleogene (bP) horizon was between 20 Hz and 30 Hz and corresponded to an interval velocity of between 3100 m s^{-1} and 3500 m s^{-1} (**figure 7.8c**). From **equations 6.3 & 6.4** the lowest vertical resolution would arise from an average velocity of 3500 m s^{-1} and frequency of 20 Hz, giving a vertical resolution of approximately 44 m (measurement error = ± 22 m). The frequency at the deepest point of the base post-rift sedimentary succession (≈ Ak horizon) was between 40 Hz and 60 Hz and corresponded to an interval velocity of between 2300 m s^{-1} and 2500 m s^{-1} (**Figure 7.9c**). The lowest vertical resolution, calculated using a velocity of 2500 m s^{-1} and frequency of 40 Hz, therefore, is approximately 16 m (measurement error = ± 8 m). The error associated with vertical measurements of the base syn- and post-rift horizons on the observed (interpreted) seismic sections, therefore, is small (± 22 m or less) relative to the vertical scale of the models (km).

7.3.2 Depth-converted geometries

The geometry of the rift imaged on profile 1 is broadly symmetrical, and comprises three fault-bounded blocks that dip gently to the east between 6° and 8° (**Figure 7.8**). Fault blocks are deformed internally by small-offset faults (subsidiary faulting; **Figure 7.8**). The rift reaches a maximum depth of approximately 4 km and the post-rift sedimentary succession is asymmetrical, and reaches a maximum thickness of 1 km above the centre of the rift (**Figure 7.8**).

Rift geometry is strongly asymmetrical on profile 2 (**Figure 7.9**). The hanging-wall dip-slope is over 25 km long, dips gently to the east at approximately 8°, and is largely unfaulted (**Figure 7.9**). Deformation is concentrated along the eastern rift margin where two fault-bounded 'rider' blocks are situated above the shallowly-dipping (45° to 60°) eastern rift margin fault (**Figure 7.9**). The upper surface of the western rider block is sub-horizontal. However, the rider block immediately adjacent to the eastern rift margin fault is significantly tilted (26°) towards the west representing a substantial amount of non-recoverable, ductile strain (at the scale of observation) expressed as

rotational deformation. The rift reaches a maximum depth of 4.5 km, and the post-rift sedimentary succession is asymmetrical, attaining a maximum thickness of 0.7 km above the centre of the rift.

7.4 Modelling approach

Depth converted seismic sections (**Figures 7.8 & 7.9**) were modelled using the flexural-cantilever forward model (**Section 7.2**; e.g. Kusznir & Egan 1989; Egan 1990; Kusznir *et al.* 1991; Kusznir & Ziegler 1992; Roberts, *et al.* 1993; Kusznir *et al.* 1995). Initial modelling was conducted on the section adjacent to the K1 well (profile 1; **Figure 7.1**) in order to constrain the model using the K1 well subsidence history plot (**Figure 7.2**). Subsequently, parameters obtained from profile 1 were applied to profile 2 which crossed the Sarnoo Hills field area (profile 2: **Figure 7.1**). The software package used (Badley Geoscience's Stretch software package) was exceptionally versatile and modelled the geometrical, thermal, and isostatic response of the lithosphere to extension, and incorporated erosion. All of the model parameters could be varied, including: 1) the location, orientation, dip, and heave of an array of faults; 2) crustal thickness; 3) effective elastic thickness (T_e); 4) depth to detachment; 5) width and offset of the zone of pure-shear deformation (pure-shear width) relative to each fault; 6) asthenosphere temperature; 7) amount of syn-deformational sedimentation, either as a percentage (0% to 100%) or to a uniform bathymetry; 8) amount of erosion; 9) crustal and mantle densities; 10) duration of post-rift thermal subsidence, and; 11) initial topography or bathymetry. The versatility of the software facilitated generation of models that were tailor-made to each seismic depth-section. However, the abundance of input variables alludes to multiple possible valid solutions, and models should be constrained using as many geological factors as possible.

7.4.1 Model parameters

Flexural-cantilever forward models were generated at a lateral resolution of 0.4 km across a total profile length of 200 km. In accordance with work in the Sanchor Basin (Kaila *et al.* 1990), a crustal thickness of 32 km and 15 km upper crustal thickness (fault detachment depth) were used during modelling (**Figure 7.10**; **Table 7.1**). Geometrical input parameters related to geological structures (distance along profile, dip, and heave of faults) were constrained from seismic depth-sections (**Figure 7.11**). A narrow pure-shear width was used (60 km) to reflect that the Barmer Basin is a narrow rift, with the zone of pure-shear deformation for each individual fault initiated 20 km into the fault footwall. 'Standard' parameters were used for the density of the crust (ρ_c) and mantle (ρ_m),

namely 2.8 g cm^{-3} and 3.3 g cm^{-3} respectively, as well as an asthenosphere temperature (T_A) of 1333°C (e.g. McKenzie 1978; **Figure 7.10**; **Table 7.1**). Models were conducted with no initial bathymetry or topography.

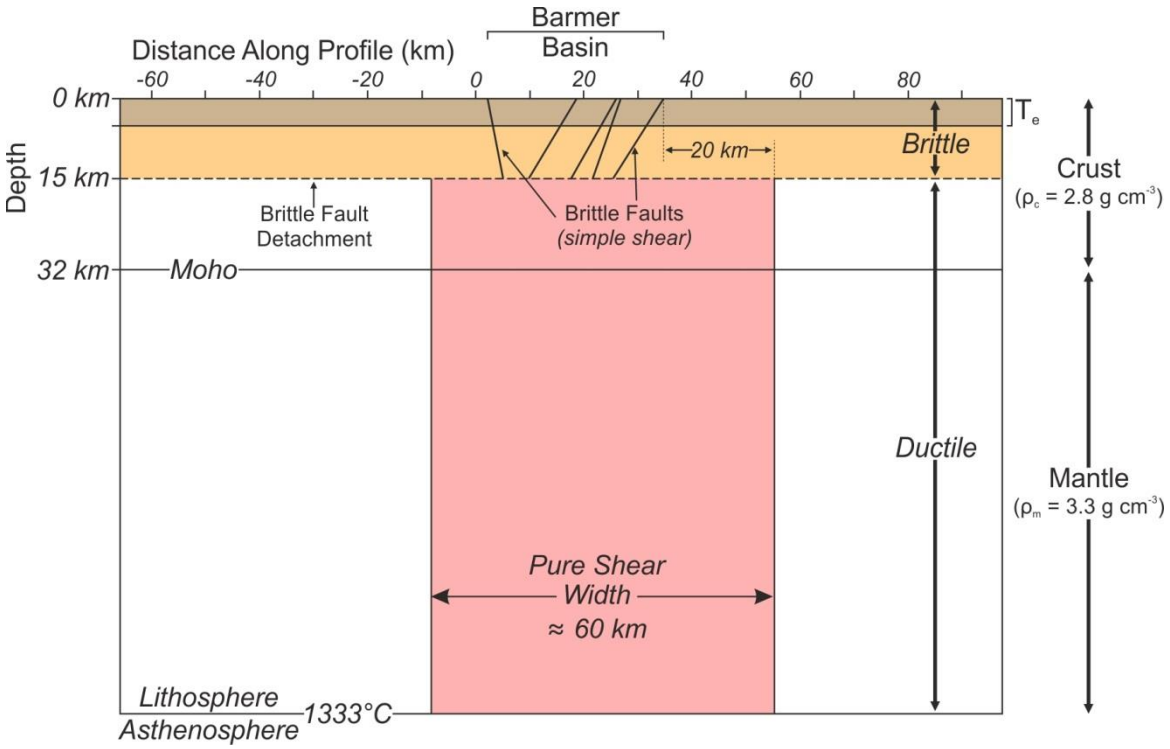

Figure 7.10 – Schematic diagram of profile 1 prior to extensional deformation depicting the input parameters for both modelled profiles (c.f. **Table 7.1**).

Parameter	Value
Crustal Thickness	32 km
Detachment Depth	15 km
Pure Shear Width	60 km
Crustal Density (ρ_c)	2.8 g cm^{-3}
Mantle Density (ρ_m)	3.3 g cm^{-3}
Asthenosphere Temperature (T_A)	1333°C
Density of Eroded Material	2.0 g cm^{-3}
Average Surface Porosity of Sediment	0.57
Average Compaction Decay Constant of Sediment	0.41 km^{-1}

Table 7.1 – Parameters used in flexural-cantilever forward models

The effective elastic thickness (T_e) of the lithosphere during the main Barmer Basin rift event is unknown. Initial, rudimentary investigations into an appropriate value of effective elastic thickness (T_e) were conducted for profile 1 using an instantaneous rift with no sediment fill. Models of instantaneous rifts were generated using various values of effective elastic thickness (3 km, 5 km,

7 km, & 9 km), and the results were compared with the base syn-rift geometry of profile 1 (bP horizon on **Figure 7.8**) for equivalence. Satisfactory values of effective elastic thickness will generate a profile that closely reproduces the dip and relative depths of all fault blocks within the rift. Erosion and post-rift subsidence were not accounted for in any of the models, and a direct comparison of absolute depth/elevation between profiles is, therefore, inappropriate. As such, the applicable value of effective elastic thickness (T_e) was assessed and constrained further during the modelling procedure when sediment loading and erosion were also considered.

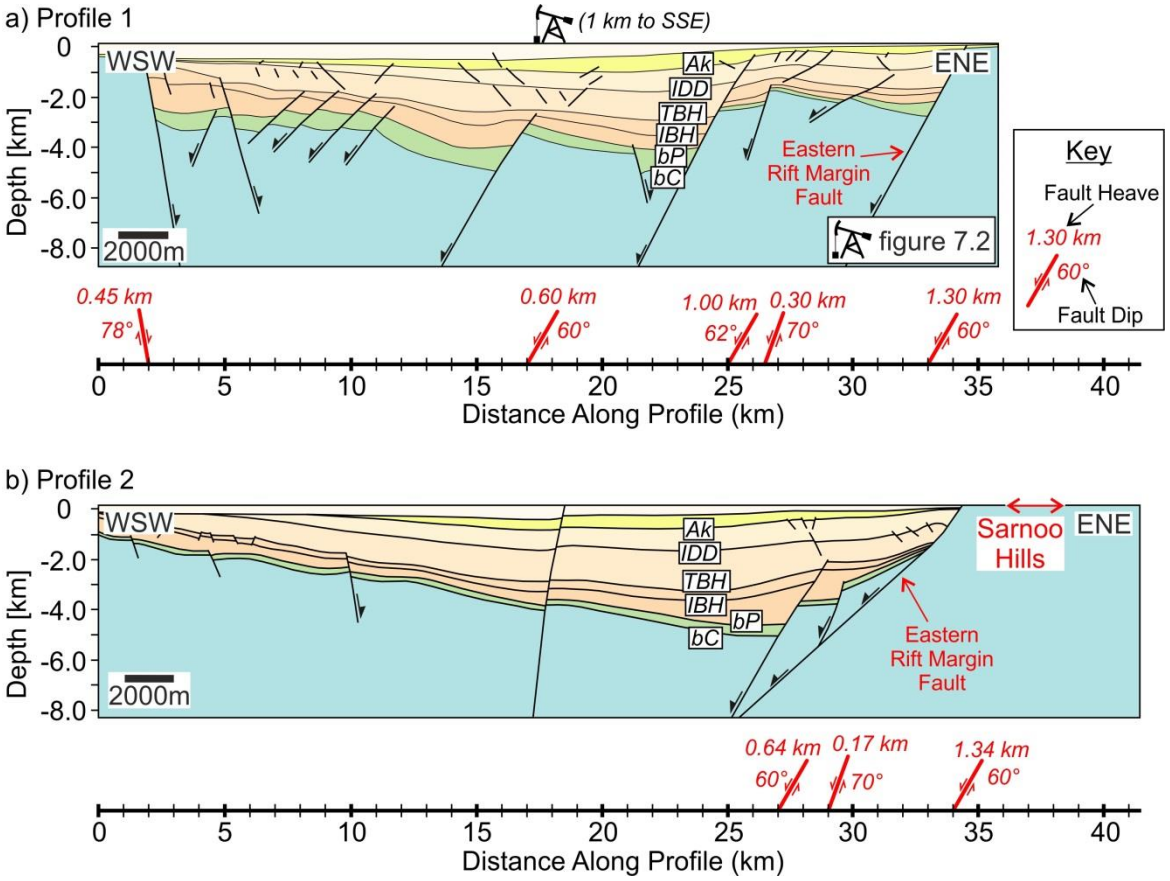

Figure 7.11 – Observed geometrical properties of profile 1 **(a)** and profile 2 **(b)**. For section locations see **figure 7.1**, and for key to colours and horizon labels see **figure 7.8**. The position of outcrop exposure in the Sarnoo Hills is also shown on **(b)**.

Compaction of sediment was accounted for by approximating the bulk sedimentary succession as 60% mudstone and 40% sandstone (c.f. **Figure 5.4**), producing an average surface porosity of 0.57 ('$\emptyset_0$' in **Equation 5.4**) and average compaction decay constant of 0.41 km^{-1} ('c' in **Equation 5.4**; Sclater & Christie 1980). Eroded material was assumed to be removed from the model completely and attributed a density of 2.0 g cm^{-3}. The presence of thick coal successions within the latest syn-rift sedimentary succession in the rift, namely the early- to middle-Eocene Akli

Formation (≈ Ak horizon; Dolson *et al.* in press), indicates deposition at or near to the local base-level at the close of rifting, and was used as a bathymetric marker. Base-level in the model is assumed to correspond with the Present Day surface of each profile, which have negligible topographical relief (profile 1: 68 m < Z < 121 m; profile 2: 106 m < Z < 159 m), and are attributed an elevation of 0 m.

7.4.2 Forward-modelling procedure

Deformation during the main Barmer Basin rift event was approximated as a single, instantaneous rift event, that is all fault-controlled (tectonic) subsidence occurred spontaneously, and was followed by 50 Myr of post-rift thermal subsidence in accordance with the K1 well subsidence history plot (**Figure 7.2**). The early, rift-oblique (≈ northwest-southeast) extensional event identified in the Sarnoo Hills (**Chapter 4**) has not been incorporated into the models due to the poorly-constrained age and the highly oblique nature of deformation relative to the modelled profiles (061°). The base syn-rift succession is, therefore, taken as the base-Paleogene (bP) horizon (**Figures 7.8 & 7.9**), and model results have attempted to reproduce the geometry of the rift at this horizon. The 14 Myr duration of rifting (non-instantaneous) and post-rift uplift and erosion (< 600 m) were also not incorporated into the models.

At the time of instantaneous rifting, 100% of the available accommodation space was filled by syn-rift sediment (**Figures 7.12a & 7.13a**). In order to reproduce the required depth on both modelled profiles, artificial heave was added to the eastern rift margin fault by an amount constrained experimentally. The addition of artificial fault heave results in greater flexural uplift of the fault footwall, which is partially eroded during the modelling procedure. Subsequently, the location of the fault preserved at the upper surface of the model after erosion will be laterally offset from the location of the fault defined along the undeformed profile due to the dip of the fault. To account for this and accurately reproduce the observed, Present Day geometry of the rift, which has undergone erosion, the addition of artificial fault heave needs to be accompanied by adjusting the position of the fault along each modelled profile accordingly.

Figure 7.12 (*next page*) – Individual stages of the best-fit profile 1 model. Geometrical input parameters (distance along profile and heave of faults) are shown in **(a)**. For profile location see **figure 7.1** and for the model parameters see **Table 7.1**, & **Figure 7.10**. Modelling undertaken using Badley Geoscience's STRETCH software. Images are 2X vertically exaggerated.

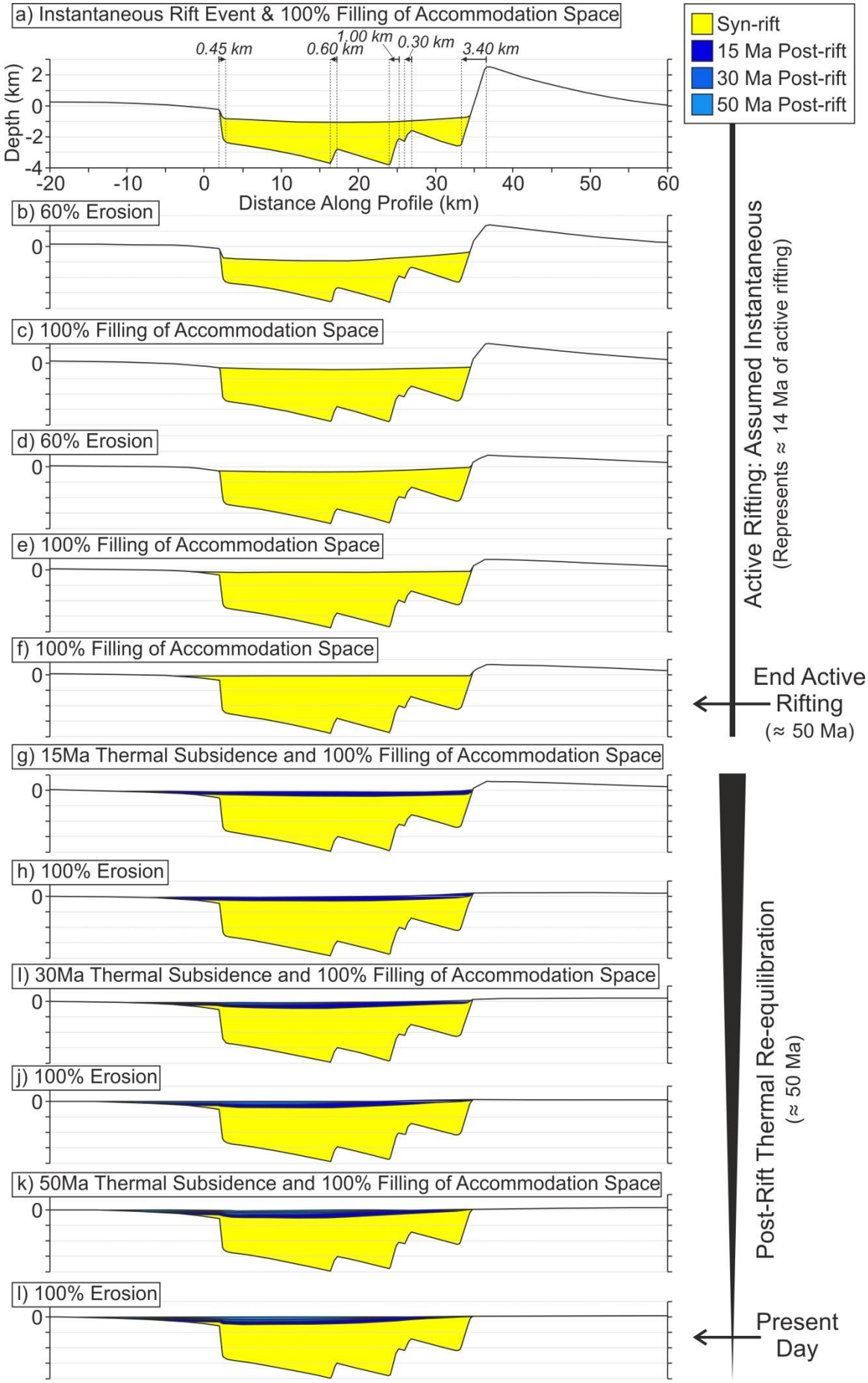
a) Instantaneous Rift Event & 100% Filling of Accommodation Space
0.45 km
0.60 km
1.00 km
0.30 km
3.40 km
Depth (km)
Distance Along Profile (km)
b) 60% Erosion
c) 100% Filling of Accommodation Space
d) 60% Erosion
e) 100% Filling of Accommodation Space
f) 100% Filling of Accommodation Space
g) 15Ma Thermal Subsidence and 100% Filling of Accommodation Space
h) 100% Erosion
I) 30Ma Thermal Subsidence and 100% Filling of Accommodation Space
j) 100% Erosion
k) 50Ma Thermal Subsidence and 100% Filling of Accommodation Space
l) 100% Erosion
Syn-rift
15 Ma Post-rift
30 Ma Post-rift
50 Ma Post-rift
Active Rifting: Assumed Instantaneous
(Represents ≈ 14 Ma of active rifting)
End Active Rifting
(≈ 50 Ma)
Post-Rift Thermal Re-equilibration
(≈ 50 Ma)
Present Day

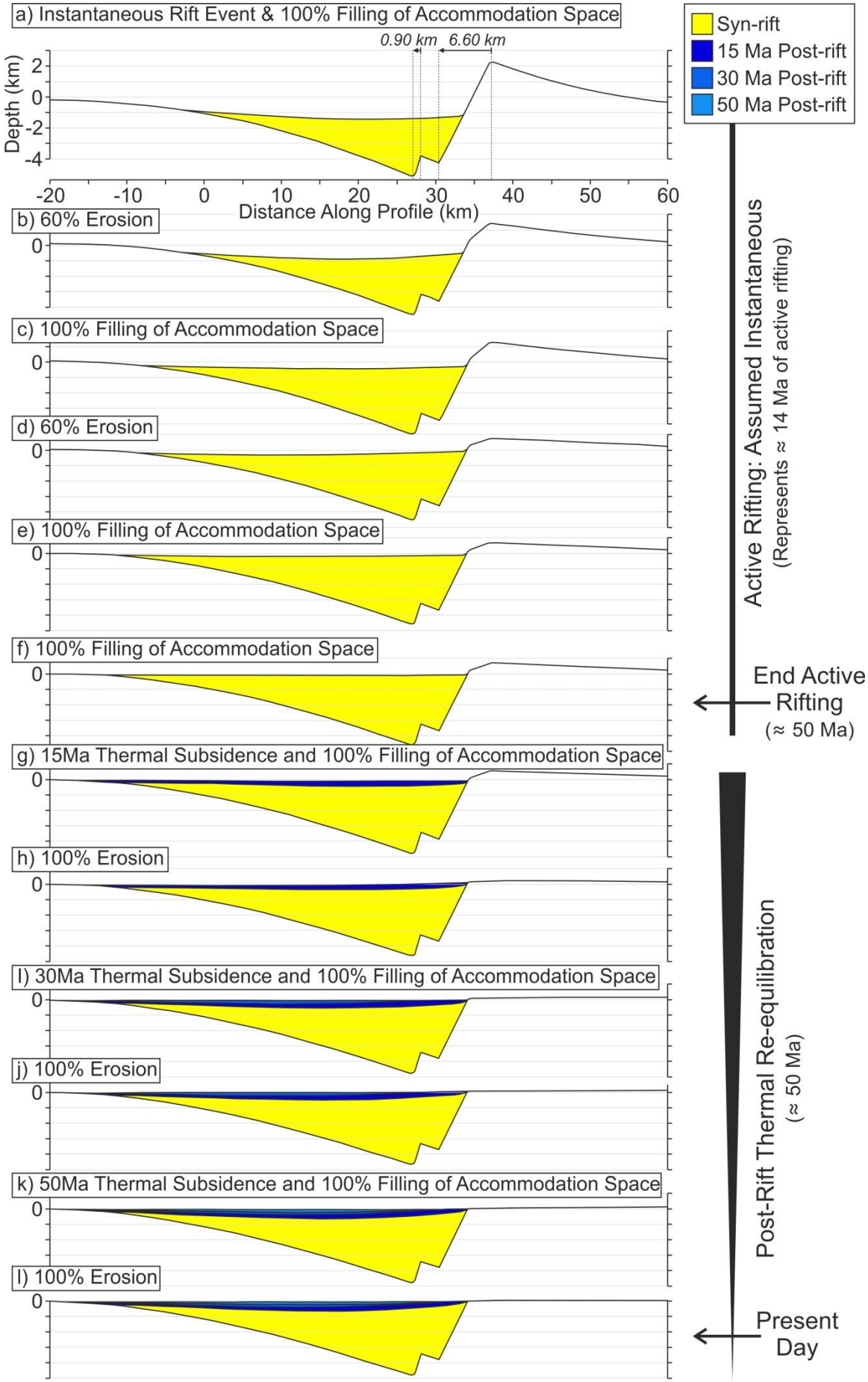
a) Instantaneous Rift Event & 100% Filling of Accommodation Space
0.90 km
6.60 km
Depth (km)
2
0
-2
-4
-20
-10
0
10
20
30
40
50
60
Distance Along Profile (km)
b) 60% Erosion
c) 100% Filling of Accommodation Space
d) 60% Erosion
e) 100% Filling of Accommodation Space
f) 100% Filling of Accommodation Space
g) 15Ma Thermal Subsidence and 100% Filling of Accommodation Space
h) 100% Erosion
i) 30Ma Thermal Subsidence and 100% Filling of Accommodation Space
j) 100% Erosion
k) 50Ma Thermal Subsidence and 100% Filling of Accommodation Space
l) 100% Erosion
Syn-rift
15 Ma Post-rift
30 Ma Post-rift
50 Ma Post-rift
Active Rifting: Assumed Instantaneous
(Represents ≈ 14 Ma of active rifting)
End Active Rifting
(≈ 50 Ma)
Post-Rift Thermal Re-equilibration
(≈ 50 Ma)
Present Day

Figure 7.13 (*previous page*) - Individual stages of the best-fit profile 2 model. Geometrical input parameters (distance along profile and heave of faults) are shown in **(a)**. For profile location see **figure 7.1** and for the model parameters see **Table 7.1**, & **Figure 7.10**. Modelling undertaken using Badley Geoscience's STRETCH software. Images are 2X vertically exaggerated.

The positive load applied by the addition of syn-rift sediment during instantaneous rifting was compensated for flexurally, generating further accommodation space. Footwall crests uplifted as a result of flexural rebound in response to crustal thinning were partially eroded (**Figures 7.12b & 7.13b**), before the addition of further syn-rift sediment in two additional stages (**Figures 7.12c & 7.13c**). This process of loading, partially eroding, and filling of the available accommodation space was continued until the necessary thickness of syn-rift sediment was reproduced throughout the rift (**Figures 7.12d-f & 7.13d-f**). Upon deposition of the desired thickness of syn-rift sediment, the top of the syn-rift sedimentary succession needed to be sub-horizontal and situated near to the local base-level (0 m) in order to reproduce the bathymetry of the thick coal successions within the Akli Formation at the close of rifting (≈ 0 m; c.f. Dolson *et al.* in press; **Figures 7.12f & 7.13f**). The degree of partial erosion required to elevate the top of the syn-rift sedimentary succession to the local base-level was constrained experimentally using an iterative modelling approach. Reproducing the correct thickness of syn-rift sediment throughout the rift with a final sub-horizontal surface at or near to the local base-level, despite the irregular isostatic uplift resulting from laterally variable amounts of footwall erosion, provide a tight series of model constraints, thus reducing ambiguity in the results.

The model stages described above approximate active rifting and result in a completely infilled continental rift with partially eroded rift shoulders. However, it is critical to note that, in reality, the final rift geometry represents a finite (14 Myr) duration of active rifting. The modelling software allowed the rift to be filled to a user-defined bathymetry during instantaneous rifting. However, instantaneously filling the rift does not reflect the more realistic process of a progressively eroded and filled rift during non-instantaneous rifting. The additional stages incorporated into the modelling procedure (loading, partially eroding, and filling) approximated a gradual (low strain-rate), rather than abrupt (high strain-rate) isostatic balancing of the lithosphere during active rifting.

Subsequently, the model was subjected to 50 Myr of post-rift thermal subsidence, partitioned into two 15 Myr stages and a final 20 Myr stage, with 100% erosion of any material exposed above base-level (0 m) between each period of thermal subsidence, to reflect the gradual and continued erosion of topography (**Figures 7.12g-l & 7.13g-l**). Following the modelling procedure outlined, a successful model would be left eroded almost completely to the local base-level in order to reproduce the negligible Present Day topographical relief of each profile without the need for additional erosion (**Figures 7.12l & 7.13l**).

7.5 Results

Numerous elements were evaluated to assess the success or failure of a model, including: 1) a geometrical comparison of the base syn- and post-rift surfaces approximated by the model and observed on seismic depth-sections (bP & Ak surfaces respectively); 2) the plausibility of footwall uplift and maximum erosion rates; 3) realistic values of bending stress (≤ 3 kB; Kusznir *et al.* 1995), and; 4) restoration of the top syn-rift succession to base-level (0 m) at the close of rifting. A model was deemed to be an acceptable approximation of the observed profile if a good match of all of these parameters was reproduced.

7.5.1 Elastic thickness

Initial investigations into an appropriate value of the effective elastic thickness revealed that the geometries reproduced using effective elastic thicknesses (T_e) of 3 km and 9 km were unsatisfactory approximations of the observed geometry of the rift imaged on profile 1 (**Figures 7.14b & e**). However, effective elastic thickness (T_e) values of 5 km and 7 km reproduced satisfactory geometrical approximations (**Figures 7.14c & d**). An effective elastic thickness (T_e) of 7 km very closely approximated the dip and relative depths of the two most easterly fault blocks (**Figures 7.14d**). However, the dip of the westernmost fault block is poorly approximated. Alternatively, a T_e of 5 km closely approximates the dip of all three fault blocks, with minor disparities in relative fault-block depths (**Figures 7.14c**), suggesting a T_e value of 5 km is most appropriate.

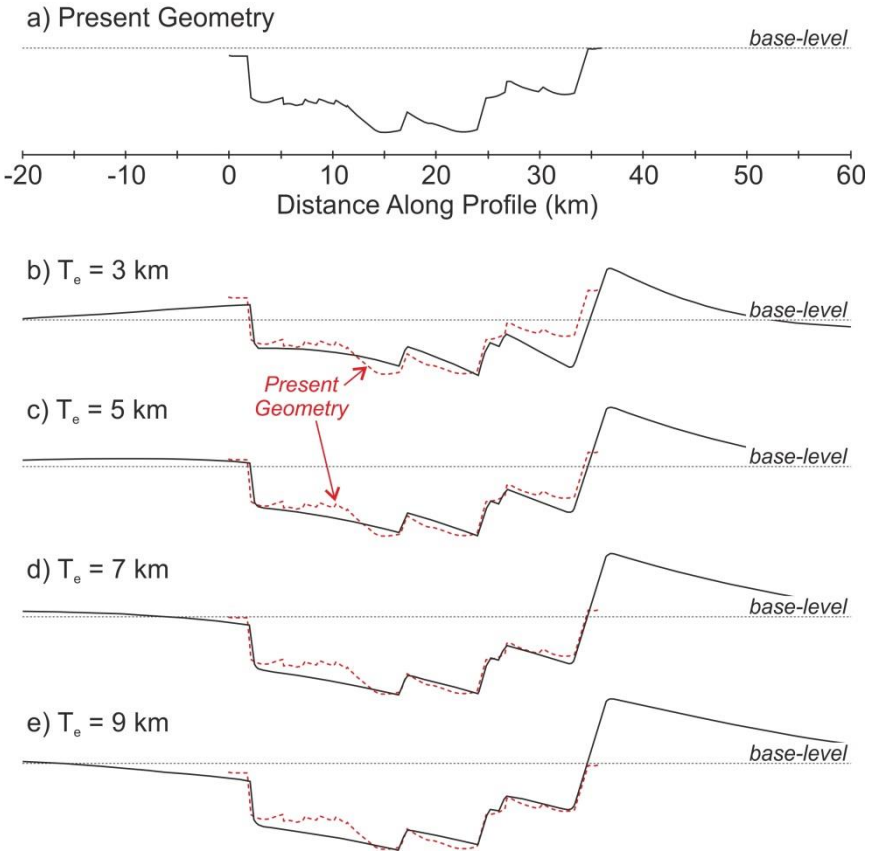

Figure 7.14 – Geometrical comparison (relative depth and dip of fault blocks) between Present Day geometry of the rift (dashed red profiles) and the geometry of the rift in instantaneously modelled rifts with no sediment fill (solid black profiles), conducted using various values of elastic thickness (T_e). Profiles are 2X vertically exaggerated

7.5.2 Forward models

At the close of active rifting, symmetrical (profile 1; **Figure 7.15a**) and asymmetrical (profile 2; **Figure 7.16a**) rift basins immediately overlie narrow (60 km), near-symmetrical zones of raised Moho topography that persist until the Present Day (**Figures 7.15b & 7.16b**). A good approximation of the broad rift geometry was achieved for profile 1 (**Figure 7.17a**) using the geometrical input parameters specified (**Figure 7.11a**) and an effective elastic thickness (T_e) of 5 km. When syn-deformational sediment infill and erosion were included, T_e values of 6 km and 7 km were unsatisfactory. The model poorly reproduced the small-scale geometry of the westernmost fault-block, the depth of the central fault block, and the base of the post-rift sedimentary succession in the centre of the rift (**Figure 7.17a**). In order to reproduce the depth of the rift, fault heave removed by erosion and extensional deformation below the resolution of the seismic data needed to be accounted for. This was achieved by the addition of a significant amount

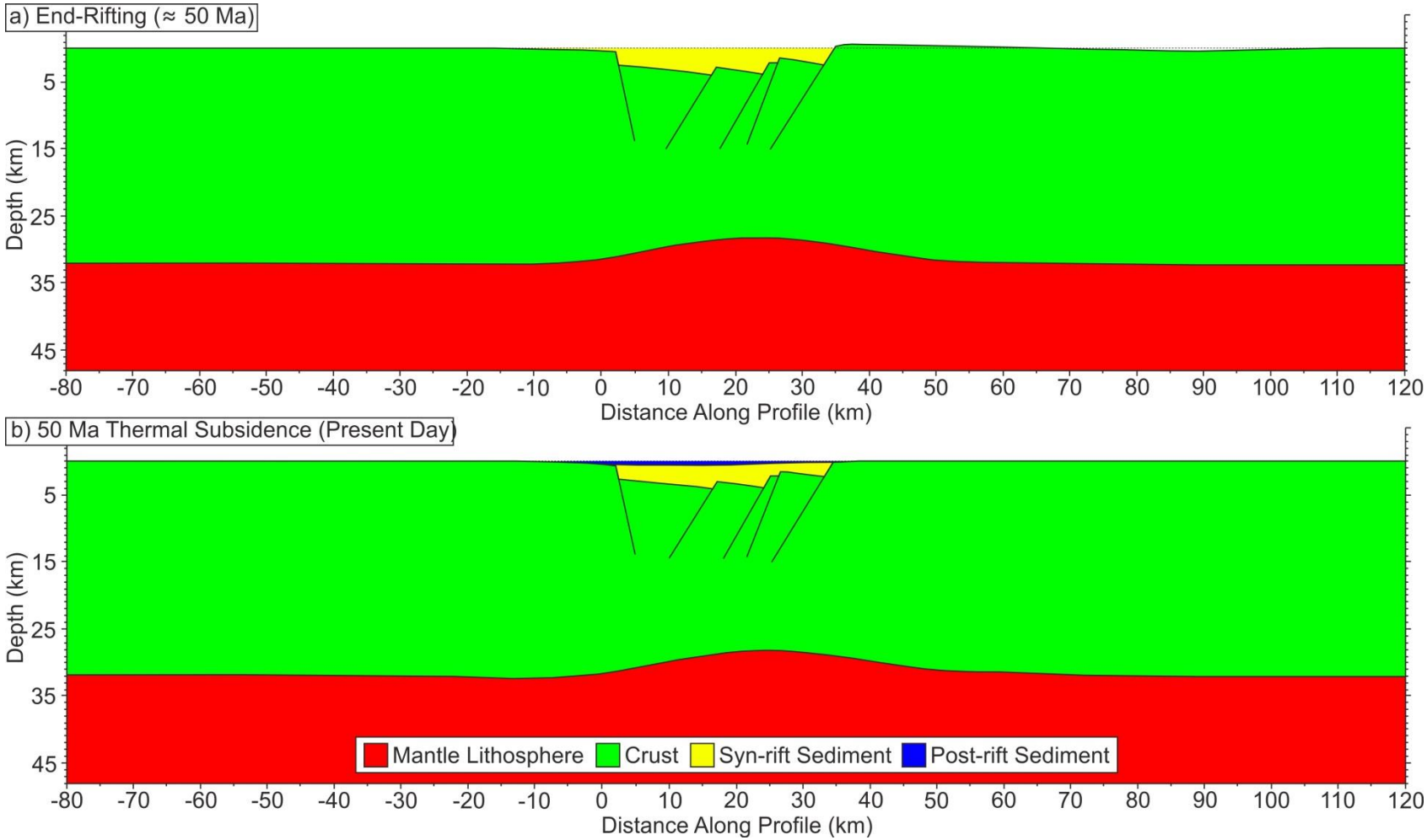

Figure 7.15 – Crustal structure of profile 1 at the end of active rifting **(a)** and the Present Day **(b)**. For profile location see **figure 7.1** and for the model input parameters see **Table 7.1**, & **Figure 7.10**. Modelling undertaken using Badley Geoscience's STRETCH software and images are shown with no vertical exaggeration. Yellow = syn-rift sediment; blue = post-rift sediment; green = crust; red = mantle lithosphere.

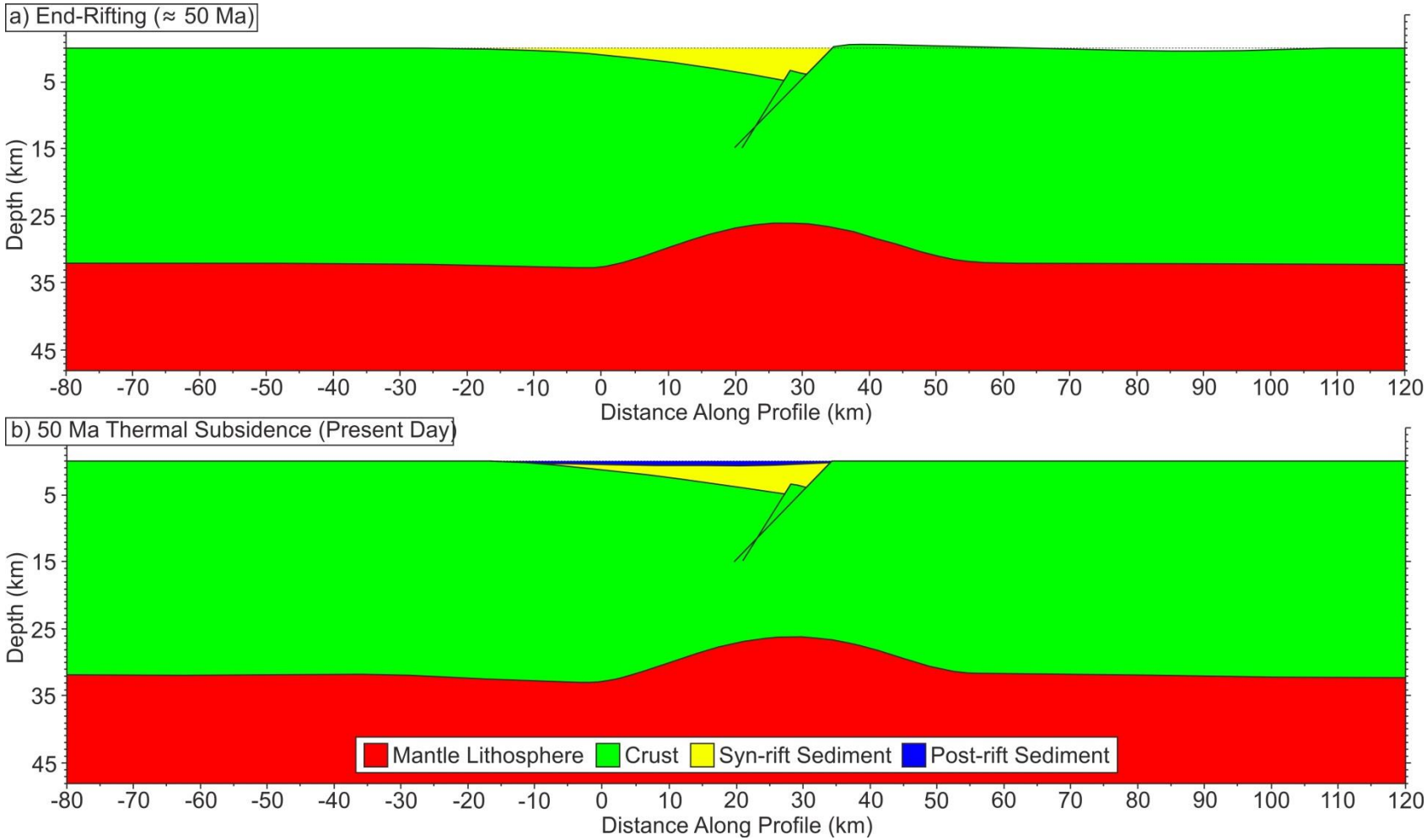

Figure 7.16 – Crustal structure of profile 2 at the end of active rifting **(a)** and the Present Day **(b)**. For profile location see **figure 7.1** and for the model input parameters see **Table 7.1**, & **Figure 7.10**. Modelling undertaken using Badley Geoscience's STRETCH software and images are shown with no vertical exaggeration. Yellow = syn-rift sediment; blue = post-rift sediment; green = crust; red = mantle lithosphere.

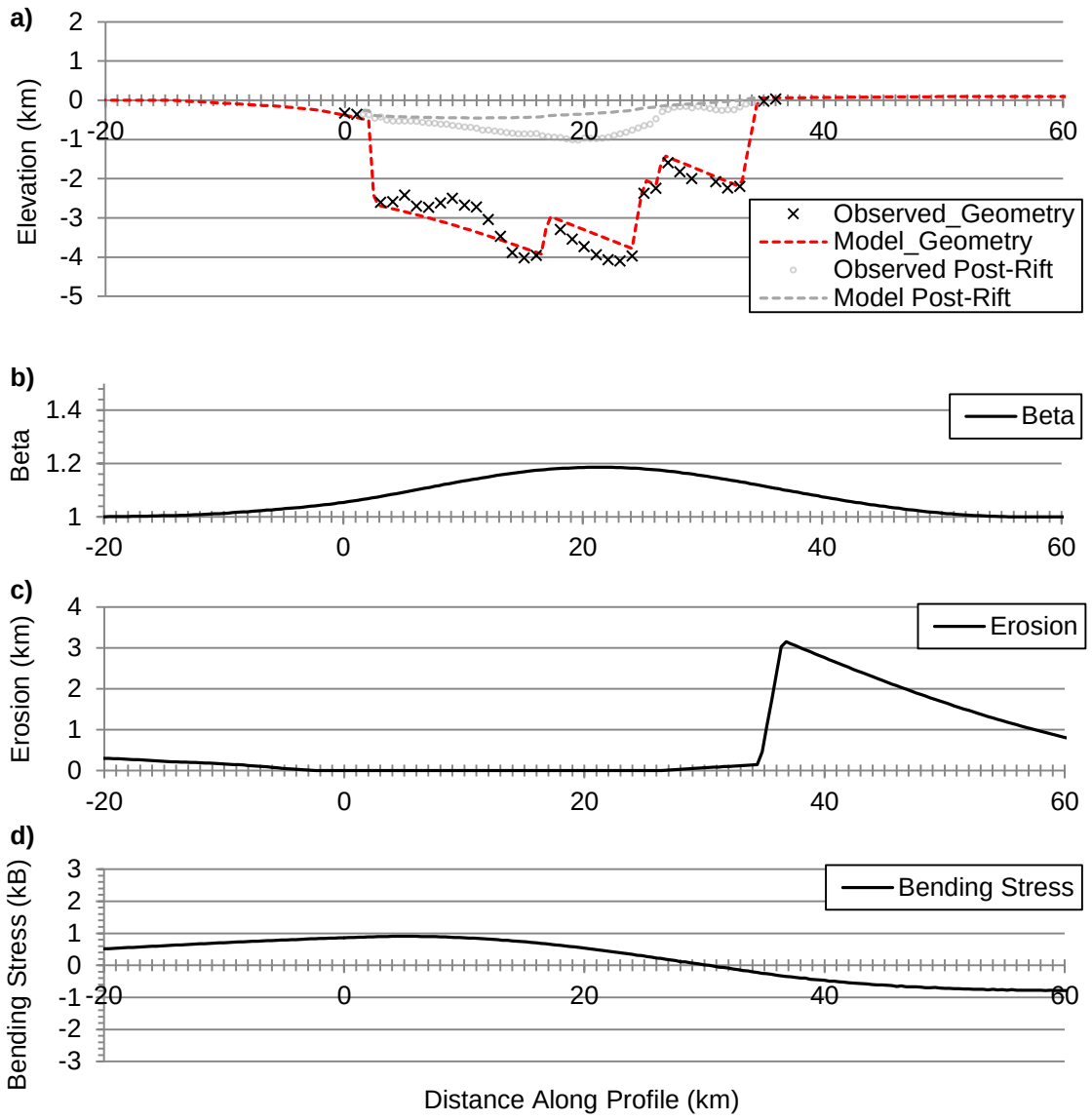

Figure 7.17 – Results of the best-fit profile 1 model. **(a)** Geometrical comparison between the observed and modelled base-syn-rift geometry (black crosses and dashed red line) and base post-rift geometry (grey circles and dashed grey line). For profile location see **figure 7.1**.Profiles are approximately 3X vertically exaggerated; **(b), (c), & (d)** Present Day erosion, stretching (β) factor, and bending stress profiles respectively

of artificial heave (≈ 2.1 km) to the eastern rift margin fault system (3.4 km modelled heave vs. 1.3 km observed heave). However, at the lateral resolution of the model (0.4 km), the heave preserved along the eastern rift margin was comparable to the heave observed on seismic depth-sections (**Figure 7.17a**). The model predicts a significant amount of total erosion (< 3 km) along the eastern rift margin and no erosion within the rift itself, with the exception of a small (< 0.1 km) amount of erosion above the terrace adjacent to the eastern rift margin (**Figure 7.17c**). Maximum stretching (β) factor and bending stresses are 1.186 and 0.906 kB/-0.792 kB respectively, with

maximum stretching (β) factor situated beneath the centre of the rift approximately 22.4 km along profile (**Figure 7.17b**).

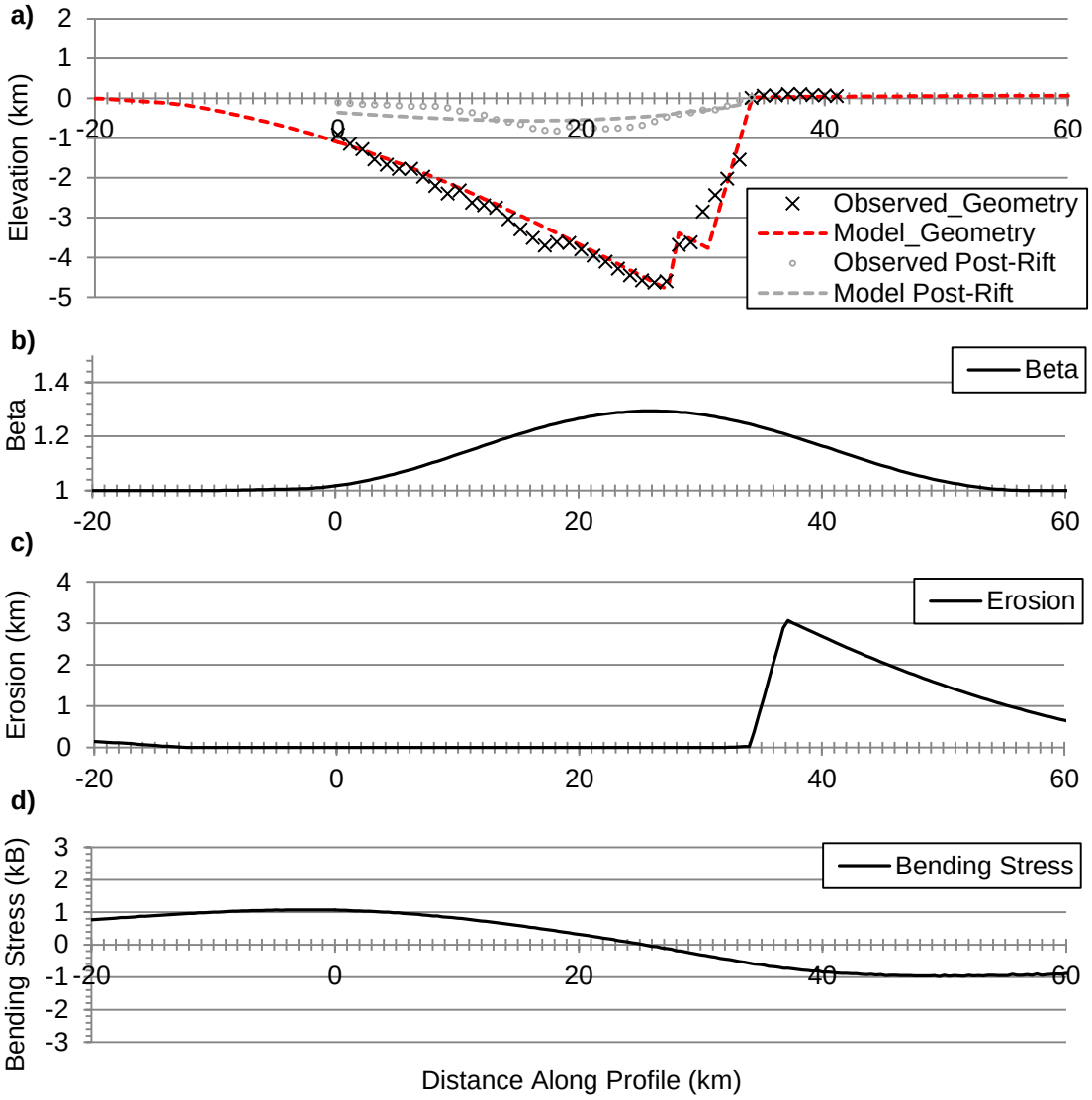

Figure 7.18 – Results of the best-fit profile 2 model. **(a)** Geometrical comparison between the observed and modelled base-syn-rift geometry (black crosses and dashed red line) and base post-rift geometry (grey circles and dashed grey line). For profile location see **figure 7.1**.Profiles are approximately 3X vertically exaggerated; **(b), (c), & (d)** Present Day erosion, stretching (β) factor, and bending stress profiles respectively

As with profile 1, a good approximation of the observed rift geometry was achieved for profile 2 (**Figure 7.18a**). However, the flexural-cantilever model approximates simple-shear deformation in the shallow crust using an elastic dislocation model (Kusznir *et al.* 1991), which does not include ductile strain within the zone of simple-shear deformation (rotated rider block; **Figure 7.9d**), and the input parameters needed to be simplified to successfully approximate rift geometry

(**Figure 7.18a**). This simplification process included the removal of the fault between the two rider blocks (**Figure 7.11b**), and essentially projected all deformation accommodated by this fault, and internally within the rotated rider block, onto the eastern rift margin fault system. As with profile 1, an unusually large amount of artificial heave (5.3 km) needed to be added to the eastern rift-margin fault system in order to reproduce the depth of the rift (6.6 km modelled heave vs. 1.3 km observed heave). However, the additional extension accommodated by the fault that was removed for simplification purposes is included within the substantial disparity between the modelled and observed fault heave, as well as rotational deformation accommodated within the rotated rider block. The model predicts a significant amount of total erosion (< 3 km) along the eastern rift margin and no erosion within the rift itself (**Figure 7.18c**). Maximum stretching (β) factor and bending stresses are 1.294, and 1.073 kB/-0.981 kB respectively, with the maximum stretching (β) factor situated beneath the centre of the rift approximately 26.4 km along profile (**Figure 7.18b**).

7.6 Lithosphere-scale deformation during the Barmer Basin rift event

The good approximation of the observed rift geometries was reproduced using the flexural-cantilever model with a crustal thickness of 32 km, a detachment depth of 15 km, 'standard' lithosphere parameters (ρ_c = 2.8 g cm^{-3}; ρ_m = 3.3 g cm^{-3}; T_A = 1333°C; e.g. McKenzie 1978), and an effective elastic thickness of 5 km. This modelling experiment suggests that the northwest Indian lithosphere deformed by coupled simple- and pure-shear deformation in the shallow and deep lithosphere respectively during the main Barmer Basin rift event (e.g. Kusznir & Egan1989; Egan 1990; Kusznir *et al.* 1991; Kusznir & Ziegler 1992; Roberts, *et al.* 1993; Kusznir *et al.* 1995). The positive correlation between model and observed profiles (**Figures 7.17 & 7.18**) demonstrates that deformation in the Barmer Basin near to the Cretaceous-Paleogene boundary can satisfactorily be approximated by lithosphere extension above 'normal' temperature asthenosphere (≈ 1333°C) and crust of average thickness (32 km) and geothermal gradient (≈ 30°C km^{-1}). The lithosphere had a finite flexural strength (T_e = 5 km) similar to that estimated for many other examples of continental lithosphere extension. The comparable positioning of post-rift thermal subsidence packages on observed and modelled sections indicates the zone of pure-shear deformation was positioned below the rift, and was not laterally offset from the zone of over-lying simple-shear deformation.

The models produced tolerable values of crustal thinning (β-factor < 1.294), footwall uplift and erosion (< 3 km), and bending stress (< 1.073) supporting that the model results are plausible.

The models presented indicate that lithosphere flexure during deformation elevated the eastern rift margin above the local base-level, accounting for the lack of preservation of syn-rift sediment. Substantial topographical relief may have existed during active rifting, and the geomorphology of the Barmer Basin near to the Cretaceous-Paleogene boundary may have been similar to that observed in the Great Rift Valley of east Africa today (e.g. Rosendahl 1987; Morley 1999a). The asymmetrical geometry of the post-rift sedimentary succession on both seismic depth-sections (**Figures 7.8d & 7.9d**) suggests topographical relief endured at the end of active rifting and footwall uplift was not eroded completely to base level. The negative load applied by continued erosion of uplifted material along the eastern rift-margin would have induced continued post-rift isostatic uplift, accounting for the thinning and asymmetry of post-rift thermal subsidence packages towards the eastern rift margin. However, the preservation of a post-rift sedimentary succession of up to 500 m in thickness adjacent to the eastern rift margin indicates that, at some time between the end of rifting and the Present Day, subsidence rates exceeded erosionally-induced isostatic uplift rates.

7.7 Discussion

The Barmer Basin is commonly assumed to cross the Precambrian Marwar Craton (Balakrishnan *et al.* 2009), likely associated with cold and dense lithosphere, and the Réunion Plume, associated with elevated asthenosphere temperature, is commonly assumed to have been situated beneath northwest India at the Cretaceous-Paleogene boundary (Morgan 1971; Cox 1989; White & McKenzie 1989; Plummer & Belle 1995; Sen & Chandrasekharam 2011). The successful approximation of the Barmer Basin rift using the flexural-cantilever forward model of lithosphere extension, using crust of average thickness (32 km) above 'normal' temperature asthenosphere (≈ 1333°C), indicates rifting of standard continental lithosphere in the absence of a mantle plume is a plausible alternative interpretation. However, the abundance of variables within the model, and poorly known parameters for the northwest Indian region at the Cretaceous-Paleogene boundary, indicate that the successful models presented are solutions within a suite of multiple possible valid solutions. In this investigation, a generic or 'standard' value was used where a parameter was unknown (e.g. T_A, ρ_c, or ρ_m), and the findings should be re-appraised when more appropriate values become available. Further to this, many factors are unaccounted for in the simple models

presented, including: 1) crustal magmatic accretion (underplating); 2) variable stretching with depth; 3) unusually cold and dense mantle beneath the Marwar Craton, 4) the presence or absence of an asthenosphere thermal perturbation during rifting (postulated Réunion Plume), and; 5) temporal variations in effective elastic thickness (T_e), and such factors should be incorporated into a more detailed geodynamical investigation. Further to this, the models presented are two-dimensional and do not include out-of-plane movement or the three-dimensional dispersion of loads, and further investigations should attempt to model the flexural response of the lithosphere in three-dimensions.

The models predict a substantial amount of footwall uplift along the eastern rift margin. Such flexural-isostatic uplift was previously unrecognised. However, the large amount of footwall uplift (< 3 km) predicted along the eastern rift margin by both models (**Figures 7.17b & 7.18b**) is unexpectedly large, and represents a maximum figure. In reality, such uplift is unlikely and numerous factors would reduce this amount, including the onset of thermal subsidence during non-instantaneous (progressive) rifting and strain accommodation by non-recoverable, ductile (rotational) deformation within structurally complex sections of the eastern rift margin, such as accommodation zones. Despite this, complete erosion of the maximum 3 km of footwall uplift during the 14 Myr duration of rifting represents a maximum erosion rate of 0.2143 mm $year^{-1}$ which is not unreasonable. The rift is likely to have comprised a significant topographical feature with sub-aerial, high-relief rift-shoulders and, at times, exposed footwall crests within the rift (c.f. **Figure 6.15**). Erosion of uplifted footwall material will have formed an important source of sediment, and locally derived sediment may comprise a substantial component of the syn-rift sedimentary succession. It follows that sedimentary environments and sediment facies distributions within the Barmer Basin, especially during the early-stages of rift evolution, were likely to have been structurally and geodynamically controlled.

The early, oblique (northwest-southeast) extensional event exposed at outcrop in the Sarnoo Hills (**Chapter 4**) has not been incorporated into the models presented due to the poor constraint on the age of deformation and the oblique orientation of the extension direction relative to the modelled profiles. It is unknown whether the lithosphere had thermally and isostatically re-equilibrated from this deformational event. Reactivation of a thermally or structurally weakened lithosphere during

the main Barmer Basin rift event would have substantial implications for the evolution of the basin, and may have controlled the location of rifting. Further to this, post-rift uplift and erosion related to the recent collision between the Indian and Eurasian continents is also not accounted for in the models presented. The observed thickness and geometry of post-rift thermal subsidence sedimentary successions represents the combined effect of deformation in the foreland of the collision zone and thermal relaxation, not thermal relaxation alone. Disparities between the observed and modelled sections, for example the poorly matched depths of the central fault block and post-rift thermal subsidence package in the centre of the rift on profile 1, may be explained by post-rift deformation, such as extensional reactivation of rift-basement faulting or lithosphere flexure in the foreland of the India-Eurasia collision zone.

7.8 Summary

This chapter has investigated the structural, thermal, and flexural isostatic response of the lithosphere during the Paleogene Barmer Basin rift event, and lithosphere-scale deformational processes. Two seismically imaged cross-sections were depth-converted and modelled using the flexural-cantilever forward model of lithosphere extension. Model results suggest 5 km to 7 km was an appropriate range of values for the effective elastic thickness (T_e), with a value of 5 km deemed most appropriate when sediment loading and erosion were incorporated into the modelling process. Subsequently, extension of average thickness (32 km) crust with a depth to detachment of 15 km, above asthenosphere of 'normal' temperature (1333°C) reproduced a good approximation of the rift geometry, while predicting reasonable values of crustal thinning ($\beta < 1.294$), footwall uplift and erosion (< 3 km), and bending stress (< 1.073). The large amount of footwall uplift and erosion predicted by the model (< 3 km) is a maximum estimate, and would be reduced by non-instantaneous rifting and structural complexities including non-recoverable (ductile) deformation. The close match between model and observed profiles validate that shallow deformational processes constrained from outcrop and subsurface investigations are compatible with deformational processes at the lithosphere-scale, and demonstrates that a model of coupled simple- and pure-shear deformation in the shallow and deep lithosphere respectively is an appropriate approximation of Paleogene extension in the Barmer Basin. The concomitance between the post-rift thermal subsidence sedimentary succession and the rift indicates that the zone of pure-shear deformation was situated beneath the rift. The rift may have comprised a

significant topographical feature, with erosion of uplifted footwall material contributing to the syn-rift sedimentary succession, and sedimentary environments and sediment facies distributions within the Barmer Basin during early-stage rifting were likely structurally-controlled.

Despite the satisfactory results, the models presented are rudimentary, and the results are one solution within a suite of possible valid solutions dependent upon the input parameters. Further to this, the early, oblique (northwest-southeast) extensional event exposed at outcrop in the Sarnoo Hills is unaccounted for in the models presented, and reactivation of a thermally or structurally weakened lithosphere would have had substantial implications for Barmer Basin rift evolution.

8 Discussion of results

Early rift-oblique extension; Rift-perpendicular Paleogene extension; Subsurface structural complications; Lithosphere-scale processes; Regional context and implications; Implications for hydrocarbon exploration.

The poor understanding of Barmer Basin rift evolution and the context of the rift within the northwest Indian region needs to be improved. Further to this, the origin of rift-oblique faults and structural complications imaged throughout the subsurface of the Barmer Basin is elusive. In **Chapter 1** it was stated that the aims of this thesis were:

1. To further the current understanding of the structural evolution of the Barmer Basin.
2. To investigate the origin of poorly understood structural complications and rift-oblique faults imaged throughout the subsurface of the Barmer Basin.
3. To place Barmer Basin rift evolution within the wider context of the northwest Indian region.
4. To assess how the findings can aid ongoing hydrocarbon exploration within the Barmer Basin.

To achieve these aims a progressive and integrated basin analysis was undertaken, which spanned three scales of investigation, namely the outcrop (small), basin (seismic), and lithospheric scales. Work was conducted with the initial objective of gaining an understanding of the structure of the rift exposed at outcrop (**Chapters 3 & 4**) with the investigation expanded into the subsurface upon constructing an outcrop-based structural framework for the Barmer Basin (**Chapters 5 & 6**). Finally, the flexural response of the lithosphere to extension was investigated, and shallow deformational processes were shown to be compatible with deformational processes at the lithosphere-scale using the flexural-cantilever forward model (**Chapter 7**). In this discussion the combined results of the basin analysis presented in previous chapters, conducted in an attempt to fulfil the research aims, are discussed.

8.1 Early northwest-southeast extension

The description of structures exposed in the Sarnoo Hills (**Chapter 4**) provides a detailed account of rift-oblique faults in the Barmer Basin, and outcrop-based evidence for rift-oblique (≈ northwest-

southeast) extensional tectonics that preceded the main, rift-perpendicular (≈ northeast-southwest) extensional event in the Barmer Basin during the Paleogene Period. Northwest-southeast extensional tectonics were previously unrecognised in northwest India. Structural activity on southwest-trending, rift-oblique faults throughout the subsurface (**Chapter 5**) substantiates that extension was regional, and that the northwest-extension observed in the Sarnoo Hills was not locally derived from, for example, gravity-induced footwall collapse (e.g. Hesthammer & Fossen 1999). In this section, the age and plate tectonic origin of northwest-southeast extension are discussed.

8.1.1 Age

The age of deformation is poorly constrained. However, the Aptian to Albian age estimate for the Ghaggar-Hakra Formation (**Section 4.6**), and probable Maastrichtian age of intrusions, which are occasionally exposed within existing fault planes, crudely constrains the deformational event exposed in the Sarnoo Hills to have occurred between the Aptian and Maastrichtian stages. Sedimentological features allude to deposition of the Ghaggar-Hakra Formation within a rapidly subsiding alluvial plain attributed to tectonic destabilisation of the Marwar Craton, the origin of which is unknown (**Chapter 4**). It is suggested that Ghaggar-Hakra Formation deposition was triggered by the onset of rapid extension-induced subsidence in the Barmer region during the Lower Cretaceous Epoch, and the fluvial succession exposed is a manifestation of rift-oblique (≈ northeast-southwest) extensional tectonics. The Lower Cretaceous Ghaggar-Hakra Formation, therefore, provides a critical temporal marker for the onset of rift-oblique extensional tectonics in the Barmer region, and further constrains rift-oblique extension to the late Lower Cretaceous Epoch. The pre-rift tectono-stratigraphical relationship between the Ghaggar-Hakra Formation sedimentary succession and the fault network exposed in the Sarnoo Hills does not invalidate the link between active tectonism and deposition. Rather it implies that the fluvial systems preserved within exposures of the Ghaggar-Hakra Formation in the Sarnoo Hills represent a fluvial system that flowed towards areas of active fault-induced subsidence elsewhere in the Barmer region, prior to the migration of deformation into the Sarnoo Hills.

8.1.2 Plate tectonic origin and implications

Based on the plate-tectonic setting of the Barmer Basin and northwest Indian rifts (**Section 2.3.1**), late Lower Cretaceous extensional tectonics are related to the multiple rift events associated with

the fragmentation of the Gondwanan supercontinent during the Mesozoic Era. Placing the northwest-southeast extensional event exposed in the Sarnoo Hills (**Chapter 4**) into the regional tectonic framework indicates differential movements (< 150 km relative motion) between the Greater Indian and Madagascan continents during the separation of east and west Gondwana (**Figure 2.19**; Bastia *et al.*, 2010; Reeves, 2014) are the likely plate-tectonic driver of rift-oblique (≈ northwest-southeast) extension in the Barmer Basin during the late Lower Cretaceous Epoch.

Over a transition period between 145 Ma and 118 Ma, ocean growth occurred to the south of the Greater Indian continent at the expense of spreading in the Somali Basin to the north (**Figure 2.19b**), driven by the failure of the Greater Indian and Madagascan continent to keep pace with the southwards migrating Australian and Antarctic continent (Reeves 2014). Transtension between the Greater Indian and Madagascan continents is most likely to have occurred during the Lower Cretaceous Epoch as a result of a clockwise rotation of the Antarctic continent relative to the African continent, and the establishment of the spreading centre between the Greater Indian and Antarctic continents (Bastia *et al.*, 2010; Reeves, 2014). Differential movements between the Greater Indian and Madagascan continents, therefore, are associated with plate boundary relocation from within the Somali Basin to between the Greater Indian and Antarctic continents (**Figure 2.19b**).

Tensional stresses transmitted through the Greater Indian continent during plate-boundary relocation may have induced rifting in the northwest Indian region, with relative plate motions that were favourable for northwest-southeast extensional deformation in the Barmer Basin (**Figure 8.1a**). The northwest-southeast extensional event exposed in the Sarnoo Hills (**Chapter 4**), and the early rift-oblique (southwest-trending) depocentres (sub-basins) evident in the Barmer Basin subsurface (**Chapter 5**), therefore, are likely associated with plate reorganisations during the Lower Cretaceous Epoch. More specifically, rift-oblique sub-basins in the Barmer Basin may be intracontinental manifestations of transtension between the Greater Indian and Madagascan continents (**Figures 2.19b & 8.1a**; e.g. Bastia *et al.*, 2010; Reeves, 2014). Equivalent structures may occur in the Kachchh (Kutch) and Cambay basins (e.g. Biswas, 1982; Biswas, 1987; Gombos *et al.*, 1995), and may also be hidden beneath thick Deccan-related volcanics on the broad west Indian continental shelf (Reeves, 2014).

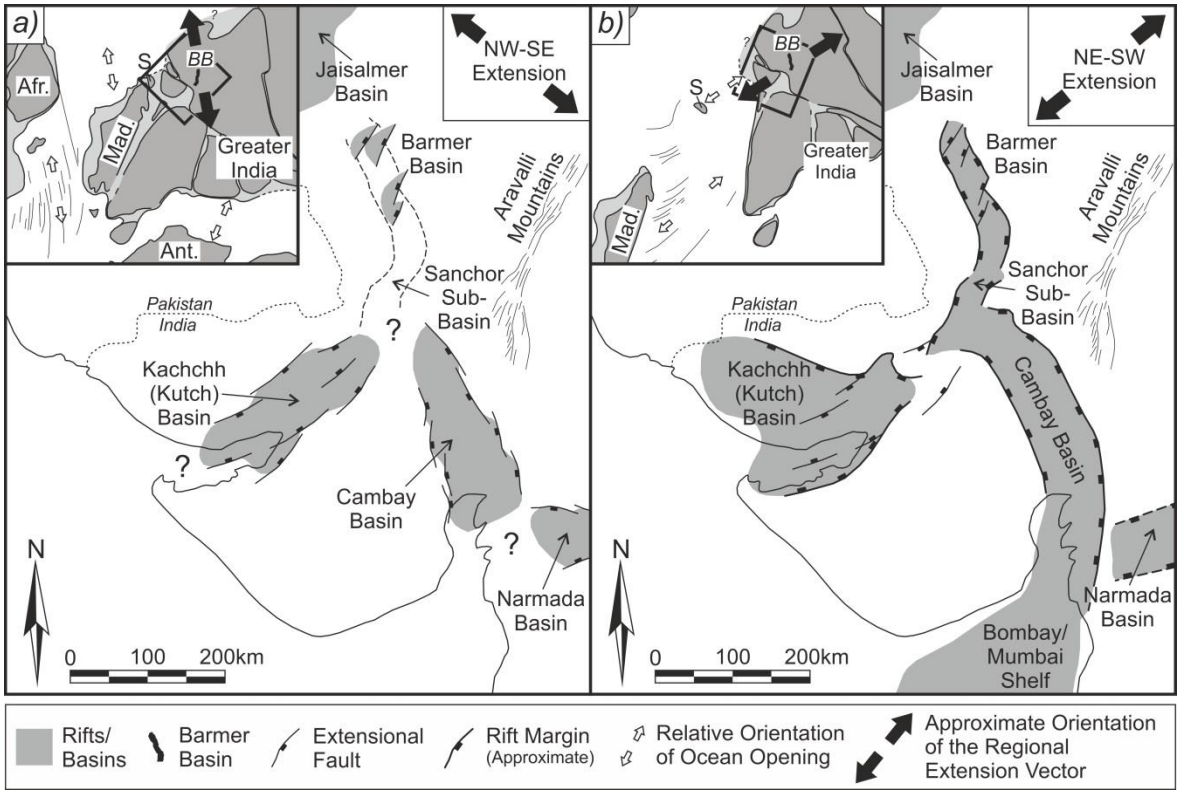

Figure 8.1 – **(a)** Transtension between the Greater Indian and Madagascan continents during the separation of east and west Gondwana may have generated northwest-southeast extension throughout northwest India, manifest as rift-oblique faults and depocentres in the Barmer Basin. Plate reconstruction at 120 Ma inset (after Reeves 2014); **(b)** Failed rifting in the Gop and Laxmi basins, and successful rifting of the Seychelles microcontinent in response to plate boundary reorganisations, generated northeast-southwest extension throughout northwest India and the majority of subsidence in the Barmer Basin. Plate reconstruction at 66 Ma inset (after Reeves 2014). BB = Barmer Basin; S = Seychelles; Afr = Africa; Mad. = Madagascar; Ant. = Antarctica.

The spreading centre in the Somali Basin to the north of the Greater Indian continent became extinct by 120 Ma, coincident with the 120 Ma age estimate of the basalts underlying the Ghaggar-Hakra formation in the Sarnoo Hills (Sharma 2007). Upon abandonment of the spreading centre in the Somali Basin, northern (Africa-Greater India-Madagascar) and southern (South America-Antarctica-Australia) Gondwanan continents were formed and persisted until separation of the Greater Indian and Madagascan continents in the Coniacian age (88 Ma; Storey *et al.* 1995). The documentation of mid-Cretaceous extension in the Barmer Basin, linked to external plate boundary forces, indicates that extension throughout northwest India was long lived, resulted from far-field plate reorganisations, and was established prior to the main phase of Deccan eruptions (≈ 65 Ma).

The development of rift-oblique depocentres in the Barmer region during the Lower Cretaceous Epoch suggests that the Present Day Barmer Basin is underlain by a Cretaceous (or older?) rift system orientated northeast-southwest (**Figure 8.2**). Extension-induced subsidence in the Barmer

region during the Lower Cretaceous Epoch may have captured established regional drainage systems (**Figure 8.2**), accounting for the high sediment input within deposits of the Ghaggar-Hakra Formation exposed in the Sarnoo Hills, and formed an analogous or equivalent fluvial system to the Present Day Luni River (**Figure 4.25**).

8.2 Rift-perpendicular extension during Paleogene rifting

The description and kinematic analysis of faulting exposed in the Barmer Hills (**Chapter 3**) substantiated the common assumption that deformation in the Barmer Basin accommodated regional, rift-perpendicular (≈ northeast-southwest) extension during the Paleogene Barmer Basin rift event. In this section the plate tectonic origin and the expression of rift-perpendicular, Paleogene extension at outcrop exposure in the Sarnoo Hills are discussed.

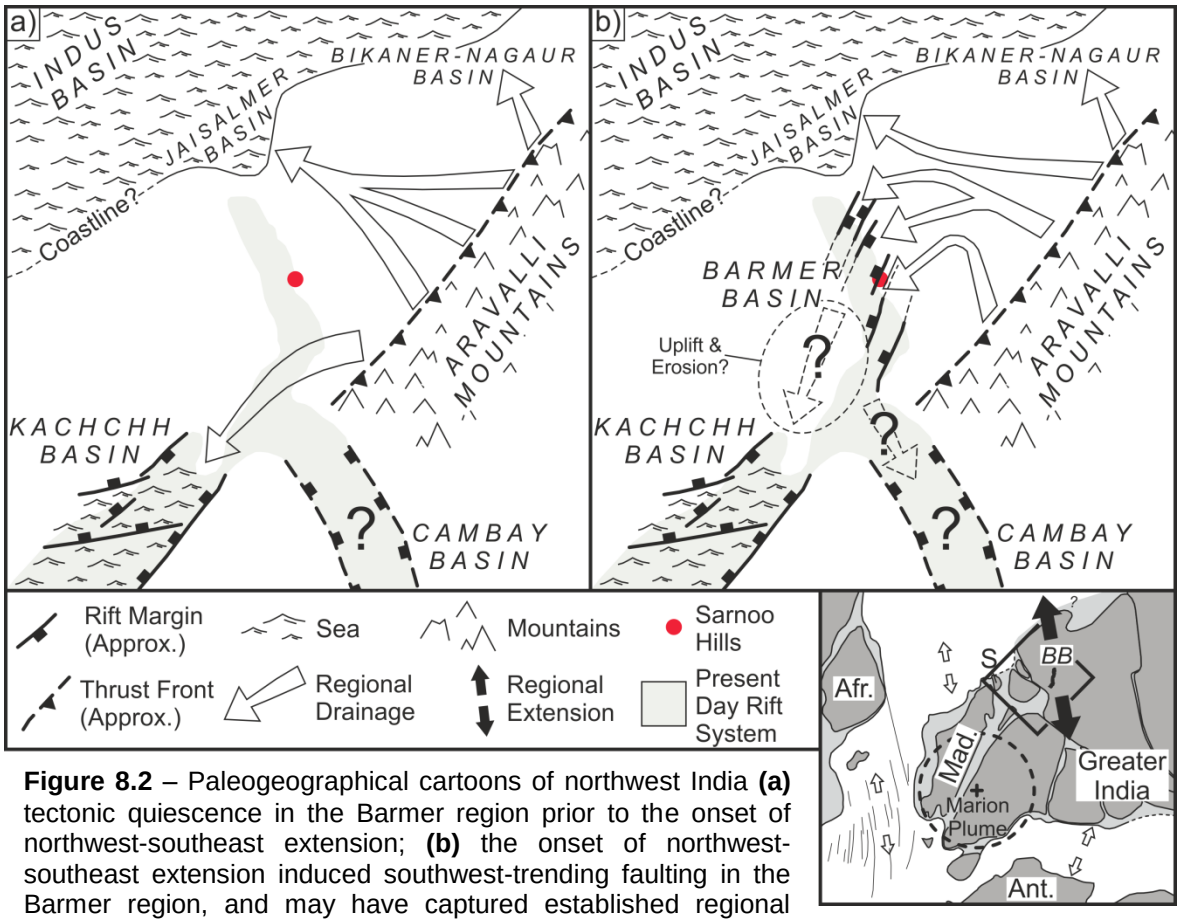

Figure 8.2 – Paleogeographical cartoons of northwest India **(a)** tectonic quiescence in the Barmer region prior to the onset of northwest-southeast extension; **(b)** the onset of northwest-southeast extension induced southwest-trending faulting in the Barmer region, and may have captured established regional drainage systems within early rift-oblique rift systems. Plate reconstruction at 120 Ma inset (after Reeves 2014). Afr. = Africa; S = Seychelles microcontinent; Mad. = Madagascar; BB = Barmer Basin; Ant. = Antarctica.

8.2.1 Plate-tectonic origin

The northeast-southwest orientated divergence of the Greater Indian and Madagascan continents during the Upper Cretaceous Epoch, and subsequently the Greater Indian continent and Seychelles microcontinent during the early Paleogene Period (Reeves 2014), indicates the regional extension vector was northeast-southwest orientated (**Figure 8.1b**). Northeast-southwest orientated regional extension is sub-parallel to the rift-perpendicular Paleocene extensional deformation exposed in the Barmer Hills (**Chapter 3**). Placing the observations within the currently understood regional tectonic framework, therefore, suggests the main phase of subsidence in the Barmer Basin, the Barmer Basin rift event (**Figure 8.1b**), is an intra-continental northerly manifestation of attempted rifting in the Gop and Laxmi basins (e.g. Malod *et al.* 1997; Chaubey *et al.* 2002; Collier *et al.* 2008; Yatheesh *et al.* 2009), and subsequent separation of the Seychelles microcontinent from northwest India (**Figure 8.1b**).

Separation of the Seychelles microcontinent from northwest India was associated with a major relocation of the plate boundary between the Greater Indian and African continents. Attempted rifting in the Gop and Laxmi basins, followed by successful rifting of the Seychelles microcontinent from northwest India occurred at the expense of spreading in the Mascarene Basin (Torsvik *et al.* 2013; Eagles & Hoang 2014). Northeast-southwest orientated extensional deformation throughout northwest India at the Cretaceous-Paleogene boundary, therefore, is linked to the fragmentation of the Greater Indian continent in the wake of rapid northwards continental migration, and establishment of the Carlsberg Ridge between the Seychelles microcontinent and northwest India. The potential for contemporaneous Maastrichtian rifting in the Barmer, Gop, and Laxmi basins alludes to a period of rifting throughout northwest India that pre-dated the main phase of Deccan eruptions (≈ 65Ma; Chenet *et al.* 2007).

8.2.2 The expression of northeast-southwest extension in the Sarnoo Hills exposure

Evolution of the rift-oblique Sarnoo Hills fault network during late-Lower Cretaceous extensional deformation indicates the fault network was inherent in the crust during rift-perpendicular Paleogene extension. However, little evidence of fault reactivation is observed in the Sarnoo Hills. The high degree of involvement of pre-existing structures, the juvenile nature, and zig-zag geometry of the fault network exposed in the Sarnoo Hills (**Chapter 4**) indicates that southwest-

striking faults, which were perpendicular to early northwest-southeast extension, did not become dominant, nor were structural irregularities (zig-zag's) obliterated and 'smoothed-out' as expected to occur during fault network maturation (**Section 4.6**). Due to the lack of development of efficient, through-going, southwest-striking faults, the zig-zag nature of the juvenile fault network would have actively hindered sinistral-oblique reactivation of southwest-striking faults during northeast-southwest orientated Paleogene extension. Northeast-southwest extension is expressed in the Sarnoo Hills, however, as distributed, low-strain deformation, such as the predominance of rift-parallel extensional fractures (**Figure 4.16**).

Despite a lack of evidence for reactivation of faults within the Sarnoo Hills fault network, the complete syn-rift sedimentary succession at the base of the rift-oblique rift-margin fault immediately adjacent to the Sarnoo Hills (**Figure 4.6**) indicates that this fault was active for the duration of Paleogene rifting. It is speculated that, during the main Barmer Basin rift event (≈ northeast-southwest), sinistral-oblique reactivation of the rift margin fault would have been favourable to overcoming (obliterating) irregularities inherited from early rift-oblique (≈ northwest-southeast) extension in the juvenile Sarnoo Hills fault network. Such a hypothesis implies that faults in the Sarnoo Hills remained inactive during Paleogene rifting, accounting for the lack of evidence for oblique reactivation of southwest-striking faults.

8.3 Subsurface structural complications and rift oblique faults

Exposure of two distinct extensional structural regimes on the Barmer Basin rift margins (**Chapters 3 & 4**) that can be correlated with temporally variable depocentres in the subsurface (**Chapter 5**), indicates that rift evolution resulted from the superimposition of two discrete, non-coaxial extensional events (e.g. Keep & McClay 1997; Bonini *et al.* 1997; Morley *et al.* 2007; Henza *et al.* 2010; Henza *et al.* 2011). Structural complications and rift-oblique faults interpreted throughout the subsurface of the Barmer Basin were demonstrated to result from the incorporation of rift-oblique faults into the evolving rift-parallel fault systems during Paleogene rifting (**Chapters 5 & 6**). However, some of the observations presented could also be accounted for by uniaxial transtensional (oblique) rifting or a significant rotation of the stress field local to a long-lived pre-existing crustal weakness during a single deformational event. In this section these alternative hypotheses are discussed, alongside the applicability of the findings throughout the Barmer Basin.

8.3.1 Transtensional (oblique) rifting

Features including: 1) the rift-oblique (northwest) extension direction exposed at outcrop in the Sarnoo Hills (**Chapter 4**); 2) the dominance of rift-oblique faults during the early-stages of rifting, with rift-parallel faults becoming dominant with continued extension (**Chapters 5 & 6**), and; 3) bipolar structural domains in the northern Barmer Basin (rift margin vs mid-rift; **Figure 2.20**), could be interpreted to suggest rift evolution under a single episode of uniaxial transtensional (oblique) rifting (e.g. Withjack & Jamison 1986; McClay & White 1995; Clifton *et al.* 2000; Clifton & Schlische 2001; McClay *et al.* 2002; Autin *et al.* 2013). However, the spatial variation in oblique faulting throughout the rift, namely rift-oblique faulting prevalent in the north, but absent in the south (**Figure 2.20**), and the incorporation of a rift-oblique fault into the eastern rift margin, are inconsistent with such models. Further to this, the incorporation of a rift-oblique fault into the eastern rift margin (**Figures 5.25 & 5.26**), requires that a rift-oblique fault be present prior to rift margin evolution. As such, the inheritance of a rift-oblique fault into the eastern rift margin, and the long-lived activity of this fault throughout evolution of the Barmer Basin, indicates that: 1) southwest-striking, rift-oblique faults existed prior to the main Barmer Basin rift event; 2) rift-oblique faults were favourable for reactivation, and; 3) in some cases rift-oblique faults were active for the duration of rifting. Additionally, the spatial variation of rift-oblique faulting within the rift can be attributed to the presence or absence of pre-existing faults, and the favourability of these faults for reactivation during Paleogene rifting. Rift evolution over a crust containing spatially variable pre-existing structures, namely a pre-structured crust, provides a robust alternative to transtensional (oblique) rifting.

8.3.2 Localised stress field rotation during rifting

Significant stress-field rotations have been observed during rifting in the East African Rift System (Morley 2010). Stress-field rotation occurs locally to long-lived, weak pre-existing strength anisotropies within the crust, and may result in pure extension of faults orientated obliquely to the extension direction, that is extension-oblique faults may exhibit normal sense dip-slip displacement rather than normal sense oblique-slip displacement. Such a hypothesis satisfactorily explains the formation of two, non-coaxial extensional structural regimes during a single extensional event, as exposed on opposing rift margins of the Barmer Basin (**Chapters 3 & 4**), and is in accordance with the existence of a rift-oblique fault prior to evolution of the eastern rift margin (**Chapter 5**;

Figure 5.26). Without conclusive constraint on the age of rift-oblique (≈ northwest-southeast) extension, as exposed in the Sarnoo Hills (**Chapter 4**), it is hard to support or refute this alternative hypothesis. However, it is not the favoured interpretation because the Ghaggar-Hakra Formation is suggested to represent deposition within a rapidly subsiding alluvial plain in an actively extending region (**Section 8.1.1**), crudely constraining the rift-oblique (≈ northwest-southeast) extensional event exposed in the Sarnoo Hills to the late Lower Cretaceous Epoch.

8.3.3 Applicability of findings throughout the rift

Incorporation of rift-oblique faults into the evolving rift-parallel fault systems during Paleogene rifting (**Chapters 5 & 6**; e.g. Keep & McClay 1997; Bonini *et al.* 1997; Morley *et al.* 2007), provides a robust explanation for structural complications and poorly understood rift-oblique faults interpreted in the subsurface throughout the Barmer Basin. In accordance with previous work, inherited rift-oblique faults were dominant during early rifting, and became inactive with continued extension as rift-parallel fault systems became established and dominant (**Chapters 5 & 6**; e.g. Morley 1995; Lezzar *et al.* 2002; Morley *et al.* 2004; Bellahsen & Daniel 2005). It is noteworthy that without detailed chronostratigraphical constraint on the sedimentary succession within deep, undrilled depocentres and early rift-oblique sub-basins, it is not currently possible to differentiate between the sedimentary succession deposited during early rift-oblique extension (≈ northwest-southeast), and the early-stage sedimentary succession deposited within rift-oblique depocentres during the incipient stages of rift-perpendicular (≈ northeast-southwest) Paleogene rifting.

The complex interplay and numerous factors that dictate the reactivation of weak structures inherent in the crust (**Section 2.1.5.1**), including: 1) the strength of the fabric relative to intact rock; 2) the orientation (dip and strike) of the fabric relative to the stress field, and 3) the sense of slip upon reactivation (Morley *et al.* 2004), does not indicate that the relationships described in previous chapters, namely the incorporation and long-lived involvement of a pre-existing, rift-oblique fault within rift-parallel fault systems (**Chapter 5**), or early reactivation of rift-oblique faults followed by rapid inactivity during the early stages of rifting (**Chapter 6**), are ubiquitous throughout the Barmer Basin. In order to understand the degree of involvement of an inherited fault within the evolving rift-parallel fault systems, a detailed investigation of each individual rift-oblique fault should be undertaken.

8.4 Lithosphere-scale processes

Rudimentary flexural-cantilever forward models of lithosphere extension, conducted with 'standard' lithosphere parameters (e.g. ρ_c, ρ_m, T_A) in the absence of alternative, well-constrained parameters, produced satisfactory approximations of the Barmer Basin rift geometry. However, crust weakened by rift-oblique extensional deformation prior to Paleogene rifting, rifting above a mantle thermal anomaly, and rifting of cratonic lithosphere were not accounted for during modelling. In this section, the potential effect of incorporating these modifications into forward models of lithosphere extension is discussed.

8.4.1 Crust weakened by early rifting

The early rift-oblique extensional event exposed at outcrop along the eastern rift margin of the Barmer Basin, in the Sarnoo Hills (**Chapter 4**) is poorly constrained, both spatially and temporally, but is suggested to have occurred during the late-Lower Cretaceous Epoch (**Section 8.1.1**), approximately 60 Ma prior to Paleogene rifting. Early rifting would be associated with a thermal and mechanical weakening of the lithosphere. The thermal perturbation associated with rifting decays exponentially with time (McKenzie 1978), and the thermal perturbation associated with early rifting would have largely re-equilibrated by the Maastrichtian. However, changes to the mechanical properties of the lithosphere resulting from early rifting are permanent. Post-rift processes are often associated with a strengthening of the lithosphere in the centre of the rift, resulting in subsequent deformation favoured along the rift margins (e.g. Cloetingh *et al.* 2003) or in areas of lesser extension during early rifting (Reemst & Cloetingh 2000). During the earliest stages of deformation strain localises onto weaknesses in the lithosphere, such as lithosphere sutures, molten magmatic bodies, or salt. The presence of a relative mechanical weakness along the margins of early rifts situated beneath the Barmer Basin at the onset of Paleogene extension, therefore, would: 1) likely exert a primary control on the location of Paleogene rifting and the present day Barmer Basin, despite the highly oblique orientation, and; 2) would account for the superimposition of rift systems that formed in response to two non-coaxial extensional deformational events separated by 60 Ma. It is expected that the high strength of the Marwar Craton, across which the Barmer Basin is situated (Balakrishnan *et al.* 2009), the adversity of cratonic lithosphere to deform, or the presence of a lithospheric weakness that pre-dated Mesozoic extension in the Barmer Basin, would accentuate the effects of strain localisation, and the superimposition of deformational events.

8.4.2 Rifting above anomalously hot asthenosphere (1500°C)

In the absence of well-founded evidence supporting anomalously hot asthenosphere, flexural-cantilever forward models were performed using a 'standard' asthenosphere temperature (1333°C). However, it is commonly assumed that the Réunion mantle plume was situated beneath northwest India at the Cretaceous-Paleogene boundary, and would be associated with anomalously high temperature asthenosphere (T_A < 1500°C). Although the Barmer Basin is situated outside the limits of the Deccan Large Igneous Province (DLIP; **Figure 2.18 inset**), the rift is situated within the inferred limits of the Réunion mantle plume head (e.g. Cox 1989; White & McKenzie 1989). High asthenosphere temperature during rifting is associated with greater syn-rift uplift, supressed syn-rift deposition, thick post-rift thermal subsidence packages, and excessive volcanism dependent upon the amount of crustal thinning (White & McKenzie 1989; Kusznir & Ziegler 1992). In the context of the Barmer Basin, rifting above an asthenosphere thermal perturbation implies greater footwall uplift (& erosion) during rifting, a comparatively thin syn-rift sedimentary succession that may contain significant erosional unconformities, and a thick post-rift thermal subsidence sedimentary succession. The low amount of crustal thinning calculated during forward-modelling (β < 1.294; **Chapter 7**) is unlikely to have generated excessive volcanism at surface (e.g. White & McKenzie 1989), but would promote the accretion of magma to the lithosphere (underplating) if the asthenosphere were anomalously hot.

Despite multiple, rift-related unconformities within the sedimentary succession of the Barmer Basin, the preservation of a thick (< 6 km) succession of Paleocene to Eocene syn-rift sediments is not in accordance with rifting above anomalously hot asthenosphere at the Cretaceous-Paleogene boundary. This is supported further by the relatively thin post-rift thermal subsidence sedimentary succession. However, the onset of compressional deformation related to the collision between the Greater Indian and Eurasian continents was coincident with the end of active rifting in the Barmer Basin, and likely supressed subsidence during post-rift thermal relaxation. This deduction is supported by the significant regional post-rift unconformity throughout the southern Barmer Basin (Base Miocene Unconformity; Compton 2009; Dolson *et al.* in press). In the Barmer Basin, therefore, the thickness of sediments deposited during post-rift thermal subsidence, or the rate of thermal subsidence, should not be used to approximate asthenosphere temperature.

8.4.3 Rifting of cratonic lithosphere

The Barmer Basin is commonly assumed to traverse the Marwar Craton (e.g. Balakrishnan *et al.* 2009). Cratonic lithosphere may be between 180 km and 250 km in thickness (Poudjom Djomani *et al.* 2001), and is often assumed to be cold and dense. Lithosphere-scale geodynamical models of deformation were conducted using 'standard' values of crustal and mantle density (ρ_c & ρ_m), namely 2.8 g cm^{-3} and 3.3 g cm^{-3} respectively, in the absence of well-constrained alternative values, and a crustal thickness of 32 km based upon work conducted immediately to the south of the Barmer Basin, in the Sanchor sub-basin (Kaila *et al.* 1990; **Chapter 7**). However, the Sanchor Basin is at the periphery of the Marwar Craton and be unrepresentative of the craton interior.

Increased crustal thickness does not affect the flexural strength of the lithosphere, which is dictated by the effective elastic thickness (T_e), and the detailed geometries and relative depths of fault blocks within the rift should be unaffected by changing crustal thickness alone. A more important factor is the detachment depth of faulting, which is controlled by the depth of the transition between brittle and ductile deformation, which is in-turn controlled by the composition and geothermal gradient of the crust. A deeper detachment depth may be expected for cold, cratonic lithosphere due to the low geothermal gradient. A deeper detachment depth is associated with greater syn-rift uplift due to thermal buoyancy, thin basins, and supressed post-rift deposition (Kusznir & Egan 1989). Both the narrow width of the Barmer Basin, and the thin post-rift sedimentary succession, suggest a deeper detachment depth may be applicable to Paleogene deformation in the Barmer Basin. However the thickness of the post-rift sedimentary succession does not reflect thermal subsidence alone and should not be used to approximate post-rift thermal relaxation.

8.5 Regional context and implications

The rift-oblique (≈ northwest-southeast) extensional structural regime exposed along the central eastern rift margin of the Barmer Basin, in the Sarnoo Hills (**Chapter 4**), is suggested to have occurred during the late Lower Cretaceous Epoch and, therefore, pre-dated the rift-perpendicular (≈ northeast-southwest; **Chapter 3**) Paleogene Barmer Basin rift event. Rift-oblique sub-basins that formed during early rift-oblique extension may be obscured beneath the Barmer Basin (**Chapter 5**) and, although lithosphere and asthenosphere parameters were poorly constrained, extensional deformation of average thickness crust (32 km) and 'normal' temperature' asthenosphere (1333°C) using the flexural-cantilever forward model produced satisfactory approximations of the rift

geometry (**Chapter 7**). In this section the implications of the findings are discussed within the context of the northwest Indian region.

8.5.1 Pre-Paleogene rift system

In conjunction with established rifting elsewhere in northwest India (Kachchh, Cambay, and Narmada basins; **Section 2.2.2**), the discovery of northwest-southeast extensional deformation in the Barmer Basin that pre-dated the onset of Paleogene extension demonstrates that rifting was established throughout northwest India prior to the Cretaceous-Paleogene boundary, and possibly formed a pre-Paleogene series of rifts that evolved from at least the Lower Cretaceous Epoch. Rift segments may not have been linked directly, and may instead have formed a linked series of isolated pockets of extension (rift-segments) as occurs during the earliest stages of continental-rift evolution (Nelson *et al.*, 1992). The temporal correlation of non-coaxial extensional events exposed at outcrop in the Barmer Basin with distinct stages of the plate-tectonic evolution of the Greater Indian continent, namely: 1) northwest-southeast regional extension (**Chapter 4**) during the south-easterly drift of the Greater Indian continent prior to separation of the Greater Indian and Madagascan continents during the Upper Cretaceous Epoch, and; 2) northeast-southwest regional extension (**Chapter 3**) in the wake of the rapid north-easterly drift of the Greater Indian continent after successful separation of the Greater Indian and Madagascan continents, demonstrates that rifting throughout northwest India can satisfactorily be explained within an entirely plate-tectonic framework (e.g. Sharma, 2007).

The common assumption that the arrival of the Réunion mantle plume triggered rifting is only one of two options. The commonly overlooked alternative hypothesis that rifting triggered volcanism (e.g. Sheth 2005a; Sheth 2005b; Sheth 2007; Sharma 2007) is also entirely practicable, with one possibility being rifting triggered by tensional forces transmitted through the Greater Indian plate as a result of variable ‘slab pull’ and ‘ridge push’ interactions between the leading edge of the Greater Indian continent subducting beneath the Eurasian continent, and the spreading centre in the Mascarene Basin, during rapid northwards migration. It is foreseeable that an established Mesozoic rift-system throughout northwest India could: 1) accommodate and localise tensional strain transmitted through the Greater Indian continent, triggering rifting throughout northwest India at the Cretaceous-Paleogene boundary, and; 2) may have represented a more efficient location for extension, driving the relocation of the plate boundary between the Greater Indian and African

continents from within the Mascarene Basin, to between northwest India and the Seychelles microcontinent.

8.5.2 Plume induced rifting?

The common assumption that the Réunion Mantle Plume triggered rifting throughout west India at the Cretaceous-Paleogene boundary (Morgan 1971; Plummer & Belle 1995; Sen & Chandrasekharam 2011) is not consistent with the interpretation presented herein of early, possibly late Lower Cretaceous Epoch northwest-southeast extension in the Barmer Basin (**Chapter 4**), or the formation of pre-Deccan rift-systems throughout northwest India. A mantle-plume origin for the Deccan Traps has been questioned, with many aspects of the Deccan geology inconsistent with that predicted by the plume-head model (Sheth 2005a; Sheth 2005b; Sheth 2007), and it is suggested that the two non-coaxial episodes of rifting observed within early deposits of the Barmer Basin are better explained by a model of plate reorganisations that initiated long before the arrival of the Réunion Mantle Plume (e.g. Sharma 2007; Collier *et al.* 2008). This, combined with a lack of evidence for significant pre-Deccan regional unconformities, and only minor Deccan-age volcanism within the Barmer Basin (Basu *et al.* 1993; Sen *et al.* 2012), suggests that rifting did not occur above anomalously hot asthenosphere, despite the rift being situated within the inferred limits of the Réunion plume-head (**Figure 2.19d**; e.g. Cox 1989; White & McKenzie 1989).

An alternative to the plume head model (c.f. Campbell & Griffiths 1990) has been suggested for the Deccan province (Sheth 2005b) in which fertile mantle released during rifting accounts for the excessive Deccan volcanism, rather than decompression melting of anomalously hot asthenosphere caused by a mantle plume. Similar models involving high mantle fertility beneath Iceland (Foulger *et al.* 2005; Foulger & Anderson 2005) and heat accumulation beneath the Karoo Large Igneous Province (Hastie *et al.* 2014), provide further support for the generation of excessive volcanism during rifting in the absence of a mantle plume. It is suggested that such models should be given consideration as viable alternatives to explain the geology of these regions, rather than a widespread acceptance of the plume head model that has, in the case of the Deccan, been shown to poorly explain many aspects of the regional geology (Sheth 2005a; Sheth 2007).

8.5.3 Early interaction between the Indian and Eurasian continents

The onset of collision between the Greater Indian and Eurasian continents is widely cited to have occurred near to the Paleocene-Eocene boundary (≈ 56 Ma; Patriat & Achache 1984; Beck *et al.* 1995; Leech *et al.* 2005; Green *et al.* 2008; Liebke *et al* 2013), and indicates the latest stages of active extensional deformation in the Barmer Basin (early- to middle Eocene Akli Formation; **Chapter 6**; **Figure 6.16**) coincided or post-dated the onset of collision. However, an earlier collision near to the Cretaceous-Paleogene boundary (≈ 66 Ma) has also been proposed (Liebke *et al* 2013 and references therein), and inversion structures are observed in the Barmer Basin within late Paleocene deposits (≈ 58 Ma; Kelly *et al.* 2014 Dolson *et al.* in press). Further to this, inversion structures 800 km south of Sri Lanka were suggested to result from resistance between the underthrusting Indian plate and the overriding Eurasian plate (Lowell 1995), indicating that compressional forces were transmitted significant distances into the foreland of the collision zone (< 3000 km).

Throughout this work the structural evolution of the Barmer Basin is assumed to have responded to regional extensional deformation alone. However, the potential for an early collision between the Greater Indian and Eurasian continents suggests deformation in the foreland of the collision zone may have been significant during Paleogene rifting. If this is the case, it is likely that a complex interplay existed between regional extension and deformation in the foreland of the collision zone. However, compressional structures in the Barmer Basin are rare, and often subtle, indicating that extensional deformation with an extension direction that was perpendicular to the direction of convergence, predominated over compressional deformation. Paleogene rifting, therefore, may have been driven by a combination of regional extension in the wake of the rapidly northwards migrating Greater Indian continent, and extension driven by the early interactions between the Greater Indian and Eurasian continents, for example lateral evacuation in the foreland of the collision zone (e.g. Impactogen; c.f. Segnor *et al.* 1978; Allen & Allen 2005).

8.6 Implications for hydrocarbon exploration

The Barmer Basin is a prolific oil and gas producing province, with the current estimate of reserves amounting to approximately eight billion barrels of stock tank oil in place (STOIIP), across thirty-six discoveries. The reservoirs range from high-quality quartzose fluvial sandstones, through lacustrine turbidites and diatomites, to basement granites and rhyolites (Dolson *et al.* in press). Recent

improvements in the understanding of the sedimentary succession of the Barmer Basin indicate that some of the discovered hydrocarbons occur in the Lower Cretaceous Ghaggar-Hakra Formation, which is exposed along the central eastern rift margin, in the Sarnoo Hills (**Chapter 4**). As such, the Ghaggar-Hakra Formation must constitute a significant reservoir in the basin and has the potential to become a major exploration play. The improved understanding of the structural evolution of the Barmer Basin, as well as the preliminary characterisation of the Ghaggar-Hakra Formation sedimentary succession exposed in the Sarnoo Hills, contribute to the current understanding of the hydrocarbon system within the Barmer Basin. In this section, the findings presented in previous chapters are discussed with reference to on-going hydrocarbon exploration in the Barmer Basin. Specifically, the findings of outcrop and seismic work are used to: 1) refine the current poor understanding of the pre-Paleogene (Ghaggar-Hakra Formation) sedimentary succession in the subsurface of the Barmer Basin and speculate on reservoir and source rock distributions; 2) to assess how the formation of complex structural geometries arising from the superimposition of non-coaxial rifting events could have influenced the style and distribution of syn-rift sedimentation during Paleogene rifting, and; 3) to speculate on how structural complications during Paleogene rifting may have formed reproducible trapping styles throughout the Barmer Basin.

8.6.1 The pre-Paleogene sedimentary succession in the Barmer Basin

The discovery of rift-oblique (≈ northwest-southeast) extensional deformation at outcrop exposure in the Sarnoo Hills (**Chapter 4**), and early rift-oblique depocentres in the subsurface of the central Barmer Basin (**Chapter 5**), alludes to pre-Paleogene sub-basins in the subsurface of the Barmer Basin. Rift-oblique rift-systems may be obscured beneath the present day Barmer Basin (**Figure 8.3**). Further to this, deposition of the Ghaggar-Hakra Formation within an actively extending terrane (**Chapter 4**; **Section 8.1.1**) implies that the Ghaggar-Hakra Formation may exhibit syn-rift tectono-stratigraphical relationships in the subsurface of the Barmer Basin (**Figure 8.3**) contrary to previous suggestions (e.g. Compton 2009). However, stratigraphical constraints on the sedimentary succession within rift-oblique rift-systems are limited due to a paucity of core data, and rift-oblique rift-systems are deeply buried where seismic imaging on current data is poor. Moreover, confirmation that a viable source rock is present within the pre-Paleogene sedimentary succession and a detailed understanding of the structure of rift-oblique rift-

systems are poorly constrained. In this sub-section, the findings of work presented in previous chapters are used to: 1) refine the current poor understanding of the pre-Paleogene (Ghaggar-Hakra Formation) sedimentary succession in the subsurface of the Barmer Basin and speculate on reservoir and source rock distributions, and; 2) to evaluate the seismic resolution of potential reservoir intervals exposed in the Sarnoo Hills on currently available subsurface seismic data using seismic forward modelling.

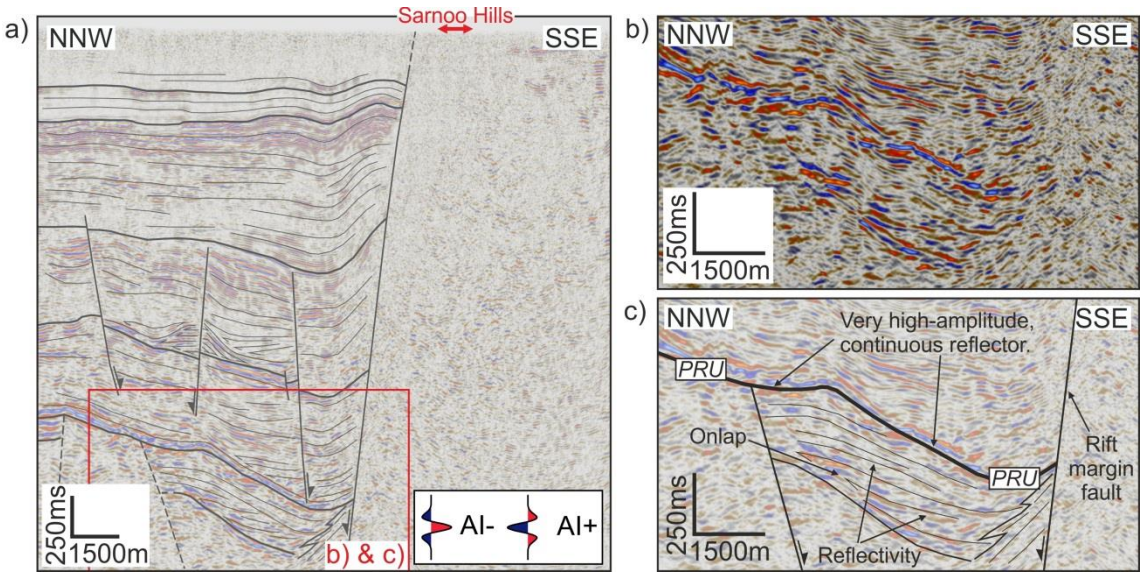

Figure 8.3 – Reflectivity below the current interpretation of the base syn-rift sedimentary succession (PRU) adjacent to outcrop exposure in the Sarnoo Hills, possibly displaying seismo-stratigraphical relationships (onlap). Such features may represent rift-oblique sub-basins obscured beneath the Barmer Basin. For section location see **figure 4.1**. PRU = pre-rift unconformity.

8.6.1.1 The pre-Paleogene (Ghaggar-Hakra Formation) sedimentary succession

Despite the likely presence of an active hydrocarbon system buried beneath the Barmer Basin (Dolson *et al.* in press; Farrimond *et al*. in review), the pre-Paleogene sedimentary succession is poorly understood due to negligible exposure and poor seismic resolution in the deeper sections of the rift. Exposure of the Lower Cretaceous Ghaggar-Hakra Formation in the Sarnoo Hills (**Chapter 4**) provides important insights into pre-Paleogene sedimentary succession. The outcrop revealed three fluvial sandstone successions, namely the Darjaniyon-ki Dhani, Sarnoo, and Nosar sandstones, separated by thick packages of floodplain mudstones and siltstones (**Figure 4.23**). Deposition on the rift margin, in the Sarnoo Hills, commenced within immature, braided fluvial systems in mobile, erosive channels, as demonstrated by the Darjaniyon-ki Dhani Sandstone, and evolved into a larger, meandering fluvial system, the Sarnoo Sandstone. Stacked accreting channel

systems and highly erosive bases indicated deposition of the youngest Nosar Sandstone occurred within a large, rapidly migrating fluvial system that was dominantly braided. The intervening floodplain mudstones and siltstones occur in unusually thick packages (≤ 30 m), with rooted horizons alluding to sub-aerial exposure and the beginning of pedogenesis. However, the paucity of well-developed palaeosols indicates a lack of long-term floodplain stability, and it was suggested that the preservation of a high proportion of fine deposits relative to the sandstone successions resulted from floodplain aggradation due to deposition within a rapidly subsiding alluvial plain in an actively extending region (**Chapter 4**). The sandstone successions demonstrate good reservoir potential at outcrop, especially the well-sorted Sarnoo Sandstone (sar; **Figure 4.23**) which is dominated by well-rounded, monomictic, quartzitic clasts. However, variable cementation, poor sorting, and compaction reduce reservoir quality.

Limited exposure of the Ghaggar-Hakra Formation sedimentary succession in the Sarnoo Hills due to uplift and erosion of the rift shoulder (**Chapter 7**) precludes attaining a detailed spatio-temporal understanding of the Ghaggar-Hakra Formation fluvial system. The sedimentary succession exposed indicates a large-scale braided fluvial system (Nosar Sandstone) was established from a series of comparatively small-scale braided and meandering fluvial systems (Darjaniyon-ki Dhani and Sarnoo sandstones respectively). Although erosion has removed much of the succession, it is conceivable that the Ghaggar-Hakra Formation sedimentary succession exposed in the Sarnoo Hills continued to grow, and comprised a large braided fluvial system with a high bedload, as alluded to by the Nosar Sandstone. However, the Sarnoo Hills are situated on the rift margin of the Barmer Basin, in the immediate footwall of a major southwest-striking, rift-oblique fault that was active during both Lower Cretaceous Epoch rift-oblique (northwest-southeast) extension and rift-perpendicular (northeast-southwest) extension during the Paleogene Period (**Chapter 5**). Active faulting results in uplift of the footwall relative to the hanging-wall, which subsides, and the formation of the basic building block of continental rift-basins, a half-graben (**Figure 2.9a**; e.g. Rosendahl 1987; Kusznir & Egan 1989; Morley 1995). The preservation of syn-rift fluvial deposits within the immediate rift-margin footwall of the Barmer Basin, in the Sarnoo Hills, therefore, is unusual.

During continental rifting, footwall uplift is expected to shutdown active deposition on exposed footwall crests and deviate fluvial systems around the uplifted footwall high (e.g. Gawthorpe & Leeder 2000). Despite being situated within the immediate footwall of the rift-margin, which is likely to have been flexurally uplifted during deformation (e.g. Egan 1990), and tectono-stratigraphical relationships indicating that deposition pre-dated deformation, fluvial deposition exposed in the Sarnoo Hills is inferred to have been tectonically induced (**Chapter 4**; **Section 8.1.1**), that is the Ghaggar-Hakra Formation is syn-rift. During the incipient stages of deformation in the Gulf of Suez rift (rift-initiation), deposition and progradation of coarse-grained (Gilbert-type) deltas over a monoclinal flexure (growth fold) above a blind normal fault generated unfaulted, basinwards-thickening syn-rift sedimentary packages, prior to breaching of the monocline structure and the formation of the characteristic half-graben geometry (**Figure 8.4**; Gupta *et al.* 1999; Sharp *et al.* 2000). Such a scenario accounts for the preservation of syn-rift fluvial sedimentation in the Sarnoo Hills, which displays pre-rift tectono-stratigraphical relationships with the exposed fault network (**Figure 8.4d**), and alludes to a thick succession of clastic progradational deposits proximal to the rift margin near to the Sarnoo Hills (**Figure 8.3**). The possible presence of thick successions of clastic deposits proximal to the rift margins, such as Gilbert-type deltas (**Figure 8.4**), near to the Sarnoo Hills and elsewhere in the Barmer region, undoubtedly represent promising potential reservoir intervals within the pre-Paleogene sedimentary succession of the Barmer Basin.

The presence of lacustrine mudstones and siltstones within the Ghaggar-Hakra Formation in the subsurface of the Barmer Basin (Dolson *et al.* in press), indicate that in some areas of the Barmer region subsidence rates exceeded sedimentation rates during the Lower Cretaceous Epoch. Where subsidence rates exceeded sedimentation rates, lacustrine deposits represent high source rock potential. Paleogeographical reconstructions of the Greater Indian continent during the late Lower Cretaceous Epoch (**Figure 2.19b**) indicate the Barmer Basin was land-locked, analogous to rift-segments within the western branch of the East African Rift System (e.g. Lake Malawi, Lake Rukwa, and Lake Tanganyika; Nelson *et al.* 1992), and source rocks of lacustrine origin are most-likely type 1 (algal) kerogen and oil-prone.

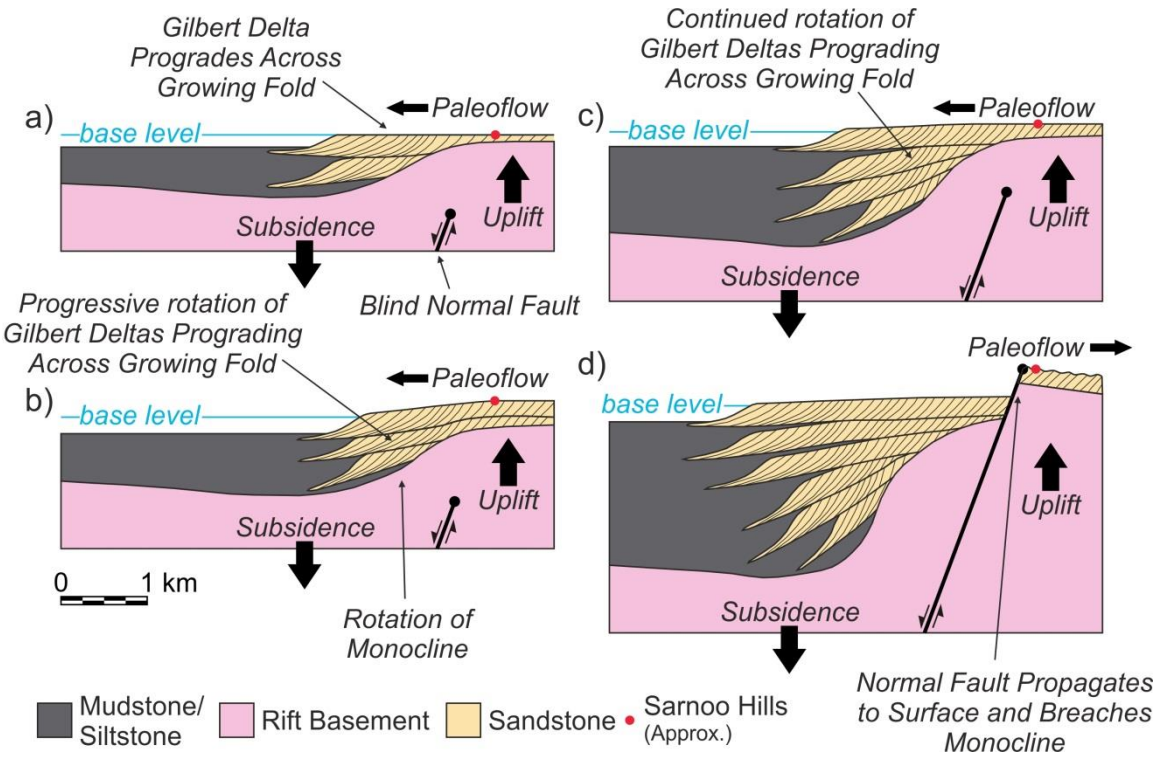

Figure 8.4 – Schematic cross-section illustrating the sequential evolution of a prograding Gilbert-type delta over a monoclinal flexure (growth fold) above a blind normal fault (after Gupta *et al.* 1999). Key to colours and symbols inset. The fluvial systems of the Ghaggar-Hakra Formation in the Sarnoo Hills are interpreted to be syn-rift, but display pre-rift tectono-stratigraphical relationships with the exposed fault network. Formation of a monoclonal flexure above a blind normal fault, prior to breaching of the monocline and uplift of the footwall crest, accounts for deposition of the Ghaggar-Hakra Formation within an actively extending terrane, and preservation of a syn-rift sedimentary succession within the immediate footwall of a major, rift-margin fault system.

The observations suggest that pre-Paleogene graben or half-graben structures are likely to occur beneath the Barmer Basin (**Figure 8.3**) and contain the key components of an oil-prone hydrocarbon play (source & reservoir). Sand-prone sedimentology proximal to the rift margins where subsidence rates were relatively low (e.g. Ghaggar-Hakra Formation in the Sarnoo Hills), is likely to have transitioned down-dip (e.g. relay-ramps or hanging-wall dip-slopes) into more mud-prone lake-margin facies (e.g. deltas), and eventually into sand-poor facies within a lacustrine setting where subsidence rates were high. In this manner, the distribution and thickness of sand-prone facies within the pre-Paleogene sedimentary succession of the Barmer Basin (e.g. fluvial or deltaic sediments), which comprise target reservoir intervals, will vary laterally due to tectonically-induced variations in subsidence rates, as observed in many global rift systems such as the East African Rift System (e.g. Rosendahl 1987; Morley 1995; Morley 1999a; Lezzar *et al.* 2002;) Gulf of Suez (e.g. Gawthorpe *et al.* 1990; Gupta *et al.* 1999; Sharp *et al.* 2000; Young *et al.* 2000; Jackson *et al.* 2005) and the Gulf of Corinth (e.g. Gawthorpe *et al.* 1994). Sand-prone facies of notable

thickness are most likely to be present on the margins of lakes defined by active southwest-striking faults (**Figure 8.5**). Within the pre-Paleogene sedimentary succession of the Barmer Basin fluvial to deltaic sandstone reservoirs are likely to be coupled with a lacustrine type 1 (algal) kerogen source rock. It is foreseeable that the migration of hydrocarbons up-dip and away from hanging-wall depocentres, where oil-prone lacustrine source rocks were deposited, could charge reservoirs within sand-prone, lake-margin facies (e.g. deltas). Trapping styles are likely stratigraphical, fault margin, or a combination of the two.

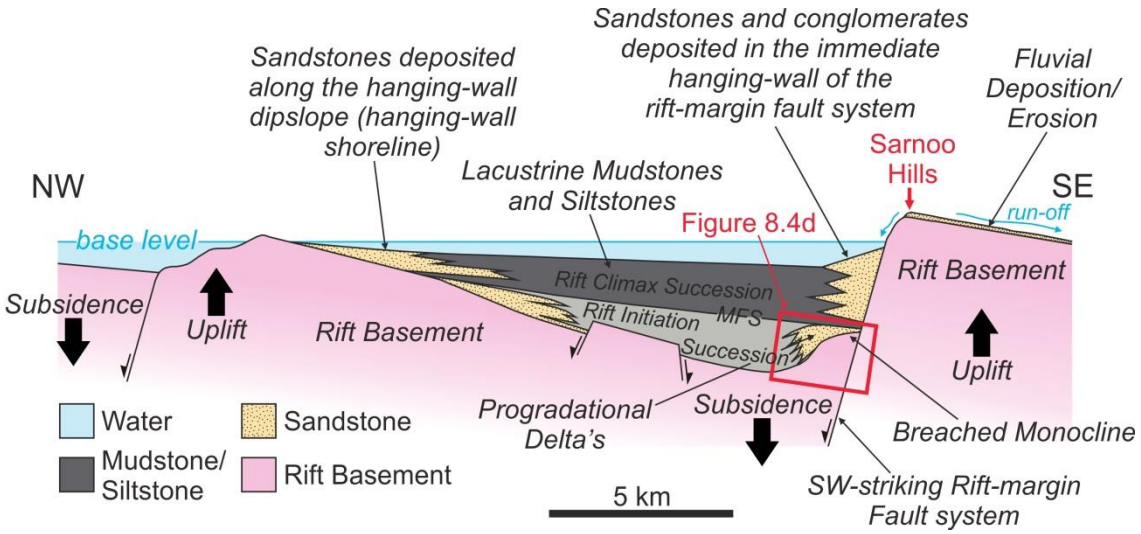

Figure 8.5 – Schematic diagram depicting tectonically-induced variations in subsidence rates and the associated lateral variations in gross depositional environments, sedimentary architectures, and sedimentary thicknesses (modified from Jackson *et al.* 2005). Key to colours inset and the approximate location of **Figure 8.4d** is indicated. Sand prone facies comprising target intervals for hydrocarbon exploration occur along the lake margins. It is speculated that the scenario depicted is representative of the pre-Paleogene sedimentary succession within rift-oblique rift-systems buried beneath a thick succession of Paleogene sediments in the subsurface of the Barmer Basin (e.g. **Figure 8.3**). Critically, substantial sedimentological and thickness variations are likely to occur between the pre-Paleogene sedimentary succession in the subsurface of the Barmer Basin and exposures of the Lower Cretaceous Ghaggar-Hakra Formation in the Sarnoo Hills, situated within the uplifted crest of the rift-margin fault system. The approximate location of the Sarnoo Hills is indicated. MFS = Major Flooding Surface.

8.6.1.2 Seismic resolution of the Ghaggar-Hakra Formation on currently available seismic data

This investigation has undertaken a preliminary characterisation of the Lower Cretaceous Ghaggar-Hakra Formation sedimentary succession based upon exposure in the Sarnoo Hills. However, the resolution gap between individual components of the sedimentary succession at outcrop, and the vertical resolution of industry-standard subsurface seismic data (**Section 6.3.2**) precludes a direct correlation between outcrop exposure and subsurface data. Here this resolution gap is assessed

quantitatively using seismic forward modelling. Despite the potentially substantial lateral facies variations within the Ghaggar-Hakra Formation (**Figure 8.5**), seismic forward models were conducted to replicate the sedimentary succession exposed in the Sarnoo Hills, because: 1) there is no alternative constraint on the seismic-scale architecture of the Ghaggar-Hakra Formation, and; 2) the sandstone successions demonstrate good reservoir potential, which may be targeted during on-going exploration in the Barmer Basin, and it is valuable to evaluate the resolvability of similar intervals on industry-standard subsurface seismic data.

On both two- and three-dimensional seismic data, the frequency of the seismic signal at the base of the sedimentary succession (PRU or bC) is approximately 20 Hz, and corresponds to a maximum compressional (primary or P) wave velocity of 3500 m s^{-1} constrained from interval velocity well-logs (**Figure 5.5**). A schematic, scaled geological model was constructed of the Ghaggar-Hakra Formation based on exposure in the Sarnoo area, which covered a depth of 0.15 km and spanned a width of 5 km (**Figure 8.6a**). Each unit was attributed a density (ρ) and a compressional wave velocity (V_p), and an acoustic impedance and reflectivity coefficient were calculated for each unit and for each interface respectively. Subsequently, 350 seismic traces were generated across the model (≈ 14.3 m trace spacing) for different frequencies using an input 'Ricker' wavelet (**Figures 8.6b-e**). Synthetic seismic images are presented with a vertical axis in time, and seismic traces are normal (North American) polarity, whereby a downward increase in acoustic impedance (positive reflection coefficient) is represented by a peak. Models were conducted with no background noise.

The interface between the Nosar Sandstone (nos; > 30 m) and the Ghaggar-Hakra Formation undivided (gha; < 60 m) is detected at all frequencies, and is represented by a continuous reflector characterised by a negative reflectivity coefficient (trough; **Figures 8.6b-e**). Where the Sarnoo Sandstone succession (sar) is 20 m in thickness, the succession is resolvable, that is the upper and lower contacts are visible as distinct signals, using a signal frequency of 80 Hz (**Figure 8.6b**) and 60 Hz (**Figure 8.6c**), is largely resolvable using a signal frequency of 40 Hz (**Figure 8.6d**), and is detectable using a signal frequency of 20 Hz (**Figure 8.6e**). The Darjaniyon-ki Dhani sandstone succession (dar; < 5 m) is unresolvable at all frequencies, and largely un-detectable using signal frequencies of 80 Hz (**Figure 8.6b**) and 60 Hz (**Figure 8.6c**). The interface between the basalt (B^B)

and the Ghaggar-Hakra Formation undivided (gha) is detected at all frequencies, and is represented by a continuous reflector characterised by a positive reflectivity coefficient (peak; **Figures 8.6b-e**). The 'pull-down' effect of the gha - B^B interface in the north of the models (left of images; **Figures 8.6b-e**) is a result of the thick succession (< 50 m) of low-velocity gha mudstones and siltstones, and the absence of sar in the north of the Sarnoo area (Karentia Hills; **Figure 4.2**).

The models indicate that individual channelised sandstone successions within the Ghaggar-Hakra Formation, which demonstrate potentially good reservoir quality at outcrop and represent target intervals for hydrocarbon exploration, will be undetectable within the deep sedimentary succession of the Barmer Basin using currently available seismic data (frequency < 20 Hz). However, the base Nosar Sandstone (nos-gha) and base Ghaggar-Hakra Formation undivided (gha-B^B) interfaces will be imaged, represented by continuous reflectors characterising negative and positive reflectivities respectively (**Figure 8.6e**). Even if individual sandstone successions were resolvable on currently available seismic data, the sandstone successions consist of stacked fluvial channels, and the individual architectural elements of each succession, such as channel geometries or sand bars which may be targeted during hydrocarbon exploration, would remain unresolvable.

8.6.2 Structural control on sedimentation within the Barmer Basin during Paleogene rifting

Sedimentation within the Barmer Basin during Paleogene rifting was tectonically controlled (**Chapter 7**; Dolson *et al.* in press), and the formation of atypical accommodation zones and unusual structural geometries resulting from structural inheritance (**Chapter 5**; **Figure 5.26**) will have had an atypical influence on sedimentation. It is essential to understand the geometrical evolution of an array of faults in three-dimensions in order to predict gross-depositional environments, sedimentary architectures, and the thickness of basin fill sediments, which are often structurally controlled in extensional terranes (Gawthorpe & Leeder 2000). Such predictions underpin geological models within sedimentary basins, and outline areas that should be evaluated for prospectivity during hydrocarbon exploration. Here, predictions of gross-depositional environments and sedimentary architectures for the atypical accommodation structure demonstrated to occur along the central eastern rift margin of the Barmer Basin (**Chapter 5**; **Figure 5.26**) are discussed, and are visually compared with the predictions made using

conventional structural models (e.g. Morley *et al.* 1990; Gawthorpe & Hurst 1993; Faulds & Varga 1998).

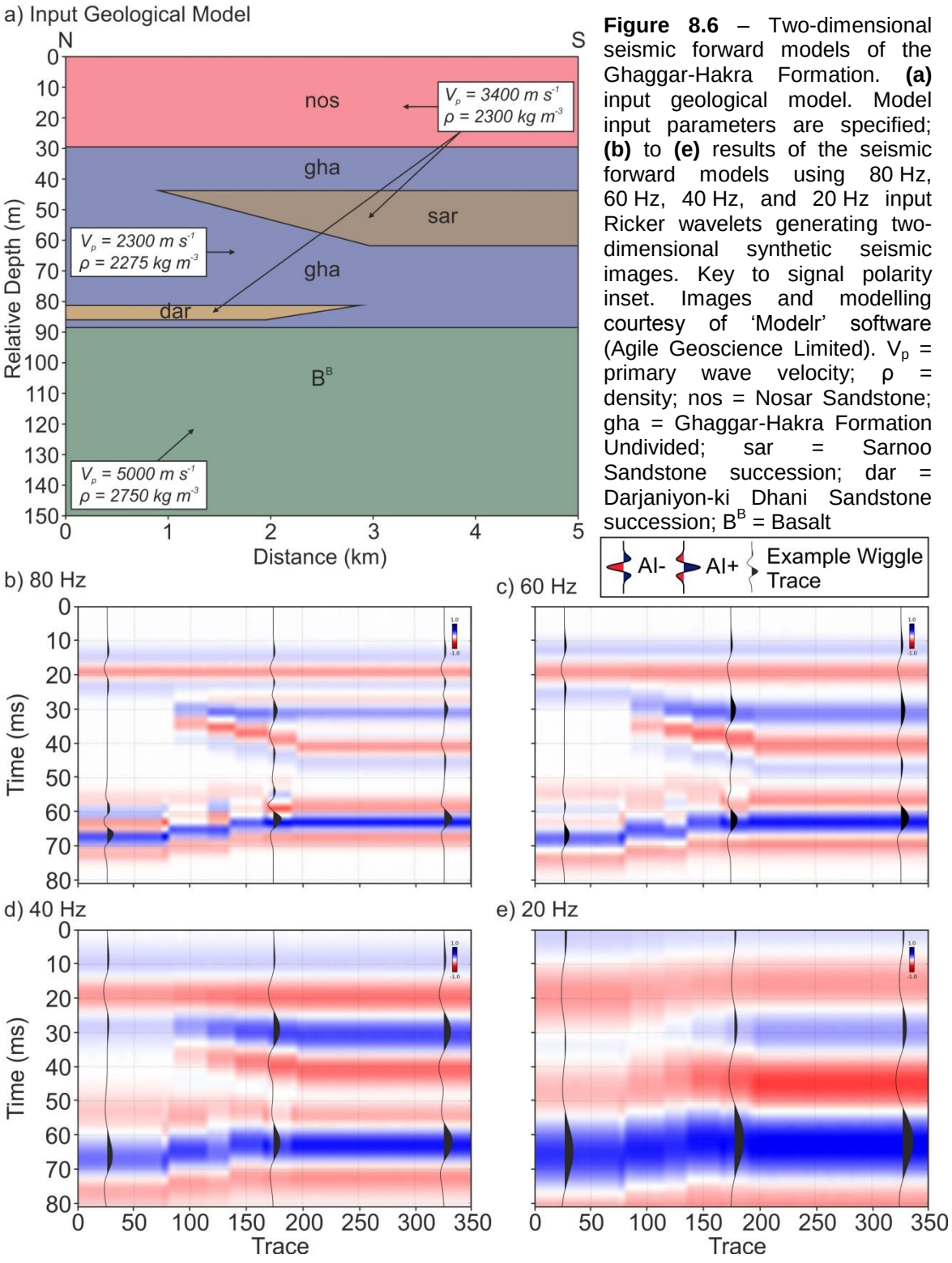

Figure 8.6 – Two-dimensional seismic forward models of the Ghaggar-Hakra Formation. **(a)** input geological model. Model input parameters are specified; **(b)** to **(e)** results of the seismic forward models using 80 Hz, 60 Hz, 40 Hz, and 20 Hz input Ricker wavelets generating two-dimensional synthetic seismic images. Key to signal polarity inset. Images and modelling courtesy of 'Modelr' software (Agile Geoscience Limited). V_p = primary wave velocity; ρ = density; nos = Nosar Sandstone; gha = Ghaggar-Hakra Formation Undivided; sar = Sarnoo Sandstone succession; dar = Darjaniyon-ki Dhani Sandstone succession; B^B = Basalt

During Paleogene rifting, flexural isostatic uplift elevated the rift margins of the Barmer Basin (**Chapter 7**). Sediment routing on the rift-margins during Paleogene rifting, therefore, would be sub-aerial and fluvial, and the uplifted footwall crests of the evolving, rift-parallel, rift-margin faults would form barriers to fluvial systems entering the evolving Barmer Basin depocentres. The supressed topography associated with relay ramps commonly guides sediment routing systems (e.g. rivers) into continental rift basins via the relay ramp structure (Gawthorpe & Hurst 1993; Gawthorpe & Leeder 2000). It is highly likely, therefore, that the southeast-dipping relay-ramp associated with the atypical accommodation structure situated along the central eastern rift margin of the Barmer Basin ('Southern Terrace' on **Figure 5.26**) was a major location of sediment input into the evolving rift. The evolution of the unusual eastern rift margin accommodation structure was associated with the establishment of the main rift-parallel fault systems during the late Paleocene to early Eocene epochs, and the formation of a basin-wide lake during deposition of the Barmer Hill Formation (Compton 2009; Dolson *et al.* in press; Farrimond *et al.* in review). It follows that the relay-ramp would have formed a topographically favourable (low-relief) pathway connecting fluvial systems on the rift margin to the Barmer Basin Lake. However, the relay ramp (Southern Terrace) dips to the southeast, rather than to the northwest as predicted by conventional structural models (e.g. Morley *et al.* 1990; Gawthorpe & Hurst 1993; Faulds & Varga 1998) and gross-depositional environments, sedimentary architectures, and the thickness of basin fill sediments in the east Barmer Basin are likely to be substantially different to that predicted.

Fluvially-dominated sediments on the rift margins would transition down-ramp through delta top and delta front sub-environments, and eventually into lacustrine deposits (**Figure 8.7**). The Barmer Basin Lake was non-marine during the late Paleocene to early Eocene epochs (Dolson *et al.* in press), indicating the effect of tidal currents and waves were negligible, and the delta environment was fluvially dominated. Sand-prone sedimentary facies are likely to become more disparate down-ramp (towards the south), with stacked belts of fluviatile sandstones at the northern end of the relay ramp where subsidence rates were low ('1' & '2' on **Figure 8.7**), transitioning into increasingly isolated, channelised successions within fluvially dominated delta-top sediments, and finally into more distal delta front ('3' on **Figure 8.7**) and lacustrine mudstones and siltstones ('4' on **Figure 8.7**) towards the southern end of the relay ramp where subsidence rates were high. Progradation of the delta into the Barmer Basin Lake would have resulted in coarsening-upwards

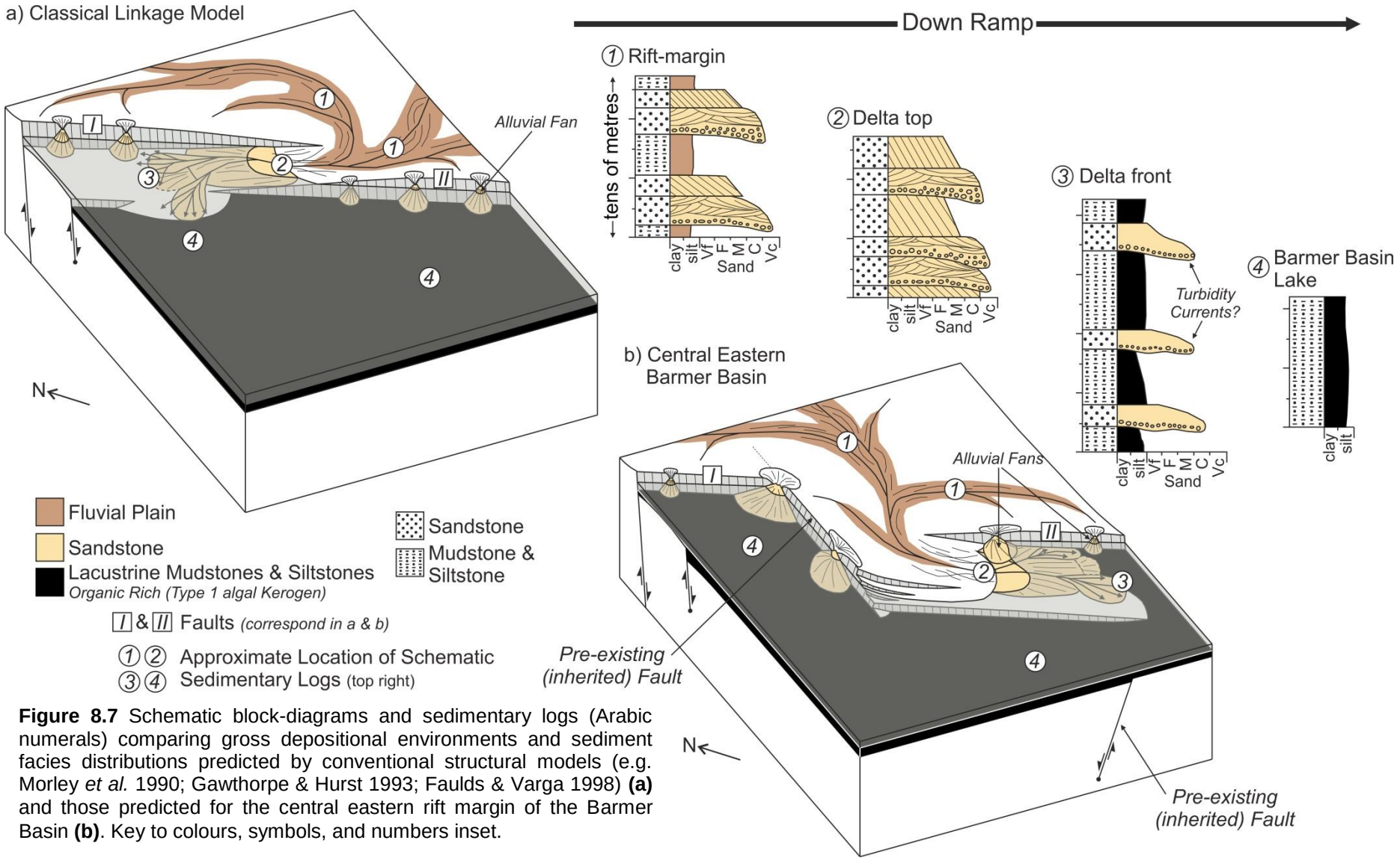

Figure 8.7 Schematic block-diagrams and sedimentary logs (Arabic numerals) comparing gross depositional environments and sediment facies distributions predicted by conventional structural models (e.g. Morley *et al.* 1990; Gawthorpe & Hurst 1993; Faulds & Varga 1998) **(a)** and those predicted for the central eastern rift margin of the Barmer Basin **(b)**. Key to colours, symbols, and numbers inset.

successions. Tectonically-induced variations in subsidence rates in conjunction with fluctuations in relative lake-level (e.g. Milankovitch cycles), suggests river avulsion and lobe switching would have been common, and coarsening-upwards progradational successions will be stacked and cyclic. The fluvial to lacustrine transition is also likely to be associated with turbiditic facies towards the southern end of the ramp ('3' on **Figure 8.7**), and deposits proximal to the evolving eastern rift-margin fault system, such as alluvial fans and Gilbert-type deltas. In conjunction with down-ramp facies variations, variable, tectonically-controlled subsidence and deposition rates will also be manifest through variable sediment thicknesses. Additionally, the main depocentres associated with the unusual eastern rift margin accommodation structure were situated at the base of the reactivated rift-oblique fault (e.g. Bellahsen & Daniel 2005) and along the western edge of the relay ramp (**Figure 8.7b**). Substantial disparities, therefore, are likely to exist between the gross-depositional environments and sedimentary architectures predicted using conventional structural models (**Figure 8.7a** e.g. Morley *et al.* 1990; Gawthorpe & Hurst 1993; Faulds & Varga 1998), and those predicted to occur along the central eastern rift margin of the Barmer Basin (**Figure 8.7b**).

The atypical eastern rift margin accommodation structure demonstrate that structural complexities in the Barmer Basin, which result from the incorporation of pre-existing faults into the evolving extension-perpendicular fault systems (structural inheritance), make prediction of depositional systems, and the associated hydrocarbon systems, more complex than for 'simple' rifts. The possible presence of stacked fluvial channels and delta lobes, as well as turbiditic successions and proximal rift-margin facies, such as Gilbert-type deltas and alluvial fans, on the southeast-dipping, rift-internal, eastern rift-margin relay ramp, suggest copious sand-prone sedimentary intervals of potential reservoir quality may occur within the rift adjacent to the eastern rift margin of the central Barmer Basin (**Figure 8.7b**). The proximity and up-dip nature of such potential reservoir intervals to proven, oil-prone, type 1 (algal) kerogen lacustrine source rocks (Farrimond *et al.* in review), deposited as part of the Barmer Hill Formation within the Barmer Basin Lake, allude to a high hydrocarbon charge potential.

8.6.3 A reproducible trapping style throughout the Barmer Basin

The timing of trap formation relative to source rock maturation is a critical consideration in any hydrocarbon play. The structural relationships demonstrated in this investigation, namely the progressive dominance of extension-perpendicular (rift-parallel) faults at the expense of extension-

oblique faults that are dominant during early rifting (e.g. Morley 1995; Lezzar *et al.* 2002; Morley *et al.* 2004; Bellahsen & Daniel 2005; **Figure 2.13**; **Chapters 5 & 6**), provide critical temporal insights into the formation of structures throughout the Barmer Basin with high trapping potential. Here, a generic model of hydrocarbon trap formation during Paleogene rifting in the Barmer Basin is speculated based upon the improved understanding of the structural evolution of the Barmer Basin presented in this work and the current understanding of the active hydrocarbon system within the Barmer Basin (e.g. Compton 2009; Dolson *et al.* in press; Farrimond *et al.* in review; Sunder *et al.* 2013).

During incipient rifting, the early dominance of rift-oblique faults would have elevated pre- or early-Paleogene fluvial sandstone successions of proven high reservoir quality (Lathi, Ghaggar-Hakra, and Fatehgarh formations) within the footwall crests of active rift-oblique faults (**Figure 8.8a**). Subsequently, the evolution (**Figure 8.8b**) and establishment (**Figures 8.8c**) of rift-parallel faults rendered rift-oblique faults inactive (**Figure 8.8d**), and resulted in the formation of a basin-wide lake (Barmer Basin Lake) during the late Paleocene to early Eocene epochs, within which the Barmer Hill Formation type 1 (algal) kerogen source rock was deposited (**Figures 8.8c & d**; Dolson *et al.* in press; Farrimond *et al.* in review). Inactivity of rift-oblique faults, but continued activity of rift-parallel faults resulted in burial of rift-oblique faults beneath a thick succession of lacustrine deposits (**Figures 8.8d**; e.g. Kaameshwari Fault; **Chapter 6**). Lacustrine mudstones and siltstones form good barriers to fluid flow (seal or cap rock), and would have encased fluvial sandstones of high reservoir quality, situated within up-thrown crests of rift-oblique fault-blocks, against the Barmer Hill Formation source rock within the adjacent hanging-wall depocentre (**Figure 8.8e**).

Burial of fluvial sandstone with proven high reservoir quality (e.g. Lathi, Ghaggar-Hakra, and Fatehgarh formations) adjacent to oil-prone, type 1 (algal) kerogen source rock (Barmer Hill Formation), beneath a lacustrine mudstone and siltstone cap-rock (Barmer Hill and Dharvi Dungar formations) would have formed a structure with a high hydrocarbon trapping potential (**Figure 8.8e**). Critically, trap formation, that is inactivity and burial of rift-oblique faults, is envisaged to have been shallow where source rocks were immature. Burial during continued Paleogene rifting, with subsidence accommodated on the established rift-parallel fault systems, could have lowered inactive rift-oblique faults, and the associated immature hydrocarbon play (source,

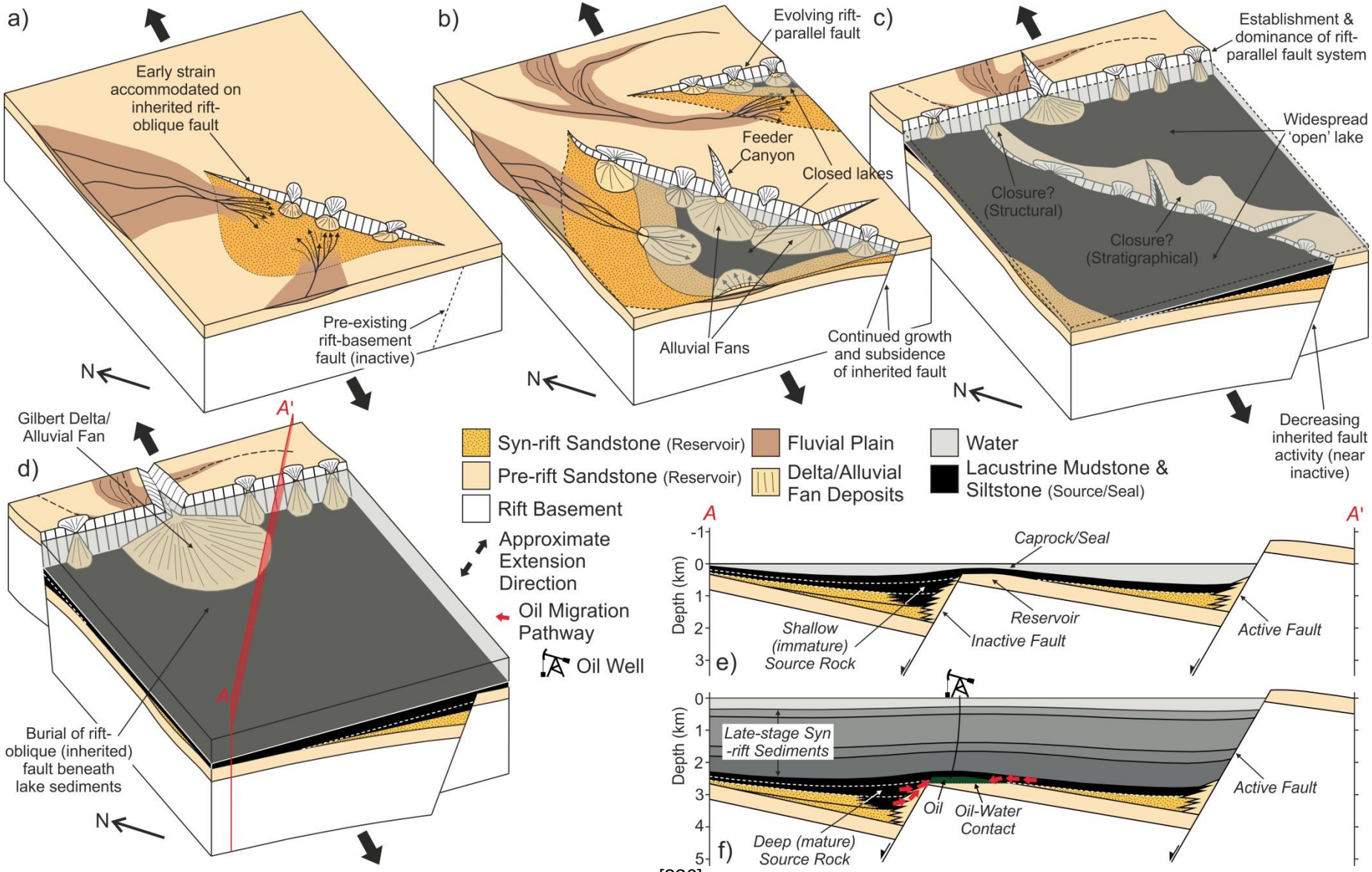
a)
Early strain accommodated on inherited rift-oblique fault
Pre-existing rift-basement fault (inactive)
N
b)
Evolving rift-parallel fault
Feeder Canyon
Closed lakes
Alluvial Fans
Continued growth and subsidence of inherited fault
N
c)
Establishment & dominance of rift-parallel fault system
Widespread 'open' lake
Closure? (Structural)
Closure? (Stratigraphical)
Decreasing inherited fault activity (near inactive)
N
d)
Gilbert Delta/ Alluvial Fan
A
A'
Burial of rift-oblique (inherited) fault beneath lake sediments
N
Syn-rift Sandstone (Reservoir)
Pre-rift Sandstone (Reservoir)
Rift Basement
Approximate Extension Direction
Oil Migration Pathway
Oil Well
Fluvial Plain
Delta/Alluvial Fan Deposits
Water
Lacustrine Mudstone & Siltstone (Source/Seal)
A
A'
Depth (km)
-1
0
1
2
3
Caprock/Seal
Shallow (immature) Source Rock
Reservoir
Inactive Fault
Active Fault
e)
Depth (km)
0
1
2
3
4
5
Late-stage Syn -rift Sediments
Oil
Oil-Water Contact
Active Fault
Deep (mature) Source Rock
f)

Figure 8.8 (*previous page*) **–** A reproducible trapping style throughout the Barmer Basin. **(a)** to **(d)** Initial strain during Paleogene rifting was accommodated on rift-oblique faults, which became inactive upon establishment of rift-parallel fault systems. Establishment of rift-parallel fault systems buried inactive rift-oblique faults beneath lacustrine mudstones and siltstones; **(e)** Schematic cross-section of **(d)** depicting shallow trap formation during the early-stage structural evolution of the Barmer Basin where source rocks are immature; **(f)** as (e) with continued subsidence within the hanging-wall of an established rift-parallel fault system. Source rocks within the oil window may charge reservoirs within traps situated in the uplifted footwall crests of rift-oblique fault blocks if a suitable migration pathway exists.

reservoir, seal, & trap), into the oil window. Expulsion of oil from the Barmer Hill Formation source rock, situated within the hanging-wall depocentre of the inactive rift-oblique fault, upon source rock maturation could have charged the reservoir situated in the crest of the adjacent rift-oblique fault-block if a suitable migration pathway were present (e.g. fault plane, up-dip migration; **Figure 8.8f**).

8.7 Summary

This chapter discussed the combined results of previous work, which was undertaken to investigate the early-stage structural evolution of the Barmer Basin, placed the findings within the wider context of the northwest Indian region, and applied the findings to ongoing hydrocarbon exploration within the Barmer Basin. Rift-oblique (≈ northwest-southeast) extensional deformation exposed along the central eastern rift margin in the Sarnoo Hills (**Chapter 4**), that pre-dated rift-perpendicular Paleogene extension exposed along the western rift margin in the Barmer Hills (**Chapter 3**), was suggested to have occurred during the late Lower Cretaceous Epoch and is an intracontinental manifestation of transtension between the Greater Indian and Madagascan continents during Gondwana fragmentation. Subsequently, late Maastrichtian to Eocene rift-perpendicular (≈ northwest-southeast) extension was driven by a major relocation of the plate boundary between the Greater Indian and African continents during the fragmentation of northwest India in the wake of the rapid northward migration of the Greater Indian continent. The present day structural architecture of the Barmer Basin, therefore, resulted from the superimposition of two non-coaxial extensional events. The presence of a relative mechanical weakness in the lithosphere inherited from Lower Cretaceous rifting may have defined the location of Paleogene rifting, and resulted in the superimposition of Lower Cretaceous and Paleogene rift systems. Structural complications and rift-oblique faults interpreted in the subsurface throughout the Barmer Basin are manifestations of structural inheritance.

In conjunction with established rifting elsewhere in northwest India (Kachchh, Cambay, and Narmada basins), the documentation of pre-Paleogene rifting in the Barmer Basin indicates that extension throughout northwest India was long lived and established prior to the Cretaceous-Paleogene boundary. Non-coaxial extensional events in the Barmer Basin can be correlated with distinct stages of the plate-tectonic evolution of the Greater Indian continent, suggesting that rifting throughout northwest India can satisfactorily be explained within an entirely plate-tectonic framework. The common assumption that the Réunion Mantle Plume triggered rifting throughout northwest India at the Cretaceous-Paleogene boundary (Morgan, 1971; Plummer & Belle, 1995; Sen & Chandrasekharam, 2011), therefore, is not consistent with the results presented previously, namely: 1) the documentation of early, possibly late Lower Cretaceous rifting in the Barmer Basin; 2) established rifting throughout northwest India prior to the main phase of Deccan eruptions, and; 3) the preservation of a thick (< 6 km) syn-rift sedimentary succession within the Barmer Basin, despite the presence of multiple rift-related unconformities.

Rift-oblique rift-systems may be obscured beneath the present day Barmer Basin that contain a poorly constrained pre-Paleogene sedimentary succession, equivalent to the Ghaggar-Hakra Formation exposed in the Sarnoo Hills, which are buried beneath a thick succession of Paleogene sediments in the subsurface of the Barmer Basin. Deposition of the Ghaggar-Hakra Formation within an actively extending terrane during the Lower Cretaceous Epoch alludes to laterally variable gross depositional environments, sedimentary architectures, and sediment thicknesses within the pre-paleogene sedimentary succession of the Barmer Basin. Sand-prone intervals are speculated to be present at the margins of non-marine lakes within half-graben defined by southwest-striking fault systems. Within the pre-Paleogene sedimentary succession, fluvial to deltaic sandstone reservoirs may be coupled with a lacustrine type 1 (algal) kerogen source rock. However, target reservoir intervals (< 20 m) within the pre-Paleogene sedimentary succession exposed in the Sarnoo Hills are unresolvable on currently available seismic data (< 73.75 m at 20 Hz).

Structural complexities in the Barmer Basin during Paleogene rifting, which result from the incorporation of pre-existing faults into the evolving extension-perpendicular fault systems (structural inheritance), make prediction of depositional systems, and the associated hydrocarbon systems, difficult. However, based upon the appreciation of a common temporal relationship

between rift-oblique and rift-parallel faulting and the current understanding of the active hydrocarbon system within the Barmer Basin, a reproducible structural trapping style was speculated that may be applicable throughout the Barmer Basin. Trap formation is envisaged to have been shallow. However, continued subsidence accommodated on rift-parallel fault systems may have buried inactive rift-oblique fault systems. Upon entering the oil window, source rock maturation may charge the pre-formed trap if a suitable migration pathway exists.

9 Conclusions

The structural evolution of the Barmer Basin was poorly understood, and the context of the rift within the northwest Indian region was previously unknown. The integrated basin analysis conducted in this work has covered three scales of investigation, namely the outcrop (small), basin (seismic), and lithospheric scales, and investigated the early-stage structural evolution of the Barmer Basin, placed the findings within the wider context of the northwest Indian region, and applied the findings to ongoing hydrocarbon exploration within the Barmer Basin. In this concluding chapter the main results of the work discussed in this thesis are summarised, and subsequently some suggestions for further research are made.

9.1 The early-stage structural evolution of the Barmer Basin

9.1.1 Rift-oblique (≈ northwest-southeast) extension during the late Lower Cretaceous Epoch

High resolution geological mapping along the eastern rift margin, in the Sarnoo Hills, characterised a rift-oblique fault network exposed nowhere else in the region. Geometrical analysis of the exposed fault network in conjunction with analysis of structural data indicated fault network evolution during northwest-southeast extensional deformation, a distinctly different extensional structural regime to that expected within the north-northwest trending Barmer Basin. Outcrop exposure in the Sarnoo Hills, therefore, provides direct evidence of northwest-southeast extensional tectonics that were previously unknown in northwest India. The age of northwest-southeast extensional deformation remains poorly constrained. However, subsurface sediment thickness maps in the central Barmer Basin indicated substantial thickening of the earliest syn-rift sedimentary succession across rift-oblique faults that are parallel to southwest-striking faults exposed at outcrop in the Sarnoo Hills, prior to the establishment of rift-parallel depocentres. The northwest-southeast orientated extensional event exposed along the eastern rift margin in the Sarnoo Hills, therefore, pre-dated the northeast-southwest orientated Paleogene Barmer Basin rift event.

In conjunction with geological mapping, graphical sedimentary logging of the sedimentary succession exposed in the Sarnoo Hills characterised Lower Cretaceous sediments that accumulated prior to Paleogene rifting. Graphical logs were used to establish a broad depositional

framework for each mapping unit, which were subsequently combined into a depositional model for the exposed succession. Deposition occurred within a maturing upwards fluvial system, with the high proportion of floodplain deposits preserved within the succession suggesting floodplain aggradation, possibly due to rapid subsidence or a high sediment supply. Deposition likely marked a sudden change to long-lived stability on the craton interior, and it is suggested that the Ghaggar-Hakra Formation is a temporal marker for the onset of the poorly age constrained rift-oblique (≈ northwest-southeast) extensional event exposed in the Sarnoo Hills. Northwest-southeast extensional deformation, therefore, is suggested to have occurred during the late Lower Cretaceous Epoch, supporting that the deformational event exposed in the Sarnoo Hills pre-dates Paleogene rifting in the Barmer Basin

Northwest-southeast extensional deformation in the Barmer Basin during the late Lower Cretaceous Epoch coincides with, and is sub-parallel to, the inferred extension direction during a period of significant plate boundary re-organisations associated with the fragmentation of the Gondwanan supercontinent, and transtension between the Greater Indian and Madagascan continents. Within the currently understood regional tectonic framework, therefore, northwest-southeast extensional deformation in the Barmer Basin during the late Lower Cretaceous Epoch is likely an intra-continental manifestation of transtension between the Greater Indian and Madagascan continents during Gondwana fragmentation. Equivalent structures may occur elsewhere in the West Indian Rift System, possibly in the Kachchh and Cambay basins.

9.1.2 Rift-perpendicular (≈ northeast-southwest) extension during the Paleogene Period

High resolution mapping of a rift-parallel section of the western rift margin fault system was conducted in the Barmer Hills, alongside collection of a suite of structural data. Geometrical analysis of the exposed fault system, as well as a multi-component kinematic analysis including analysis of fault-plane-slickenline and extensional fracture data, in conjunction with construction of fault-plane solutions, indicated the exposed fault network evolved during northeast-southwest extensional deformation. Tectono-stratigraphical relationships indicated fault activity occurred during Paleogene rifting in the Barmer Basin. Analysis of the western rift margin fault system in the Barmer Hills, therefore, validated the common assumption that the regional extension vector during Paleogene rifting was approximately rift-perpendicular (≈ northeast-southwest). Rift-perpendicular

extension was supported further by the tendency of late-stage faults to form in a rift-parallel orientation within the middle Eocene Epoch Akli Formation, mapped in the shallow subsurface (< 1 km) above the Kaameshwari Fault using three-dimensional seismic data. Placing northeast-southwest extension during the early Paleogene Period into the regional tectonic framework suggested rift-perpendicular extension in the Barmer Basin was driven by a major relocation of the plate boundary between the Greater Indian and African continents during the fragmentation of northwest India in the wake of the rapid northward migration of the Greater Indian continent.

Lithosphere-scale flexural-cantilever forward models were conducted across the central Barmer Basin in order to investigate the flexural response of the lithosphere during Paleogene rifting, and validate that shallow deformational processes constrained from outcrop and subsurface investigations are compatible with deformational processes at the lithosphere-scale. An effective elastic thickness (T_e), of 5 km was constrained experimentally, and extension of 'normal' thickness (32 km) lithosphere with a depth to detachment of 15 km, above asthenosphere of 'normal' temperature (1333°C) reproduced a good approximation of the rift geometry, while predicting reasonable values of crustal thinning ($\beta < 1.294$), footwall uplift and erosion (< 3 km), and bending stress (< 1.073). The combined results of outcrop and subsurface investigations, therefore, are compatible with deformation at the lithosphere-scale, and a model of coupled simple- and pure-shear deformation in the shallow and deep lithosphere respectively is an appropriate approximation of Paleogene extension in the Barmer Basin. Although the 3 km of footwall uplift is a maximum estimate, the rift was likely a significant topographical feature, and the syn-rift sedimentary succession is likely to contain a substantial component of eroded footwall material. Further to this, substantial syn-rift topography indicates that sedimentary environments and sediment facies distributions within the Barmer Basin during early-stage rifting were likely structurally-controlled.

9.1.3 The early-stage structural evolution of the Barmer Basin rift

The exposure of two-distinct structural regimes on opposing rift margins of the Barmer Basin rift that can be correlated with temporally variable depocentres in the subsurface indicates that rift evolution resulted from the superimposition of two discrete, non-coaxial extensional events. Mechanical (strain) weakening of the lithosphere during late Lower Cretaceous rifting may have defined the location of Paleogene rifting, accounting for the superimposition of two near-perpendicular extensional events.

9.2 Structural complications within the Barmer Basin

At the outcrop scale, in the Sarnoo Hills, the exposed fault network displays an unusual zig-zag geometry due to the incorporation of pre-existing, extension-oblique rift-basement faults within the evolving extension perpendicular fault systems. The juvenile fault network provides important outcrop-based insights into the interaction between pre-existing, extension-oblique faults favourable for reactivation, and evolving, extension-perpendicular faults during the incipient stages of fault network evolution. The findings are likely to be applicable across multiple scales and within other extensional provinces affected by structural inheritance.

In the subsurface of the central Barmer Basin an unusual eastern rift margin accommodation structure imaged on two-dimensional seismic data comprises right-stepping, rift-parallel, rift margin fault systems separated by a significant rift-oblique (southwest-trending) fault. A large southeast-dipping ramp is situated within the rift adjacent to the eastern rift margin and at the southern end of the rift-oblique, rift-margin fault. This structure is unusual and would not be predicted by conventional accommodation zone, transfer zone, or extensional structural models. Structural and seismic-stratigraphical relationships indicated that the rift-oblique fault was active during late Lower Cretaceous, rift-oblique (≈ northwest-southeast) extension, was incorporated (via inheritance) into the eastern rift margin during Paleogene rifting (≈ northeast-southwest), and formed an atypical accommodation structure as a result of structural inheritance.

In the subsurface of the north Barmer Basin a number of highly oblique (east-northeast-west-southwest) faults were active contemporaneously with rift-parallel (≈north-northwest-south-southeast) faults during rift-perpendicular Paleogene extension. Exposure of a northwest-southeast orientated, late Lower Cretaceous extensional structural regime along the eastern rift margin (Sarnoo Hills) suggests rift-oblique faults and unusual structural geometries in the north of the Barmer Basin result from the inheritance of pre-existing faults into the evolving rift-parallel (≈north-northwest-south-southeast) fault systems during Paleogene extension. It is suggested that structural complications throughout the Barmer Basin, comprising rift-oblique fault patterns, reflect the inheritance of faults active during northwest-southeast extension during the late Lower Cretaceous Epoch. However, a slight variation in the orientation of structural complications in the subsurface of the northern Barmer Basin and the fault network exposed in the Sarnoo Hills, east-

northeast-west-southwest and northeast-southwest respectively, alludes to the inheritance of additional basement fabrics during rift-perpendicular, Paleogene extension.

The interpretation that structural complications in the Barmer Basin subsurface result from structural inheritance was clarified and refined by investigating the three-dimensional tectono-stratigraphical evolution of the rift-oblique (≈ north-south) Kaameshwari Fault using three-dimensional seismic data. The Kaameshwari Fault accommodated significant fault-controlled subsidence during incipient Paleogene rifting, but became largely inactive during the mid-Paleocene Epoch. The cessation of Kaameshwari Fault activity was coeval with the establishment of the main rift-parallel, rift-margin fault systems, suggesting the rift-oblique (≈ north-south) Kaameshwari Fault was orientated obliquely (non-ideal) to the extension direction. It follows that the Kaameshwari Fault comprises an inherited structure providing further support to previous suggestions. However, despite a substantial thickening of sediments within the Cretaceous depositional interval towards the south (< 400ms), a pronounced lack of thickness variations across the Kaameshwari Fault indicates tectonic inactivity of the Kaameshwari Fault during late Lower Cretaceous rift-oblique (≈ northwest-southeast) extension. Southwest trending faults, therefore, were likely only one of multiple trends of weak pre-existing fabrics that were inherited during the Paleogene Barmer Basin rift event.

9.3 Regional context of the Barmer Basin within the northwest Indian region

The discovery of northwest-southeast extensional deformation at outcrop exposure in the Barmer Basin, and the associated rift-oblique rift-systems interpreted in the subsurface, indicated established pre-Paleogene rifting in the Barmer Basin. In conjunction with active rifting elsewhere in the West Indian Rift System (Kachchh, Cambay, and Narmada basins), pre-Paleogene sub-rifts in the Barmer Basin may have formed within a northwest Indian rift system that evolved from at least the Lower Cretaceous Epoch. Rifting throughout northwest India, therefore, was established prior to the Cretaceous-Paleogene boundary. The temporal correlation of non-coaxial extensional events exposed at outcrop in the Barmer Basin with distinct stages of the plate-tectonic evolution of the Greater Indian continent demonstrates that rifting throughout northwest India can satisfactorily be explained within an entirely plate-tectonic framework.

The formation of a pre-Deccan rift system throughout northwest India, as well as evolution of the Barmer Basin from two discrete, non-coaxial extensional events that can satisfactorily be accounted for within a model of external plate boundary forces, is not in accordance with the common assumption that rifting in the northwest Indian region near to the Cretaceous-Paleogene boundary was triggered by the arrival of the Réunion mantle plume. The two non-coaxial episodes of rifting observed within the Barmer Basin are better explained by a model of plate reorganisations that initiated long before the arrival of the Réunion Mantle Plume. This, combined with a lack of evidence for significant pre-Deccan regional unconformities, and only minor Deccan-age volcanism within the Barmer Basin, suggested that rifting did not occur above anomalously hot asthenosphere, despite the rift being situated within the inferred limits of the Réunion plume-head. The potential for an early collision between the Greater Indian and Eurasian continents (66 Ma) also suggests that Paleogene rifting could have been driven by a combination of regional extension in the wake of the rapidly northwards migrating Greater Indian continent, and extension driven by the early interactions between the Greater Indian and Eurasian continents.

9.4 Implications of the findings for hydrocarbon exploration in the Barmer Basin

Based on a preliminary sedimentological analysis of the Ghaggar-Hakra Formation sedimentary succession exposed in the Sarnoo Hills, deposition was suggested to have occurred within an actively extending terrane. Pre-Paleogene graben or half-graben structures are likely to be buried beneath a thick succession of Paleogene sediments in the Barmer Basin, and contain the key components of an oil-prone hydrocarbon play (source & reservoir). Sand-prone intervals are speculated to be present at the margins of non-marine lakes within half-graben defined by southwest-striking fault systems. However, target sandstone intervals of high reservoir quality at surface (< 20 m) are unresolvable on currently available seismic data (< 73.75 m at 20 Hz).

The formation of atypical structural geometries in the Barmer Basin during Paleogene rifting, which result from the incorporation of pre-existing faults into the evolving extension-perpendicular fault systems (structural inheritance), make prediction of depositional systems, and the associated hydrocarbon systems, difficult. However, the improved understanding of structural complications in the subsurface of the Barmer Basin and the appreciation of a common temporal relationship between rift-oblique and rift-parallel faulting suggested potential hydrocarbon traps formed during

early rifting at shallow depths where any source rock would be immature. It is conceivable that the establishment and dominance of rift-parallel faults with continued extension, and the resultant burial of inactive rift-oblique faults, could subside the immature hydrocarbon trap into the oil window and charge the pristine trap if a suitable migration pathway were present.

9.5 Recommendations for further research

This work represents an initial investigation into the early-stage structural evolution of the Barmer Basin rift, and discusses the context of the rift within the northwest Indian region. The findings elucidate poorly understood structural complications interpreted throughout the subsurface of the Barmer Basin, provide critical insights into previously unrecognised regional tectonic processes, and are applicable to hydrocarbon exploration within the Barmer Basin. However, there is considerable scope for continued research within the Barmer Basin and the northwest Indian region to clarify and refine the findings of the integrated basin analysis presented. In this section, some suggestions of future research are made that will build upon the findings of this investigation.

9.5.1 Age of northwest-southeast extensional deformation

The age of the northwest-southeast extensional deformational event exposed along the eastern rift margin of the Barmer Basin is poorly constrained. Many of the conclusions of this work are hinged on the inferred link between the onset of Ghaggar-Hakra Formation deposition and the northwest-southeast extensional event exposed in the Sarnoo Hills. It is essential, therefore, that any continued investigations attempt to date the Ghaggar-Hakra Formation, as well as the northwest-southeast extensional event exposed in the Sarnoo Hills. Such an investigation would incorporate palynological investigation of the exposed sedimentary succession in an attempt to verify and further constrain the Middle Jurassic to Lower Cretaceous age estimate of previous work (Baksi & Naskar 1981), in conjunction with dating of the igneous material that is both extrusive and underlies the Ghaggar-Hakra Formation, and is intrusive and observed within fault planes, thus crudely constraining deformation. Further to improving upon the current Ghaggar-Hakra Formation age estimate, a detailed characterisation of the sedimentary succession, including: 1) analysis of the sediment source provenance; 2) palaeocurrent analysis; 3) detailed biostratigraphical analysis; 4) investigation of the validity of the assumption of floodplain aggradation by looking for indicators of floodplain stability and palaeosol development, and; 5) maximum burial depth, is essential to improve the current understanding of tectono-stratigraphical relationships during the late Lower

Cretaceous as well as the amount of footwall erosion associated with Paleogene rifting. A wealth of subsurface core data could also be employed to extend the investigation into the subsurface in locations where the Ghaggar-Hakra Formation has been penetrated. An improved age estimate of the deformational event exposed in the Sarnoo Hills would support or refute the alternative hypothesis that rift-oblique extension exposed in the Sarnoo Hills is a manifestation of a rotated stress-field local to a long-lived weak pre-existing fabric during Paleogene rifting.

9.5.2 Deep undrilled depocentres

The poor sedimentological characterisation and lack of chronostratigraphical differentiation within deep, undrilled depocentres throughout the rift needs to be improved upon to unequivocally prove early rift-oblique extension. If such depocentres were drilled during hydrocarbon exploration, and core and wireline data were available, an attempt could be made to date and characterise the sedimentary succession within such depocentres.

9.5.3 Further investigation of subsurface rift-oblique faults

The interpretation that structural complications variably imaged throughout the rift on subsurface data resulted from the inheritance of pre-existing rift-oblique faults into the evolving rift-parallel fault systems was corroborated by a detailed investigation of one such rift-oblique fault, the Kaameshwari Fault, using three-dimensional seismic data. The investigation presented included a geometrical analysis of fault systems, analysis of seismic-stratigraphical relationships, and a tectono-stratigraphical analysis of faulting using sediment thickness maps. However, a structural analysis of the Kaameshwari Fault incorporating construction of backstripped fault displacement profiles for a suite of closely spaced seismic horizons was not attempted. Further investigations of other rift-oblique faults should be conducted to characterise and assess the variability of fault reactivation within the Barmer Basin. The abundance of rift-oblique faults throughout the Barmer Basin subsurface provides abundant study areas and opportunities, and in conjunction with 70% coverage of the rift by three-dimensional seismic data, indicates a large dataset is available to perform such analyses. In particular, a detailed structural analysis should attempt to characterise the slip behaviour of rift-oblique faults, and by constructing backstripped displacement profiles for closely-spaced, well-constrained seismic horizons, the temporal evolution of fault-slip can be defined. Demonstrating that fault-displacement during deposition of early pre-Paleogene stratigraphical intervals was symmetrical, and that displacement during Paleogene stratigraphical

intervals is distinctly asymmetrical, would present a strong argument supporting the evolution of rift-oblique faults during pre-Paleogene rift-oblique (≈ northwest-southeast) extension and the subsequent oblique-slip reactivation of these faults during Paleogene rifting.

9.5.4 Continued lithosphere-scale investigations

At the lithosphere-scale, more detailed investigations must use well-constrained parameters, such as the crustal and mantle densities (ρ_c & ρ_m), crustal thickness, depth to detachment, degree of lithosphere magmatic accretion (underplating), asthenosphere temperature during rifting (T_A), and the amount of rift-margin uplift and erosion. The presence of a wide-angled seismic survey that images the present-day structure of the northwest Indian crust in its entirety would greatly improve the understanding of lithosphere-scale processes in the Barmer Basin and northwest Indian region at the Cretaceous-Paleogene boundary, and would facilitate an improved estimation of the poorly constrained parameters used in this investigation. Further to geometrical parameters, a more detailed investigation of lithosphere-scale deformation needs to incorporate gravity data and magnetic surveys to constrain the models and construct tailor-made geodynamical flexural-cantilever forward models. Subsequently, geodynamical models could be used in conjunction with detailed gravity and magnetic modelling. Such a study will enable a critical evaluation of the findings presented here, and more importantly constrain the state of the northwest Indian lithosphere during extensional deformation near to the Cretaceous-Paleogene boundary.

9.5.5 Interactions between the Greater Indian and Eurasian continents

The potential for an early collision between the Greater Indian and Eurasian continents indicates a better understanding of the effect of the collision between the Greater Indian and Eurasian continents within the evolving Barmer Basin needs to be attained. Inversion structures are recognised within the Barmer Basin, but are poorly understood, and detailed investigations of inversion structures at all levels of the syn-rift sedimentary succession should be undertaken. The paucity of outcrop within the Barmer Basin, and lack of exposed inversion structures, precludes field-based investigations. However, detailed structural and stratigraphical investigation of inversion structures within the subsurface of the Barmer Basin using the large, three-dimensional seismic dataset would improve the current understanding of the interplay between regional extension and deformation in the foreland of the Greater India-Eurasia collision. With improved age constraint on the syn-rift sedimentary succession inversion structures could be dated using tectono-

stratigraphical relationships, such as onlap/offlap relationships of seismic reflectors of well-constrained age onto inversion-related monoclonal folds.

9.6 The early-stage structural evolution of the Barmer Basin rift

The early-stage structural evolution of the Barmer Basin rift is demonstrably the result of two extensional events of different orientation, as indicated by sedimentological and structural analyses, and tectono-stratigraphical relationships. Extensional structures in the Barmer Basin are complicated and unique, and further the current understanding of extensional fault system and rift-system evolution in the presence of pre-existing, weak crustal structures that are favourable for reactivation. Further to this, the discovery of early, possibly late Lower Cretaceous rifting in the Barmer Basin demonstrated rifting throughout northwest India was established long before the Cretaceous-Paleogene boundary and the postulated arrival of the Réunion mantle plume, counter to the common assumption that rifting throughout northwest India was plume-induced, and initiated near to the Cretaceous-Paleogene boundary. The findings are applicable globally in other extensional provinces where pre-existing weak structures are present, and support that rifting throughout northwest India has a long history that can satisfactorily be explained within an entirely plate-tectonic framework. It is therefore not necessary to invoke a mantle plume beneath northwest India at the Cretaceous-Paleogene boundary, and based upon the integrated basin analysis presented, it is suggested that the commonly overlooked alternative that continental rifting triggered Deccan volcanism is more applicable to the northwest Indian region.

References

Akhtar, K., Ahmad, A.H.M., 1991. Single-cycle cratonic quartzarenites produced by tropical weathering: the Nimar sandstone (Lower Cretaceous), Narmada basin, India. Sedimentary Geology 71, 23-32.

Ali, J.R., Aitchison, J.C., 2014. Greater India's northern margin prior to its collision with Asia. Basin Research 26, 73-84.

Allen, P.A., Allen, J.R. 2005. Basin Analysis: Principles and Applications. 2nd Edition. Wiley-Blackwell, Oxford, UK, pp.560.

Allen, P.A., Allen, J.R. 2013. Basin Analysis: Principles and Application to Petroleum Play Assessment. 3rd Edition. Wiley-Blackwell, Oxford, UK, pp.642.

Anders, M.H., Schlische, R.W., 1994. Overlapping Faults, Intrabasin Highs, and the Growth of Normal Faults. The Journal of Geology 102, 163-180.

Angelier, J., 1984. Tectonic Analysis of Fault Slip Data Sets. Journal of Geophysical Research 89(B7), 5835-5848.

Angelier, J., 1990. Inversion of field data in fault tectonics to obtain the regional stress – III. A new rapid direct inversion method by analytical means. Geophysical Journal International 103(2), 363-376.

Angelier, J., Tarantola, A., Valette, B., Manoussis, S., 1982. Inversion of field data in fault tectonics to obtain the regional stress – I. Single phase fault populations: a new method of computing the stress tensor. Geophysical Journal International 69(3), 607-621.

Armitage, J.J., Collier, J.S., Minshull, T.A., 2010. The importance of rift history for volcanic margin formation. Nature 465, 913-917, doi: 10.1038/nature09063.

Armitage, J.J., Collier, J.S., Minshull, T.A., Henstock, T.J., 2011. Thin oceanic crust and flood basalts: India-Seychelles breakup, Geochemistry, Geophysics, Geosystems 12, Q0AB07, doi:10 1029/2010GC003316.

Autin, J., Bellahsen, N., Leroy, S., Husson, L., Beslier, M-O., d'Acremont, E., 2013. The role of structural inheritance in oblique rifting: insights from analogue models and application to the Gulf of Aden. Tectonophysics 607, 51-64.

Baksi, S.K., Naskar, P., 1981. Fossil Plants from the Sarnu Hill Formation, Barmer Basin, Rajasthan. Palaeobotanist 27, 107-111.

Balakrishnan, T.S., Unnikrishnan, P., Murty, A.V.S., 2009. The Tectonic Map of India and Contiguous Areas. Journal of the Geological Society of India 74, 158-170.

Bastia, R., Reeves, C., Pundarika Rao, D., D'Silva, K., Radhakrishna, M., 2010. Paleogeographic Reconstruction of East Gondwana and Evolution of the Indian Continental Margin. DCS-DST news, August 2010, 2-8.

Basu, A.R., Renne, P.R., DasGupta, D.K., Teichmann, F., Poreda, R.J., 1993. Early and Late Alkali Igneous Pulses and a High-^{3}He Plume origin for the Deccan Flood Basalts. Science 261, 902-906.

Beck, R.A., Burbank, D.W., Sercombe, W.J., Riley, G.W., Barndt, J.K., Berry, J.R., Afzal, J., Khan, A.M., Jurgen, H., Metje, J., Cheema, A., Shafique, N.A., Lawrence, R.D., Asif Khan, M., 1995. Stratigraphic evidence for an early collision between northwest India and Asia. Nature 373, 55-58.

Bellahsen, N., Daniel, J.M., 2005. Fault reactivation control on normal fault growth: an experimental study. Journal of Structural Geology, 27, 769-780.

Bellahsen, N., Fournier, M., d'Acremont, E., Leroy, S., Daniel, J.M., 2006. Fault reactivation and rift-localisation: Northeastern Gulf of Aden margin. Tectonics 25, TC1007, doi:10.1029/2004TC001626.

Bellahsen, N., Husson, L., Autin, J., Leroy, S., d'Acremont, E., 2013. The effect of thermal weakening and buoyancy forces on rift-localization: Field evidences from the Gulf of Aden oblique rifting. Tectonophysics 607, 80-97.

Biswas, S.K., 1982. Rift Basins in Western Margin of India and Their Hydrocarbon Prospects with Special Reference to Kutch Basin. American Association of Petroleum Geologists 66(10), 1497-1513.

Biswas, S.K., 1987. Regional tectonic framework, structure and evolution of the western marginal basins of India. Tectonophysics 135, 307-327.

Bond, C.E., Lunn, R.J., Shipton, Z.K., Lunn, A.D., 2012. What makes an expert effective at interpreting seismic images? Geology 40, 75-78.

Bonini, M., Souriot, T., Boccaletti, M., Brun, J.P., 1997. Successive orthogonal and oblique extension episodes in a rift zone: Laboratory experiments with application to the Ethiopian Rift. Tectonics 16(2), 347-362.

Borges, M.R., Sen, G., Hart, G.L., Wolff, J.A., Chandrasekharam, D., 2014. Plagioclase as recorder of magma chamber processes in the Deccan Traps: Sr-isotope zoning and implications for Deccan eruptive event. Journal of Asian Earth Sciences 84, 95- 101.

Bott, M.H.P., 1959. The mechanisms of oblique slip faulting. Geological Magazine 96, 109-117.

Bridge, J.S., 2003. Rivers and Floodplains: Forms, Processes, and Sedimentary Record. Wiley-Blackwell, Oxford, UK, 504pp.

Brune, S., Popov, A.A., Sobolev, S.V., 2012. Modeling suggests that oblique extension facilitates rifting and continental break-up. Journal of Geophysical Research 117, B08402.

Buddin, T.S., Kane, S.J., Williams, G.D., Egan, S.S., 1997. A sensitivity analysis of 3-dimensional restoration techniques using vertical and inclined shear constructions. Tectonophysics 269. 33-50.

Byerlee, J.D., 1968. Brittle-ductile transition in rocks. Journal of Geophysical Research 73(14), 4741-4750.

Campbell, I.H., Griffiths, R.W., 1990. Implications of mantle plume structure for the evolution of flood basalts. Earth and Planetary Science Letters 99, 79-93.

Cande, S.C., Stegman, D.R., 2011. Indian and African plate motions driven by the push force of the 472 Réunion plume head. Nature 475, 47 – 52.

Cande, S.C., Patriat, P., Dyment, J., 2010. Motion between the Indian, Antarctic and African plates in the early Cenozoic. Geophysical Journal International 183, 127-149.

Cartwright, J.A., Trudgill, B.D., Mansfield, C.S., 1995. Fault growth by segment linkage: an explanation for scatter in maximum displacement and trace length data from the Canyonlands Grabens of SE Utah. Journal of Structural Geology 17(9), 1319-1326.

Chalapathi Rao, N.V., Lehmann, B., 2011. Kimberlites, flood basalts and mantle plumes: New insights from the Deccan Large Igneous Province. Earth-Science Reviews 107, 315-324.

Chattopadhyay, A., Chakra, M., 2013. Influence of pre-existing pervasive fabrics on fault patterns during orthogonal and oblique rifting: An experimental approach. Marine and Petroleum Geology 39, 74-91.

Chaubey, A.K., Gopala Rao, D., Srinivas, K., Ramprasad, T., Ramana, M.V., Subrahmanyam, V., 2002. Analysis of multichannel seismic reflection, gravity and magnetic data along a regional profile across the central-western continental margin of India. Marine Geology 182, 303-323.

Chenet, A.L., Quidelleur, X., Fluteau, F., Courtillot, V., Bajpai, S., 2007. ^{40}K-^{40}Ar dating of the Main Deccan large igneous province: Further evidence of KTB age and short duration. Earth and Planetary Science Letters 263, 1-15.

Childs, C., Watterson, J., Walsh, J.J., 1995. Fault overlap zones within developing normal fault systems. Journal of the Geological Society 152, 535-549.

Childs, C., Nicol, A., Walsh, J.J., Watterson, J., 1996. Growth of vertically segmented normal faults. Journal of Structural Geology 18(12), 1389-1397.

Chowdhary, L.R., 1975. Reversal of Basement-Block Motions in Cambay Basin, India, and its Importance in Petroleum Exploration. The American Association of Petroleum Geologists Bulletin 59(1), 85-96.

Clemson, J., 2014. Base Cretaceous and base Paleogene horizon interpretations for the Barmer Basin. Unpublished data.

Clarke, S.M., 2011. Outcrop studies in the Barmer Basin, Rajasthan, India. Keele University, unpublished report.

Clifton, A.E., Schlische, R.W., 2001. Nucleation, growth and linkage of faults in oblique rift zones: Results from experimental clay models and implications for maximum fault size. Geology 29(5), 455-458.

Clifton, A.E., Schlische, R.W., Withjack, M.O., Ackermann, R.V., 2000. Influence of rift-obliquity on fault population systematics: results of experimental clay models. Journal of Structural Geology 22, 1491-1509.

Cloetingh, S., Spadini, G., Van Wees J.D., Beekman, F., 2003. Thermo-mechanical modelling of Black Sea Basin (de)formation. Sedimentary Geology 156, 169-184.

Collier, J.S., Sansom, V., Ishizuka, O., Taylor, R.N., Minshull, T.A., Whitmarsh, R.B., 2008. Age of Seychelles-India break-up. Earth and Planetary Science Letters 272, 264-277.

Compton, P.M., 2009. The geology of the Barmer Basin, Rajasthan, India, and the origins of its major oil reservoir, the Fatehgarh Formation. Petroleum Geoscience 15, 117-130.

Conneally, J., Childs, C., Walsh, J.J., 2014. Contrasting origins of breached relay zone geometries. Journal of Structural Geology 58, 59-68.

Contreras, J., Anders, M.H., Scholz, C.H., 2000. Growth of a normal fault system; observations from the Laka Malawi basin of the east African rift. Journal of Structural Geology 22, 159-168.

Cooke, M.L., Madden, E.H., 2014. Is the Earth Lazy? A review of work minimization in fault evolution. Journal of Structural Geology 66, 334-346.

Corti, G., 2012. Evolution and characteristics of continental rifting: Analog modelling-inspired view and comparison with examples from the East African Rift System. Tectonophysics 522-523, 1-33.

Cowie, P.A., Scholz, C.H., 1992. Displacement-length scaling relationship for faults: data synthesis and discussion. Journal of Structural Geology 14(10), 1149-1156.

Cowie, P.A., Vanneste, C., Sornette, D., 1993. Statistical Physics Model for the Spatiotemporal Evolution of Faults. Journal of Geophysical Research 98(B12), 21,809-21,821.

Cowie, P.A., Gupta, S., Dawers, N.H., 2000. Implications of fault array evolution for synrift depocentre development: Insights from a numerical fault growth model. Basin Research 12, 241-261.

Cox, K.G., 1989. The role of mantle plumes in the development of continental drainage patterns. Nature 342, 873-877.

Crider, J.G., Peacock, D.C.P., 2004. Initiation of brittle faults in the upper crust: a review of field observations. Journal of Structural Geology 26, 691-707.

Daniels, J.M., 2003. Floodplain aggradation and pedogenesis in a semiarid environment. Geomorphology 56, 225-242.

Davis, J.C., 1986. Statistics and data analysis in geology. 2nd Edition, John Wiley and Sons, Chichester, UK. pp.646.

Dawers, N.H., Anders, M.H., 1995. Displacement-length scaling and fault linkage. Journal of Structural Geology 17, 607-614.

Doblas, M., 1998. Slickenside kinematic indicators. Tectonophysics 295, 187-197.

Dolson, J., Burley, S.D., Sunder, V.R., Kothari, V., Naidu, B., Whiteley, N.P., Farrimond, P., Taylor, A., Direen, N., Ananthakrishnan, B., in press. The Discovery of the Barmer Basin, Rajasthan, India, and its Petroleum Geology. The American Association of Petroleum Geologists Bulletin (in press).

Eagles, G., Hoang, H.H., 2014. Cretaceous to present kinematics of the Indian, African and Seychelles plates. Geophysical Journal International 196, 1-14.

Egan, S.S., 1990. The flexural isostatic response of the lithosphere to extensional tectonics. Tectonophysics 202, 291-308.

Farrimond, P. Naidu, B.S., Burley, S.D., Dolson, J., Whiteley, N., Kothari, V., in review. Geochemical characterization of oils and their source rocks in the Barmer Basin, Rajasthan, India (in review).

Faulds, J.E., Varga, R.J., 1998. The role of accommodation zones and transfer zones in the regional segmentation of extended terranes, in Faulds, J.E., and Stewart, J.H., eds.,

Accommodation Zones and Transfer Zones: The Regional Segmentation of the Basin and Range Province: Boulder, Colorado, Geological Society of America Special Paper 323.

Fletcher, R., Kusznir, N.J., Roberts, A.M., Hunsdale, R., 2013. The formation of a failed continental breakup basin: The Cenozoic development of the Faroe-Shetland Basin. Basin Research 25, 532-553.

Fossen, H., 2010. Structural Geology. Cambridge University Press, Cambridge, UK. 480pp.

Fossen, H., Johansen, T.E.S., Hesthammer, J., Rotevatn, A., 2005. Fault interaction in porous sandstone and implications for reservoir management; examples from southern Utah. American Association of Petroleum Geologists Bulletin 89(12), 1593-1606.

Foulger, G.R., Anderson, D.L., 2005. A cool model for the Iceland hotspot. Journal of Volcanology and Geothermal Research 141, 1-22.

Foulger, G.R., Natland, J.H., Anderson, D.L., 2005. A source for Icelandic magmas in remelted Iapetus crust. Journal of Volcanology and Geothermal Research 141, 23-44.

Fürisch, F.T., Pandey, D.K., 2003. Sequence stratigraphic significance of sedimentary cycles and shell concentrations in the Upper Jurassic-Lower Cretaceous of Kachchh, western India. Palaeogeography, Palaeoclimatology, Palaeoecology 193, 285-309.

Gawthorpe, R.L., Hurst, J.M., 1993. Transfer zones in extensional basins: their structural style and influence on drainage development and stratigraphy. Journal of the Geological Society 150, 1137-1152.

Gawthorpe, R.L., Leeder, M.R., 2000. Tectono-sedimentary evolution of active extensional basins. Basin Research 12, 195-218.

Gawthorpe, R.L., Hurst, J.M., Sladen, C.P., 1990. Evolution of Miocene Footwall-derived Coarse-Grained Deltas, Gulf of Suez, Egypt: Implications for Exploration. American Association of Petroleum Geologists Bulletin 74(7), 1077-1086.

Gawthorpe, R.L., Fraser, A.J., Collier, R.E.L., 1994. Sequence stratigraphy in active extensional basins: implications for the interpretation of ancient basin-fills. Marine and Petroleum Geology 11(6), 642-658.

Giba, M., Walsh, J.J., Nicol, A., 2012. Segmentation and growth of an obliquely reactivated normal fault. Journal of Structural Geology 39, 253-267.

Gibbs, A.D., 1983. Balanced cross-section construction from seismic sections in areas of extensional tectonics. Journal of Structural Geology 5(2), 153-160.

Gombos, Jr. A.M., Powell, W.G., Norton, I.O., 1995. The tectonic evolution of western India and its impact on hydrocarbon occurrences: an overview. Sedimentary Geology 96, 119-129.

Green, O.R., Searle, M.P., Corfield, R.I., Corfield, R.M., 2008. Cretaceous-Tertiary Carbonate Platform Evolution and the Age of the India-Asia Collision along the Ladakh Himalaya (Northwest India). The Journal of Geology 116, 331-353.

Groshong, R.H., 2006. 3-D Structural Geology. 2nd Edition. Springer, pp.400. ISBN: 978-3-540-31055-6.

Gupta, S., Cowie, P.A., Dawers, N.H., Underhill, J.R., 1998. A mechanism to explain rift-basin subsidence and stratigraphic patterns through fault-array evolution. Geology 26(7), 595-598.

Gupta, S., Underhill, J.R., Sharp, I.R., Gawthorpe, R.L., 1999. Role of fault interactions in controlling synrift sediment dispersal patterns: Miocene, Abu Alaqa Group, Suez Rift, Sinai, Egypt. Basin Research 11, 167-189.

Hammond, J.O.S., Collier, J.S., Kendall, J.-M., Helffrich, G., Rümpker, G., 2012. Plume scar in the mantle lithosphere beneath the Seychelles revealed by seismic imaging. Earth and Planetary Science Letters 355-356, 20-31.

Hardy, S., McClay, K., 1999. Kinematic modelling of extensional fault-propagation folding. Journal of Structural Geology 21, 695-702.

Hart, B.S., 2012. An Introduction to Seismic Interpretation. American Association of Petroleum Geologists Discovery Series No.16. 1st Edition. American Association of Petroleum Geologists, pp.215. ISBN: 978-1-588-61396-7.

Hastie, W.W., Watkeys, M.K., Aubourg, C., 2014. Magma flow in dyke swarms of the Karoo LIP: Implications for the mantle plume hypothesis. Gondwana Research 25, 736-755.

Heine, C., Brune, S., 2014. Oblique rifting of the Equatorial Atlantic: Why there is no Saharan Atlantic Ocean. Geology 42(3), 211-214.

Henza, A.A., Withjack, M.O., Schlische, R.W., 2010. Normal-fault development during two-phases of non-coaxial extension: An experimental study. Journal of Structural Geology 32, 1656-1667.

Henza, A.A., Withjack, M.O., Schlische, R.W., 2011. How do the properties of a pre-existing normal-fault population influence fault development during a subsequent phase of extension? Journal of Structural Geology 33, 1312-1324.

Hesthammer, J., Fossen, H., 1999. Evolution and geometries of gravitational collapse structures with examples from the Statfjord Field, northern North Sea. Marine and Petroleum Geology 16, 259-281.

Hodgkinson, K.M., Stein, R.S., King, G.C.P., 1996. The 1954 Rainbow Mountain-Fairview Peak-Dixie Valley earthquakes: a triggered normal faulting sequence. Journal of Geophysical Research 101(B11), 25,459-25,471.

Hooper, P., Widdowson, M., Kelley, S., 2010. Tectonic setting and timing of the final Deccan flood basalt eruptions. Geology 38, 839-842.

Huang, Q., Angelier, J., 1989. Inversion of field data in fault tectonics to obtain the regional stress – II. Using conjugate fault sets within heterogeneous families for computing palaeostress axes. Geophysical Journal International 96(1), 139-149.

Jackson, C.A.L., Gawthorpe, R.L., Carr, I.D., Sharp, I.R., 2005. Normal faulting as a control on the stratigraphic development of shallow marine syn-rift sequences: the Nukhul and Lower Rudeis Formations, Hammam Faraun fault block, Suez Rift, Egypt. Sedimentology 52, 313-338.

Jaeger, J.C., Cook, N.G.W., Zimmerman, R., 2007. Fundamentals of Rock Mechanics, 4th Edition. Blackwell Publishing, Oxford, UK, 488pp.

Jain, M., Tandon, S.K., Singhvi, A.K., Mishra, S., Bhatt, S.C., 2005. Quaternary alluvial stratigraphical development in a desert setting: a case study from the Luni River basin, Thar Desert of western India. Fluvial Sedimentology VII, International Association of Sedimentologists. Special Publication 35, 349-371.

Jaitly, A.K., Ajane, R., 2013. Comments on Placenticeras Mintoi (Vredenburg, 1906) from the Bagh Beds (Late Cretaceous), Central India with Special Reference to Turonian Nodular Limestone Horizon. Journal of the Geological Society of India 81, 565-574.

Kaila, K.L., Tewari, H.C., Krishna, V.G., Dixit, M.M., Sarkar, D., Reddy, M.S., 1990. Deep seismic sounding studies in the north Cambay and Sanchor basins, India. Geophysical Journal International 103, 621-637.

Kale, V.S., Singhvi, A.K., Mishra, P.K., Banerjee, D., 2000. Sedimentary records and luminescence chronology of late Holocene palaefloods in the Luni River, Thar Desert, northwest India. Catena 40, 337-358.

Kamb, W.B., 1959. Ice petrofabrics observations from Blue Glacier, Washington in relation to theory and experiment. Journal of Geophysical Research 64, 1891-1909.

Kearey, P., Brooks, M., 1991. An Introduction to Geophysical Exploration, 2nd Edition. Blackwell Scientific Publications, Oxford, UK, 263pp.

Keep, M., McClay, K.R., 1997. Analogue modelling of multiphase rift systems. Tectonophysics 273, 239-270.

Kelly, M.J., Najman, Y., Mishra, P., Burley, S., Clemson, J., Copley, A., Clarke, S., 2014. Timing and tectonics of the India-Asia collision: Constraints from the Barmer Basin, Rajasthan. Poster presentation at the 29th Himalayan-Karakoram-Tibet workshop, Lucca (Italy).

Kerr, A.C., Khan, M., Mahoney, J.J., Nicholson, K.N., Hall, C.M., 2010. Late Cretaceous alkaline sills of the south Tethyan suture zone, Pakistan: Initial melts of the Réunion hotspot? Lithos 117, 161-171.

Khosla, A., Kapur, V.V., Sereno, P.C., Wilson, J.A., Wilson, G.P., Dutheil, D., Sahni, A., Singh, M.P., Kumar, S., Rana, R.S., 2003. First Dinosaur Remains from the Cenomanian-Turonian Nimar Sandstone (Bagh Beds), District Dhar, Madhya Pradesh, India. Journal of the Palaeontological Society of India 48, 115-127.

Kim, Y-S., Sanderson, D.J., 2005. The relationship between displacement and length of faults: a review. Earth-Science Reviews 68, 317-334.

Krishna, J., 1987. An overview of the Mesozoic stratigraphy of Kachchh and Jaisalmer basins. Journal of the Palaeontological Society of India 32, 136-149.

Kusznir, N.J., Egan, S.S., 1989. Simple-Shear and Pure-Shear Models of Extensional Sedimentary Basin Formation: Application to the Jeanne d'Arc Basin, Grand Banks of Newfoundland. in Tankard, A.J., & Balkwill, H.R., eds., Extensional Tectonics of the North Atlantic Margins. American Association of Petroleum Geologists Memoir 46, 305-322..

Kusznir, N.J., Ziegler, P.A., 1992. The mechanics of continental extension and sedimentary basin formation: A simple-shear/pure-shear flexural-cantilever model. Tectonophysics 215, 117-131.

Kusznir, N.J., Marsden, G., Egan, S.S., 1991. A flexural-cantilever simple-shear/pure-shear model of continental lithosphere extension: applications to the Jeanne d'Arc Basin, Grand Banks and Viking Graben, North Sea. in Roberts, A.M., Yielding, G., & Freeman, B., eds., The Geometry of Normal Faults, Geological Society Special Publication 56, 41-60.

Kusznir, N.J., Roberts, A.M., Morley, C.K., 1995. Forward and reverse modelling of rift basin formation. in Lambaise, J.J., ed., Hydrocarbon Habitat in Rift Basins, Geological Society Special Publication 80, 33-56.

Kusznir, N.J., Hunsdale, R., Roberts, A.M., 2004. Timing of depth-dependent lithosphere stretching on the S. Lofoten rifted margin offshore mid-Norway: pre-breakup or post-breakup? Basin Research 16, 279-296.

Kristensen, M.B., Childs, C., Korstgård, J.A., 2008. The 3D geometry of small-scale relay zones between normal faults in soft sediments. Journal of Structural Geology 30, 257-272.

Leech, M.L., Singh, S., Jain, A.K., Klemperer, S.L., Manickavasagam, R.M., 2005. The onset of India-Asia continental collision: Early, steep subduction required by the timing of UHP metamorphism in the western Himalaya. Earth and Planetary Science Letters 234, 83-97.

Lezzar, K.E., Tiercelin, J-J., Le Turdu, C., Cohen, A.S., Reynolds, D.J., Le Gall, B., Scholz, C.A., 2002. Control of normal fault interaction on the distribution of major Neogene sedimentary depocentres, Lake Tanganyika, East African rift. The American Association of Petroleum Geologists Bulletin, 86(6), 1027-1059.

Li, L., Clift, P.D., Stephenson, R., Nguyen, H.T., 2014. Non-uniform hyper-extension in advance of seafloor spreading on the Vietnam continental margin and the SW South China Sea. Basin Research 26, 106-134.

Liebke, U., Appel, E., Ding, L., Zhang, Q., 2013. Age constraints on the India-Asia collision derived from secondary remanences of Tethyan Himalayan sediments from the Tingri area. Journal of Asian Earth Sciences 62, 329-340.

Lowell, J.D., 1995. Mechanics of basin inversion from worldwide examples. Journal of the Geological Society Special Publication 88, 39-57.

Malod, J.A., Droz, L., Mustafa Kemel, B., Patriat, P., 1997. Early spreading and continental to oceanic basement transition beneath the Indus deep-sea fan: northeastern Arabian Sea. Marine Geology 141, 221-235.

Mamtani, M.A., Karanth, R.V., Merh, S.S., Greiling, R.O., 2000. Tectonic Evolution of the Southern Part of Aravalli Mountain Belt and its Environs: Possible Causes and Time Constraints. Gondwana Research, 3(2), 175-187.

Marrett, R., Allmendinger, R.W., 1990. Kinematic analysis of fault-slip data. Journal of Structural Geology 12(8), 973-986.

McClay, K.R., White, M.J., 1995. Analogue modelling of orthogonal and oblique rifting. Marine and Petroleum Geology 12, 137-151.

McClay, K., Khalil, S., 1998. Extensional hard linkages, eastern Gulf of Suez, Egypt. Geology 26(6), 563-566.

McClay, K.R., Dooley, T., Whitehouse, P., Mills, M., 2002. 4-D evolution of rift-systems: Insights from scaled physical models. The American Association of Petroleum Geologists Bulletin 86(6), 935-959.

McKenzie, D., 1978. Some remarks on the development of sedimentary basins. Earth and Planetary Science Letters 40, 25-32.

McLeod, A.E., Dawers, N.H., Underhill, J.R., 2000. The propagation and linkage of normal faults: insights from the Strathspey-Brent-Statfjord fault array, northern North Sea. Basin Research 12, 263-284.

Meredith, D.J., Egan, S.S., 2002. The geological and geodynamic evolution of the eastern Black Sea basin: insights from 2-D and 3-D tectonic modelling. Tectonophysics 350, 157-179.

Miall, A., 1996. The geology of Fluvial Deposits; Sedimentary Facies, Basin Analysis, and Petroleum Geology. Springer, London, UK, 582pp.

Misra, A.A., Bhattacharya, G., Mukherjee, S., Bose, N., 2014. Near N-S paleo-extension in the western Deccan region, India: Does it link strike-slip tectonics with India-Seychelles rifting? International Journal of Earth Sciences (Geologische Rundschau), DOI 10.1007/s00531-014-1021-x.

Morgan, W.J., 1971. Convection Plumes in the Lower Mantle. Nature 230, 42-43.

Morley, C.K., 1995. Developments in the structural geology of rifts over the last decade and their impact on hydrocarbon exploration. in Lambaise, J.J., ed., Hydrocarbon Habitat in Rift Basins, Geological Society Special Publication 80, 1-32.

Morley, C.K., 1999a. Patterns of Displacement along Large Normal Faults: Implications for Basin Evolution and Fault Propagation, Based on Examples from East Africa. American Association of Petroleum Geologists Bulletin 83(4), 613-634.

Morley, C.K., 1999b. How successful are analogue models in addressing the influence of pre-existing fabrics on rift structure? Journal of Structural Geology 21, 1267-1274.

Morley, C.K., 2010. Stress re-orientation along zones of weak fabrics in rifts: An explanation for pure extension in 'oblique' rift segments. Earth and Planetary Science Letters 297, 667-673.

Morley, C.K., Gabdi, S., Seusutthiya, K., 2007. Fault superimposition and linkage resulting from stress changes during rifting: Examples from 3D seismic data, Phitsanulok Basin, Thailand. Journal of Structural Geology 29, 646-663.

Morley, C.K., Nelson, R.A., Patton, T.L., Munn, S.G., 1990. Transfer Zones in the East African Rift System and Their Relevance to Hydrocarbon Exploration in Rifts. American Association of Petroleum Geologists Bulletin 74(8), 1234-1253.

Morley, C.K., Haranya, C., Phoosongsee, W., Pongwapee, S., Kornsawan, A., Wonganan, N., 2004. Activation of rift oblique and rift parallel pre-existing fabrics during extension and their effect on deformation style: examples from the rifts of Thailand. Journal of Structural Geology 26, 1803-1829.

Mukhopadhyay, D.K., 2011. Analysis and significance of mesoscopic structures in and around Barmer Basin, Rajasthan. IIT Roorke, unpublished report.

Nelson, R.A., Patton, T.L., Morley, C.K., 1992. Rift-Segment Interaction and its Relation to Hydrocarbon Exploration in Continental Rift Systems. American Association of Petroleum Geologists Bulletin 76(8), 1153-1169.

Nieto-Samaniego, A.F., Alaniz-Alvarez, S.A., 1997. Origin and tectonic interpretation of multiple fault patterns. Tectonophysics 270, 197-206.

Nixon, C.W., Sanderson, D.J., Dee, S.J., Bull, J.M., Humphreys, R.J., Swanson, M.H., 2014. Fault interactions and reactivation within a normal-fault network at Milne Point, Alaska. American Association of Petroleum Geologists Bulletin 98(10), 2081-2107.

Pandey, D.K., Fürisch, F.T., Sha, J.G., 2009. Interbasinal marker intervals – a case study from the Jurassic basins of Kachchh and Jaisalmer, western India. Science in China Series D: Earth Sciences 52(12), 1924-1931, doi: 10.1007/s11430-009-0158-0.

Pandey, D.K., Choudhary, S., Bahadur, T., Swami, N., Poonia, D., Sha, J., 2012. A review of the Lower – lowermost Upper Jurassic facies and stratigraphy of the Jaisalmer Basin, western Rajasthan, India. Volumina Jurassica 10, 61-82.

Pareek, H.S., 1981. Petrochemistry and Petrogenesis of the Malani Igneous Suite, India. Geological Society of America Bulletin 92(2), 206-273.

Patriat, P., Achache, J., 1984. India-Eurasia collision chronology has implications for crustal shortening and driving mechanism of plates. Nature 311, 615-621.

Peacock, D.C.P., Sanderson, D.J., 1991. Displacements, segment linkage and relay ramps in normal fault zones. Journal of Structural Geology 13, 721-733.

Peacock, D.C.P., Sanderson, D.J., 1994. Geometry and Development of Relay Ramps in Normal Fault Systems. American Association of Petroleum Geologists Bulletin 78(2), 147-165.

Plummer, Ph.S., Belle, E.R., 1995. Mesozoic tectono-stratigraphic evolution of the Seychelles microcontinent. Sedimentary Geology 96, 73-91.

Poudjom Djomani, Y.H., O'Reilly, S.Y., Griffin, W.L., Morgan, P., 2001. The density structure of subcontinental lithosphere through time. Earth and Planetary Science Letters 184, 605-621.

Rai, J., Singh, A., Pandey, D.K., 2013. Early to Middle Albian age calcareous nannofossils from Pariwar Formation of Jaisalmer Basin, Rajasthan, western India and their significance. Current Science 105(11), 1604-1611.

Rainbird, R.H., Ernst, R.E., 2001. The sedimentary record of mantle-plume uplift, in Ernst, R.E., and Buchan, K.L., eds., Mantle Plumes: Their Identification Through Time: Boulder, Colorado, Geological Society of America Special Paper 352, pp. 227-245

Raju, A.T.R., 1968. Geological Evolution of Assam and Cambay Tertiary Basins of India. The American Association of Petroleum Geologists Bulletin 52(2), 2422-2437.

Reches, Z., Lockner, D.A., 1994. Nucleation and growth of faults in brittle rocks. Journal of Geophysical Research 99(B9), 18159-18173.

Reemst, P., Cloetingh, S., 2000. Polyphase rift evolution of the Vøring margin (mid-Norway): Constraints from forward tectonostratigraphic modelling. Tectonics 19(2), 225-240.

Reeve, M.T., Bell, R.E., Jackson, C.A-L., 2014. Origin and significance of intra-basement seismic reflections offshore western Norway. Journal of the Geological Society 171, 1-4.

Reeves, C., 2014. The position of Madagascar within Gondwana and its movements during Gondwana dispersal. Journal of African Earth Sciences 94, 45-57.

Reeves, C., de Wit, M., 2000. Making ends meet in Gondwana: retracing the transforms of the Indian Ocean and reconnecting continental shear zones. Terra Nova 12(6), 272-280.

Roberts, A.M., Yielding, G., 1991. Deformation around basin-margin faults in the North Sea/mid-Norway rift. in Roberts, A.M., Yielding, G., & Freeman, B., eds., The Geometry of Normal Faults, Geological Society Special Publication 56, 61-78.

Roberts, A.M., Lundin, E.R., Kusznir, N.J., 1997. Subsidence of the Vøring Basin and the influence of the Atlantic continental margin. Journal of the Geological Society 154, 551-557.

Roberts, A.M., Kusznir, N.J., Yielding, G., Styles, P., 1998. 2D flexural backstripping of extensional basins: the need for a sideways glance. Petroleum Geoscience 4, 327-338.

Roberts, A.M., Yielding, G., Kusznir, N.J., Walker, I., Dorn-Lopez, D., 1993. Mesozoic extension in the North Sea: constraints from flexural backstripping, forward modelling and fault populations. In Parker, J.R., ed., Petroleum Geology of Northwest Europe: Proceedings of the 4th Conference. The Geological Society, London, 1123-1136.

Rohrman, M., 2007. Prospectivity of volcanic basins: Trap delineation and acreage de-risking. The American Association of Petroleum Geologists Bulletin 91(6), 915-939.

Rosendahl, B.R., 1987. Architecture of Continental Rifts with Special Reference to East Africa. Annual Review of Earth and Planetary Sciences 15, 445-503.

Rouby, D., Fossen, H., Cobbold, P.R., 1996. Extension, Displacement, and Block Rotation in the Larger Gullfaks Area, Northern North Sea: Determined from Map View Restoration. American Association of Petroleum Geologists Bulletin 80(2), 875-890.

Roy, A.B., 2003. Geological and Geophysical Manifestations of the Réunion Plume-Indian Lithosphere Interactions – Evidence from Northwest India. Gondwana Research 6(3), 487-500.

Roy, A.B., Jakhar, S.R., 2002. Geology of Rajasthan (Northwest India): Precambrian to Recent. Scientific Publishers (India), Jodhpur, pp.421.

Schlische, R.W., 1991. Half-graben basin filling models: new constraints on continental extensional basin development. Basin Research 3. 123-141.

Schlische, R.W., Young, S.S., Ackerman, R.V., Gupta, A., 1996. Geometry and scaling relations of a population of very small rift-related normal faults. Geology 24, 683-686.

Schultz-Ela, D.D., 1992. Restoration of cross-sections to constrain deformation processes of extensional terranes. Marine and Petroleum Geology 9, 372-388.

Sclater, J.G., Christie, P.A.F., 1980. Continental stretching: An explanation of the Post-Mid-Cretaceous subsidence of the central North Sea Basin. Journal of Geophysical Research: Solid Earth 85(B7), 3711-3739.

Scott, D.H., Rosendahl. B.R., 1989. North Viking Graben: An East African Perspective. American Association of Petroleum Geologists Bulletin 73(2), 155-165.

Segnor, A.M.C., Burke, K., Dewey, J.F., 1978. Rifts at high angles to orogenic belts: tests for their origin and the Upper Rhine Graben as an example. American Journal of Science 278, 24-40.

Sen, G., Chandrasekharam, D., 2011. Deccan Traps flood basalt province: an evaluation of the thermochemical plume model, in Ray, J., Sen, G., Ghosh, B., eds.,Topics in Igneous Petrology. Springer, Netherlands, 29-53.

Sen, A., Pande, K., Hegner, E., Sharma, K.K., Dayal, A.M., Sheth, H.C., Mistry, H., 2012. Deccan volcanism in Rajasthan: ^{40}Ar-^{39}Ar geochronology and geochemistry of the Tavidar volcanic suite. Journal of Asian Earth Sciences 59, 127-140.

Sharma, K.K., 2004. The Neoproterozoic Malani magmatism of the northwestern Indian Shield: Implications for crust-building processes. Journal of Earth System Science 113(4), 795-807.

Sharma, K.K., 2007. K-T magmatism and basin tectonism in western Rajasthan, India: Results from extensional tectonics and not from Réunion plume activity, in Foulger, G.R., and Jurdy, D.M., eds., Plates, plumes and planetary processes: Geological Society of America Special Paper 430, 775-784, doi: 10.1130/2007.2430(35).

Sharp, I.R., Gawthorpe, R.L., Underhill, J.R., Gupta, S., 2000. Fault-propagation folding in extensional settings: Examples of structural style and synrift sedimentary response from the Suez rift, Sinai, Egypt. Geological Society of America Bulletin 112(12), 1877-1899.

Sheth, H.C., 2005a. From Deccan to Réunion: no trace of a mantle plume, in Foulger, G.R., Natland, J.H., Presnall, D.C. and Anderson, D.L., eds., Plates, plumes and paradigms: Boulder, Colorado, Geological Society of America Special Paper 388, 477-501, doi: 10.1130/2005.2388(29).

Sheth, H.C., 2005b. Were the Deccan Flood Basalts Derived in Part from Ancient Oceanic Crust Within the Indian Continental Lithosphere? Gondwana Research 8(2), 109-127.

Sheth, H.C., 2007. Plume-related regional prevolcanic uplift in the Deccan Traps: Absence of evidence, evidence of absence, in Foulger, G.R., and Jurdy, D.M., eds., Plates, plumes and planetary processes: Geological Society of America Special Paper 430, 785-813, doi: 10.1130/2007.2430(36).

Sheth, H.C., Chandrasekharam, D., 1997. Plume-rift interaction in the Deccan volcanic province. Physics of the Earth and Planetary Interiors 99, 179-187.

Sheth, H.C., Pande, K., 2014. Geological and $^{40}Ar/^{39}Ar$ age constraints on late-stage Deccan rhyolitic volcanism, inter-volcanic sedimentation, and the Panvel flexure from the Dongri area, Mumbai. Journal of Asian Earth Sciences 84, 167-175.

Simonetti, A., Bell, K., Viladkar, S.G., 1995. Isotopic data from the Amba Dongar carbonatite complex, west–central India: evidence for an enriched mantle source. Chemical Geology (Isotope Geoscience Section) 122, 185–198.

Simonetti, A., Goldstein, S.L., Schmidberger, S.S., Viladkar, S.G., 1998. Geochemical and Nd, Pb, and Sr Isotope Data from Deccan Alkaline Complexes-Inferences for Mantle Sources and Plume–Lithosphere Interaction. Journal of Petrology 39, 1847-1864.

Singh, N.P., 2006. Mesozoic lithostratigraphy of the Jaisalmer Basin, Rajasthan. Journal of the Palaeontological Society of India 51(2), 1-25.

Singh, N.P., 2007. Cenozoic lithostratigraphy of the Jaisalmer Basin, Rajasthan. Journal of the Palaeontological Society of India 52(2), 129-154.

Sisodia, M.S., Singh, U.K., 2000. Depositional Environment and hydrocarbon prospects of the Barmer Basin, Rajasthan, India. Nafta, Zagreb (Croatia) 51(9), 309-326.

Srivastava, R.K., Kumar, S., Sinha, A.K., Chalapathi Rao, N.V., 2014. Petrology and geochemistry of high-titanium and low titanium mafic dykes from the Damodar valley, Chhotanagpur Gneissic Terrain, eastern India and their relation to Cretaceous mantle plume(s). Journal of Asian Earth Sciences 84, 34-50.

Storey, M., Mahoney, J.J., Saunders, A.D., Duncan, R.A., Kelley, S.P., Coffin, M.F., 1995. Timing of Hot Spot-Related Volcanism and the Breakup of Madagascar and India. Science 267, 852-855.

Sunder, V.R., Raine, R., Taylor, A., Whiteley, N.J., Burley, S.D., Kothari, V., 2013. The Mesozoic to Cenozoic stratigraphy of the Barmer Basin, Rajasthan, India. Unpublished report.

Torsvik, T.H., Pandit, M.K., Redfield, T.F., Ashwal, L.D., Webb, S.J., 2005. Remagnetization of Mesozoic limestones from the Jaisalmer basin, NW India. Geophysical Journal International 161, 57-64.

Torsvik, T.H., Carter, L.M., Ashwal, L.D., Bhushan, S.K., Pandit, M.K., Jamtveit, B., 2001. Rodinia refined or obscured: palaeomagnetism of the Malani igneous suite (NW India). Precambrian Research 108, 319-333.

Torsvik, T.H., Amundsen, H., Hartz, E.H., Corfu, F., Kusznir, N., Gaina, C., Doubrovine, P.V., Steinberger, B., Ashwal, L.D., Jamtveit, B., 2013. A Precambrian microcontinent in the Indian Ocean. Nature Geoscience 6, 223-227.

Tron, V., Brun, J-P., 1991. Experiments on oblique rifting in brittle-ductile systems. Tectonophysics 188, 71-84.

Trudgill, B., Cartwright, J., 1994. Relay-ramp forms and normal-fault linkages, Canyonlands National Park, Utah. Geological Society of America Bulletin 106, 1143-1157.

Turcotte, D.L., Schubert, G., 2002. Geodynamics, 2nd Edition. Cambridge University Press, Cambridge, UK. 472pp.

Vijaya Rao, V., Rajendra Prasad, B., Reddy, P.R., Tewari, H.C., 2000. Evolution of Proterozoic Aravalli Delhi Fold Belt in the northwestern Indian Shield from seismic studies. *Tectonophysics*, 327, 109-130.

Wallace, R.E., 1951. Geometry of shearing stress and relation to faulting. Journal of Geology 59, 118-130.

Walsh J.J., Watterson, J., 1988. Analysis of the relationship between displacements and dimensions of faults. Journal of Structural Geology 10(3), 239-247.

Walsh, J.J., Watterson, J., 1989. Displacement gradients on fault surfaces. Journal of Structural Geology 11, 307-316.

Walsh, J.J., Watterson, J., Bailey, W.R., Childs, C., 1999. Fault relays, bends and branch-lines. Journal of Structural Geology 21, 1019-1026.

Walsh, J.J., Nicol, A., Childs, C., 2002. An alternative model for the growth of faults. Journal of Structural Geology 24, 1669-1675.

Walsh, J.J., Bailey, W.R., Childs, C., Nicol, A., Bonson, C.G., 2003. Formation of segmented normal faults: a 3-D perspective. Journal of Structural Geology 25, 1251-1262.

Watterson, J., 1986. Fault Dimensions, Displacements and Growth. Pure and Applied Geophysics 124(1-2), 365-373.

Wernicke, B., 1985. Uniform-sense normal simple-shear of the continental lithosphere. Canadian Journal of Earth Sciences 22, 108-125.

Whipp, P.S., Jackson, C.A-L., Gawthorpe, R.L., Dreyer, T., Quinn, D., 2014. Fault array evolution above a reactivated rift-fabric; a subsurface example from the northern Horda Platform fault array, Norwegian North Sea. Basin Research 26, 523-549.

White, R., McKenzie, D., 1989. Magmatism at Rift Zones: The Generation of Volcanic Continental Margins and Flood Basalts. Journal of Geophysical Research 94(B6), 7685-7729.

Willemse, E.J.M., 1997. Segmented normal faults: correspondence between three-dimensional mechanical models and field data. Journal of Geophysical Research 102(B1), 675-692.

Williams, G.D., Kane, S.J., Buddin, T.S., Richards, A.J., 1997. Restoration and balance of complex folded an faulted rock volumes: flexural flattening, jigsaw fitting and decompaction in three dimensions. Tectonophysics 273, 203-218.

Withjack, M.O., Jamison, W.R., 1986. Deformation Produced by Oblique Rifting. Tectonophysics 126, 99-124.

Withjack, M.O., Olson, J., Peterson, E., 1990. Experimental models of extensional forced folds. American Association of Petroleum Geologists Bulletin 74(7), 1038-1054.

Yatheesh, V., Bhattacharya, G.C., Dyment, J., 2009. Early oceanic opening off Western India-Pakistan margin: The Gop Basin revisited. Earth and Planetary Science Letters 284, 399-408.

Younes, A.I., McClay, K., 2002. Development of accommodation zones in the Gulf of Suez – Red Sea rift, Egypt. The American Association of Petroleum Geologists Bulletin 86(6), 1003-1026.

Young, M.J., Gawthorpe, R.L., Sharp, I.R., 2000. Sedimentology and sequence stratigraphy of a transfer zone coarse-grained delta, Miocene Suez Rift, Egypt. Sedimentology 47, 1081-1104.

Appendix A

Structural data from the Barmer Hills

A1 Fault-plane measurements

UTM Zone 42N		Strike	Dip	Dip Direction	UTM Zone 42N		Strike	Dip	Dip Direction
Eastings	Northings				Eastings	Northings			
0738989	2849554	353	71	E	0738945	2849014	089	66	S
0738989	2849554	131	32	SW	0738902	2848975	275	79	N
0739172	2849055	283	70	N	0738928	2849524	351	58	E
0739157	2849063	296	73	NE	0738901	2849492	342	57	E
0739133	2849076	309	49	NE	0738890	2849602	102	60	S
0739137	2849075	293	50	NE	0738766	2849814	333	58	NE
0739150	2849116	110	45	SSW	0738752	2849834	334	66	NE
0739149	2849130	175	62	W	0738739	2849859	322	62	NE
0739147	2849143	198	50	W	0738702	2849900	324	63	NE
0739113	2849092	292	72	N	0738718	2849869	340	61	E
0739058	2849096	279	73	N	0738634	2849888	338	43	NE
0739002	2849113	291	41	N	0738610	2849928	319	63	NE
0738817	2849308	174	56	W	0738565	2849939	344	74	E
0738926	2849425	293	50	N	0738511	2849944	016	78	E
0738934	2849428	002	52	E	0738476	2850067	324	73	NE
0738943	2849431	005	60	E	0738367	2850253	246	41	NNW
0739077	2849408	159	52	W	0738357	2850274	163	47	WSW
0739301	2849010	286	77	N	0738354	2850278	207	44	WNW
0739282	2849013	286	65	N	0738319	2850300	129	77	SW
0738986	2849027	109	72	SW	0738356	2850311	141	59	SW

A2 Extensional fracture plane measurements

UTM Zone 42N		Strike	Dip	Dip Direction	UTM Zone 42N		Strike	Dip	Dip Direction
Eastings	Northings				Eastings	Northings			
0739044	2849435	010	67	E	0738984	2849612	344	60	E
0739044	2849435	186	71	W	0738984	2849612	080	53	S
0739044	2849435	006	77	E	0738984	2849612	078	57	S
0739044	2849435	199	62	W	0738954	2849637	319	72	NE
0739030	2849445	202	59	NW	0738954	2849637	321	80	NE
0739030	2849445	028	73	SE	0738954	2849637	314	77	NE
0739030	2849445	039	82	SE	0738954	2849637	132	79	SW
0739030	2849445	210	81	NW	0738894	2849728	308	72	NE
0738997	2849469	331	83	NE	0738894	2849728	305	71	NE
0738997	2849469	330	70	NE	0738894	2849728	305	79	NE
0738997	2849469	329	81	NE	0738894	2849728	319	84	NE
0738997	2849469	321	70	NE	0738887	2849752	051	61	SE
0739011	2849476	161	82	SW	0738887	2849752	062	63	SE
0738978	2849554	046	77	SE	0738887	2849752	069	69	SE
0738990	2849589	253	86	N	0738887	2849752	059	81	SE
0738990	2849589	204	46	NW	0738897	2849749	043	76	SE
0738990	2849589	075	89	S	0738897	2849749	068	73	SE
0738990	2849589	148	74	SW	0738897	2849749	051	80	SE

UTM Zone 42N		Strike	Dip	Dip Direction	UTM Zone 42N		Strike	Dip	Dip Direction
Eastings	Northings				Eastings	Northings			
0738897	2849749	067	68	SE	0739701	2848746	315	83	NE
0738907	2849738	059	72	SE	0739701	2848746	319	82	NE
0738907	2849738	062	72	SE	0739012	2849034	169	63	W
0738907	2849738	050	81	SE	0739012	2849034	168	59	W
0738907	2849738	056	79	SE	0739012	2849034	174	63	W
0739240	2849185	170	73	W	0739012	2849034	170	60	W
0739240	2849185	184	85	W	0738782	2849424	324	62	NE
0739240	2849185	161	79	W	0738782	2849424	335	68	NE
0739240	2849185	179	85	W	0738782	2849424	317	68	NE
0739150	2849116	172	62	W	0738782	2849424	330	65	NE
0739150	2849116	164	54	W	0738915	2849577	202	66	NW
0739150	2849116	158	58	SW	0738915	2849577	192	68	W
0739150	2849116	160	64	SW	0738915	2849577	204	64	NW
0739147	2849143	198	56	W	0738915	2849577	218	52	NW
0739147	2849143	193	52	W	0738771	2849860	223	67	NW
0739147	2849143	194	56	W	0738771	2849860	226	61	NW
0739147	2849143	200	65	NW	0738771	2849860	226	58	NW
0738817	2849308	005	79	E	0738771	2849860	234	48	NW
0738817	2849308	001	73	E	0738754	2849866	329	60	NE
0738817	2849308	184	68	W	0738754	2849866	323	60	NE
0738876	2849317	354	46	E	0738696	2849884	324	54	NE
0738876	2849317	359	48	E	0738696	2849884	314	62	NE
0738876	2849317	109	76	S	0738696	2849884	324	63	NE
0738876	2849317	103	72	S	0738696	2849884	325	58	NE
0738876	2849317	120	73	SW	0738666	2849886	309	62	NE
0738876	2849317	111	71	S	0738666	2849886	294	66	NNE
0738876	2849317	115	70	S	0738666	2849886	301	65	NE
0738876	2849317	121	68	SW	0738666	2849886	301	65	NE
0738899	2849346	186	57	W	0738610	2849928	311	60	NE
0738899	2849346	190	61	W	0738610	2849928	316	09	NE
0738899	2849346	189	62	W	0738610	2849928	218	46	NW
0738899	2849346	188	64	W	0738610	2849928	203	52	NW
0738926	2849425	284	47	N	0738565	2849939	336	83	NE
0738926	2849425	275	47	N	0738565	2849939	347	70	ENE
0738926	2849425	288	47	N	0738565	2849939	340	73	ENE
0738926	2849425	292	47	N	0738565	2849939	346	74	E
0738943	2849431	296	61	N	0738565	2849939	061	79	SE
0738943	2849431	306	78	NE	0738565	2849939	058	82	SE
0738943	2849431	296	62	NE	0738565	2849939	071	48	S
0738943	2849431	303	61	NE	0738565	2849939	072	62	SSE
0738943	2849431	022	70	E	0738511	2849944	167	68	W
0738943	2849431	007	72	E	0738511	2849944	351	62	E
0738943	2849431	351	65	E	0738511	2849944	012	67	E
0738943	2849431	355	46	E	0738511	2849944	007	71	E
0739077	2849408	222	73	NW	0738498	2849988	341	73	NE
0739077	2849408	217	77	NW	0738498	2849988	161	71	SW
0739077	2849408	184	60	W	0738498	2849988	328	82	NE
0739077	2849408	180	80	W	0738498	2849988	167	66	SW
0739701	2848746	322	80	NE	0738511	2849993	358	83	E
0739701	2848746	327	81	NE	0738511	2849993	328	72	NE

UTM Zone 42N		Strike	Dip	Dip Direction	UTM Zone 42N		Strike	Dip	Dip Direction
Eastings	Northings				Eastings	Northings			
0738511	2849993	342	72	E	0738319	2850300	119	80	SW
0738511	2849993	352	86	E	0738319	2850300	150	74	SW
0738497	2850012	154	66	WSW	0738319	2850300	146	50	SW
0738497	2850012	356	72	E	0738449	2850278	128	61	SW
0738497	2850012	339	67	NE	0738449	2850278	335	65	NE
0738497	2850012	343	80	NNE	0738449	2850278	334	62	NE
0738492	2850032	182	62	W	0738449	2850278	341	55	NE
0738492	2850032	191	73	W	0738495	2850376	146	79	SW
0738492	2850032	192	74	W	0738495	2850376	152	77	SW
0738492	2850032	008	58	E	0738495	2850376	316	73	NE
0738476	2850067	336	60	NE	0738495	2850376	329	81	NE
0000000	0000000	166	75	W	0738451	2850391	332	63	NE
0000000	0000000	178	62	W	0738451	2850391	323	60	NE
0000000	0000000	168	90		0738451	2850391	336	86	ENE
0000000	0000000	135	78	SW	0738451	2850391	332	78	NE
0738476	2850067	330	62	NE	0738526	2850096	301	77	NE
0738476	2850067	327	89	NE	0738526	2850096	301	80	NE
0738476	2850067	343	59	E	0738526	2850096	295	81	N
0738442	2850088	293	77	N	0738526	2850096	332	76	ENE
0738442	2850088	303	78	NNE	0738602	2850097	323	68	NE
0738442	2850088	304	78	NNE	0738602	2850097	327	72	NE
0738442	2850088	298	72	NNE	0738602	2850097	322	65	NE
0738411	2850119	087	73	S	0738602	2850097	320	74	NE
0738411	2850119	090	72	S	0738710	2850032	304	69	NE
0738411	2850119	084	64	S	0738710	2850032	316	72	NE
0738411	2850119	113	62	SSW	0738710	2850032	172	65	W
0738399	2850141	150	85	SW	0738710	2850032	178	64	W
0738399	2850141	341	73	ENE	0738702	2849866	176	50	N
0738399	2850141	189	62	W	0738702	2849866	178	55	W
0738399	2850141	166	70	SW	0738702	2849866	172	50	W
0738396	2850181	290	65	NNE	0738702	2849866	172	40	W
0738396	2850181	311	72	NE	0738738	2849794	164	40	WSW
0738396	2850181	302	61	NE	0738738	2849794	322	68	ENE
0738396	2850181	312	61	NE	0738738	2849794	311	71	ENE
0738396	2850181	314	64	NE	0738738	2849794	315	62	ENE
0738396	2850181	311	72	NE	0738773	2849737	299	70	NE
0738396	2850181	306	68	NE	0738773	2849737	313	58	NE
0738396	2850181	321	79	NE	0738773	2849737	308	58	NE
0738357	2850274	154	62	SW	0738773	2849737	316	70	NE
0738357	2850274	128	70	SW	0738759	2849691	338	60	ENE
0738357	2850274	144	52	SW	0738759	2849691	339	68	ENE
0738357	2850274	126	83	SW	0738759	2849691	334	59	ENE
0738319	2850300	118	70	SSW	0738759	2849691	333	65	ENE

A3 Fault-plane slickenline measurements

Eastings	Northings	Fault Plane			Pitch (from strike)	Lineation		Slip-Sense
		Strike	Dip	Dip Direction		Plunge	Trend	
0739157	2849063	296	73	NE	116	59	083	Normal
0739133	2849076	309	49	NE	110	45	069	Normal
0739137	2849075	303	48	NE	100	48	048	Normal
0739150	2849116	138	52	SW	096	51	234	Normal
0739149	2849130	175	62	W	053	44	207	Normal
0739147	2849143	198	50	W	031	23	219	Normal
0739058	2849096	279	73	N	139	38	085	Normal
0739002	2849113	256	48	N	131	34	037	Normal
0739002	2849113	279	41	N	099	41	020	Normal
0739002	2849113	290	42	N	122	36	060	Normal
0738926	2849425	293	50	N	046	32	326	Normal
0738945	2849014	089	66	S	119	54	232	Normal
0738890	2849602	102	60	S	084	60	180	Normal
0738752	2849834	346	68	E	099	66	097	Normal
0738739	2849859	322	62	NE	086	62	040	Normal
0738718	2849869	340	61	E	083	60	056	Normal
0738634	2849888	338	42	NE	073	39	045	Normal
0738610	2849928	319	63	NE	077	61	021	Normal
0738565	2849939	344	74	E	080	71	040	Normal
0738511	2849944	016	78	E	087	78	089	Normal
0738367	2850253	246	41	NNW	102	39	349	Normal
0738357	2850274	163	47	WSW	086	46	246	Normal
0738354	2850278	207	44	WNW	049	32	246	Normal
0738319	2850300	129	77	SW	086	86	202	Normal
0738356	2850311	141	59	SW	110	53	267	Normal

Appendix B

Sarnoo Hills Cross-sections

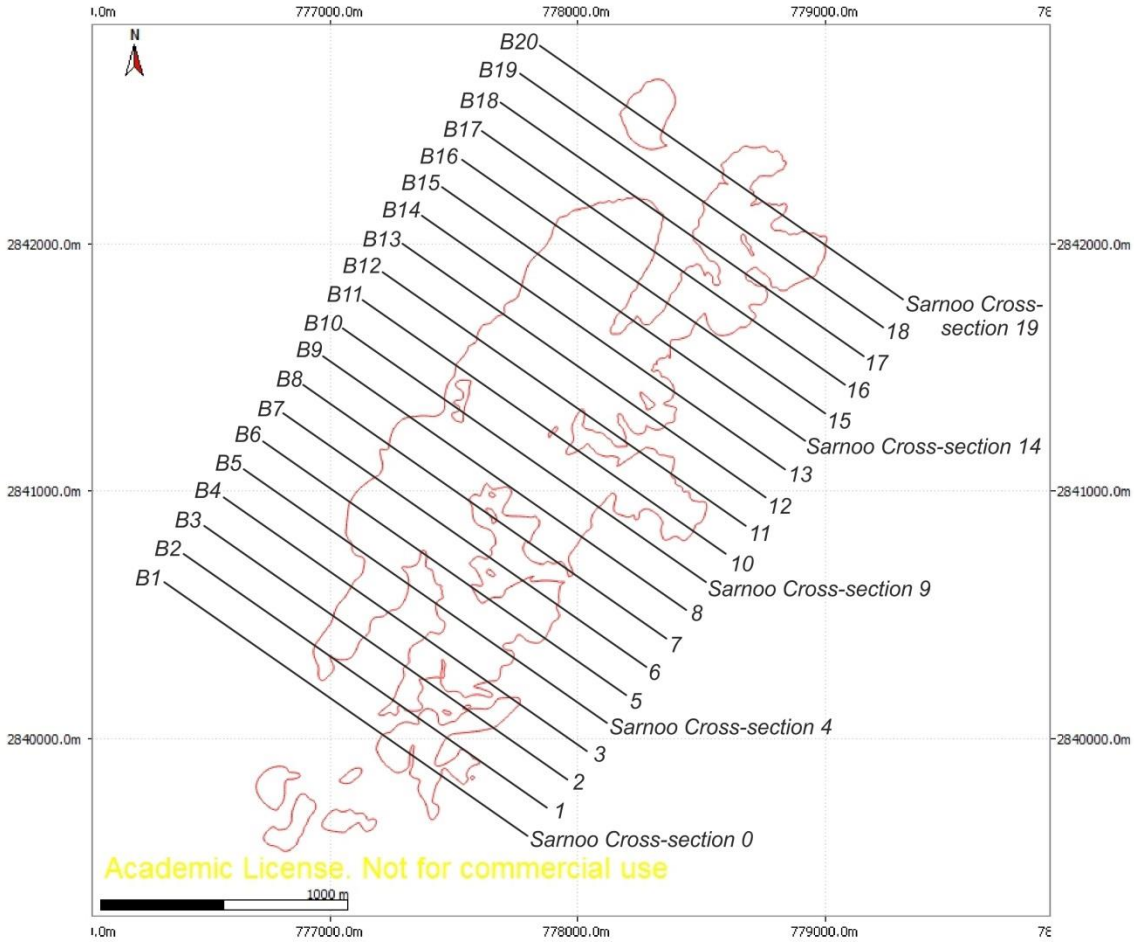

B1: Sarnoo Cross-section 0

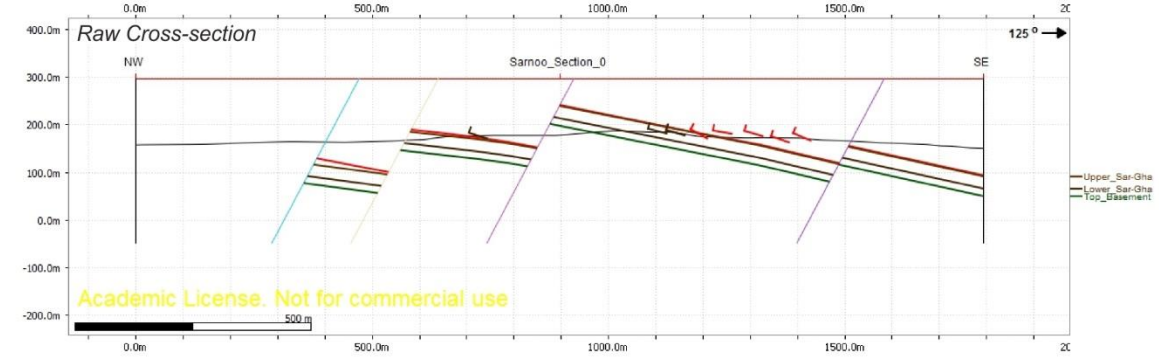

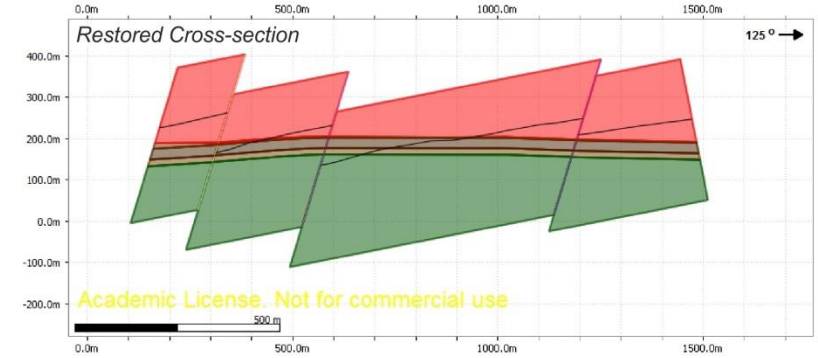

B2: Sarnoo Cross-section 1

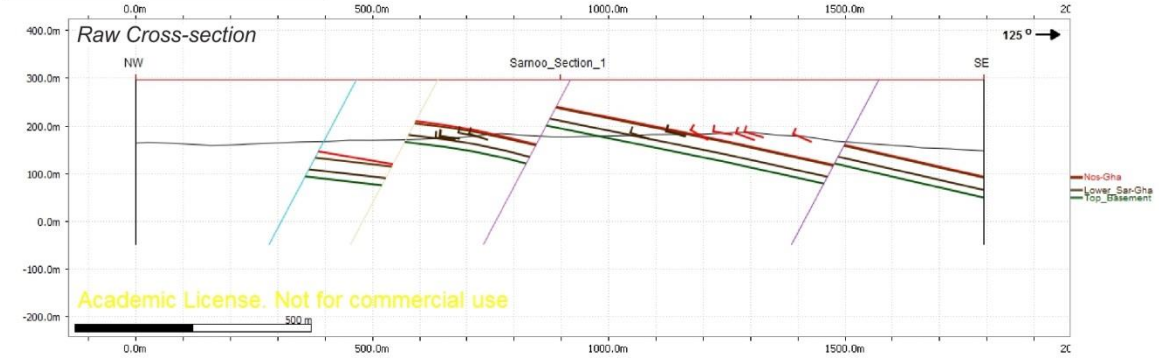

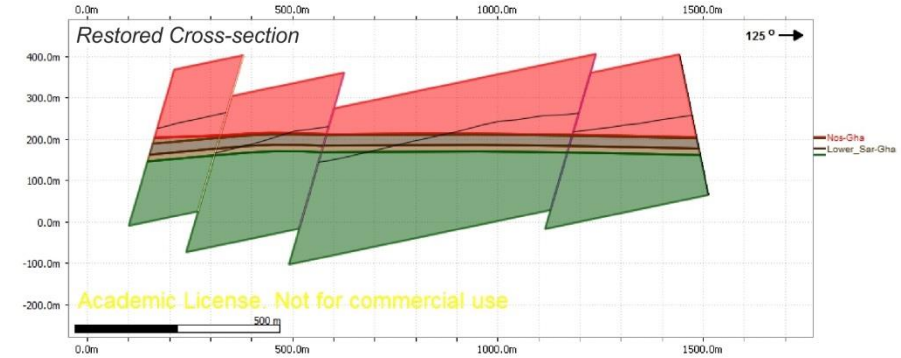

B3: Sarnoo Cross-section 2

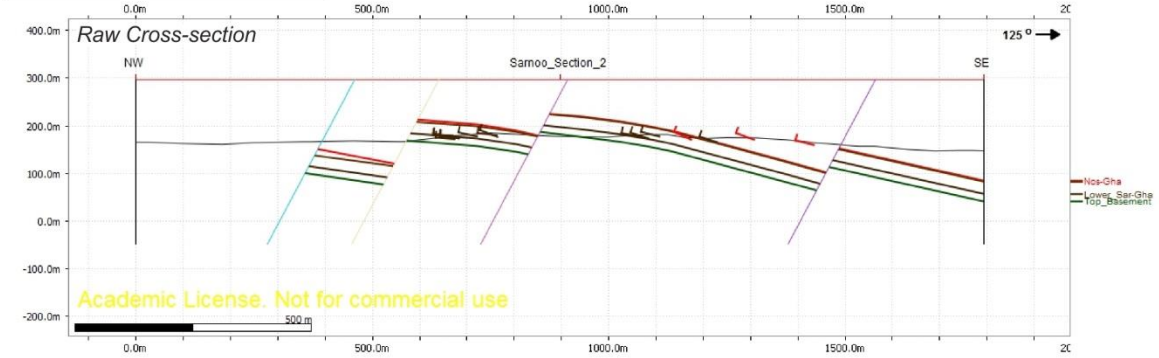

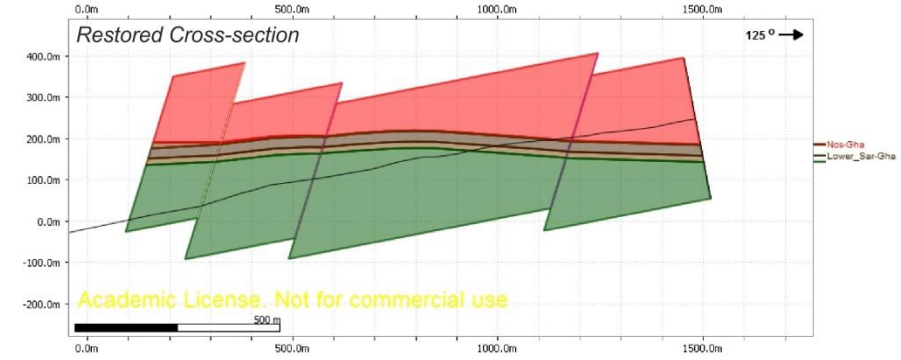

B4: Sarnoo Cross-section 3

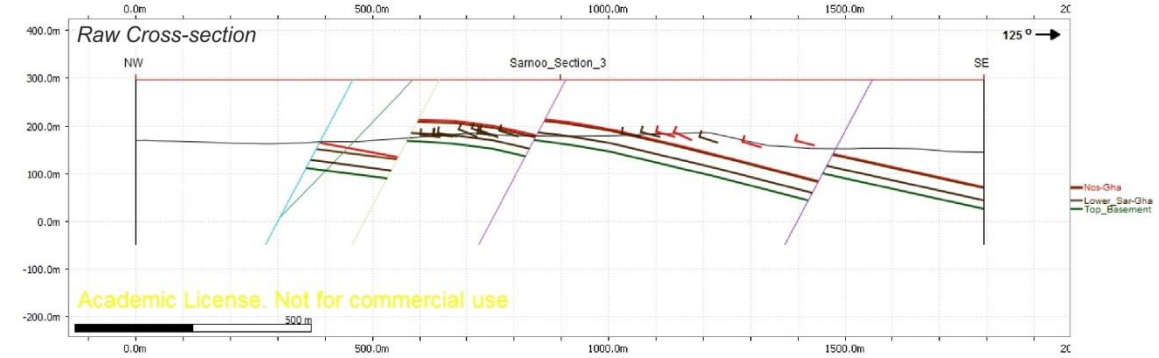

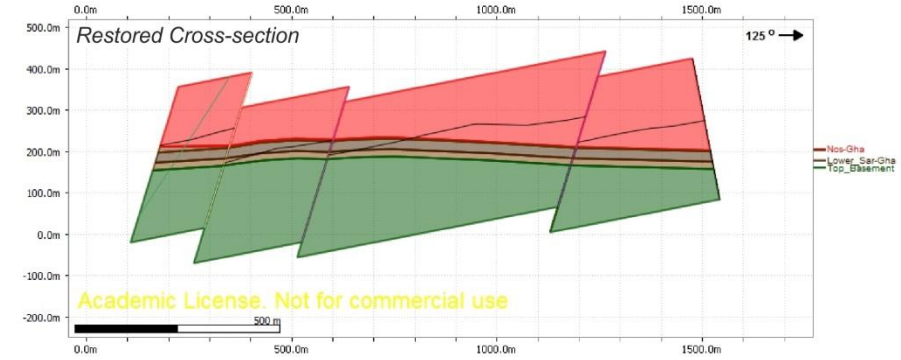

B5: Sarnoo Cross-section 4

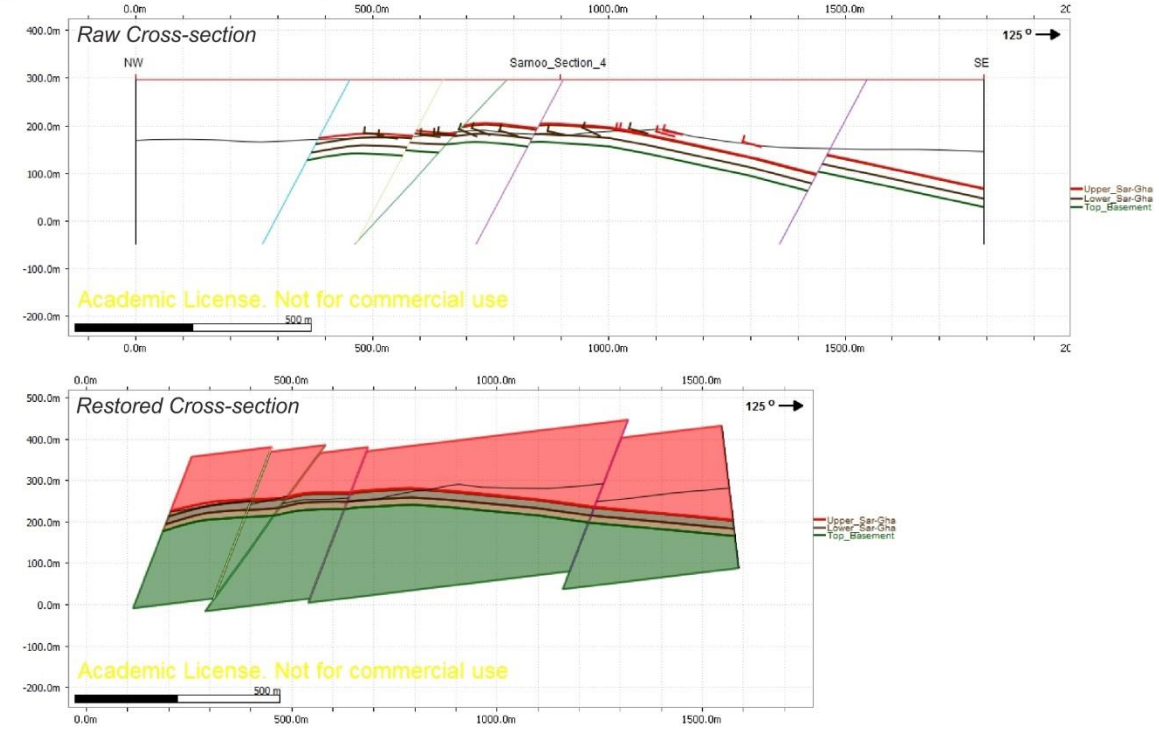

B6: Sarnoo Cross-section 5

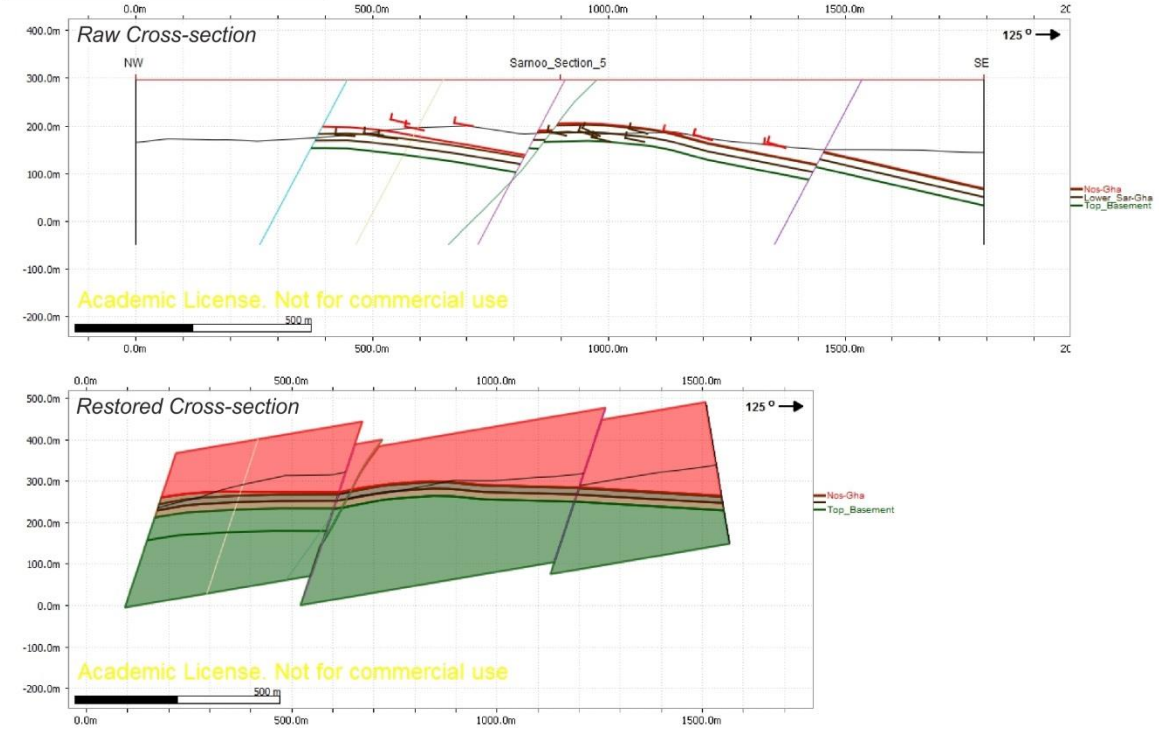

B7: Sarnoo Cross-section 6

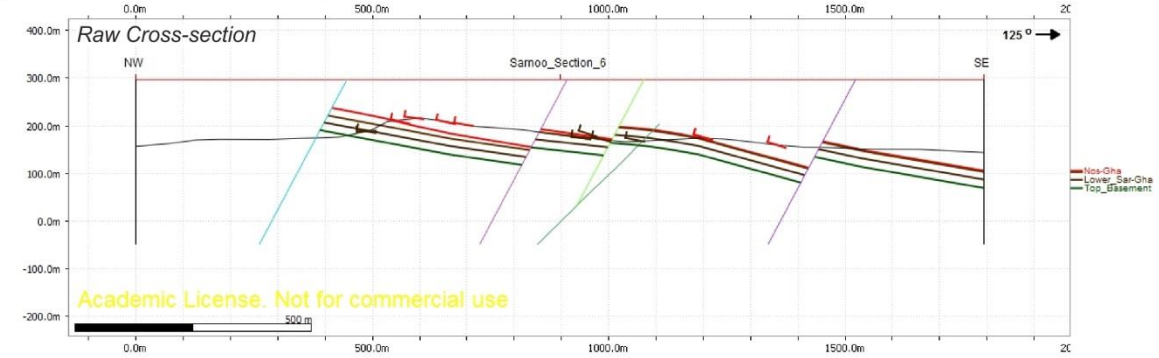

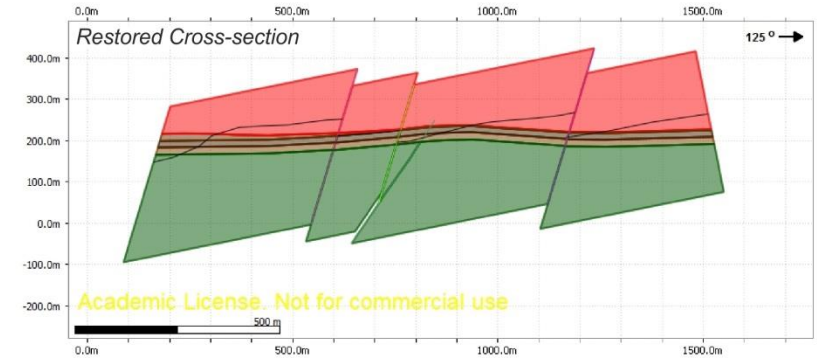

B8: Sarnoo Cross-section 7

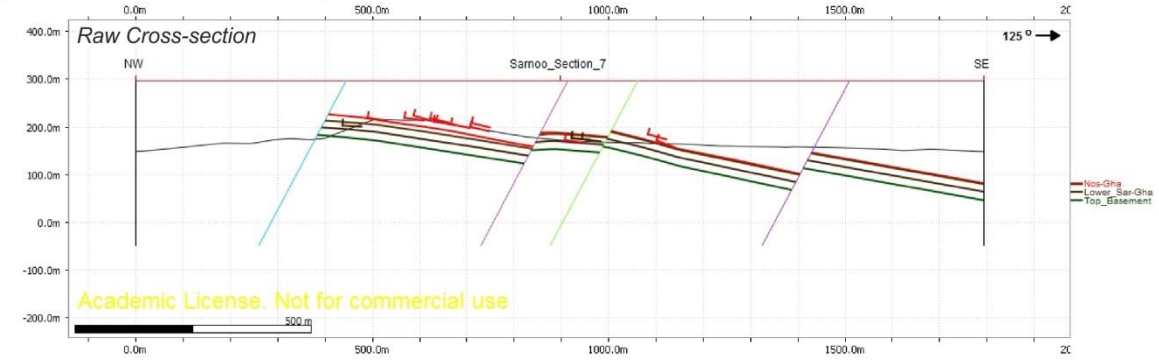

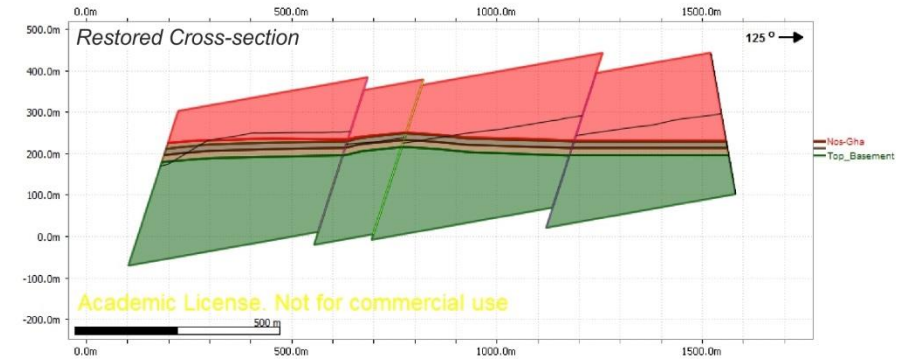

B9: Sarnoo Cross-section 8

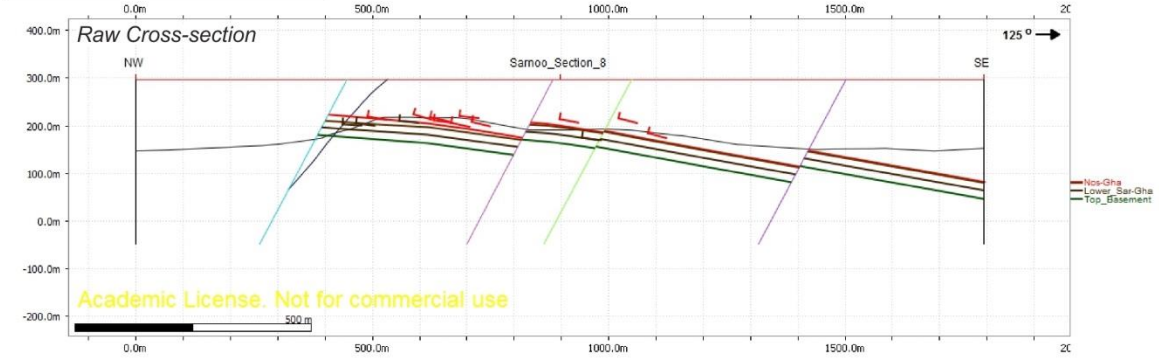

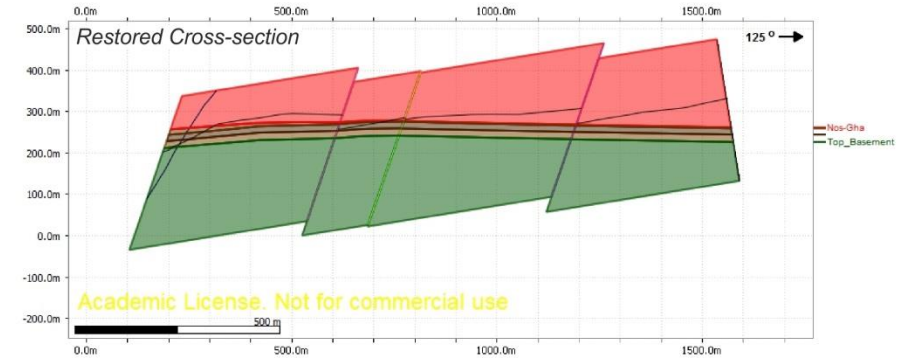

B10: Sarnoo Cross-section 9

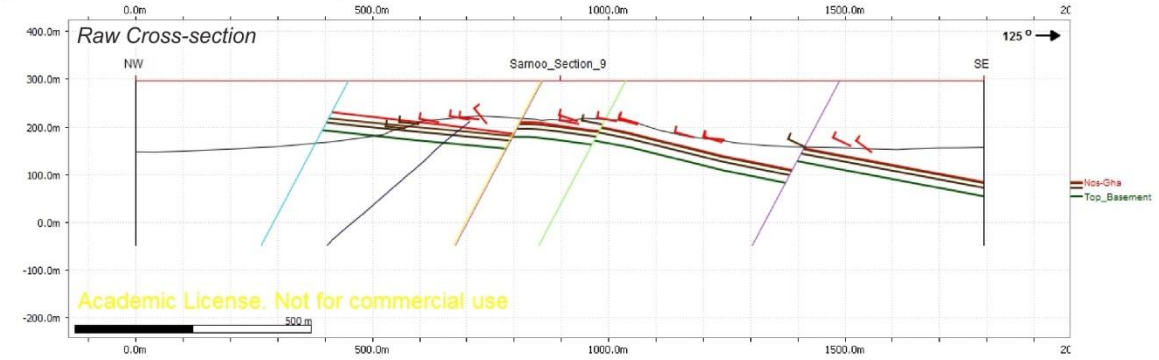

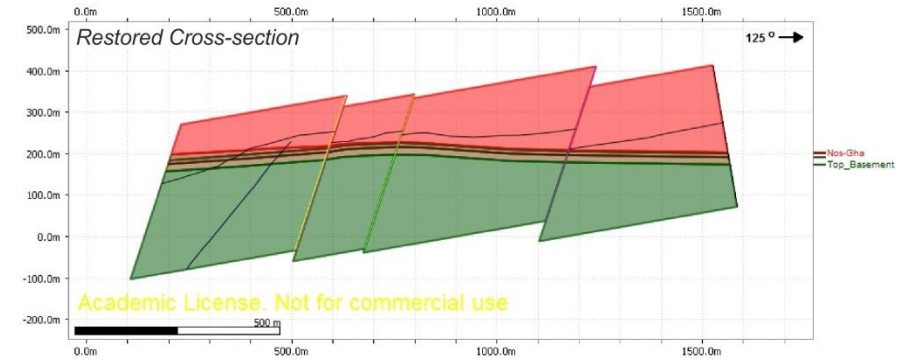

B11: Sarnoo Cross-section 10

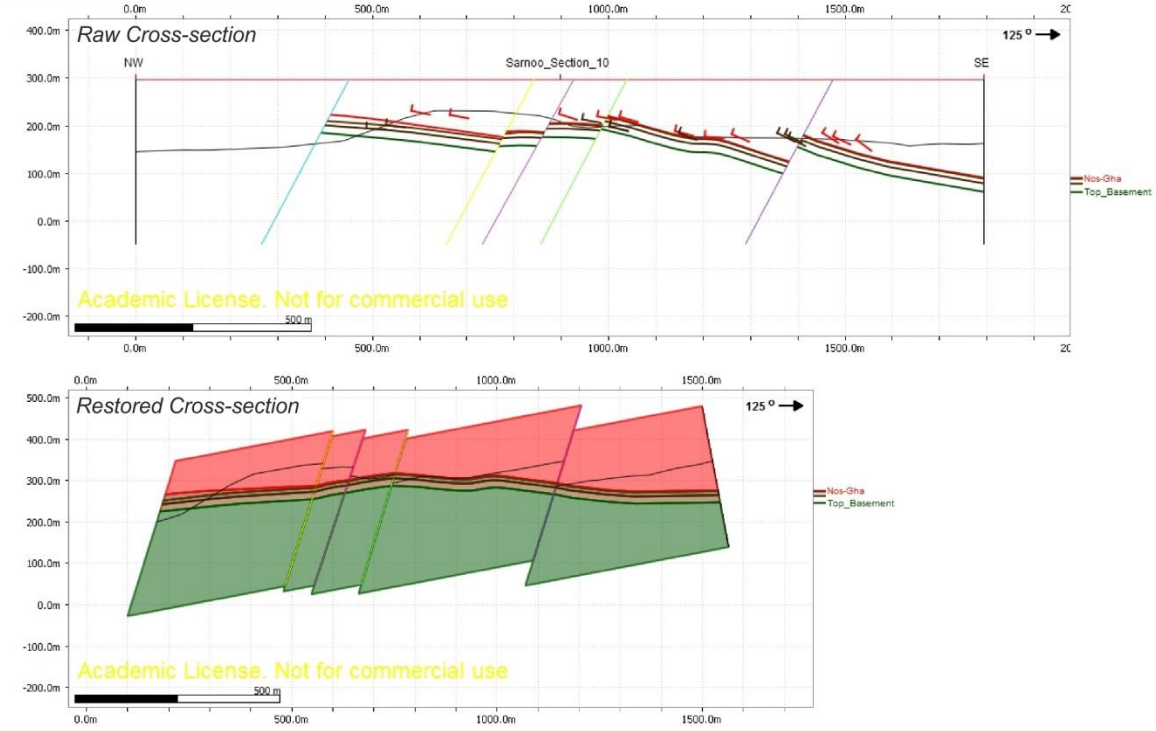

B12: Sarnoo Cross-section 11

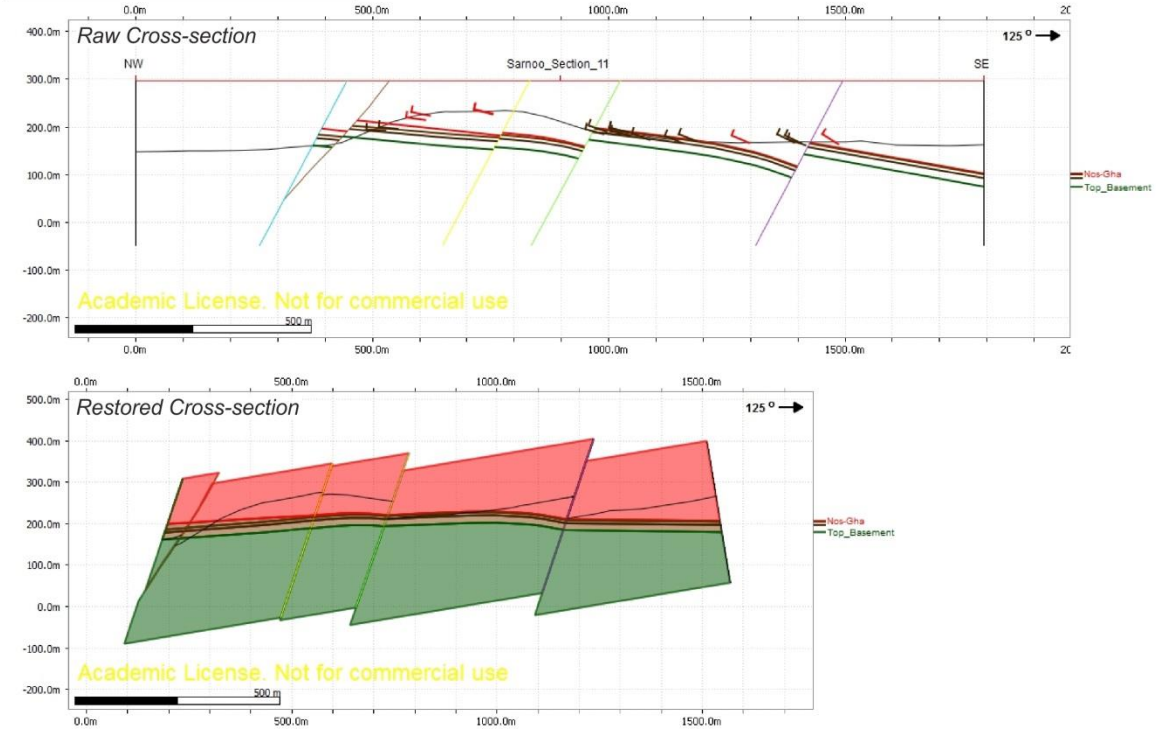

B13: Sarnoo Cross-section 12

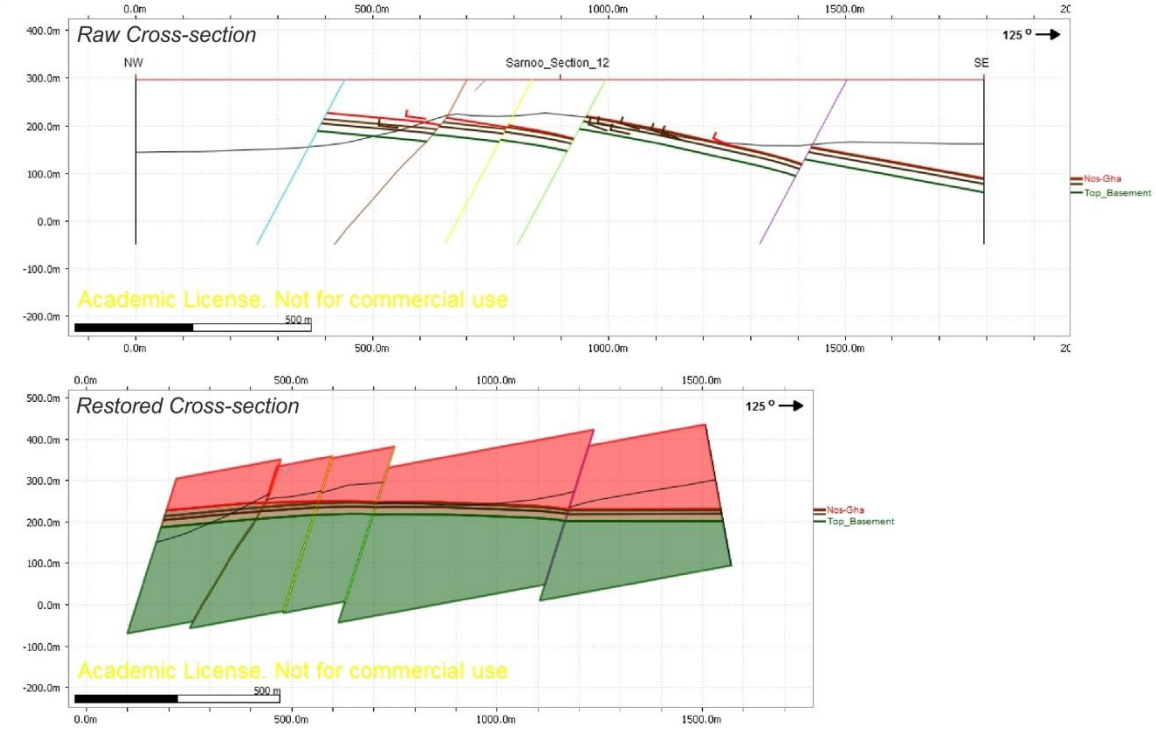

B14: Sarnoo Cross-section 13

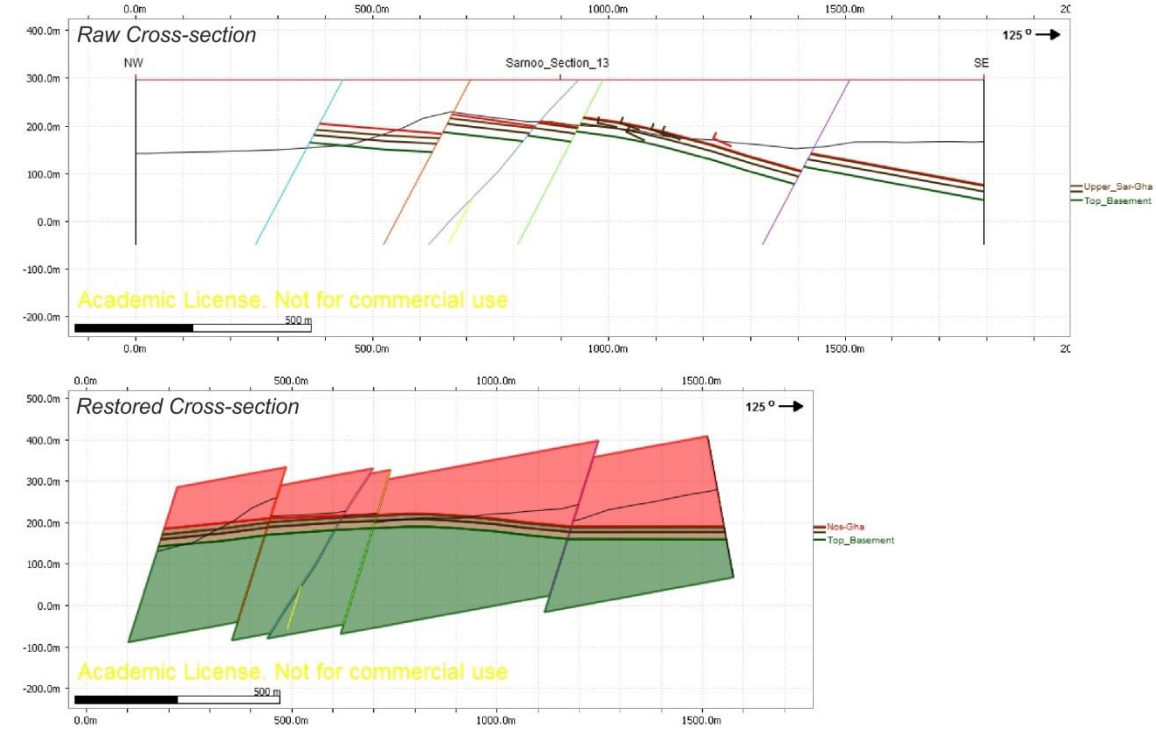

B15: Sarnoo Cross-section 14

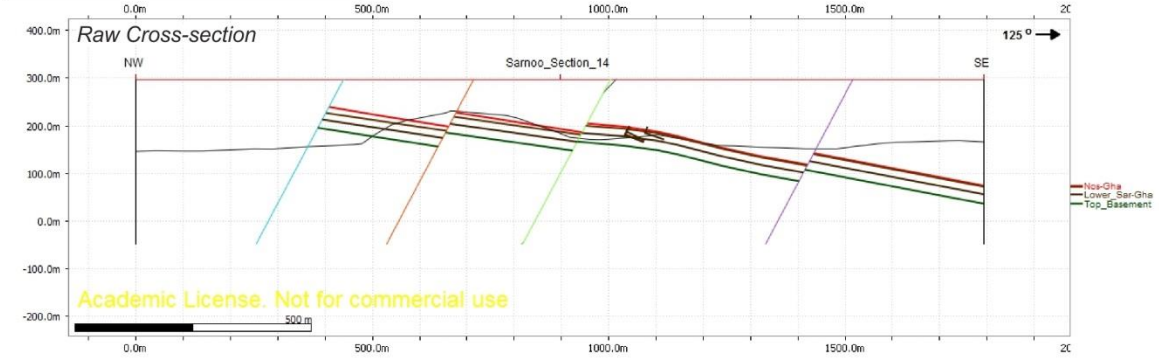

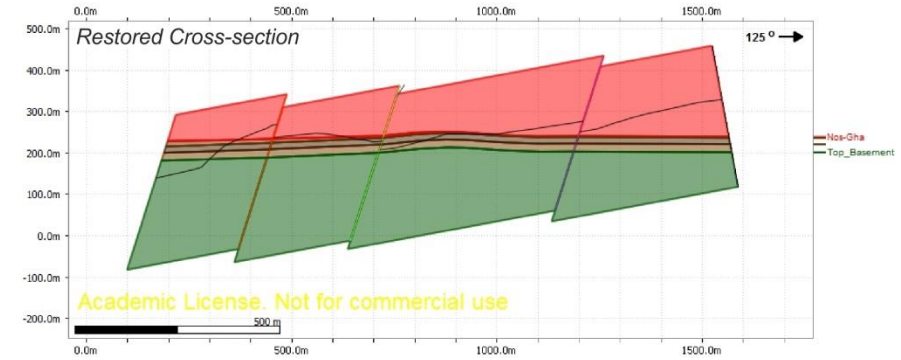

B16: Sarnoo Cross-section 15

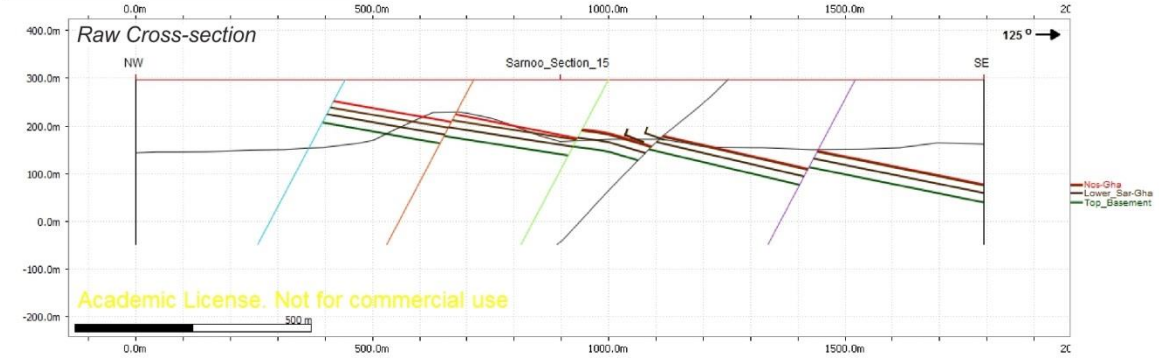

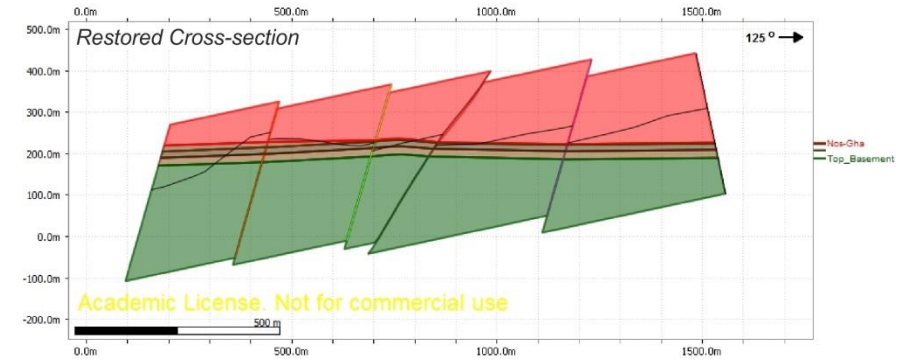

B17: Sarnoo Cross-section 16

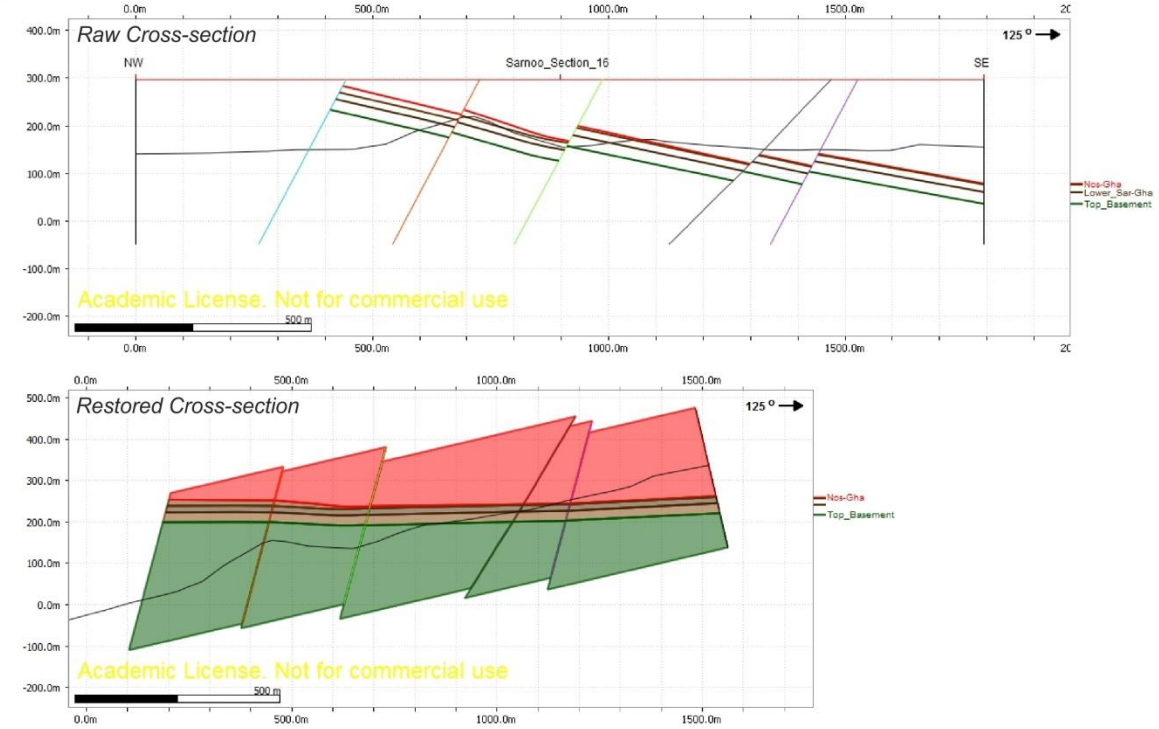

B18: Sarnoo Cross-section 17

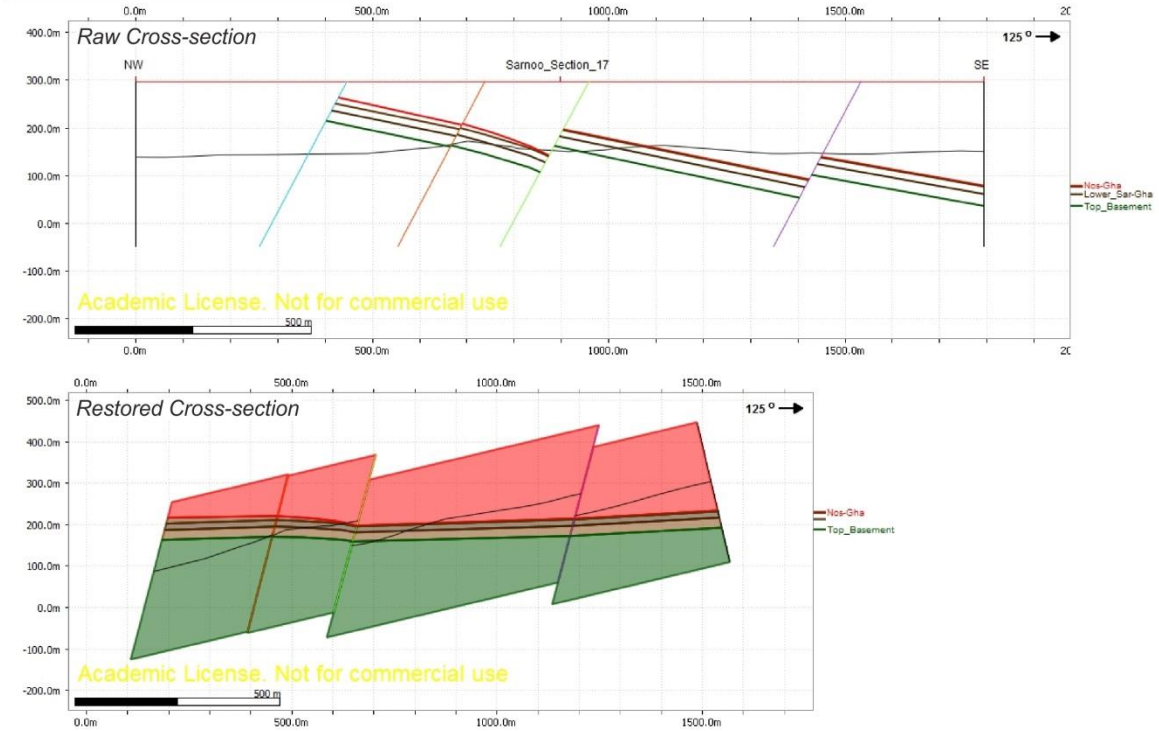

B19: Sarnoo Cross-section 18

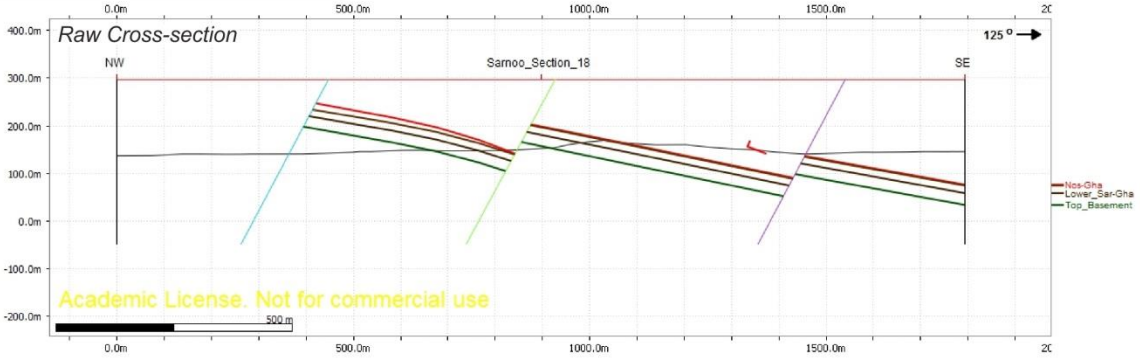

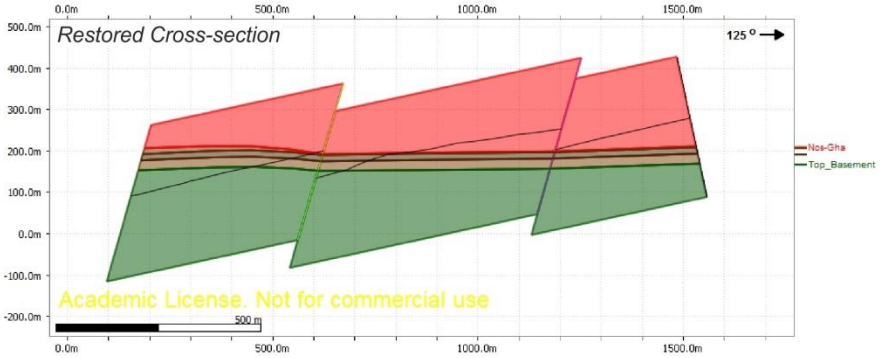

B20: Sarnoo Cross-section 19

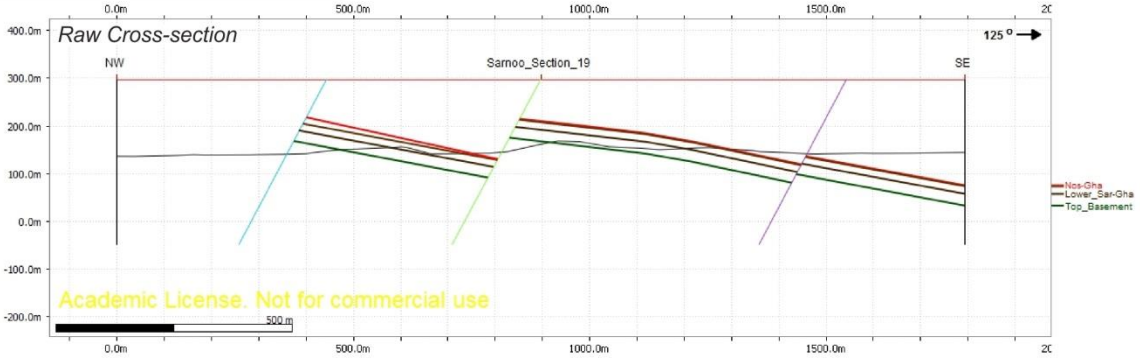

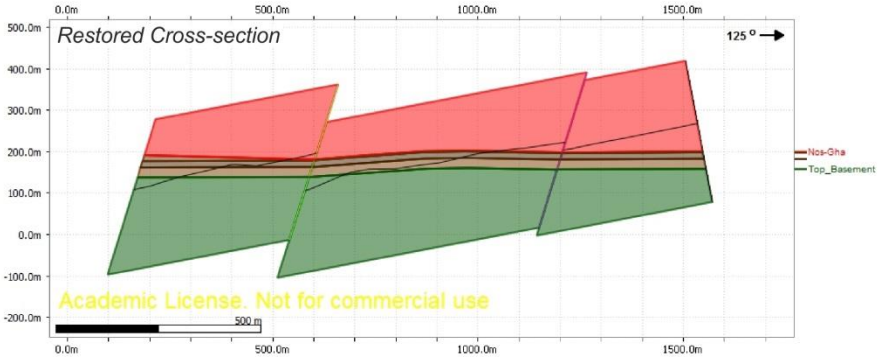

Appendix C

Structural data from the Sarnoo Hills

C1 Bedding measurements

UTM Zone 42N		Strike	Dip	Dip Direction	UTM Zone 42N		Strike	Dip	Dip Direction
Eastings	Northings				Eastings	Northings			
0777379	2841276	004	10	E	0777454	2840548	030	25	SE
0777288	2841195	018	04	E	0777439	2840653	039	13	SE
0777215	2841038	293	18	NE	0777526	2840663	042	18	SE
0777215	2841038	053	10	SE	0777224	2840628	047	21	SE
0777101	2840954	048	05	SE	0777285	2840612	046	17	SE
0777687	2841631	063	07	SE	0777598	2840791	056	06	SE
0777564	2841305	038	10	SE	0777598	2840791	010	10	E
0777624	2841279	069	13	SE	0777615	2840741	044	14	SE
0777330	2841163	032	10	SE	0777654	2840672	057	12	SE
0777261	2840979	033	13	SE	0777657	2840900	036	08	SE
0777354	2841060	068	09	S	0777841	2840426	053	08	SE
0777445	2841082	047	08	SE	0777884	2840476	033	18	SE
0777487	2841008	025	14	SE	0777584	2841530	024	03	SE
0777386	2840989	081	18	S	0777529	2841379	006	07	E
0777464	2841123	027	13	SE	0777486	2841268	051	06	SE
0777466	2841049	014	13	E	0777215	2840860	040	12	SE
0777553	2841097	052	14	SE	0777126	2840884	023	06	SE
0777458	2841177	011	18	E	0777102	2840798	015	08	SE
0777586	2841188	329	15	NE	0777155	2840717	327	17	NE
0777658	2841249	022	52	ESE	0777176	2840683	077	13	SW
0777823	2841474	044	16	SE	0777139	2840644	048	03	SE
0777823	2841474	036	10	SE	0777071	2840549	080	10	SSE
0777677	2841497	061	13	SE	0777071	2840549	049	02	SE
0777742	2841608	051	08	SE	0777025	2840461	049	08	SE
0778252	2840927	024	26	SE	0777001	2840424	032	06	SE
0778354	2840906	020	26	ESE	0776957	2840378	025	05	SE
0778357	2840829	032	37	SE	0776962	2840263	025	18	SE
0778292	2840996	036	26	SE	0777024	2840390	026	12	SE
0778369	2841095	025	19	SE	0777120	2840450	027	21	SE
0778223	2841094	066	26	SSE	0777175	2840534	075	08	SSE
0778281	2841009	026	26	SE	0777175	2840606	039	22	SE
0778057	2840960	034	17	SE	0777669	2840065	022	15	SE
0778082	2840989	109	20	S	0777478	2840244	034	24	SE
0778324	2841306	018	25	E	0777511	2840195	035	18	SE
0778257	2841399	043	24	SE	0777412	2840269	044	14	SE
0778244	2841421	028	22	SE	0777397	2840319	028	10	SE
0778197	2841466	038	19	SE	0777326	2840186	026	18	SE
0778066	2841315	049	12	SE	0777306	2840024	018	13	E
0778040	2841361	044	20	SE	0777306	2840024	033	17	SE
0778015	2841337	048	16	SE	0777199	2839938	038	15	SE
0778088	2841270	056	21	SE	0777101	2839859	037	24	SE
0778153	2841241	021	23	ESE	0776834	2839591	072	17	SSE
0778111	2841129	019	22	ESE	0776917	2839673	050	30	SE
0777988	2841209	086	23	S	0776883	2839729	067	16	SSE
0777988	2841209	056	14	SE	0777520	2840073	030	20	SE
0777907	2841193	016	11	ESE	0777346	2839994	010	32	E

UTM Zone 42N		Strike	Dip	Dip Direction	UTM Zone 42N		Strike	Dip	Dip Direction
Eastings	Northings				Eastings	Northings			
0777841	2841186	036	18	SE	0777166	2839654	043	30	SE
0777887	2841109	079	15	S	0777006	2839665	013	17	E
0777798	2841121	055	11	SE	0777067	2839643	068	10	SE
0777921	2841076	030	16	SE	0777438	2839825	026	19	SE
0777904	2841055	040	14	SE	0777425	2840020	047	10	SE
0778056	2841064	041	15	SE	0777451	2839942	033	16	SE
0777866	2840892	038	15	SE	0777523	2839866	039	23	SE
0777705	2840905	022	08	SE	0777509	2840500	041	12	SE
0777815	2840789	036	21	SE	0777353	2840875	054	10	SE
0777749	2840556	070	20	SSE	0777713	2841053	068	22	SSE
0777749	2840556	020	16	SE	0778342	2841657	004	24	E
0777621	2840484	041	12	SE	0778342	2841657	015	23	E
0777595	2840575	020	15	SE	0778317	2841617	012	27	E
0777512	2840491	038	14	SE	0778185	2841533	018	12	E
0777709	2840318	048	17	SE	0778371	2841624	017	20	E
0777547	2840406	058	16	SE	0778354	2840948	035	32	SE

C2 Fault-plane measurements

UTM Zone 42N		Strike	Dip	Dip Direction	UTM Zone 42N		Strike	Dip	Dip Direction
Eastings	Northings				Eastings	Northings			
0778219	2841029	231	67	NW	0777968	2841905	251	76	N
0777957	2840837	066	64	SSE	0777968	2841905	273	43	N
0777914	2840717	194	60	W	0777956	2841894	274	50	N
0777860	2840800	252	63	S	0777956	2841894	270	45	N
0777863	2840864	068	42	SSE	0777956	2841894	265	60	N
0777900	2840991	270	63	N	0777947	2841883	282	49	N
0777900	2840991	257	39	N	0777947	2841883	276	62	N
0777871	2841013	228	65	NW	0777947	2841883	276	85	N
0777871	2841013	356	48	E	0777947	2841883	270	87	N
0777714	2840534	158	51	SW	0777947	2841883	272	61	N
0777385	2840761	230	61	NW	0777947	2841883	273	53	N
0777385	2840761	218	47	NW	0777947	2841883	100	80	S
0777232	2840853	230	62	NW	0777947	2841883	095	86	S
0776842	2839836	224	76	NW	0777934	2841864	261	60	N
0776842	2839836	200	80	W	0777917	2841860	267	61	N
0776842	2839836	209	82	W	0777917	2841860	257	56	N
0776807	2839848	196	67	W	0777917	2841860	238	56	NNW
0776789	2839848	263	44	N	0777917	2841860	251	68	N
0776789	2839848	268	49	N	0777881	2841825	276	59	N
0776789	2839848	164	50	W	0777881	2841825	266	61	N
0776743	2839779	221	38	NW	0777881	2841825	262	69	N
0776742	2839763	216	46	NW	0777866	2841806	031	85	SE
0776742	2839763	207	43	NW	0777818	2841740	252	56	N
0776779	2839796	038	86	SE	0777818	2841740	268	50	N
0776779	2839796	224	40	NE	0777836	2841720	221	68	NW
0776745	2839596	263	81	N	0777809	2841696	064	58	SE
0777338	2839957	181	36	W	0777809	2841696	274	60	N
0777026	2839631	254	40	NNW	0777809	2841696	232	70	NW
0777395	2839836	229	78	NW	0777813	2841677	266	66	N
0777395	2839836	232	84	NW	0777813	2841677	258	45	N

UTM Zone 42N		Strike	Dip	Dip Direction	UTM Zone 42N		Strike	Dip	Dip Direction
Eastings	Northings				Eastings	Northings			
0777897	2840598	296	66	N	0778053	2841660	231	62	NW
0777897	2840598	166	78	W	0778053	2841660	225	33	NW
0777842	2840575	135	67	SW	0778051	2841679	255	78	NNW
0777792	2840505	264	52	N	0778051	2841679	082	58	S
0777792	2840505	088	64	S	0778051	2841679	101	82	S
0777674	2840342	286	72	N	0778112	2841813	043	57	SE
0777674	2840342	297	60	NNE	0778112	2841813	066	56	SE
0777720	2840314	299	67	N	0778121	2841840	231	62	NW
0777688	2840297	173	89	W	0778121	2841840	263	84	N
0777439	2840371	266	51	N	0778121	2841840	084	80	S
0777504	2840479	307	74	NNE	0778131	2841884	262	48	N
0777470	2840786	240	78	NW	0778131	2841884	157	82	SW
0777495	2840810	238	77	NW	0778156	2841942	252	56	NW
0777495	2840810	122	88	S	0777638	2841528	287	70	N
0777408	2840869	117	72	W	0777609	2841448	243	62	NW
0777408	2840869	244	63	NW	0777609	2841448	236	55	NW
0777408	2840869	105	66	S	0777609	2841448	265	58	N
0777416	2840946	253	62	NNW	0777613	2841416	246	48	N
0777807	2841045	249	48	N	0777613	2841416	267	34	N
0777766	2841078	245	67	NW	0777576	2841381	224	42	NW
0777629	2841142	030	75	ESE	0777580	2841365	312	82	NE
0777639	2841164	027	78	ESE	0777580	2841357	256	83	N
0777611	2841092	160	57	SW	0777567	2841257	269	54	N
0777586	2841064	180	20	W	0777578	2841229	265	48	N
0777586	2841064	180	32	W	0777534	2841220	145	47	SW
0777783	2841288	164	86	W	0777460	2841213	156	60	SW
0777789	2841283	206	68	NW	0777375	2841222	064	47	S
0777789	2841283	328	78	NNE	0777362	2841212	256	43	NW
0777812	2841386	043	65	SE	0777345	2841203	252	70	NW
0777812	2841386	086	69	S	0777325	2841110	248	47	N
0777812	2841386	174	28	W	0777312	2841072	277	48	N
0777866	2841423	159	82	W	0777200	2840916	120	80	SW
0777866	2841423	218	74	NW	0777233	2840848	245	74	NW
0777866	2841423	226	76	NW	0777233	2840848	217	40	NW
0777866	2841423	111	78	S	0777233	2840848	254	53	NW
0777930	2841468	263	64	N	0777289	2840934	108	62	S
0777942	2841491	266	76	N	0777296	2840990	248	46	NW
0777928	2841532	030	62	SE	0777296	2840990	244	47	NW
0778085	2841510	211	52	NE	0777296	2840990	221	78	NW
0778090	2841447	305	84	NNW	0777492	2840949	052	75	SE
0778090	2841447	100	82	SSW	0777526	2840942	240	67	NW
0778069	2841413	255	48	N	0777526	2840942	238	57	NW
0777994	2841414	018	82	E	0777526	2840942	262	79	N
0777994	2841414	039	66	SE	0777526	2840942	257	80	NE
0777994	2841414	073	67	SE	0777485	2840910	221	51	NW
0777994	2841414	308	80	NE	0777485	2840910	206	40	NW
0777994	2841414	120	78	SW	0777567	2840520	185	42	W
0777914	2841316	155	35	SW	0777716	2840542	150	56	SW
0778072	2841072	197	89	W	0777796	2840617	127	62	SW
0777961	2840989	252	52	NW	0777893	2841573	114	75	SW

UTM Zone 42N		Strike	Dip	Dip Direction	UTM Zone 42N		Strike	Dip	Dip Direction
Eastings	Northings				Eastings	Northings			
0778844	2841937	258	32	N	0777831	2841505	144	44	SW
0778688	2841892	174	76	W	0777825	2841493	174	46	W
0778703	2841797	207	42	NW	0777930	2841465	263	61	N
0778616	2841932	267	62	NW	0777903	2841455	257	59	N
0778597	2841927	225	36	NW	0777903	2841455	268	59	N
0778589	2842030	237	59	NW	0777881	2841448	138	46	SW
0778589	2842030	178	86	W	0777881	2841448	257	68	N
0778589	2842030	176	81	W	0777881	2841448	280	49	N
0778589	2842030	359	81	E	0777881	2841448	215	75	NW
0778600	2842034	230	25	NW	0777829	2841382	180	28	W
0778600	2842034	233	28	NW	0777829	2841382	176	36	W
0778600	2842034	247	52	NW	0777829	2841382	174	32	W
0778600	2842034	243	25	NW	0777829	2841382	164	25	SW
0778600	2842034	238	71	NW	0777832	2841390	108	80	S
0778600	2842034	255	40	N	0777832	2841390	167	72	W
0778600	2842034	242	84	NW	0777819	2841385	038	63	SE
0778600	2842034	246	38	NW	0777819	2841385	046	62	SE
0778600	2842034	231	30	NW	0777819	2841385	044	60	SE
0778602	2842063	277	76	N	0777819	2841385	037	51	SE
0778602	2842063	256	71	N	0777702	2841393	258	48	NNE
0778602	2842063	270	64	N	0777702	2841393	238	56	NW
0778602	2842063	277	71	N	0777646	2841371	256	53	N
0778602	2842063	267	76	N	0777646	2841371	259	66	N
0778602	2842063	278	75	N	0777762	2841442	278	77	N
0778602	2842063	272	78	N	0777761	2841480	233	62	NW
0778602	2842063	271	78	N	0777773	2841554	266	50	N
0778602	2842063	280	58	N	0777786	2841557	269	57	N
0778602	2842063	286	69	N	0777785	2841584	144	50	SW
0778751	2841944	178	47	W	0777785	2841584	138	46	SW
0778869	2841919	241	50	N	0777779	2841592	143	51	SW
0778457	2841675	125	76	SW	0777783	2841613	129	79	SW
0778457	2841675	180	72	W	0777798	2841627	134	78	SW
0778396	2841741	163	62	SW	0777798	2841627	306	69	NE
0778396	2841741	165	60	W	0777798	2841631	197	71	W
0778414	2841775	207	58	NW	0777975	2841748	271	71	N
0778414	2841775	211	60	NW	0778049	2841765	220	42	NW
0778414	2841775	160	84	W	0778049	2841765	223	48	NW
0777959	2841617	260	43	N	0778049	2841765	237	52	NW
0777959	2841617	276	51	N	0778071	2841756	041	50	SE
0777959	2841617	268	89	N	0778057	2841741	051	50	SE
0778003	2841662	093	72	S	0778058	2841763	035	62	SE
0777997	2841661	068	76	SE	0778058	2841763	238	55	NW
0777950	2841622	049	64	SE	0778047	2841748	034	57	SE
0777827	2841633	228	68	NW	0778028	2841693	275	59	N
0777827	2841633	078	89	S	0778081	2841838	275	66	N
0777827	2841633	341	76	E	0778081	2841838	076	85	S
0777830	2841694	086	68	S	0778081	2841838	076	85	S
0777830	2841694	268	89	N	0778081	2841838	276	55	N
0777846	2841697	086	71	S	0778083	2841848	290	38	N
0777854	2841694	081	83	S	0778060	2841871	215	63	NW

UTM Zone 42N		Strike	Dip	Dip Direction	UTM Zone 42N		Strike	Dip	Dip Direction
Eastings	Northings				Eastings	Northings			
0777894	2841712	254	48	NW	0778111	2841963	262	46	N
0777894	2841712	231	64	NW	0778145	2842004	241	68	N
0777898	2841744	240	56	NW	0778147	2842010	230	35	NW
0778577	2842114	350	87	E	0778062	2841961	268	56	N
0778576	2842078	236	57	NW	0778297	2842497	244	58	N
0778579	2842076	206	40	NW	0777718	2840508	243	60	NW
0778593	2842070	260	77	N	0777695	2840498	242	73	NW
0778593	2842070	266	76	N	0777695	2840498	266	55	N
0778593	2842070	065	57	E	0777855	2840801	068	70	S
0778533	2841860	168	47	W	0777856	2840867	061	49	SE
0778526	2841859	264	46	N	0777787	2840977	220	61	NW
0778502	2841853	164	86	W	0777940	2840974	241	55	NW
0778502	2841853	289	53	N	0777959	2840988	270	69	N
0778502	2841853	236	35	NNW	0777959	2840988	232	52	NW
0778549	2841819	166	82	W	0778227	2841044	226	64	NW
0778504	2841807	294	69	N	0778669	2841873	129	48	SW
0778504	2841807	329	79	NE	0778398	2841346	215	55	W
0778504	2841807	164	70	W	0778210	2841573	221	40	NW
0778510	2841783	168	87	W	0778210	2841573	205	42	NW
0778537	2841774	246	50	N	0778489	2841843	298	61	N
0778505	2841760	165	81	W	0778489	2841843	294	46	N
0778496	2841764	318	25	NE	0778489	2841843	104	85	S
0778486	2841765	157	67	SW	0778489	2841843	292	61	NNW
0778486	2841765	154	49	SW	0778489	2841843	090	80	S
0778266	2842072	244	53	N	0778082	2841556	248	83	NW
0778208	2841985	254	47	NW	0778082	2841556	269	53	N
0778208	2841985	267	62	N	0777838	2841423	048	74	SE
0778181	2842031	268	70	N	0777838	2841423	038	58	SE
0778181	2842031	276	48	N	0777838	2841423	184	59	W
0778181	2842031	248	48	N	0777740	2841264	223	77	NW
0778137	2842024	269	58	N	0777740	2841264	304	71	NE
0778080	2842011	259	39	N	0777740	2841264	120	87	SW
0778080	2842011	271	60	N	0777740	2841264	223	72	NW
0777968	2841905	287	40	N	0777740	2841264	308	61	NE
0777914	2841317	143	56	SW	0777740	2841264	327	61	NE
0777914	2841317	127	49	SW	0777710	2841229	211	79	NW
0777914	2841317	127	39	SW	0777710	2841229	131	88	SE
0777914	2841317	162	52	W	0777710	2841229	138	87	SE
0777914	2841317	147	48	SW					

C3 Extensional fracture plane measurements

UTM Zone 42N		Strike	Dip	Dip Direction	UTM Zone 42N		Strike	Dip	Dip Direction
Eastings	Northings				Eastings	Northings			
0777419	2841122	235	81	NW	0778504	2841807	294	64	N
0777419	2841122	210	84	NW	0778504	2841807	220	71	NW
0777441	2841038	170	85	W	0778504	2841807	215	77	NW

UTM Zone 42N		Strike	Dip	Dip Direction	UTM Zone 42N		Strike	Dip	Dip Direction
Eastings	Northings				Eastings	Northings			
0777441	2841038	173	70	W	0778504	2841807	078	80	S
0777347	2841053	197	72	W	0778537	2841774	142	87	SW
0777759	2841340	114	84	W	0778537	2841774	140	83	SW
0778229	2841271	192	60	W	0778537	2841774	154	64	SW
0778229	2841271	201	84	W	0778537	2841774	074	76	SSE
0778349	2841309	174	53	W	0778496	2841764	170	78	W
0777676	2840449	307	69	NE	0778496	2841764	347	90	
0777676	2840449	187	72	W	0778496	2841764	206	69	W
0777676	2840449	240	75	NW	0778486	2841765	179	66	W
0777635	2840383	278	68	N	0778486	2841765	112	80	S
0777635	2840383	194	66	W	0778486	2841765	169	70	W
0777674	2840342	296	86	NNE	0778266	2842072	054	60	SE
0777674	2840342	188	70	W	0778208	2841985	288	62	N
0777688	2840297	192	67	W	0778208	2841985	151	72	SW
0777688	2840297	167	76	SW	0778208	2841985	092	72	S
0777688	2840297	188	77	W	0778190	2842005	155	51	SW
0777555	2840214	188	57	W	0778190	2842005	258	74	NNW
0777555	2840214	177	60	W	0778190	2842005	150	57	SW
0777478	2840438	300	62	NE	0778038	2841974	157	86	W
0777478	2840438	298	68	NNE	0778038	2841974	165	89	W
0777478	2840438	137	67	SW	0778038	2841974	320	76	NE
0777474	2840852	086	56	S	0778038	2841974	011	82	E
0777724	2841071	177	80	W	0778038	2841974	079	73	S
0777599	2841023	156	69	SW	0778038	2841974	328	78	NE
0777599	2841023	152	78	SW	0777934	2841864	341	80	ENE
0777789	2841283	003	80	E	0777934	2841864	340	86	E
0777812	2841386	046	52	SE	0777934	2841864	087	46	S
0777812	2841386	034	48	SE	0777934	2841864	146	74	SW
0777812	2841386	195	43	W	0777934	2841864	106	80	SW
0777930	2841468	106	90		0777934	2841864	207	81	NW
0778085	2841510	201	84	W	0777894	2841847	345	83	NE
0777994	2841414	358	73	E	0777894	2841847	334	55	NE
0777994	2841414	331	70	NE	0777894	2841847	269	71	N
0777994	2841414	121	88	NE	0777894	2841847	345	76	NE
0777904	2841295	124	74	SW	0777894	2841847	031	78	SE
0777904	2841295	131	55	SW	0777894	2841847	328	83	NE
0778016	2841077	203	76	W	0777894	2841847	051	80	SE
0778016	2841077	190	84	W	0777881	2841825	266	75	N
0778016	2841077	214	66	NW	0777866	2841806	333	70	NE
0778016	2841077	192	78	W	0777866	2841806	340	75	ENE
0778844	2841937	172	84	W	0777866	2841806	347	78	ENE
0778721	2841769	163	78	W	0777866	2841806	047	66	SE
0778721	2841769	145	78	SW	0777866	2841806	026	83	SE
0778721	2841769	144	80	SW	0777866	2841806	188	80	W
0778616	2841932	158	73	SW	0777866	2841806	066	50	SE
0778616	2841932	162	82	SW	0778051	2841679	335	71	NE
0778616	2841932	162	76	SW	0778051	2841679	114	65	SW
0778593	2841969	158	63	SW	0778051	2841679	010	88	E
0778593	2841969	159	65	SW	0778051	2841679	351	81	W
0778593	2841969	110	49	S	0778095	2841773	066	59	SE

UTM Zone 42N		Strike	Dip	Dip Direction	UTM Zone 42N		Strike	Dip	Dip Direction
Eastings	Northings				Eastings	Northings			
0778589	2842030	171	72	W	0778095	2841773	333	64	NE
0778589	2842030	203	78	NW	0778095	2841773	316	88	NE
0778589	2842030	026	62	ESE	0778095	2841773	060	85	SE
0778589	2842030	180	89	W	0778095	2841773	240	85	NW
0778589	2842030	031	80	NW	0778103	2841791	241	59	NW
0778589	2842030	035	58	SE	0778103	2841791	235	67	NW
0778589	2842030	054	69	SE	0778103	2841791	236	71	NW
0778754	2842018	253	83	NW	0778103	2841791	142	84	SW
0778754	2842018	250	84	NW	0778114	2841858	156	87	W
0778754	2842018	064	89	SE	0778114	2841858	349	82	NE
0778754	2842018	171	83	W	0778114	2841858	345	75	NE
0778754	2842018	064	80	SE	0778131	2841884	340	88	E
0778754	2842018	084	75	S	0778131	2841884	350	83	E
0778869	2841919	157	85	WSW	0778156	2841942	240	75	NW
0778869	2841919	209	50	WNW	0777613	2841416	356	64	E
0778869	2841919	166	80	SW	0777613	2841416	006	80	E
0778869	2841919	196	57	W	0777580	2841357	182	85	W
0778869	2841919	072	67	SE	0777570	2841291	360	77	E
0778869	2841919	258	80	N	0777570	2841291	211	65	NW
0778869	2841919	338	70	NE	0777570	2841291	314	85	NE
0778869	2841919	232	67	NW	0777570	2841291	299	81	NE
0778869	2841919	258	82	NW	0777578	2841229	189	86	W
0778869	2841919	161	65	SW	0777578	2841229	324	67	NE
0778869	2841919	167	76	SW	0777578	2841229	186	86	W
0778869	2841919	175	71	W	0777578	2841229	184	89	W
0778457	2841675	159	82	SW	0777499	2841211	329	77	NE
0778457	2841675	162	63	SW	0777499	2841211	146	78	SW
0778457	2841675	329	90		0777499	2841211	325	90	
0778396	2841741	168	86	W	0777499	2841211	343	90	
0778396	2841741	356	76	E	0777499	2841211	160	77	SW
0778396	2841741	164	85	W	0777460	2841213	162	40	SW
0778317	2841617	339	89	NE	0777460	2841213	246	83	N
0778317	2841617	180	83	W	0777460	2841213	160	61	WSW
0777959	2841617	214	88	W	0777460	2841213	074	86	S
0777959	2841617	222	88	NW	0777410	2841233	173	60	WSW
0777959	2841617	221	75	NW	0777410	2841233	178	65	W
0777959	2841617	269	84	N	0777410	2841233	170	65	W
0777959	2841617	086	74	S	0777375	2841222	173	83	W
0777959	2841617	053	80	SE	0777375	2841222	136	72	SW
0777959	2841617	212	72	NW	0777375	2841222	160	87	SW
0777959	2841617	275	80	N	0777375	2841222	352	88	E
0778005	2841614	344	68	NE	0777319	2841096	253	78	N
0778005	2841614	063	83	NW	0777319	2841096	121	85	SW
0778005	2841614	096	79	S	0777180	2840920	022	85	E
0778005	2841614	342	68	E	0777180	2840920	030	75	SE
0778054	2841580	005	68	E	0777180	2840920	028	82	SE
0778054	2841580	015	66	E	0777180	2840920	207	87	W
0778054	2841580	173	61	W	0777180	2840920	036	79	SE
0778054	2841580	017	69	E	0777180	2840920	199	86	W
0778054	2841580	085	70	S	0777173	2840884	211	64	NW

UTM Zone 42N		Strike	Dip	Dip Direction	UTM Zone 42N		Strike	Dip	Dip Direction
Eastings	Northings				Eastings	Northings			
0778054	2841580	131	54	SW	0777173	2840884	189	61	W
0778063	2841583	319	85	NE	0777173	2840884	246	80	NW
0778063	2841583	340	85	NE	0777173	2840884	232	84	NW
0778063	2841583	262	72	N	0777173	2840884	067	82	SE
0778063	2841583	064	58	S	0777173	2840884	207	73	WNW
0778018	2841557	312	67	NE	0777620	2840490	152	86	W
0778018	2841557	168	71	W	0777620	2840490	199	63	NW
0778018	2841557	167	90		0777620	2840490	150	85	SW
0778018	2841557	098	62	S	0777620	2840490	196	43	W
0777997	2841541	261	80	N	0777620	2840490	140	90	
0777997	2841541	016	82	E	0777664	2840519	317	89	NE
0777997	2841541	134	74	SW	0777664	2840519	213	65	NW
0777997	2841541	200	72	W	0777664	2840519	318	82	NE
0777997	2841541	354	80	E	0777664	2840519	236	64	NW
0777997	2841541	008	78	E	0777893	2841573	126	82	SW
0777997	2841541	358	77	E	0777893	2841573	139	87	SW
0777997	2841541	091	72	S	0777893	2841573	318	83	NE
0777974	2841541	224	71	NW	0777893	2841573	167	88	W
0777974	2841541	336	90		0777827	2841395	049	52	SE
0777974	2841541	308	84	NE	0777827	2841395	026	50	SE
0777974	2841541	120	89	SW	0777827	2841395	026	57	SE
0777974	2841541	301	78	NE	0777724	2841381	164	88	W
0778003	2841662	156	87	E	0777724	2841381	336	87	E
0778003	2841662	037	64	SE	0777724	2841381	138	78	SW
0778003	2841662	163	80	W	0777724	2841381	014	83	E
0777950	2841622	308	88	NE	0777765	2841262	051	84	SE
0777950	2841622	137	82	SW	0777765	2841262	174	80	W
0777950	2841622	308	88	NE	0777765	2841262	252	83	W
0777950	2841622	106	70	S	0777765	2841262	033	77	SE
0777827	2841633	147	86	SW	0777765	2841262	030	67	SE
0777827	2841633	211	77	NW	0777765	2841262	154	87	W
0777827	2841633	156	84	NE	0777783	2841613	151	87	WSW
0777827	2841633	342	82	E	0777783	2841613	119	78	SW
0777827	2841633	221	71	NW	0777783	2841613	325	86	NE
0777830	2841682	084	62	S	0777783	2841613	160	86	WSW
0777830	2841682	016	76	ESE	0777783	2841613	138	89	SW
0777830	2841682	282	79	N	0777783	2841613	136	72	SW
0777830	2841682	009	82	E	0777798	2841627	129	73	SW
0777830	2841682	001	81	E	0777798	2841627	110	64	S
0777830	2841682	346	86	NE	0777798	2841627	103	73	S
0777830	2841682	161	83	SW	0777798	2841631	101	77	S
0777854	2841694	188	89	W	0777798	2841631	107	62	S
0777854	2841694	032	87	E	0777798	2841631	116	58	SW
0777854	2841694	018	70	ESE	0777798	2841631	285	82	N
0777898	2841744	164	89	SW	0777798	2841631	278	82	N
0777898	2841744	017	89	SE	0777798	2841631	101	79	S
0777898	2841744	024	86	SE	0777798	2841631	100	82	S
0777898	2841744	166	82	W	0777798	2841631	120	68	SW
0777937	2841770	348	81	E	0777798	2841631	127	37	SE
0777937	2841770	348	82	E	0777798	2841631	278	56	N

UTM Zone 42N		Strike	Dip	Dip Direction	UTM Zone 42N		Strike	Dip	Dip Direction
Eastings	Northings				Eastings	Northings			
0777937	2841770	160	89	W	0778111	2841950	351	87	E
0777937	2841770	168	88	W	0778111	2841950	169	85	W
0777937	2841770	341	81	E	0778111	2841950	340	83	E
0778646	2842242	291	80	N	0778111	2841950	201	70	NW
0778646	2842242	216	70	NW	0778111	2841950	348	86	NE
0778646	2842242	086	77	S	0778118	2841010	201	78	W
0778577	2842114	176	73	W	0778118	2841010	184	85	W
0778577	2842114	172	82	W	0778118	2841010	199	77	W
0778577	2842114	165	81	W	0778118	2841010	198	83	W
0778577	2842114	223	84	NW	0778258	2841047	223	63	NW
0778577	2842114	054	80	SE	0778258	2841047	207	49	W
0778577	2842114	242	45	NW	0778258	2841047	245	78	NW
0778577	2842114	168	83	W	0778258	2841047	200	70	W
0778577	2842114	173	86	W	0778572	2841687	156	69	SW
0778577	2842114	259	62	N	0778572	2841687	166	78	SW
0778577	2842114	040	84	SE	0778572	2841687	143	83	SW
0778576	2842078	229	78	NW	0778572	2841687	333	85	NE
0778576	2842078	327	62	NE	0778572	2841687	143	82	SW
0778576	2842078	218	70	NW	0778572	2841687	143	68	SW
0778576	2842078	221	63	NW	0778398	2841346	213	48	W
0778593	2842070	173	82	W	0778398	2841346	190	60	W
0778593	2842070	160	73	W	0778398	2841346	218	48	W
0778533	2841860	177	52	W	0778264	2841153	356	87	E
0778533	2841860	193	54	W	0778264	2841153	191	81	W
0778502	2841853	179	77	W	0778264	2841153	167	82	W
0778502	2841853	266	57	N	0778238	2841127	182	73	W
0778502	2841853	176	81	W	0778238	2841127	189	71	W
0778502	2841853	251	72	N	0778238	2841127	179	83	W
0778502	2841853	172	71	W	0778238	2841127	171	80	W
0778516	2841824	051	80	SE	0778238	2841127	168	84	W
0778516	2841824	295	73	NE	0778228	2841118	276	87	N
0778516	2841824	286	72	N	0778228	2841118	194	74	W
0778516	2841824	164	73	W	0778228	2841118	178	82	W
0778516	2841824	260	62	N	0778489	2841843	174	60	W
0778516	2841824	274	68	N	0778489	2841843	186	58	W
0778504	2841807	215	77	NW	0778489	2841843	172	65	W
0777982	2841452	026	70	SE	0778489	2841843	182	68	W
0777982	2841452	209	76	SW	0778489	2841843	178	64	W

C4 Fault-plane slickenline measurements

Eastings	Northings	Fault Plane			Pitch (from strike)	Lineation		Slip-Sense
		Strike	Dip	Dip Direction		Plunge	Trend	
0776789	2839848	268	49	N	080	48	343	Normal
0776789	2839848	164	50	W	102	48	272	Normal
0776742	2839763	207	43	NW	103	42	315	Normal
0776779	2839796	038	86	SE	093	85	158	Normal

Eastings	Northings	Fault Plane			Pitch (from strike)	Lineation		Slip-Sense
		Strike	Dip	Dip Direction		Plunge	Trend Strike	
0776779	2839796	224	40	NE	082	40	303	Normal
0777338	2839957	181	36	W	072	35	260	Normal
0777395	2839836	229	78	NW	082	75	284	Normal
0777395	2839836	232	84	NW	076	74	254	Normal
0777897	2840598	296	66	N	069	58	343	Normal
0777897	2840598	166	78	W	092	78	268	Normal
0777792	2840505	088	64	S	097	63	195	Normal
0777674	2840342	286	72	N	073	65	332	Normal
0777674	2840342	297	60	NNE	073	56	356	Normal
0777720	2840314	299	67	N	072	61	351	Normal
0777688	2840297	173	89	W	083	83	184	Normal
0777439	2840371	266	51	N	086	50	348	Normal
0777495	2840810	122	88	S	106	74	294	Normal
0777408	2840869	244	63	NW	083	62	318	Normal
0777408	2840869	105	66	S	104	62	229	Normal
0777416	2840946	253	62	NNW	075	59	314	Normal
0777766	2841078	245	67	NW	084	66	322	Normal
0777724	2841071	247	77	N	104	72	022	Normal
0777586	2841064	180	32	W	112	30	295	Normal
0777783	2841288	164	86	W	096	83	308	Normal
0777789	2841283	206	68	NW	110	59	339	Normal
0777789	2841283	328	78	NNE	094	77	075	Normal
0777812	2841386	086	69	S	136	40	247	Normal
0777812	2841386	174	28	W	095	27	269	Normal
0777866	2841423	159	82	W	150	29	335	Normal
0777866	2841423	226	76	NW	084	74	291	Normal
0777866	2841423	111	78	S	119	54	272	Normal
0777942	2841491	266	76	N	046	44	380	Normal
0777928	2841532	030	62	SE	093	52	125	Normal
0778069	2841413	255	48	N	077	46	325	Normal
0777994	2841414	039	66	SE	087	66	121	Normal
0777914	2841316	155	35	SW	098	35	255	Normal
0778072	2841072	197	89	W	076	76	203	Normal
0777961	2840989	252	52	NW	098	52	355	Normal
0778844	2841937	258	32	N	078	31	334	Normal
0778688	2841892	174	76	W	098	74	294	Normal
0778703	2841797	207	42	NW	099	42	309	Normal
0778616	2841932	267	62	NW	072	57	322	Normal
0778597	2841927	225	36	NW	085	36	308	Normal
0778589	2842030	237	59	NW	079	58	306	Normal
0778589	2842030	178	86	W	109	71	346	Normal
0778589	2842030	176	81	W	108	70	329	Normal
0778589	2842030	359	81	E	030	29	004	Normal
0778600	2842034	230	25	NW	096	25	326	Normal
0778600	2842034	233	28	NW	097	28	330	Normal
0778600	2842034	247	52	NW	071	48	308	Normal
0778600	2842034	243	25	NW	094	25	337	Normal
0778600	2842034	238	71	NW	082	70	301	Normal
0778600	2842034	255	40	N	083	41	335	Normal
0778600	2842034	242	84	NW	083	81	283	Normal

Eastings	Northings	Fault Plane			Pitch (from strike)	Lineation		Slip-Sense
		Strike	Dip	Dip Direction		Plunge	Trend Strike	
0778600	2842034	246	38	NW	089	39	334	Normal
0778600	2842034	231	30	NW	087	31	317	Normal
0778602	2842063	277	76	N	061	58	301	Normal
0778602	2842063	256	71	N	053	59	280	Normal
0778602	2842063	270	64	N	060	52	308	Normal
0778602	2842063	277	71	N	074	66	326	Normal
0778602	2842063	267	76	N	074	69	307	Normal
0778602	2842063	278	75	N	062	60	301	Normal
0778602	2842063	272	78	N	050	48	286	Normal
0778602	2842063	271	78	N	067	64	299	Normal
0778602	2842063	280	58	N	059	46	321	Normal
0778602	2842063	286	69	N	050	46	310	Normal
0778751	2841944	178	47	W	121	38	310	Normal
0778869	2841919	241	50	N	071	50	318	Normal
0778457	2841675	125	76	SW	116	60	280	Normal
0778396	2841741	165	60	W	127	44	311	Normal
0777959	2841617	260	43	N	099	43	003	Normal
0777959	2841617	276	51	N	073	49	340	Normal
0777959	2841617	268	89	N	081	81	276	Normal
0778018	2841557	357	86	E	168	12	176	Normal
0778003	2841662	093	72	S	098	71	208	Thrust???
0778003	2841662	093	72	S	114	60	239	Normal
0777827	2841633	228	68	NW	071	61	275	Normal
0777827	2841633	078	89	S	081	81	082	Normal
0777827	2841633	341	76	E	070	66	013	Normal
0777830	2841694	086	68	S	084	67	159	Normal
0777830	2841694	268	89	N	080	80	277	Normal
0777846	2841697	086	71	S	104	66	215	Normal
0777854	2841694	081	83	S	101	78	232	Normal
0777894	2841712	231	64	NW	087	64	315	Normal
0777898	2841744	240	56	NW	077	55	309	Normal
0778577	2842114	350	87	E	053	53	355	Normal
0778579	2842076	206	40	NW	120	34	333	Normal
0778593	2842070	260	77	N	071	67	294	Normal
0778593	2842070	266	76	N	073	68	306	Normal
0778533	2841860	168	47	W	105	45	280	Normal
0778526	2841859	264	46	N	087	46	350	Normal
0778502	2841853	164	86	W	120	60	337	Normal
0778502	2841853	289	53	N	061	45	336	Normal
0778502	2841853	236	35	NNW	097	35	335	Normal
0778549	2841819	166	82	W	126	53	335	Normal
0778504	2841807	294	69	N	066	58	334	Normal
0778504	2841807	329	79	NE	067	65	352	Normal
0778504	2841807	164	70	W	111	62	303	Normal
0778510	2841783	168	87	W	119	60	342	Normal
0778505	2841760	165	81	W	134	45	335	Normal
0778496	2841764	318	25	NE	024	10	340	Normal
0778486	2841765	157	67	SW	141	35	320	Normal
0778486	2841765	154	49	SW	115	42	280	Normal
0778208	2841985	254	47	NW	088	47	341	Normal

Eastings	Northings	Fault Plane			Pitch (from strike)	Lineation		Slip-Sense
		Strike	Dip	Dip Direction		Plunge	Trend Strike	
0778208	2841985	267	62	N	080	60	337	Normal
0778181	2842031	276	48	N	055	38	320	Normal
0778181	2842031	248	48	N	071	45	311	Normal
0778137	2842024	269	58	N	071	54	326	Normal
0778080	2842011	259	39	N	076	38	331	Normal
0778080	2842011	271	60	N	071	55	327	Normal
0777968	2841905	251	76	N	081	73	310	Normal
0777968	2841905	273	43	N	072	40	339	Normal
0777956	2841894	274	50	N	078	49	346	Normal
0777956	2841894	270	45	N	072	42	336	Normal
0777947	2841883	282	49	N	077	48	353	Normal
0777947	2841883	276	85	N	073	72	293	Normal
0777947	2841883	270	87	N	070	70	280	Normal
0777947	2841883	272	61	N	077	58	336	Normal
0777947	2841883	273	53	N	082	52	351	Normal
0777947	2841883	095	86	S	089	86	177	Normal
0777934	2841864	261	60	N	078	58	329	Normal
0777917	2841860	267	61	N	082	60	341	Normal
0777917	2841860	257	56	N	080	54	331	Normal
0777917	2841860	238	56	NNW	099	55	344	Normal
0777917	2841860	251	68	N	088	68	336	Normal
0777881	2841825	276	59	N	094	59	013	Normal
0777881	2841825	266	61	N	082	60	341	Normal
0777866	2841806	031	85	SE	071	70	044	Normal
0777818	2841740	268	50	N	078	49	340	Normal
0777836	2841720	221	68	NW	103	64	344	Normal
0777809	2841696	064	58	SE	098	57	168	Normal
0777809	2841696	274	60	N	094	60	011	Normal
0777809	2841696	232	70	NW	082	68	301	Normal
0777813	2841677	258	45	N	092	45	350	Normal
0778053	2841660	225	33	NW	094	33	320	Normal
0778051	2841679	255	78	NNW	079	74	303	Normal
0778051	2841679	082	58	S	112	56	194	Normal
0778051	2841679	101	82	S	097	79	235	Normal
0778112	2841813	066	56	SE	066	49	117	Normal
0778121	2841840	263	84	N	076	75	285	Normal
0778121	2841840	084	80	S	130	49	253	Normal
0778131	2841884	262	48	N	069	44	322	Normal
0778131	2841884	157	82	SW	140	40	331	Normal
0777609	2841448	243	62	NW	073	58	300	Normal
0777609	2841448	236	55	NW	078	53	306	Normal
0777609	2841448	265	58	N	070	52	320	Normal
0777613	2841416	246	48	N	063	42	298	Normal
0777613	2841416	267	34	N	060	29	322	Normal
0777576	2841381	224	42	NW	107	40	336	Normal
0777580	2841357	256	83	N	080	78	290	Normal
0777567	2841257	269	54	N	090	54	358	Normal
0777578	2841229	265	48	N	084	48	345	Normal
0777534	2841220	145	47	SW	106	41	271	Normal
0777375	2841222	064	47	S	101	46	170	Normal

Eastings	Northings	Fault Plane			Pitch (from strike)	Lineation		Slip-Sense
		Strike	Dip	Dip Direction		Plunge	Trend Strike	
0777362	2841212	256	43	NW	092	43	349	Normal
0777325	2841110	248	47	N	077	46	319	Normal
0777233	2840848	217	40	NW	100	40	320	Normal
0777233	2840848	254	53	NW	071	50	315	Normal
0777289	2840934	108	62	S	108	58	234	Normal
0777296	2840990	248	46	NW	083	46	328	Normal
0777296	2840990	244	47	NW	080	47	320	Normal
0777296	2840990	221	78	NW	094	78	330	Normal
0777492	2840949	052	75	SE	118	58	206	Normal
0777526	2840942	240	67	NW	079	65	305	Normal
0777526	2840942	238	57	NW	067	51	291	Normal
0777526	2840942	262	79	N	061	59	282	Normal
0777526	2840942	257	80	NE	067	65	281	Normal
0777485	2840910	206	40	NW	094	40	302	Normal
0777893	2841573	114	75	SW	125	52	275	Normal
0777930	2841465	263	61	N	072	55	318	Normal
0777903	2841455	268	59	N	082	58	342	Normal
0777881	2841448	138	46	SW	119	39	267	Normal
0777881	2841448	257	68	N	086	68	338	Normal
0777881	2841448	280	49	N	056	38	324	Normal
0777881	2841448	215	75	NW	088	76	299	Normal
0777829	2841382	180	28	W	105	28	288	Normal
0777829	2841382	176	36	W	109	35	290	Normal
0777829	2841382	174	32	W	094	32	269	Normal
0777829	2841382	164	25	SW	107	24	273	Normal
0777832	2841390	167	72	W	023	22	174	Normal
0777819	2841385	038	63	SE	091	63	130	Normal
0777819	2841385	046	62	SE	097	61	149	Normal
0777819	2841385	044	60	SE	091	60	134	Normal
0777819	2841385	037	51	SE	100	50	140	Normal
0777702	2841393	258	48	NNE	087	48	344	Normal
0777702	2841393	238	56	NW	099	56	344	Normal
0777646	2841371	256	53	N	087	53	341	Normal
0777646	2841371	259	66	N	085	65	338	Normal
0777761	2841480	233	62	NW	083	61	310	Normal
0777786	2841557	269	57	N	077	54	336	Normal
0777785	2841584	144	50	SW	100	48	249	Normal
0777785	2841584	138	46	SW	100	45	242	Normal
0777779	2841592	143	51	SW	093	41	237	Normal
0777783	2841613	129	79	SW	097	77	252	Normal
0777798	2841627	134	78	SW	157	22	308	Normal
0777798	2841627	306	69	NE	060	54	339	Normal
0777798	2841631	197	71	W	080	68	260	Normal
0777894	2841712	254	48	NW	060	40	304	Normal
0778049	2841765	220	42	NW	089	42	309	Normal
0778049	2841765	223	48	NW	099	47	327	Normal
0778049	2841765	237	52	NW	083	52	316	Normal
0778057	2841741	051	50	SE	103	48	160	Normal
0778044	2841794	058	67	SE	108	60	189	Normal
0778081	2841838	275	66	N	087	66	359	Thrust??

Eastings	Northings	Fault Plane			Pitch (from strike)	Lineation		Slip-Sense
		Strike	Dip	Dip Direction		Plunge	Trend Strike	
0778081	2841838	076	85	S	128	52	250	Normal
0778081	2841838	076	85	S	099	80	227	Thrust??
0778081	2841838	276	55	N	088	56	002	Thrust??
0778111	2841963	262	46	N	083	46	343	Normal
0778147	2842010	230	35	NW	109	33	343	Normal
0778297	2842497	244	58	N	095	58	344	Normal
0777718	2840508	243	60	NW	069	53	296	Normal
0777695	2840498	266	55	N	069	49	321	Normal
0777959	2840988	270	69	N	039	36	287	Normal
0777959	2840988	232	52	NW	055	40	274	Normal
0778227	2841044	226	64	NW	093	63	323	Normal
0778210	2841573	221	40	NW	083	39	301	Normal
0778210	2841573	205	42	NW	081	42	283	Normal
0778489	2841843	298	61	N	066	52	345	Normal
0778489	2841843	294	46	N	069	41	355	Normal
0778489	2841843	104	85	S	114	66	273	Normal
0778489	2841843	292	61	NNW	064	51	337	Normal
0778489	2841843	090	80	S	132	47	259	Normal
0778082	2841556	248	83	NW	074	72	274	Normal
0777982	2841452	353	87	E	119	61	166	Normal
0777997	2841457	286	87	N	099	80	083	Normal
0777997	2841457	212	79	NW	083	77	268	Normal
0777914	2841317	143	56	SW	097	56	245	Normal
0777914	2841317	127	49	SW	109	45	245	Normal
0777914	2841317	127	39	SW	120	33	255	Normal
0777914	2841317	162	52	W	092	52	256	Normal
0777914	2841317	147	48	SW	100	47	253	Normal

Appendix D

Kaameshwari study area 100 m fault segment strike data

D1 Base Cretaceous (bC) horizon

Eastings	Northings	Fault Segment Strike	Eastings	Northings	Fault Segment Strike	Eastings	Northings	Fault Segment Strike
0775787	2815647	237	0773068	2817726	355	0766553	2827475	144
0775698	2815618	266	0773051	2817824	346	0766612	2827391	146
0775595	2815620	276	0773027	2817921	346	0766669	2827308	145
0775496	2815635	281	0773001	2818020	345	0766724	2827226	147
0775398	2815656	283	0772977	2818114	345	0766782	2827141	144
0775301	2815678	281	0772950	2818208	344	0766842	2827058	145
0775205	2815700	285	0772923	2818304	344	0766900	2826977	144
0775106	2815724	283	0772896	2818400	345	0766958	2826898	144
0775010	2815751	287	0772871	2818496	345	0767015	2826817	146
0774915	2815778	284	0772842	2818593	342	0767083	2826744	129
0774817	2815800	281	0772822	2818691	354	0767166	2826687	120
0774721	2815816	277	0772823	2818789	007	0767252	2826636	122
0774620	2815830	279	0772830	2818889	002	0767337	2826583	122
0774520	2815847	280	0772834	2818990	003	0767423	2826529	122
0774422	2815866	282	0772831	2819090	355	0767503	2826474	126
0774322	2815884	279	0772818	2819190	350	0767584	2826421	121
0774223	2815904	284	0772806	2819287	356	0767670	2826367	123
0774124	2815926	282	0772803	2819383	360	0767755	2826309	126
0774028	2815948	284	0772809	2819482	007	0767837	2826252	124
0773934	2815980	293	0772823	2819582	008	0767919	2826197	125
0773842	2816020	294	0772835	2819684	006	0768001	2826140	125
0773752	2816062	295	0772846	2819784	006	0768083	2826083	125
0773667	2816112	305	0772857	2819883	005	0768169	2826029	120
0773588	2816171	308	0772866	2819983	005	0768255	2825980	119
0773509	2816232	307	0772871	2820084	360	0768342	2825931	119
0773439	2816304	324	0772873	2820185	002	0768430	2825880	121
0773381	2816385	324	0772876	2820284	002	0768517	2825831	119
0773327	2816466	328	0772877	2820384	359	0768603	2825782	120
0773277	2816553	333	0772873	2820483	356	0768690	2825730	122
0773235	2816646	337	0772866	2820581	356	0768777	2825682	116
0773196	2816739	337	0772858	2820681	354	0768865	2825636	119
0773165	2816832	346	0772851	2820781	357	0768952	2825587	119
0773141	2816929	346	0772844	2820881	355	0769040	2825538	119
0773116	2817027	346	0772837	2820981	357	0769129	2825489	118
0773100	2817124	356	0772829	2821081	354	0769216	2825442	119
0773094	2817223	357	0772818	2821180	354	0769302	2825392	121
0773089	2817323	357	0772816	2821280	004	0769389	2825341	119
0773087	2817423	360	0772823	2821381	004	0769476	2825290	122
0773085	2817524	357	0772825	2821481	358	0769561	2825235	123
0773077	2817626	355	0772819	2821581	355	0769645	2825182	122

Eastings	Northings	Fault Segment Strike	Eastings	Northings	Fault Segment Strike	Eastings	Northings	Fault Segment Strike
0769730	2825130	121	0768184	2821881	164	0770672	2819067	202
0770495	2825748	169	0768209	2821784	167	0770636	2818974	200
0770495	2825650	190	0768229	2821685	169	0770602	2818881	201
0770476	2825551	192	0768252	2821584	166	0770550	2818796	221
0770458	2825455	188	0768274	2821486	169	0770481	2818720	223
0770436	2825359	198	0768288	2821392	174	0770413	2818649	224
0770401	2825264	203	0768292	2821295	181	0770339	2818584	233
0770363	2825172	202	0768290	2821193	181	0770259	2818526	234
0770320	2825082	209	0768288	2821092	182	0770178	2818471	237
0770267	2824998	215	0768284	2820992	183	0770094	2818419	240
0770209	2824917	216	0768280	2820892	182	0770006	2818365	237
0770138	2824849	237	0768276	2820792	183	0769924	2818311	237
0770055	2824794	236	0768272	2820692	182	0769844	2818251	230
0769970	2824742	241	0768267	2820592	184	0769766	2818185	228
0769890	2824686	229	0768263	2820490	181	0769690	2818120	231
0769816	2824621	228	0768263	2820390	180	0769623	2818047	215
0769743	2824554	228	0768263	2820291	179	0769571	2817964	209
0769674	2824479	218	0768266	2820192	178	0769547	2817870	181
0769613	2824399	218	0768269	2820094	178	0769546	2817769	181
0769550	2824321	219	0768271	2819994	179	0769520	2817678	211
0769487	2824241	218	0768270	2819893	183	0769465	2817596	216
0769427	2824163	217	0768263	2819793	185	0769406	2817513	215
0769369	2824082	215	0768253	2819693	185	0769347	2817430	216
0769309	2823999	217	0768242	2819593	187	0769288	2817352	219
0769248	2823916	216	0768231	2819494	186	0769232	2817272	211
0769190	2823834	215	0768218	2819395	189	0769183	2817185	208
0769133	2823753	215	0768202	2819296	189	0769136	2817096	208
0769075	2823672	216	0768185	2819196	190	0769097	2817004	198
0769012	2823596	223	0768168	2819098	189	0769105	2816911	152
0768941	2823527	229	0768166	2819002	175	0769151	2816821	153
0768867	2823462	228	0768179	2818902	171	0769189	2816728	163
0768794	2823395	228	0768194	2818802	171	0769220	2816634	161
0768719	2823327	228	0768210	2818704	171	0769251	2816539	163
0768645	2823260	228	0768225	2818605	172	0769282	2816442	162
0768569	2823192	229	0768240	2818505	171	0769309	2816347	166
0768491	2823127	231	0768259	2818407	167	0769332	2816250	169
0768411	2823069	237	0768283	2818310	165	0769351	2816153	169
0768328	2823014	235	0768309	2818213	165	0769364	2816058	175
0768246	2822955	233	0768334	2818115	166	0769367	2815957	182
0768173	2822886	220	0768359	2818019	165	0769362	2815856	185
0768108	2822809	221	0768394	2817929	153	0769349	2815755	190
0768049	2822730	213	0768441	2817840	151	0769331	2815657	191
0768010	2822642	195	0768490	2817750	152	0769312	2815560	191
0767994	2822549	184	0768536	2817661	153	0769293	2815460	191
0768003	2822456	166	0768586	2817578	145	0769274	2815361	190
0768035	2822359	157	0768644	2817495	145	0769255	2815263	192
0768072	2822266	159	0770799	2819415	194	0769236	2815164	191
0768105	2822171	162	0770777	2819346	200	0769228	2815066	177
0768134	2822073	165	0770742	2819254	202	0769232	2814968	179
0768159	2821977	166	0770707	2819161	199	0769229	2814868	184

Eastings	Northings	Fault Segment Strike	Eastings	Northings	Fault Segment Strike	Eastings	Northings	Fault Segment Strike
0769224	2814768	183	0769296	2811021	207	0773290	2812401	290
0769218	2814668	184	0769247	2810935	212	0773197	2812437	292
0769213	2814566	182	0769196	2810847	209	0773104	2812471	288
0769209	2814465	183	0769158	2810755	196	0773009	2812506	293
0769189	2814370	202	0769128	2810660	199	0772917	2812546	293
0769149	2814278	205	0769093	2810567	202	0772832	2812596	307
0769109	2814186	202	0769057	2810474	201	0772753	2812653	305
0769078	2814090	194	0769021	2810380	201	0772667	2812713	305
0769051	2813996	198	0768985	2810287	201	0772586	2812774	310
0769023	2813902	196	0768949	2810194	202	0772514	2812840	315
0768989	2813807	202	0768925	2810098	186	0772457	2812921	334
0768951	2813714	202	0768914	2809998	186	0772417	2813012	339
0768912	2813622	203	0768905	2809896	184	0772385	2813110	345
0768874	2813530	202	0768902	2809797	180	0772360	2813207	345
0768843	2813436	195	0768918	2809699	162	0772342	2813300	353
0768822	2813339	190	0768958	2809610	148	0772330	2813401	354
0768804	2813239	191	0769012	2809527	146	0772318	2813505	353
0768785	2813140	191	0769070	2809446	142	0772304	2813600	350
0768770	2813043	186	0769128	2809367	145	0772286	2813699	350
0768762	2812945	184	0769188	2809285	143	0772268	2813800	351
0768752	2812845	186	0769250	2809205	142	0772254	2813896	353
0768739	2812745	188	0769310	2809124	145	0772241	2813993	351
0768723	2812646	191	0769370	2809042	143	0772229	2814092	355
0768703	2812548	191	0769430	2808961	143	0772235	2814191	011
0768682	2812448	192	0769491	2808884	140	0772262	2814284	022
0768658	2812352	196	0769554	2808807	141	0772308	2814374	031
0768632	2812255	194	0769617	2808729	141	0772344	2814465	010
0768607	2812156	194	0769680	2808650	141	0772346	2814564	354
0768584	2812060	192	0769742	2808570	143	0772330	2814665	348
0768562	2811963	193	0769803	2808492	140	0772314	2814765	353
0768539	2811866	195	0769865	2808417	141	0772304	2814866	355
0768526	2811770	180	0771265	2809488	343	0772298	2814965	358
0768528	2811670	177	0771233	2809584	341	0772308	2815064	013
0768534	2811569	176	0771203	2809682	344	0764999	2823805	156
0768540	2811468	176	0771174	2809780	342	0765043	2823714	153
0768548	2811368	175	0771141	2809877	340	0765088	2823619	155
0768555	2811268	177	0771098	2809969	332	0765128	2823531	156
0768559	2811168	178	0771055	2810059	337	0765168	2823442	155
0768563	2811067	177	0771006	2810148	326	0765206	2823346	162
0768568	2810967	177	0770937	2810222	307	0765232	2823250	167
0768583	2810868	166	0770858	2810282	307	0765253	2823152	168
0768604	2810771	170	0770777	2810348	312	0765270	2823054	173
0768622	2810675	170	0770708	2810423	324	0765281	2822954	175
0768641	2810578	168	0770654	2810507	330	0765288	2822853	177
0768662	2810478	167	0770605	2810597	333	0765289	2822753	182
0768689	2810381	162	0770560	2810689	335	0765287	2822655	181
0768722	2810289	158	0770515	2810782	333	0765284	2822555	182
0769380	2811304	191	0770470	2810874	335	0765286	2822458	176
0769359	2811209	193	0770426	2810964	333	0765294	2822361	175
0769333	2811113	197	0773386	2812368	289	0765303	2822261	174

Eastings	Northings	Fault Segment Strike	Eastings	Northings	Fault Segment Strike	Eastings	Northings	Fault Segment Strike
0765307	2822161	182	0762360	2824599	189	0763797	2820365	174
0765303	2822059	183	0762350	2824500	182	0763809	2820263	172
0765296	2821959	185	0762340	2824401	189	0763821	2820164	175
0765288	2821859	185	0762326	2824301	188	0763833	2820065	172
0765282	2821759	183	0762316	2824201	184	0763845	2819967	174
0765278	2821658	182	0762307	2824100	186	0763853	2819868	178
0765277	2821558	179	0762294	2824002	189	0763858	2819767	176
0765280	2821458	178	0762274	2823903	193	0763864	2819667	176
0765290	2821360	169	0762253	2823805	192	0763870	2819568	178
0765317	2821265	160	0762233	2823708	191	0763876	2819470	175
0765351	2821172	160	0762215	2823610	190	0763884	2819370	175
0765388	2821080	156	0762197	2823511	191	0763890	2819270	179
0765431	2820988	154	0762172	2823412	197	0763892	2819170	179
0765476	2820899	153	0762140	2823319	200	0763894	2819069	179
0765521	2820811	152	0762101	2823228	207	0763895	2818966	180
0765567	2820722	154	0762056	2823137	206	0763896	2818865	179
0765611	2820631	154	0762018	2823045	199	0763897	2818766	180
0765657	2820542	152	0762005	2822950	176	0763908	2818668	168
0765704	2820452	153	0762020	2822855	167	0763932	2818569	164
0765755	2820366	146	0762050	2822757	159	0763962	2818474	161
0765814	2820284	143	0762092	2822666	152	0763992	2818377	164
0765874	2820208	141	0762134	2822577	157	0764025	2818282	158
0765935	2820132	141	0762165	2822484	166	0764056	2818193	163
0765997	2820051	144	0762192	2822388	162	0764085	2818098	163
0766059	2819972	140	0762228	2822293	157	0764114	2818002	163
0766121	2819892	144	0762272	2822208	149	0764147	2817909	158
0766180	2819810	145	0762338	2822140	124	0764190	2817817	151
0766238	2819729	144	0762417	2822082	129	0764230	2817725	163
0766296	2819648	145	0762497	2822022	123	0764251	2817630	172
0766354	2819566	144	0762590	2821970	115	0764264	2817529	173
0766412	2819484	146	0762682	2821929	113	0764277	2817430	173
0766469	2819401	146	0762771	2821890	114	0764290	2817330	173
0766526	2819319	144	0762855	2821833	133	0764303	2817228	173
0766585	2819239	144	0762929	2821765	133	0764309	2817127	180
0766658	2819176	117	0762997	2821695	138	0764309	2817026	180
0766746	2819135	113	0763057	2821617	146	0764310	2816927	179
0766839	2819095	113	0763114	2821535	144	0764322	2816826	168
0766931	2819056	113	0763174	2821455	143	0764343	2816731	167
0767023	2819016	113	0763237	2821373	142	0764358	2816637	175
0767116	2818980	110	0763300	2821296	138	0764364	2816536	178
0767208	2818943	113	0763360	2821220	146	0764369	2816434	176
0767301	2818906	111	0763419	2821138	143	0764380	2816335	172
0767395	2818871	110	0763488	2821061	132	0764397	2816236	169
0763995	2825942	157	0763563	2820994	132	0764404	2816138	182
0764039	2825844	155	0763634	2820925	137	0764401	2816035	181
0764081	2825744	160	0763694	2820848	147	0764397	2815932	184
0764118	2825641	161	0763740	2820759	159	0764383	2815835	193
0762372	2824902	176	0763769	2820663	167	0764361	2815739	193
0762374	2824799	182	0763784	2820566	176	0761883	2822703	217
0762370	2824700	182	0763789	2820467	178	0761843	2822634	205

Eastings	Northings	Fault Segment Strike	Eastings	Northings	Fault Segment Strike	Eastings	Northings	Fault Segment Strike
0761802	2822546	205	0761205	2821192	154	0762158	2816344	156
0761771	2822449	192	0761246	2821101	157	0762201	2816254	153
0761756	2822349	185	0761287	2821005	157	0762248	2816164	153
0761747	2822249	186	0761330	2820914	153	0762293	2816074	154
0761736	2822150	186	0761377	2820825	153	0762330	2815982	163
0761738	2822052	172	0761423	2820732	154	0762356	2815885	167
0761755	2821953	168	0761466	2820643	154	0762381	2815785	165
0761776	2821854	167	0761512	2820555	150	0762412	2815688	160
0761792	2821757	174	0761567	2820471	144	0762445	2815591	162
0761805	2821658	171	0761630	2820385	143	0762486	2815496	151
0761821	2821557	171	0761688	2820301	148	0762537	2815410	147
0761834	2821458	174	0761742	2820221	143	0762589	2815327	149
0761850	2821359	168	0761802	2820140	144	0762642	2815245	145
0761870	2821261	169	0761860	2820058	146	0762695	2815159	152
0761891	2821166	166	0761647	2819814	197	0762745	2815072	148
0761911	2821068	171	0761619	2819718	196	0762793	2814984	154
0761929	2820966	168	0761605	2819622	182	0762847	2814893	145
0761947	2820869	172	0761615	2819521	167	0762904	2814808	148
0761961	2820774	171	0761638	2819423	167	0762957	2814725	148
0761978	2820673	170	0761663	2819329	163	0763010	2814638	150
0761994	2820574	172	0761697	2819236	157	0763061	2814554	147
0762006	2820487	172	0761737	2819142	157	0763113	2814472	148
0760889	2823970	172	0761774	2819046	160	0763166	2814387	148
0760907	2823871	167	0761804	2818951	164	0763216	2814301	151
0760925	2823771	172	0761828	2818856	167	0763269	2814214	146
0760935	2823672	176	0761847	2818753	171	0763324	2814125	150
0760943	2823573	174	0761865	2818655	167	0763377	2814038	148
0760952	2823474	176	0761885	2818561	169	0763430	2813953	148
0760957	2823370	178	0761900	2818466	173	0763483	2813868	148
0760963	2823269	174	0761898	2818372	188	0763533	2813784	151
0760970	2823168	178	0761873	2818273	200	0763584	2813698	149
0760976	2823065	174	0761840	2818174	197	0759812	2823369	160
0760998	2822968	162	0761819	2818077	188	0759839	2823271	170
0761028	2822873	163	0761808	2817978	184	0759854	2823170	173
0761058	2822778	162	0761797	2817879	189	0759857	2823069	184
0761079	2822678	174	0761786	2817778	183	0759842	2822970	193
0761091	2822581	172	0761786	2817677	177	0759807	2822877	209
0761099	2822480	178	0761791	2817577	177	0759763	2822788	204
0761096	2822379	186	0761798	2817474	175	0759720	2822702	209
0761081	2822278	191	0761804	2817373	177	0759680	2822629	208
0761064	2822176	187	0761810	2817271	177	0758607	2822588	155
0761059	2822079	178	0761814	2817171	178	0758645	2822495	160
0761059	2821983	182	0761822	2817070	173	0758680	2822398	161
0761062	2821880	174	0761847	2816976	156	0758708	2822305	165
0761072	2821776	175	0761889	2816886	153	0758732	2822208	166
0761082	2821677	174	0761933	2816792	157	0758751	2822107	174
0761096	2821579	171	0761974	2816698	156	0758759	2822009	176
0761109	2821478	174	0762017	2816607	153	0758766	2821908	176
0761130	2821381	161	0762061	2816525	151	0758775	2821806	173
0761165	2821285	159	0762110	2816437	150	0758790	2821708	170
0758809	2821614	168	0758828	2821513	169	0758856	2821416	158

D2 Base Paleogene (bP) horizon

Eastings	Northings	Fault Segment Strike	Eastings	Northings	Fault Segment Strike	Eastings	Northings	Fault Segment Strike
0766698	2827607	139	0769872	2824350	217	0768601	2820059	191
0766760	2827531	142	0769813	2824268	215	0768582	2819962	191
0766827	2827453	138	0769757	2824183	212	0768564	2819862	190
0766898	2827380	134	0769704	2824099	212	0768545	2819763	191
0766966	2827307	140	0769651	2824013	211	0768524	2819665	193
0767028	2827226	144	0769600	2823927	211	0768500	2819567	194
0767090	2827147	141	0769548	2823841	211	0768474	2819471	197
0767151	2827069	143	0769486	2823761	225	0768447	2819374	194
0767210	2826988	145	0769409	2823699	238	0768421	2819279	197
0767278	2826915	130	0769324	2823653	245	0768389	2819185	200
0767359	2826851	127	0769237	2823608	241	0768367	2819088	186
0767437	2826786	132	0769148	2823555	238	0768367	2818988	174
0767511	2826719	132	0769064	2823504	240	0768381	2818889	169
0767586	2826649	134	0768983	2823446	229	0768398	2818791	171
0767657	2826581	134	0768904	2823381	233	0768417	2818692	168
0767730	2826512	134	0768826	2823321	233	0768437	2818592	169
0767807	2826446	127	0768746	2823260	232	0768462	2818497	161
0767888	2826388	124	0768666	2823200	234	0768502	2818407	151
0767969	2826332	125	0768590	2823136	226	0768546	2818317	155
0768054	2826279	119	0768525	2823061	215	0768593	2818226	151
0768145	2826232	115	0768470	2822977	212	0768642	2818137	151
0768237	2826191	113	0768416	2822894	214	0768689	2818051	151
0768333	2826155	108	0768369	2822807	202	0768730	2817962	160
0768426	2826122	111	0768340	2822709	192	0768763	2817869	161
0768518	2826089	108	0768326	2822608	185	0768793	2817772	165
0768616	2826059	105	0768330	2822509	171	0768824	2817677	158
0768712	2826031	107	0768353	2822414	161	0768864	2817586	155
0768806	2825999	110	0768397	2822325	148	0768909	2817496	151
0768903	2825966	109	0768447	2822238	153	0768957	2817407	152
0768999	2825930	112	0768479	2822144	170	0769008	2817320	147
0769089	2825885	121	0768499	2822045	168	0769061	2817238	148
0769175	2825831	122	0768512	2821948	177	0769115	2817153	147
0769260	2825778	122	0768516	2821849	178	0769172	2817069	145
0769346	2825726	121	0768517	2821749	180	0769233	2816995	136
0769432	2825674	121	0768520	2821649	177	0769297	2816918	144
0769517	2825620	124	0768523	2821550	180	0769353	2816834	147
0769599	2825563	125	0768523	2821451	180	0769402	2816748	153
0769682	2825506	124	0768524	2821352	178	0769442	2816656	160
0770585	2825254	186	0768525	2821249	180	0769475	2816562	161
0770575	2825150	186	0768527	2821148	178	0769504	2816467	165
0770556	2825054	196	0768528	2821050	180	0769535	2816370	160
0770517	2824966	212	0768532	2820950	175	0769572	2816278	156
0770445	2824899	241	0768546	2820849	168	0769611	2816182	158
0770363	2824843	231	0768573	2820754	161	0769639	2816088	170
0770288	2824779	228	0768598	2820659	170	0769645	2815995	183
0770212	2824714	231	0768615	2820558	171	0769633	2815897	191
0770134	2824653	233	0768629	2820459	174	0769615	2815796	189
0770061	2824583	219	0768631	2820360	183	0769593	2815696	197
0769997	2824505	221	0768623	2820258	186	0769560	2815602	202
0769933	2824428	218	0768614	2820157	185	0769523	2815509	201

Eastings	Northings	Fault Segment Strike	Eastings	Northings	Fault Segment Strike	Eastings	Northings	Fault Segment Strike
0769484	2815415	203	0769319	2810683	141	0773825	2815604	287
0769449	2815323	199	0769384	2810603	140	0773731	2815635	289
0769424	2815230	191	0769444	2810525	145	0773640	2815672	295
0769428	2815133	165	0769492	2810438	157	0773553	2815723	306
0769450	2815036	169	0769526	2810343	163	0773476	2815791	317
0769470	2814939	168	0769554	2810248	164	0773408	2815862	316
0769486	2814840	174	0769575	2810148	171	0773341	2815934	317
0769498	2814738	173	0769589	2810051	172	0773275	2816010	321
0769508	2814637	175	0769600	2809954	175	0773217	2816090	326
0769508	2814539	185	0769611	2809852	173	0773156	2816168	318
0769490	2814443	197	0769627	2809753	169	0773090	2816247	322
0769466	2814342	190	0769650	2809658	163	0773025	2816323	316
0769450	2814242	188	0769687	2809566	153	0772961	2816398	323
0769438	2814146	186	0769734	2809476	153	0772907	2816484	332
0769425	2814048	189	0769779	2809384	155	0772871	2816577	346
0769406	2813947	192	0769824	2809294	151	0772853	2816673	352
0769383	2813848	195	0769870	2809207	153	0772844	2816774	357
0769353	2813755	200	0769919	2809119	149	0772840	2816874	358
0769322	2813661	198	0769973	2809035	146	0772824	2816972	343
0769285	2813569	207	0770031	2808954	143	0772793	2817070	342
0769240	2813481	208	0770091	2808874	144	0772767	2817167	348
0769192	2813390	207	0770149	2808794	145	0772749	2817264	351
0769150	2813298	202	0770210	2808712	142	0772731	2817361	347
0769111	2813206	204	0770268	2808630	147	0772724	2817460	004
0769076	2813112	198	0776339	2815451	268	0772728	2817557	360
0769051	2813014	191	0776241	2815446	265	0772724	2817653	356
0769047	2812918	174	0776141	2815445	273	0772721	2817755	002
0769073	2812824	155	0776039	2815451	275	0772727	2817857	004
0769118	2812737	150	0775940	2815455	270	0772723	2817957	351
0769148	2812643	173	0775842	2815449	262	0772707	2818055	351
0769158	2812541	177	0775745	2815431	258	0772691	2818156	351
0769156	2812442	185	0775647	2815412	259	0772676	2818258	353
0769139	2812342	195	0775550	2815389	255	0772663	2818357	352
0769114	2812247	195	0775454	2815364	256	0772650	2818455	352
0769096	2812150	187	0775359	2815336	252	0772647	2818554	005
0769085	2812052	185	0775260	2815306	254	0772655	2818652	005
0769072	2811954	190	0775161	2815286	264	0772666	2818751	007
0769058	2811857	185	0775063	2815277	265	0772679	2818852	008
0769048	2811758	187	0774965	2815270	267	0772691	2818951	006
0769033	2811658	189	0774866	2815266	268	0772702	2819050	006
0769021	2811558	187	0774768	2815269	275	0772704	2819149	357
0769007	2811458	189	0774671	2815295	295	0772700	2819249	359
0768991	2811357	189	0774577	2815338	294	0772696	2819351	357
0768978	2811255	186	0774488	2815376	293	0772694	2819449	360
0768976	2811156	175	0774398	2815412	292	0772695	2819547	002
0769006	2811068	148	0774305	2815448	290	0772699	2819649	003
0769065	2810992	135	0774209	2815480	286	0772702	2819748	360
0769134	2810918	139	0774111	2815510	288	0772696	2819848	354
0769199	2810840	142	0774016	2815542	288	0772688	2819950	357
0769258	2810762	144	0773920	2815574	288	0772680	2820048	354

Eastings	Northings	Fault Segment Strike	Eastings	Northings	Fault Segment Strike	Eastings	Northings	Fault Segment Strike
0765293	2824024	146	0766684	2819510	145	0762227	2821646	168
0765348	2823941	147	0766743	2819424	145	0762250	2821548	166
0765404	2823857	145	0766805	2819340	143	0760965	2824089	191
0765463	2823773	144	0766874	2819273	123	0760949	2823990	187
0765515	2823688	153	0766960	2819227	114	0760938	2823889	185
0765554	2823599	159	0767052	2819187	113	0760931	2823788	184
0765587	2823503	163	0767147	2819161	099	0760926	2823687	182
0765609	2823407	172	0767248	2819149	094	0760923	2823587	181
0765625	2823310	169	0767348	2819141	095	0760921	2823488	180
0765642	2823210	172	0767447	2819133	095	0760920	2823386	181
0765645	2823113	184	0767545	2819120	100	0760919	2823286	180
0765635	2823012	187	0767641	2819096	108	0760927	2823187	172
0765619	2822911	191	0767734	2819057	116	0760947	2823089	165
0765596	2822814	195	0767822	2819007	123	0760980	2822994	157
0765571	2822718	194	0767910	2818962	110	0761018	2822902	158
0765543	2822623	200	0762658	2825087	179	0761052	2822806	162
0765518	2822526	189	0762659	2824986	180	0761076	2822709	170
0765506	2822427	184	0762658	2824886	181	0761088	2822611	176
0765500	2822327	184	0762650	2824786	187	0761091	2822510	180
0765493	2822230	184	0762630	2824688	195	0761082	2822410	190
0765483	2822129	187	0762602	2824589	197	0761062	2822311	193
0765472	2822023	186	0762576	2824492	192	0761039	2822213	193
0765472	2821922	174	0762549	2824397	200	0761020	2822113	188
0765488	2821826	166	0762514	2824302	200	0761008	2822015	185
0765508	2821734	170	0762480	2824206	199	0761004	2821914	180
0765523	2821637	173	0762449	2824110	197	0761009	2821813	174
0765526	2821539	184	0762425	2824012	191	0761026	2821714	167
0765508	2821441	197	0762405	2823913	192	0761054	2821618	162
0765493	2821341	180	0762384	2823814	192	0761084	2821524	162
0765510	2821243	160	0762364	2823714	191	0761115	2821429	162
0765548	2821152	154	0762341	2823615	194	0761148	2821333	160
0765596	2821066	147	0762316	2823520	196	0761185	2821239	157
0765645	2820982	152	0762291	2823424	194	0761224	2821147	157
0765695	2820897	147	0762264	2823326	196	0761264	2821055	156
0765751	2820815	144	0762239	2823231	194	0761306	2820962	156
0765812	2820729	145	0762215	2823133	193	0761341	2820867	163
0765872	2820644	145	0762194	2823034	191	0761369	2820770	164
0765926	2820565	146	0762175	2822934	191	0761396	2820675	165
0765979	2820481	149	0762156	2822836	191	0762596	2822467	144
0766036	2820395	144	0762137	2822735	190	0762654	2822388	144
0766095	2820314	143	0762120	2822636	189	0762716	2822309	140
0766158	2820234	140	0762106	2822536	187	0762786	2822231	136
0766219	2820156	144	0762095	2822434	186	0762854	2822157	139
0766280	2820080	139	0762092	2822334	178	0762923	2822085	132
0766343	2820003	143	0762097	2822234	176	0762998	2822018	132
0766406	2819918	143	0762112	2822135	166	0763080	2821955	122
0766466	2819837	144	0762133	2822040	169	0763165	2821897	127
0766517	2819756	151	0762155	2821940	166	0763244	2821836	128
0766571	2819674	142	0762179	2821842	166	0763320	2821775	129
0766628	2819594	147	0762204	2821744	166	0763398	2821713	127

Eastings	Northings	Fault Segment Strike	Eastings	Northings	Fault Segment Strike	Eastings	Northings	Fault Segment Strike
0763477	2821654	126	0765175	2816882	163	0764107	2815696	164
0763555	2821589	133	0765202	2816785	167	0764132	2815599	166
0763633	2821520	131	0765211	2816685	182	0764153	2815500	170
0763705	2821450	136	0761940	2819863	147	0764166	2815401	175
0763768	2821374	145	0761995	2819779	146	0764178	2815304	171
0763826	2821292	145	0762050	2819695	149	0764202	2815207	162
0763884	2821206	147	0762105	2819609	145	0764232	2815110	163
0763942	2821126	141	0762161	2819528	145	0764263	2815013	162
0764005	2821045	143	0762212	2819443	152	0764296	2814918	159
0764067	2820963	142	0762264	2819352	150	0764328	2814823	164
0764117	2820881	154	0762317	2819266	147	0764350	2814725	171
0764152	2820789	165	0762374	2819187	142	0764373	2814630	163
0764175	2820689	169	0762432	2819102	149	0764400	2814532	165
0764196	2820589	167	0762484	2819013	151	0764430	2814435	161
0764213	2820489	174	0762530	2818927	153	0764459	2814339	165
0764218	2820387	180	0762577	2818839	151	0764480	2814240	171
0764218	2820288	180	0762626	2818749	152	0764500	2814143	166
0764216	2820188	182	0762670	2818660	156	0764522	2814046	168
0764211	2820084	184	0762707	2818568	161	0764545	2813949	166
0764211	2819983	176	0762739	2818468	164	0764559	2813851	177
0764225	2819882	169	0762764	2818372	167	0764562	2813749	180
0764244	2819785	168	0762793	2818281	158	0764555	2813647	187
0764268	2819689	165	0762834	2818189	154	0764543	2813549	186
0764286	2819591	174	0762883	2818098	150	0764526	2813450	193
0764297	2819491	173	0762929	2818011	155	0764501	2813352	196
0764312	2819388	171	0762970	2817921	156	0764475	2813257	195
0764322	2819295	178	0763010	2817830	156	0764452	2813159	191
0764209	2818952	174	0763055	2817737	152	0764441	2813058	181
0764219	2818848	175	0763104	2817648	150	0764460	2812964	155
0764234	2818746	169	0763153	2817564	150	0764508	2812879	148
0764277	2818656	140	0763209	2817478	144	0764564	2812794	145
0764345	2818579	138	0763271	2817397	140	0764619	2812710	149
0764416	2818508	132	0763330	2817320	144	0764658	2812618	164
0764487	2818435	139	0763388	2817240	144	0764678	2812516	174
0764555	2818362	135	0763447	2817154	148	0764684	2812415	180
0764623	2818286	141	0763500	2817070	148	0764684	2812316	180
0764687	2818202	144	0763552	2816987	148	0764681	2812217	183
0764745	2818121	145	0763608	2816897	149	0764676	2812118	183
0764795	2818036	154	0763660	2816810	150	0764670	2812018	183
0764839	2817942	155	0763709	2816726	149	0765484	2814218	176
0764884	2817849	153	0763755	2816636	156	0765494	2814115	173
0764927	2817760	155	0763799	2816544	153	0765505	2814015	174
0764973	2817664	153	0763842	2816454	155	0765523	2813915	166
0765018	2817572	155	0763885	2816364	155	0765552	2813817	162
0765051	2817479	165	0763926	2816270	158	0765569	2813718	179
0765071	2817377	173	0763967	2816177	154	0765572	2813618	178
0765082	2817276	174	0764004	2816087	161	0765571	2813516	184
0765099	2817178	167	0764034	2815992	164	0765575	2813415	172
0765122	2817079	167	0764059	2815893	168	0765593	2813314	168
0765147	2816980	165	0764082	2815794	167	0765605	2813213	179

Eastings	Northings	Fault Segment Strike	Eastings	Northings	Fault Segment Strike	Eastings	Northings	Fault Segment Strike
0765599	2813112	187	0766663	2809131	192	0758603	2822613	160
0765586	2813013	188	0766644	2809028	189	0758636	2822516	163
0766779	2810253	172	0761369	2817882	192	0758667	2822418	162
0766792	2810149	173	0761346	2817775	192	0758697	2822321	165
0766802	2810046	176	0761317	2817670	200	0758725	2822221	164
0766803	2809942	182	0761268	2817585	222	0758750	2822121	169
0766799	2809837	182	0760247	2823635	175	0758772	2822020	167
0766791	2809734	186	0760262	2823531	168	0758793	2821916	169
0766780	2809633	187	0760273	2823429	178	0758810	2821815	172
0766764	2809532	191	0760270	2823321	185	0758823	2821714	173
0766737	2809431	199	0760258	2823220	188	0758836	2821610	173
0766707	2809332	195	0760240	2823121	193	0758848	2821509	174
0766683	2809232	191	0760212	2823017	197			

D3 Akli (Ak) horizon

Eastings	Northings	Fault Segment Strike	Eastings	Northings	Fault Segment Strike	Eastings	Northings	Fault Segment Strike
0769597	2808111	322	0768514	2809794	189	0768731	2812196	211
0769546	2808186	329	0768517	2809695	168	0768684	2812106	203
0769496	2808273	331	0768546	2809601	158	0768659	2812009	186
0769452	2808365	337	0768590	2809511	151	0768664	2811909	169
0769416	2808461	342	0768638	2809423	152	0768680	2811806	174
0769399	2808560	358	0768682	2809332	157	0768687	2811706	179
0769403	2808661	007	0768711	2809237	170	0768678	2811607	191
0769410	2808762	360	0768724	2809137	175	0768656	2811508	194
0769406	2808863	355	0768731	2809042	177	0768629	2811410	197
0769394	2808962	351	0768882	2810717	148	0768606	2811313	190
0769386	2809064	360	0768916	2810623	173	0768592	2811212	185
0769388	2809166	003	0768922	2810521	181	0768587	2811110	180
0769383	2809265	351	0768922	2810417	178	0768584	2811010	184
0769366	2809365	350	0768939	2810313	163	0768555	2810917	211
0769360	2809465	003	0768976	2810216	155	0768507	2810828	206
0769371	2809565	010	0769021	2810124	153	0768461	2810737	207
0769392	2809665	013	0769050	2810026	174	0768422	2810644	199
0769415	2809765	013	0769057	2809922	178	0768393	2810544	193
0769095	2809206	325	0768544	2813128	163	0768370	2810445	193
0769039	2809297	331	0768554	2813039	182	0770293	2809308	144
0768987	2809390	331	0768550	2812938	183	0770326	2809235	162
0768935	2809483	331	0768560	2812838	167	0770350	2809134	172
0768880	2809572	325	0768584	2812739	166	0770358	2809031	179
0768807	2809648	307	0768619	2812643	154	0770360	2808926	179
0768449	2810175	178	0768664	2812551	153	0770378	2808825	161
0768475	2810079	152	0768713	2812462	149	0770420	2808730	152
0768518	2809990	156	0768763	2812377	150	0770471	2808639	150
0768530	2809896	189	0768772	2812286	198	0768558	2815561	181

Eastings	Northings	Fault Segment Strike	Eastings	Northings	Fault Segment Strike	Eastings	Northings	Fault Segment Strike
0768554	2815462	184	0769885	2810933	192	0771119	2810483	110
0768543	2815362	190	0769854	2810838	203	0771215	2810447	110
0768518	2815269	200	0769814	2810747	202	0771308	2810411	112
0768477	2815179	209	0769781	2810650	196	0771373	2810350	156
0768427	2815088	209	0769754	2810550	193	0771413	2810260	157
0768394	2814995	190	0769741	2810454	183	0771455	2810165	155
0768386	2814897	180	0769742	2810356	176	0771500	2810075	151
0768407	2814800	156	0769763	2810259	158	0771549	2809988	149
0768452	2814713	151	0769803	2810166	155	0771600	2809902	150
0768499	2814628	151	0769846	2810072	155	0771650	2809814	151
0768551	2814542	147	0769876	2809977	170	0771698	2809726	152
0768606	2814458	147	0769889	2809877	175	0771736	2809634	163
0768661	2814375	146	0769892	2809778	181	0771769	2809538	159
0768713	2814289	151	0769888	2809680	184	0771810	2809446	154
0768754	2814197	160	0769891	2809579	173	0772384	2811360	173
0768784	2814102	165	0769907	2809480	168	0772410	2811265	156
0768809	2814008	165	0769932	2809385	162	0772450	2811175	157
0768834	2813910	167	0769970	2809289	155	0772470	2811078	180
0768863	2813810	159	0770014	2809199	153	0772468	2810976	183
0768899	2813717	158	0770058	2809113	152	0772467	2810875	178
0768932	2813623	163	0770105	2809023	153	0772480	2810776	167
0768963	2813526	162	0770724	2809606	178	0772516	2810684	149
0768994	2813431	162	0770727	2809493	178	0772573	2810601	142
0769014	2813335	176	0770735	2809384	174	0772635	2810521	142
0769024	2813239	171	0770641	2811850	167	0772699	2810445	138
0769063	2813154	139	0770660	2811752	171	0772772	2810376	128
0769132	2813083	132	0770675	2811653	173	0772853	2810314	127
0769206	2813015	132	0770688	2811553	172	0772923	2810243	144
0769279	2812944	136	0770697	2811453	178	0772975	2810158	154
0769349	2812872	136	0770962	2811247	296	0773172	2812194	008
0769401	2812790	159	0770871	2811286	290	0773186	2812296	008
0769411	2812697	189	0770776	2811308	276	0773203	2812400	011
0769403	2812598	181	0770706	2811267	206	0773225	2812502	013
0769427	2812507	147	0770664	2811176	205	0773319	2812586	168
0769491	2812434	132	0770618	2811088	210	0773340	2812479	170
0769562	2812363	138	0770564	2811004	215	0773348	2812372	182
0769615	2812280	157	0770530	2810918	186	0773337	2812266	189
0769655	2812187	157	0770565	2810849	121	0773315	2812162	194
0769691	2812093	162	0770651	2810803	117	0773279	2812062	205
0769723	2811997	162	0770715	2810736	157	0773137	2813012	167
0769756	2811902	159	0770762	2810651	145	0773159	2812908	169
0769799	2811811	151	0770817	2810562	151	0773170	2812801	178
0769841	2811719	160	0770839	2810466	185	0772847	2813886	117
0769871	2811624	166	0770832	2810362	183	0772928	2813825	137
0769886	2811525	176	0770824	2810261	186	0772992	2813745	147
0769892	2811425	176	0770817	2810163	183	0773042	2813657	154
0769897	2811326	178	0770813	2810062	182	0773081	2813564	160
0769904	2811228	175	0770812	2809961	179	0773099	2813464	179
0769908	2811130	180	0770929	2810553	110	0773054	2814619	204
0769901	2811030	187	0771023	2810518	110	0773011	2814528	206

Eastings	Northings	Fault Segment Strike	Eastings	Northings	Fault Segment Strike	Eastings	Northings	Fault Segment Strike
0772965	2814438	208	0768090	2813985	169	0769661	2815403	246
0772911	2814355	217	0768104	2813881	175	0771100	2817198	193
0772844	2814280	227	0768119	2813781	167	0771070	2817098	201
0772768	2814213	230	0768147	2813685	159	0771018	2817006	217
0772686	2814155	239	0768179	2813588	165	0770943	2816936	238
0772600	2814104	240	0768196	2813496	176	0770860	2816874	228
0772512	2814056	242	0768045	2814620	360	0770786	2816797	219
0772422	2814010	244	0767577	2814779	345	0770718	2816714	219
0771843	2814578	153	0767559	2814887	357	0770648	2816641	229
0771883	2814486	161	0767562	2814992	007	0770646	2817337	147
0771897	2814389	181	0769177	2814194	358	0770700	2817236	157
0771884	2814290	194	0770212	2814567	198	0771036	2820380	201
0771861	2814193	192	0770154	2814482	231	0771001	2820283	198
0771851	2814093	179	0770061	2814428	249	0770985	2820185	180
0771851	2813992	182	0769830	2814111	210	0770999	2820086	164
0771847	2813892	183	0769765	2814019	222	0771032	2819992	157
0771841	2813794	184	0769560	2815004	013	0771073	2819899	157
0771829	2813696	190	0769598	2815111	027	0771112	2819806	158
0771808	2813599	195	0769660	2815206	039	0771151	2819714	156
0771780	2813502	197	0771171	2816122	118	0771187	2819620	162
0771734	2813412	217	0771257	2816072	122	0771224	2819525	155
0771665	2813341	233	0771346	2816023	117	0771265	2819433	157
0771582	2813287	241	0771438	2815978	114	0771300	2819340	162
0771500	2813232	231	0771519	2815917	140	0771329	2819242	165
0771426	2813166	225	0771584	2815840	139	0771354	2819144	166
0771355	2813094	224	0771646	2815759	146	0771369	2819048	176
0770268	2813626	190	0771704	2815673	147	0771374	2818948	178
0770257	2813521	182	0771756	2815584	153	0771375	2818849	181
0770332	2813205	136	0771798	2815493	157	0771369	2818751	186
0770397	2813120	149	0771841	2815400	154	0771357	2818651	187
0770450	2813024	154	0771884	2815305	157	0771334	2818552	199
0770484	2812926	167	0771924	2815213	156	0771293	2818459	209
0770501	2812824	173	0771969	2815123	151	0771239	2818376	218
0769024	2812888	200	0772018	2815030	152	0771181	2818299	216
0768968	2812797	224	0772068	2814937	151	0771115	2818223	225
0768371	2812097	006	0770027	2816694	211	0771043	2818150	224
0768369	2812220	353	0769961	2816620	233	0770971	2818080	228
0767849	2812700	338	0769875	2816568	245	0770894	2818012	230
0767818	2812804	349	0769785	2816522	240	0770818	2817945	227
0767812	2812910	005	0769732	2816448	191	0770752	2817875	219
0767841	2813010	027	0769726	2816350	177	0770693	2817795	214
0767620	2813228	341	0769735	2816251	173	0770631	2817712	218
0767583	2813325	337	0769747	2816152	174	0770572	2817629	213
0767544	2813422	339	0769756	2816051	176	0770522	2817541	206
0767505	2813516	336	0769763	2815949	177	0768085	2815888	017
0767479	2813613	354	0769768	2815849	177	0768121	2815979	026
0767484	2813713	012	0769775	2815749	175	0768165	2816070	026
0768025	2814284	179	0769772	2815650	187	0768214	2816156	033
0768036	2814182	168	0769752	2815551	195	0768267	2816241	031
0768064	2814084	161	0769716	2815460	208	0768319	2816328	031

Eastings	Northings	Fault Segment Strike	Eastings	Northings	Fault Segment Strike	Eastings	Northings	Fault Segment Strike
0768369	2816414	029	0768058	2819260	064	0766727	2816329	327
0768416	2816499	029	0768155	2819302	068	0766671	2816411	324
0768466	2816588	031	0768253	2819336	074	0766614	2816493	327
0768504	2816680	012	0768354	2819362	077	0766563	2816580	332
0768513	2816778	359	0768454	2819392	070	0766519	2816667	334
0768524	2816877	014	0768551	2819408	093	0766476	2816756	336
0768558	2816970	027	0768594	2819362	183	0766435	2816846	335
0768602	2817060	025	0768575	2819271	200	0766393	2816937	335
0768639	2817154	018	0768554	2819169	184	0766354	2817032	340
0768669	2817249	016	0768524	2819070	210	0766319	2817126	339
0768697	2817345	017	0768453	2819006	245	0766284	2817221	340
0768726	2817440	016	0768551	2818439	013	0766249	2817315	339
0768757	2817536	020	0768575	2818540	014	0766219	2817410	347
0768794	2817631	023	0768600	2818640	015	0766194	2817508	344
0768615	2817775	200	0768627	2818736	016	0766167	2817603	345
0768577	2817677	201	0768655	2818829	018	0766143	2817697	346
0768539	2817582	203	0768699	2818919	033	0766123	2817797	351
0768499	2817490	203	0768759	2819005	038	0766108	2817897	353
0768462	2817392	199	0768827	2819075	052	0766095	2817996	353
0768426	2817294	201	0768899	2819142	043	0766088	2818097	359
0768390	2817197	199	0768948	2819230	016	0766094	2818196	009
0768351	2817103	206	0768963	2819330	001	0766124	2818288	026
0769254	2818014	172	0768943	2819425	335	0766167	2818377	026
0769258	2817913	184	0768911	2819521	348	0765865	2813561	107
0769232	2817817	207	0768893	2819623	352	0765965	2813529	108
0769190	2817724	201	0768900	2819720	016	0766064	2813496	110
0769159	2817624	193	0768919	2819817	006	0766162	2813457	114
0769618	2818207	018	0768914	2819917	348	0766259	2813412	116
0769666	2818307	034	0768891	2820017	347	0766350	2813363	121
0769739	2818392	047	0768887	2820116	008	0766432	2813300	134
0769646	2818895	002	0768919	2820211	029	0766429	2814639	328
0769404	2819253	021	0768971	2820296	034	0766374	2814733	331
0769453	2819363	027	0768232	2819576	351	0766326	2814835	338
0769345	2819665	029	0768232	2819679	009	0766293	2814940	348
0769402	2819750	038	0768251	2819781	012	0764383	2814825	162
0769476	2819826	050	0768271	2819882	010	0764416	2814724	162
0769560	2819884	062	0767780	2815426	320	0764453	2814623	157
0769654	2819927	069	0767711	2815504	317	0764487	2814526	163
0769751	2819963	070	0767641	2815571	310	0764515	2814426	166
0768321	2818128	013	0767559	2815630	301	0764535	2814323	173
0768334	2818227	002	0767467	2815676	292	0764540	2814216	181
0768335	2818334	359	0767378	2815717	298	0764536	2814111	183
0768332	2818439	359	0767291	2815766	301	0763956	2815433	280
0768338	2818542	007	0767209	2815822	308	0763862	2815451	283
0768358	2818645	015	0767133	2815886	312	0763761	2815459	267
0767417	2818782	074	0767060	2815953	314	0763661	2815443	254
0767519	2818814	072	0766989	2816024	316	0763559	2815422	262
0767620	2818844	075	0766919	2816097	317	0763456	2815415	272
0767721	2818872	075	0766853	2816170	319	0764224	2815414	118
0767821	2818899	075	0766788	2816248	320	0764310	2815347	139

Eastings	Northings	Fault Segment Strike	Eastings	Northings	Fault Segment Strike	Eastings	Northings	Fault Segment Strike
0764370	2815259	153	0763996	2820085	342	0763021	2819881	170
0764653	2815689	110	0763955	2820178	330	0763061	2819791	143
0764752	2815654	109	0763894	2820259	316	0763126	2819717	134
0764845	2815606	125	0763815	2820326	305	0762155	2819931	138
0764929	2815542	129	0763672	2820127	186	0762227	2819855	132
0765002	2815475	137	0763664	2820026	184	0762041	2820680	189
0763035	2816620	127	0763660	2819926	181	0762038	2820571	174
0763110	2816554	136	0763654	2819828	185	0762055	2820461	168
0763171	2816469	152	0763647	2819727	184	0762064	2820354	184
0763227	2816386	140	0763637	2819627	187	0761522	2820015	270
0763299	2816325	121	0763614	2819528	199	0761408	2820009	263
0763389	2816279	113	0763577	2819436	205	0761296	2820010	277
0763485	2816244	107	0763547	2819343	191	0761043	2820163	308
0763581	2816218	104	0763551	2819245	165	0760968	2820251	330
0763680	2816198	099	0763567	2819148	176	0760814	2818721	348
0763778	2816170	113	0763575	2819049	174	0760806	2818826	003
0763868	2816130	114	0763583	2818948	176	0760811	2818934	001
0763962	2816093	109	0763571	2818849	199	0760811	2819043	359
0764057	2816060	109	0763540	2818753	197	0760810	2819148	360
0764149	2816022	116	0763547	2818660	153	0760811	2819254	001
0764226	2815983	118	0763589	2818571	157	0761964	2819569	305
0763261	2816992	114	0763620	2818474	166	0761893	2819637	323
0763355	2816949	115	0763635	2818372	178	0761838	2819721	330
0763441	2816898	127	0763622	2818276	200	0761793	2819812	337
0763518	2816829	136	0763569	2818198	228	0761755	2819908	340
0763577	2816744	154	0763517	2818119	198	0761721	2820003	341
0763618	2816650	159	0763505	2818023	176	0761693	2820100	347
0763665	2816560	147	0762264	2818173	021	0761669	2820200	346
0763725	2816481	138	0762323	2818269	043	0761647	2820299	349
0764848	2819235	106	0762257	2818465	027	0761632	2820399	354
0764946	2819210	103	0762313	2818548	040	0761629	2820502	002
0765045	2819182	108	0762397	2818617	060	0761618	2820602	346
0765141	2819151	107	0762484	2818682	047	0761592	2820701	344
0765234	2819118	113	0762554	2818756	040	0761551	2820794	329
0765324	2819079	113	0761884	2818984	105	0761494	2820880	323
0765413	2819034	121	0761995	2818935	123	0761434	2820959	322
0765496	2818975	131	0762152	2819416	176	0761381	2821043	333
0764720	2819051	320	0762167	2819299	168	0761348	2821137	349
0764677	2819138	347	0762199	2819196	157	0761463	2821920	174
0764651	2819235	343	0762669	2819460	098	0761450	2821820	201
0764595	2819314	306	0762754	2819410	142	0761576	2821718	138
0764513	2819366	298	0762817	2819325	144	0761640	2821636	147
0764421	2819415	298	0762896	2819258	118	0761691	2821547	154
0764331	2819474	310	0762890	2820526	170	0761755	2821480	118
0764259	2819543	318	0762908	2820430	168	0761836	2821454	095
0764200	2819622	330	0762945	2820337	149	0761802	2821259	147
0764149	2819713	331	0763006	2820255	137	0761858	2821173	147
0764093	2819801	324	0763045	2820170	173	0761919	2821088	142
0764051	2819890	347	0763045	2820070	187	0761975	2821000	153
0764026	2819987	344	0763026	2819976	196	0761075	2821157	003

Eastings	Northings	Fault Segment Strike	Eastings	Northings	Fault Segment Strike	Eastings	Northings	Fault Segment Strike
0761066	2821254	348	0759633	2821326	056	0760622	2823713	149
0761060	2821354	005	0759711	2821387	048	0761004	2823106	312
0761084	2821456	021	0759746	2821465	356	0761138	2822572	360
0761113	2821557	010	0759717	2821549	327	0761138	2822667	360
0761124	2821659	004	0759662	2821634	327	0761014	2823947	178
0761110	2821760	340	0759604	2821718	324	0761021	2823840	175
0761066	2821851	329	0759543	2821797	322	0761254	2823989	135
0761010	2821937	325	0759477	2821874	317	0761310	2823904	158
0761314	2821397	321	0759407	2821945	314	0761335	2823808	174
0761247	2821476	319	0759333	2822014	312	0761337	2823709	184
0761722	2821935	140	0759199	2822031	060	0761353	2823610	158
0760496	2821988	065	0759245	2822099	001	0761391	2823514	159
0760582	2822038	055	0759239	2822191	353	0761431	2823420	155
0760671	2822087	066	0759223	2822290	348	0761482	2823334	143
0760768	2822122	075	0759205	2822391	352	0761537	2823251	150
0760866	2822140	084	0759181	2822488	341	0761555	2823157	187
0760967	2822136	101	0759146	2822580	337	0761813	2822574	107
0761065	2822125	092	0759101	2822667	327	0761911	2822543	109
0761369	2822525	132	0759053	2822753	335	0762000	2822495	127
0761432	2822446	150	0759684	2823149	150	0762078	2822431	132
0761479	2822358	154	0759713	2823055	176	0762052	2822594	128
0761532	2822273	143	0759707	2822958	190	0762122	2822517	147
0761604	2822201	126	0759674	2822865	209	0762176	2822428	150
0761683	2822149	120	0759812	2822884	158	0761963	2822309	147
0759869	2820591	063	0759852	2822787	158	0762013	2822232	147
0759947	2820616	077	0759895	2822687	156	0762068	2822151	145
0760049	2820641	076	0759929	2822587	166	0762124	2822065	149
0759888	2820413	154	0759941	2822483	181	0762176	2821978	150
0759935	2820323	151	0759939	2822373	181	0762225	2821890	153
0759991	2820234	144	0759940	2822265	178	0762273	2821803	148
0760065	2820163	122	0759115	2821701	150	0761970	2824472	162
0760151	2820108	123	0759170	2821614	145	0761987	2824378	177
0760232	2820047	131	0759225	2821528	150	0761996	2824279	173
0761106	2820494	306	0759274	2821443	150	0762028	2824186	149
0761035	2820556	316	0759325	2821357	149	0762077	2824096	153
0760959	2820618	302	0759384	2821274	140	0762115	2824003	163
0760867	2820663	292	0759451	2821218	117	0762137	2823909	172
0760772	2820708	299	0759492	2821153	171	0762144	2823811	178
0760684	2820757	299	0759521	2821058	155	0762158	2823710	167
0760598	2820799	293	0759563	2820968	155	0762197	2823618	147
0760509	2820842	299	0759606	2820877	156	0762256	2823534	143
0760418	2820892	299	0759642	2820786	162	0762315	2823456	142
0760335	2820942	303	0759668	2820691	169	0762359	2823371	163
0760254	2820999	308	0760068	2823417	078	0762375	2823272	179
0760176	2821061	310	0760166	2823417	101	0762373	2823173	183
0760097	2821126	309	0760264	2823402	096	0762369	2823074	181
0760014	2821189	306	0760363	2823388	099	0762371	2822972	177
0759937	2821253	312	0760467	2823379	092	0762383	2822871	170
0759867	2821322	317	0760570	2823385	081	0762417	2822777	150
0759545	2821274	063	0760664	2823403	077	0762469	2822691	148

Eastings	Northings	Fault Segment Strike	Eastings	Northings	Fault Segment Strike	Eastings	Northings	Fault Segment Strike
0762519	2822606	151	0764530	2820895	142	0766554	2826361	163
0762549	2822513	172	0764591	2820815	144	0766592	2826270	152
0762556	2822416	180	0764653	2820735	140	0766630	2826181	162
0762555	2822317	182	0764716	2820657	142	0766664	2826089	157
0762553	2822216	180	0764777	2820576	144	0766703	2825994	157
0762561	2822116	171	0764848	2820500	129	0766733	2825905	167
0762570	2822017	179	0762706	2824951	169	0766646	2825494	338
0762565	2821914	187	0762738	2824836	160	0766618	2825589	349
0762533	2821827	215	0763061	2824199	007	0766594	2825688	344
0762467	2821763	236	0763085	2824298	020	0766556	2825782	332
0762409	2821697	204	0763129	2824395	028	0766509	2825867	329
0762398	2821607	173	0763182	2824492	029	0766457	2825952	329
0762409	2821505	175	0763230	2824587	023	0766429	2826050	360
0762410	2821406	183	0763339	2824359	137	0766467	2826131	052
0762404	2821305	184	0763392	2824274	158	0766116	2824133	360
0762391	2821205	191	0763448	2824187	137	0766118	2824238	002
0762388	2821107	172	0763537	2824744	125	0766120	2824345	360
0762410	2821012	161	0763615	2824685	131	0766120	2824438	360
0762447	2820920	155	0763692	2824633	118	0766100	2824535	340
0762506	2820842	132	0763773	2824576	133	0766066	2824639	344
0762577	2820770	139	0763839	2824500	144	0766033	2824730	335
0762639	2820686	148	0763895	2824413	151	0765995	2824817	339
0762900	2822181	142	0763938	2824320	159	0765967	2824914	349
0762958	2822098	148	0763978	2824230	152	0765941	2825012	341
0763002	2822003	162	0764029	2824143	147	0765913	2825107	347
0763023	2821898	176	0764079	2824056	155	0765884	2825208	341
0763018	2821797	191	0764125	2823966	152	0765856	2825303	347
0762992	2821700	198	0764184	2823885	135	0765826	2825399	339
0762974	2821598	183	0764244	2823808	149	0765814	2825509	334
0762991	2821496	158	0764291	2823718	154	0765769	2825610	337
0763039	2821407	145	0764335	2823625	155	0765737	2825716	349
0763096	2821323	147	0764363	2823530	173	0766907	2825068	148
0763149	2821235	151	0764371	2823433	178	0766961	2824984	146
0763188	2821148	161	0764028	2822898	112	0767016	2824905	145
0763186	2821713	124	0764116	2822851	125	0767075	2824820	145
0763272	2821673	103	0764198	2822791	128	0767128	2824733	153
0763365	2821657	097	0764276	2822725	132	0767176	2824645	149
0763466	2821633	110	0764349	2822654	137	0767224	2824557	153
0763561	2821598	111	0764419	2822580	137	0767276	2824470	146
0763657	2821554	118	0764492	2822517	123	0767332	2824392	141
0763741	2821497	131	0764572	2822473	115	0767381	2824309	155
0763823	2821439	120	0764646	2822414	142	0767413	2824210	171
0763905	2821381	131	0764707	2822330	146	0767438	2824117	159
0763977	2821309	139	0764763	2822240	150	0767963	2823972	132
0764043	2821227	143	0764806	2822149	160	0768041	2823907	127
0764118	2821172	107	0764842	2822055	159	0768125	2823856	115
0764215	2821139	111	0766441	2826736	135	0768216	2823816	112
0764306	2821090	127	0766499	2826659	152	0768304	2823772	122
0764388	2821035	120	0766531	2826567	169	0769822	2823642	012
0764465	2820973	138	0766541	2826462	180	0769846	2823739	016

Eastings	Northings	Fault Segment Strike	Eastings	Northings	Fault Segment Strike	Eastings	Northings	Fault Segment Strike
0769869	2823834	012	0770124	2822410	014	0766660	2820359	011
0769903	2823926	028	0770146	2822505	013	0767551	2820971	012
0769959	2824009	040	0770182	2822602	027	0767585	2821073	025
0770024	2824084	042	0770235	2822692	034	0767360	2821251	012
0770088	2824162	037	0770296	2822770	042	0767399	2821351	030
0770157	2824239	046	0770367	2822840	049	0767459	2821434	042
0770242	2824295	069	0770443	2822905	049	0767530	2821506	047
0770328	2824338	057	0770514	2822976	041	0767608	2821581	046
0770401	2824404	040	0770583	2823051	044	0767689	2821645	058
0770461	2824485	032	0770653	2823123	045	0767761	2821711	037
0770512	2824568	032	0770722	2823197	041	0767803	2821803	012
0770576	2824648	045	0770792	2823272	045	0767832	2821905	020
0770651	2824717	050	0770869	2823340	053	0767875	2822001	027
0770725	2824781	048	0770952	2823395	060	0768221	2822394	359
0770794	2824846	045	0771041	2823447	060	0768461	2821874	330
0770867	2824912	051	0771131	2823490	070	0768420	2821976	345
0768861	2821991	353	0771225	2823522	073	0768397	2822086	352
0768851	2822096	356	0771325	2823547	079	0768381	2822197	352
0768851	2822201	004	0771422	2823576	066	0768442	2820918	148
0768855	2822300	360	0771514	2823613	070	0768492	2820820	159
0769020	2822487	022	0771610	2823654	063	0768529	2820718	161
0769070	2822578	034	0772587	2822065	207	0768578	2820623	143
0769127	2822669	031	0772525	2821987	230	0768707	2820694	057
0769179	2822751	034	0772455	2821916	219	0768803	2820755	058
0769236	2822828	039	0772398	2821830	208	0768684	2820883	340
0769302	2822904	043	0772351	2821739	207	0768659	2820986	352
0769379	2822969	056	0772295	2821654	219	0768641	2821094	348
0769468	2823021	064	0772221	2821580	231	0768629	2821201	359
0769556	2823066	060	0772144	2821517	229	0768625	2821309	357
0769643	2823116	061	0772062	2821456	237	0768783	2821252	120
0769728	2823167	057	0771974	2821404	243	0768881	2821193	123
0769810	2823223	054	0771884	2821359	244	0768974	2821131	125
0769891	2823285	051	0771790	2821314	245	0769053	2821054	144
0769978	2823342	062	0771697	2821272	246	0767553	2822874	071
0770064	2823400	050	0773061	2821258	216	0767651	2822894	086
0770143	2823453	062	0772975	2821206	263	0767750	2822896	092
0770225	2823503	055	0772871	2821201	271	0767852	2822886	099
0770310	2823552	064	0772767	2821209	277	0767928	2823006	132
0770399	2823594	066	0771608	2820169	224	0767996	2822934	142
0770496	2823620	084	0771522	2820104	242	0768062	2822863	132
0770596	2823632	083	0771421	2820059	249	0768143	2822805	120
0770679	2823642	084	0771315	2820032	263	0768236	2822760	111
0770027	2821653	326	0766528	2819572	006	0768329	2822720	115
0769985	2821742	342	0766542	2819668	010	0768421	2822681	111
0769959	2821838	347	0766559	2819763	010	0768515	2822644	111
0769952	2821940	004	0766577	2819864	010	0768606	2822606	115
0769964	2822042	009	0766593	2819966	007	0768702	2822567	111
0769992	2822137	023	0766607	2820066	008	0768795	2822525	118
0770037	2822225	032	0766620	2820167	007	0768878	2822474	125
0770087	2822313	027	0766638	2820263	014	0769119	2822290	136

Eastings	Northings	Fault Segment Strike		Eastings	Northings	Fault Segment Strike		Eastings	Northings	Fault Segment Strike
0769193	2822224	127		0770743	2820281	161		0775125	2813579	053
0769273	2822163	128		0770778	2820187	159		0775591	2813665	049
0769346	2822097	136		0772035	2820001	119		0775688	2813724	068
0769417	2822021	137		0772128	2819951	117		0775783	2814052	067
0769489	2821951	129		0772219	2819901	120		0775881	2814083	077
0769572	2821889	126		0772298	2819844	131		0775978	2814113	069
0769643	2821824	142		0772366	2819773	141		0776079	2814155	067
0769704	2821748	141		0772423	2819691	150		0776137	2813587	182
0769771	2821668	140		0772477	2819605	146		0776135	2813480	180
0769835	2821594	138		0772528	2819516	154		0776119	2813385	200
0769908	2821528	126		0772566	2819421	162		0776089	2813290	195
0769982	2821463	135		0772590	2819323	170		0776055	2813194	204
0770048	2821384	145		0772604	2819224	174		0776012	2813107	209
0770111	2821301	140		0772618	2819121	171		0775970	2813018	201
0770172	2821222	145		0775641	2816334	108		0775934	2812924	201
0770225	2821141	149		0775746	2816318	090		0775895	2812823	202
0770282	2821056	144		0775845	2816348	056		0777088	2814442	235
0770343	2820969	146		0775934	2816411	054		0777000	2814392	246
0770396	2820886	149		0774920	2814700	084		0776908	2814350	245
0770442	2820802	153		0775027	2814702	094		0776817	2814306	244
0770488	2820709	153		0774789	2813206	029		0776725	2814269	252
0770538	2820622	147		0774845	2813294	036		0776629	2814242	256
0770596	2820541	142		0774910	2813375	042		0776529	2814214	253
0770652	2820458	150		0774976	2813450	040		0776432	2814188	257
0770702	2820372	150		0775045	2813518	052		0776334	2814163	255